Benzene-Based 1D, 2D and 3D Molecular Architectures for Organic Electronics

Dissertation zur Erlangung des Grades

„Doktor der Naturwissenschaften"

am Fachbereich Chemie, Pharmazie und Geowissenschaften

der Johannes Gutenberg-Universität Mainz

Florian Schlütter

geboren in Suhl

Mainz im Jahr 2013

Dekan: ████████████████

1. Berichterstatter: ██████████████

2. Berichterstatter: ████████████████

3. Berichterstatter: ███████████████

Tag der mündlichen Prüfung: 26.11.2013

v

Für meine Eltern

„Habe nun, ach! Philosophie,
Juristerei und Medizin,
Und leider auch Theologie!
Durchaus studiert, mit heißem Bemühn,
Da steh ich nun, ich armer Tor!
Und bin so klug als wie zuvor.“

Johann Wolfgang von Goethe

Table of Contents

Index of Abbreviations

2D WAXS	two-dimensional wide-angle X-ray scattering
AcOH	acidic acid
AFM	atomic force microscopy
bipy	2,2'-bipyridine
BuLi	butyl lithium
br	broad signal (NMR)
COD	cycloocta-1,5-diene
COSY	correlation spectroscopy
COT	cyclooctatetraene
CV	cyclic voltammetry
d	doublet (NMR)
dd	doublet of doublets (NMR)
DDQ	2,3-dichloro-5,6-dicyano-1,4-benzoquinone
DFT	density functional theory
DLS	dynamic light scattering
DMF	*N*,*N*-dimethylformamide
DMSO	dimethyl sulfoxide
DSC	differential scanning calorimetry
ESI	electron spray ionization
FD MS	field desorption mass spectrometry
GNR	graphene nanoribbon
h	hour
H, H COSY	two-dimensional correlated proton NMR spectroscopy
HBC	hexa-*peri*-hexabenzocoronene
HOMO	highest occupied molecular orbital
HPLC	high performance liquid chromatography
HR ESI	high resolution electron spray ionization
HSQC	heteronuclear single quantum coherence
LDA	lithium di-*iso*-propylamide
LUMO	lowest unoccupied molecular orbital
m	multiplet (NMR)
MALDI-TOF	matrix-assisted laser desorption/ionization time-of-flight

Me	methyl
min	minute
MS	mass spectrometry
NMR	nuclear magnetic resonance
NOESY	nuclear *Overhauser* enhancement spectroscopy
OFET	organic field-effect transistor
OLED	organic light emitting diode
OPP	oligo(*para*phenylene)
OPV	organic photovoltaics
*o*DCB	1,2-dichlorobenzene
PAH	polycyclic aromatic hydrocarbon
Ph	phenyl
PL	photoluminescence
ppm	parts per million
PPE	poly(*para*phenyleneethynylene)
PPP	poly(*para*phenylene)
PPV	poly(*para*phenylenevinylene)
PS	poly(styrene)
q	quartet (NMR)
RT	room temperature
s	singlet (NMR)
STM	scanning tunneling microscopy
t	triplet (NMR)
^{t}Bu	*tert*-butyl
TCB	1,2,4-trichlorobenzene
TCNQ	7,7,8,8-tetracyanoquinodimethane
TD-DFT	time-dependent DFT calculations
THF	tetrahydrofuran
TGA	thermogravimetric analysis
TLC	thin layer chromatography
TMS	trimethylsilyl
UHV	ultrahigh vacuum
UV-vis	ultraviolet-visible

1 Introduction

1.1 Organic Electronics

Cost, availability and sustainability of energy will be the most important factors influencing the human society in the 21st century by their significant impact on the quality of our life, the stability of our environment, the growth of global economies and the relationships between countries.[1, 2] Thus, research is more and more focused on the development of novel energy-harvesting and energy-saving devices, such as solar cells, light-emitting diodes and transistors.[3] In the last decades, the central element of microelectronics was silicon, which allowed for a miniaturization of devices, *e.g.*, processors in such way that recent Pentium i7 chips contain up to 1.1 billion transistors. Through the replacement of silicon by organic molecules or polymers, researchers around the world hope to provide new materials for various electronic applications. The primary advantage of such organic materials over their inorganic counterparts is their simple and cost-effective processing by large-scale roll-to-roll production with the help of dip-coating, spin-casting and inkjet printing.[4] However, the goal is thereby not necessarily to attain or even exceed the level of performance of inorganic semiconductors (silicon is still the best for several applications) but more to benefit from their unique characteristics combining the electrical properties of (semi)conductors with the properties of plastics, such as low-costs, the versatility of chemical synthesis, the ease of processing and a certain mechanical flexibility.[5] This led to several intriguing new results in the past years, such as ultrahigh charge carrier mobilities in polymeric transistors or the integration of such transistors with an organic light-emitting diode (OLED).[6-8]

Figure 1-1. Examples of organic electronics. Left: Flexible display based on an organic field-effect transistor. Middle: Flexible blue emitting OLED. Right: Suspended mirrorwall prototype made with Philips Lumiblade OLEDs (Philips 2009).[9]

OLEDs are already used for flat-panel displays in cell phones, televisions and computer screens as well as for lighting applications (Figure 1-1). They are composed of a fluorescent organic material, which is either a polymer or a small molecule dye emitting light by applying an electric current. This active organic layer is usually located between two electrodes, one of which must be transparent to light. Additional layers thereby assist the charge injection and the transport from the electrodes to the active layer to improve the device performance.[9]

Devices based on organic molecules and polymers have the advantages of being lighter, are more robust and are considerably cheaper to produce than single crystals or amorphous silicon analogues.

The ability of processing such organic molecules at lower temperatures over large areas, *e.g.*, by inject printing, may provide unique technologies and generate new applications.[4]

Such devices already entered the commercial market, most notably the displays of several mobile and television applications. Dye-sensitized solar cells, a special type of organic solar cells, were moreover the first organic photovoltaic products on the market, due to their high efficiency and stability.[2] According to a recent outlook, the total market of organic electronics will grow from $16.04 billion in 2013 to $76.79 billion in 2023.[10] Every 18 months the charge mobility of transistors made from organic materials significantly increases, and is now at the point where it competes with amorphous silicon, at a fraction of the cost.[11, 12]

1.2   One-dimensional Polyphenylene Scaffolds for Multidimensional Systems

The key building block of all herein discussed molecular entities is the simplest aromatic compound, namely benzene (**1-1**, Figure 1-2). It consists of six sp^2-hybridized carbon atoms arranged in a hexagon and was initially discovered by *Faraday* in 1825.[13] Its exact structure, however, remained the topic of intense discussions for several years.[14, 15] In 1865, *Kekulé* proposed for the first time the concept of aromaticity by his cyclic structure of benzene.[16] The aromatic π-sextet was later on introduced by *Robinson* and further improved by *Hückel's* molecular orbital theory in 1931.[17, 18] A facile system for the prediction of stability of larger aromatic systems was postulated in 1964 by *Clar*.[19] Due to its structural anisotropy and chemical versatility, benzene is an ideally suited modular repeating unit for the construction of macro- and supramolecular structures by covalent and
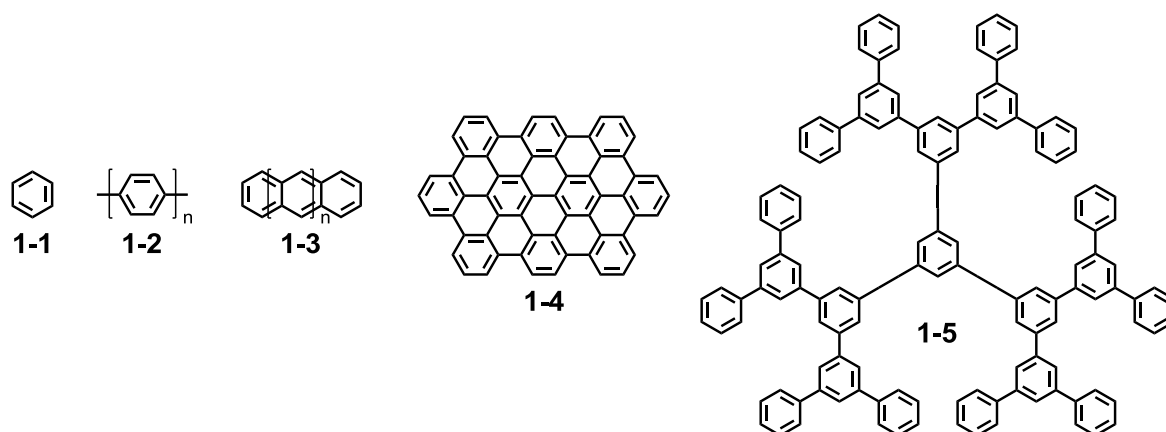
Figure 1-2. One-, two- and three dimensional polyphenylene structures.

non-covalent bonds with different sizes and shapes.[2, 20, 21] By the repeated connection of benzene units, a series of π-conjugated scaffolds with varying size and dimensionality is obtained. These comprise, for instance, linear poly(*para*phenylenes) (PPP) **1-2** and poly[*n*]acenes **1-3** with one-dimensional (1D) architectures, graphene or polycyclic aromatic hydrocarbons (PAHs) such as **1-4** with two-dimensional (2D) architectures and three-dimensional (3D) polyphenylene dendrimes **1-5**.[21] The following discussion refers to the most relevant examples of each category.

1.2.1 One-dimensional Polyphenylene Architectures

The dicovery of *Shirakawa*, *MacDiarmid* and *Heeger*, that poly(acetylene),[22, 23] a plastic material, is able to conduct electric current upon doping through the addition of elemental iodine, led to a breakthrough for organic semiconductors.[24-26]

A wide range of new semiconductor materials have emerged, which are essentially based on polyphenylene structures (Figure 1-3). This includes besides PPPs **1-2**, poly(*para*phenylenevinylene) (PPV, **1-6**) and poly(*para*phenyleneethynylene) (PPE, **1-7**). Their manifold applications comprise optoelectronic devices, such as organic solar cells,[27-30] organic field-effect transistors (OFETs),[6, 8, 31-35] OLEDs,[7, 36-38] and sensors.[39-42] All structures consist of a rigid chain with conjugated single- (σ-bond) and multiple bonds (π-bond). In general, the electronic structures of these types of polymers originate from the sp^{2}p$_z$ hybridized wavefunctions of the carbon atoms in the repeating unit.[43]
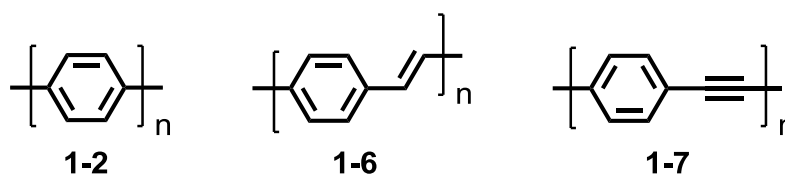
Figure 1-3. Examples of polyphenylene based polymers.

(a)

(b)
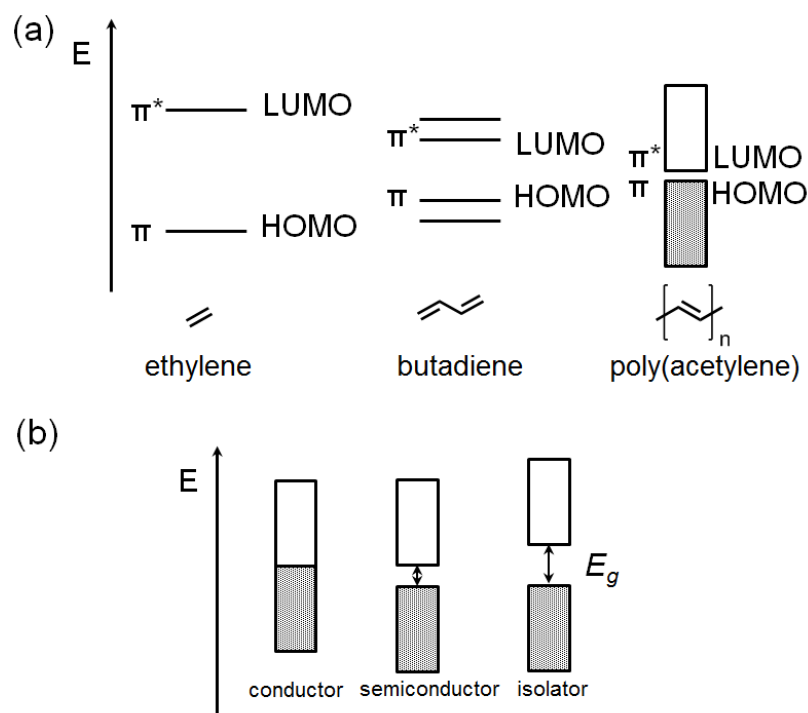
Figure 1-4. (a) Schematic representation of the energy differences of molecular orbitals. (b) Band gap differences of electrical conductors, semiconductors and isolators.

Polyphenylene polymers are described by energy bands that arise from the individual molecular orbitals of the repeating units, whose energy difference can no longer be discerned and hence lead to a band-type structure (Figure 1-4 a). The σ-bonds hold the structure together, whereas the π-bonds are the origin of the properties that characterize π-conjugated polymers as semiconductors.[24, 43-45] The delocalization of the electrons along the polymer chain is determined by the overlap of the π-orbitals. The distance between the highest occupied molecular orbital (HOMO) and lowest unoccupied molecular orbital (LUMO) is defined as the band gap (E_g).[2, 43] It describes the amount of energy needed to raise an electron from its ground state to an excited state. Insulators have large band gaps, whereas electrical conductors have a vanished band gap. Semiconductors, such as π-conjugated polymers are small band gap materials (Figure 1-4 b). The E_g defines thereby their utilization in optoelectronic devices and is usually located between 2 to 3 eV for polyphenylene architectures.[2, 46, 47]

The polymers in Figure 1-3 were made soluble and processible by the virtue of alkyl or alkoxy side chains. Due to the steric repulsion between the solubilizing chains, a decreased overlap of the π-orbitals together with an increased E_g is observed. This is displayed by a hypsochromic shift of the absorption and emission properties. To obtain solubility and thus processability without undesired absorption and emission shifts, short carbon bridges were
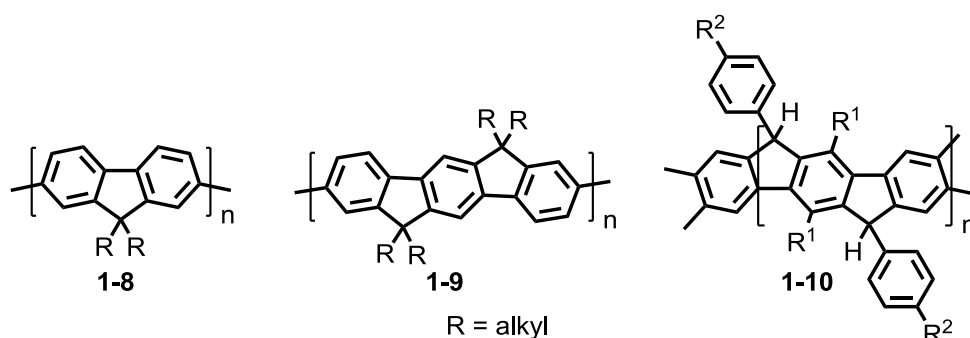
Figure 1-5. Structures of poly(fluorene) **1-8**, poly(indenofluorene) **1-9** and ladder-type polyphenylene **1-10**.

attached between some or all of the benzene rings.[48, 49] *Yoshino* and coworkers achieved this by the synthesis of poly(fluorene) **1-8** for the first time (Figure 1-5).[50] By the emergence of modern transition metal-mediated cross-coupling reactions, the molecular weights of these materials could be significantly increased. This concept was further extended by *Müllen* and coworkers with the synthesis of alkyl-substituted poly(indenfluorenes) **1-9**.[51] These polymers showed a strong blue emission with maxima around 430 nm, which made them attractive candidates for the use in OLEDs.[48, 49] The next step in the concept of bridged PPPs was the transition from step-ladder to ladder-type polyphenylenes (**1-10**) with methine-bridges developed by *Scherf* and *Müllen*.[52-54] Twisting along the polymer chain was minimized by complete bridging of all phenylenes with each of the respective neighboring units.[21] The key synthesis step is thereby the polymer analogous *intra*molecular *Friedel-Crafts* alkylation of polyalcohol **1-12** which is obtained upon reduction of precursor polymer **1-11** (Scheme 1-1).
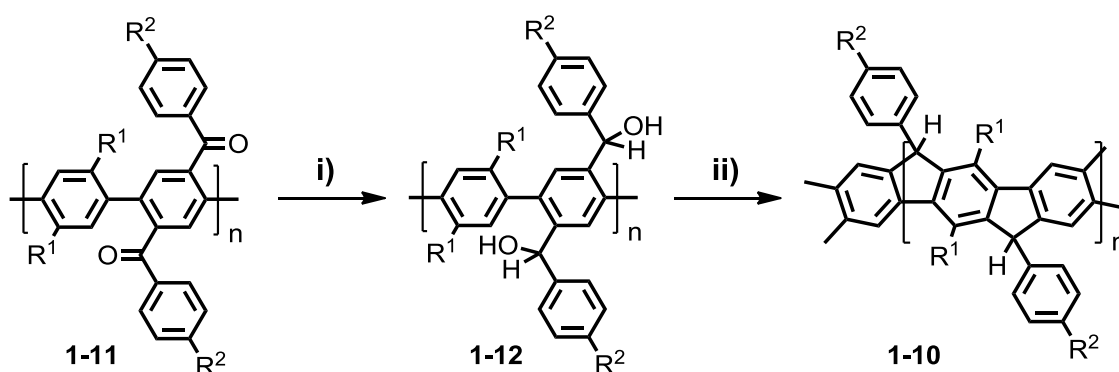
Scheme 1-1. Schematic representation of the synthesis of ladder-type polyphenylene **1-10** developed by *Scherf* and *Müllen*.[52-54] Conditions: i) LiAlH$_4$; ii) BF$_3$.

This step could be carried out quantitatively and regioselectively. By this method polymers with up to 50 000 g/mol have been obtained. The increased π-conjugation resulting from the planarization led to an optimization of the photophysical properties of PPPs. The

successful stiffening of the PPP backbone was revealed by a small Stokes shift (150 cm^{-1}).

In addition to a well-defined chemistry, PPP-type polymers allow for an effective emission-color tuning from UV-blue to blue by increasing the number of aryl-aryl bridges[55] - stretching from the UV emission of PPP,[56] over poly(fluorene)[57] (emitting in the UV blue) and poly(indenofluorene)[51] (emitting further in the visible) to ladder-type PPPs[58, 59] yielding a deep blue emission matching the sensitivity of the human eye for blue. Therefore, these types of polymers are appealing candidates for OLED and lighting applications.[60-62]

In combination with the variations of this bridging methods developed by *Swager*[63] and *Tour*,[64-66] the rigidification of the PPP backbone, however, can be considered as the starting point toward 2D polyphenylene ribbon-type structures.

1.2.2 Two-dimensional Polyphenylene Architectures

In contrast to the 1D structures, 2D architectures are covalently linked networks of monomers with periodic bonding in two orthogonal directions.[67] A very prominent example of 2D structures is the monolayer of the carbon allotrope graphite, denoted as graphene, and whose optical, electronic and mechanical properties attracted intense contemporary interest.[68-72] *Geim* and *Novoselov* reported in 2004 the microexfoliation of graphene from graphite *via* a scotch tape. Further top-down methods for the preparation of graphene are epitaxial growth[73] or pyrolytic decomposition techniques.[74, 75]
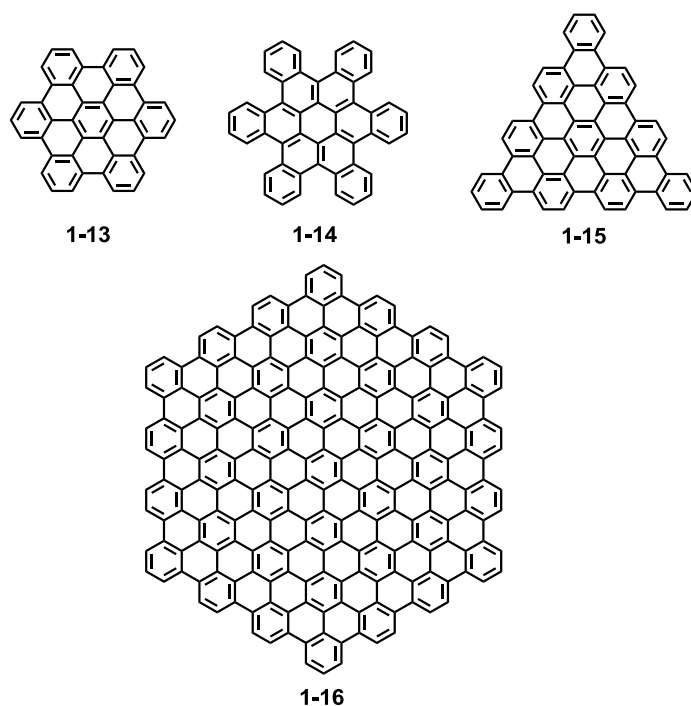
Figure 1-6. Structures of 2D nanographene examples synthesized by *Müllen* and *Nuckolls*.[82-85]

Since its experimental realization, graphene has been extensively studied as a substitute for doped silicon in transistors, caused by its high charge carrier mobility and its low thickness.[76, 77] Due to the lack of a band gap, however, graphene transistors cannot be put in the "off" state.[78] Nevertheless, there are several concepts available for opening a band gap such as the lateral confinement to graphene materials. The resulting structurally precise nanographenes, that can be regarded as 2D cutouts of the graphene lattice, have been basically derived by the bottom-up fabrication *via* synthetic approaches (Figure 1-6).[79-85] *Müllen* and coworkers utilized, for example, well-characterized, soluble oligophenylene precursors, which were converted in the so-called *Scholl* reaction,[86-88] an *intra*molecular, oxidative cyclodehydrogenation using different types of Lewis acids into the respective nanographenes.[89-91] This method allowed for the synthesis of a broad variety of nanographenes, such as hexa-*peri*-hexabenzocoronene **1-13** (HBC), hexa-*cata*-hexabenzocoronene **1-14**, triangle-shaped **1-15** and the so-far largest nanographene C_{222} **1-16** (Figure 1-6).[82-85] The *intra*molecular cyclodehydrogenation of the carefully designed dendritic precursors was achieved in a single reaction comprising the formation of up to 54(!) $C(sp^2)-C(sp^2)$ bonds (for **1-16**) at exact positions. The decreased solubility limited, however, the characterization of the larger molecules to mass spectrometry and microscopy techniques. Besides **1-14** with its cove edges, the depicted molecules have the same armchair edge structure. Nanographenes fused with additional C−C double bonds, which act as zig-zag edges, have also been produced.[92, 93] It is known that the variation of the edge structure can provide a powerful tool to alter the optoelectronic properties of graphene molecules.[81]

1.2.2.1   Shape-persistent π-Conjugated Macrocycles

A special type of 2D oligophenylene structures and therefore an important family of compounds are shape-persistent π-conjugated macrocycles. Their study combines aspects of solution-based organic synthesis, polymer science and supramolecular chemistry and hence forms a link between these individual fields of research.[94-97] Organic chemistry provides defined and analytically pure compounds, whereas polymer chemistry allows for the formation of polydisperse compounds with different chain lengths. Due to their monodisperse structures with few degrees of conformational freedom, mimicking an infinite polymer chain without perturbing end groups, π-conjugated macrocycles are interesting for fundamental studies but also have potential applications in organic optoelectronics and nanotechnology.[98-101]
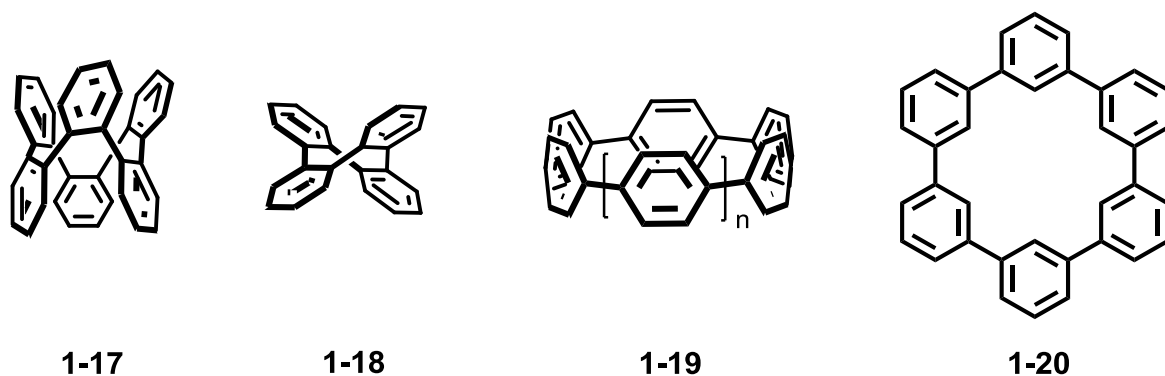
Figure 1-7. Structures of cyclo-*o*-hexaphenylene **1-17**, cyclo-*o*-tetraphenylene **1-18**, cyclo-*p*-hexaphenylene **1-19** and cyclo-*m*-hexaphenylene **1-20**.

In recent years, a broad variety of large macrocycles with several nanometers in diameter were reported. The properties of these structures were basically determined by their spatial arrangement and *inter*molecular interactions. Not fully π-conjugated, flexible macrocycles, such as cyclodextrines and calixarenes are not able to constantly maintain their inner cavity.[102-104] Due to their rigidity, however, shape-persistent macrocycles are composed of an inner cavity, which is separated from the environment. This architecture can lead to the assembly of columnar 1D nanotubes,[105-110] 2D porous networks at interfaces,[79, 96, 97, 111-116] and 3D host-guest complexes.[108, 109, 117-123] Owing to the great variety of macrocyles with π-conjugated arene backbones, the following overview is limited to a few selected examples.

Since the pioneering work of *Staab* in the 1960s,[124-127] macrocycles, being exclusively constructed from directly connected aromatic units, became scientifically relevant. Depending on the substitution pattern of the aryl moiety, different geometries can be obtained (Figure 1-11). Utilizing a 1,2-functionalized aryl led, *e.g.*, to the formation of highly twisted cyclo-*o*-hexaphenylene **1-17** and cyclo-*o*-tetraphenylene (COT) **1-18**. The latter one is furthermore designated as cyclooctatetraphenylene (COT) and its derivatives were extensively investigated by *Iyoda* and *Rajca* as a consequence of their chirality and liquid crystallinity.[128-133]

Switching to a 1,4-substituted benzene led to cyclo-*p*-hexaphenylene (CPP) **1-19** and its larger derivatives, such as [7]-, [8]-, [9]-, [12]-, [14]-, [15]-, [16]- and [18]-CPP, which can be considered as the smallest segments of armchair carbon nanotubes.[134-143]

The formation of cyclo-*m*-hexaphenylene **1-20**, however, required a 1,3-functionalized aryl precursor. The optimization of the reaction conditions by *Staab* and *Müllen* is exemplified in Scheme 1-2.[110, 124] By utilizing Grignard monomer **1-21** the formation of various linear
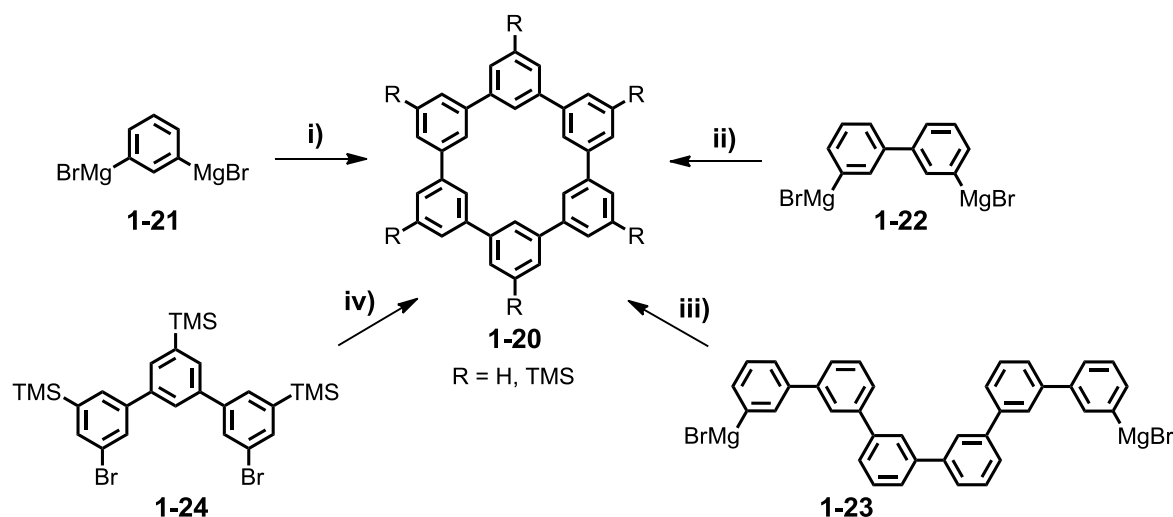
Scheme 1-2. Schematic representation of the cyclo-*m*-phenylene **1-20** synthesis optimization by *Staab*[124] and *Müllen*.[110] Conditions: i) CuCl$_2$, 1.1%; ii) CuCl$_2$, 11%; iii) CuCl$_2$, 45%; iv) bis(cycloocta-1,5-diene)nickel(0), cycloocta-1,5-diene, 2,2'-bipyridine, 58%.

oligomers was obtained, which significantly reduced the amount of formed macrocycle **1-20** (1.1%). The yield of **1-20** was, however, increased by one order of magnitude (11%) when using dimer **1-22**, due to the reduced number of coupling steps. Further decreasing the number of C−C bond formations to one *intra*molecular connection by utilizing hexamer **1-23** afforded **1-20** in 45% yield. *Staab* and coworkers could thereby show that by decreasing the number of coupling steps, the cyclization yield is significantly increased.[124] This example illustrates the strengths and the weaknesses of the two basic macrocylization concepts. The utilization of a simple monomer leads to a small amount of macrocyle together with a complex mixture of oligomers. On the other hand, the application of a linear oligomer, which is obtained in a multistep sequence prior to the cyclization, reduces the total number of cyclization steps and thus increases the macrocycle yield. The level of complexity increases, however, by further expanding the ring size. To overcome these problems, *Müllen* and coworkers adapted in a more recent approach a repetitive convergent strategy for the optimized synthesis of **1-20** (Scheme 1-2).[110] They synthesized a preorganized trimer **1-24** which was subsequently cyclodimerized by the *Yamamoto* reaction thus affording **1-20** in 58% yield. By utilizing highly diluted reaction mixtures for the final cyclization, the unfavored *intra*molecular C−C bond formation was facilitated and *inter*molecular reactions were suppressed. This strategy has been introduced by *Moore* in 1994 for the formation of macrocycle **1-25** using a sequence of *Sonogashira-Hagihara* reactions thus affording **1-25** in 75% yield (Figure 1-8). It was thereby much more efficient than the statistical approach of *Staab* for the same cyle (4.6% for **1-25**).[106, 144]
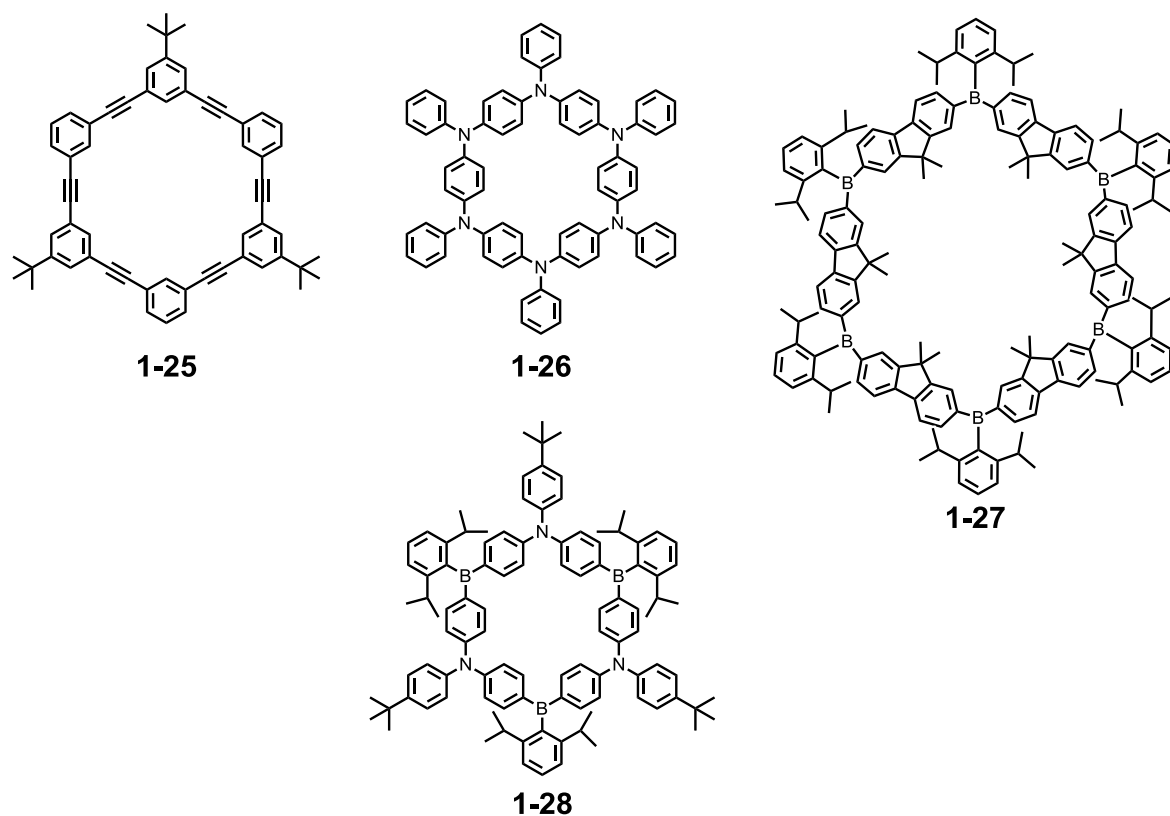
Figure 1-8. Structures of macrocycles synthesized by *Moore*,[106] *Tanaka* and *Ito*,[145, 146] and *Jäkle*.[100, 101]

The macrocycle synthesis could be successfully extended toward heteroatom-linked aryls (Figure 1-8). *Tanaka* and *Ito* prepared, for example, hexaaza[1$_6$]paracyclophane **1-26** *via* a convergent sequence of *Buchwald-Hartwig* amination reactions in 7% yield over three steps.[145] Due to its redox-active triarylamine centers, **1-26** was oxidizable up to a hexacation species. *Jäkle* and coworkers modified this procedure for the synthesis of the boron analogue **1-27** by exploiting a complex sequence of stannyl/boron and silyl/boron exchange reactions, which provided **1-27** in 31% yield over three steps. Combining the aspects of electron-rich hexaazacyclophane **1-26** and electron-deficient boracyclophane **1-27**, *Jäkle* and coworkers synthesized very recently π-expanded borazine **1-28**.[101] Besides its appealing structure, **1-28** can be applied as sensor for anions and is a potential candidate for ambipolar charge transport applications.

In addition to the statistical synthesis and *Moore*`s convergent approach, template-directed cyclizations allowed for the synthesis of macrocycles with larger cavities.[109, 119-121, 147-150] This concept has been developed, among others, by *Anderson* and coworkers in 1990 and will be explained for a few examples in the following.[151, 152] It has been demonstrated for the synthesis of zinc porphyrin macrocycle **1-31** that already smaller precursors can be successfully cyclized by this method thus avoiding demanding multistep syntheses of the linear oligomers (Scheme 1-3).
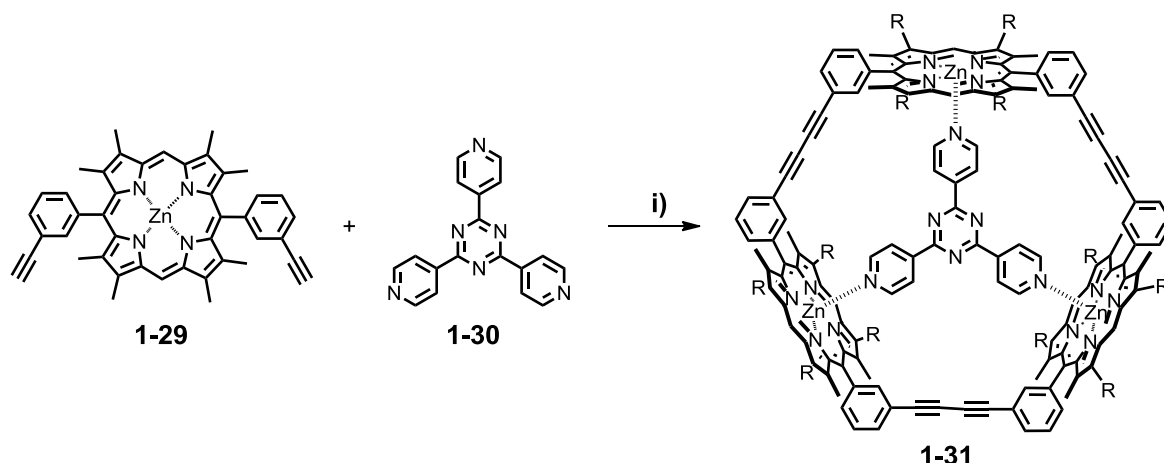
Scheme 1-3. Schematic representation of the template-directed synthesis of macrocycle **1-31** by *Anderson*.[151] Conditions: i) CuCl, TMEDA, air, 50%.

By coordinating three molecules of **1-29** to the template 2,4,6-tri(pyridin-4-yl)-1,3,5-triazine (**1-30**), the porphyrins were forced into close spatial contact thus increasing the propensity of the three subsequent *intra*molecular reactions toward **1-31**. This approach resulted in a remarkable cyclization yield of 50%. While **1-29** showed a *meta*-substitution of the peripheral acetylenes, *Anderson* utilized this concept also for the cyclization of *para*-connected porphyrins toward macrocycles with larger cavities.[120, 148] *Müllen* and coworkers expanded this strategy toward dodeca-2,7-carbazole and dodeca-2,7-fluorene rings, which is illustrated for oligofluorene macrocycle **1-35** in Scheme 1-4.[109, 149] In contrast to *Anderson's* approach, they covalently attached a fluorene trimer endcapped with chlorine atoms (**1-32**) to a zinc porphyrin template (**1-33**). Precursor **1-34** was subsequently cyclized by the *Yamamoto* reaction in a highly diluted reaction mixture. Finally, the template was removed from the cavity by a simple hydrolysis to provide macrocycle **1-35** in 1.5% yield, which was in the same range as for the similarly prepared dodeca-2,7-carbazole ring. Investigation of **1-35** by scanning tunneling microscopy (STM) on highly oriented pyrolytic graphite (HOPG) revealed a diameter of 4.0 nm and a self-assembly of the macrocycles to a hexagonal packing (Scheme 1-4, inset).

Based on the template-directed approach, *Höger* and coworkers were able to synthesize all-hydrocarbon spoked wheels with diameters of 4, 6.9 and 7.9 nm (Scheme 1-5).[115, 118, 119, 150, 153] The "template" (**1-36**) was accessed by a sixfold *Sonogashira-Hagihara* coupling of a hexahalo hexaphenylbenzene with a preformed spoke followed by deprotection of the terminal acetylenes.[153] The diameter of the macrocycle was thereby controlled by the length of the respective spokes. Utilizing the *Glaser*
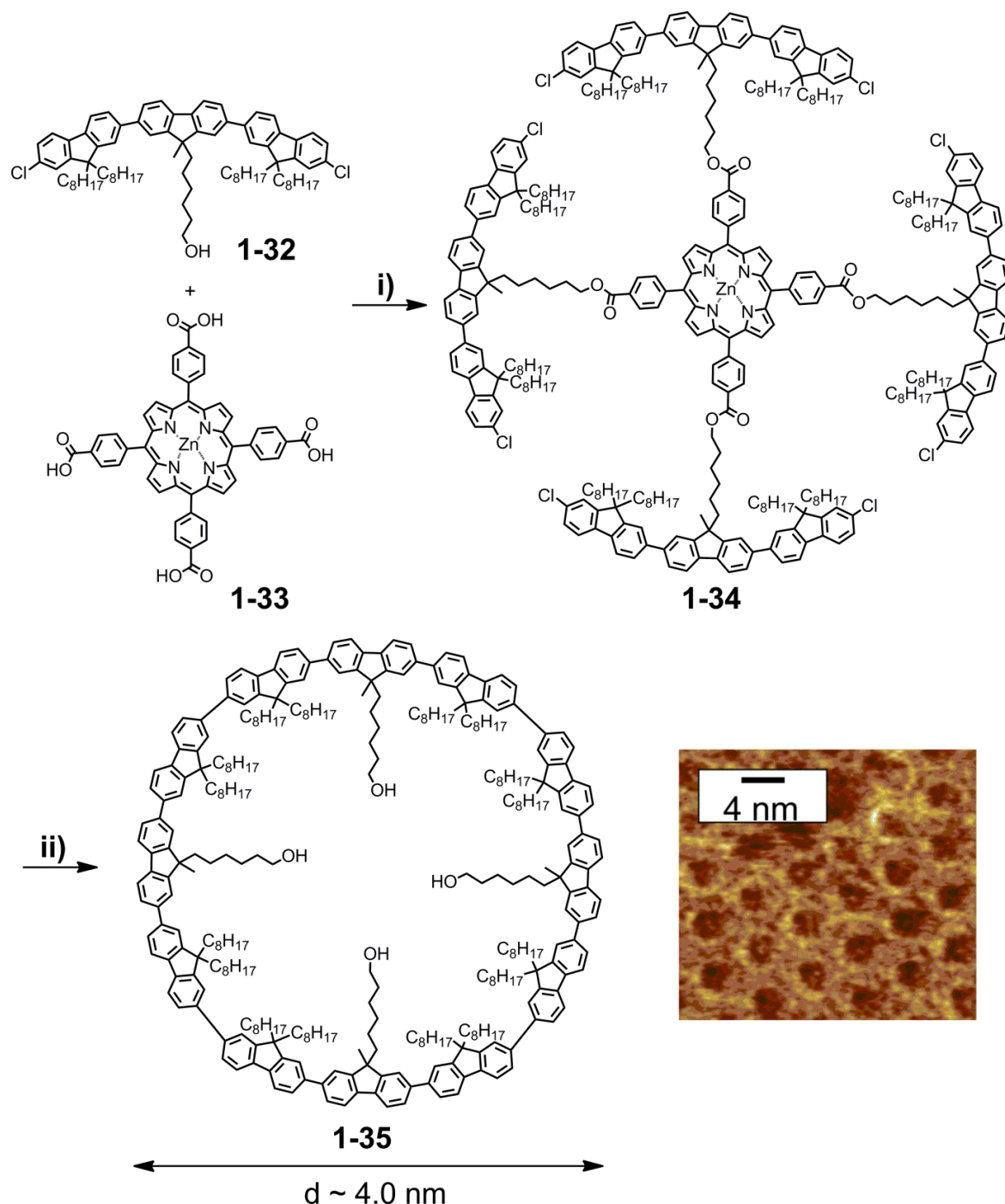
Scheme 1-4. Schematic representation of the synthesis of oligo(fluorene) macrocycle **1-35** synthesized by *Müllen*.[149] Conditions: i) PPh$_3$, diethyl azodicarboxylate, 65%; ii) (a) bis(cycloocta-1,5-diene)nickel(0), cycloocta-1,5-diene, 2,2'-bipyridine; (b) KOH, 1.5%. Inset: STM image of a 2D layer of **1-35** on HOPG.

reaction, the *intra*molecular coupling of **1-36** was achieved in a highly diluted reaction mixture to afford **1-37** in 75% yield. The calculated diameters of the obtained macrocycles, were in excellent agreement with the diameters revealed by STM (Scheme 1-5, inset).

The key to the high cyclization yields of the three examples was basically a low concentration of molecules in the reaction mixtures in combination with a high local
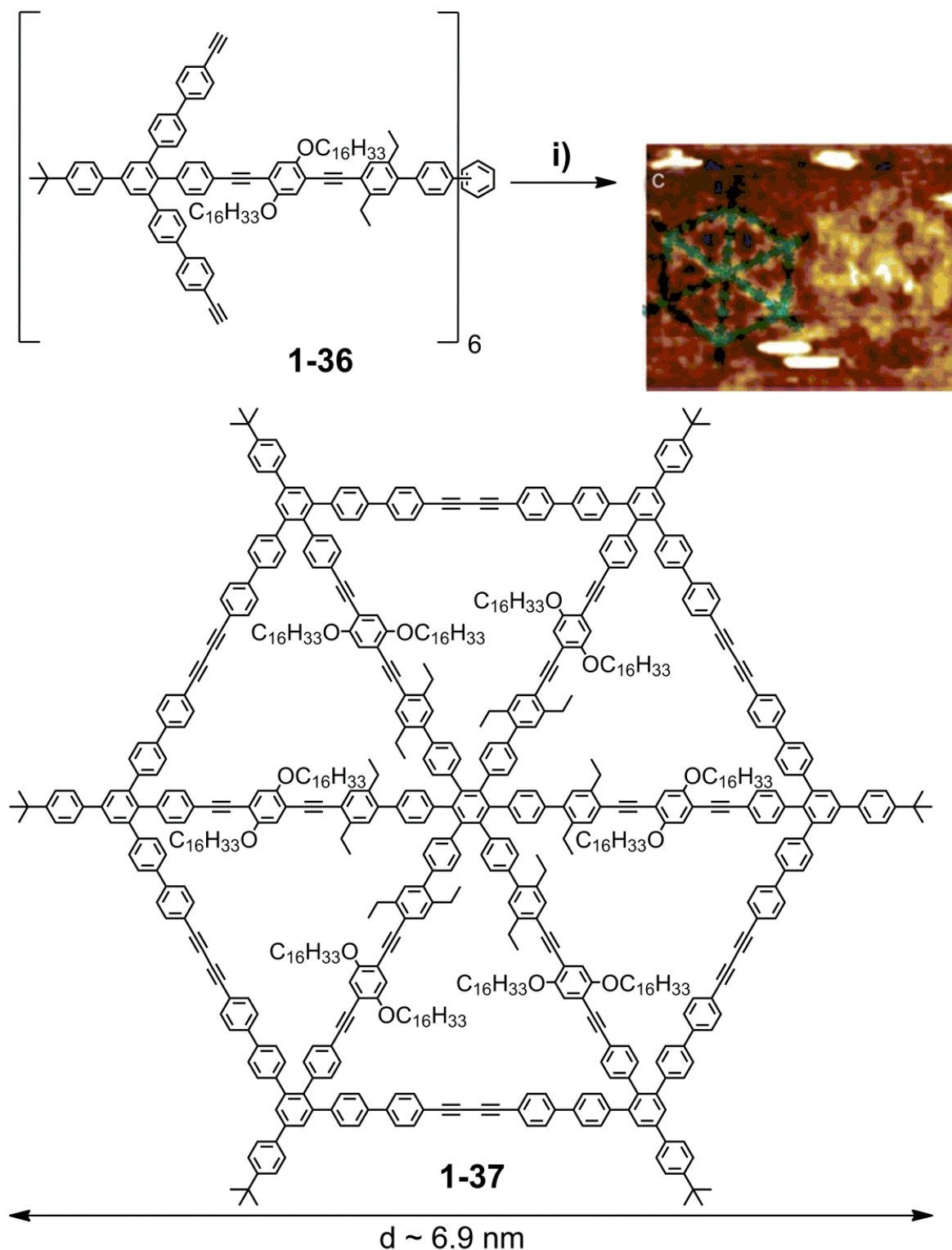
Scheme 1-5. Schematic representation of *Höger`s* template-directed macrocycle synthesis of spoked-wheel macrocycle **1-37**.[115] Conditions: i) CuCl, CuCl$_2$, pyridine, DBU, 75%. Inset: STM image of **1-37** immobilized on HOPG.

concentration of reactive terminal groups. This was accomplished by reducing the number of possible relative orientations of the reacting molecules through the connection to the template.

1.2.2.2   Graphene Nanoribbons

As already mentioned above, the lateral confinement of graphene induces a band gap. Graphene nanoribbons (GNRs), being 2D cutouts of graphene that exhibit a large aspect ratio of length over width, are known to possess a band gap.[77, 154] Several top-down fabrication methods have been reported, such as lithographic patterning[155-158] or mechanical exfoliation of graphene.[159]
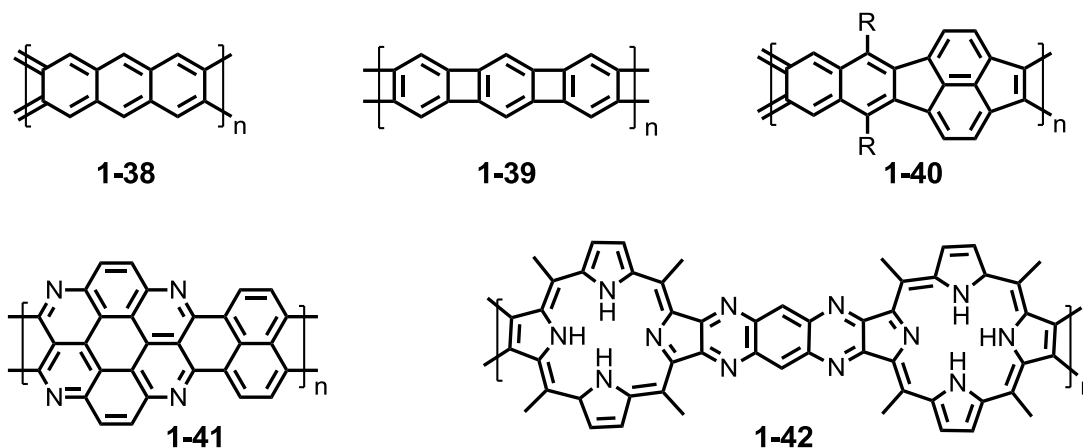
Figure 1-9. Structures of early examples of ribbon-type polymers.

The synthesis of ladder-type PPPs was basically the starting point for the chemical synthesis of GNRs (see above). The simplest approach for the formation of GNRs is thereby the linear annelation of benzenes leading to poly(acenes) **1-38** (Figure 1-9).[160, 161] According to *Clar`s* rule only one electron sextet can be assigned to **1-38**, thus reflecting the instability of higher, unsubstituted acenes.[19]

The connection of the benzene rings *via* a cyclobutadiene moiety led to the formation of double-stranded [N]phenylenes (**1-39**), which have been extensively studied by *Vollhardt* and coworkers.[162-169] A [N]phenylene consists thereby of N benzene rings which are separated by [N-1] intervening four-membered rings. Due to the alternating arrangement of aromatic benzenes and antiaromatic cyclobutadienes, unusual electronic properties have been revealed for **1-39**. This includes an incrementally decreasing bathochromical shift of the longest-wavelength absorption with increasing chain length.

Applying transition metal-catalyzed aryl-aryl couplings and subsequent ring-closure reactions led to alternative ribbon-types such as **1-40** with six- and five-membered ring combinations.[21, 170]

Early work on stable, heteroatom-containing ribbons **1-41** goes back until the 1960s.[171-174] They were obtained *via* polycondensations under harsh conditions. Due to the lack of

solubilizing side chains, only insoluble hardly characterizable polymeric materials were obtained.

In addition, fully π-conjugated porphyrin polymers (**1-42**) have been reported by *Crossely*.[175] The macrocyclic units were thereby fused through pyrazine rings. Their extended π-conjugation in combination with the metal-chelating ability of the porphyrin makes such material potentially interesting as molecular wires.

Müllen and coworkers developed in recent years a bottom-up approach for the synthesis of structurally defined GNRs overcoming the solubility problems of earlier examples. In a two-step procedure, initially well-soluble dendronized poly(*para*phenylene) precursors were synthesized by *Diels-Alder* cycloaddition[176-178] or Pd-catalyzed aryl-aryl couplings.[179, 180] Due to the close spatial arrangement of the benzene rings, the precursors adopt a similar topology as the target molecules. In the second step, the precursors were planarized through oxidative *intra*molecular cyclodehydrogenation toward the desired GNRs.[154] By this reproducible synthetic strategy, GNRs with precise lateral and longitudinal dimensions have been fabricated (Figure 1-10, top).

The *Suzuki-Miyaura* polycondensation of hexaphenylbenzene monomers was used for the synthesis of nanoribbon **1-43** consisting of up to 20 repeating units.[180] High efficiencies for the cyclodehydrogenation toward **1-43** were shown and its structure was studied by electron and scanning tunneling microscopy (STM).

Laterally extended nanoribbon **1-44** was prepared by *Yamamoto* polymerization, which circumvented the intrinsic sensitivity of A_2B_2-type polycondensations to stoichiometry (see Chapter 3 for further details). By this method the length of the GNRs has been expanded to approximately 30 nm, having optical band gaps of up to 1.12 eV.[178] Whereas **1-43** and **1-44** illustrate the solution-based synthesis of GNRs, a very recent trend addresses the surface-assisted fabrication of graphene structures under STM control and ultrahigh vacuum (UHV) conditions.[181-184] By this method chevron-type GNR **1-45** and linearly fused poly(anthryl) derivative **1-69** were accessible (Figure 1-10, bottom).[182] This technique, involving most likely radical reaction mechanisms both for the polymerization and the cyclodehydrogenation step, is situated somewhere between synthetic polymer and surface chemistry. Moreover, the solubility problems of the GNRs are efficiently avoided by the surface concept.

solution

1-43

R = alkyl

1-44

surface

1-45   **1-46**
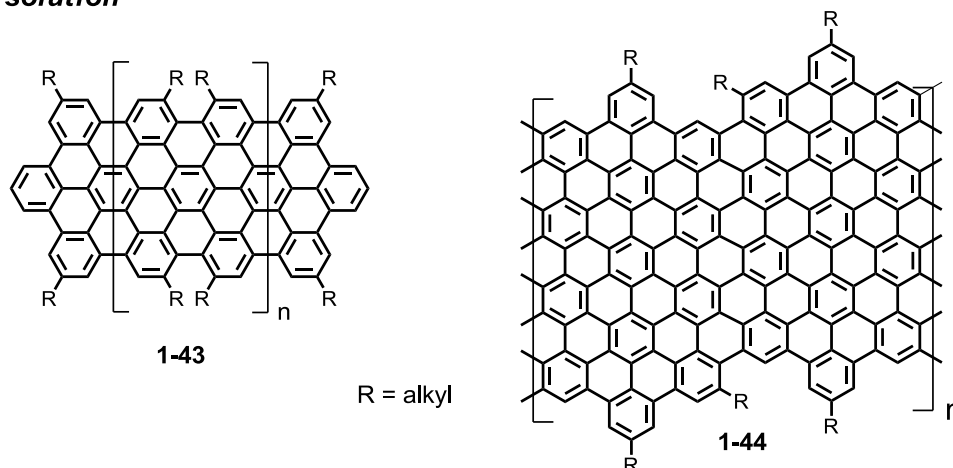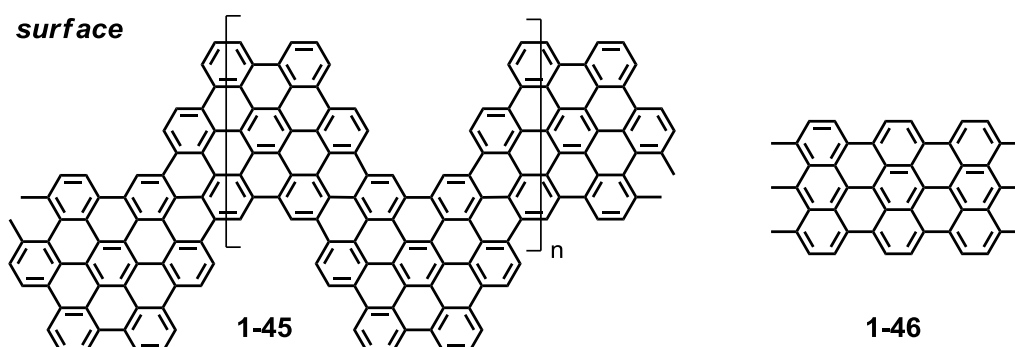
Figure 1-10. Top: Selected Examples of GNRs obtained by *intra*molecular cyclodehydrogenation of polyphenylene precursors. Bottom: Examples of GNRs obtained by surface-assisted polymerization and cyclodehydrogenation.

1.2.3   Three-dimensional Polyphenylene Architectures

The transition from 2D to 3D architectures implies the definition of another important class of benzene-based materials, namely hyperbranched polymers. This term describes polymers that feature a high degree of branching but are nevertheless not cross-linked.[21]

1-47   **1-48**
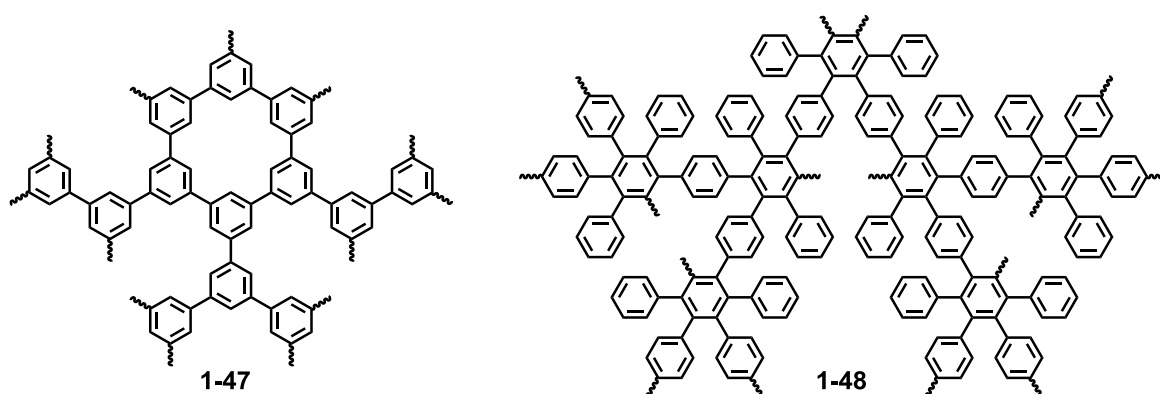
Figure 1-11. Selected Examples of hyperbranched polyphenylene polymers.

If the reaction occurs between two *B* groups of one monomer and the *A* functions of two other monomers, a molecule containing one *A* group and four *B* groups results.[20, 21]

After multiple repetition of this procedure, a macromolecule is formed which comprises a multitude of branches and *B* functions but only a single *A* group. Based on statistical and sterical considerations, not all available *B* groups are converted in reactions with *A* functions of a further monomer. This leads to the inevitable formation of defects and hence to polydispersity.[20, 21] In contrast to dendrimers, being monodisperse hyperbranched molecules prepared by multistep reactions, hyperbranched polymers have generally less defined structures and broad molecular weight distributions.

The first hyperbranched polyphenylenes were described by *Kim* and *Webster*.[185, 186] They utilized transition metal-mediated polycondensation reactions of a phenylene based *AB*$_2$-monomer for the synthesis of **1-47** (Figure 1-11). The advantage of this polymer lies in its high thermal stability as well as in the possibility of influencing the properties by functionalization.

Besides cross-coupling procedures, *Diels-Alder* cycloadditions of *AB*$_2$-monomer have been utilized for the synthesis of hyperbranched polymer **1-48** by *Müllen* and coworkers.[187] The advantage, in comparison with **1-47**, lies in the higher density of benzene rings and in the higher molecular weight. In addition, this method was extensively utilized for the preparation of polyphenylene dendrimers,[20, 21, 188] which is, however, beyond the scope of this Chapter.
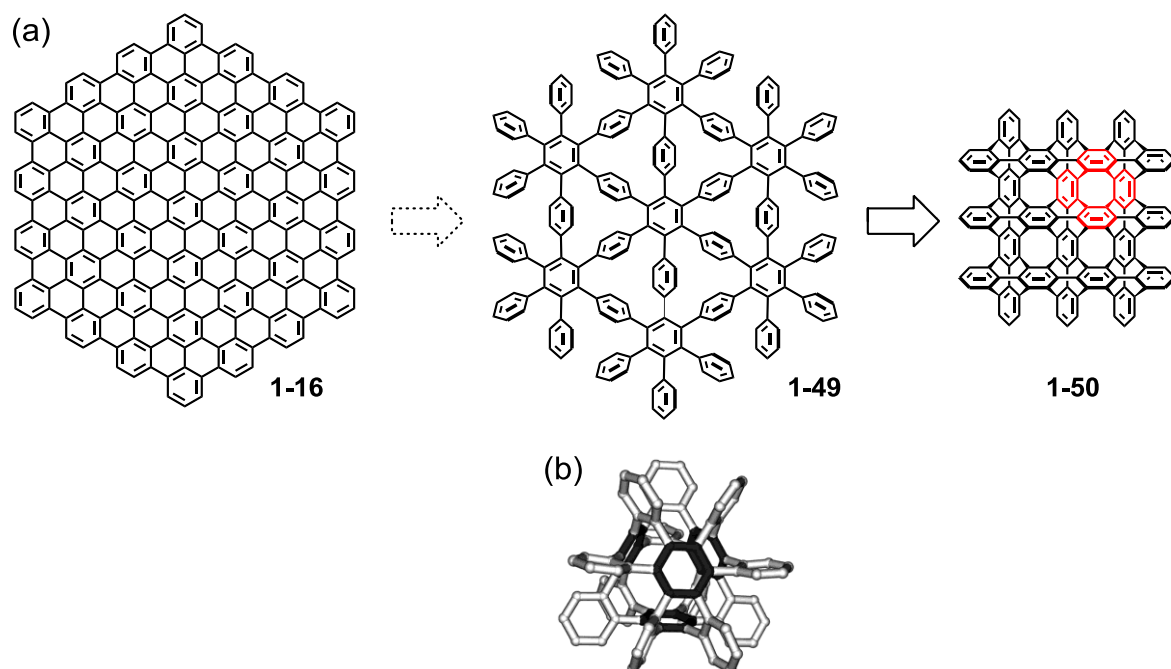
Scheme 1-6. (a) Schematic representation of the structural relationship between a graphene sheet **1-16**, aromatic ring layer **1-49** and cubic graphite **1-50**. The smallest subunit cyclo-*o*-tetraphenylene **1-18** is highlighted in red. (b) Three-dimensional representation of a subunit of cubic graphite.[188]

In connection with 3D polyphenylene structures, it is appropriate to refer to cubic carbon phases.[189, 190] Theoretically predicted cubic graphite can be entirely constructed from benzene rings. By braking one-sixth of the C−C bonds in a graphene sheet (*e.g.* C_{222} **1-16**) it is transformed into the aromatic ring layer **1-49** (Scheme 1-6 a), which leads to three-fourths of freely rotatable benzene rings.[191] This geometry enables the formation of *inter*molecular C−C bonds between the tilted benzene rings with identical neighboring sheets. As a result of this, all carbon atoms of the connected sheets become equivalent and consequently the benzenes part of three equivalent PPP chains (**1-50**, Scheme 1-6 a and b).[191] This arrangement leads to the formation of COT (**1-18**) as the smallest subunit (Scheme 1-6 b and c).[188] Cubic graphite is still an elusive material but has sparked considerable interest, as a result of its predicted useful properties, such as high mechanical and thermal stability.[21] This together with the presence of large diffusion channels for ions and its high predicted maximum charge storage capacity makes cubic graphite to a potential candidate for supercapacitors and electrochromic displays.[188, 191, 192] Several efforts were made to approach the unique architecture of cubic graphite by synthesizing adequate "phenylogues".[193] This comprised basically the utilization of polyphenylene dendrimers as suitable precursor or subunits thereof.
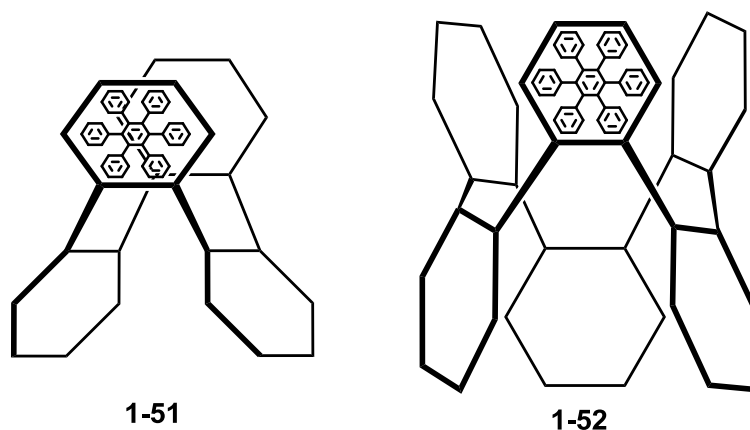
Figure 1-12. Hexaphenylbenzene cycles **1-51** and **1-52** synthesized by *Pascal Jr.*

For example, *Pascal Jr.* and coworkers linked hexaphenylbenzene (HPB) to cycles with different sizes that mimic the connection pattern of the benzene rings in cubic graphite (Figure 1-12).[193-195] The synthesis of **1-51** and **1-52** was achieved by a sequence of sterically demanding *Diels-Alder* reactions. The highly twisted benzene rings increased the solubility of these molecules in organic solvents. The crystal structure of **1-51** revealed the formation of infinite channels in the solid state.
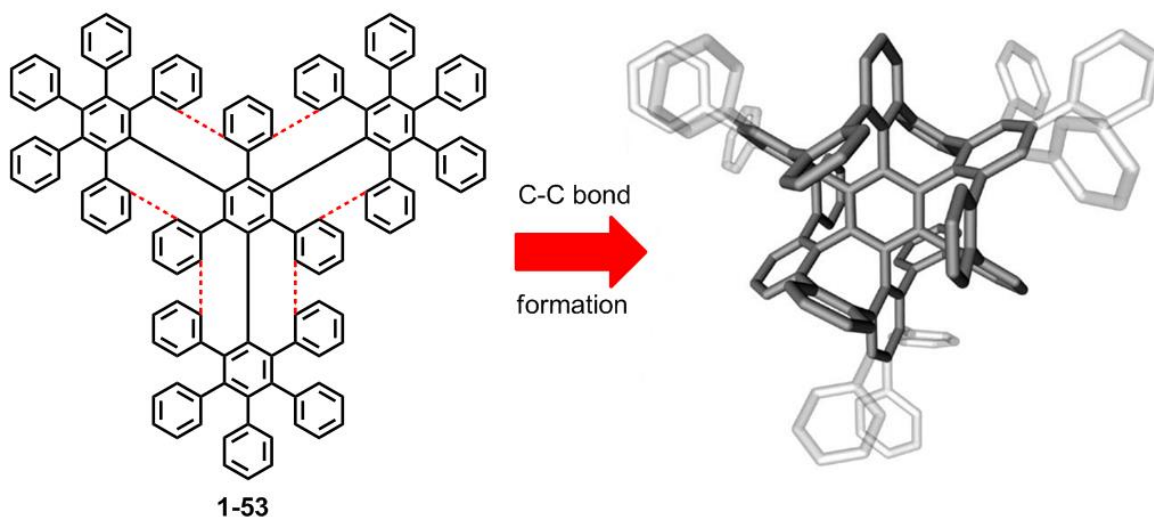
Scheme 1-7. Schematic representation of the necessary C−C bond formations from **1-53** toward a subunit of cubic graphite.[192]

Extremely crowded polyphenylene dendrimer **1-53** was designed as precursor for cubic graphite by *Müllen* and coworkers (Scheme 1-7). Due to the steric repulsion between the individual dendrons, the *Diels-Alder* reaction for the preparation of **1-53** had to be carried out under very drastic conditions. The phenyl rings of **1-53** adopt a conformation that might enable the synthesis of a subunit of cubic graphite *via* a spatially restricted cyclodehydrogenation between its inner benzene rings (Scheme 1-7, red bonds).[188]
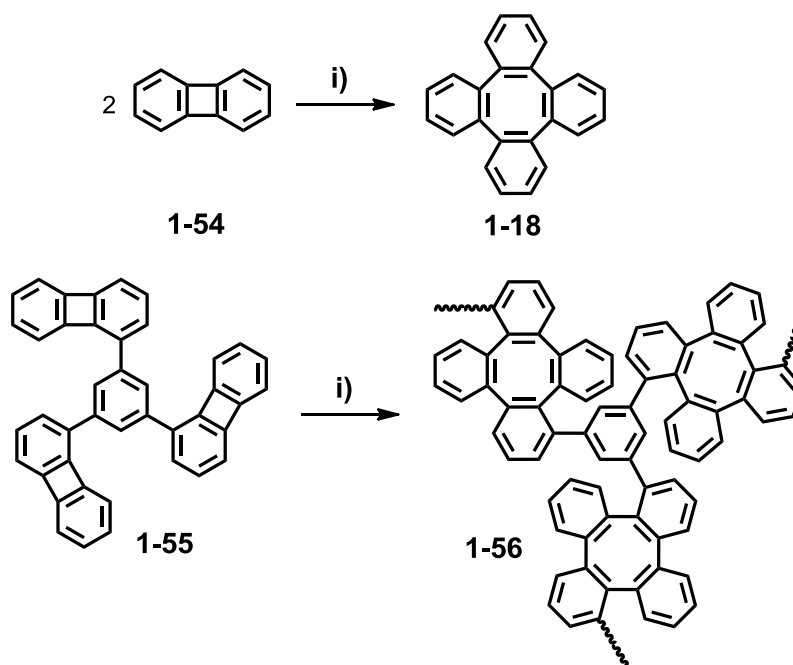
Scheme 1-8. Top: Thermally induced dimerization of biphenylene **1-54** to cyclo-*o*-tetraphenylene **1-18**. Bottom: Thermally induced polymerization of **1-55** to tetraphenylene polymer **1-56**.[196] Conditions: i) 400 °C.

Moreover, a 3D polyphenylene structure containing cyclo-*o*-tetraphenylene (**1-18**) units has been synthesized by the group of *Müllen* (Scheme 1-8).[196] This method was based on the thermally induced dimerization of biphenylene **1-54** to cyclo-*o*-tetraphenylene **1-18**, which proceeds in high yields and without the need of catalysts.[197] Three biphenylene moieties were attached to a benzene moiety leading to *A₃*-monomer tris(biphenylenyl)benzene **1-55**. The successful polymerization of **1-55** could be proven by solid-state NMR techniques. The insolubility of polymer **1-56** in organic solvents, however, prevented further characterization and the utilization of the material.

1.3   Triarylamines in Organic Electronics

As it has been shown above, the incorporation of heteroatoms to polyphenylene structures either by doping or by utilizing the heteroatoms as linkers is a beneficial concept for altering the electronic properties of the materials. In this regard triarylamines, being composed of three aryl units attached to a central nitrogen atom, emerged in the field of organic electronics as an important class of benzene-based materials in recent years.[198, 199] Due to their electron-rich character and their good hole-transport abilities, triarylamines received considerable attention as hole-transport materials (HTMs) in OLEDs and OFETs.[36, 199-202] Moreover, this type of molecules exhibits enhanced two-photon absorption cross sections and nonlinear responses,[203, 204] and has thus potential applications in optical data storage,[205] in scanning excitation microscopy,[206] and optical power limitation.[207]

Two characteristic properties of triarylamines make them desirable in the field of organic electronics. (1) The sp^2-hybridized nitrogen bears a lone pair in its p-orbital which induces a tetrahedral conformation and results in its pronounced tendency toward oxidation compared with its boron and carbon counterparts (Figure 1-13). The lone pair is also accessible for further chemical transformations. The electron-donating properties result (2) in the ability to transport positive charges *via* radical cation centers.
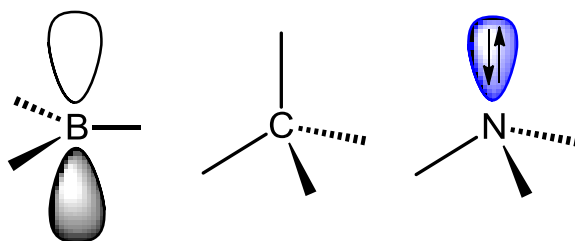
Figure 1-13. Comparison of the geometrical features of B, C and N.

Stable radicals are thereby required which can undergo an infinite number of redox cycles.[200] The crucial influence of the position *para* to the central nitrogen is thereby shown by the oxidation of triphenylamine **1-57** (Scheme 1-9). After having formed radical cation **1-58**, the subsequent dimerization toward tetraphenylbenzidine **1-60** occurs at the unsubstituted *para*-postion (**1-59**). This pathway is, however, very unfavorable for an efficient hole-transport.
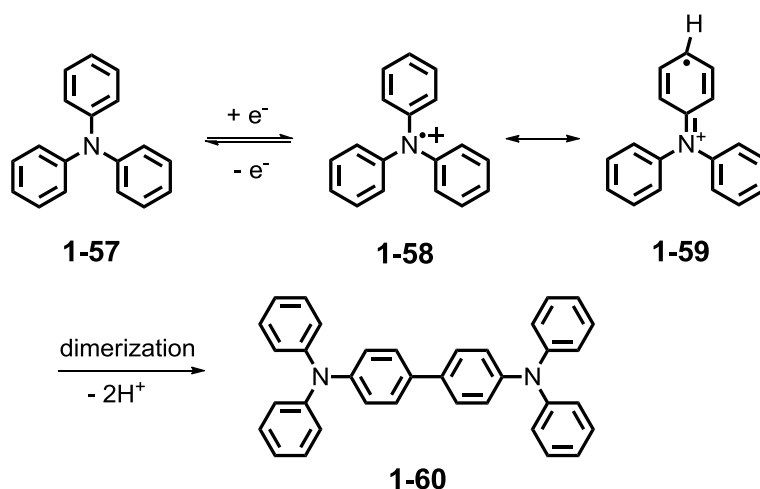
Scheme 1-9. Schematic representation of the oxidative dimerization of triphenylamine to tetraphenylbenzidine.

As already discussed, during the last decades the interest in organic electronic devices including OLEDs, OFETs and organic solar cells, in particular dye-sensitized solar cells (DSSC) has been significantly increased. Tremendous progress has been made in improving their key parameters.[2, 3, 9, 36, 38, 208-211] Since the operation mechanism of these devices requires the transport of charge carriers among various device components, research has been focused on the development of suitable charge-transporters, such as HTMs. High current densities at low driving voltages and excellent stability are thereby two of the key requirements that HTMs have to fulfill to find application in new electronic components. To meet this requirements materials have to be developed that form thermally stable amorphous states, showing reasonable hole-transport mobilities, and match the energy levels of the other device components (see Chapter 3 and 5).[212] For example, two of the widely used HTMs in OLEDs are $N^4,N^{4'}$-di(naphthalen-1-yl)-$N^4,N^{4'}$-diphenyl-[1,1'-biphenyl]-4,4'-diamine (**NPB**) and $N^4,N^{4'}$-diphenyl-$N^4,N^{4'}$-di-m-tolyl-[1,1'-biphenyl]-4,4'-diamine (**TPD**, Figure 1-14 top) with hole-mobilities in the range of 10^{-3} to 10^{-4} cm^2 V^{-1} s^{-1}. The easy synthesis by *Ullmann* coupling or *Buchwald-Hartwig* amination and the simple purification *via* sublimation, enables the preparation of both compounds in high purity and on a multigram scale.[213, 214]
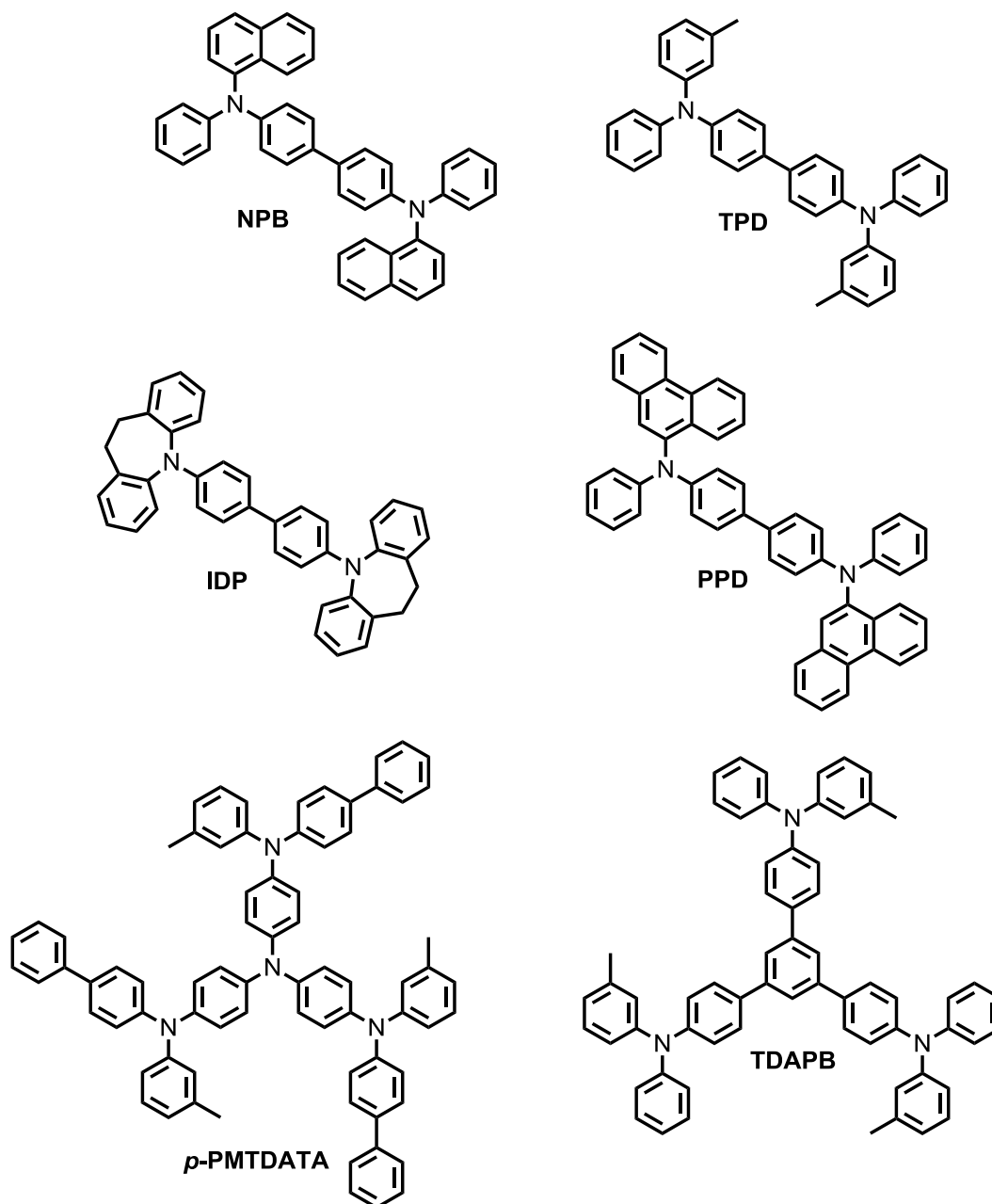
Figure 1-14. Top: Structures of the commonly used HTMs **NPB** and **TPD** with low T_g. Middle: Structures of HTMs **IDP** and **PPD** showing an increased T_g. Bottom: Starburst HTMs designed by *Shirota* and coworkers.

However, their low glass transition temperature (T_g) below 100 °C affects their morphological stability at the operating temperature of OLEDs by interdiffusion of the different layers.[215] Thus, several research groups focused on increasing T_g of the HTM and to hinder the crystallization tendency of this small organic molecules for a higher thermal durability of the devices. This was achieved, *e.g.*, by introducing bulky substituents to the molecule to hinder rotation or by increasing the number of π-electrons (Figure 1-14, middle).[216] This design principle could be demonstrated for **IDP** ($T_g = 110$ °C) and **PPD** ($T_g = 152$ °C).[216, 217]
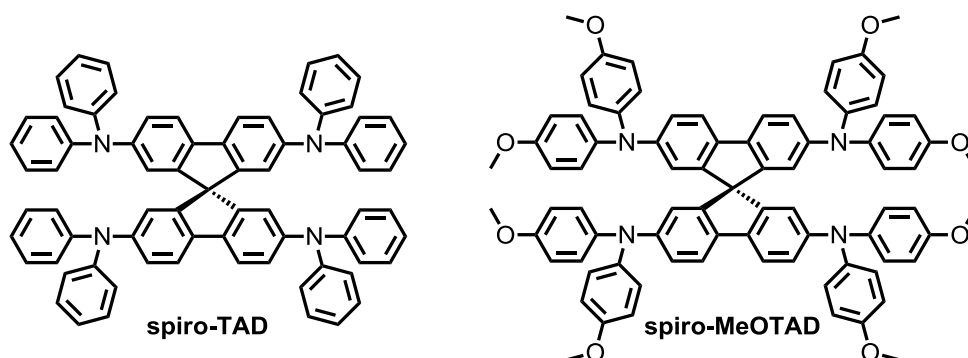
Figure 1-15. Examples of two spiro-linked HTMs.

Pioneering work of *Shirota* and coworkers led to amorphous HTMs with increased T_g showing starburst geometries (Figure 1-14, bottom).[218-222] The introduction of bulky substituents in a star-shaped fashion, enlarged the molecular size and increased thereby the number of conformers, which was shown for **p-PMTDATA** and **TDAPB**, being thermally much more stable than the extensively used **NPB** and **TPD**.

The processability and thermal stability of HTMs based on triarylamines was further increased by the specific introduction of spiro centers to modify the steric demand, while retaining their electronic properties.[212, 223] By using spiro-linked molecules as hole-transport layer (HTL) in OLEDs, such as **spiro-TAD** or **spiro-MeOTAD** (Figure 1-15) the electroluminescence (EL) efficiency was enhanced due to a strongly reduced crystallinity caused by the sterically demanding highly twisted conformation. The suppression of exciplex formation in this type of HTMs was found to be beneficial for the hole-transport process. In addition, **spiro-MeOTAD** is to date the most commonly used molecular hole-conductor in solid-state DSSCs introduced for the first time by *Grätzel* and coworkers in 1998 (for further details see Chapter 5).[224, 225] The low conductivity of **spiro-MeOTAD** (10^{-5} S cm^{-1}) and its crystallization tendency, however, hamper the maximum power conversion efficiency and the durability of sDSSCs.[226] This clearly demonstrates that there is still enough space for further improvements.

More recently bridged triarylamines were reported by the groups of *Ma* and *Lai* (Figure 1-16).[203, 227-230] By planarizing the triphenylamine core upon introduction of three dimethylmethylene tethers, the dihedral angle between the phenyl ring plane and the central nitrogen was decreased which results in an enhanced overlapping of the lone pair p-orbital on the nitrogen with the π-orbitals of the phenyl rings. Moreover, the bridges provide the possibility for the introduction of further solubilizing groups. The so-called *N*-heterotriangulenes were initially developed by *Hellwinkel* in the 1970s (for synthetic details see Chapter 3).[231-234] The attachment of bulky phenyl substituents to the bridges in-
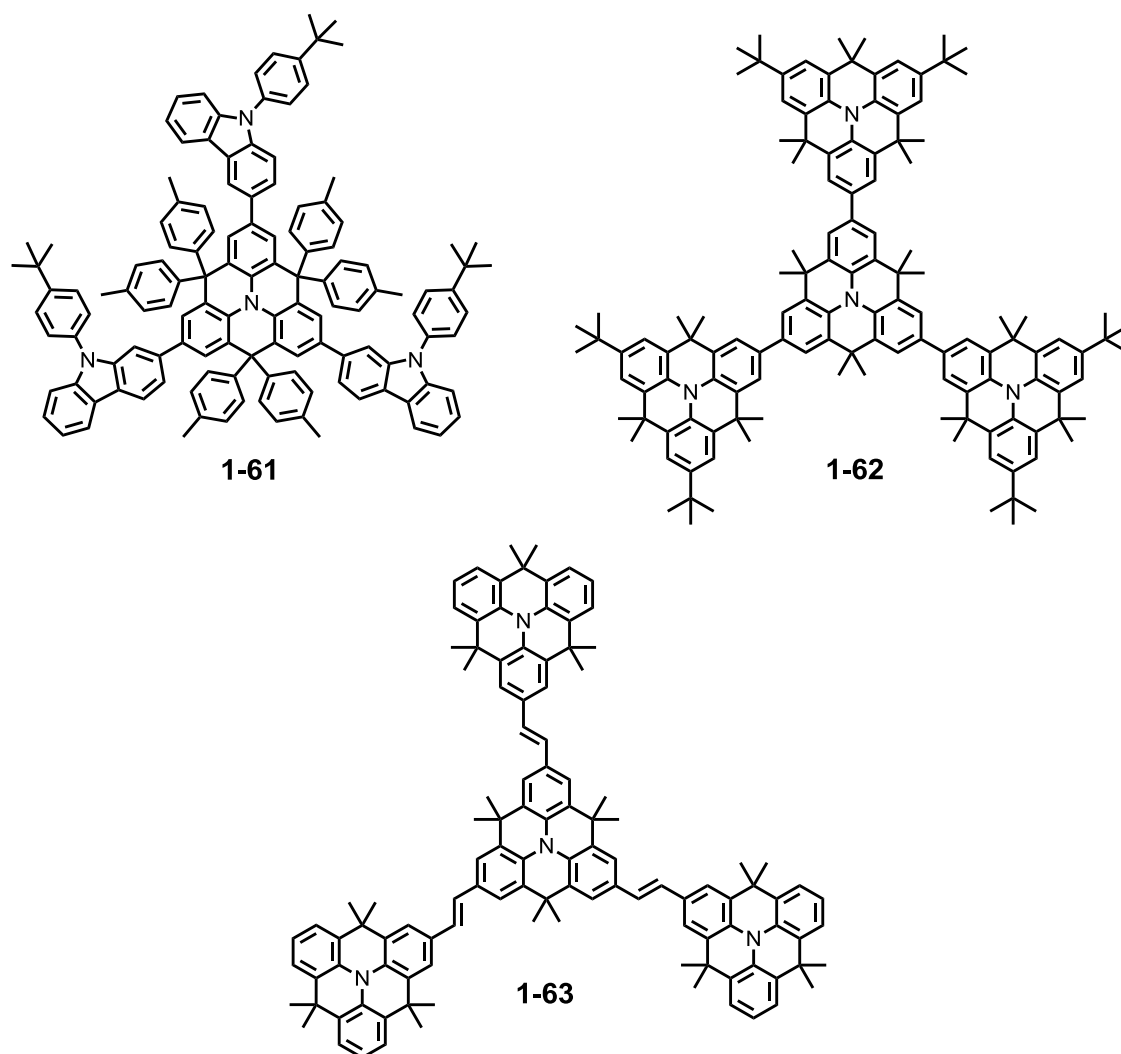
Figure 1-16. Examples of *N*-heterotriangulene structures reported by *Ma* and *Lai*.[203, 227-230]

creased the thermal stability of **1-61** (T_g up to 270 °C).[229] Although the hole-mobilities were lower than that of the standard **NPB**, a significantly improved OLED performance was revealed when using **1-61** as HTL.

In addition, *Lai* and coworkers combined *Shirota`s* starburst concept with *Hellwinkel`s* dimethylmethylene bridged *N*-heterotriangulenes.[230] The dimethylmethylene bridged structures showed decreased oxidation potentials thus leading to an increased HOMO level in comparsion to their non-planarized analogues. By utilizing trimers **1-62** and **1-63** in double-layer OLEDs, a significantly enhanced performance was observed for **1-62** compared with non-planarized **TPD**. The authors attributed this behavior to a better hole-carrier hopping between the *N*-heterotriangulene subunits, which finally increased the overall hole-mobility of the materials.

Structures **1-61**, **1-62** and **1-63** are examples for the versatility of *N*-heterotriangulenes as building blocks for the construction of sophisticated functional architectures, which will be one of the major objectives in this work.

1.4   Devices and Characterization Methods

By taking a closer look to organic optoelectronic devices, such as OFETs and organic solar cells, the properties are directly connected with the molecular order of the organic material, which is induced by non-covalent interactions.[235-237]

Due to these aspects, important characterization techniques as well as device characteristics useful for a deeper understanding of the intrinsic materials properties will be briefly introduced in the following parts. However, OFET details can be found in Chapter 3 and the Experimental Part.

1.4.1   Dye-Sensitized Solar Cells
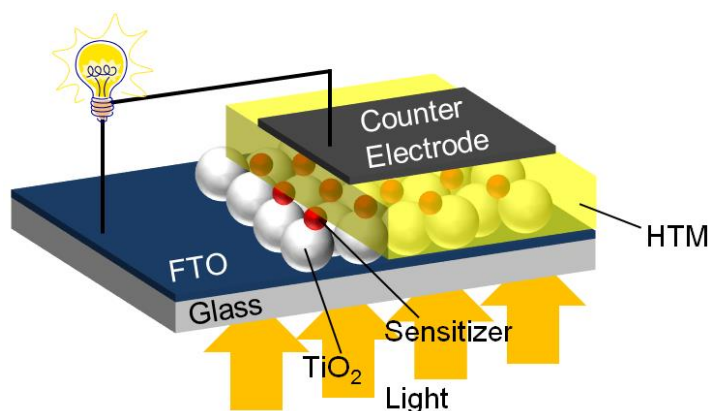
Figure 1-17. Device structure of a solid-state dye-sensitized solar cell.

Nowadays, organic photovoltaics is divided into three main solar cell types, namely flat-heterojunction cells, bulk-heterojunction cells and dye-sensitized solar cells (DSSCs).[2] Whereas the first two cell architectures are of minor importance for the herein presented results, the working principle of DSSCs, also named after its developer as *Grätzel* cells, will be discussed in more detail. DSSCs basically resemble the photosynthesis in Nature (Figure 1-17). Instead of chlorophyll in the plants, a dye in the DSSC absorbs light which leads to electron excitation. Subsequently the electrons are injected into the conduction band of an inorganic semiconductor. The oxidized dye molecules are recovered by a liquid electrolyte system for liquid DSSCs or a solid HTM for solid-state DSSCs (sDSSCs) which transports the positive charges to the counter electrode where they recombine with electrons. Semiconductor and HTM are connected by an external circuit *via* the electrodes.[2, 211, 238] Unlike the other two solar cell types, a DSSC contains a fluorine-doped tin oxide (FTO) covered glass as anode and an inorganic oxide wide band gap semiconductor, such as mesoporous titanium dioxide with a dye monolayer on the surface. There are several parameters indicating the performance of a DSSC. Besides the power
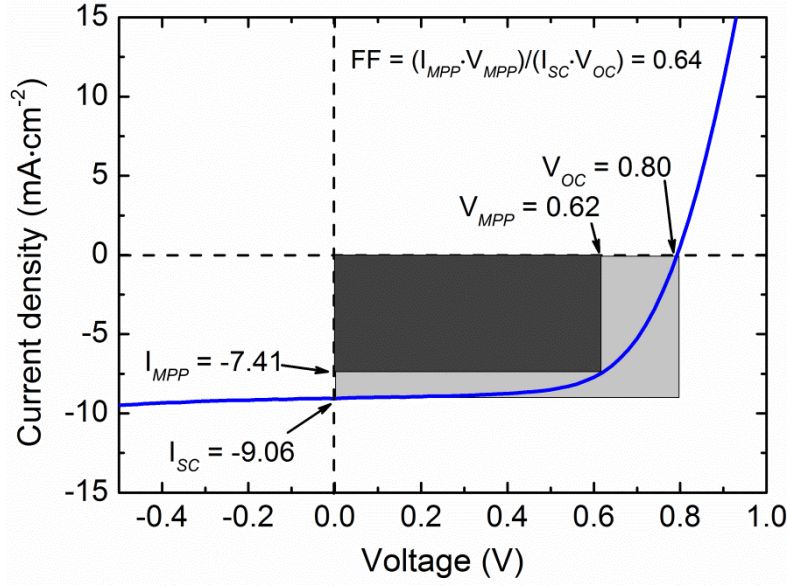
Figure 1-18. Typical I-V curve of a DSSC.

conversion efficiency (PCE), the open-circuit voltage (V_{OC}), the short-circuit current (I_{SC}) and the fill factor (FF) are main performance values for comparing different DSSCs, which can be extracted from an I-V curve displaying the photocurrent density versus the photovoltage (Figure 1-18). The V_{OC} is thereby obtained at zero output current and the I_{SC} accordingly at zero output voltage. Whereas the V_{OC} is determined by the distance between the conduction band of TiO_2 and the HOMO level of the HTM, the I_{SC} is mainly driven by the absorption behavior of the sensitizer and by the efficiency of the electron injection and the dye regeneration process.

$$PCE = \frac{P_{out}}{P_{in}} = FF \frac{V_{OC} \cdot I_{SC}}{P_{in}} \qquad (2)$$

$$FF = \frac{V_{MPP} \cdot I_{MPP}}{V_{OC} \cdot I_{SC}} \qquad (3)$$

The PCE is the ratio of the maximum electrical output power (P_{out}) of the device under illumination and the incident light intensity (P_{in}) according to equation (2). This can be further expressed by using FF, V_{OC} and I_{SC}. The fill factor (FF) is thereby defined as the ratio of current-voltage at the maximum power point (V_{MPP}, I_{MPP}) and the product of V_{OC} and I_{SC} (equation (3)). This is graphically determined by ratio of the dark grey rectangle and the light grey rectangle (Figure 1-18). In an ideal solar cell both rectangles are more or less congruent.

1.4.2   Scanning Tunneling Microscopy
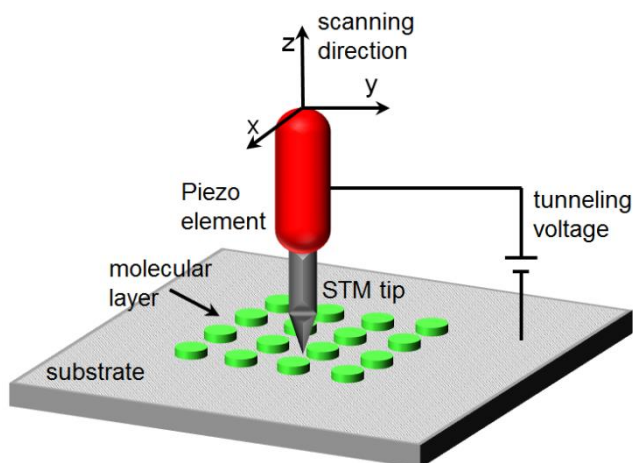
Figure 1-19. Schematic representation of a scanning tunneling microscope.

Since its invention in 1982, scanning tunneling microscopy (STM) has become a versatile technique for the generation of real-space images of surfaces and organic materials with sub-nanometer resolution.[239-241] STM provides thereby a topographical map displaying the tunneling current in a plane across a conductive sample, such as a metal surface or highly oriented pyrolytic graphite (HOPG). The STM tip is brought into close proximity to the sample surface (~1 nm) and a bias voltage is applied. By scanning the surface point by point, the probability of electron tunneling between the tip and the surface is probed (Figure 1-19).[241] The measured tunneling current provides insights about the local physical properties of the sample. Besides UHV conditions, STM experiments can be carried out in the presence of air and liquids thus enabling the investigation of the self-assembly of organic molecules at the gas/solid and liquid/solid interface.[112]

The sample can be scanned either in the constant height or constant current mode. In the constant height mode, the STM tip scans in a horizontal plane above the sample and the tunnel current changes upon variations in topography and the electronic properties of the surface. In the constant current mode, however, the tunneling current is kept at a given value by regulating the tip sample distance. If the system detects a change in the tunneling current while scanning the surface, the STM tip is adjusted in the appropriate z-direction thus recording a quasi-topographical map of the sample.

The STM technique is not only limited to visualization of molecules adsorbed or deposited on surfaces but can be used to observe and control their chemical reactions at the atomic level. In the context of polyphenylene structures, recent work made use of the STM to study for the growth of *N*-heterotriangulene networks[242] (see Chapter 3) and GNRs[181, 182] (Figure 1-10) from low molecular weight precursors.

1.4.3   Two-dimensional Wide-angle X-ray Scattering
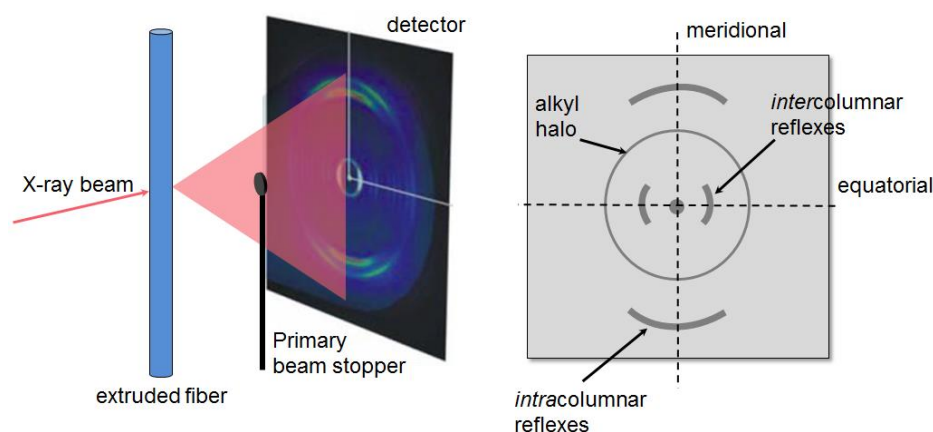
Figure 1-20. Right: Schematic representation of the experimental 2D WAXS setup for the measurement of extruded fibers. Right: Typical reflexes obtained for disquotic liquid crystals.

Liquid crystalline (LC) materials are characterized by a high degree of structural order on the microscopic scale, which arises from π-π interactions, van der Waals forces, dipole-dipole and electrostatic interactions. The liquid crystalline (LC) mesophase is located between the crystalline and the isotropic liquid phase and hence comprise characteristics of both. Such materials are typically composed of a central disc-like rigid core that is decorated with long alkyl chains on the periphery. Two-dimensional wide-angle X-ray scattering (2D WAXS) provides insights into the supramolecular organization of those materials (Figure 1-20 left).[243]

The material is therefore extruded to fibers at elevated temperatures, which can lead to the orientation of the molecules along the extrusion direction. The incident X-ray beam is scattered at the fiber and the reflection pattern is recorded (Figure 1-20 right). The observed meridional reflexes provide information about the *intra*columnar order, such as π-π stacking distances. Whereas the equatorial reflexes give insights into the packing lattice of the columns and thus the *inter*columnar interactions. It has however to be taken into account that the shear forces during the extrusion process significantly influence the orientation of the molecules.

The synthetic procedures and literature examples together with the characterization methods represent the basis for the synthesis of benzene-based materials of different dimensionality. In the following the structure of the presented work will be precisely discussed and the methodologies will be explained.

1.5   References

[1]   S. S. Penner, J. Haraden, S. Mates, *Energy* **1992**, *17*, 883-899.

[2]   C. Li, M. Y. Liu, N. G. Pschirer, M. Baumgarten, K. Müllen, *Chem. Rev.* **2010**, *110*, 6817-6855.

[3]   B. O`Regan, M. Grätzel, *Nature* **1991**, *353*, 737-740.

[4]   A. Teichler, J. Perelaer, U. S. Schubert, *J. Mater. Chem. C* **2013**, *1*, 1910-1925.

[5]   R. S. Ashraf, Ph.D. thesis, Friedrich-Schiller University Jena **2005**.

[6]   H. Sirringhaus, N. Tessler, R. H. Friend, *Science* **1998**, *280*, 1741-1744.

[7]   A. Dodabalapur, Z. Bao, A. Makhija, J. G. Laquindanum, V. R. Raju, Y. Feng, H. E. Katz, J. Rogers, *Appl. Phys. Lett.* **1998**, *73*, 142-144.

[8]   H. N. Tsao, D. M. Cho, I. Park, M. R. Hansen, A. Mavrinskiy, D. Y. Yoon, R. Graf, W. Pisula, H. W. Spiess, K. Müllen, *J. Am. Chem. Soc.* **2011**, *133*, 2605-2612.

[9]   G. M. Farinola, R. Ragni, *Chem. Soc. Rev.* **2011**, *40*, 3467-3482.

[10]   http://www.idtechex.com, in *Printed, Organic & Flexible Electronics Forecasts, Players & Opportunities 2013-2023*.

[11]   M. Kastler, Ph.D. thesis, Johannes Gutenberg-University Mainz **2006**.

[12]   http://www.phys.unsw.edu.au, in *Introduction to Organic Electronics*.

[13]   M. Faraday, *Philos. Trans. R. Soc. London* **1825**, *115*, 440-466.

[14]   M. Randic, *Chem. Rev.* **2003**, *103*, 3449-3605.

[15]   A. T. Balaban, P. V. Schleyer, H. S. Rzepa, *Chem. Rev.* **2005**, *105*, 3436-3447.

[16]   A. Kekulé, *Bull. Soc. Chim. Fr.* **1865**, *3*, 98-100.

[17]   J. W. Armit, R. Robinson, *J. Chem. Soc.* **1925**, *127*, 1604-1618.

[18]   E. Hückel, *Z. Phys.* **1931**, *70*, 204-286.

[19]   E. Clar, *The Aromatic Sextet*, John Wiley & Sons, London, **1972**.

[20]   M. D. Watson, A. Fechtenkötter, K. Müllen, *Chem. Rev.* **2001**, *101*, 1267-1300.

[21]   A. J. Berresheim, M. Müller, K. Müllen, *Chem. Rev.* **1999**, *99*, 1747-1785.

[22]   C. K. Chiang, C. R. Fincher, Y. W. Park, A. J. Heeger, H. Shirakawa, E. J. Louis, S. C. Gau, A. G. Macdiarmid, *Phys. Rev. Lett.* **1977**, *39*, 1098-1101.

[23]   H. Shirakawa, E. J. Louis, A. G. Macdiarmid, C. K. Chiang, A. J. Heeger, *J. Chem. Soc., Chem. Commun.* **1977**, 578-580.

[24]   A. J. Heeger, *Angew. Chem., Int. Ed.* **2001**, *40*, 2591-2611.

[25]   A. G. MacDiarmid, *Angew. Chem., Int. Ed.* **2001**, *40*, 2581-2590.

[26]   H. Shirakawa, *Angew. Chem., Int. Ed.* **2001**, *40*, 2575-2580.

[27]   N. S. Sariciftci, L. Smilowitz, A. J. Heeger, F. Wudl, *Science* **1992**, *258*, 1474-1476.

[28]   G. Yu, J. Gao, J. C. Hummelen, F. Wudl, A. J. Heeger, *Science* **1995**, *270*, 1789-1791.

[29]   J. Y. Kim, K. Lee, N. E. Coates, D. Moses, T. Q. Nguyen, M. Dante, A. J. Heeger, *Science* **2007**, *317*, 222-225.

[30]   D. Mühlbacher, M. Scharber, M. Morana, Z. G. Zhu, D. Waller, R. Gaudiana, C. Brabec, *Adv. Mater.* **2006**, *18*, 2884-2889.

[31]   R. D. McCullough, R. D. Lowe, *J. Chem. Soc., Chem. Commun.* **1992**, 70-72.

[32]   H. Sirringhaus, P. J. Brown, R. H. Friend, M. M. Nielsen, K. Bechgaard, B. M. W. Langeveld-Voss, A. J. H. Spiering, R. A. J. Janssen, E. W. Meijer, P. Herwig, D. M. de Leeuw, *Nature* **1999**, *401*, 685-688.

[33]   H. E. Katz, Z. N. Bao, S. L. Gilat, *Acc. Chem. Res.* **2001**, *34*, 359-369.

[34]   W. Pisula, A. Menon, M. Stepputat, I. Lieberwirth, U. Kolb, A. Tracz, H. Sirringhaus, T. Pakula, K. Müllen, *Adv. Mater.* **2005**, *17*, 684-689.

[35]   M. I, M. Heeney, C. Bailey, K. Genevicius, M. I, M. Shkunov, D. Sparrowe, S. Tierney, R. Wagner, W. M. Zhang, M. L. Chabinyc, R. J. Kline, M. D. Mcgehee, M. F. Toney, *Nat. Mater.* **2006**, *5*, 328-333.

[36]   C. W. Tang, S. A. Vanslyke, *Appl. Phys. Lett.* **1987**, *51*, 913-915.

[37]   E. J. Meijer, D. M. de Leeuw, S. Setayesh, E. van Veenendaal, B. H. Huisman, P. W. M. Blom, J. C. Hummelen, U. Scherf, J. Kadam, T. M. Klapwijk, *Nat. Mater.* **2003**, *2*, 834-834.

[38]   T. M. Figueira-Duarte, P. G. Del Rosso, R. Trattnig, S. Sax, E. J. W. List, K. Müllen, *Adv. Mater.* **2010**, *22*, 990-993.

[39]   D. T. McQuade, A. E. Pullen, T. M. Swager, *Chem. Rev.* **2000**, *100*, 2537-2574.

[40]   O. S. Wolfbeis, *J. Mater. Chem.* **2005**, *15*, 2657-2669.

[41]   M. Berggren, A. Richter-Dahlfors, *Adv. Mater.* **2007**, *19*, 3201-3213.

[42]   J. Isaksson, P. Kjall, D. Nilsson, N. D. Robinson, M. Berggren, A. Richter-Dahlfors, *Nat. Mater.* **2007**, *6*, 673-679.

[43]   A. J. Heeger, *Chem. Soc. Rev.* **2010**, *39*, 2354-2371.

[44]   S. C. Simon, Ph.D. thesis, Johannes Gutenberg-University Mainz **2010**.

[45]   J. Roncali, *Chem. Rev.* **1997**, *97*, 173-205.

[46]   F. Hide, M. A. DiazGarcia, B. J. Schwartz, A. J. Heeger, *Acc. Chem. Res.* **1997**, *30*, 430-436.

[47]   R. H. Friend, R. W. Gymer, A. B. Holmes, J. H. Burroughes, R. N. Marks, C. Taliani, D. D. C. Bradley, D. A. Dos Santos, J. L. Bredas, M. Logdlund, W. R. Salaneck, *Nature* **1999**, *397*, 121-128.

[48]   A. C. Grimsdale, K. Müllen, *Adv. Polym. Sci.* **2006**, *199*, 1-82.

[49]   A. C. Grimsdale, K. Müllen, *Adv. Polym. Sci.* **2008**, *212*, 1-48.

[50]   M. Fukuda, K. Sawada, K. Yoshino, *J. Polym. Sci., Part A: Polym. Chem.* **1993**, *31*, 2465-2471.

[51]   S. Setayesh, D. Marsitzky, K. Müllen, *Macromolecules* **2000**, *33*, 2016-2020.

[52]   U. Scherf, K. Müllen, *Makromol. Chem., Rapid Commun.* **1991**, *12*, 489-497.

[53]   U. Scherf, K. Müllen, *Polymer* **1992**, *33*, 2443-2446.

[54]   U. Scherf, K. Müllen, *Synthesis* **1992**, 23-38.

[55]   S. Nau, N. Schulte, S. Winkler, J. Frisch, A. Vollmer, N. Koch, S. Sax, E. J. W. List, *Adv. Mater.* **2013**, *25*, 4420-4424.

[56]   J. Grimme, M. Kreyenschmidt, F. Uckert, K. Müllen, U. Scherf, *Adv. Mater.* **1995**, *7*, 292-295.

[57]   U. Scherf, E. J. W. List, *Adv. Mater.* **2002**, *14*, 477-487.

[58]   J. Jacob, S. Sax, T. Piok, E. J. W. List, A. C. Grimsdale, K. Müllen, *J. Am. Chem. Soc.* **2004**, *126*, 6987-6995.

[59]   J. Jacob, S. Sax, M. Gaal, E. J. W. List, A. C. Grimsdale, K. Müllen, *Macromolecules* **2005**, *38*, 9933-9938.

[60]   J. Grüner, P. J. Hamer, R. H. Friend, H. J. Huber, U. Scherf, A. B. Holmes, *Adv. Mater.* **1994**, *6*, 748-752.

[61]   J. Grüner, H. F. Wittmann, P. J. Hamer, R. H. Friend, J. Huber, U. Scherf, K. Müllen, S. C. Moratti, A. B. Holmes, *Synth. Met.* **1994**, *67*, 181-185.

[62]   A. Kühler, J. Grüner, R. H. Friend, K. Müllen, U. Scherf, *Chem. Phys. Lett.* **1995**, *243*, 456-461.

[63]   M. B. Goldfinger, T. M. Swager, *J. Am. Chem. Soc.* **1994**, *116*, 7895-7896.

[64]   J. M. Tour, J. J. S. Lamba, *Macromol. Symp.* **1994**, *77*, 389-394.

[65]   J. M. Tour, J. J. S. Lamba, *J. Am. Chem. Soc.* **1993**, *115*, 4935-4936.

[66]   J. J. S. Lamba, J. M. Tour, *J. Am. Chem. Soc.* **1994**, *116*, 11723-11736.

[67]   J. W. Colson, W. R. Dichtel, *Nat. Chem.* **2013**, *5*, 453-465.

[68]   K. S. Novoselov, A. K. Geim, S. V. Morozov, D. Jiang, Y. Zhang, S. V. Dubonos, I. V. Grigorieva, A. A. Firsov, *Science* **2004**, *306*, 666-669.

[69]   A. K. Geim, K. S. Novoselov, *Nat. Mater.* **2007**, *6*, 183-191.

[70]   J. C. Meyer, A. K. Geim, M. I. Katsnelson, K. S. Novoselov, T. J. Booth, S. Roth, *Nature* **2007**, *446*, 60-63.

[71]   C. Lee, X. D. Wei, J. W. Kysar, J. Hone, *Science* **2008**, *321*, 385-388.

[72]   A. K. Geim, *Science* **2009**, *324*, 1530-1534.

[73]   C. Berger, Z. M. Song, X. B. Li, X. S. Wu, N. Brown, C. Naud, D. Mayou, T. B. Li, J. Hass, A. N. Marchenkov, E. H. Conrad, P. N. First, W. A. de Heer, *Science* **2006**, *312*, 1191-1196.

[74]   X. S. Li, W. W. Cai, J. H. An, S. Kim, J. Nah, D. X. Yang, R. Piner, A. Velamakanni, I. Jung, E. Tutuc, S. K. Banerjee, L. Colombo, R. S. Ruoff, *Science* **2009**, *324*, 1312-1314.

[75]   P. Y. Huang, C. S. Ruiz-Vargas, A. M. van der Zande, W. S. Whitney, M. P. Levendorf, J. W. Kevek, S. Garg, J. S. Alden, C. J. Hustedt, Y. Zhu, J. Park, P. L. McEuen, D. A. Müller, *Nature* **2011**, *469*, 389-392.

[76]   F. Schwierz, *Nat. Nanotechnol.* **2010**, *5*, 487-496.

[77]   C. Bronner, S. Stremlau, M. Gille, F. Brausse, A. Haase, S. Hecht, P. Tegeder, *Angew. Chem., Int. Ed.* **2013**, *52*, 4422-4425.

[78]   I. Meric, M. Y. Han, A. F. Young, B. Ozyilmaz, P. Kim, K. L. Shepard, *Nat. Nanotechnol.* **2008**, *3*, 654-659.

[79]   M. Bieri, M. Treier, J. M. Cai, K. Ait-Mansour, P. Ruffieux, O. Groning, P. Groning, M. Kastler, R. Rieger, X. Feng, K. Müllen, R. Fasel, *Chem. Commun.* **2009**, 6919-6921.

[80]   J. Cai, P. Ruffieux, R. Jaafar, M. Bieri, T. Braun, S. Blankenburg, M. Muoth, A. P. Seitsonen, M. Saleh, X. Feng, K. Müllen, R. Fasel, *Nature* **2010**, *466*, 470-473.

[81]   L. Chen, Y. Hernandez, X. L. Feng, K. Müllen, *Angew. Chem., Int. Ed.* **2012**, *51*, 7640-7654.

[82]   X. L. Feng, J. S. Wu, M. Ai, W. Pisula, L. J. Zhi, J. P. Rabe, K. Müllen, *Angew. Chem., Int. Ed.* **2007**, *46*, 3033-3036.

[83]   S. X. Xiao, M. Myers, Q. Miao, S. Sanaur, K. L. Pang, M. L. Steigerwald, C. Nuckolls, *Angew. Chem., Int. Ed.* **2005**, *44*, 7390-7394.

[84]   C. D. Simpson, J. D. Brand, A. J. Berresheim, L. Przybilla, H. J. Räder, K. Müllen, *Chem. Eur. J.* **2002**, *8*, 1424-1429.

[85]   C. D. Simpson, G. Mattersteig, K. Martin, L. Gherghel, R. E. Bauer, H. J. Räder, K. Müllen, *J. Am. Chem. Soc.* **2004**, *126*, 3139-3147.

[86]   R. Scholl, C. Seer, *Liebigs Ann. Chem.* **1912**, *394*, 111-177.

[87]   R. Scholl, C. Seer, *Ber. Dtsch. Chem. Ges.* **1911**, *44*, 1233-1240.

[88]   R. Scholl, C. Seer, R. Weitzenbock, *Ber. Dtsch. Chem. Ges.* **1910**, *43*, 2202-2209.

[89]   D. J. Jones, B. Purushothaman, S. M. Ji, A. B. Holmes, W. W. H. Wong, *Chem. Commun.* **2012**, *48*, 8066-8068.

[90]   L. Y. Zhai, R. Shukla, R. Rathore, *Org. Lett.* **2009**, *11*, 3474-3477.

[91]   B. T. King, J. Kroulik, C. R. Robertson, P. Rempala, C. L. Hilton, J. D. Korinek, L. M. Gortari, *J. Org. Chem.* **2007**, *72*, 2279-2288.

[92]   Z. Wang, Z. Tomović, M. Kastler, R. Pretsch, F. Negri, V. Enkelmann, K. Müllen, *J. Am. Chem. Soc.* **2004**, *126*, 7794-7795.

[93]   M. Kastler, J. Schmidt, W. Pisula, D. Sebastiani, K. Müllen, *J. Am. Chem. Soc.* **2006**, *128*, 9526-9534.

[94]   J. M. Tour, *Chem. Rev.* **1996**, *96*, 537-553.

[95]   J. S. Moore, *Acc. Chem. Res.* **1997**, *30*, 402-413.

[96]   M. Iyoda, *Pure Appl. Chem.* **2010**, *82*, 831-841.

[97]   M. Iyoda, J. Yamakawa, M. J. Rahman, *Angew. Chem., Int. Ed.* **2011**, *50*, 10522-10553.

[98]   C. Grave, A. D. Schlüter, *Eur. J. Org. Chem.* **2002**, 3075-3098.

[99]   W. Zhang, J. S. Moore, *Angew. Chem., Int. Ed.* **2006**, *45*, 4416-4439.

[100] P. K. Chen, F. Jäkle, *J. Am. Chem. Soc.* **2011**, *133*, 20142-20145.

[101] P. K. Chen, R. A. Lalancette, F. Jäkle, *Angew. Chem., Int. Ed.* **2012**, *51*, 7994-7998.

[102] I. Baxter, A. Ben-Haida, H. M. Colquhoun, P. Hodge, F. H. Kohnke, D. J. Williams, *Chem. Eur. J.* **2000**, *6*, 4285-4296.

[103] S. H. Chiu, A. R. Pease, J. F. Stoddart, A. J. P. White, D. J. Williams, *Angew. Chem., Int. Ed.* **2002**, *41*, 270-274.

[104] S. H. Chiu, S. J. Rowan, S. J. Cantrill, J. F. Stoddart, A. J. P. White, D. L. Williams, *Chem. Eur. J.* **2002**, *8*, 5170-5183.

[105] D. Venkataraman, S. Lee, J. S. Zhang, J. S. Moore, *Nature* **1994**, *371*, 591-593.

[106] J. S. Zhang, D. J. Pesak, J. L. Ludwick, J. S. Moore, *J. Am. Chem. Soc.* **1994**, *116*, 4227-4239.

[107] S. Lahiri, J. L. Thompson, J. S. Moore, *J. Am. Chem. Soc.* **2000**, *122*, 11315-11319.

[108] Y. Tobe, A. Nagano, K. Kawabata, M. Sonoda, K. Naemura, *Org. Lett.* **2000**, *2*, 3265-3268.

[109] S. H. Jung, W. Pisula, A. Rouhanipour, H. J. Räder, J. Jacob, K. Müllen, *Angew. Chem., Int. Ed.* **2006**, *45*, 4685-4690.

[110] W. Pisula, M. Kastler, C. Yang, V. Enkelmann, K. Müllen, *Chem. Asian J.* **2007**, *2*, 51-56.

[111] L. Zöphel, K. S. Mali, P. S. Reddy, M. Wagner, S. De Feyter, W. Pisula, K. Müllen, *Chem. Eur. J.* **2012**, *18*, 3264-3276.

[112] S. De Feyter, F. C. De Schryver, *Chem. Soc. Rev.* **2003**, *32*, 139-150.

[113]   K. Tahara, S. Furukawa, H. Uji-I, T. Uchino, T. Ichikawa, J. Zhang, W. Mamdouh, M. Sonoda, F. C. De Schryver, S. De Feyter, Y. Tobe, *J. Am. Chem. Soc.* **2006**, *128*, 16613-16625.

[114]   S. Furukawa, K. Tahara, F. C. De Schryver, M. Van der Auweraer, Y. Tobe, S. De Feyter, *Angew. Chem., Int. Ed.* **2007**, *46*, 2831-2834.

[115]   D. Mössinger, D. Chaudhuri, T. Kudernac, S. Lei, S. De Feyter, J. M. Lupton, S. Höger, *J. Am. Chem. Soc.* **2010**, *132*, 1410-1423.

[116]   K. Tahara, H. Yamaga, E. Ghijsens, K. Inukai, J. Adisoejoso, M. O. Blunt, S. De Feyter, Y. Tobe, *Nat. Chem.* **2011**, *3*, 714-719.

[117]   Y. Tobe, N. Utsumi, A. Nagano, K. Naemura, *Angew. Chem., Int. Ed.* **1998**, *37*, 1285-1287.

[118]   M. Fischer, G. Lieser, A. Rapp, I. Schnell, W. Mamdouh, S. De Feyter, F. C. De Schryver, S. Höger, *J. Am. Chem. Soc.* **2004**, *126*, 214-222.

[119]   S. Höger, *Chem. Eur. J.* **2004**, *10*, 1320-1329.

[120]   M. Hoffmann, J. Karnbratt, M. H. Chang, L. M. Herz, B. Albinsson, H. L. Anderson, *Angew. Chem., Int. Ed.* **2008**, *47*, 4993-4996.

[121]   J. E. Lovett, M. Hoffmann, A. Cnossen, A. T. J. Shutter, H. J. Hogben, J. E. Warren, S. I. Pascu, C. W. M. Kay, C. R. Timmel, H. L. Anderson, *J. Am. Chem. Soc.* **2009**, *131*, 13852-13859.

[122]   B. Schmaltz, A. Rouhanipour, H. J. Räder, W. Pisula, K. Müllen, *Angew. Chem., Int. Ed.* **2009**, *48*, 720-724.

[123]   K. Tahara, K. Inukai, J. Adisoejoso, H. Yamaga, T. Balandina, M. O. Blunt, S. De Feyter, Y. Tobe, *Angew. Chem., Int. Ed.* **2013**, *52*, 8373-8376.

[124]   H. A. Staab, F. Binnig, *Chem. Ber.* **1967**, *100*, 293-305.

[125]   H. A. Staab, H. Bräunling, *Tetrahedron Lett.* **1965**, 45-49.

[126]   H. Bräunling, F. Binnig, H. A. Staab, *Chem. Ber.* **1967**, *100*, 880-888.

[127]   H. Meyer, H. A. Staab, *Liebigs Ann. Chem.* **1969**, *724*, 30-33.

[128]   A. Rajca, A. Safronov, S. Rajca, C. R. Ross, J. J. Stezowski, *J. Am. Chem. Soc.* **1996**, *118*, 7272-7279.

[129]   A. Rajca, A. Safronov, S. Rajca, R. Shoemaker, *Angew. Chem., Int. Ed.* **1997**, *36*, 488-491.

[130]   S. M. H. Kabir, M. Hasegawa, Y. Kuwatani, M. Yoshida, H. Matsuyama, M. Iyoda, *J. Chem. Soc., Perkin Trans. 1* **2001**, 159-165.

[131]   A. Rajca, H. Wang, P. Bolshov, S. Rajca, *Tetrahedron* **2001**, *57*, 3725-3735.

[132]   A. Rajca, S. Rajca, M. Pink, M. Miyasaka, *Synlett* **2007**, 1799-1822.

[133]   A. Rajca, S. Rajca, *Angew. Chem., Int. Ed.* **2010**, *49*, 672-674.

[134]   R. Jasti, J. Bhattacharjee, J. B. Neaton, C. R. Bertozzi, *J. Am. Chem. Soc.* **2008**, *130*, 17646-17647.

[135]   R. Jasti, C. R. Bertozzi, *Chem. Phys. Lett.* **2010**, *494*, 1-7.

[136]   T. J. Sisto, M. R. Golder, E. S. Hirst, R. Jasti, *J. Am. Chem. Soc.* **2011**, *133*, 15800-15802.

[137]   E. S. Hirst, R. Jasti, *J. Org. Chem.* **2012**, *77*, 10473-10478.

[138]   T. J. Sisto, R. Jasti, *Synlett* **2012**, 483-489.

[139]   A. V. Zabula, A. S. Filatov, J. L. Xia, R. Jasti, M. A. Petrukhina, *Angew. Chem., Int. Ed.* **2013**, *52*, 5033-5036.

[140]   H. Takaba, H. Omachi, Y. Yamamoto, J. Bouffard, K. Itami, *Angew. Chem., Int. Ed.* **2009**, *48*, 6112-6116.

[141]   H. Omachi, S. Matsuura, Y. Segawa, K. Itami, *Angew. Chem., Int. Ed.* **2010**, *49*, 10202-10205.

[142]   S. Yamago, Y. Watanabe, T. Iwamoto, *Angew. Chem., Int. Ed.* **2010**, *49*, 757-759.

[143]   E. Kayahara, Y. Sakamoto, T. Suzuki, S. Yamago, *Org. Lett.* **2012**, *14*, 3284-3287.

[144]   H. A. Staab, K. Neunhoeffer, *Synthesis* **1974**, 424-424.

[145]   A. Ito, Y. Yokoyama, R. Aihara, K. Fukui, S. Eguchi, K. Shizu, T. Sato, K. Tanaka, *Angew. Chem., Int. Ed.* **2010**, *49*, 8205-8208.

[146]   T. F. Yang, K. Y. Chiu, H.-C. Cheng, J. W. Lee, M. Y. Kuo, Y. O. Su, *J. Org. Chem.* **2012**, *77*, 8627–8633.

[147]   S. Höger, A. D. Meckenstock, H. Pellen, *J. Org. Chem.* **1997**, *62*, 4556-4557.

[148]   M. Hoffmann, C. J. Wilson, B. Odell, H. L. Anderson, *Angew. Chem., Int. Ed.* **2007**, *46*, 3122-3125.

[149]   S. C. Simon, B. Schmaltz, A. Rouhanipour, H. J. Räder, K. Müllen, *Adv. Mater.* **2009**, *21*, 83-85.

[150]   A. V. Aggarwal, S. S. Jester, S. M. Taheri, S. Förster, S. Höger, *Chem. Eur. J.* **2013**, *19*, 4480-4495.

[151] H. L. Anderson, J. K. M. Sanders, *Angew. Chem., Int. Ed.* **1990**, *29*, 1400-1403.

[152] H. L. Anderson, C. A. Hunter, M. N. Meah, J. K. M. Sanders, *J. Am. Chem. Soc.* **1990**, *112*, 5780-5789.

[153] D. Mössinger, J. Hornung, S. Lei, S. De Feyter, S. Höger, *Angew. Chem., Int. Ed.* **2007**, *46*, 6802-6806.

[154] M. G. Schwab, Ph.D. thesis, Johannes Gutenberg-University Mainz **2011**.

[155] M. Y. Han, B. Özyilmaz, Y. B. Zhang, P. Kim, *Phys. Rev. Lett.* **2007**, *98*, 206805.

[156] B. Özyilmaz, P. Jarillo-Herrero, D. Efetov, P. Kim, *Appl. Phys. Lett.* **2007**, *91*, 192107.

[157] D. V. Kosynkin, A. L. Higginbotham, A. Sinitskii, J. R. Lomeda, A. Dimiev, B. K. Price, J. M. Tour, *Nature* **2009**, *458*, 872-875.

[158] Z. Yan, Y. Liu, J. Lin, Z. Peng, G. Wang, E. Pembroke, H. Zhou, C. Xiang, A.-R. O. Raji, E. L. G. Samuel, T. Yu, B. I. Yakobson, J. M. Tour, *J. Am. Chem. Soc.* **2013**, *135*, 10755-10762.

[159] X. L. Li, X. R. Wang, L. Zhang, S. W. Lee, H. J. Dai, *Science* **2008**, *319*, 1229-1232.

[160] V. R. Sastri, R. Schulman, D. C. Roberts, *Macromolecules* **1982**, *15*, 939-947.

[161] T. Horn, S. Wegener, K. Müllen, *Macromol. Chem. Phys.* **1995**, *196*, 2463-2474.

[162] B. C. Berris, Y. H. Lai, K. P. C. Vollhardt, *J. Chem. Soc., Chem. Commun.* **1982**, 953-954.

[163] B. C. Berris, G. H. Hovakeemian, Y. H. Lai, H. Mestdagh, K. P. C. Vollhardt, *J. Am. Chem. Soc.* **1985**, *107*, 5670-5687.

[164] M. Hirthammer, K. P. C. Vollhardt, *J. Am. Chem. Soc.* **1986**, *108*, 2481-2482.

[165] L. Blanco, H. E. Helson, M. Hirthammer, H. Mestdagh, S. Spyroudis, K. P. C. Vollhardt, *Angew. Chem., Int. Ed.* **1987**, *26*, 1246-1247.

[166] H. Schwager, S. Spyroudis, K. P. C. Vollhardt, *J. Organomet. Chem.* **1990**, *382*, 191-200.

[167] R. H. Schmidtradde, K. P. C. Vollhardt, *J. Am. Chem. Soc.* **1992**, *114*, 9713-9715.

[168] K. P. C. Vollhardt, *Pure Appl. Chem.* **1993**, *65*, 153-156.

[169] P. I. Dosa, Z. Gu, D. Hager, W. L. Karney, K. P. C. Vollhardt, *Chem. Commun.* **2009**, 1967-1969.

[170] J. Sakamoto, J. van Heijst, O. Lukin, A. D. Schlüter, *Angew. Chem., Int. Ed.* **2009**, *48*, 1030-1069.

[171] J. K. Stille, F. W. Harris, R. O. Rakutis, H. Mukamal, *J. Polym. Sci., Part B: Polym. Lett.* **1966**, *4*, 791-793.

[172] J. K. Stille, M. E. Freeburger, *J. Polym. Sci., Part B: Polym. Lett.* **1967**, *5*, 989-992.

[173] K. Imai, M. Kurihara, L. Mathias, J. Wittmann, W. B. Alston, J. K. Stille, *Macromolecules* **1973**, *6*, 158-162.

[174] R. Kellman, C. S. Marvel, *J. Polym. Sci., Part A: Polym. Chem.* **1975**, *13*, 2125-2131.

[175] M. J. Crossley, P. L. Burn, *J. Chem. Soc., Chem. Commun.* **1991**, 1569-1571.

[176] Z. B. Shifrina, M. S. Averina, A. L. Rusanov, M. Wagner, K. Müllen, *Macromolecules* **2000**, *33*, 3525-3529.

[177] Y. Fogel, M. Kastler, Z. H. Wang, D. Andrienko, G. J. Bodwell, K. Müllen, *J. Am. Chem. Soc.* **2007**, *129*, 11743-11749.

[178] M. G. Schwab, A. Narita, Y. Hernandez, T. Balandina, K. S. Mali, S. De Feyter, X. L. Feng, K. Müllen, *J. Am. Chem. Soc.* **2012**, *134*, 18169-18172.

[179] L. Dössel, L. Gherghel, X. L. Feng, K. Müllen, *Angew. Chem., Int. Ed.* **2011**, *50*, 2540-2543.

[180] X. Y. Yang, X. Dou, A. Rouhanipour, L. J. Zhi, H. J. Räder, K. Müllen, *J. Am. Chem. Soc.* **2008**, *130*, 4216-4217.

[181] L. Talirz, H. Sode, J. M. Cai, P. Ruffieux, S. Blankenburg, R. Jafaar, R. Berger, X. Feng, K. Müllen, D. Passerone, R. Fasel, C. A. Pignedoli, *J. Am. Chem. Soc.* **2013**, *135*, 2060-2063.

[182] J. M. Cai, P. Ruffieux, R. Jaafar, M. Bieri, T. Braun, S. Blankenburg, M. Muoth, A. P. Seitsonen, M. Saleh, X. L. Feng, K. Müllen, R. Fasel, *Nature* **2010**, *466*, 470-473.

[183] S. Blankenburg, J. M. Cai, P. Ruffieux, R. Jaafar, D. Passerone, X. Feng, K. Müllen, R. Fasel, C. A. Pignedoli, *ACS Nano* **2012**, *6*, 2020-2025.

[184] M. Treier, C. A. Pignedoli, T. Laino, R. Rieger, K. Müllen, D. Passerone, R. Fasel, *Nat. Chem.* **2011**, *3*, 61-67.

[185] Y. H. Kim, O. W. Webster, *J. Am. Chem. Soc.* **1990**, *112*, 4592-4593.

[186] Y. H. Kim, O. W. Webster, *Macromolecules* **1992**, *25*, 5561-5572.

[187] F. Morgenroth, K. Müllen, *Tetrahedron* **1997**, *53*, 15349-15366.

[188]   D. Türp, T. T. T. Nguyen, M. Baumgarten, K. Müllen, *New J. Chem.* **2012**, *36*, 282-298.

[189]   J. Gibson, M. Holohan, H. L. Riley, *J. Chem. Soc.* **1946**, 456-461.

[190]   H. L. Riley, *J. Chem. Phys. Phys. Chim. Biol.* **1950**, *47*, 565-572.

[191]   R. H. Baughman, C. Cui, *Synth. Met.* **1993**, *55*, 315-320.

[192]   D. Wasserfallen, G. Mattersteig, V. Enkelmann, K. Müllen, *Tetrahedron* **2006**, *62*, 5417-5420.

[193]   X. F. Shen, D. M. Ho, R. A. Pascal, *J. Am. Chem. Soc.* **2004**, *126*, 5798-5805.

[194]   X. F. Shen, D. M. Ho, R. A. Pascal, *Org. Lett.* **2003**, *5*, 369-371.

[195]   Q. L. Song, C. W. Lebeis, X. F. Shen, D. M. Ho, R. A. Pascal, *J. Am. Chem. Soc.* **2005**, *127*, 13732-13737.

[196]   L. Mindach, K. Müllen, *Adv. Mater.* **1996**, *8*, 504-507.

[197]   L. Friedman, D. F. Lindow, *J. Am. Chem. Soc.* **1968**, *90*, 2324-2328.

[198]   F. Ullmann, *Chem. Ber.* **1903**, *36*, 2382-2384.

[199]   Y. Shirota, H. Kageyama, *Chem. Rev.* **2007**, *107*, 953-1010.

[200]   M. Thelakkat, *Macromol. Mater. Eng.* **2002**, *287*, 442-461.

[201]   W. M. Zhang, J. Smith, R. Hamilton, M. Heeney, J. Kirkpatrick, K. Song, S. E. Watkins, T. Anthopoulos, I. McCulloch, *J. Am. Chem. Soc.* **2009**, *131*, 10814-10815.

[202]   J. Veres, S. D. Ogier, S. W. Leeming, D. C. Cupertino, S. M. Khaffaf, *Adv. Funct. Mater.* **2003**, *13*, 199-204.

[203]   Z. Fang, X. H. Zhang, Y. H. Lai, B. Liu, *Chem. Commun.* **2009**, 920-922.

[204]   N. S. Makarov, S. Mukhopadhyay, K. Yesudas, J. L. Bredas, J. W. Perry, A. Pron, M. Kivala, K. Müllen, *J. Phys. Chem. A* **2012**, *116*, 3781-3793.

[205]   D. A. Parthenopoulos, P. M. Rentzepis, *Science* **1989**, *245*, 843-845.

[206]   W. Denk, J. H. Strickler, W. W. Webb, *Science* **1990**, *248*, 73-76.

[207]   J. E. Ehrlich, X. L. Wu, I. Y. S. Lee, Z. Y. Hu, H. Rockel, S. R. Marder, J. W. Perry, *Opt. Lett.* **1997**, *22*, 1843-1845.

[208]   T. S. Qin, W. Wiedemair, S. Nau, R. Trattnig, S. Sax, S. Winkler, A. Vollmer, N. Koch, M. Baumgarten, E. J. W. List, K. Müllen, *J. Am. Chem. Soc.* **2011**, *133*, 1301-1303.

[209]   R. Trattnig, T. M. Figueira-Duarte, D. Lorbach, W. Wiedemair, S. Sax, S. Winkler, A. Vollmer, N. Koch, M. Manca, M. A. Loi, M. Baumgarten, E. J. W. List, K. Müllen, *Opt. Express* **2011**, *19*, A1281-A1293.

[210]   C. L. Wang, H. L. Dong, W. P. Hu, Y. Q. Liu, D. B. Zhu, *Chem. Rev.* **2012**, *112*, 2208-2267.

[211]   A. Hagfeldt, G. Boschloo, L. C. Sun, L. Kloo, H. Pettersson, *Chem. Rev.* **2010**, *110*, 6595-6663.

[212]   U. Bach, K. De Cloedt, H. Spreitzer, M. Grätzel, *Adv. Mater.* **2000**, *12*, 1060-1063.

[213]   T. Yamamoto, M. Nishiyama, Y. Koie, *Tetrahedron Lett.* **1998**, *39*, 2367-2370.

[214]   Z. Fang, Ph.D. thesis, National University of Singapore **2008**.

[215]   L. S. Hung, C. H. Chen, *Mater. Sci. Eng., R* **2002**, *39*, 143-222.

[216]   D. F. O'Brien, P. E. Burrows, S. R. Forrest, B. E. Koene, D. E. Loy, M. E. Thompson, *Adv. Mater.* **1998**, *10*, 1108-1112.

[217]   Y. Sato, S. Ichinosawa, T. Ogata, M. Fugono, Y. Murata, *Synth. Met.* **2000**, *111*, 25-29.

[218]   Y. Shirota, T. Kobata, N. Noma, *Chem Lett* **1989**, 1145-1148.

[219]   W. Ishikawa, H. Inada, H. Nakano, Y. Shirota, *J. Phys. D: Appl. Phys.* **1993**, *26*, B94-B99.

[220]   W. Ishikawa, K. Noguchi, Y. Kuwabara, Y. Shirota, *Adv. Mater.* **1993**, *5*, 559-561.

[221]   T. Noda, H. Ogawa, N. Noma, Y. Shirota, *Adv. Mater.* **1997**, *9*, 720-722.

[222]   Y. Shirota, K. Okumoto, H. Inada, *Synth. Met.* **2000**, *111*, 387-391.

[223]   J. Salbeck, N. Yu, J. Bauer, F. Weissortel, H. Bestgen, *Synth. Met.* **1997**, *91*, 209-215.

[224]   U. Bach, D. Lupo, P. Comte, J. E. Moser, F. Weissortel, J. Salbeck, H. Spreitzer, M. Grätzel, *Nature* **1998**, *395*, 583-585.

[225]   U. Bach, Y. Tachibana, J. E. Moser, S. A. Haque, J. R. Durrant, M. Grätzel, D. R. Klug, *J. Am. Chem. Soc.* **1999**, *121*, 7445-7446.

[226]   I. K. Ding, J. Melas-Kyriazi, N. L. Cevey-Ha, K. G. Chittibabu, S. M. Zakeeruddin, M. Grätzel, M. D. McGehee, *Org. Electron.* **2010**, *11*, 1217-1222.

[227]   Z. Fang, T. L. Teo, L. P. Cai, Y. H. Lai, A. Samoc, M. Samoc, *Org. Lett.* **2009**, *11*, 1-4.

[228] Z. Q. Jiang, Y. H. Chen, C. L. Yang, Y. Cao, Y. T. Tao, J. G. Qin, D. G. Ma, *Org. Lett.* **2009**, *11*, 1503-1506.

[229] Z. Q. Jiang, T. L. Ye, C. L. Yang, D. Z. Yang, M. R. Zhu, C. Zhong, J. G. Qin, D. G. Ma, *Chem. Mater.* **2011**, *23*, 771-777.

[230] Z. Fang, V. Chellappan, R. D. Webster, L. Ke, T. F. Zhang, B. Liu, Y. H. Lai, *J. Mater. Chem.* **2012**, *22*, 15397-15404.

[231] D. Hellwinkel, M. Melan, *Chem. Ber.* **1971**, *104*, 1001-1016.

[232] D. Hellwinkel, M. Melan, *Chem. Ber.* **1974**, *107*, 616-626.

[233] D. Hellwinkel, M. Melan, W. Egan, C. R. Degel, *Chem. Ber.* **1975**, *108*, 2219-2231.

[234] D. Hellwinkel, G. Aulmich, M. Melan, *Chem. Ber.* **1980**, *113*, 358-384.

[235] M. Mas-Torrent, C. Rovira, *Chem. Rev.* **2011**, *111*, 4833-4856.

[236] L. Zöphel, Ph.D. thesis, Johannes Gutenberg-University Mainz **2012**.

[237] W. P. Wu, Y. Q. Liu, D. B. Zhu, *Chem. Soc. Rev.* **2010**, *39*, 1489-1502.

[238] C. Li, H. Wonneberger, *Adv. Mater.* **2012**, *24*, 613-636.

[239] G. Binnig, H. Rohrer, *Helv. Phys. Acta* **1982**, *55*, 726-735.

[240] G. Binnig, H. Rohrer, C. Gerber, E. Weibel, *Appl. Phys. Lett.* **1982**, *40*, 178-180.

[241] P. Samori, J. P. Rabe, *J. Phys.: Condens. Matter* **2002**, *14*, 9955-9973.

[242] M. Bieri, S. Blankenburg, M. Kivala, C. A. Pignedoli, P. Ruffieux, K. Müllen, R. Fasel, *Chem. Commun.* **2011**, *47*, 10239-10241.

[243] W. Pisula, Z. Tomovic, C. Simpson, M. Kastler, T. Pakula, K. Müllen, *Chem. Mater.* **2005**, *17*, 4296-4303.

2 Objectives and Motivation

Through extensive research efforts in synthetic chemistry and engineering, new technologies have been developed to exploit the potential of organic semiconductors. Nevertheless, silicon`s charge carrier mobility in combination with its long-term stability have yet to be reached. There is much more research to be done to improve the performance of organic materials and to answer fundamental questions in the device processing.

Since the 1980s a versatile toolbox of aryl-aryl bond forming reactions has become available to synthetic chemists, which enabled the development of large libraries of molecules and polymers.[1, 2] Based on this, the search for new types of one-, two- and three-dimensional benzene-rich architectures is the major intersection of the herein presented research efforts. Within the scope of this work, the syntheses, the study of the properties along with possible optoelectronic applications will be covered.

The initial focus is upon the selective functionalization and utilization of planarized triarylamines toward sophisticated and functional multi-dimensional structures. The *N*-heterotriangulene has been chosen as structural motif due to its electron-rich properties and reversible redox behavior which is stabilized upon planarization. Its improved π-conjugation, the easy introduction of solubilizing groups at the bridges and its particularly activated positions, *para* to the central nitrogen are further benefits compared to broadly used triphenylamines.[3] Once a chemical substance becomes application relevant, one has to think of designing the synthesis to be as easy, inexpensive and efficient as possible. Thus, *N*-heterotriangulene is ideally suited due to its facile accessibility. Although a few types of dendritic structures based on *N*-heterotriangulene have been reported, it has not been applied for the formation of oligomeric and polymeric semiconductors.[4-6] Consequently, the selective functionalization of *N*-heterotriangulene toward different types of monomers plays a key role in the first part of the work (Scheme 2-1). The architecture of the resulting polymer is thereby determined by the substitution pattern of the monomer. While an *AA*-type monomer is expected to polymerize in a linear fashion, an *A₂B*-type monomer will lead to hyperbranched structures. Highly versatile transition metal-mediated cross-coupling procedures shall be used for polymerization. An efficient charge transport along the polymer backbone as well as among the individual chains by close π-π distances are believed to be crucial for organic field-effect transistors (OFETs).[7-9] Hyperbranched
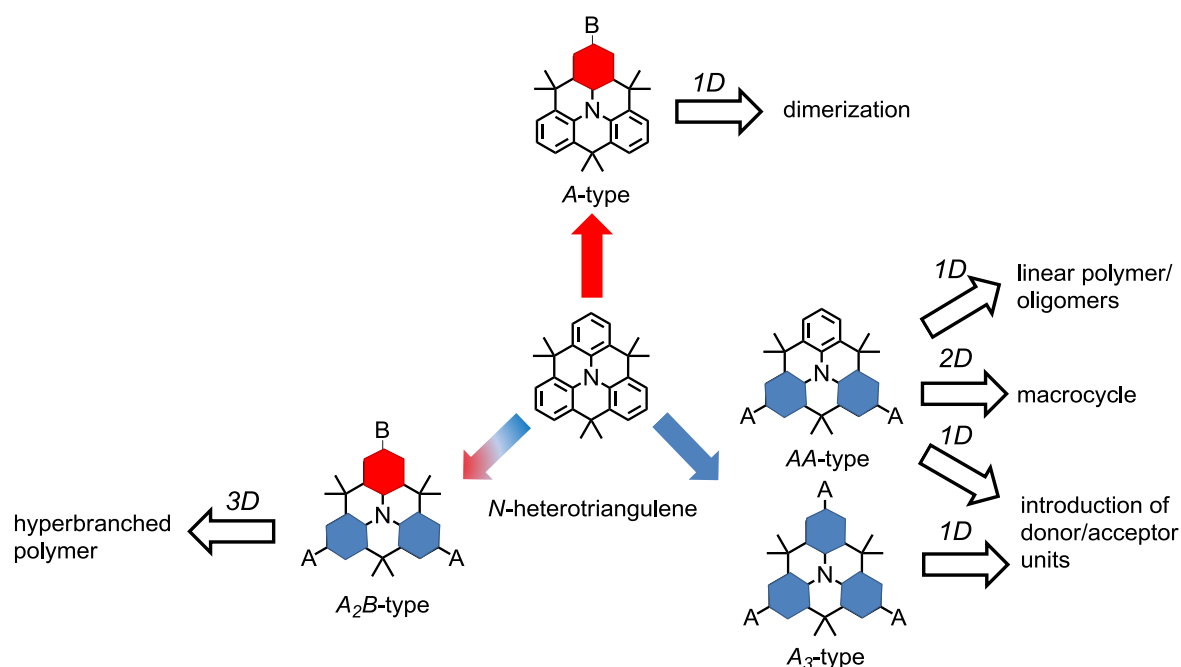
Scheme 2-1. Schematic representation of the symmetric and asymmetric functionalization strategy of *N*-heterotriangulene toward architectures with different dimensionality.

polymers allow charge transport along the backbone in two- and three-dimensional directions, while charge carriers in linear polymers are limited to two dimensions. Moreover, the long-term stability of organic (polymeric) semiconductors influences the performance of OFETs to a great extent. In this regard, the comparative aspect of the two types of *N*-heterotriangulene polymers with each other and with the "fruit-fly" among polymeric semiconductors, poly(3-hexylthiophene) (P3HT),[10, 11] will be a major issue.

The polymerization of *AA*- and *A$_2$B*-type monomers is moreover expected to provide hexameric macrocycles as byproducts, due to the C_3 symmetry of the *N*-heterotriangulene. Hence, the second chapter is dedicated to the controlled formation of a new π-conjugated macrocycle being entirely composed of *N*-heterotriangulenes. As a consequence of the assembly of *N*-heterotriangulenes with the reactive sides in an inherent angle of 120°, the resulting macrocycle is nearly planar, shape-persistent and highly symmetric. As discussed in the Introduction, numerous synthetic strategies toward macrocycles are available (Scheme 2-2). One possibility is to use a simple *AA*-type monomer for a direct cyclohexamerization. This route can in principle be applied to solution- and surface-assisted procedures. In the first case, however, the accompanying formation of linear oligomers is expected. While the second approach requires rather exotic conditions, it might be beneficial for the macrocylization process owing to the surface-confinement of the reactive precursors. Within the experimental scope of these investigations, both methods will be discussed. *Moore`s* repetitive convergent strategy,[12] can moreover help to
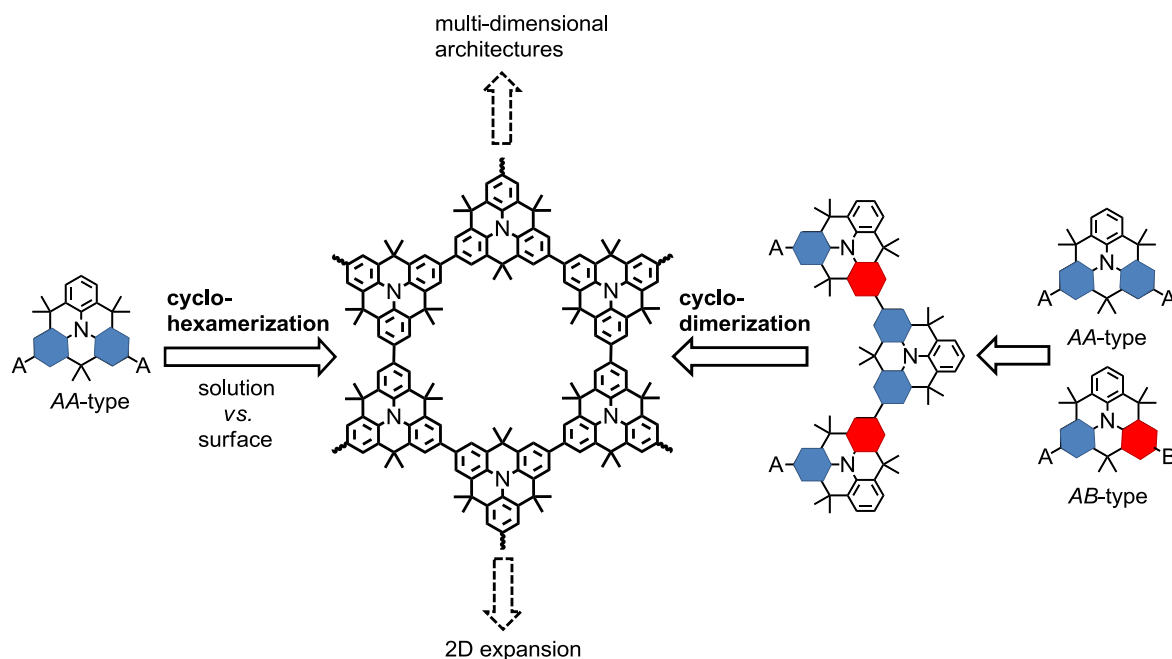
Scheme 2-2. Schematic representation of different macrocyclization attempts and utilization of the hexameric macrocycles as building block.

produce macroscopic quantities of the *N*-heterotriangulene macrocycle to enable its photophysical and electronic characterization. The central cavity of the macrocycle is expected to act as host for suitable guest molecules, which can be relevant from the viewpoint of non-covalent interactions and self-assembly. Due to the presence of six activated positions at the periphery, the two-dimensional expansion of the macrocycle toward honeycomb-structured networks is conceivable, bridging the gap between the hyperbranched polymer from the first part and the macrocyclic arrangement.

Stable electron donors, such as *N*-heterotriangulenes, are particularly useful as hole-transport materials (HTMs) for organic photovoltaics, in particular as dye regenerator in solid-state dye-sensitized solar cells (sDSSCs). Due to low electric conductivities and the high crystallization tendency of state-of-the-art small molecule HTMs, the maximum power conversion efficiency and durability of sDSSCs are hampered. The *N*-heterotriangulene unit with its facile synthesis and functionalization provides multiple options to construct various electron-rich materials potentially useful as HTMs (Scheme 2-1). Thus, in the third part of this work, several *N*-heterotriangulene derivatives have been prepared and investigated in sDSSCs to compare their HTM performance with their commonly used standard counterparts. The obtained results shall guide future molecular design of new HTMs displaying superior performances in sDSSCs.
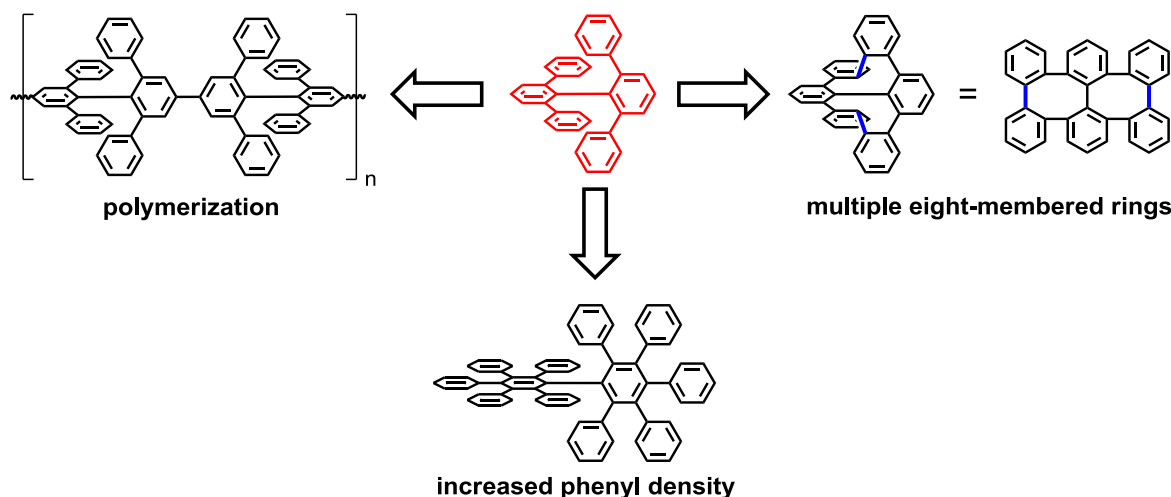
Scheme 2-3. Schematic representation of the potential utilization of 2,2',6,6'-tetraphenyl-1,1'-biphenyl.

Apart from hole-transport applications, organic semiconductors are attractive candidates for the use as emissive materials in OLEDs. Research in this area has been focused over the past years on PPPs, due to their strong blue emissions. These materials raised moreover a fundamental interest of the relation between steric congestion of the benzene units and the resulting reactivity together with the accompanied properties. Hence, considerable efforts have been devoted to 2,2',6,6'-tetraphenyl-1,1'-biphenyl as versatile building block for increasing the benzene density along the PPP backbone and to provide access to unprecedented polyaromatic architectures (Scheme 2-3). Although the parent compound has been reported, its electronic characteristics and functionalized derivatives have not been studied, most likely due to its demanding and low yielding synthesis.[13-15] An alternative pathway toward this structural motif shall be therefore targeted in this work. The polymerization of 2,2',6,6'-tetraphenyl-1,1'-biphenyl might provide a new class of poly(*para*phenylene) (PPP) whose intrinsic rigidity and steric congestion is expected to alter the electronic characteristics, such as the effective π-conjugation length (Scheme 2-3, left). A striking feature of 2,2',6,6'-tetraphenyl-1,1'-biphenyl is that it bridges the gap between one-dimensional PPPs and three-dimensional benzene-based structures. Due to its unique geometry, it is both a model compound and a potential precursor for the theoretical carbon allotrope cubic graphite. Hence, connecting the peripheral phenyls *via* their *ortho*-positions toward multiple eight-membered rings, could provide access to small segments of cubic graphite (Scheme 2-3, right). Using 2,2',6,6'-tetraphenyl-1,1'-biphenyl to further increase the phenyl density could help to gain insights into the structure-property relationship of new, sterically congested carbon-rich frameworks (Scheme 2-3, bottom). While the transition between one- and three-dimensional benzene-based structures is
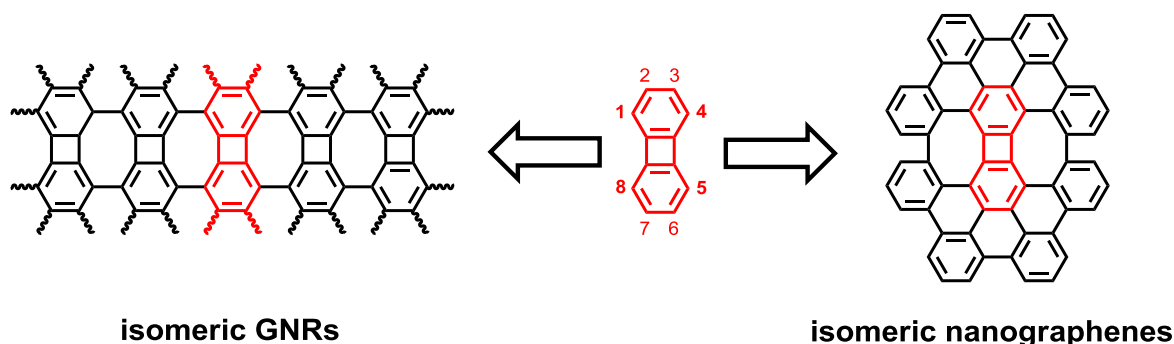
Scheme 2-4. Schematic representation of the chemical expansion of biphenylene toward isomeric graphene structures.

addressed previously, the focus turns in the final chapter toward their two-dimensional counterparts. The primary concern is at the development of synthetic pathways toward isomeric graphene nanoribbons (GNRs) and nanographenes. GNRs are two-dimensional cutouts of graphene that exhibit a large aspect ratio of length over width.[16, 17] They are known to "open" the band gap of semi-metallic graphene, thus making them appealingcandidates for carbon-based electronics.[18, 19] Besides the precise control of the edge structure of GNRs, the implementation of defects by different ring sizes constitutes an alternative pathway to modulate the band gap. A viable possibility is the combination of eight-, six- and four-membered rings within one chain, giving rise to predicted band gaps of approximately 1.1 eV for infinitely long ribbons.[20] The desired geometry, width, length and edge structure is thereby defined by the biphenylene monomer (Scheme 2-4). To enable the targeted polymerization toward such GNRs, a functionalization of the biphenylene moiety at its hardly accessible 1,4,5,8-positions is crucial. The developed biphenylene monomers can be applied to solution and surface-assisted polymerization procedures, both of which shall be discussed. Controlling the substitution pattern of biphenylene allows for further modifications of the GNR width and hence of the electronic properties. In addition, the preparation of model compounds which reflect the topology of the infinite isomeric GNRs constitutes another objective of this project.

More generally, the main target of this work is not only to synthesize new molecules, but, more importantly, also to provide systematic studies of the structure-property relationships for various types of benzene-based architectures with different dimensionalities. For selected materials, the processing conditions will be optimized and subsequently tested as active component in organic electronic devices, such as OFETs and DSSCs. Analytical techniques, for example STM and 2D WAXS will be used to study the supramolecular

organization, which is correlated to the molecular architecture. The interplay between the particular molecular structure, the intrinsic optoelectronic properties, and the supramolecular order in the solid state and the resulting device performance will be thereby emphasized. These findings might provide useful guidelines for future developments of novel organic semiconductor materials for device applications.

2.1   References

[1]   A. Suzuki, *Angew. Chem., Int. Ed.* **2011**, *50*, 6722-6737.

[2]   E. I. Negishi, *Angew. Chem., Int. Ed.* **2011**, *50*, 6738-6764.

[3]   Y. Shirota, H. Kageyama, *Chem. Rev.* **2007**, *107*, 953-1010.

[4]   Z. Fang, T. L. Teo, L. P. Cai, Y. H. Lai, A. Samoc, M. Samoc, *Org. Lett.* **2009**, *11*, 1-4.

[5]   Z. Fang, X. H. Zhang, Y. H. Lai, B. Liu, *Chem. Commun.* **2009**, 920-922.

[6]   Z. Fang, V. Chellappan, R. D. Webster, L. Ke, T. F. Zhang, B. Liu, Y. H. Lai, *J. Mater. Chem.* **2012**, *22*, 15397-15404.

[7]   M. Mas-Torrent, C. Rovira, *Chem. Rev.* **2011**, *111*, 4833-4856.

[8]   H. Klauk, *Chem. Soc. Rev.* **2010**, *39*, 2643-2666.

[9]   Z. B. Henson, K. Müllen, G. C. Bazan, *Nat. Chem.* **2012**, *4*, 699-704.

[10]   H. Sirringhaus, P. J. Brown, R. H. Friend, M. M. Nielsen, K. Bechgaard, B. M. W. Langeveld-Voss, A. J. H. Spiering, R. A. J. Janssen, E. W. Meijer, P. Herwig, D. M. de Leeuw, *Nature* **1999**, *401*, 685-688.

[11]   R. J. Kline, M. D. McGehee, E. N. Kadnikova, J. S. Liu, J. M. J. Frechet, *Adv. Mater.* **2003**, *15*, 1519-1522.

[12]   J. S. Zhang, D. J. Pesak, J. L. Ludwick, J. S. Moore, *J. Am. Chem. Soc.* **1994**, *116*, 4227-4239.

[13]   S. Ozasa, Y. Fujioka, J. Kikutake, E. Ibuki, *Chem. Pharm. Bull.* **1983**, *31*, 1572-1581.

[14]   Y. Fujioka, S. Ozasa, K. Sato, E. Ibuki, *Chem. Pharm. Bull.* **1985**, *33*, 22-29.

[15]   L. Tong, H. Lau, D. M. Ho, R. A. Pascal, *J. Am. Chem. Soc.* **1998**, *120*, 6000-6006.

[16]   M. G. Schwab, Ph.D. thesis, Johannes Gutenberg-University Mainz **2011**.

[17]   C. Bronner, S. Stremlau, M. Gille, F. Brausse, A. Haase, S. Hecht, P. Tegeder, *Angew. Chem., Int. Ed.* **2013**, *52*, 4422-4425.

[18]   F. Schwierz, *Nat. Nanotechnol.* **2010**, *5*, 487-496.

[19]   Z. Q. Wei, D. B. Wang, S. Kim, S. Y. Kim, Y. K. Hu, M. K. Yakes, A. R. Laracuente, Z. T. Dai, S. R. Marder, C. Berger, W. P. King, W. A. de Heer, P. E. Sheehan, E. Riedo, *Science* **2010**, *328*, 1373-1376.

[20]   A. Rajca, A. Safronov, S. Rajca, C. R. Ross, J. J. Stezowski, *J. Am. Chem. Soc.* **1996**, *118*, 7272-7279.

3 *N*-Heterotriangulene Polymers

## 3.1   Linear *N*-Heterotriangulene Polymer

3.1.1   Introduction

The emergence of π-conjugated polymers as functional materials for organic electronics more than two decades ago has sparked considerable attention due to the generation of new scientific concepts and the potential for new technologies.[1-6] Since π-conjugated polymers behave as organic semiconductors they have led to successful realizations of flexible large-area displays[7-12] polymer based photovoltaic cells[13] and electronic circuits for low-cost radio-frequency identification tags.[14-16] They are likewise important as sensing materials for water, organic vapors and explosives either by fluorescence quenching or by conductivity changes upon exposure to a suitable analyte.[17-20]

Although significant improvements in the charge carrier mobility have nowadays been achieved, reaching almost ($\mu_{sat} \sim 0.1-6.2$ cm^2 V^{-1} s^{-1}) the benchmark of amorphous silicon, there are still both physical and technological issues to be faced.[21-25] While amorphous polymers such as poly(triarylamines) (**PTAAs**) cannot compete with crystalline semiconductors in terms of charge carrier mobilities (10^{-3} to 10^{-2} cm^2 V^{-1} s^{-1}), their facile and reproducible processability together with their robust electrical performance make these materials particularly appealing for device applications.[26, 27]

3.1.2   Synthesis and Characterization

In line with the above considerations, dimethylmethylene bridged triphenylamine, so-called *N*-heterotriangulene (Scheme 3-1) was identified as a promising, however, relatively poor investigated molecule for organic (polymeric) semiconductors.[28-34] Its crucial air stability is provided by the low lying HOMO level ($E_{HOMO} = -5.14$ eV), which is slightly enhanced compared with triphenylamine ($E_{HOMO} = -5.19$ eV).[35] Due to the dimethylmethylene tethers good solubility in organic solvents is provided without the need of additional solubilizing groups (*i.e.* long alkyl chains).

The straightforward synthetic route toward *N*-heterotriangulene **3-4** is shown in Scheme 3-1.[28-34] It starts with an *Ullmann*-type aromatic amination between commercially available methyl 2-iodobenzoate and methyl 2-aminobenzoate **3-1** using high boiling diphenyl ether as a solvent. Triester **3-2** was subsequently reacted under Grignard conditions with CH$_3$MgI resulting in the respective triol **3-3** in moderate yields. In this step, a broad variety
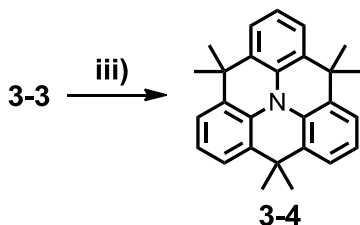
Scheme 3-1. Synthetic route toward the *N*-heterotriangulene **3-4**.[32-34] Conditions: i) methyl 2-iodobenzoate, Cu, CuI, K_2CO_3, diphenyl ether 190 °C, 50%; ii) CH_3I, Mg, Et_2O/toluene, reflux, 32%; iii) H_3PO_4, RT, 83%.

of aliphatic and aromatic substituents can be introduced by simply generating the respective organometallic species and reacting with triester **3-2**, revealing the versatility of this reaction sequence.[36, 37] Acid catalyzed threefold *intra*molecular *Friedel-Crafts* alkylation using phosphoric acid led subsequently to *N*-heterotriangulene **3-4** in an overall yield of 13%. Gratifyingly, this synthetic route is rather robust and can be applied on a multi gram scale.

The X-ray crystallographic structure of single crystals grown by slow evaporation of a chloroform solution of **3-4** clearly reveals the planarization induced by the bridging dimethylmethylene groups (Figure 3-1).
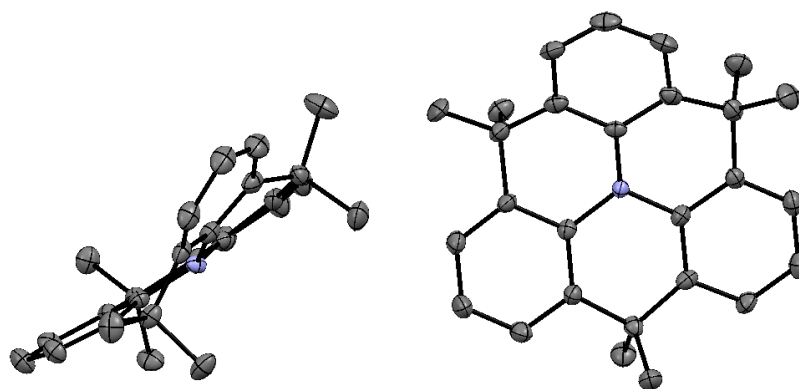
Figure 3-1. X-ray crystallographic structure of **3-4** (nitrogen atoms blue, carbon atoms grey, hydrogen atoms omitted for clarity).

For the polymerization of **3-4** toward a liner π-conjugated polymer, different techniques are feasible. Thus, A_2B_2-type polycondensations, *e.g.*, *Suzuki-Miyaura* or *Stille* polymerization procedures revealed several drawbacks which will be addressed in the following (Figure 3-2):

- the necessity of an additional reaction step for the introduction of a second functional group toward *AB*-, *AA*- and *BB*-monomers,

- precise control of the equimolar ratio between the two functional groups, referring to the *Carothers'* law,[38]

- stoichiometric deviations significantly alter the conversion and decrease simultaneously the polymer chain length,

- the lack of reproducibility,

- the necessity of extended reaction times to achieve high molecular weights as a result of the intrinsic kinetics of the polycondensation mechanism.
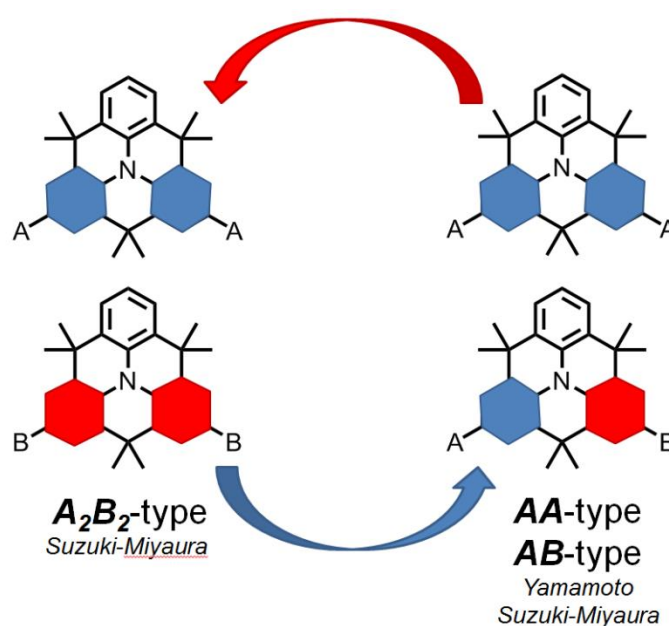
Figure 3-2. Schematic representation illustrating the systematic design of a suitable *A₂B₂*-type (*Suzuki-Miyaura* reaction) and *AA*-type monomer (*Yamamoto* reaction).

In order to avoid these detrimental effects, an efficient *AA*-type coupling method was targeted. In this context one of the most versatile methods for the synthesis of rigid π-conjugated polymers from an *AA*-type monomer is the Ni^0-mediated *Yamamoto* dehalogenation polycondensation.[39-43] This procedure avoids precise weighing due to the necessity of a bifunctionalized monomer, which enhances the conversion rate of the stepwise growth and the reproducibility. Thus, **3-4** was brominated using two equivalents of *N*-bromosuccinimde (NBS) at its activated positions, *para* to the central nitrogen (Scheme 3-2). By performing the reaction at lower temperatures, a sufficient selectivity for the formation of dibromo *N*-heterotriangulene **3-5** was achieved. After column chromatographic separation and repeated crystallization, highly pure **3-5** was obtained in 77% yield.
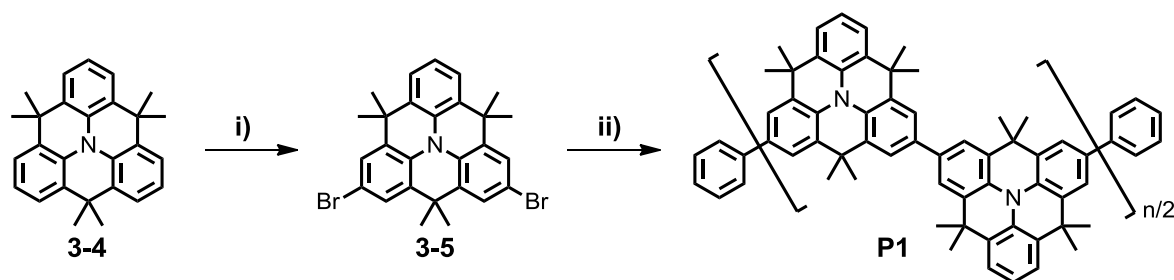
Scheme 3-2. Synthetic route toward *N*-heterotriangulene polymer **P1**. Conditions: i) 2 equiv. NBS, CHCl$_3$, 0 °C to RT, 2h, 77%; ii) bis(cycloocta-1,5-diene)nickel(0), cycloocta-1,5-diene, 2,2'-bipyridine, toluene/DMF, 85 °C, 2 days, endcapping with bromobenzene, 66%.

Subsequently, the polymerization reaction of monomer **3-5** was conducted in a standard *Yamamoto* protocol utilizing an overall 12/1 mixture of toluene/DMF.[39, 40] The active Ni^0 complex was prepared under glovebox conditions from a stoichiometric mixture of bis(cycloocta-1,5-diene)nickel(0), cycloocta-1,5-diene and 2,2'-bipyridine in a toluene/DMF solvent mixture. The deep-purple complex solution was subsequently activated at 65 °C for 30 min in the absence of light. Due to the 120° angle between the two bromo substituents in **3-4**, the formation of macrocycles was expected which occurs as a side-reaction if too low precursor concentrations are used.[44-46] For this purpose, the concentration was set to 25×10^{-3} M and the monomer solution was added quickly to the activated Ni^0 complex. After gently heating the reaction for two days in the dark at 85 °C to avoid gelation and to keep the polymer in solution, the active polymer chains were endcapped using an excess of bromobenzene. Quenching and decomposition of nickel residues were achieved by dropping the reaction mixture into dilute methanolic hydrochloric acid. The crude polymer was filtered, reprecipitated and subjected to Soxhlet extraction with acetone and *n*-hexane to remove the low molar mass fractions.

The molecular weight of **P1** was estimated by size-exclusion chromatography (SEC) in THF using poly(styrene) as standard. The SEC method is based on the relative determination of molecular weights by comparing the elution volume of the analyte to a calibration curve derived from a polymer standard with a defined molecular weight distribution. According to its hydrodynamic volume, the analyte is separated by a column filled with poly(styrene) beads and detected by a refractive index (RI) or UV-vis detector. With the relation between the size and the molecular weight of the standard, the unknown molecular weight of the analyte can be estimated. With this method a weight-average molecular weight (M_w) of 18 000 g/mol (polydispersity index (PDI) = 1.7) was obtained for **P1**, which corresponds to a molecular structure of approximately 49 *N*-
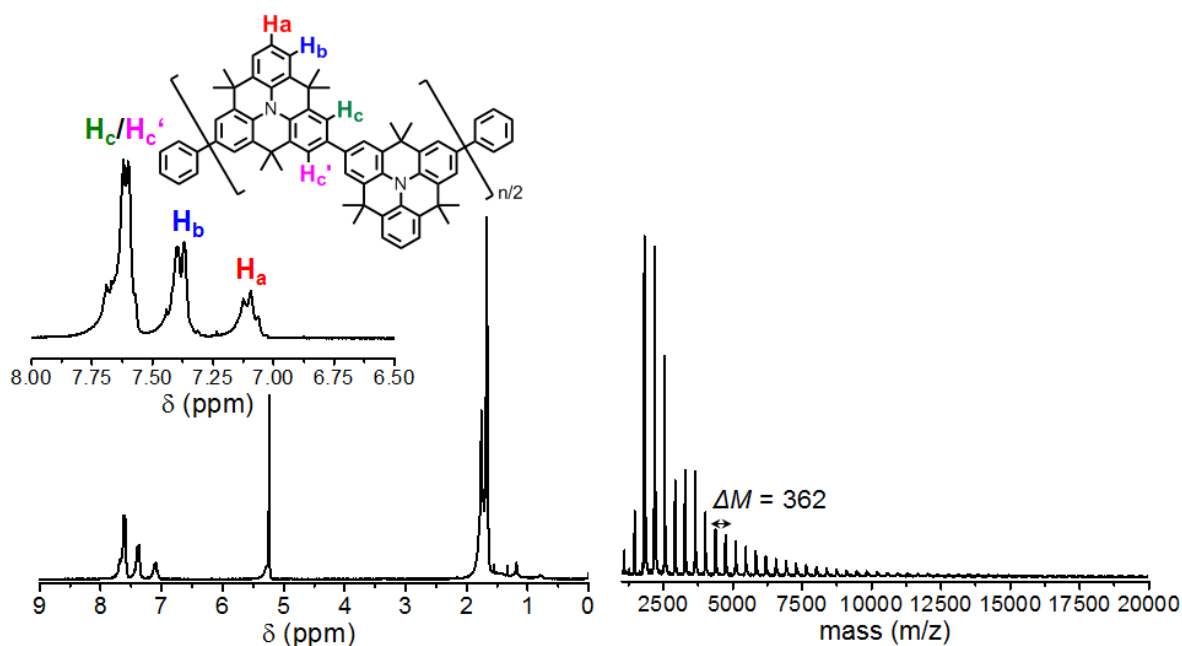
Figure 3-3. Left: ^{1}H NMR spectrum of **P1** in CD$_2$Cl$_2$ at 25 °C. Inset: Zoom into the aromatic region with proton assignment. Right: MALDI-TOF MS of **P1** (linear mode, matrix: dithranol).

heterotriangulene units which is a reasonable value for poly(triarylamine)s.[27] With the help of MALDI-TOF MS a molecular weight up to 20 000 g/mol was detected revealing successful removal of the bromine functionalities (Figure 3-3, right). The peaks are separated by a mass difference of 362 corresponding to the molecular weight of the *N*-heterotriangulene repeating unit. The spectrum exhibited an exponential decline of the peak intensities due to differences in the ionization process of the individual polymer chains. Lower molecular weight species are easily desorbed by the applied laser and reach the detector in larger amounts leading to saturation. The polymer chains having a higher molecular weight desorb less efficiently resulting in less intense signals. Although MALDI-TOF MS do not reflect the actual molecular weight distribution of a polymer, it is, however, a versatile analytic method for determination of the polymerization progress and for end group analysis.[47, 48] The differences in the molar mass values obtained by SEC and by MALDI-TOF MS reflect the difficulties in determining absolute molecular weights of polymers. However, other techniques, such as dynamic light scattering, were impeded by the strong absorption and fluorescence of **P1** at the available wavelengths, which prevented an accurate measurement.

The *N*-heterotriangulene polymer **P1** displayed high solubility in organic solvents, *e.g.*, THF, dichloromethane, toluene and 1,2-dichlorobenzene enabling its characterization by ^{1}H NMR spectroscopy. The ^{1}H NMR spectrum revealed broad signals between 7.8 and 7.0 ppm corresponding to aromatic protons of the *N*-heterotriangulene subunits and a broad

signal at 1.7 ppm as a result of the bridging dimethylmethylene groups, with correct signal intensities (Figure 3-3, left). Moreover, thermogravimetric analysis (TGA, Figure 3-15, for further remarks see below) revealed a high thermal stability up to 400 °C (decomposition temperature at 5% weight loss is 456 °C).

3.1.3   Optoelectronic Properties

3.1.3.1   *Solution Studies*

The following experiments (dilute solution and thin film studies) were conducted in collaboration with ███████████████ in the group of ███████████████ at the NanoTecCenter Weiz, Austria.

Investigation of the electronic properties was performed with the help of cyclic voltammetry (CV) at room temperature in dichloromethane (Figure 3-4 right). The CV experiment was performed with a 1 mM solution of **P1** in anhydrous dichloromethane under argon atmosphere using *n*-Bu$_4$NPF$_6$ as conductive salt. Ferrocene has been added as internal standard to normalize the cyclovoltagram. While the current flow was measured, the voltage was ramped with a speed of 50 mV s^{-1}. The HOMO level of **P1** in solution was estimated using the onset oxidation potential relative to the ferrocene standard according to equation (1).[49]

$$E^{HOMO} = \left[\left(E_{onset}^{ox} - E_{onset}^{reference} \right) + 4.8 \right] eV \qquad (1)$$

This resulted in a HOMO of 5.01 eV (see Table 3-1).

The photophysical properties of **P1** were initially investigated in diluted solutions (1 × 10^{-5} M, Figure 3-4 left, Table 3-1). The longest wavelength transitions in absorption were found at 382 and 323 nm for a toluene solution of **P1** (Figure 3-5 left, black line). By changing the solvent to chloroform, no significant change in absorption occurred (Figure 3-5 left, red line). However, the photoluminescence spectra of both solutions showed significant differences (Figure 3-5 left). In general, changes of the solvent composition influence fluoresecence properties (*e.g.* the spectral shape or the spectral position) more dramatically than the related absorption characteristics.[50] In order to study these differences the solutions of **P1** were measured under different pre-conditions. Figure 3-5 displays the fluorescence spectra of toluene (left) and chloroform (right) solutions which were prepared under ambient conditions (solid black line), under yellow light and kept in dark until the measurements (blue dashed line) and exposed to UV-light (~10 s, with wavelengths of 254 nm and 366 nm, red dashed/dotted line).
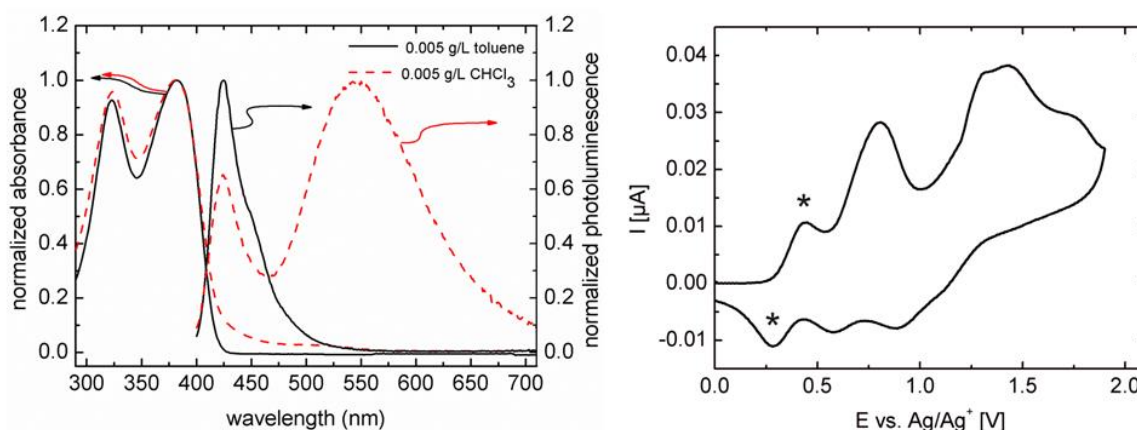
Figure 3-4. Left: UV-vis absorption and photoluminescence emission spectra of **P1** in toluene (solid black line, 1×10^{-5} M) and in $CHCl_3$ (dashed red line, 1×10^{-5} M). Right: Cyclic voltammogram of **P1** reported *vs.* ferrocene (anodic scans are shown, 10^{-3} M, 0.1 M *n*-Bu_4NPF_6 in CH_2Cl_2 at a scan rate of 50 mV/s). The asterisks denote the Fc^+/Fc oxidation/reduction process.

Table 3-1. Selected photophysical data of **P1**.

| Solvent	$\lambda_{abs,max}$ (nm)	$\lambda_{PL,max}$ (nm)	E_g^{opt} [a] (eV)	E_{HOMO} (eV)	E_{LUMO} [d] (eV)
Toluene	323, 382	425	2.9	-5.1[b]	-2.2
$CHCl_3$	324, 382	424, 547	2.9	-5.0[c]	-2.1

[a] $E_g^{opt} = h \cdot c / \lambda_{0.1max}$. [b] Obtained by ultraviolet photoelectron spectroscopy. [c] The HOMO level was calculated from the measured first oxidation potential. [d] LUMO levels were calculated from the optical band gap E_g^{opt} and the respective HOMO levels.

In contrast to the toluene solutions, the chloroform solution spectra exhibited a significant influence of the ambient/UV-light exposure. A second peak appeared at around ~550 nm and the initial blue emission at 424 nm decreased. The corresponding inset depicts a color change of the $CHCl_3$ solution from colorless to brown solution when exposed to ambient light. The observed effects can be ascribed to the dissociation of chloroform induced by UV-light at which hydrochloric acid is formed and protonation of the central nitrogen occurs (Scheme 3-3 a).[51-53] This could lead to an *intra*molecular charge-transfer (ICT) of the protonated *N*-heterotriangulene units (electron acceptors) with the remaining unprotonated (electron donors) units, resulting in a lowered LUMO and a lifted HOMO level of **P1** causing the observed bathochromic shift in emission. Even if the chloroform solution was prepared under yellow light and kept in dark, a non-negligible emission from 500 to 650 nm appeared, which is, however, not as pronounced as for solutions exposed to UV light.
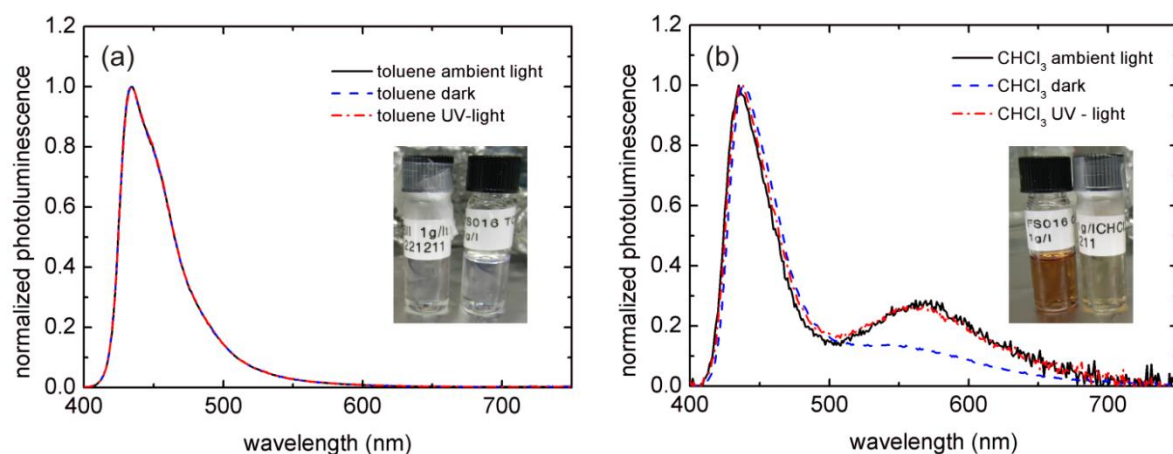
Figure 3-5. Photoluminescence emission spectra of a solution of **P1** (a) in toluene (3×10^{-3} M) and (b) in CHCl$_3$ after preparation under ambient conditions (black solid line), in dark (blue dashed line) and after exposure to UV-light (red dashed/dotted line). Inset: Corresponding solutions when prepared under ambient light (left) and in dark (right).

The reversibility of this process was tested by the addition of triethylamine to the chloroform solution exposed prior to UV light resulting in a color change from red to colorless (Scheme 3-3 b). This behavior might make **P1** particularly attractive for applications as stimuli-responsive material in, *e.g.*, optical pH-sensors.[54]
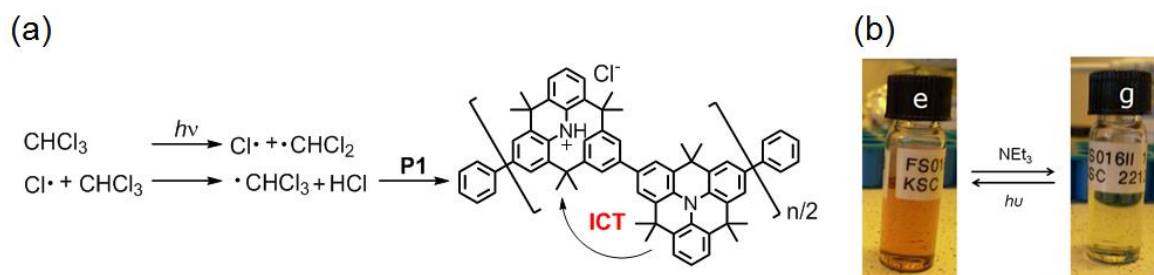
Scheme 3-3. (a) Schematic representation of the dissociation of CHCl$_3$ and subsequent protonation of **P1**.[51-53] (b) Reversible switching between protonated and deprotonated state.

3.1.3.2   *Thin Film Studies*

The topographic image of a typical film of **P1** is shown in Figure 3-6 a after spin-coating from toluene and annealing at 120 °C for one hour in high vacuum (p ~ 4×10^{-5} mbar). The root-mean-squared roughness of ~0.4 nm reflects a very smooth film formation. An amorphous, disordered morphology was confirmed by X-ray diffraction analysis, which was revealed by the absence of scattering patterns.

The UV-vis absorption and emission spectra of **P1** films spin-coated from 3 g/L toluene and chloroform solutions are shown in Figure 3-6 b. The absorption maxima of **P1** films were detected at 383 nm and 325 nm, respectively, indicating no significant aggregation of
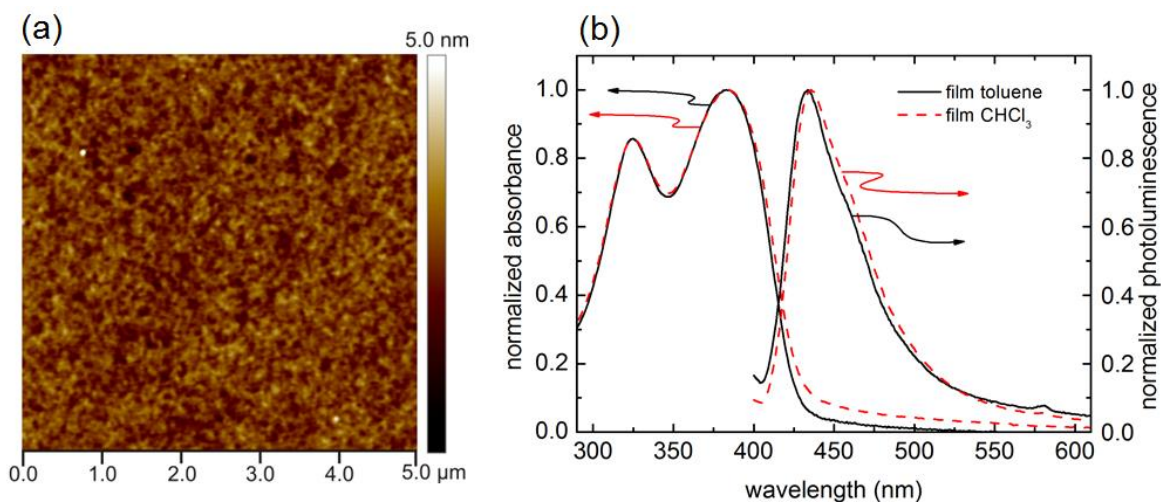
Figure 3-6. (a) AFM topographic image of a typical **P1** film on SiO$_2$ (spin-coating from toluene (3 g/L), scan size 5 μm × 5 μm). (b) UV-vis absorption and photoluminescence emission spectra of **P1** films prepared from toluene (solid black line) and CHCl$_3$ (dashed red line) solutions.

P1 in the solid state. The emission spectra revealed no protonation effects during the spin-coating process, indicated by similar maxima at 434 nm and 436 nm for the film spin-coated from toluene and chloroform, respectively. This can be explained by the fact that the solutions for film deposition were prepared and spin-coated under inert atmosphere in absence of UV-light and subsequently dried under high vacuum (p ~ 4 × 10^{-5} mbar) at 120 °C to remove residual solvents. With the help of ultraviolet photoelectron spectroscopy (UPS), the energy levels of **P1** and their alignment with respect to the gold Fermi-level were determined. In addition, these values were compared with P3HT, one of the most widely investigated p-type polymers. The low binding energy onset is 0.7 eV below the Fermi-level (E_F) (Figure 3-8 a, top). This led to an ionization energy (IE) of 5.1 eV, together with the work function (Φ = 4.4 eV, Figure 3-8 a, top) determined from the secondary electron cut-off. This result is in good agreement with the HOMO level (E_{HOMO} = −5.0 eV) calculated from the CV data. Using the optical band gap (E_g^{opt}) obtained by UV-vis absorption measurements in thin films (Table 3-1), the lowest unoccupied molecular orbital (LUMO) was estimated (E_{LUMO} = −2.1 eV). In contrast to that, the secondary electron cut-off for P3HT was found at 4.2 eV with respect to the Fermi level (E_F) and, combined with the binding energy of 0.4 eV below the Fermi level, the corresponding IE could be determined to 4.6 eV (Figure 3-8, bottom). The LUMO of P3HT can be estimated (E_{LUMO} = −2.6 eV) by using the optical gap energy of 1.9 eV, which was determined from UV-vis absorption measurements in solid state (film of 3 g/l toluene, not shown). Moreover, the semiconductor/gold interface is a relevant parameter
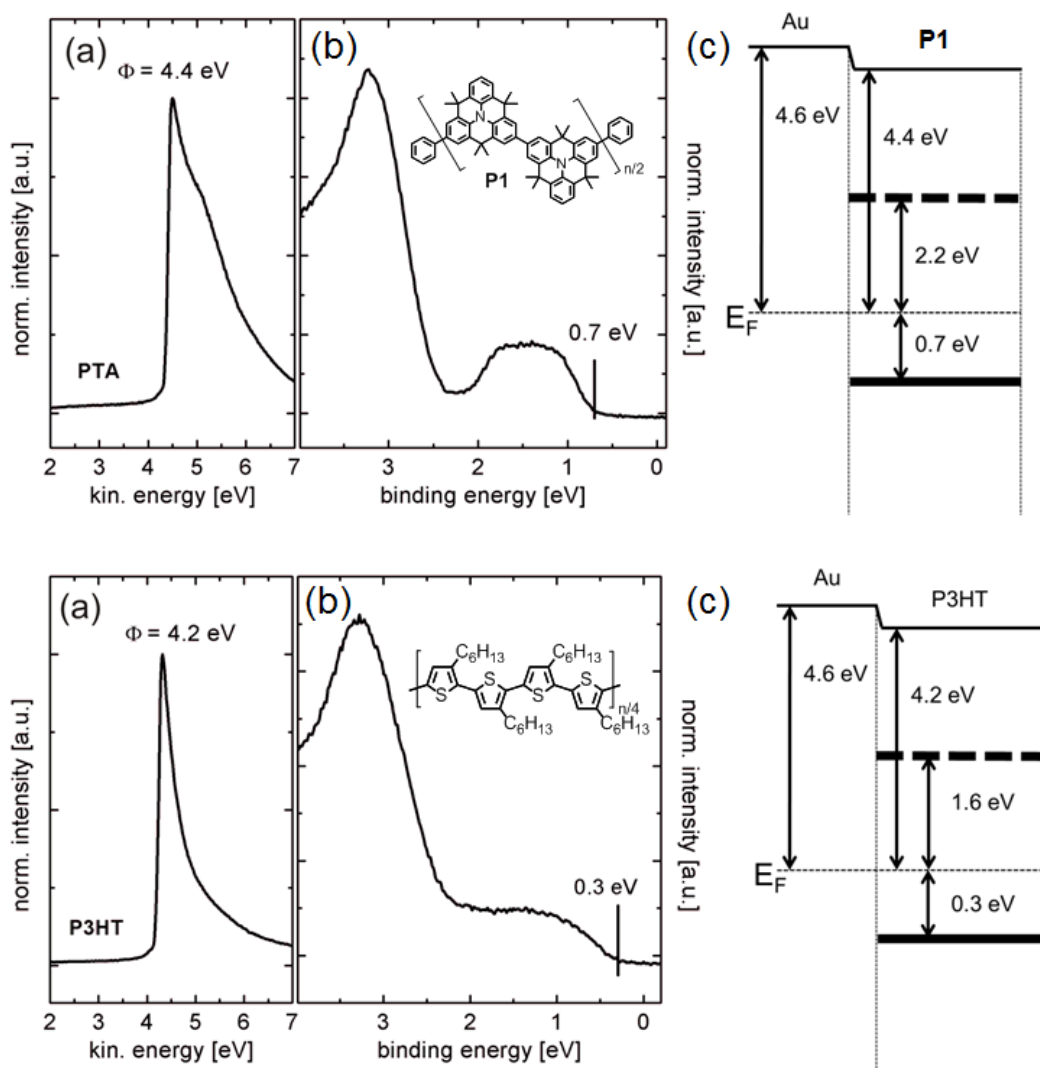
Figure 3-7. (a) Secondary electron cut-off and (b) valence region UPS of **P1** (top) and P3HT (bottom) on Au/SiO$_2$ substrates. (c) Schematic energy levels of **P1** (top) and P3HT (bottom) with respect to Au.

for OFETs in order to correlate the charge injection properties with the electrical characteristics. For this purpose the work function of gold was determined. This resulted in a rather low value of 4.6 eV, which might be explained by contaminations of hydrocarbons due to handling in air and exposure to chemicals used in the lift-off process, reducing the surface dipole ($\Delta\Phi$) and thereby the work function.[55] Hence, the hole injection barrier between gold and **P1** was calculated to be 0.7 eV with a $\Delta\Phi = -0.2$ eV (Figure 3-7).

3.1.4 OFET Performance

3.1.4.1 *Optimization of the Device Parameters*

The semiconductive properties of *N*-heterotriangulene polymer **P1** in organic field-effect transistors (OFETs) were tested in collaboration with ▮▮▮▮▮▮▮▮▮▮▮▮ in the group of ▮▮▮▮▮▮▮▮▮▮ at the NanoTecCenter Weiz, Austria.
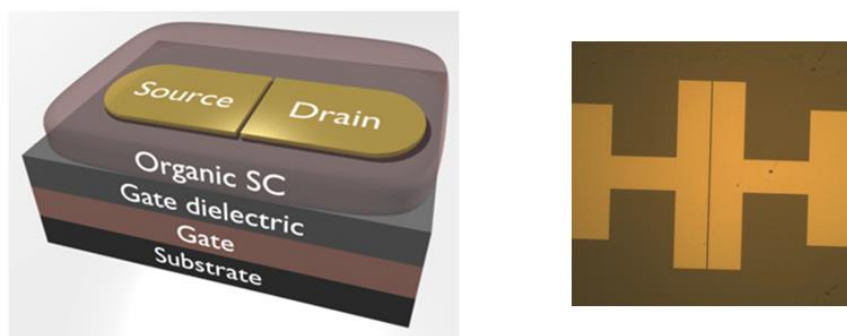
Figure 3-8. Left: OFET geometry: bottom-gate/bottom-contact. Source and drain electrodes both from metallic gold. Dielectric from SiO_2. Gate electrode: heavily doped silicon wafer.[56] Right: Top view of a BG/BC OFET fabricated from **P1** as the active layer.

Besides the organic semiconductor, the device performance strongly depends on additional factors, *e.g.*, transistor design, the electrode material, the presence of oxygen, the processing, the substrate and its modifications.[16] In this study, the impact of all these factors could hardly be investigated and it has been therefore focused on the organic semiconductor as active material and the respective optimization parameters.

Investigations were carried out in a bottom-gate/bottom-contact (BG/BC) configuration using heavily doped silicon wafers as gate electrode, thermally grown SiO_2 as gate dielectric and gold as source/drain electrodes and run under argon atmosphere (Figure 3-8). Prior to the processing of **P1** from toluene by spin-coating, the gold source/drain (S/D) electrodes were structured using a conventional lift-off process. Gold electrodes were used since the gold Fermi level matches the HOMO energy of **P1**, thus holding promise for hole injection and low contact resistance.[57]

Table 3-2. Device parameters of BG/BC OFETs based on **P1** with different surface treatments.

Surface modification	HMDS treatment[a]	Mobility μ_{sat}[b] $(cm^2\ V^{-1}\ s^{-1})$	I (on/off)[c]	V_{so} (V)	S (V/dec)
O_2 plasma	-	1.8×10^{-4}	8.8×10^1	>10	15.7
UV/ozone	-	1.5×10^{-4}	2.3×10^3	−3	5.5
bare SiO_2	-	4.1×10^{-4}	4.4×10^3	−5	5.9
O_2 plasma	HMDS 15min	4.9×10^{-4}	8.3×10^2	7	8.3
UV/ozone	HMDS 5s	2.1×10^{-3}	2.8×10^4	−6	5.3
bare SiO_2	HMDS 15 min	4.2×10^{-3}	1.0×10^5	−3	4.3

[a] Different exposure times had to be used due to wetting problems. [b] μ_{sat} was calculated according to the gradual channel approximation.[58] [c] On-current extracted at $V_{GS} = -50$ V, $V_{DS} = -50$ V and off-current at $V_{GS} = 0$ V, $V_{DS} = -50$ V.
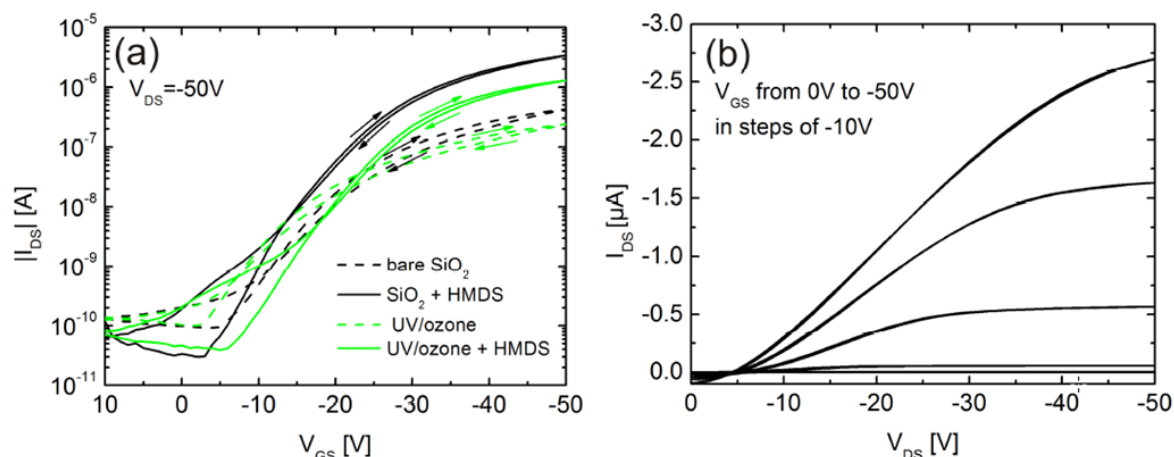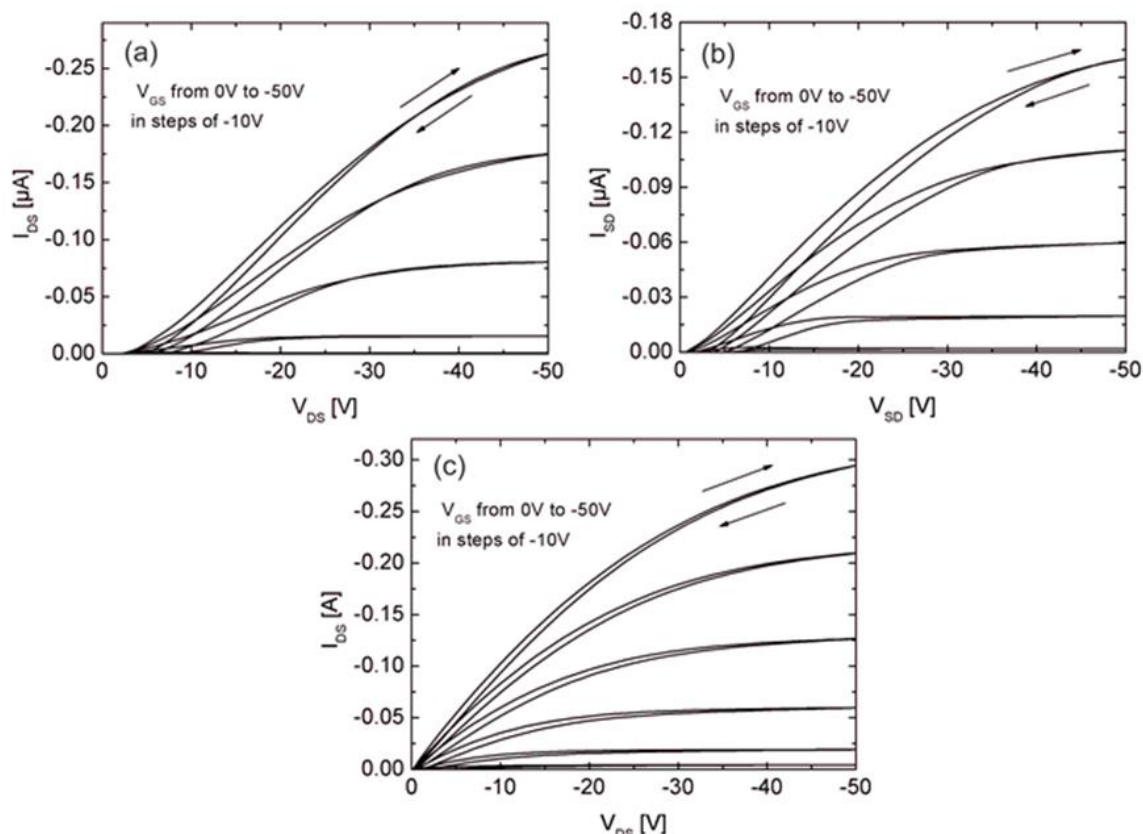
Figure 3-9. (a) Transfer characteristics of **P1** OFETs with different surface treatments: bare SiO$_2$ (dashed black line), 15 min HMDS treatment (solid black line), UV/ozone treatment with (dashed green line) and without (solid green line) HMDS. (b) Output characteristics of a typical **P1** OFET with HMDS treatment.

BG/BC OFETs based on **P1** revealed a clear p-type transport with a strong influence of the applied surface treatments (Figure 3-9 a and Table 3-2). As it has been shown for related fully amorphous semiconductors such as poly(triarylamine)s, the charge carrier mobility μ_{sat} and the on/off current ratio can be significantly influenced by hexamethyldisilazane (HMDS), octadecyltrichlorosilane (OTS) or other silane treatments.[26, 59] The reactive silane groups have been used to provide hydrophobic self-assembled monolayers (SAMs) with a well- defined, ordered surface.[26] For this purpose the surface of the dielectric (SiO$_2$) was modified by using HMDS to avoid interface trapping by silanol groups.[60] This results in the highest saturation mobility of 4.2×10^{-3} cm^2 V^{-1} s^{-1} with an on/off current ratio of ~10^5 for HMDS treated OFETs. These values are slightly higher than the charge carrier mobility obtained for a related poly(triarylamine) ($\mu_{sat} = 4.0 \times 10^{-3}$ cm^2 V^{-1} s^{-1}; $M_w = 96\ 400$ g/mol) reported by *McCulloch* and coworkers.[27] This might be explained by an increase of polymer backbone planarity, caused by an improvement in the *intra*molecular π-orbital overlap together with an enhancement of the structural organization when replacing the twisted triphenylamine by *N*-heterotriangulene.

The output characteristics of a typical device revealed a negligible hysteresis and are shown in Figure 3-9 b. A significant contact resistance was observed by the absence of a clear linear characteristic at low drain voltages, due to a too high hole injection barrier explained by the energy mismatch of the HOMO level of **P1** and the low gold work function due to storage in the presence of air. This confirmed the significant impact of the fabrication process on the properties of devices, *e.g.*, *via* changes in energy barriers at metal-organic interfaces exposed to air.[61, 62] As reported by *Rentenberger* and coworkers,

Figure 3-10. Output characteristics of **P1** OFETs with different interface treatments: (a) bare SiO$_2$; (b) UV/ozone and (c) O$_2$ plasma treatment, (L = 25 μm, W = 2.85 mm, without HMDS exposure).

the injection of charge carriers can be improved by treating the gold electrodes with UV/ozone and O$_2$ plasma inducing a thin AuO$_x$ layer which helps to increase the work function of the gold electrodes.[63, 64] By carefully screening this methods (Figure 3-10), the charge carrier mobility could be increased again (~2.1 × 10^{-3} cm^2 V^{-1} s^{-1}, Figure 3-9 a) while decreasing the polar component on the dielectric with the help of deactivating the OH-groups through UV/ozone treatment.[65, 66] This behavior of the studied OFETs clearly revealed changes of the hole injection barrier, the surface polarity and, thus, an increased/decreased charge carrier trap density, rather than morphological changes of **P1**.[26]

As studied previously, protonation of **P1** led to significant differences in the electronic properties (see above). In order to investigate the influence of this doping effect on the electrical characteristics of **P1** OFETs, toluene was replaced by chloroform as the spin-coating solvent. For this purpose BG/BC OFETs were fabricated using chloroform solutions of **P1** exposed to UV-light (~10 s, wavelengths of 254 nm and 366 nm) prior to spin-coating. They were compared with reference OFETs, spin-coated from chloroform solutions not exposed to the UV-light. The output characteristics of both devices are shown
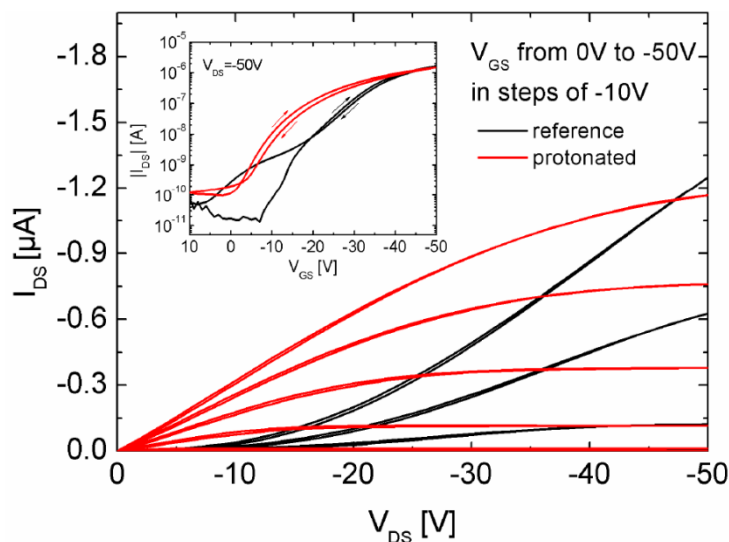
Figure 3-11. Output and transfer (inset) characteristics of **P1** OFETs with (red lines) and without (black lines) UV-light exposure of the CHCl$_3$ solution prior to spin-coating in argon atmosphere.

in Figure 3-11. As expected, the reference device (Figure 3-11, black line) showed a significant contact resistance similar to the devices fabricated from toluene solutions (Figure 3-9). In contrast to that, the transfer curve of the device prepared from a chloroform solution exposed to UV-light (Figure 3-11, red line) showed a higher off-current and a shift of V_{so} to more positive values. Both aspects can be attributed to (contact-)doping of the *N*-heterotriangulene polymer **P1**. However, further investigations are necessary in order to understand the exact underlying chemical mechanisms, which might enable the application of **P1** as the active material in pH-sensor elements.

3.1.4.2   *Stability Tests*

With respect to roll-to-roll large-area production of OFETs, ambient processing and stability are required, which enables low-cost fabrication. Organic semiconductors often degrade over time due to oxidation processes in the presence of oxygen and humidity. The ambient stability of *N*-heterotriangulene polymer **P1** was tested and benchmarked against the commonly used P3HT. Both OFET devices were fabricated in a BG/BC configuration from toluene solutions in ambient atmosphere. They were stored at identical conditions for three months, while recording their output characteristics (Figure 3-12). The output characteristics of **P1** (Figure 3-12 a) and P3HT (Figure 3-12 b) showed significant differences directly after fabrication. The source-drain channel currents (I_{DS}) are similar for both polymers, however, the values are lower compared to the **P1** devices fabricated under an inert atmosphere (see Figure 3-9). The contact resistance of the OFET based on P3HT is
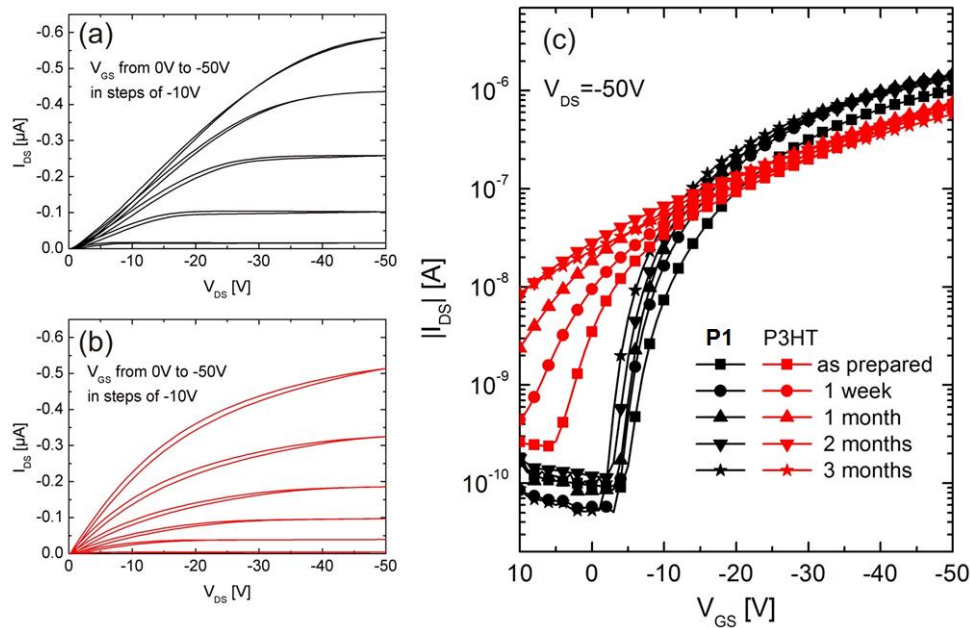
Figure 3-12. Output characteristics of **P1** (a) and P3HT (b) FETs after fabrication at ambient conditions and in the presence of light. (c) Semilogarithmic transfer characteristics of **P1** (black) and P3HT (red) as a function of time measured at ambient conditions and in the presence of light. (23-26 °C, humidity: 45-60%).

Table 3-3. Device parameters of BG/BC OFETs based on **P1** in comparison with P3HT after storage in air.

Sample	time	Mobility μ_{sat}[a] $(cm^2\ V^{-1}\ s^{-1})$	I (on/off)[b]	V_{so} (V)
P1	as prepared	6.6×10^{-4}	1.1×10^{4}	−4
	1 week	8.3×10^{-4}	2.5×10^{4}	−3
	1 month	7.6×10^{-4}	1.8×10^{4}	−3
	2 months	6.3×10^{-4}	1.1×10^{4}	−2
	3 months	6.3×10^{-4}	2.6×10^{4}	−1
P3HT	as prepared	2.5×10^{-4}	2.6×10^{3}	6
	1 week	2.7×10^{-4}	1.6×10^{3}	>10
	1 month	2.6×10^{-4}	3.2×10^{2}	>10
	2 months	2.1×10^{-4}	8.0×10^{1}	>10
	3 months	1.9×10^{-4}	6.6×10^{1}	>10

[a] μ_{sat} was calculated according to the gradual channel approximation.[58] [c] on-current I_{on} was taken at $V_{GS} = -50V$, $V_{DS} = -50V$ and off-current I_{off} at $V_{GS} = 0V$, and $V_{GS} = -10V$ (for P3HT OFETs, being fully depleted for as prepared devices), $V_{DS} = -50V$.

lower compared with the **P1**, attributed to a lower hole injection barrier of P3HT (0.3 eV, see Figure 3-7). The transfer characteristics as a function of storage time are shown in Figure 3-12 c and the extracted device parameters are listed Table 3-3. By comparing the on/off current ratios of the as-prepared samples, ~10^4 for **P1** and ~10^2 for P3HT at $V_{GS} = 0$ V were observed. However, even after 3 months of storing at ambient conditions **P1** OFETs revealed no significant changes of the charge carrier mobility (μ_{sat}) and the on/off

current ratio. Slight variations in the charge carrier mobilities and on/off ratios can be explained by varying levels of moisture and temperature during the storage of the devices. The P3HT OFETs showed, in contrast to that, a significant loss of the on/off current ratio by a factor of 40. The outstanding stability of **P1** can be attributed to the deep lying HOMO level (E_{HOMO} = 5.0 eV) and its wide band gap (E_g = 2.9 eV). As a consequence of **P1** amorphous structure, grain boundaries, acting as migration spots for water molecules which increase the density of traps, were significantly reduced.[56] The pronounced long-term stability of **P1** avoids furthermore HMDS treatment of the dielectric surface, which is usually necessary for enhancing the stability of the OFET devices.

3.2   Hyperbranched *N*-Heterotriangulene Polymer

3.2.1   Introduction

The bottom-up synthesis of two- (2D) and three-dimensional (3D) polymers is usually achieved by the condensation of monomers with two or more functionalities (average functionality >2, denoted as *AB₂*, *AB₃*, *A₂ + B₃*, etc.).[67, 68] This creates (hyper)branched structures resulting in a remarkable growth of both molecular weight and end groups.[68] In contrast to their linear analogues, π-conjugated hyperbranched polymers usually exhibit structural rigidity and extraordinary thermal stability.[69] The large number of end groups enables further modifications through various chemical reactions of the peripheral groups.[70-72] Exploring the potential of these materials is often hampered by their imperfect solution-based synthesis as a result of the available degrees of freedom of the molecules. By the addition of templates, such as single layer graphene sheets to the reaction mixture, the formation of ordered structures has been enhanced.[73-77] Moreover, on-surface reactions of confined molecular precursors were shown to be beneficial for the preparation of defect free 2D structures.[78-83] Considering confined molecules as conformationally restricted, certain degrees of freedom are impeded which reduces the possible relative orientations of molecules approaching each other. By utilizing this approach, *Müllen* and *Fasel* synthesized recently molecular thin 2D covalently linked polymers on metal surfaces based on *N*-heterotriangulenes (Figure 3-13).[84] Following the network formation with scanning tunneling microscopy (STM), excellent periodicity of the 2D polymer was revealed. The interesting properties of this network were disclosed by subsequent computational studies including a ferromagnetic half-metal character.[85] From the viewpoint of potential applications, however, the challenge of transferring the fabricated
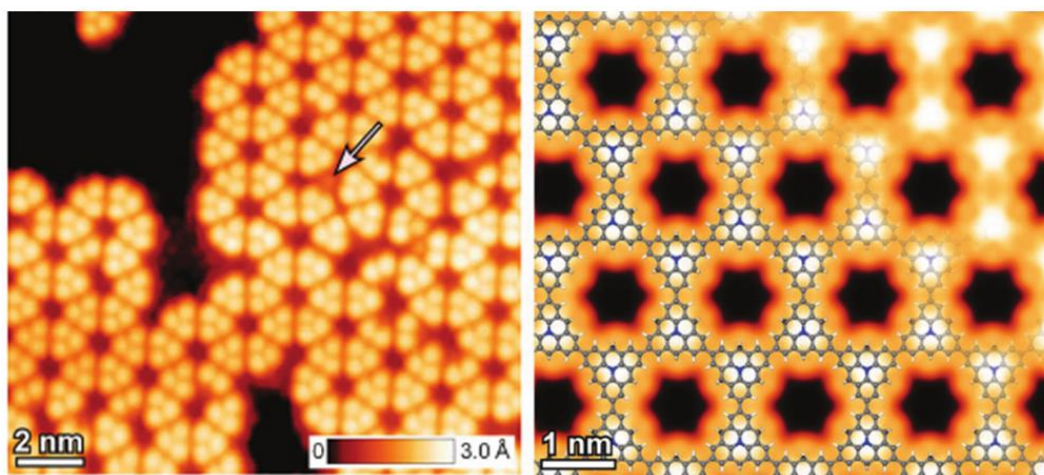
Figure 3-13. *N*-heterotriangulene covalent polymers on Ag(111). Left: STM topography of a covalent polymer formed at 300 °C. Right: Computational model of the obtained polymer network (methyl groups are replaced by hydrogen).[84]

structures from the metal surface to some technologically relevant substrates still needs to be solved. In order to generate macroscopic quantities of such hyperbranched *N*-heterotriangulene polymers which can be characterized in optoelectronic devices, *e.g.*, OFETs, a solution-based synthetic strategy was aimed. Comparison of its charge transport characteristics with those of the linear polymer **P1** might help to understand which arrangement of the *N*-heterotriangulene units is favorable for an effective charge carrier transport.

3.2.2 Synthesis and Characterization

For a bottom-up approach toward hyperbranched polymers the condensation of monomers with different functionalities is necessary. As a consequence of the *Carothers'* law, high molecular weights are only achieved at high conversions and strictly maintained stoichiometries (see above).[38] In order to avoid stoichiometric imbalances when using two or three monomers, an *A₂B* monomer was targeted bearing both functions inside one molecule. During the polymerization, the different functionalities react with each other leading to the formation of larger oligomers. The progressive expansion of these units with new monomers results commonly in precipitation after having obtained a certain molecular weight. Nevertheless, it is believed that bond formation still continues after having formed a heterogeneous reaction mixture as a result of the high local concentration of the reaction partners. This could be proven by a low content of non-reacted functional groups.[47]

Due to its broad scope and usually high conversion rates, the *Suzuki-Miyaura* cross-coupling reaction was chosen as polymerization procedure. Further advantages are the easy accessibility of the respective boronic acids and esters as well as a large variety of reported
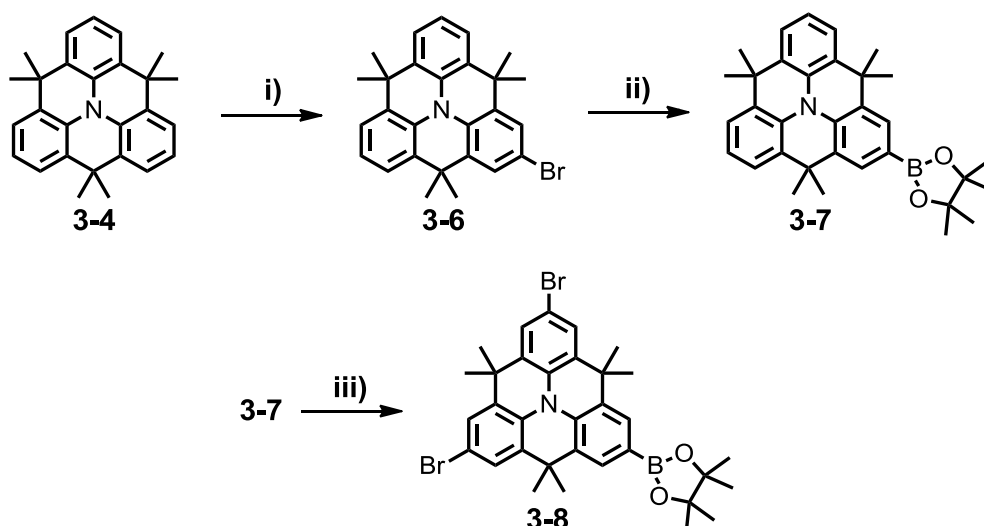
Scheme 3-4. Synthetic route toward A_2B-type monomer **3-8**. Conditions: i) 1 equiv. NBS, CHCl$_3$, 0 °C to RT, 2h, 90%; ii) Pd(dppf)Cl$_2$, KOAc, bis(pinacolato)diboron, DMF, 85 °C, 12h, 86%; iii) 2 equiv. NBS, CHCl$_3$, 0 °C to RT, 18h, 73%.

synthetic protocols.[86-90] The synthetic route toward A_2B monomer **3-8**, is shown in Scheme 3-4. While taking advantage of the *para*-directing effect of the central nitrogen, **3-4** was monobrominated by using stoichiometric amounts of NBS. Multiple bromination was reduced by performing the reaction at low temperatures and slow addition of NBS. Monobromo *N*-heterotriangulene **3-6** was subsequently used for the Pd-catalyzed *Miyaura* borylation toward **3-7**. This procedure enables the introduction of boronates under cross-coupling conditions using bis(pinacolato)diboron in combination with a weak base, such as potassium acetate which suppresses the competing *Suzuki-Miyaura* coupling.[91] Moreover, it has the advantages of introducing a boronic ester in one step in combination with the ease of purification compared with the boronic acids due to a reduced polarity, thus affording **3-7** in 86% yield. Due to the tendency of boronates to undergo protodeboronation or *ipso*-substitution, optimization of the subsequent bromination of **3-7** was required.[92] While the standard bromination procedure used for the preparation of **3-4** led mainly to *ipso*-substitution of the boronic ester, the absence of light and careful control of the NBS stoichiometry were necessary for the isolation of monomer **3-8** in a reasonable yield. In line with the *Carothers'* law, high purity of the used monomers is required to achieve high conversion rates during polymerizations.[38] For this purpose, **3-8** was two times recrystallized and carefully dried.

The A_2B-type self-polycondensation of monomer **3-8** was carried out by applying standard *Suzuki-Miyaura* conditions (Scheme 3-5).[93, 94]
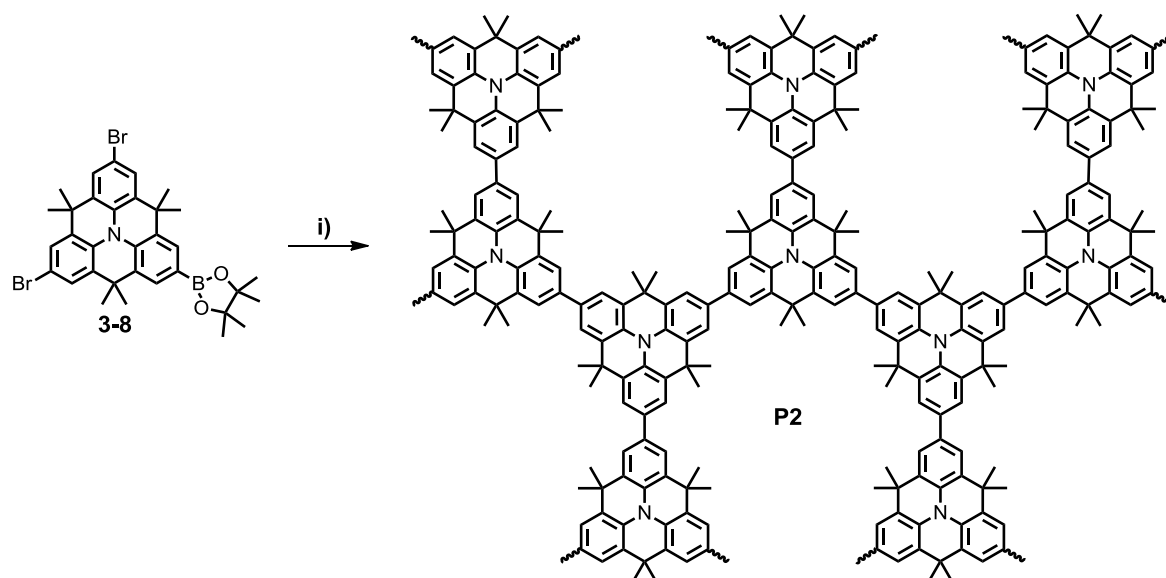
Scheme 3-5. Synthesis of the hyperbranched *N*-heterotriangulene polymer **P2**. i) Pd(PPh₃)₄, 2 M aq. Na₂CO₃, toluene, *Aliquat 336*, 90 °C, 6 days, endcapping with bromobenzene and phenylboronic acid, 70%.

The concentration of monomers during polymerization toward hyperbranched polymers plays a crucial role with respect to structural perfection of the resulting hyperbranched polymers. On the one hand, high concentrations are favorable for the formation of high molecular weights due to an enhanced probability of *inter*molecular coupling events. On the other hand, however, a substantial dilution is necessary to favor the formation of honeycomb pores, *i.e.* macrocyclic subunits. This is achieved by *intra*molecular aryl-aryl couplings of the oligomeric or polymeric species. By decreasing the concentration of the coupling partners the probability of *intra*molecular couplings is increased and the entropic handicap upon chain-end connection is lowered. As a consequence of these considerations, the Pd⁰-catalyzed *Suzuki-Miyaura* polymerization of **3-8** was performed in toluene (1×10^{-2} M) with aqueous sodium carbonate solution (2 M) as base and *Aliquat 336* as phase transfer agent. In order to avoid deactivation of the catalyst, oxygen was removed by carefully degassing the biphasic mixture with argon. Subsequently, tetrakis(triphenylphosphine)palladium(0) was added to the mixture followed by degassing again with argon. After an optimized reaction time of six days at elevated temperatures, the reactive end groups were endcapped with bromobenzene and phenylboronic acid. By dropping the reaction mixture into dilute methanolic hydrochloric acid, a pale yellow precipitate was formed which was subsequently collected by filtration. MALDI-TOF MS of the polymer revealed peaks, which are separated by a mass difference corresponding to the calculated *N*- heterotriangulene repeating units ($\Delta M = 362$ g/mol) thus proving the successful polymerization (Figure 3-14, right).
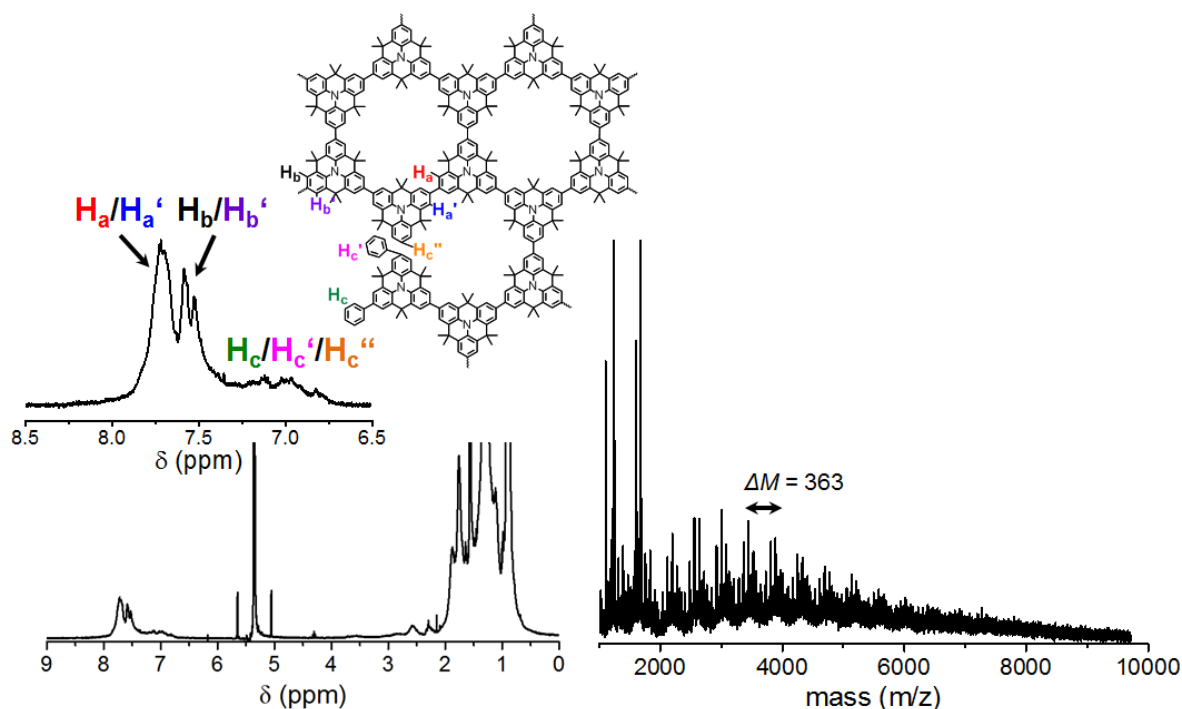
Figure 3-14. Left: ^{1}H NMR spectrum of **P2** in CD$_2$Cl$_2$ at 25 °C. Inset: Zoom into the aromatic region with proton assignment. Right: MALDI-TOF MS of **P2** (linear mode, matrix: DCTB).

Analysis of the molecular weight of **P2** by SEC in THF using a poly(styrene) standard gave a M_w of 22 400 g/mol (PDI = 2.3). This corresponds to a molecular structure of approximately 61 *N*-heterotriangulene units. Due to the different constitution and hydrodynamic radii of **P1** (DP = 49) and **P2** (DP = 61), however, a quantitative comparison between the molecular weights of both polymers was hampered.[93] The hyperbranched architecture is thereby expected to increase the hydrodynamic volume of **P2** thus leading to an overestimation of its molecular weight by SEC. The total number of repeating units of both polymers is therefore expected to be in a similar range. In order to elucidate the constitution of **P2**, NMR analysis was conducted (Figure 3-14, left). As a result of the hyperbranched nature, **P2** showed a decreased solubility in common organic solvents compared with its linear analogue **P1**, impeding ^{13}C NMR measurements. The ^{1}H NMR spectrum of **P2** showed broadened aromatic and aliphatic signals, indicating the polymeric nature. The protons of the *N*-heterotriangulene subunits located next to a branching point (H$_a$, H$_a$' and H$_b$, H$_b$', Figure 3-14, left) were detected between 7.4 and 7.9 ppm with correct signal intensities (H$_a$, H$_a$'/ H$_b$, H$_b$' ≈ 2/1). Besides that, a less distinct signal between 7.3 and 6.7 ppm was detected corresponding to the end groups of **P2**. Two different types of end groups were anticipated to induce an end group signal: (i) Due to the endcapping with an excess of bromobenzene and phenylboronic acid, a certain amount of
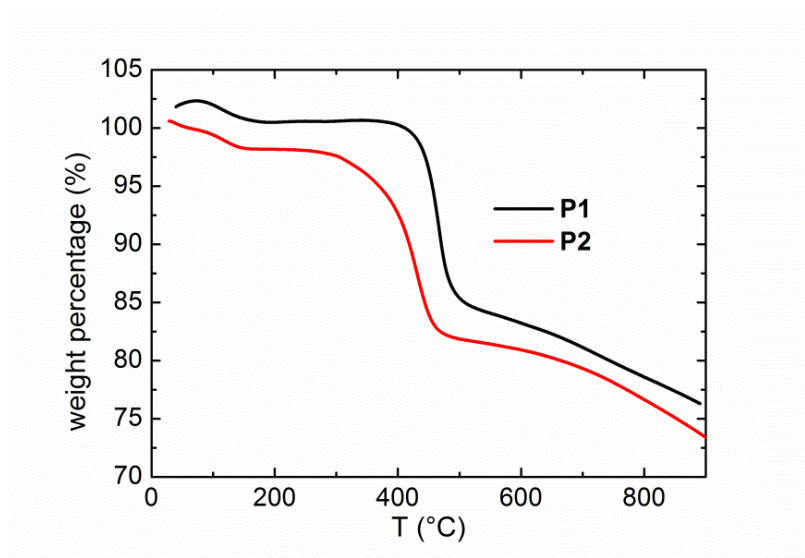
Figure 3-15. Thermogravimetric analysis of linear polymer **P1** and hyperbranched polymer **P2**.

end groups consist of benzenes (five protons per end group). (ii) During the *Suzuki-Miyaura* reaction protodehalogenation occurs as a side reaction, which led to proton endcapping (one proton per end group). The presence of residual functional groups, however, cannot be excluded despite the applied endcapping procedure (zero protons per end group). By considering (i) and (ii) as equally probable processes (average number of protons per end groups = 3), hyperbranched polymer **P2** consists of approximately 13% of end groups.

The thermal stability of **P2** was investigated by TGA and compared with the linear polymer **P1** (Figure 3-15). **P2** showed a good thermal stability up to 350 °C (decomposition temperature at 5% weight loss is 396 °C), which is slightly lower than for the linear analogue **P1**. After two degradation steps affecting 20 wt% of both polymers, further decomposition proceeds slowly. Even at temperatures of 900 °C, **P1** and **P2** still retain 70% of their initial mass, revealing the robust performance of **P1** and **P2** at ambient conditions.

3.2.3   Optoelectronic Properties

3.2.3.1   Solution Studies

The optoelectronic properties of hyperbranched polymer **P2** were investigated by UV-vis absorption and emission spectroscopy in solution and are shown in Figure 3-16 and Table 3-4. Due to the decreased solubility of **P2** in organic solvents, electrochemical measurements could not be conducted.
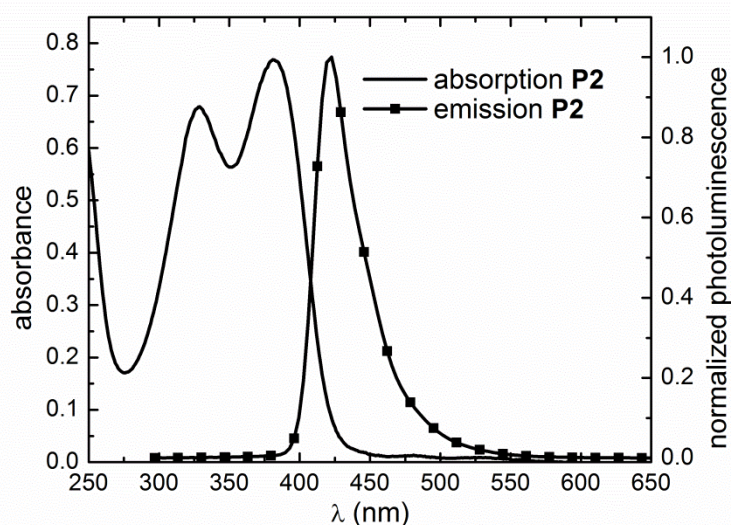
Figure 3-16. UV-vis absorption (solid line) and photoluminescence emission (symbol line) spectra of **P2** (10^{-6} M in CH_2Cl_2).

Table 3-4. Selected photophysical properties of linear polymer **P1** and hyperbranched polymer **P2**.

| Compound	$\lambda_{abs,max}$[a] (nm)	$\lambda_{PL,max}$[a] (nm)	Stokes Shift (cm^{-1})	E_g^{opt}[b] (eV)
P1	329, 391	430	2 320	2.9
P2	329, 381	423	2 610	2.9

[a] For all spectra: 10^{-6} M in CH_2Cl_2. [b] $E_g^{opt} = h \cdot c / \lambda_{0.1max}$.

The absorption spectrum of **P2** showed two characteristic absorption at 381 and 329 nm in a dichloromethane solution, corresponding to the π-π* transition of the entire π-conjugated system and the transition of the *N*-heterotriangulene subunits. In order to ensure comparability, the photophysical properties of linear polymer **P1** were measured in dichloromethane at similar concentrations as for **P2** (Table 3-4). By comparing **P2** ($\lambda_{abs,max}$ = 381 nm) with the linear polymer **P1** ($\lambda_{abs,max}$ = 391 nm), a hypsochromic shift of the longest wavelength absorption of about 10 nm is observed. The same behavior is simultaneously revealed by the emission of **P2** ($\lambda_{PL,max}$ = 423 nm) showing a hypsochromic shift of 7 nm in comparison with the linear analogue **P1** ($\lambda_{PL,max}$ = 430 nm).

To gain further insights into the electronic and conformational details of the hyperbranched polymer **P2**, the X-ray crystallographic structure of a representative section obtained by ▇▇▇▇▇▇▇▇▇▇▇▇▇ was analyzed (Figure 3-17).[35] From the bending of the *N*-heterotriangulene units of the model compound a 3D structure of **P2** is revealed. As a result of the consequently reduced interactions between the hyperbranched chains, the
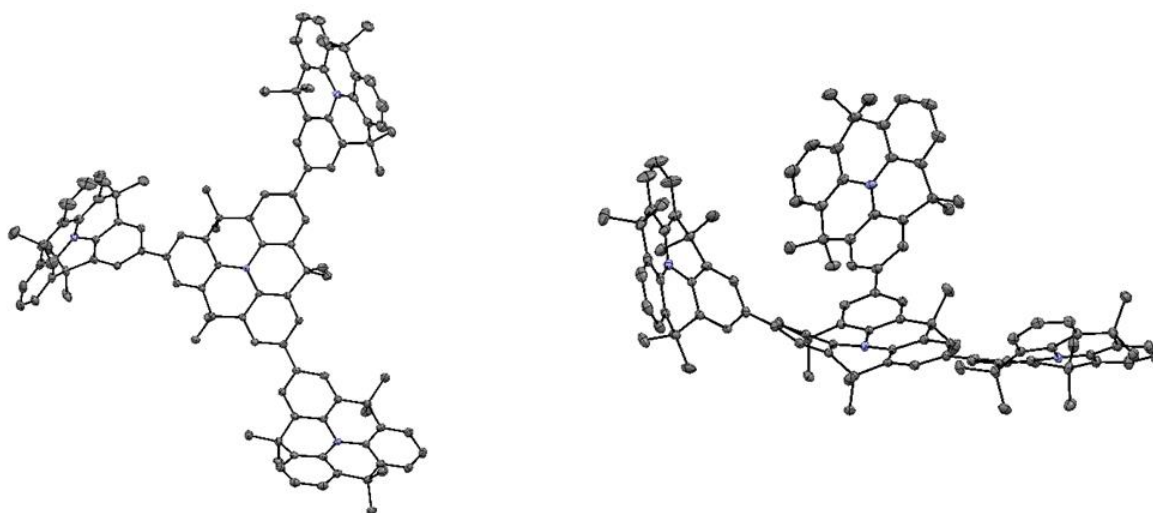
Figure 3-17. X-ray crystallographic structure of a model segment from hyperbranched polymer **P2** showing two different views (hydrogens are omitted for clarity).[35]

observed hypsochromic shift of the longest wavelength transition of **P2** compared with its linear counterpart **P1** can be explained. The large Stokes shift of **P2** (2 610 cm^{-1}) revealed furthermore a geometrical rearrangement of the π-conjugated system and thus a planarization of the hyperbranched backbone in the excited state (2 320 cm^{-1} for **P1**).

3.2.4 OFET Performance

The semiconductor properties of the hyperbranched *N*-heterotriangulene polymer **P2** in OFETs were again tested in collaboration with ▇▇▇▇▇▇▇▇▇▇▇▇▇▇ in the group of ▇▇▇▇▇▇▇▇▇▇ at the NanoTecCenter Weiz, Austria.

Investigations were carried out in a BG/BC configuration using heavily doped silicon wafers as gate electrode, thermally grown SiO$_2$ as gate dielectric and gold as S/D electrodes and run under argon atmosphere (Figure 3-8). To ensure comparability, the devices were fabricated in a similar method as reported for the linear polymer **P1**.
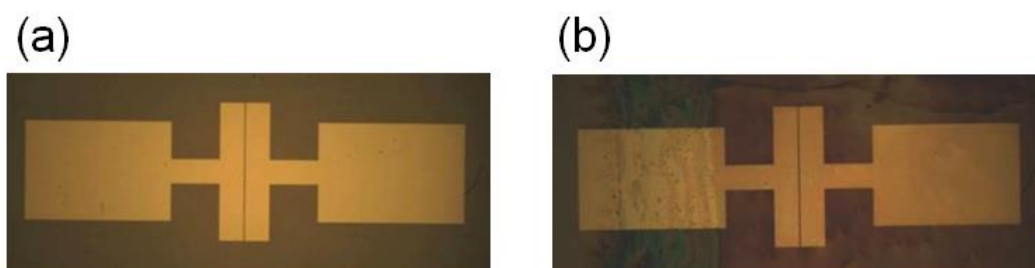

Figure 3-18. Top view of a BG/BC OFET fabricated from **P2** as the active layer by (a) spin-coating and (b) drop-casting from a toluene solution (3 g/L).

A toluene solution of **P2** (3 g/L) was spin-coated on top of a cleaned SiO$_2$ dielectric bearing structured S/D electrodes at 1000 rpm/s for 40 seconds under argon. The deposited

film of **P2** was subsequently dried for one hour at 60 °C in high vacuum (4×10^{-5} mbar) resulting in an inhomogenous layer (Figure 3-18 a).

The transistor characteristics are depicted in Figure 3-19. BG/BC OFETs revealed a p-type transport of hyperbranched polymer **P2** resulting in a low mobility of 5×10^{-5} cm^2 V^{-1} s^{-1} in the saturated regime. In addition a low on-current ($I_{on} \approx -25$ nA) is observed which is in the range of the leakage current (Figure 3-19 a, red line). Furthermore a high negative switch-on voltage ($V_{so} \approx -20$ V) is revealed. The output curve of a typical device (Figure 3-19 b) showed significant hysteresis. This together with the absence of a clear linear characteristic at low V_D can be ascribed to a high hole injection barrier as a result of the energy mismatch of the HOMO of **P2** with the gold work function. Moreover, the poor morphology of the thin films contributed to the rather weak performance. However, altering the preparation technique by fabricating the OFETs by drop-casting **P2** from a toluene solution improved neither the film formation (Figure 3-18 b) nor the respective OFET performance.
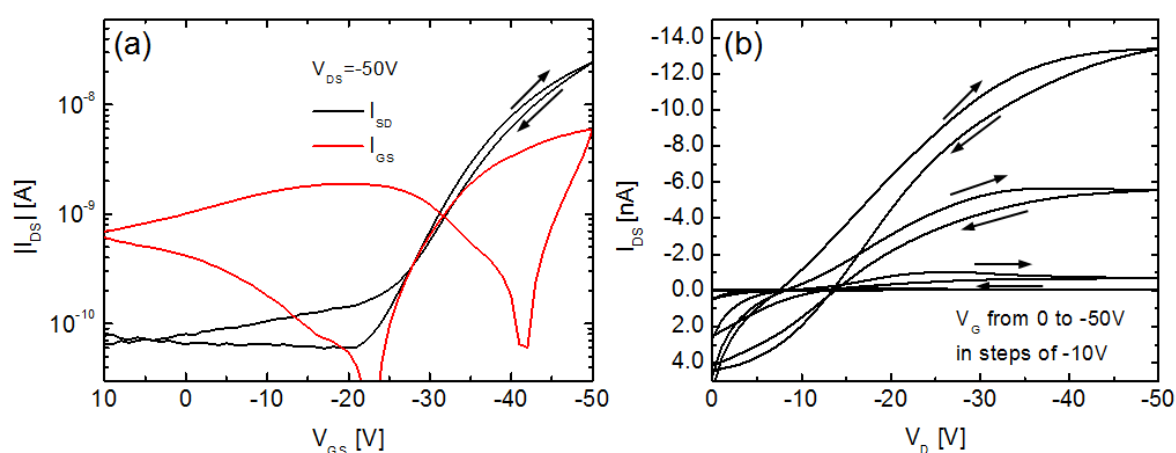
Figure 3-19. Field-effect transistor characteristics with the hyperbranched polymer **P2** as the active layer. (a) Transfer curve (black line) with leakage current at $V_{DS} = -50$ V (red line) and (b) output curve (L = 25 μm, W = 2.85 mm, without HMDS exposure).

The observed charge carrier mobility of **P2** is two orders of magnitude lower than for the linear analogue **P1** ($\mu_{sat} = 4.2 \times 10^{-3}$ cm^2 V^{-1} s^{-1}; see above). This behavior can be mainly ascribed to two crucial aspects: (1) The exceptional solubility of **P1** in organic solvents resulted in a very smooth film formation and thus allowed a reasonable hole transport. Whereas the poorer solubility of **P2** led to a significant phase separation, which can trap charges and hamper the hole transport through the film. (2) **P2** does not allow a significant π-π interaction of the polymeric species as a result of the three-dimensional nature of the hyperbranched structure. The linear configuration of **P1** ensures closer contacts between

the polymer chains than in **P2**, which facilitates the *inter*molecular charge carrier transport.[22]

Taking these aspects into account, the thin film morphology of **P2** might be improved by replacing the bridging dimethylmethylene groups in the *N*-heterotriangulene monomer by longer alkyl chains to enhance the solubility and film formation tendency of the hyperbranched polymer. The long-range order, however, can be furthermore pronounced by introducing heteroatoms at the bridge positions of the *N*-heterotriangulene, *e.g.*, sulfur or nitrogen, which should lead to a reduction of the π-π distances.

3.3   Summary

It was shown that *N*-heterotriangulene building block **3-4** can readily be functionalized in straightforward synthetic protocols. The twofold bromination of **3-4** led to an *AA*-monomer **3-5** which was successfully polymerized by a *Yamamoto* polycondensation. This resulted in a linear polymer **P1** with a reasonable molecular weight ($M_w = 20\,000$ g/mol, PDI = 1.7), which was thoroughly characterized in solution and in the solid state. A significant sensitivity of **P1** to acidic conditions, in particular to hydrochloric acid evolving from the light-induced dissociation of chloroform, was observed. Due to the protonation of the central nitrogen of the *N*-heterotriangulene units in **P1** an *intra*molecular charge-transfer between the protonated and neutral subunits is induced, which was followed by a significant color change and the appearance of an additional band in the emission spectrum. **P1** was furthermore investigated in BG/BC OFETs. By an optimization of the electrode- and dielectric-polymer interfaces with the help of HMDS and ozone treatment, a charge carrier mobility of 4.2×10^{-3} cm^2 V^{-1} s^{-1} and an on/off current ratio of ~10^5 was obtained. This revealed the potential of **P1** being a viable alternative for the best performing amorphous semiconducting polymers such as poly(triarylamine)s.[27] As a result of its deep lying HOMO level ($E_{HOMO} = 5.1$ eV) and wide band gap ($E_g = 2.9$ eV) BG/BC OFETs based on **P1** showed an excellent stability over months compared to commonly used P3HT.

In addition, the *N*-heterotriangulene unit was used for the synthesis of a hyperbranched polymer. A three-step synthesis, including a bromination and borylation sequence, led to an A_2B-type monomer **3-8**. The subsequent self-condensation of **3-8** following a *Suzuki-Miyaura* protocol resulted in hyperbranched polymer **P2** with a reasonable molecular weight ($M_w = 22\,300$ g/mol, PDI = 2.4). Investigation of the photophysical properties of **P2** in solution revealed a hypsochromic shift of the longest wavelength absorption band in

comparison with linear **P1**. This can be attributed to an increased distance between the polymers chains caused by the hyperbranched architectures. The relatively poor solubility of **P2** in organic solvents resulted in the formation of inhomogeneous films by spin-coating and drop-casting. This led to a significantly lower charge carrier mobility ($\mu_{sat} = 5 \times 10^{-5}$ cm^2 V^{-1} s^{-1}) in BG/BC OFETs for **P2** in comparison with its linear analogue **P1**. This can be further explained by closer contacts of the polymer chains in the linear configuration of **P1**. In other words the linear arrangement of **P1** is more favorable for an efficient charge transport among the polymer chains than the corresponding hyperbranched configuration in **P2**. The combination of the reasonable charge carrier mobility, the robust performance together with a good processability makes linear polymer **P1** a particularly appealing candidate for large-scale and low-cost fabrication of p-type transport layers in organic electronic devices. There is furthermore a considerable scope for the application of **P1** as an active material in pH-sensor devices.

The described polymerization procedures can potentially lead to the formation of hexameric *N*-heterotriangulene macrocycles, due to the ideal angles of 120° between the functionalities of monomers **3-5** and **3-8**. This special type of 2D architectures represents a bridge between the previously described linear (1D) and hyperbranched (3D) polymers. Its synthesis, characterization and subsequent expansion will be therefore the main objective in the following part.

3.4   References

[1]   A. J. Heeger, *Angew. Chem., Int. Ed.* **2001**, *40*, 2591-2611.

[2]   A. G. MacDiarmid, *Angew. Chem., Int. Ed.* **2001**, *40*, 2581-2590.

[3]   H. Shirakawa, *Angew. Chem., Int. Ed.* **2001**, *40*, 2575-2580.

[4]   M. D. Watson, A. Fechtenkötter, K. Müllen, *Chem. Rev.* **2001**, *101*, 1267-1300.

[5]   C. Li, M. Y. Liu, N. G. Pschirer, M. Baumgarten, K. Müllen, *Chem. Rev.* **2010**, *110*, 6817-6855.

[6]   C. L. Wang, H. L. Dong, W. P. Hu, Y. Q. Liu, D. B. Zhu, *Chem. Rev.* **2012**, *112*, 2208-2267.

[7]   T. M. Figueira-Duarte, P. G. Del Rosso, R. Trattnig, S. Sax, E. J. W. List, K. Müllen, *Adv. Mater.* **2010**, *22*, 990-993.

[8]   G. Gelinck, P. Heremans, K. Nomoto, T. D. Anthopoulos, *Adv. Mater.* **2010**, *22*, 3778-3798.

[9]   H. E. A. Huitema, G. H. Gelinck, J. B. P. H. van der Putten, K. E. Kuijk, K. M. Hart, E. Cantatore, D. M. de Leeuw, *Adv. Mater.* **2002**, *14*, 1201-1204.

[10]   A. Dodabalapur, Z. Bao, A. Makhija, J. G. Laquindanum, V. R. Raju, Y. Feng, H. E. Katz, J. Rogers, *Appl. Phys. Lett.* **1998**, *73*, 142-144.

[11]   R. Trattnig, T. M. Figueira-Duarte, D. Lorbach, W. Wiedemair, S. Sax, S. Winkler, A. Vollmer, N. Koch, M. Manca, M. A. Loi, M. Baumgarten, E. J. W. List, K. Müllen, *Opt. Express* **2011**, *19*, A1281-A1293.

[12]   H. Sirringhaus, N. Tessler, R. H. Friend, *Science* **1998**, *280*, 1741-1744.

[13]   G. Yu, J. Gao, J. C. Hummelen, F. Wudl, A. J. Heeger, *Science* **1995**, *270*, 1789-1791.

[14]   P. F. Baude, D. A. Ender, M. A. Haase, T. W. Kelley, D. V. Muyres, S. D. Theiss, *Appl. Phys. Lett.* **2003**, *82*, 3964-3966.

[15]   E. Cantatore, T. C. T. Geuns, G. H. Gelinck, E. van Veenendaal, A. F. A. Gruijthuijsen, L. Schrijnemakers, S. Drews, D. M. de Leeuw, *IEEE J. Solid-State Circuits* **2007**, *42*, 84-92.

[16]   M. Mas-Torrent, C. Rovira, *Chem. Rev.* **2011**, *111*, 4833-4856.

[17]   M. Berggren, A. Richter-Dahlfors, *Adv. Mater.* **2007**, *19*, 3201-3213.

[18]   J. T. Mabeck, G. G. Malliaras, *Anal. Bioanal. Chem.* **2006**, *384*, 343-353.

[19]   J. Isaksson, P. Kjall, D. Nilsson, N. D. Robinson, M. Berggren, A. Richter-Dahlfors, *Nat. Mater.* **2007**, *6*, 673-679.

[20]   H. R. Nie, G. N. Sun, M. Zhang, M. Baumgarten, K. Müllen, *J. Mater. Chem.* **2012**, *22*, 2129-2132.

[21]   H. Bronstein, Z. Y. Chen, R. S. Ashraf, W. M. Zhang, J. P. Du, J. R. Durrant, P. S. Tuladhar, K. Song, S. E. Watkins, Y. Geerts, M. M. Wienk, R. A. J. Janssen, T. Anthopoulos, H. Sirringhaus, M. Heeney, I. McCulloch, *J. Am. Chem. Soc.* **2011**, *133*, 3272-3275.

[22]   H. N. Tsao, D. M. Cho, I. Park, M. R. Hansen, A. Mavrinskiy, D. Y. Yoon, R. Graf, W. Pisula, H. W. Spiess, K. Müllen, *J. Am. Chem. Soc.* **2011**, *133*, 2605-2612.

[23]   Z. Y. Chen, M. J. Lee, R. S. Ashraf, Y. Gu, S. Albert-Seifried, M. M. Nielsen, B. Schroeder, T. D. Anthopoulos, M. Heeney, I. McCulloch, H. Sirringhaus, *Adv. Mater.* **2012**, *24*, 647-652.

[24]   S. H. Dong, H. T. Zhang, L. Yang, M. L. Bai, Y. Yao, H. L. Chen, L. Gan, T. Y. Yang, H. Jiang, S. M. Hou, L. J. Wan, X. F. Guo, *Adv. Mater.* **2012**, *24*, 5576-5580.

[25]   S. H. Wang, M. Kappl, I. Liebewirth, M. Müller, K. Kirchhoff, W. Pisula, K. Müllen, *Adv. Mater.* **2012**, *24*, 417-420.

[26]   J. Veres, S. D. Ogier, S. W. Leeming, D. C. Cupertino, S. M. Khaffaf, *Adv. Funct. Mater.* **2003**, *13*, 199-204.

[27]   W. M. Zhang, J. Smith, R. Hamilton, M. Heeney, J. Kirkpatrick, K. Song, S. E. Watkins, T. Anthopoulos, I. McCulloch, *J. Am. Chem. Soc.* **2009**, *131*, 10814-10815.

[28]   D. Hellwinkel, M. Melan, *Chem. Ber.* **1971**, *104*, 1001-1016.

[29]   D. Hellwinkel, M. Melan, *Chem. Ber.* **1974**, *107*, 616-626.

[30]   D. Hellwinkel, M. Melan, W. Egan, C. R. Degel, *Chem. Ber.* **1975**, *108*, 2219-2231.

[31]   D. Hellwinkel, G. Aulmich, M. Melan, *Chem. Ber.* **1980**, *113*, 358-384.

[32]   Z. Fang, T. L. Teo, L. P. Cai, Y. H. Lai, A. Samoc, M. Samoc, *Org. Lett.* **2009**, *11*, 1-4.

[33]   Z. Fang, X. H. Zhang, Y. H. Lai, B. Liu, *Chem. Commun.* **2009**, 920-922.

[34]   Z. Fang, V. Chellappan, R. D. Webster, L. Ke, T. F. Zhang, B. Liu, Y. H. Lai, *J. Mater. Chem.* **2012**, *22*, 15397-15404.

[35] M. Kivala, K. Müllen, *unpublished results*.

[36] Z. Q. Jiang, Y. H. Chen, C. L. Yang, Y. Cao, Y. T. Tao, J. G. Qin, D. G. Ma, *Org. Lett.* **2009**, *11*, 1503-1506.

[37] Z. Q. Jiang, T. L. Ye, C. L. Yang, D. Z. Yang, M. R. Zhu, C. Zhong, J. G. Qin, D. G. Ma, *Chem. Mater.* **2011**, *23*, 771-777.

[38] W. H. Carothers, *Trans. Faraday Soc.* **1936**, *32*, 39-53.

[39] T. Yamamoto, *Prog. Polym. Sci.* **1992**, *17*, 1153-1205.

[40] T. Yamamoto, *Bull. Chem. Soc. Jpn.* **1999**, *72*, 621-638.

[41] T. Kanbara, N. Saito, T. Yamamoto, K. Kubota, *Macromolecules* **1991**, *24*, 5883-5885.

[42] K. Chmil, U. Scherf, *Makromol. Chem., Rapid Commun.* **1993**, *14*, 217-222.

[43] A. C. Grimsdale, K. Müllen, *Adv. Polym. Sci.* **2006**, *199*, 1-82.

[44] C. Grave, A. D. Schlüter, *Eur. J. Org. Chem.* **2002**, 3075-3098.

[45] W. Zhang, J. S. Moore, *Angew. Chem., Int. Ed.* **2006**, *45*, 4416-4439.

[46] W. Pisula, M. Kastler, C. Yang, V. Enkelmann, K. Müllen, *Chem. Asian J.* **2007**, *2*, 51-56.

[47] M. G. Schwab, Ph.D. thesis, Johannes Gutenberg-University Mainz **2011**.

[48] B. Tieke, *Makromolekulare Chemie. Eine Einführung.*, Wiley-VCH Verlag GmbH & Co. KGaA, Weinheim, **2005**.

[49] J. F. Rusling, S. L. Suib, *Adv. Mater.* **1994**, *6*, 922-930.

[50] W. L. Wang, R. Helgeson, B. Ma, F. Wudl, *J. Org. Chem.* **2000**, *65*, 5862-5867.

[51] S. Hautecloque, *J. Photochem.* **1980**, *12*, 187-196.

[52] P. E. Hoggard, A. J. Bridgeman, H. Kunkely, A. Vogler, *Inorg. Chim. Acta* **2004**, *357*, 639-643.

[53] S. Kappaun, S. Horner, A. M. Kelterer, K. Waich, F. Grasse, M. Graf, L. Romaner, F. Niedermair, K. Müllen, A. C. Grimsdale, R. Saf, E. J. W. List, E. Zojer, C. Slugovc, *Macromol. Chem. Phys.* **2008**, *209*, 2122-2134.

[54] O. S. Wolfbeis, *J. Mater. Chem.* **2005**, *15*, 2657-2669.

[55] S. Rentenberger, A. Vollmer, E. Zojer, R. Schennach, N. Koch, *J. Appl. Phys.* **2006**, *100*.

[56] A. Klug, A. Meingast, G. Wurzinger, A. Blumel, K. Schmoltner, U. Scherf, E. J. W. List, *Proc. SPIE* **2011**, *8118*, 811809.

[57] L. Zöphel, Ph.D. thesis, Johannes Gutenberg-University Mainz **2012**.

[58] G. Horowitz, R. Hajlaoui, H. Bouchriha, R. Bourguiga, M. Hajlaoui, *Adv. Mater.* **1998**, *10*, 923-927.

[59] J. Veres, S. Ogier, S. Leeming, B. Brown, D. Cupertino, *Mater. Res. Soc. Symp. Proceed.* **2002**, *708*, 243-250.

[60] M. H. Yoon, C. Kim, A. Facchetti, T. J. Marks, *J. Am. Chem. Soc.* **2006**, *128*, 12851-12869.

[61] A. Wan, J. Hwang, F. Amy, A. Kahn, *Org. Electron.* **2005**, *6*, 47-54.

[62] D. Natali, M. Caironi, *Adv. Mater.* **2012**, *24*, 1357-1387.

[63] S. Rentenberger, A. Vollmer, E. Zojer, R. Schennach, N. Koch, *J. Appl. Phys.* **2006**, *100*, 053701.

[64] B. Stadlober, U. Haas, H. Gold, A. Haase, G. Jakopic, G. Leising, N. Koch, S. Rentenberger, E. Zojer, *Adv. Funct. Mater.* **2007**, *17*, 2687-2692.

[65] J. Veres, S. Ogier, G. Lloyd, D. de Leeuw, *Chem. Mater.* **2004**, *16*, 4543-4555.

[66] S. C. Lim, S. H. Kim, J. H. Lee, M. K. Kim, D. J. Kim, T. Zyung, *Synth. Met.* **2005**, *148*, 75-79.

[67] D. Yan, C. Gao, H. Frey, *Hyperbranched Polymers: Synthesis, Properties, and Applications, Wiley Series on Plastics Engineering and Technology*, John Wiley & Sons, New York, **2011**.

[68] J. M. Koenen, S. Jung, A. Patra, A. Helfer, U. Scherf, *Adv. Mater.* **2012**, *24*, 681-686.

[69] A. J. Berresheim, M. Müller, K. Müllen, *Chem. Rev.* **1999**, *99*, 1747-1785.

[70] P. C. Che, Y. N. He, X. G. Wang, *Macromolecules* **2005**, *38*, 8657-8663.

[71] H. Mori, D. C. Seng, M. F. Zhang, A. H. E. Müller, *Langmuir* **2002**, *18*, 3682-3693.

[72] H. Mori, D. C. Seng, H. Lechner, M. F. Zhang, A. H. E. Müller, *Macromolecules* **2002**, *35*, 9270-9281.

[73] E. L. Spitler, W. R. Dichtel, *Nat. Chem.* **2010**, *2*, 672-677.

[74] J. W. Colson, A. R. Woll, A. Mukherjee, M. P. Levendorf, E. L. Spitler, V. B. Shields, M. G. Spencer, J. Park, W. R. Dichtel, *Science* **2011**, *332*, 228-231.

[75] E. L. Spitler, B. T. Koo, J. L. Novotney, J. W. Colson, F. J. Uribe-Romo, G. D. Gutierrez, P. Clancy, W. R. Dichtel, *J. Am. Chem. Soc.* **2011**, *133*, 19416-19421.

[76]   D. N. Bunck, W. R. Dichtel, *Chem. Eur. J.* **2013**, *19*, 818-827.

[77]   J. W. Colson, W. R. Dichtel, *Nat. Chem.* **2013**, *5*, 453-465.

[78]   J. M. Cai, P. Ruffieux, R. Jaafar, M. Bieri, T. Braun, S. Blankenburg, M. Muoth, A. P. Seitsonen, M. Saleh, X. L. Feng, K. Müllen, R. Fasel, *Nature* **2010**, *466*, 470-473.

[79]   M. Bieri, M. Treier, J. M. Cai, K. Ait-Mansour, P. Ruffieux, O. Groning, P. Groning, M. Kastler, R. Rieger, X. Feng, K. Müllen, R. Fasel, *Chem. Commun.* **2009**, 6919-6921.

[80]   D. F. Perepichka, F. Rosei, *Science* **2009**, *323*, 216-217.

[81]   M. O. Blunt, J. C. Russell, N. R. Champness, P. H. Beton, *Chem. Commun.* **2010**, *46*, 7157-7159.

[82]   G. Franc, A. Gourdon, *Phys. Chem. Chem. Phys.* **2011**, *13*, 14283-14292.

[83]   C. A. Palma, P. Samori, *Nat. Chem.* **2011**, *3*, 431-436.

[84]   M. Bieri, S. Blankenburg, M. Kivala, C. A. Pignedoli, P. Ruffieux, K. Müllen, R. Fasel, *Chem. Commun.* **2011**, *47*, 10239-10241.

[85]   E. J. Kan, W. Hu, C. Y. Xiao, R. F. Lu, K. M. Deng, J. L. Yang, H. B. Su, *J. Am. Chem. Soc.* **2012**, *134*, 5718-5721.

[86]   J. J. Yin, M. P. Rainka, X. X. Zhang, S. L. Buchwald, *J. Am. Chem. Soc.* **2002**, *124*, 1162-1163.

[87]   G. Altenhoff, R. Goddard, C. W. Lehmann, F. Glorius, *Angew. Chem., Int. Ed.* **2003**, *42*, 3690-3693.

[88]   S. D. Walker, T. E. Barder, J. R. Martinelli, S. L. Buchwald, *Angew. Chem., Int. Ed.* **2004**, *43*, 1871-1876.

[89]   T. E. Barder, S. D. Walker, J. R. Martinelli, S. L. Buchwald, *J. Am. Chem. Soc.* **2005**, *127*, 4685-4696.

[90]   K. L. Billingsley, T. E. Barder, S. L. Buchwald, *Angew. Chem., Int. Ed.* **2007**, *46*, 5359-5363.

[91]   T. Ishiyama, M. Murata, N. Miyaura, *J. Org. Chem.* **1995**, *60*, 7508-7510.

[92]   D. Qiu, F. Y. Mo, Z. T. Zheng, Y. Zhang, J. B. Wang, *Org. Lett.* **2010**, *12*, 5474-5477.

[93]   A. D. Schlüter, *J. Polym. Sci., Part A: Polym. Chem.* **2001**, *39*, 1533-1556.

[94]   X. Y. Yang, X. Dou, K. Müllen, *Chem. Asian J.* **2008**, *3*, 759-766.

4 *N*-Heterotriangulene Macrocycles

4.1   Introduction

Exploring the potential of shape-persistent π-conjugated macrocycles is usually hampered by demanding synthetic sequences with commonly low overall yields.[1-13] To enhance the macrocycle formation, different strategies have been pursued. Besides one-pot cyclizations of simple monomers[2, 12, 14-20] and template-directed cyclizations,[21-26] the main synthetic method is the utilization of oligomeric precursor molecules to limit the macrocycle formation to one or two *intra*molecular ring closure reactions (see Chapter 1 for details).[27] In addition to that, the direct assembly of molecular precursors confined on surfaces can be considered as an alternative method for the generation of sophisticated molecular architectures.[28] With this bottom-up method ultranarrow graphene nanoribbons (GNRs),[29] honeycomb networks,[30-33] poly(phenylene) and poly(fluorene) nanowires,[34, 35] and transition metal phthalocyanine sheets were successfully fabricated.[28, 36]
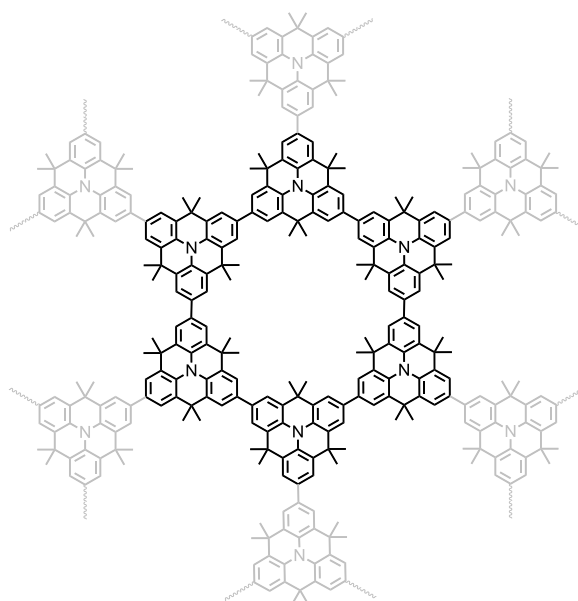
Figure 4-1. Structure of a potential fraction of a hyperbranched *N*-heterotriangulene network.[33] The macrocyclic subunit is highlighted.

In this chapter, these three methods were used for the synthesis of a π-conjugated macrocycle based on the aforementioned *N*-heterotriangulene moiety (see above) to study the impact of the synthetic approach on the outcome of the macrocyclization. Besides the already mentioned comparative aspects, the aesthetically appealing structure of a π-conjugated macrocycle based on *N*-heterotriangulene units and the connection to the

already described linear and hyperbranched polymers (**P1** and **P2**) were further motivations for these efforts (Figure 4-1). The cyclic arrangement of the *N*-heterotriangulenes raises the question to which extent the photophysical properties, *e.g.*, the photoluminescence quantum yields (PLQY) will be altered in comparison to the linear one. It influences furthermore the molecular ordering in the solid state and thus the hole transport properties relevant to organic electronics.[8] Liquid crystallinity which can be anticipated from the flat geometry of the *N*-heterotriangulene subunit as well as self-assembly on surfaces remain thus important issues to be explored. The same holds for the inclusion of guest molecules and their impact on the molecular self-organization.

## 4.2   Synthetic Approaches toward *N*-Heterotriangulene Macrocycles

4.2.1   Solution-Based One-Step Macrocycle Synthesis

As mentioned before, a 120° substitution pattern of the functional groups is required for the highly selective formation of six-membered macrocycles. Owing to its C_3 symmetry and straightforward functionalization of the activated positions *para* to the central nitrogen, *N*-heterotriangulene **3-4** is an ideal building block for the construction of six-membered macrocycles.
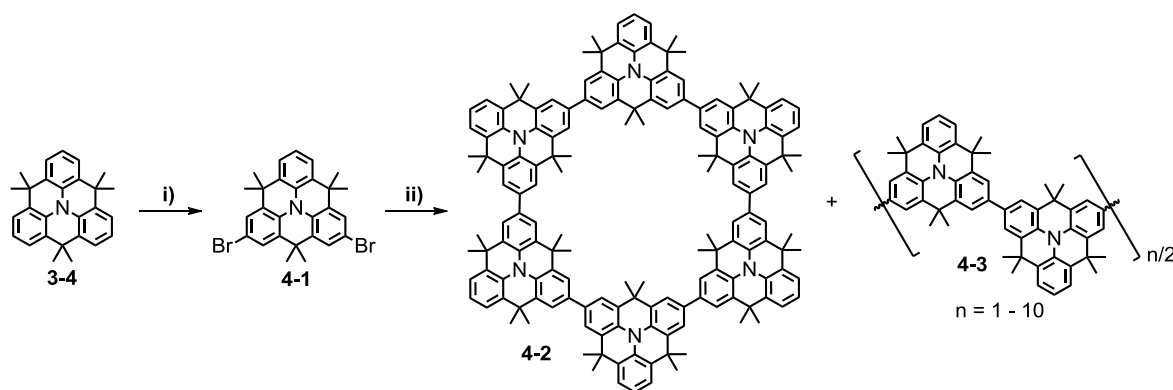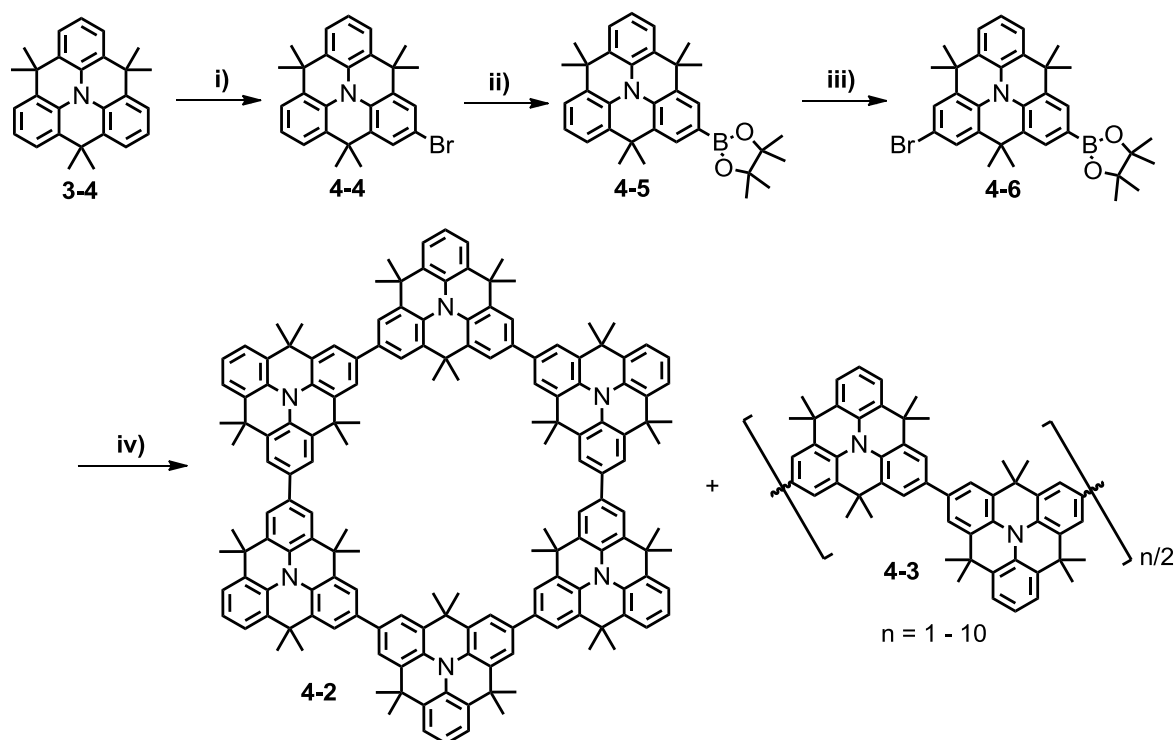

Scheme 4-1. Synthetic route of the one-step *Yamamoto* macrocyclization. Conditions: i) 2 equiv. NBS, CHCl$_3$, 0 °C to RT, 2h, 77%; ii) bis(cycloocta-1,5-diene)nickel(0), cycloocta-1,5-diene, 2,2'-bipyridine, toluene/DMF, c = 4 × 10^{-3} or 3.5 × 10^{-4} M, 85 °C, 2 days.

On the basis of the functionalization strategy discussed in the previous chapter, a bis-functionalized *N*-heterotriangulene precursor was aimed for a direct macrocycle synthesis. For this purpose **3-4** was brominated using two equivalents of NBS referring to the established procedure (see above). Dibromo *N*-heterotriangulene **4-1**, with an angle of 120°
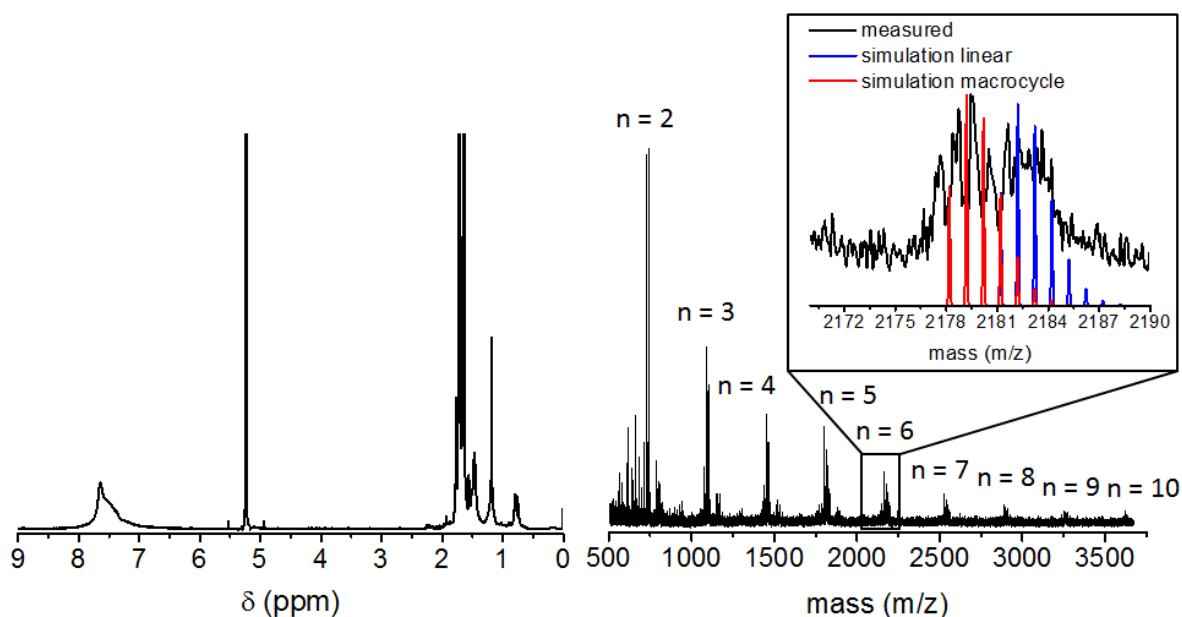
Figure 4-2. ^{1}H NMR spectrum (left) in CD_2Cl_2 at 25 °C and MALDI-TOF MS (right, matrix: dithranol) of the oligomeric mixture obtained by the *Yamamoto* reaction of **4-1**. The inset shows a magnification of the region corresponding to hexameric species together with the simulated isotopic pattern of the six-membered macrocycle and the linear hexamer.

between both bromines was thus obtained in 77% yield (Scheme 4-1). For the cyclohexamerization of **4-1**, the Ni^0-mediated *Yamamoto* reaction was used in a 5/1 mixture of toluene/DMF.[37, 38] The formation of linear oligomers is an unavoidable side reaction in macrocycle synthesis if too high concentrations are used.[4, 5, 39] Therefore, the concentration was set to 4×10^{-3} M and the solution of **4-1** was slowly added over the course of two hours to the active nickel complex to ensure pseudo high-dilution conditions. After running the reaction for two days, it was quenched and the nickel residues were decomposed using dilute methanolic hydrochloric acid. Analysis of the obtained crude product by SEC revealed a broad oligomer distribution. MALDI-TOF MS showed moreover a complex mixture of species with up to 10 *N*-heterotriangulene units (Figure 4-2, right). The isotopic pattern of the hexameric peak (n = 6) revealed two distributions with a mass difference of two Dalton corresponding to macrocycle **4-2** and the linear hexamer (n = 6). The relative signal intensities suggest no preference for the macrocyclization. Further analysis of the corresponding mass spectrum provided no evidence for the formation of larger macrocycles under the applied reaction conditions. To quantify the amount of macrocycle **4-2** formed during the one-step reaction, the hexameric fraction was enriched with the help of repeated preparative size-exclusion chromatography (SEC). ^{1}H NMR spectroscopy revealed a broad signal in the aromatic region and less distinct aliphatic signals corresponding to the less symmetric linear hexamer (Figure 4-2, left).

Scheme 4-2. Synthetic route of the one-step *Suzuki-Miyaura* macrocyclization. Conditions: i) 1 equiv. NBS, CHCl$_3$, 0 °C to RT, 2h, 90%; ii) Pd(dppf)Cl$_2$, KOAc, bis(pinacolato)diboron, DMF, 85 °C, 12h, 86%; iii) 1 equiv. NBS, CHCl$_3$, 0 °C to RT, 18h, 75%; iv) Pd(PPh$_3$)$_4$, 2 M aq. K$_2$CO$_3$, toluene, ethanol, c = 4 × 10^{-4} M, 85 °C, 2 days.

By considering the intrinsic sensitivity of NMR spectroscopy (the accuracy limit is usually around 5%) the obtained yield of macrocycle **4-2** was not higher than 5%. To further enhance the *intra*molecular bond formation, the reaction was repeated using higher diluted reaction mixtures. However, the results were not significantly influenced by the concentration. In order to study the effect of the applied cross-coupling procedure on the macrocyclization the *Suzuki-Miyaura* reaction was furthermore tested. For this purpose the established protocol for the formation of **3-8** was adapted for the synthesis of *AB*-monomer **4-6** (see Chapter 3 and Scheme 4-2). *N*-heterotriangulene **3-4** was initially monobrominated, followed by a Pd-catalyzed *Miyaura* borylation toward **4-5**. Final bromination of boronate **4-5** led to **4-6** in good overall yields. *AB*-monomer **4-5** was subjected to the *Suzuki-Miyaura* coupling in a 2.5/1 toluene/ethanol mixture using aqueous K$_2$CO$_3$ as base.[10] The concentration of the organic phase was set to 4 × 10^{-4} M. After running the reaction for two days, thin-layer chromatography and FD-MS indicated full conversion and the reaction was quenched. Analysis of the crude mixture by MALDI-TOF MS revealed again oligomers with up to 10 *N*-heterotriangulene units and no preferential formation of the hexameric species, which was very similar to the results obtained *via* the *Yamamoto* reaction.
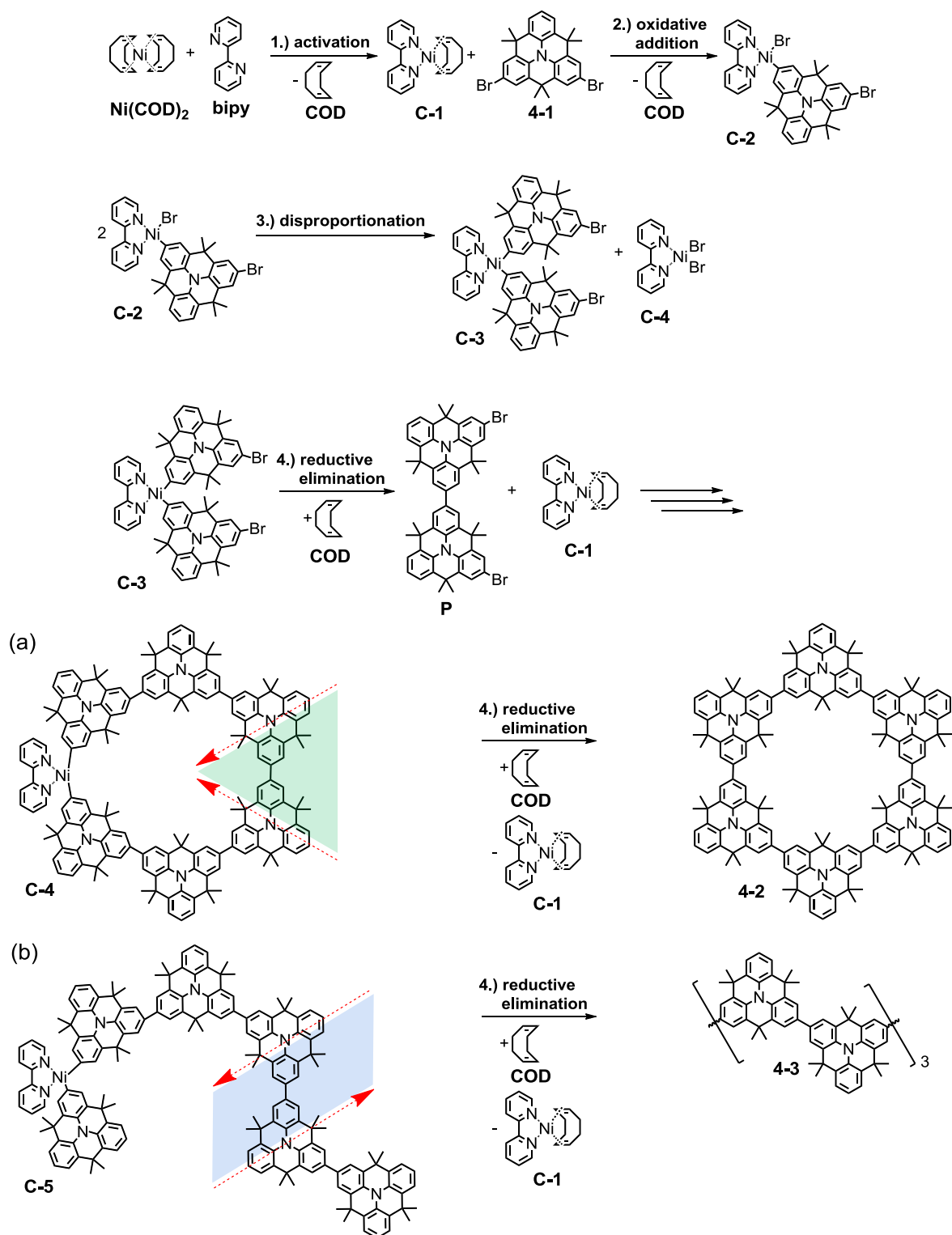
Scheme 4-3. Proposed reaction mechanism during the formation of **4-2** and **4-3** *via Yamamoto* reaction. The molecular main axis is indicated by a dashed red arrow. (a) Two *N*-heterotriangulenes are linked in the cyclic configuration if their two main axes differ by 60° (green triangle). (b) Two *N*-heterotriangulenes are linked in the linear configuration if their two main axes are antiparallel (blue parallelogram).

These findings suggest an unfavored pathway of the cyclohexamerization in a solution-based cross-coupling reaction, which will be discussed in the following on the basis of the *Yamamoto* reaction.

The corresponding reaction sequence is depicted in Scheme 4-3. The thermal activation of bis(cycloocta-1,5-diene)nickel(0) (**Ni(COD)₂**) occurs initially *via* the replacement of one cycloocta-1,5-diene (**COD**) by the 2,2'-bipyridine (**bipy**) ligand to result in **C-1**. Subsequent insertion of the nickel atom into the carbon-bromine bond of **4-1** leads to formation of Ni^{II}-complex **C-2**.[39-42] A disproportionation of two molecules of **C-2** yields **C-3** with the two *N*-heterotriangulenes at the Ni^{II} center. As a result of the formation of inactive complex **C-4** in stoichiometric amounts, the Ni^0-species is consumed during the course of the reaction. The reductive elimination leads to the cross-coupling product (**P**) followed by a release of the reactivated complex **C-1** which is available for a new cycle.[39] This procedure is subsequently repeated involving analogous *inter*molecular reaction sequences, which lead to the formation of a hexamer.

To understand the preferential formation of the linear oligomers, the definition of a "molecular main axis" is required (Scheme 4-3, dashed red arrows). According to this definition, two *N*-heterotriangulene molecules can be said to be linked in the cyclic or linear manner if their two main axes differ by 60° or 180°, respectively. By comparing two successive axes it is thus possible to determine the relative bonding configuration (cyclic or linear).

During the course of the repetitive *Yamamoto* reaction sequence, two situations are thus possible (Scheme 4-3 a and b): (a) To obtain a predefined macrocyclic geometry in **C-4**, every *N*-heterotriangulene inside the growing oligomer has to arrange in a 60° configuration to each other (Scheme 4-3 a, green triangle). In this case, macrocycle **4-2** is formed by an *intra*molecular bond formation upon reductive elimination. (b) The rotation of only one molecule around the $C(sp^2)-C(sp^2)$ single bond results in an antiparallel main axis as depicted in **C-5** (Scheme 4-3 b, blue parallelogram) preventing the macrocyclization. After reductive elimination linear oligomers (**4-3**) are formed by an *inter*molecular bond formation. They can be further extended if no protodehalogenation has occurred during the cycle.

In a cyclohexamerization the statistical probability of situation (a) is intrinsically lower than for situation (b). By considering a simple "hit and stick" model for unconfined molecules, the probability of forming a macrocycle is thereby $(0.5)^5 = 3.1\%$. This assumption is based on their conformational and orientational degrees of freedom allowing

two possible orientations per added molecule, whereas only one of them is leading to the respective macrocycle. The predicted probability is consistent with the NMR investigations of the hexameric fraction showing less than 5% of macrocyclic species (see above).

4.2.2 Surface-Assisted One-Step Macrocycle Synthesis

Based on the *Ullmann* reaction,[29, 33, 35, 43, 44] a chemistry-driven protocol for the generation of *N*-heterotriangulene honeycomb networks on metal surfaces has been recently established by *Müllen* together with *Fasel* and coworkers.[33] The formation of the defect-free networks was attributed to the confinement of the motion of the *N*-heterotriangulenes to two dimensions, thus enforcing planar growth. These restrictions are particularly favorable for the bottom-up assembly of macrocyclic structures. The subsequent *Ullmann* reaction has been realized by incorporating specific, comparably weak halogen-carbon bonds in a monomer building block adsorbed on a metal surface. According to *Grill* and *Hecht* the reaction mechanism of the on-surface *Ullmann* reaction consists of two crucial steps:[28] (1) Upon heating, the halogen atoms dissociate while creating reactive sites at their initial positions (activation step). (2) The reactive molecules subsequently diffuse on the metal surface and connect with each other by forming covalent $C(sp^2)-C(sp^2)$ bonds at the previous halogen positions (connection step). From recent studies on the direct growth of GNRs and graphene networks on metal surfaces it is known that the formation of the nanostructures on surfaces proceeds *via* a radical pathway.[29-31] A Further advantage of the on-surface synthesis under ultrahigh vacuum (UHV) conditions is a much broader temperature range than in solution without significant side reactions. Combining this technique with scanning tunneling microscopy (STM) allows imaging at a submolecular level and thus an *in situ* characterization.[45-47]

To study this effect on the outcome of the direct macrocyclization on an atomically flat Ag(111) surface and to compare the results with the solution-based macrocyclization, dibromo-substituted *N*-heterotriangulene **4-1** was applied for the STM-assisted surface reaction under UHV conditions. The respective STM experiments were carried out in collaboration with ████████████████████ in the group of ████████████████ at the EMPA Dübendorf, Switzerland.

Dibromo-substituted *N*-heterotriangulene **4-1** was synthesized according to the previously established procedure and was purified by column chromatography and several recrystallization steps. A rigorous purification was necessary to ensure complete removal
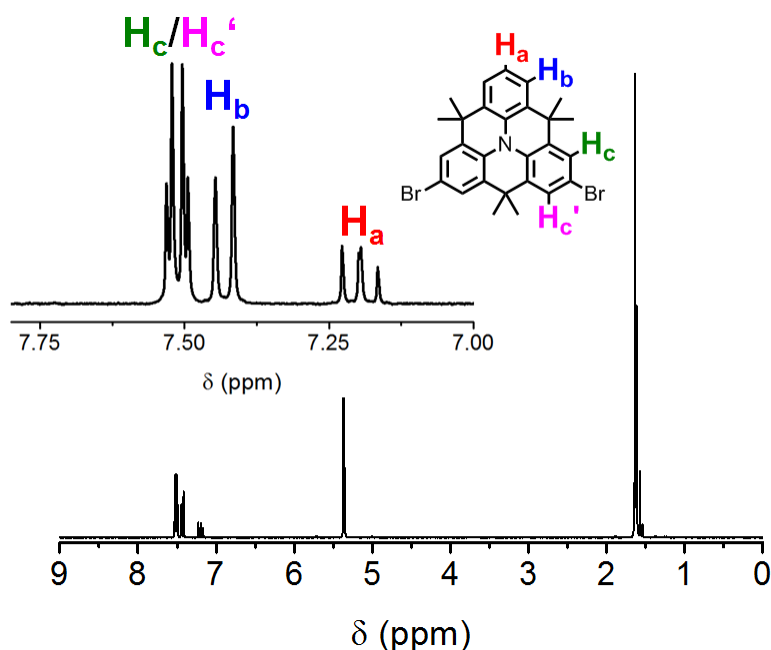
Figure 4-3. ^{1}H NMR spectrum of dibromo *N*-heterotriangulene **4-1** in CD_2Cl_2 at 25 °C. Inset: Zoom into the aromatic region with proton assignment.

of the interfering mono- and tri-brominated byproducts. The purity of **4-1** was verified by NMR spectroscopy (Figure 4-3) and further confirmed with the help of high-resolution (HR) ESI MS with a single signal at *m/z* = 522.0441 ($C_{27}H_{26}Br_2N$, calculated 522.0432). With its intermediate molecular weight of 522 g/mol, sublimation of **4-1** was accomplished at 110 °C in UHV (~10^{-7} mbar). It was deposited onto a cleaned Ag(111) crystal held at room temperature so that the molecules initially adsorb as dibrominated species. Annealing of the Ag(111) substrate at temperatures of 200 °C after molecule deposition resulted in dehalogenation of **4-1**. The *STM* images with submolecular resolution (Figure 4-4) revealed a triangular shape of the monomers with bright protrusions at the edges. The observed features were identified as the dimethylmethylene groups essentially perpendicular oriented with respect to the surface thus defining the triangular shape of the molecule, which is in agreement with previous reports.[33] The so-obtained biradical species were stabilized by coordinating to the silver atoms lifted up from their initial equilibrium position to form metal-coordination networks.[31, 33, 43] In contrast to the two-dimensional regular porous coordination networks obtained for a similar sample preparation using tribromo-substituted *N*-heterotriangulene, non-porous close-packed domains were observed owing to the lower symmetry of **4-1**.[33] No covalent bonds were formed at this stage as confirmed by the equal distances between the individual *N*-heterotriangulenes (Figure 4-4 c). The STM tip was used to perform a line profile analysis
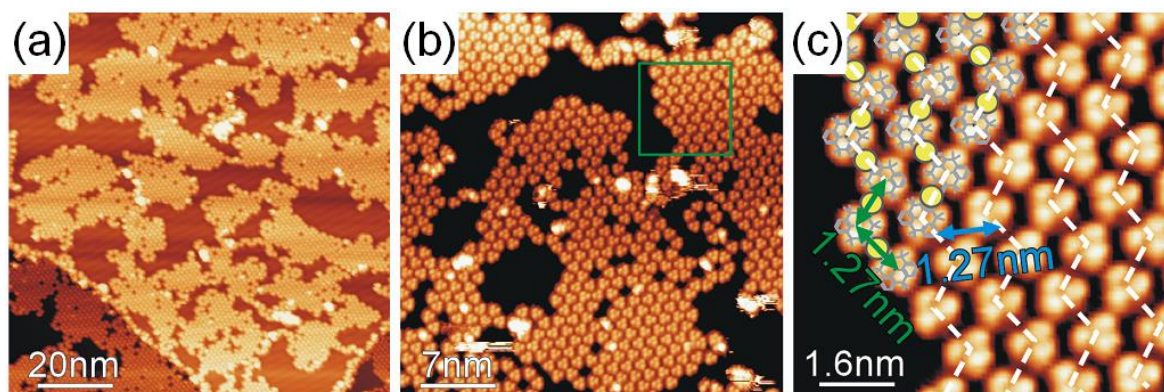
Figure 4-4. (a) STM image of metal-coordination networks of **4-1** on a Ag(111) surface after annealing at 200 °C. (b) Magnification of the STM image. (c) Zoom into the green rectangle. The distance between Ag-coordinated molecules is about 1.27 nm. Coordinating Ag atoms are shown in yellow.

across the surface-confined molecules. This yielded a distance between the linear chains of 1.27 nm (blue arrow) and an *inter*molecular center-to-center distance of 1.27 nm along the virtual Br−Br axis (green arrows). Since *inter*molecular distances of 1.20 nm were found for metal-coordination networks fabricated using tribromo-substituted *N*-heterotriangulene,[33] it is most likely that in this situation two adjacent radicals coordinate to one silver atom being slightly elevated out of the surface equilibrium position (Figure 4-4 c, depicted in yellow). However, an unambiguous assignment is difficult to make in the STM topographs, due to subtle differences between the dibromo *N*-heterotriangulene **4-1** and its diradical species. At this stage, a preorientation of the molecules toward macrocycles or linear oligomers was already observed (Figure 4-4 b).

The sample was subsequently heated to 300 °C to trigger the surface-promoted aryl-aryl coupling reaction.[30, 31] Extended nanostructures were thereby observed spreading across the metal surface as depicted in Figure 4-5 a. The relatively high annealing temperature occasionally results in methyl scission (see *e.g.* the species indicated by a red arrow in Figure 4-5 c). This might be explained by a substitution of residual hydrogen present in the UHV chamber and/or hydrogen from methyl groups of the cleaved CH_3 units in a radical process.[33]

The observed nanostructures consisted of covalently linked monomers as confirmed by the line profile analysis, revealing an apparent height of 0.25 nm and an *inter*molecular center-to-center distance of 1.00 nm along the virtual Br−Br axis. These dimensions are in agreement with the distances observed in related 2D porous covalent networks (1.00 nm) and provide additional evidence that the individual *N*-heterotriangulene moieties are now connected by C−C bonds instead of C−Ag−C bonds.[33] With respect to this, the transition
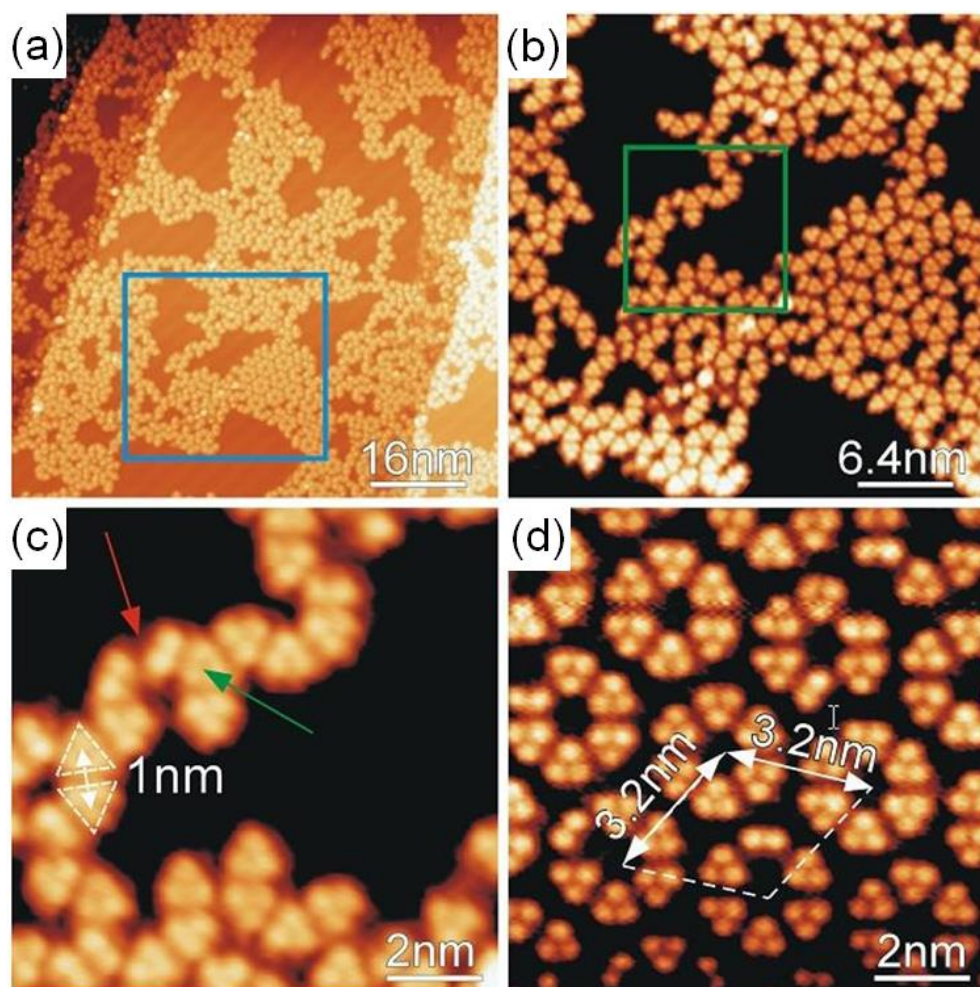
Figure 4-5. STM topographs of covalently *N*-heterotriangulene nanostructures. (a) Flat oligomeric structures and macrocycles are observed. (b) Close-up view of the area highlighted by the blue rectangle in (a) revealing submolecular contrast. (c) Zoom into the green rectangle of (b). The center-to-center distance between two covalently bonded monomers is 1.0 nm. The red arrow points to a molecule with one missing methyl unit. The green arrow points to a molecule with three neighbors. (d) Island consisting of aggregated six-membered macrocycles. The distance between macrocycles is 3.2 nm.

temperature between the metal-coordination and the covalently linked structures is found to be at approximately 250 °C. The observed nanostructures were composed of linear oligomers (Scheme 4-4 a), six-membered macrocycles (Scheme 4-4 b) and mixed chains (Scheme 4-4 c) in analogy to the results of the solution-based synthesis (see above). As a result of the ditopic nature of **4-1**, the individual *N*-heterotriangulene units were linked to two neighbors *via* covalent bonds. Occasionally the formation of three covalent bonds was observed (8 ± 1% of the monomers). In this particular case, a carbon radical appeared to attack the H−C bond of a phenyl moiety of the neighboring molecule, leading to C−H bond scission and *inter*molecular C−C bond formation. This circumstance could be furthermore explained by the presence of traces of a tri-brominated species in **4-1** which is, however,
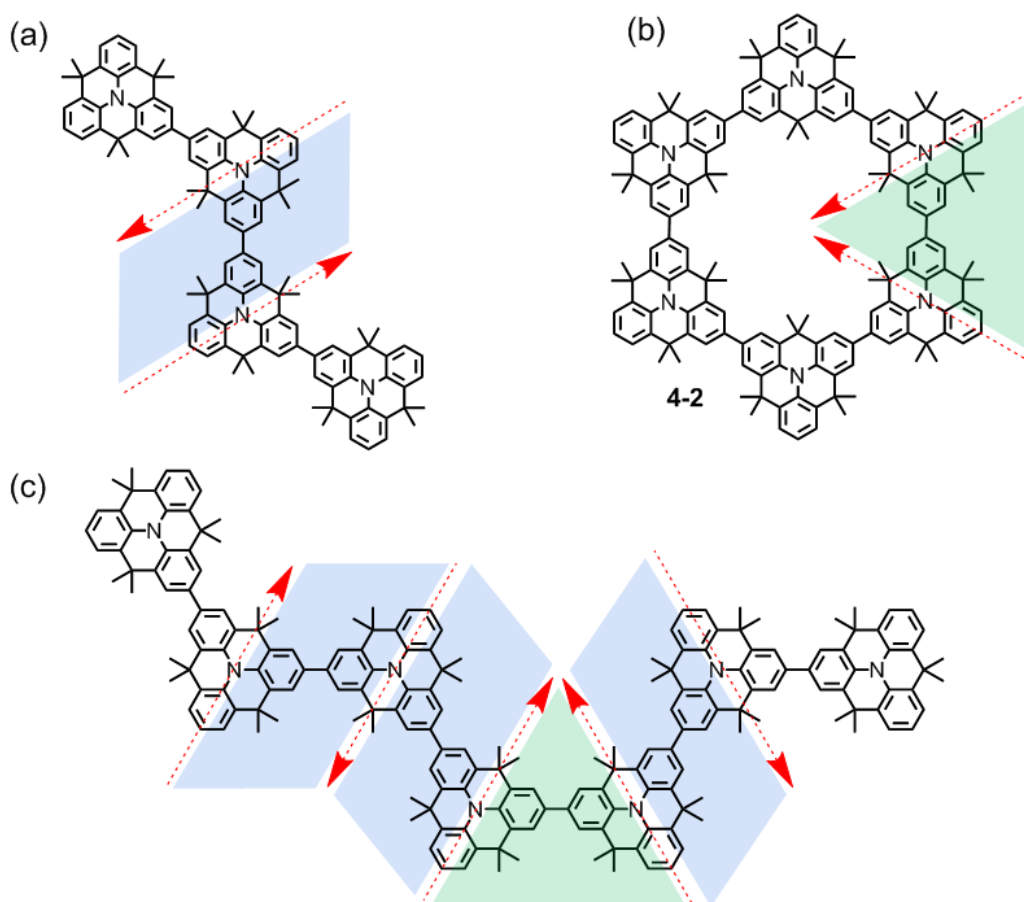
Scheme 4-4. Schematic representation of the observed nanostructures by the on-surface oligomerization of **4-1**. The molecular main axis is represented by a dashed red arrow. (a) Structure of a linear oligomer. Two monomers are linked in the linear configuration if their two main axes are antiparallel (blue parallelogram). (b) Structure of a six-membered macrocycle. Two monomers are linked in the cycle configuration if their two main axes differ by 60° (green triangle). (c) Mixed chain with links in the linear and cycle configurations.

rather unlikely. The sublimation temperature of the tri-brominated species is higher than the applied temperature for the sublimation of **4-1**, which further increased the purity of the deposited material during the sublimation process.[33] In addition, such radical induced C−H bond scissions have a reduced activation barrier on the metal surface as it was shown for the surface-mediated synthesis of GNRs.[29, 48]

The on-surface oligomerization of dibromo-substituted **4-1** on Ag(111) also led to a significant amount ($16 \pm 2\%$) of six-membered macrocycles (**4-2**), which were frequently grouped together into ordered islands forming a hexagonal lattice with a distance between macrocycles of about 3.2 nm (Figure 4-5 d). The fact that there seem to be regions where macrocycles are clustered and others where linear oligomers dominate is likely to be related to the different mobility of these two types of structures at the applied reaction temperature: Macrocycles, owing to their compact architecture, can easily diffuse on the
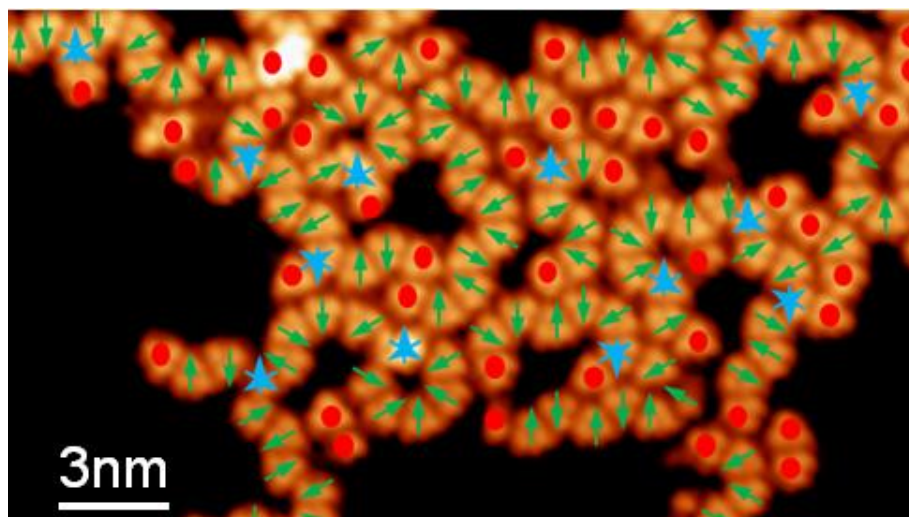
Figure 4-6. High-resolution STM image of covalently linked *N*-heterotriangulene nanostructures with additional information for data analysis. Green arrows: monomer main axes; red spots: species without identified main axes; blue triple-arrows: molecules with three covalent bonds.

surface and form close-packed clusters that are energetically favorable (van der Waals attraction). On the other hand, linear oligomers can hardly diffuse on the surface or form dense structures, due to their larger sizes and irregular shapes. The distance between the edges of two adjacent macrocycles (~0.6 nm, Figure 4-5 d) confirmed furthermore the absence of C−C bonds between the rings. To determine whether any coupling selectivity governs the *intra-* or *inter*molecular connection toward cyclic or linear direction, five representative high-resolution STM images acquired over the same sample were characterized. This corresponds to a total number of 1937 molecules. The method consisted in identifying and comparing successive monomer main axes (Scheme 4-4 and Figure 4-6). Since the main axis of a monomer can only be determined when it is covalently bonded to two clearly identified neighbors, and not in all other cases such as isolated monomers, dimers, monomers connected to three neighbors etc., the main axes of only about two thirds of the monomers could be unequivocally determined (Figure 4-6). Two successive monomers can be said to be linked in the cyclic or linear configuration if their two axes differ by 60° or 180°, respectively (Scheme 4-4). Based on this, a preference for bond formation in the cyclic configuration (60 ± 5 %) compared to the linear arrangement (40 ± 4 %) was found. In agreement with the results in solution (see above), no ring sizes smaller or larger than six- membered macrocycles (**4-2**) were observed. This suggests that the combination of the rigid *N*-heterotriangulene with the hexagonal Ag(111) surface favors the 120° angle and hence led to a certain selectivity of the reaction with respect to the macrocycle system formed.[49]

By considering a simple statistic model for the macrocyclization, a probability of only $(0.5)^4 = 6.25\%$ is obtained for the macrocyclization. In this model a step-wise macrocycle formation (monomer after monomer) is assumed, allowing two possible orientations per added molecule, whereas only one of them leads to the macrocycle. It comprises furthermore a probability of 1 for the last monomer to close the macrocycle as a result of the high reactivity of the radicals.

The difference between the predicted and the actually observed number of macrocycles suggest that the on-surface oligomerization of **4-1** is not a random process. The two possible orientations correspond to different reaction possibilities.

In a very recent study *Gottfried* and *Zhu* confirmed the validity of the herein proposed model for the preferential formation of six-membered macrocycles on metal surfaces based on C_3 symmetric precursor molecules.[49] The utilization of a 4,4''- dibromo-*m*-terphenyl gave 70% so-called "hyperbenzene" rings *vs.* 30% linear chains on a Cu(111) surface at 280 °C.

By comparing the results of the surface-assisted with the solution-based approach for the one-step synthesis of *N*-heterotriangulene macrocycle **4-2**, a clear superiority of the on-surface experiment could be identified. Applying transition-metal mediated cross-coupling procedures in solution, the *intra*molecular aryl-aryl coupling is hampered by possible rotations about the $C(sp^2)-C(sp^2)$ single bond. The *inter*molecular connection to a new monomer and the *intra*molecular coupling have an equal feasibility as expressed by a predicted probability of $(0.5)^5 = 3.1\%$. As a result of the two-dimensional confinement of the molecules on the metal surface, however, essentially no such conformational changes are possible. This results in reduced possible orientations, which favors *intra*molecular coupling events. The probability of a chain-end connection has been increased due to a reduced entropic handicap.

Moreover, a templating effect of the Ag(111) surface cannot be excluded, favoring the fabrication of the six-membered macrocycle **4-2**. Metal (111) surfaces are considered to stabilize monomers with 120° angles in the adsorbate lattice by the hexagonal orientated atoms.[49, 50]

The influence of the uplifted silver atoms from their equilibrium positions in the surface during the first steps is not yet fully understood.[31, 43] The consequent radical-induced surface reconstruction significantly influences the energy landscape for following monomers, which have a considerable impact on the preference for specific binding motifs.

4.2.3   Solution-Based Stepwise Macrocycle Synthesis

Although the surface-mediated synthesis on Ag(111) favors the formation of macrocyclic structures, the solution chemistry should allow their synthesis in macroscopic quantities. From the viewpoint of potential applications in organic molecular electronics, the challenge of transferring the generated nanostructures from the metal surface to some technologically relevant substrates still needs to be solved.
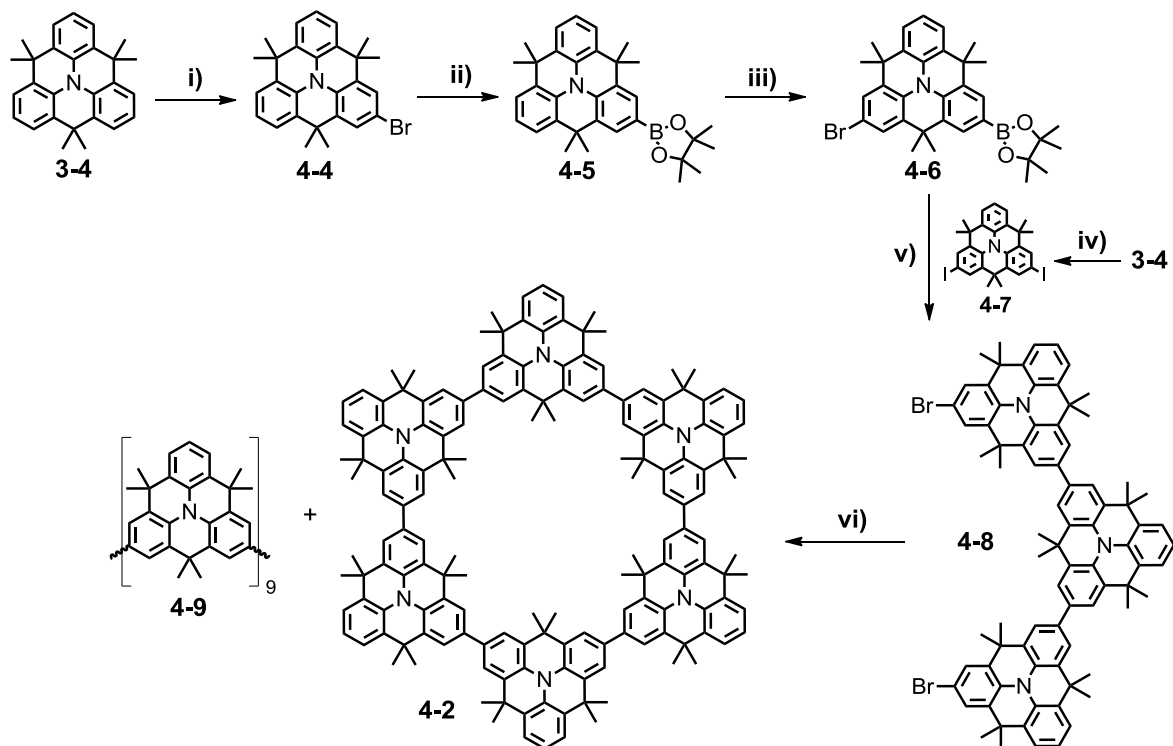
Scheme 4-5. Synthetic route of the stepwise synthesis toward *N*-heterotriangulene macrocycle **4-2**. Conditions: i) 1 equiv. NBS, CHCl$_3$, 0 °C to RT, 2h, 90%; ii) Pd(dppf)Cl$_2$, KOAc, bis(pinacolato)diboron, DMF, 85 °C, 12h, 86%; iii) 1 equiv. NBS, CHCl$_3$, 0 °C to RT, 18h, 75%; iv) 2 equiv. NIS, CHCl$_3$, 0 °C to 50 °C, 96h, 89%; v) Pd(PPh$_3$)$_4$, 2 M aq. Na$_2$CO$_3$, toluene, *Aliquat 336*, 65 °C, 3 days, 55%; vi) bis(cycloocta-1,5-diene)nickel(0), cycloocta-1,5-diene, 2,2'-bipyridine, toluene/DMF, c = 3.8 × 10^{-3} M, 85 °C, 2 days, **4-2**: 38%, **4-9**: 15%.

For the reasons above, a reliable synthetic route was aimed to obtain macroscopic quantities of the *N*-heterotriangulene macrocycle **4-2**. Since the direct synthesis utilizing a simple monomer results in insufficient amounts of **4-2**, the concept was extended to an iterative strategy (Scheme 4-5). With respect to this, a suitable linear precursor was aimed, limiting the macrocyclization to one or two *intra*molecular reaction steps.[18, 27]

The sequence started with the synthesis of *AB*-monomer **4-6** utilizing the established protocol. *N*-heterotriangulene was selectively mono-brominated to obtain **4-4**, followed by a Pd-catalyzed *Miyaura*-borylation using bis(pinacolato)diboron toward **4-5**.[51] The

subsequent mono-bromination of boronate **4-5** was accomplished in the absence of light and at 0 °C to avoid protodeboronation and *ipso*-substitution (see above).[52] This led to *AB*-monomer **4-6** after column chromatographic purification in an overall yield of 58% over three steps, enabling a gram scale synthesis. The second building block was obtained by a twofold iodination of **3-4**. The reaction was carried out referring to the previous procedure utilizing *N*-iodosuccinimide (NIS) instead of NBS leading to **4-7** in 90% yield. As a result of the decreased electrophilicity of NIS, the reaction proceeded only at temperatures above 40 °C. The subsequent *Suzuki-Miyaura* cross-coupling of **4-6** and **4-7** was carried out selectively at 65 °C utilizing aqueous sodium carbonate (2 M) as base and tetrakis(triphenylphosphine)palladium(0) as Pd^0-source.[18] The reactivity of the iodine substituents was sufficiently high to exclude thereby a possible attack of the bromine atoms at this temperature. The yield of the reaction was decreased by an inevitable formation of a deiodinated dimer, which was separated by column chromatography. Dibromo trimer **4-8** was obtained in 55% yield after final precipitation by adding a dichloromethane/methanol mixture. The described synthetic sequence allowed for the efficient preparation of precursor **4-8** on a gram scale.

With trimer **4-8** in hand, an adequate cyclodimerization method was sought. Again, the *Yamamoto* reaction was utilized due to its broad scope and versatility as it has been previously shown.[42, 53] As already discussed the concentration influences the yield and the outcome of a macrocyclization to a great extent. Thus, the reaction was run in 5/1 mixture of toluene/DMF at 85 °C at a concentration of 3.8×10^{-3} M. A toluene solution of precursor **4-8** was added slowly to the activated Ni^0-complex to ensure pseudo high-dilution conditions. In order to keep the Ni^0-complex active during the addition period which usually lasted for 1 hour, it was essential to exclude oxygen from the reaction system. This was achieved by a slight argon counterflow through the *Schlenk* flask in the course of the addition. Monitoring the reaction by thin-layer chromatography and FD-MS indicated full consumption of **4-8** after 24 hours reaction time. The reaction was, however, allowed to proceed for further 24 hours in the dark and was quenched by adding dilute hydrochloric acid. Analyzing the crude reaction mixture with MALDI-TOF MS, three major species were observed (Figure 4-7, bottom). The main peaks corresponded thereby to the six-membered macrocycle **4-2** and a nonamer species **4-9**. The third peak could be assigned to the non-functionalized precursor **4-8** as a result of protodehalogenation.

Following preliminary column chromatography to remove inorganic impurities, the
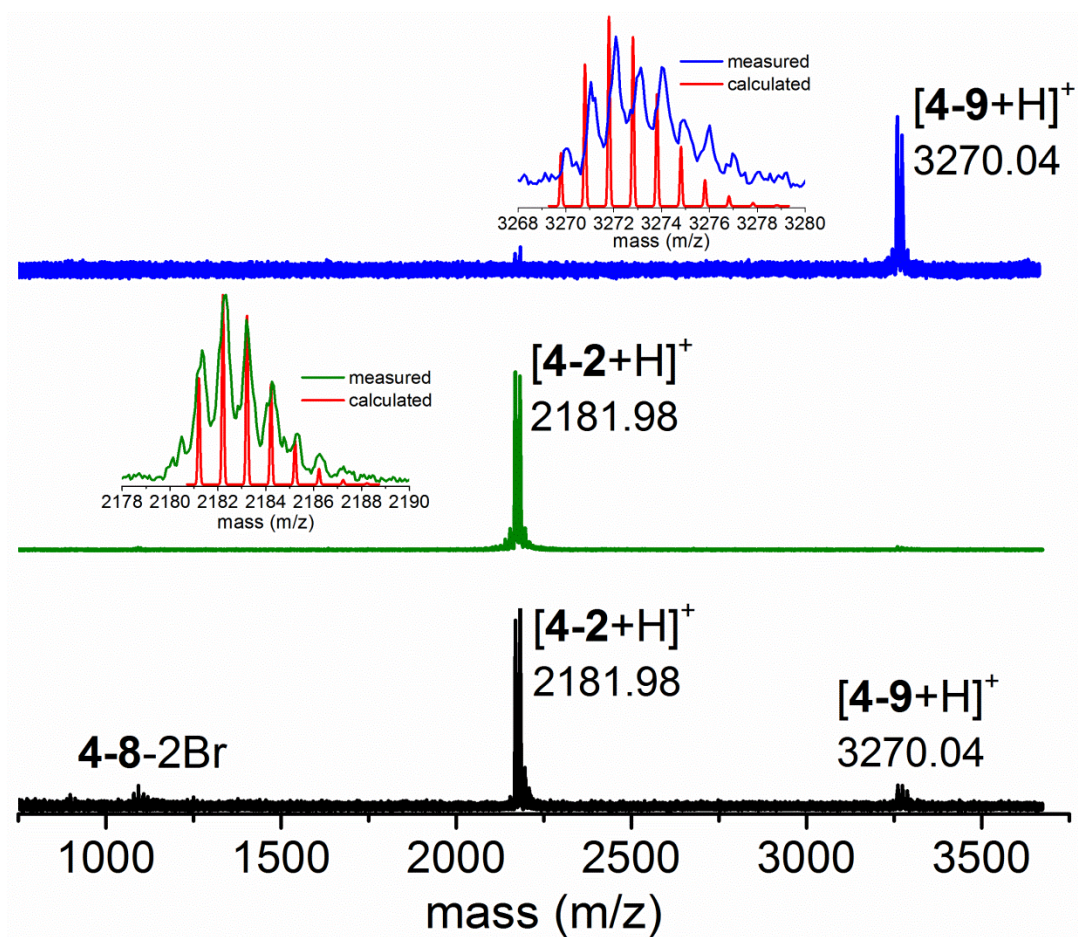
Figure 4-7. MALDI-TOF MS spectra (matrix: dithranol) of the crude reaction mixture of the *Yamamoto* cyclodimerization (bottom, black line), of the purified macrocycle **4-2** (middle, green line) and the purified linear nonamer **4-9** (top, blue line). Inset: Measured and calculated isotopic patterns of **4-2** and **4-9**.

reaction mixture was then subjected to preparative SEC to afford macrocycle **4-2** in 38% yield. The presence of the protodehalogenated precursor and nonamer **4-9** accounted for the moderate yield of the macrocyclization. They were, however, removed with the help of preparative SEC leading to **4-9** in 15% yield. The reaction mechanism discussed for dibromo *N*-heterotriangulene **4-1** can be similarly expected for the cyclodimerization of **4-8**. But as a result of the preorganized geometry of **4-8** (the monomer main axes differ for each *N*-heterotriangulene unit by 60°) and the reduced number of bond formations (one *inter-* and one *intra*molecular C−C bond formation), the yield of the macrocyclization could thus be increased allowing the preparation of **4-2** in an overall reasonable yield (12.4% over four steps) on a several hundred milligram scale.

4.2.3.1   *Characterization of the N-Heterotriangulene Macrocycle*

Macrocycle **4-2** forms a pale yellow solid that is stable at ambient temperature under air and soluble in most organic solvents, thus enabling its characterization by methods such as MALDI-TOF MS and NMR spectroscopy.
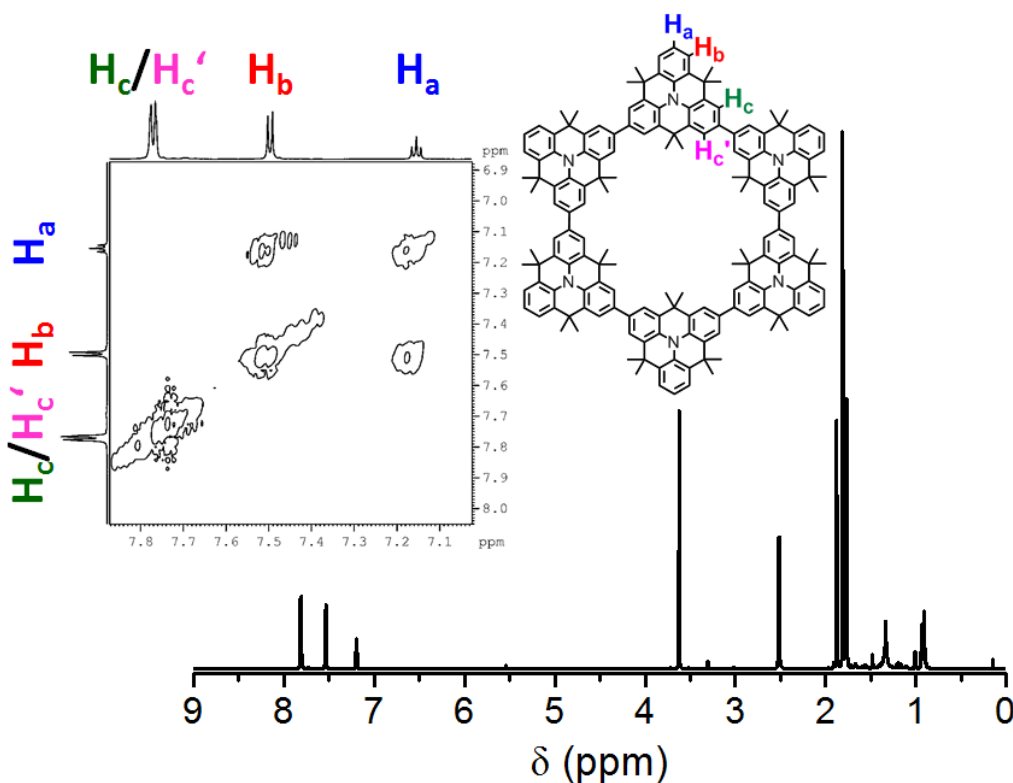
Figure 4-8. ^{1}H NMR spectrum of *N*-heterotriangulene macrocycle **4-2** in THF-d$_8$ at 25 °C. Inset: Two-dimensional proton correlation (^{1}H, ^{1}H COSY) of **4-2** with proton assignment.

MALDI-TOF MS clearly indicates the successful formation of the macrocycle with a targeted mass of 2181.98 g/mol, which was desorbed as a [M+H]$^+$ species (Figure 4-7, middle). It reveals furthermore the linear nature of nonamer **4-9** with *m/z* = 3270.04 (Figure 4-7, top). Besides the [M+H]$^+$ peak, the scisson of methyl groups depending on the power of the applied desorption laser, was observed for both compounds. The identity of **4-2** was additionally confirmed by HR ESI MS with a single signal at *m/z* = 2180.2009 (C$_{162}$H$_{150}$N$_6$, calculated 2180.2000).

The ^{1}H NMR spectrum of **4-2** in THF-d$_8$ at 25 °C is in agreement with the highly symmetric structure of the *N*-heterotriangulene macrocycle (Figure 4-8). Due to the presence of only four sets of aromatic protons with a ratio of 1 to 2 to 4, the signals were readily assigned. Thus, the triplet at 7.20 ppm was ascribed to the protons located at the periphery of the macrocycle (H$_a$). The signal at 7.54 ppm originated from their neighboring
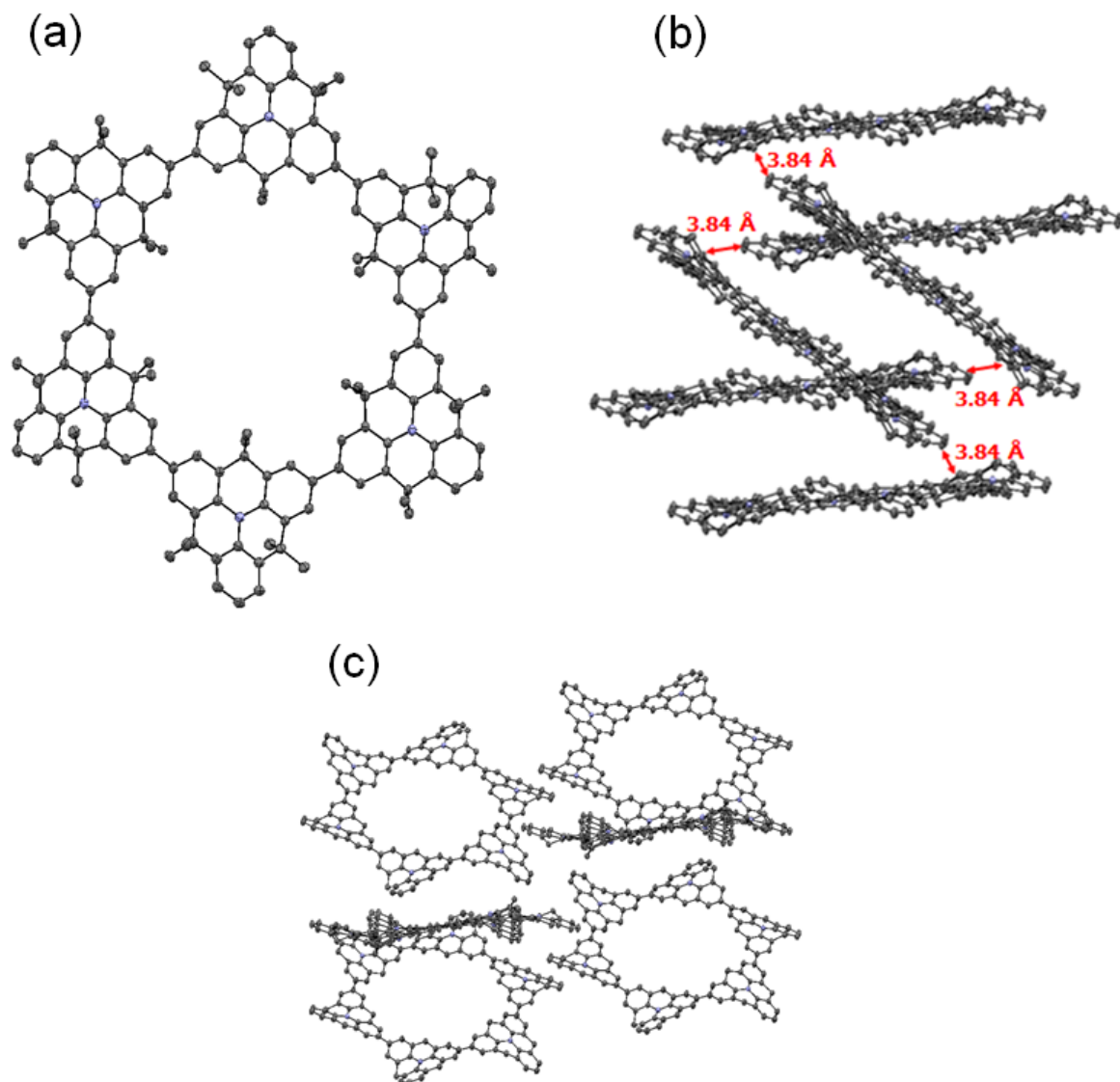
Figure 4-9. X-ray crystal structure of **4-2**. (a) Top view (nitrogen atoms in blue, carbon atoms in grey, hydrogens omitted for clarity). (b) Side view of the unit cell. The red arrows indicate the shortest distance between two macrocycles of 3.84 Å (hydrogens and methyl-groups omitted for clarity). (c) Front view of the asymmetric unit (hydrogens and methyl-groups omitted for clarity).

protons (H_b) giving rise to a doublet by an *ortho*-coupling with H_a. This was furthermore confirmed by a cross peak in the two-dimensional proton correlation (^{1}H, ^{1}H COSY) spectrum (Figure 4-8, inset). In addition, the resonances at 7.81 and 7.82 ppm were identified as two singulets corresponding to the isolated protons in close proximity to the next *N*-heterotriangulene unit (H_c/H_c'). As a result of the rigid conformation of the *N*-heterotriangulene subunits inside the macrocycle, no coupling between H_c and H_c' was observed.

It was further possible to grow single crystals of macrocycle **4-2**, suitable for X-ray diffraction (Figure 4-9). They were obtained by slow diffusion of diethyl ether vapor into a chloroform solution of **4-2**. The analysis clearly confirmed the successful cyclization

(Figure 4-9 a). As a result of the tilted *N*-heterotriangulene units, macrocycle **4-2** shows an overall bent structure with a dihedral angle between the *N*-heterotriangulene subunits ranging from 13.8(9)° to 35.5(4)°. This behavior is caused by the steric repulsion among the 24 *ortho*-protons at the neighboring *N*-heterotriangulene subunits. The nitrogen-centered cores of the six *N*-heterotriangulene moieties are almost planar as obviously no significant pyramidalization of the nitrogen takes place, which was revealed by the sum of the three C−N−C angles (358.4(5)°). Furthermore, the average N−C(sp^2) bond length of 1.43 Å is in the same range as for the unsubstituted *N*-heterotriangulene unit (1.43 Å) and does not differ significantly from that in triphenylamine (1.42 Å).[54] An average distance of 14.09 Å between the dimethylmethylene groups of two opposite *N*-heterotriangulenes was found, which correspondes to the diameter of the inner cavity of the macrocycle. This highlights the potential of **4-2** for the investigation of host-guest interactions by utilizing suitable guest molecules such as fullerenes. The crystal packing of **4-2** is shown in Figure 4-9 b and c. The macrocycle crystallized in the in the centrosymmetric space group C2/*c* as a chloroform solvate (four molecules per unit cell) and contains four independent macrocycles in the unit cell. As a result of the edge-to-face orientation, every second macrocycle is placed parallel to the other (Figure 4-9 b). This led to short distances of 3.84 Å between two rings (Figure 4-9b, red arrows).
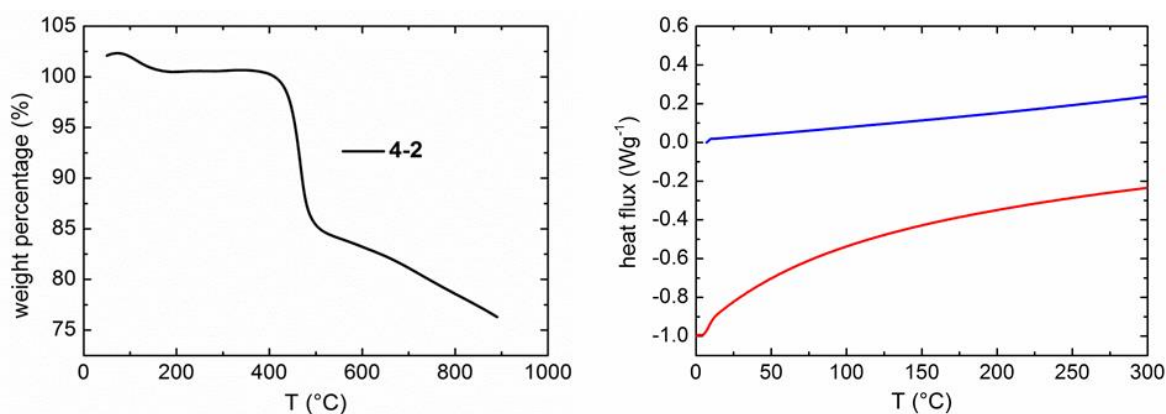

Figure 4-10. Left: Thermogravimetric analysis of *N*-heterotriangulene macrocycle **4-2**. Right: DSC traces of **4-2** applying heating/cooling rates 10 °C/min (red line = heating, blue line = cooling).

Thermal properties of π-conjugated macrocycle **4-2** were investigated with the help of TGA (Figure 4-10, left). It revealed an excellent stability of **4-2** up to 400 °C (decomposition temperature at 5% weight loss is 455 °C). Besides that, the removal of cocrystallized chloroform was observed at around 170 °C. Differential scanning calorimetry (DSC) revealed no phase transitions, confirmed by the absence of a glass transition temperature or any melting or crystallization processes (Figure 4-10, right).

Considering the good solubility of **4-2** in organic solvents such as dichloromethane, THF, toluene or 1,2-dichlorobenzene together with the excellent thermal properties, it shows a reasonable potential for processability and a high durability in optoelectronic devices.

4.2.3.2 *Self-Assembly of the N-Heterotriangulene Macrocycle in the Bulk Phase*

In order to study liquid-crystalline behavior of the *N*-heterotriangulene macrocycle, a synthetic method for the introduction of flexible, long alkyl-arms to **4-2** was aimed. They should theoretically impose discotic properties on the molecule and hence influence the molecular ordering in the solid state. This was shown to be a successful strategy for large phenylacetylene-based macrocycles synthesized by *Höger* and *Moore* as well as for a cyclohexa-*m*-phenylene by *Müllen* and coworkers.[5, 18, 55, 56]
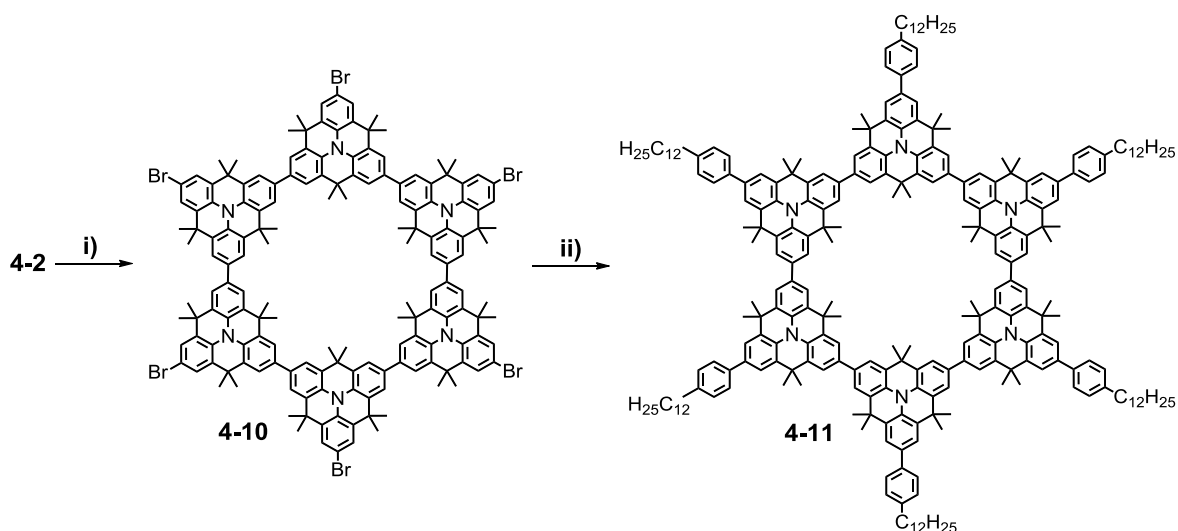

Scheme 4-6. Synthetic route toward alkyl-substituted *N*-heterotriangulene macrocycle **4-11**. Conditions: i) 6 equiv. NBS, CHCl$_3$, 0 °C to RT, 12h, 69%; ii) (4-dodecylphenyl)boronic acid, Pd(OAc)$_2$, 2-dicyclohexylphosphino-2',6'-dimethoxybiphenyl (S-Phos), K$_3$PO$_4$, toluene, H$_2$O, 130 °C, microwave irradiation, 43%.

As a result of the strong electron-donating effect of the central nitrogen in the *N*-heterotriangulene units in macrocycle **4-2**, the peripheral positions, *para* to the nitrogens, are particularly activated for electrophilic aromatic substitutions. By applying the procedure used for the halogenation of **3-4**, macrocycle **4-2** was successfully hexabrominated affording **4-10** in 69% yield (Scheme 4-6). As a result of the decreased solubility of the hexabrominated macrocycle **4-10** in organic solvents, its characterization was limited to mass spectrometry. MALDI-TOF MS revealed the successful bromination by a mass difference of 472, thus confirming that no higher brominated species have been
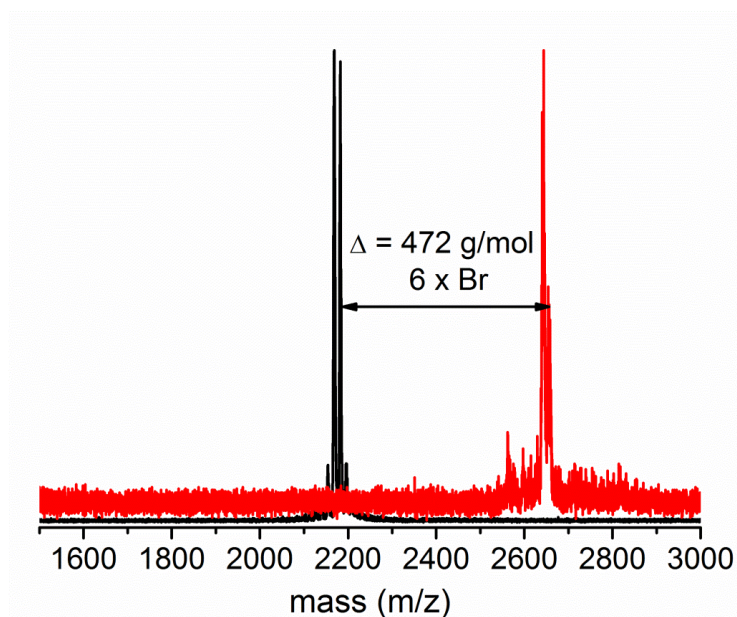
Figure 4-11. MALDI-TOF MS spectra of the hexabrominated macrocycle **4-10** (red line) showing the successful bromination **4-2** (black line, matrix: dithranol).

formed (Figure 4-11). Finally, a sixfold *Suzuki-Miyaura* reaction with **4-10** and (4-dodecylphenyl)boronic acid was conducted. Utilizing tetrakis-(triphenylphosphine)palladium(0) with aqueous sodium carbonate (2 M) as base yielded a complex mixture of three-, four- and fivefold cross-coupling products accompanied by protodehalogenation.
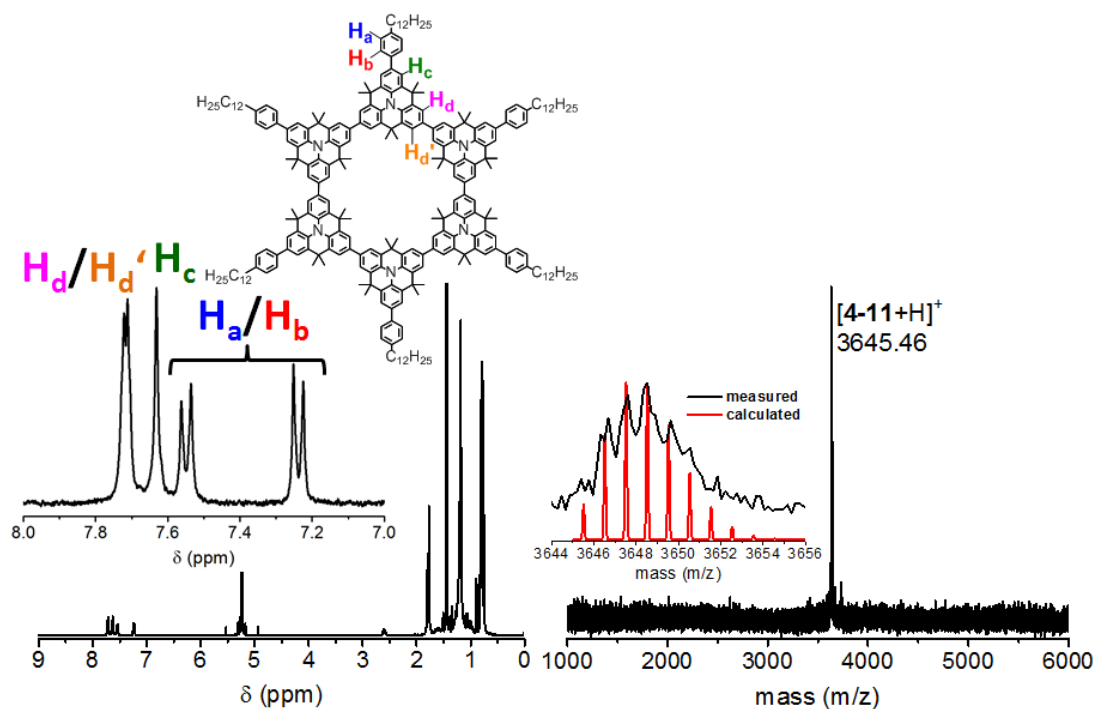
Figure 4-12. Left: ^{1}H NMR spectrum of alkyl-substituted macrocycle **4-11** in CD$_2$Cl$_2$ at 25 °C. Inset: Zoom into the aromatic region with proton assignment. Right: MALDI-TOF MS spectrum of **4-11** (matrix: dithranol).

To enhance the efficiency of the cross-coupling process, *Buchwald*'s ligand 2-dicyclohexylphosphino-2',6'-dimethoxybiphenyl (S-Phos) in combination with palladium(II)acetate was applied.[57-59] To shorten the reaction times, the reaction was carried out under microwave irradiation thus giving **4-11** in reasonable yield (43%) after column chromatographic purification. Characterization with the help of MALDI-TOF MS confirmed the successful formation of **4-11** with a targeted mass of $m/z = 3645.46$, which was desorbed as a [M+H]⁺ species (Figure 4-12, right). The successful attachment of the alkyl moieties was furthermore revealed by a vanished triplet of the peripheral hydrogen atoms, and the presence of an AA'XX' system (7.32 and 7.58 ppm) in the aromatic region of **4-11** ¹H NMR spectrum (Figure 4-12, left).
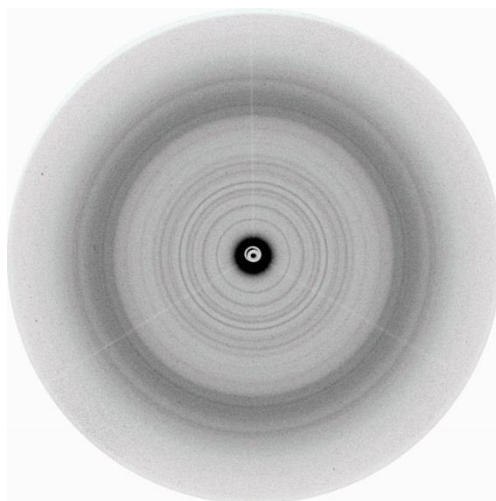

Figure 4-13. 2D WAXS diffraction pattern of an extruded sample of macrocycle **4-11** at room temperature.

The supramolecular organization of macrocycle **4-11** was studied by two-dimensional wide-angle X-ray scattering (2D WAXS) in collaboration with ████████████████ and ████████████████ at the MPI-P Mainz, Germany.[60-63] The patterns were recorded for mechanically extruded fibers obtained by a setup described in Chapter 1.[64] The 2D WAXS pattern of a fiber extruded at room temperature exhibited only anisotropic reflections in the crystalline phase, indicating a poor macroscopic alignment of the macrocycle **4-11** (Figure 4-13). The material differed distinctly from other π-conjugated macrocycles such as cyclo-2,7-dodeca-carbazole and cyclo-7,10-tris-triphenylenes, which were much higher oriented and better organized.[12, 21, 62, 63] This behavior can be mainly attributed to the perpendicular oriented dimethylmethylene groups located at the sp³-hybridzed carbon bridges of the *N*-heterotriangulene building blocks. They are hampering the π-π-stacking of the cycles and hence the tendency for self-organization into columnar superstructures. By replacing the dimethylmethylene groups with heteroatoms, *e.g.*,

nitrogen and sulfur or by sp^2-hybridized carbonyl groups these drawbacks can be overcome, making the respective macrocycles more relevant for potential applications such as ion selective channels or conducting wires.

4.2.4   Expansion of the *N*-Heterotriangulene Macrocycle

In the above part, the successful synthesis of *N*-heterotriangulene macrocycle **4-2** was described. As a logic consequence, a solution-based expansion of macrocycle **4-2** was aimed to gain further insights into the macroscopic properties of the *N*-heterotriangulene honeycomb fragments of the 2D polymer obtained on a Ag(111) surface.[33]
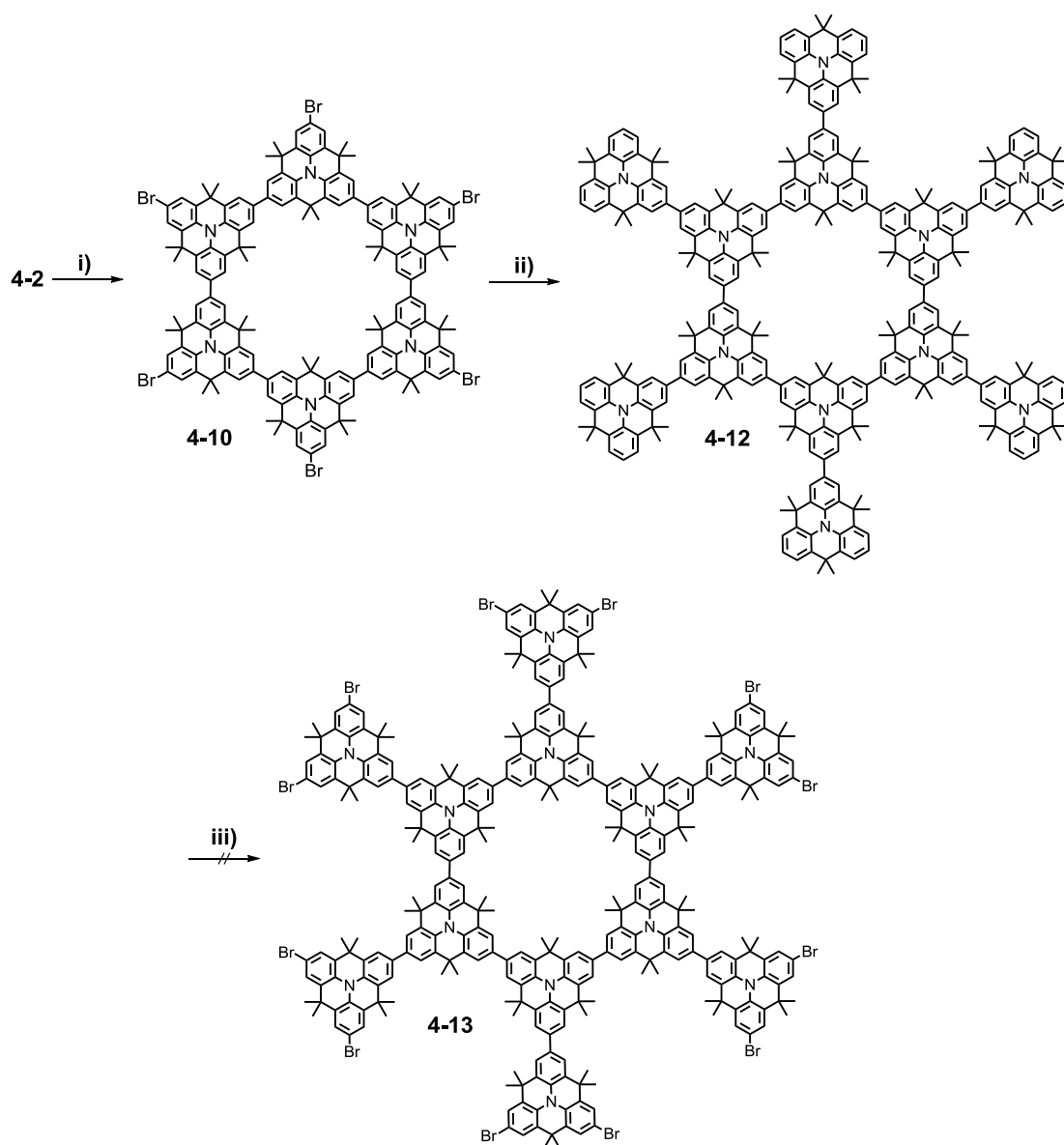
Scheme 4-7. Synthetic route toward the first-generation expanded macrocycle **4-12** and its bromination attempt. Conditions: : i) 6 equiv. NBS, CHCl$_3$, 0 °C to RT, 12h, 69%; ii) **4-5**, Pd(OAc)$_2$, 2-dicyclohexylphosphino-2',6'-dimethoxybiphenyl, K$_3$PO$_4$, toluene, H$_2$O, 130 °C, microwave irradiation, 24h, 38%; iii) 12 equiv. NBS, CHCl$_3$, 0 °C to RT, 12h.
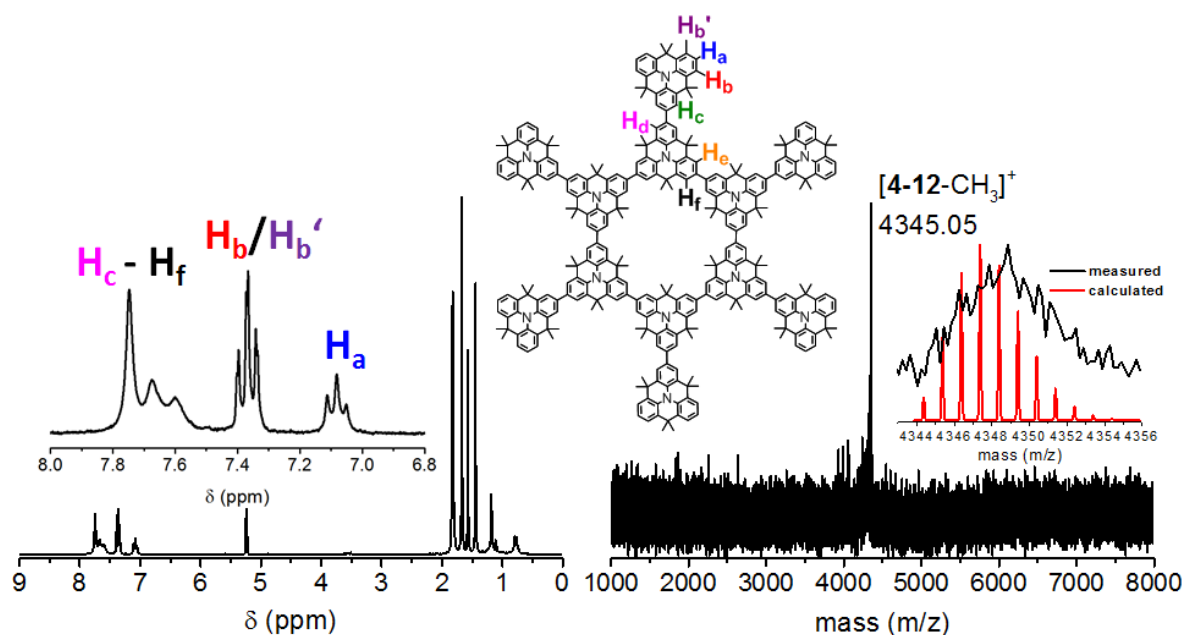
Figure 4-14. Left: ^{1}H NMR spectrum of first-generation expaneded macrocycle **4-12** in CD$_2$Cl$_2$ at 25 °C. Inset: Zoom into the aromatic region with proton assignment. Right: MALDI-TOF MS spectrum of **4-12** (matrix: DCTB).

The hexabrominated macrocycle **4-10** is a versatile precursor which can be further utilized for the generation of dendritic extensions based on macrocycle **4-2**. For this purpose, monoboronate **4-5** was reacted with **4-10** in a sixfold *Suzuki-Miyaura* reaction utilizing palladium(II)acetate together with S-Phos as ligand under microwave irradiation (Scheme 4-7).[57-59] Purification was achieved with the help of repeated column chromatography affording first-generation expanded macrocycle **4-12** in a good overall yield (26% overall yield over two steps from **4-2**). The successful attachment of the six additional *N*-heterotriangulene units was confirmed with MALDI-TOF MS showing the molecular peak of **4-12** with one bridging methyl group missing (Figure 4-14, right); a common feature for these compounds. However, HR ESI MS unambiguously confirmed the formation of **4-12** with a signal of the doubly charged species at *m/z* = 2179.19483 (C$_{323}$H$_{298}$N$_{12}$, calculated 2179.19165). Due to the symmetric structure of **4-12**, four sets of aromatic protons were found in the ^{1}H NMR spectrum (Figure 4-14, left). The signals could be assigned in a straightforward way to the respective protons upon integration. The signal at 7.12 ppm corresponds thereby to the peripheral *para*-protons (H$_a$) giving rise to a triplet. Due to the similar chemical environment of the adjacent protons (H$_b$/H$_b$'), two almost identical doublets were obtained at 7.44 and 7.47 ppm caused by the *ortho*-coupling with H$_a$. The remaining aromatic protons coincide in a broad multiplet at 7.70 ppm. The ratio between

the obtained aromatic signals corresponds to the aliphatic signals due the methyl groups (1.0 to 2.6).

For further expansion, **4-12** was subjected to the bromination procedure utilized in the previous steps to functionalize the 12 peripheral *para*-positions toward **4-13** (Scheme 4-7). Analyzing the reaction mixture by MALDI TOF MS revealed, however, a broad distribution between *m/z* 4 500 and 7 500 (*m/z* = 5 293 for $C_{324}H_{288}Br_{12}N_{12}$), which suggested a complex mixture of higher brominated species despite the slow addition of NBS at 0 °C. This observation might be attributed to an additional activation of the *N*-heterotriangulene subunits as due to an increased electron density at the non-substituted positions, thus making **4-12** inappropriate for further extensions upon selective peripheral functionalization.

Hence, the strategy was varied to a divergent approach, comprising the synthesis of a geometrically well-defined branch followed by subsequent fusion with the macrocyclic core (Scheme 4-8). This reduces the cross-coupling steps for the formation of the dendronized species (6 instead of 12) on the one hand, but requires additionally a multi-step synthesis of the branch (**4-16**).

The reaction sequence started with an unsymmetrical functionalization of *N*-heterotriangulene **3-4** referring to the previous methods. After mono-bromination of **3-4**, diiodination was readily achieved using a mixture of potassium iodide and potassium iodate in acetic acid. The subsequent *Suzuki-Miyaura* coupling with mono-boronate **4-5** was selectively carried out at 65 °C utilizing aqueous sodium carbonate (2 M) as base and tetrakis(triphenylphosphine)palladium(0). The reaction was accompanied by the formation of an undesired star-shaped tetramer caused by a simultaneous attack of the bromine atom at the applied temperature. After column chromatographic separation and recrystallization from ethanol the tetramer was successfully removed, thus affording **4-15** in 43% yield. Subsequent *Miyaura*-borylation using bis(pinacolato)diboron resulted in the targeted trimer **4-16** in 56% yield. The final sixfold *Suzuki-Miyaura* reaction with the macrocyclic core **4-10** was anticipated to proceed slowly due to the increased steric demand of **4-16**. Therefore, *Buchwald's* S-Phos ligand was again utilized together with palladium(II)acetate and potassium phosphate as base under microwave irradiation.[57-59] Monitoring the conversion by thin-layer chromatography and MALDI-TOF MS, full consumption of **4-10** was revealed after 24 hours. Besides dehalogenated macrocycle **4-2** and deborylated trimer **4-16**, a weak signal at around *m/z* = 8 800 was detected corresponding to the molecular weight of second-generation expanded macrocycle **4-17** (*m/z* = 8 723 for $C_{648}H_{600}N_{24}$).
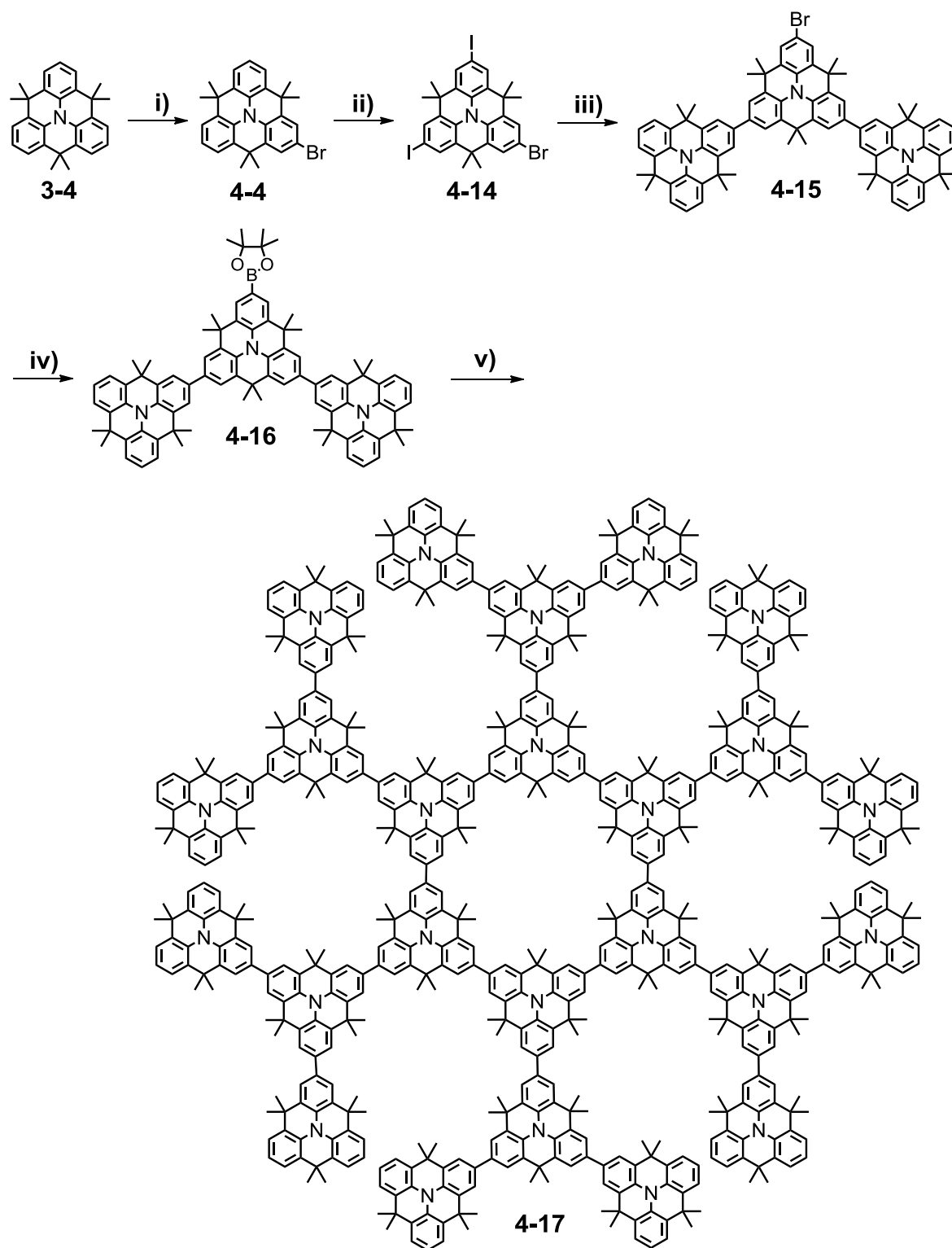
Scheme 4-8. Synthetic route toward second-generation expanded macrocycle **4-17** *via* a divergent synthesis. Conditions: i) 1 equiv. NBS, CHCl$_3$, 0 °C to RT, 2h, 90%; ii) KI, KIO$_3$, CH$_3$COOH, 85 °C, 2h, 93%; iii) **4-5**, Pd(PPh$_3$)$_4$, 2 M aq. Na$_2$CO$_3$, toluene, *Aliquat 336*, 65 °C, 4 days, 43%; iv) Pd(dppf)Cl$_2$, KOAc, bis(pinacolato)diboron, DMF, 85 °C, 12h, 56%; v) **4-10**, Pd(OAc)$_2$, 2-dicyclohexylphosphino-2',6'-dimethoxybiphenyl (S-Phos), K$_3$PO$_4$, toluene, H$_2$O, 130 °C, 24h, microwave irradiation, 18%.
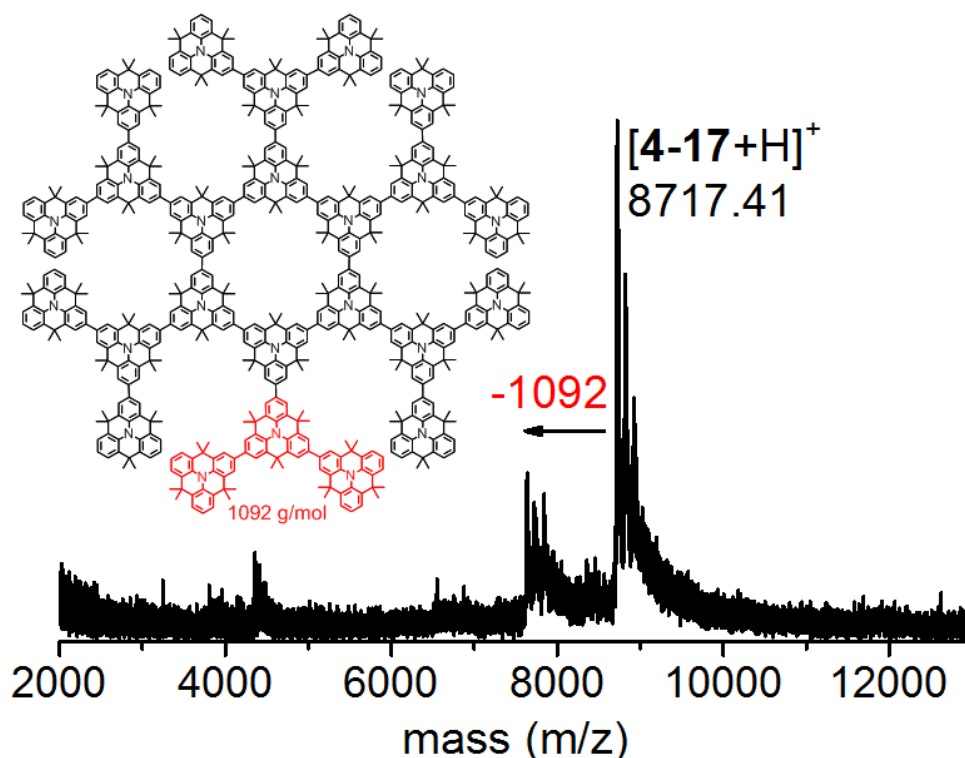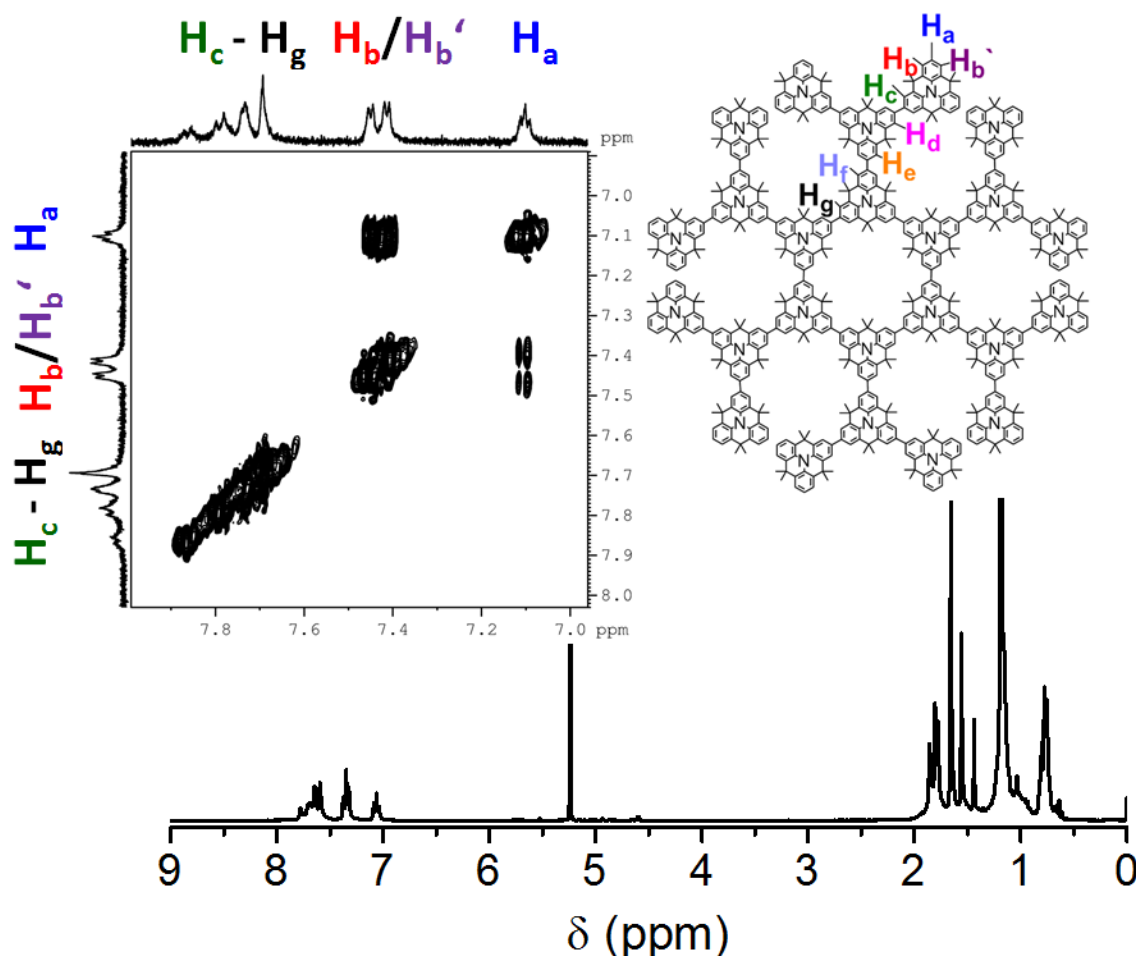
Figure 4-15. MALDI-TOF MS spectrum of second-generation expanded macrocycle **4-17** (matrix: DCTB).

As a result of strong interactions of the overall 24 nitrogen atoms of **4-17** with silica, standard column chromatography was not feasible for the separation of the reaction mixture. Due to large differences in the molecular weight and the hydrodynamic radius between **4-17** and the byproducts, preparative SEC was the suitable purification method. Macrocycle **4-17** eluted at first, followed by macrocycle **4-2** and the unsubstituted trimer, thus affording second-generation expanded macrocycle **4-17** in 18% yield after final precipitation from methanol.

MALDI-TOF MS confirmed the successful formation of **4-17** (Figure 4-15). Besides the $[M+H]^+$ peak, additional matrix adducts were observed. The power of the applied desorption laser led, as expected, to the cleavage of methyl groups. Besides these measurement artifacts, an additional peak at $m/z = 7\,625$ was observed which corresponds to a fivefold substituted macrocyclic core. Mass spectrometry, however, did not figure out if this peak occurred as a result of an incomplete cross-coupling process or as a partial cleavage during the laser induced ionization process. The identification by HR ESI MS, however, was not feasible due to a decreased ionization tendency of **4-17**.

The structure was unambiguously proven with the help of NMR spectroscopy. One-dimensional ^{1}H NMR spectroscopy resulted in a well resolved spectrum due to the regular shape of **4-17** (Figure 4-16). Thus, four sets of aromatic protons with a ratio of 1 to 2 to 2

Figure 4-16. ^{1}H NMR spectrum of second-generation expanded macrocycle **4-17** in CD$_2$Cl$_2$ at 25 °C. Inset: Two-dimensional proton correlation (^{1}H, ^{1}H COSY) of **4-17** with proton assignment.

to 8 were found. With the help of two-dimensional proton correlation (^{1}H, ^{1}H COSY) NMRspectroscopy, the signals could be assigned to the respective protons (Figure 4-16, inset). In analogy to compounds **4-2** and **4-12**, a clearly separated triplet at 7.06 ppm was observed, referring to the peripheral protons (H$_a$). As a result of the *ortho*-coupling with the neighboring protons, a cross peak is obtained between the triplet and the two doublets at 7.42 and 7.45 ppm. This identified both signals as the *meta*-protons H$_b$ and H$_b$'. The sixfold attachment of the trimer **4-16** to the macrocyclic core was consequently verified. In the presence of a smaller fragment, further signals were expected giving rise to additional cross peaks. The broad multiplet at 7.64 ppm was assigned with the help of the integrals and the absence of additional cross peaks to the remaining internal protons allowing no coupling with H$_a$, H$_b$ and H$_b$'. Moreover, correct signal intensities between the aromatic protons and the aliphatic methyl protons (1.0 to 2.6) were observed.

The large size and amorphous nature of first- and second-generation expanded macrocycles **4-12** and **4-17** did not allow for the growth of single crystals suitable for X-ray diffraction. This confirms furthermore the existence of conformational isomers. Both

compounds showed, however, a high stability over several months under ambient temperature and in the presence of light and oxygen. The good solubility of both macrocycles in organic solvents, for example, dichloromethane, THF, toluene or 1,2-dichlorobenzene enabled their photophysical and electronic characterization and, thus, the comparison with the macrocyclic core **4-2** (see below).

4.2.5 *N*-Heterotriangulene "Heptacycle"

The applied solution-based syntheses led to the successful expansion of macrocycle **4-2** toward first- and second-generation macrocycles **4-12** and **4-17**, monodisperse molecules consisting of 324 and 648 carbon atoms, respectively. In addition, macrocycle **4-17** can be considered as an "open" form of a section of the previously reported hyperbranched polymer **P2**.[33] By closing six additional *intra*molecular C−C bonds between the peripheral branches in **4-17**, a planarized molecule consisting of seven *N*-heterotriangulene macrocycles (**4-19**) is obtained (Scheme 4-9, the crucial bonds are highlighted in red). Due to its zig-zag edge structure, **4-19** can be considered as a nitrogen-substituted "supercoronene" and will be denoted in the following as "heptacycle". In contrast to oligophenylene precursors being planarized by an *intra*molecular cyclodehydrogenations in the presence of Lewis acids, which is widely referred as the *Scholl* reaction,[65-68] the crucial C−H positions in **4-17** are not in close spatial contact. To overcome this drawback, a functionalization of the positions, *para* to the central nitrogen, was aimed thus enabling the utilization of cross-coupling reactions for the *intra*molecular bond formation. It is important to note, that thereby the peripheral branches have to be forced into close proximity to allow the C−C bond formation under the applied reaction conditions.

The planarization toward "heptacycle" **4-19**, required a precursor (**4-18**) with 12 halogen atoms at the periphery. The crucial bromine atoms are highlighted in red in Scheme 4-9. By considering that 24 *para*-positions are in total available, perhalogenation was an unavoidable consequence. For this purpose, macrocycle **4-17** was reacted under the standard bromination conditions by adding 24 equivalents of NBS at 0 °C to minimize higher brominated species. The reaction progress was monitored with the help of mass spectrometry. After running the reaction for four days at room temperature, the MALDI-TOF MS revealed the consumption of the starting material together with a broad distribution between $m/z = 9\,000-13\,000$ (Figure 4-17, bottom). Besides target compound **4-18** ($m/z = 10\,531$ [M-4·CH$_3$]$^+$ for C$_{644}$H$_{586}$Br$_{24}$N$_{24}$) the presence of a broad variety of brominated species was concluded.
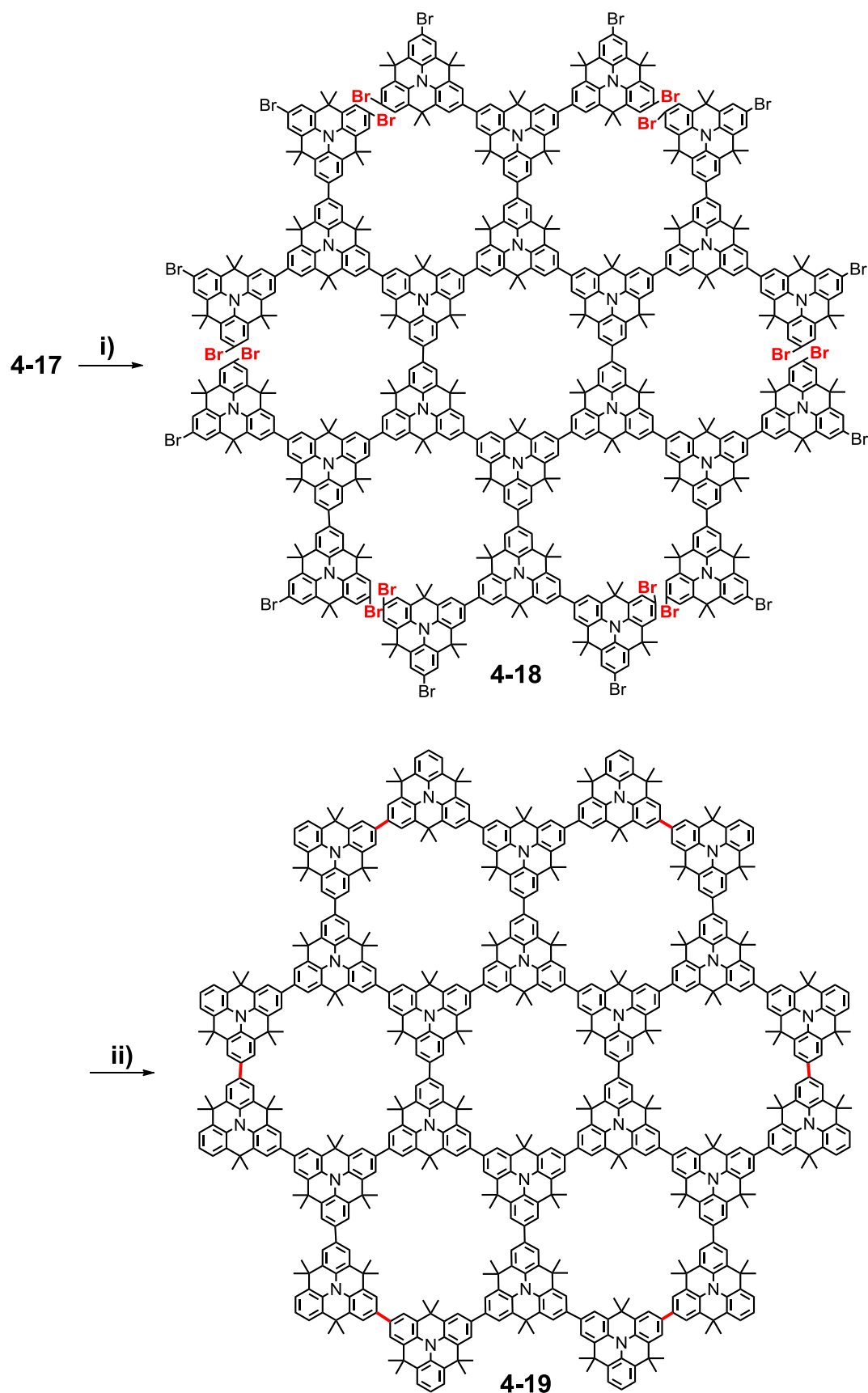
Scheme 4-9. Synthetic route toward the "heptacycle" **4-19**. The crucial bromines and C−C bonds are highlighted in red. Conditions: 24 equiv. NBS, CHCl₃, 0 °C to RT, 4 days; ii) bis(cycloocta-1,5-diene)nickel(0), cycloocta-1,5-diene, 2,2'-bipyridine, toluene/DMF, c = 3.1 × 10⁻³ M, 85 °C, 4 days.
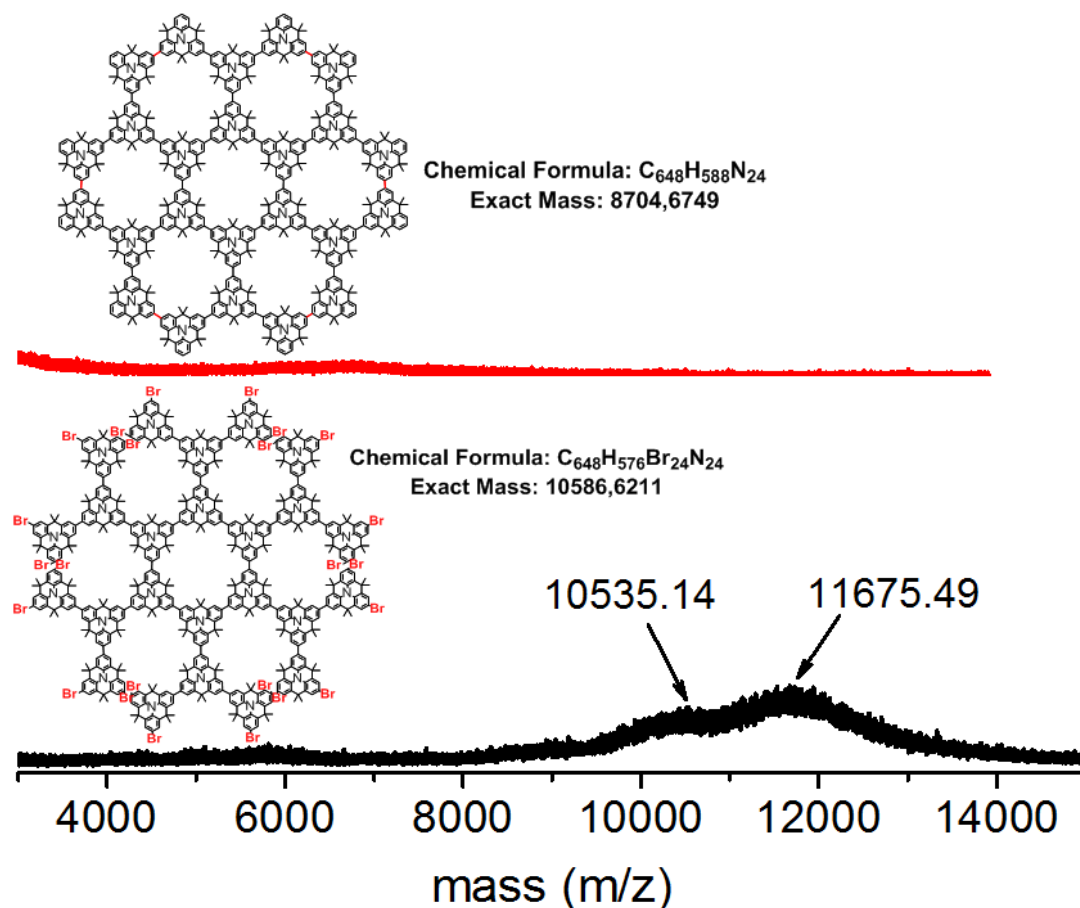
Figure 4-17. MALDI-TOF MS spectra obtained after the bromination of **4-17** (matrix: DCTB, bottom, black line) and after the *Yamamoto* cyclization attempt (matrix: DCTB + Ag⁺, top, red line).

This observation is in agreement with the results of the bromination attempts of first-generation expanded macrocycle **4-12**. As a result of the decreased solubility of the mixture, the separation of **4-18** and the higher brominated species was not feasible. Hence, the complex mixture was used for the cyclization attempt. Again, the *Yamamoto* reaction appeared to be ideally suited for the respective cyclization. It enables within one reaction the *intra*molecular C−C bond formation toward targeted heptacycle **4-19** as well as the removal of the excess bromines by protodehalogenation.[38, 53] By setting the concentration of the reaction to 3.1×10^{-3} M, the *intra*molecular bond formation was expected to be favored and an *inter*molecular connection suppressed. The reaction was run in a 3/2 mixture of toluene/DMF and the precursor mixture was slowly added to the activated Ni⁰-complex to ensure pseudo high-dilution conditions referring to the previous cyclization attempts (see above). After four days at 85 °C, the reaction was quenched by the addition of diluted hydrochloric acid. Upon preparative SEC of the crude material, a highly fluorescent fraction was obtained in a small amount. It was subjected to MALDI-TOF MS
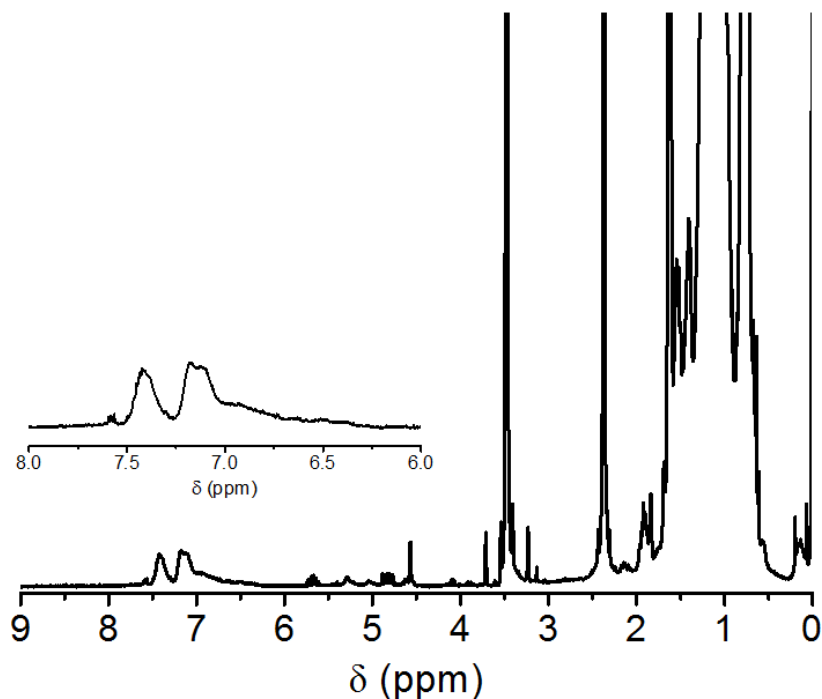
Figure 4-18. ^{1}H NMR spectrum of a fraction obtained after the *Yamamoto* cyclization attempt in THF-d$_8$ at 60 °C.

utilizing a broad variety of matrices, such as 1,8-dihydroxy-10*H*-anthracen-9-on (dithranol), 7,7,8,8-tetracyanoquinodimethane (TCNQ) and *trans*-2-[3-(4-*tert*-butylphenyl)-2-methyl-2-propenylidene]malononitrile (DCTB) in combination with various additives, *e.g.*, sodium iodide and silver nitrate. However, all combinations resulted in similar spectra, revealing neither the presence of molecular peaks of **4-19** nor **4-17** or any other non-cyclized derivatives (Figure 4-17, top). NMR measurements of the fraction were conducted in CD$_2$Cl$_2$ and THF-d$_8$ both at room and elevated temperatures. The presence of "heptacycle" **4-19** was expected to result in a clearly separated triplet in combination with two doublets for the peripheral protons and a multiplet for the residual internal protons. The spectra, however, revealed no distinct signals and a significant broadening in the aromatic region. This suggested the presence of a complex mixture of different macrocyclic species giving rise to the signal broadening (Figure 4-18). A successful formation of "heptacycle" **4-19** was expected to comprise six *intra*molecular coupling steps followed by twelve protodehalogenations of the residual bromines. From pure counting statistics, these *intra*molecular connections can be similarly considered as the solution-based macrocyclization of dibromo *N*-heterotriangulene **4-1** (see above). The additional bromine atoms intrinsically increase the probability of *intra*molecular connections, however, they raise simultaneously the probability of an *inter*molecular bond formation to a second molecule. It is very likely that this resulted in the formation of

different species with various combinations of closed and opened bonds. Moreover, an incomplete protodehalogenation process could increase the amount of possible derivatives of **4-19**. These molecules were expected to have an almost identical hydrodynamic radius accompanied by a similar adsorption behavior, hampering the separation by both preparative SEC and standard column chromatography. The analysis of these different species is furthermore limited by a surprisingly low ionization tendency under the applied mass spectrometry methods.

Due to the fact that only a complex mixture of different species was obtained, a careful analysis of the photophysical and electronic properties of **4-19** was impeded.

4.3 Photophysical and Electronic Properties of the *N*-Hetero-triangulene Macrocycles

4.3.1 UV-vis Absorption and Emission Properties

From a historic point of view, triarylamines have always been associated with their excellent characteristics in optoelectronic devices as a result of their electronic and morphological properties. Therefore, the investigation of the absorption and emission behavior of the new *N*-heterotriangulene macrocycles is of high interest with respect to their potential applications as hole-transport materials.[69-75]
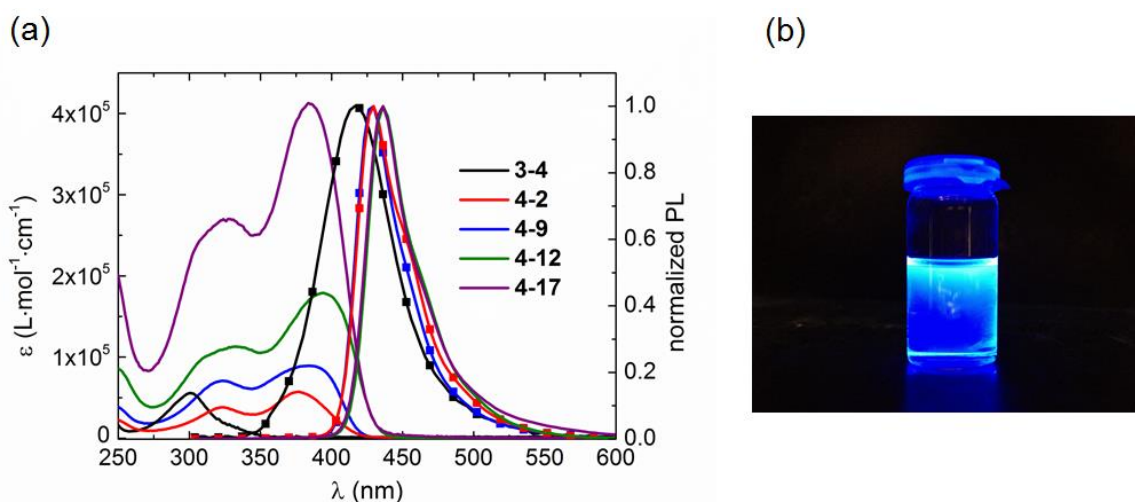
Figure 4-19. (a) UV-vis absorption (solid line) and emission (symbol line) spectra of **3-4** (black), **4-2** (red), **4-9** (blue), **4-12** (green) and **4-17** (violet). For all spectra: 1×10^{-6} M in CH_2Cl_2. (b) Photograph showing the luminescence of macrocycle **4-2** ($\lambda_{exc} = 365$ nm).

UV-vis absorption and emission properties of **4-2**, **4-12** and **4-17** were investigated in dichloromethane and compared to the data of the monomeric model compound **3-4** and the linear nonamer **4-9**. To ensure comparability, the concentration in all experiments was set

to 1×10^{-6} M. All spectra are depicted in Figure 4-19 and the obtained values are listed in Table 4-1.

Large optical band gaps (E_g^{opt}) of 2.87 to 3.59 eV were found for all compounds as a result of their eletron-rich nature. A certain flexibility of macrocycles **4-2**, **4-12** and **4-17** was reflected by the absence of a fine structure in the resulting absorption spectra, in contrast to more rigid PAH macrocycles.[12, 39, 76] Due to an extended π-conjugation in **4-2**, **4-9**, **4-12** and **4-17**, the corresponding absorption maxima at the longest wavelength are bathochromically shifted by 76 to 93 nm in comparison with *N*-heterotriangulene **3-4**. This led to a decrease of the E_g^{opt} of up to 0.72 eV caused by an enhanced electron-donating character of **4-2**, **4-9**, **4-12** and **4-17**, which raises the HOMO level.

Table 4-1. Selected photophysical data of **3-4**, **4-2**, **4-9**, **4-12** and **4-17**.

	$\lambda_{abs,max}$ [a] (nm)	$\lambda_{PL,max}$ [a,b] (nm)	$\varepsilon \times 10^{4}$ [a,c] (M^{-1} cm^{-1})	Stokes shift (cm^{-1})	E_g^{opt} [d] (eV)	Φ_{PL} [a,e]
3-4	301	416	5.6	9 180	3.59	0.02
4-2	324, 377	430	5.7	3 270	2.96	0.89
4-9	312, 383	430	8.9	2 850	2.95	0.87
4-12	333, 394	436	17.9	2 440	2.87	0.79
4-17	324, 384	436	41.2	3 110	2.91	0.53

[a] For all spectra: 10^{-6} M in CH$_2$Cl$_2$. [b] Excited at the absorption maxima. [c] Extinction coefficients of the lowest energy absorption band. [d] $E_g^{opt} = h \cdot c / \lambda_{0.1max}$ [e] Absolute PL quantum yields, uncorrected with respect to reabsorption.

The impact of the π-conjugated cyclic arrangement of six *N*-heterotriangulenes is seen in the absorption spectrum of unsubstituted **4-2**. Compared to the absorption spectrum of pristine *N*-heterotriangulene **3-4**, macrocycle **4-2** exhibited two absorption bands at 324 and 377 nm, respectively. The longest-wavelength absorption was thereby assigned to a π−π* transition of the whole π-conjugated macrocycle.[73-75] Concentration-dependent absorption spectra in the range between 2×10^{-4} and 1×10^{-6} M showed a linear relationship of the concentration and the absorbance, indicating no significant self-assembly at these conditions. This is contrast to other π-conjugated macrocycles and can be attributed again to the tetrahedral dimethylmethylene bridging units of the *N*-heterotriangulenes hampering π−π-stacking.[5, 21]

By expanding the macrocycle toward **4-12** and **4-17**, the absorption maxima of the longest wavelength transition are shifted by about 17 and 7 nm, respectively, followed by a gradually increased extinction coefficient of 179 000 to 412 000 M^{-1} cm^{-1}. These remarkable values can be attributed to the connection of 12 and 24 chromophores in

macrocycles **4-12** and **4-17**, respectively. As a result of reduced π-conjugative interactions of the macrocyclic core with the trimeric branches, a hypsochromic shift of the longest wavelength absorption maxima is observed in **4-17** compared with **4-12**. This behavior can be assigned to a significant twisting between the sterically demanding trimeric branches and the central unit in **4-17**. The linear oligomer **4-9** featured similar absorption bands at 312 and 383 nm, respectively. The slight bathochromic shift of the absorption maximum at the longest wavelength transition compared with **4-2** can be attributed to an extended π-conjugation of the nine covalently bound *N*-heterotriangulenes and a more flexible conformation of nonamer **4-9**.

The photoluminescence properties of the compounds were subsequently studied to further investigate the correlation between macrocycles **4-2**, **4-12** and **4-17** with their building unit **3-4** and the linear counterpart **4-9**. A weak emission was observed for pristine *N*-heterotriangulene **3-4** at 416 nm without a significant fine structure. The fluorescence spectrum of unsubstituted macrocycle **4-2** showed a symmetric emission at 430 nm. This is in the same range as the linear oligomer **4-9** ($\lambda_{PL,max} = 430$ nm). The comparably large *Stokes* shift of **4-2** (3 270 cm^{-1}) in contrast to **4-9** (2 850 cm^{-1}) can be attributed to a geometrical rearrangement in the excited state caused by a significant planarization of the π-conjugated system of the macrocycle. This is similarly observed for second-generation expanded macrocycle **4-17** ($\lambda_{PL,max} = 436$ nm; 3 110 cm^{-1}) compared with **4-12** ($\lambda_{PL,max} = 436$ nm; 2 440 cm^{-1}).

As discussed previously, macrocycles **4-2**, **4-12** and **4-17** and linear nonamer **4-9** featured strong blue emissions (Figure 4-19 b) which were close to the ideal value for pure blue luminescence between 440 and 450 nm.[39, 77, 78] The macrocyclic arrangement of **4-2**, **4-12** and **4-17** resulted in a significant increase in the photoluminescence quantum yield (PLQY) in comparison with *N*-heterotriangulene **3-4** ($\Phi_{PL} = 0.02$), reaching the maximum of 0.89 for **4-2**. As a result of the effectively broken overall symmetry of the *N*-heterotriangulene subunit by the cyclic π-conjugated configuration of **4-2** and the higher expanded systems **4-12** and **4-17**, the oscillator strength of the emissive transition was enhanced, while the transition energy (emission maxima) was only slightly changed. This value gradually decreased for **4-12** ($\Phi_{PL} = 0.79$) and **4-17** ($\Phi_{PL} = 0.53$) induced by a weakened oscillator strength caused by the twisting between the exterior branches and the macrocyclic backbone.

4.3.2   Electrochemical Properties

Further investigations of the electronic properties of the macrocyclic species were performed by cyclic voltammetry (CV) and rotating-disk voltammetry (RDV) together with DFT calculations. The electrochemical experiments were carried out in collaboration with ████████████████████ at the Université de Strasbourg, France. The analysis was limited to the unsubstituted macrocycle **4-2** and the first-generation expanded macrocycle **4-12** owing to low available quantities of **4-17**.
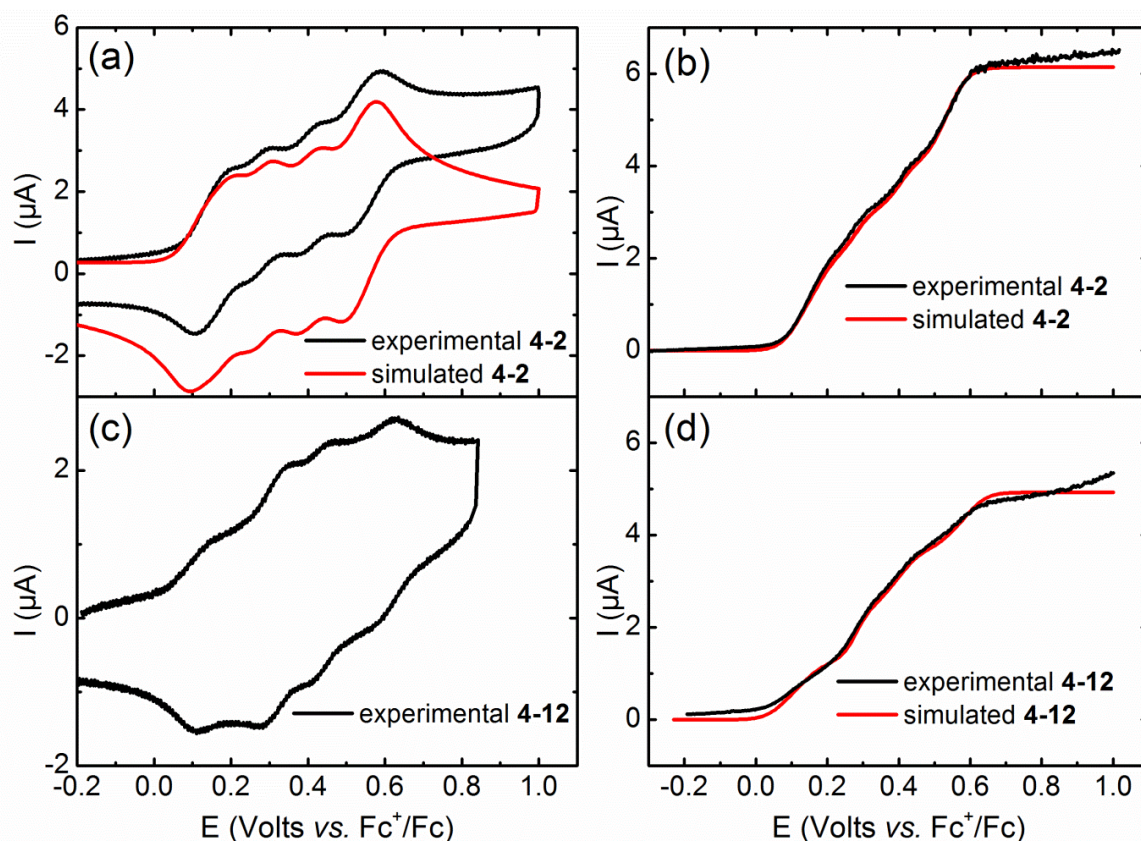
Figure 4-20. (a) Cyclic voltammetry curve of unsubstituted macrocycle **4-2** (scan rate = 0.1 V·s^{-1}, black line) and its simulation using DigiElch v 6F (red line).[80] (b) Rotating disc voltammetry curve of **4-2** (1000 rev·s^{-1}, black line) and its simulation using Digisim (v 3.03b, red line).[81] (c) Cyclic voltammetry curve of first-generation expanded macrocycle **4-12** (scan rate = 0.1 V·s^{-1}). (d) Rotating disc voltammetry curve of **4-12** (1000 rev·s^{-1}, black) and its simulation using Digisim (v 3.03b, red line).[81] For all spectra: in CH$_2$Cl$_2$ + 0.1 M *n*-Bu$_4$NPF$_6$, potentials are given *vs.* ferrocene, used as internal standard.

To ensure comparability of the results, the experiments were performed under identical conditions using 1×10^{-3} M solutions of the analyte in anhydrous dichloromethane and under argon atmosphere with *n*-Bu$_4$NPF$_6$ as conductive salt. Ferrocene has been always added at the end of the studies as internal standard.[79] Digital simulation of the electron transfers for **4-2** and **4-12** were carried out using the DigiElch software for CV studies and

Table 4-2. Selected electronic properties of **3-4**, **4-2** and **4-12**.

	$E°_{ox}$ [a] (V)	E_{HOMO} [CV][b] (eV)	E_{LUMO} [c] (eV)	E_g^{opt} [d] (eV)	E_{HOMO}^{cal} [e] (eV)	E_{LUMO}^{cal} [e] (eV)	E_g^{cal} (eV)
3-4	+0.34, +1.36	−5.14	−1.55	3.59	−4.96	−0.11	4.85
4-2	+0.14, +0.26, +0.39, +0.54	−4.94	−1.98	2.96	−4.28	−0.86	3.42
4-12	+0.12, +0.30, +0.41, +0.58	−4.92	−2.05	2.87	−7.42[f]	−0.60[f]	6.82

[a] Redox potentials from CV are reported *vs.* Fc/Fc$^+$ (0.1 M *n*-Bu$_4$NPF$_6$ in CH$_2$Cl$_2$, scan rate 100 mV s^{-1}). [b] HOMO levels were calculated from the measured first oxidation potential. [c] LUMO levels were calculated from the optical band gap E_g^{opt} and the respective HOMO levels. [d] $E_g^{opt} = h \cdot c/\lambda_{0.1max}$. [e] Calculated by DFT/B3LYP/6-31G*. [f] Calculated by semi-empirical/PM3.

the Digisim software for RDV studies.[80, 81] For the analysis, the onset of the respective oxidation wave was used.

The unsubstituted macrocycle **4-2**, with six electroactive *N*-heterotriangulene units, gave well resolved voltammograms showing four fully reversible oxidation steps under the applied measurement conditions (Figure 4-20 a and Table 4-2). This behaviour was furthermore observed by the RDV measurement (Figure 4-20 b). With the peak amplitudes and the limiting currents observed by RDV, it can be shown that the first and fourth oxidations are twice as intense as the second and third. Taking this into account the first oxidation ($E_1° = +0.14$ V) corresponded to a global two-electron transfer, which was identified by the shapes of the CV and RDV curves as an overlapping of two reversible one-electron transfers. The second ($E_2° = +0.26$ V) and third oxidations ($E_3° = +0.39$ V) were reversible one-electron transfers, whereas the fourth oxidation ($E_4° = +0.53$ V) had again the characteristics of two reversible overlapping one-electron transfers. The comparison of the peak amplitudes of **4-2** with the peak amplitude of ferrocene at similar concentration confirmed the given number of electrons exchanged for each electron transfer. These observations were furthermore verified by digital simulations of the CV and RDV output using the DigiElch and the Digisim software.[80, 81] The obtained curves (Figure 4-20 a and b) were in excellent agreement with the measured data. The reversibility of the electron transfers up to six electrons denoted a good stability of the oxidized species of **4-2** at the time scale of cyclic voltammetry.

The CV and RDV investigations of the first-generation expanded macrocycle **4-12** revealed again a well resolved voltammogram showing four reversible oxidations together with the absence of any reduction processes (Figure 4-20 c). The four oxidation steps were furthermore displayed by the respective RDV curve (Figure 4-20 d). Based on the reasonable assumption that all 12 nitrogen-centers of the *N*-heterotriangulene subunits in **4-12** are oxidized, each oxidation step is expected to involve three electrons. As a result of the symmetric nature of macrocycles **4-2** and **4-12**, the exact localization of the electron transfers at the six available *N*-heterotriangulenes could not be determined. It can be supposed, however, that the increasing charge induced by the oxidative electron transfer resulted in electrostatic repulsion, thus explaining the splitting of the oxidation steps in **4-2** and **4-12**. Moreover, the formation of π-π radical cation dimers during the oxidation process can not be excluded.[82] The reasonably decreased first oxidation potentials of **4-2** and **4-12** compared with pristine **3-4**, that is reversibly oxidized at +0.34 V, revealed a moderate communication between the *N*-heterotriangulene subunits. This is further confirmed by the relatively small potential separations.

From the first reversible oxidation potentials of **4-2** and **4-12**, the corresponding HOMO levels were calculated to be −4.94 eV and −4.92 eV, respectively (Table 4-2). This indicated that further attachment of additional *N*-heterotriangulene units to the periphery of macrocycle **4-2** did not significantly alter the ionization potential and which is an important criterion for hole-transport applications in optoelectronic devices. The expansion toward second-generation macrocycle **4-17** and "heptacycle" **4-19** is, therefore, expected to have minor or no significant influence on the respective HOMO levels.
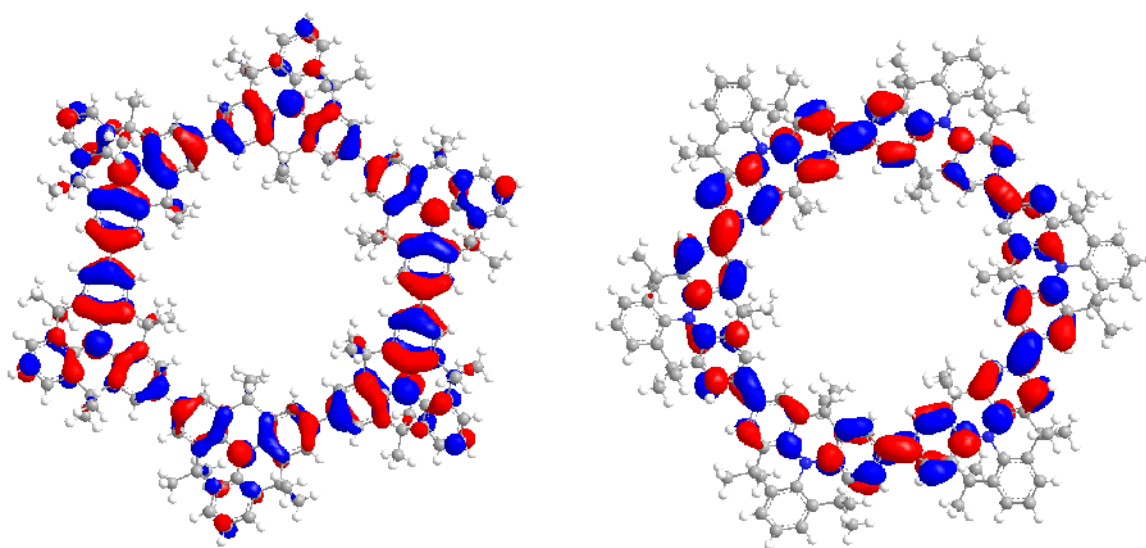
Figure 4-21. Orbital surfaces of the HOMO (left) and LUMO of the unsubstituted macrocycle **4-2** determined by DFT calculation (B3LPY/6-31G*).

DFT calculations (B3LYP/6-31G*) carried out on unsubstituted macrocycle **4-2** revealed a totally symmetric HOMO with contributions of the central nitrogen atoms as well as the internal and exocyclic phenyl rings (Figure 4-21, left). Due to the well matching HOMOs of **4-2** and **4-12** with the work function of metallic gold ($\varphi = -5.1$ eV), the charge carrier injection between the electrode and the organic semiconductor in OFETs and OLEDs could potentially be enhanced thus improving the device performance.[8, 83, 84] Furthermore, from the optical band gap E_g^{opt} and the HOMO level, the respective LUMO levels of macrocycles **4-2** ($E_{LUMO} = -1.98$ eV) and **4-12** ($E_{LUMO} = -2.05$ eV) were estimated. According to the DFT calculation on **4-2**, the LUMO is exclusively located at the bridging benzene rings ($E_{LUMO}^{cal} = -0.86$ eV; Figure 4-21, right). As expected, by extending the macrocyclic core toward **4-12**, the LUMO level remained almost unaffected. The differences in the calculated and the electrochemically measured energy levels can be mainly attributed to characteristics of the DFT calculation and the CV setup. Electrochemical measurements were performed in solution whereas the DFT calculation relates to a single molecule without any interactions with the environment. The oxidation behavior is influenced by interactions with the solvent and the counterions. Geometric changes during oxidation may further explain the differences between the experimental and theoretical results.

4.3.3   Spectroelectrochemical Properties

To further enlighten the redox behavior of *N*-heterotriangulene macrocycle **4-2**, UV-vis spectroelectrochemical measurements were conducted on a thin film of **4-2**. The experiments were carried out in collaboration with ███████████ in the group of ████████████ at the University of Strathclyde Glasgow, United Kingdom.

A dichloromethane solution of **4-2** (1 mg/mL) was drop-casted on top of an indium tin oxide (ITO) slide. The measurements were carried out under argon and in the presence of a solution of *n*-Bu$_4$NPF$_6$ (0.1 M) in anhydrous acetonitrile as supporting electrolyte. The ITO slide was used as the working electrode, a platinum wire as counter electrode and silver wire as the reference electrode. The three electrodes were immersed to a solution of the electrolyte in a sealed quartz glass cuvette. Upon repetitive cycling between 0 to 1000 mV, the UV-vis spectra were recorded between 300 to 900 nm.

The oxidation behavior is shown in Figure 4-22 top. In the potential range of 0 to 500 mV a slight decrease of the longest-wavelength absorption was detected, however, no
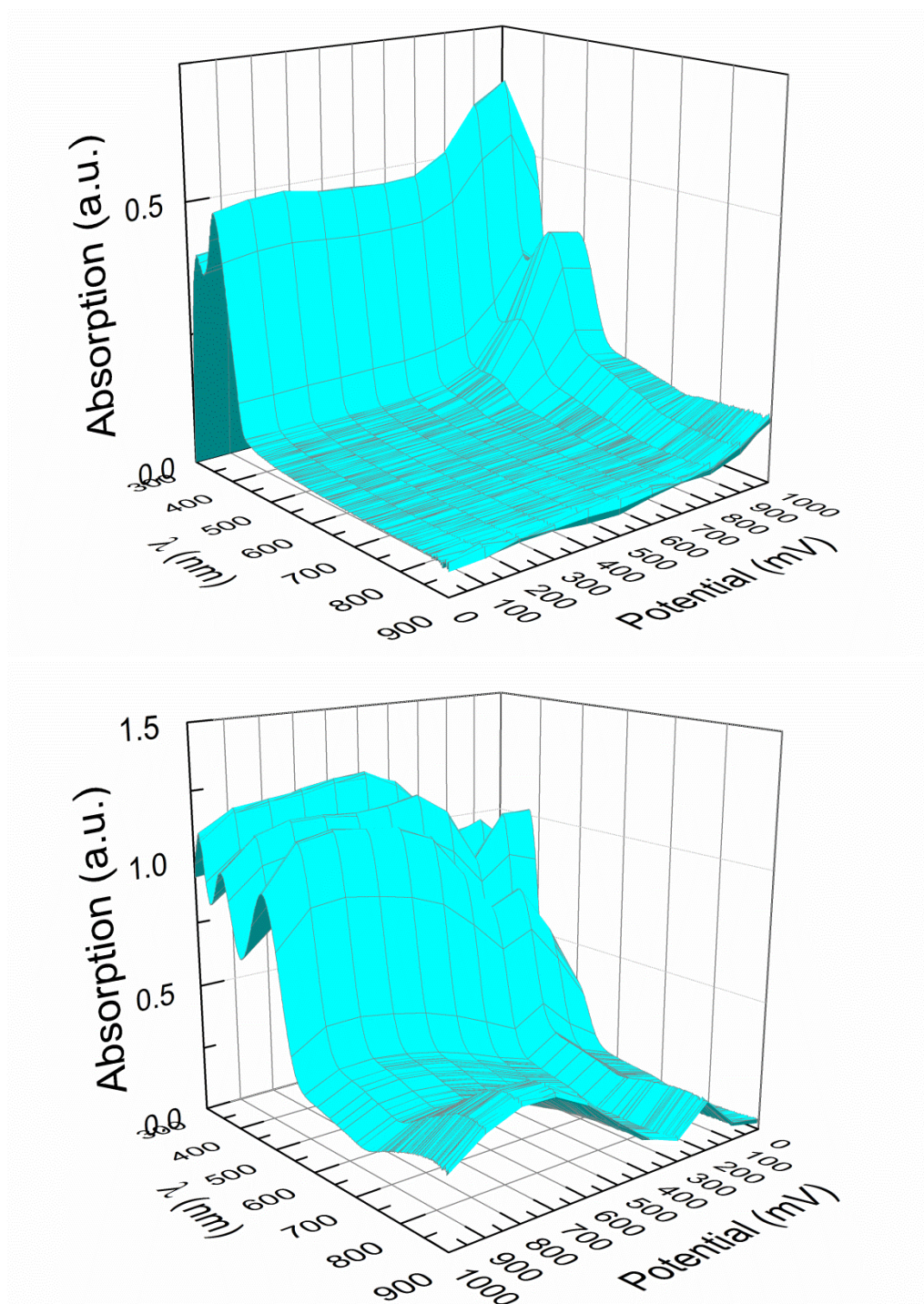
Figure 4-22. UV-vis spectroelectrochemical plots of *N*-heterotriangulene macrocycle **4-2** upon increasing (top) and reversing the potential (bottom), deposited on ITO glass, using an Ag wire reference electrode and Pt counter electrode. Experiments were conducted in a 0.1 M *n*-Bu₄NPF₆ acetonitrile solution.

significant spectral changes were observed. By further increasing the potential to 600 mV the emergence of a new absorption band at 490 nm could be detected. The appearance of this band is very similar to the oxidation behavior of *N,N,N',N'*-tetraphenylphenylenediamine and hexaaza[1₆]paracyclophane, showing absorption bands at around 500 nm during the formation of a diradical cation species.[85-87] The spectral

pattern was thus assigned to the absorption of [**4-2**]$^{2+}$, as a result of a double electron removal from the lone pair of two nitrogens on the *N*-heterotriangulene subunits. This was in agreement with the results from the CV measurements of **4-2**, revealing a global two-electron transfer as first oxidation step (see above). While moving the potential further anodically up to 1000 mV, the intensity of this band significantly increased and started to decrease after 900 mV. Moreover, a shoulder at around 650 nm was observed at these potentials. Both aspects indicated the formation of a tetracation species [**4-2**]$^{4+}$ by a second global two-eletron transfer or even the evolving of higher oxidized species. In addition, the development of a broad band in the near-IR region at around 900 nm was detected by additionally increasing the potential. This absorption is most likely a result of an intervalence charge-transfer (IVCT) between the oxidized *N*-heterotriangulene species and the residual neutral subunits.[87-89]

By reversing the potential, the absorption peak at 490 nm initially increased from 1000 to 900 mV, it plateaued thereafter from 900 to 600 mV and significantly decreased between 600 and 300 mV. The IVCT band, however, increased initially and vanished from 850 to 300 mV. Surprisingly, both transitions started to emerge again between 300 and 200 mV indicating the formation of additional radicals. By approaching 0 mV the IVCT band has been completely vanished. Besides a weak absorption at 490 nm, the initial transitions of **4-2** at 376 nm and 320 nm were fully recovered at 0 mV, suggesting a reasonable stability of **4-2** at the time scale of the measurements accompanied by an acceptable reversibility of the redox processes.

Moreover, the observed differences in the oxidation behavior of **4-2** between the CV measurements and the spectroelectrochemical data might be attributed to the characteristics of the applied measurement conditions. The CV experiments were carried out in solution, whereas the spectroelectrochemical studies were conducted in the solid state. This was shown in literature to influence the redox behavior of π-conjugated molecules and shift the oxidation onset ($E°_{ox}$) to higher potentials.[90]

4.4 Three-Component Architecture Based on the *N*-Hetero-triangulene Macrocycle 4-2

Supramolecular Chemistry, the chemistry beyond the covalent bond, has led to a broad variety of possibilities wherein researchers exploited non-covalent interactions such as hydrogen bonds, π-π- and van der Waals-interactions for the controlled fabrication of complex molecular architectures.[91-94] The research on supramolecular ordering of organic and metal organic building blocks on various surfaces studied by scanning probe techniques, such as STM and AFM, has received considerable attention over the last decade. A wide variety of structurally very diverse molecular monolayers have been reported, ranging from simple lamellar structures to nanoporous networks and from single-component systems to sophisticated multi-component hierarchically structured monolayers.[62, 63, 94-98]

Of the different types of surface supported supramolecular networks reported to date, two-dimensional porous networks are of particular interest because they offer the possibility to immobilize functional units as guest molecules in a repetitive and spatial ordered arrangement.[98] These systems might play a crucial role in future nanotechnological applications, such as molecular wires, due to the possibility of utilizing them as templates for the controlled self-assembly of single-molecule-based devices.[94, 98-100] Among numerous building blocks, dehydrobenzo[12]annulene (**DBA**) derivatives are particularly appealing candidates for the construction of flexible porous networks through directional alkyl chain interdigitation (Figure 4-23).[98, 101] By careful selecting structural and environmental factors such as the length of the peripheral alkyl chains, concentration of the **DBA** molecules in solution and the choice of the solvent and the surface, it is possible to control the structure of the resultant monolayer from a high density linear packing to a low density nanoporous network.[102]
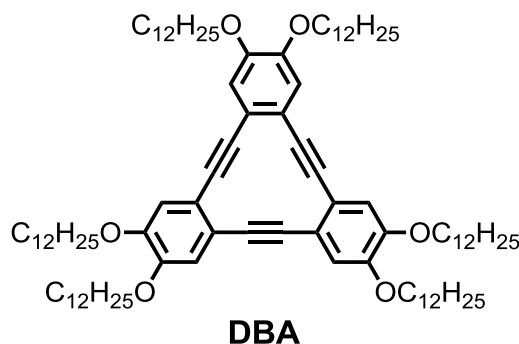
Figure 4-23. (a) Molecular structure of dehydrobenzo[12]annulene (**DBA**). (b) Alkyl chain length dependency of the 2D networks formed.[98]

Considering their flexibility in network formation, the **DBA** host networks were used to immobilize the *N*-heterotriangulene macrocycle **4-2** at the liquid/solid interface. The resultant multi-component networks formed were examined in detail using STM, in collaboration with ▮▮▮▮▮▮▮▮▮▮ in the group of ▮▮▮▮▮▮▮▮▮▮▮▮ at the Division of Molecular Imaging and Photonics of the KU Leuven, Belgium.

The surface confined porous supramolecular networks of **DBA**s have been extensively used to immobilize different type of guest molecules allowing the fabrication of complex multi-component systems.[98, 101, 103] The structural match in terms of their size and shape allowed the fabrication of a two-component network comprising of macrocycle **4-2** (diameter 2.8 nm from X-ray crystallography) as a guest immobilized in the hexagonal cavities of a host network constructed using a **DBA** derivative possessing six *n*-dodecyloxy chains (cavity size ~3.0 nm). Given the fact that the macrocycle has an intrinsic cavity with a diameter of ~1.3 nm, this two-component network could be further used to immobilize fullerenes (C_{60}). For this purpose, a tentative mechanism for the hierarchical assembly of a three-component architecture based on **4-2** was compiled (Scheme 4-10). The hierarchical nature of the self-assembly process leading to the fabrication of the three-component (**DBA/4-2/C_{60}**) network is shown in Scheme 4-10.
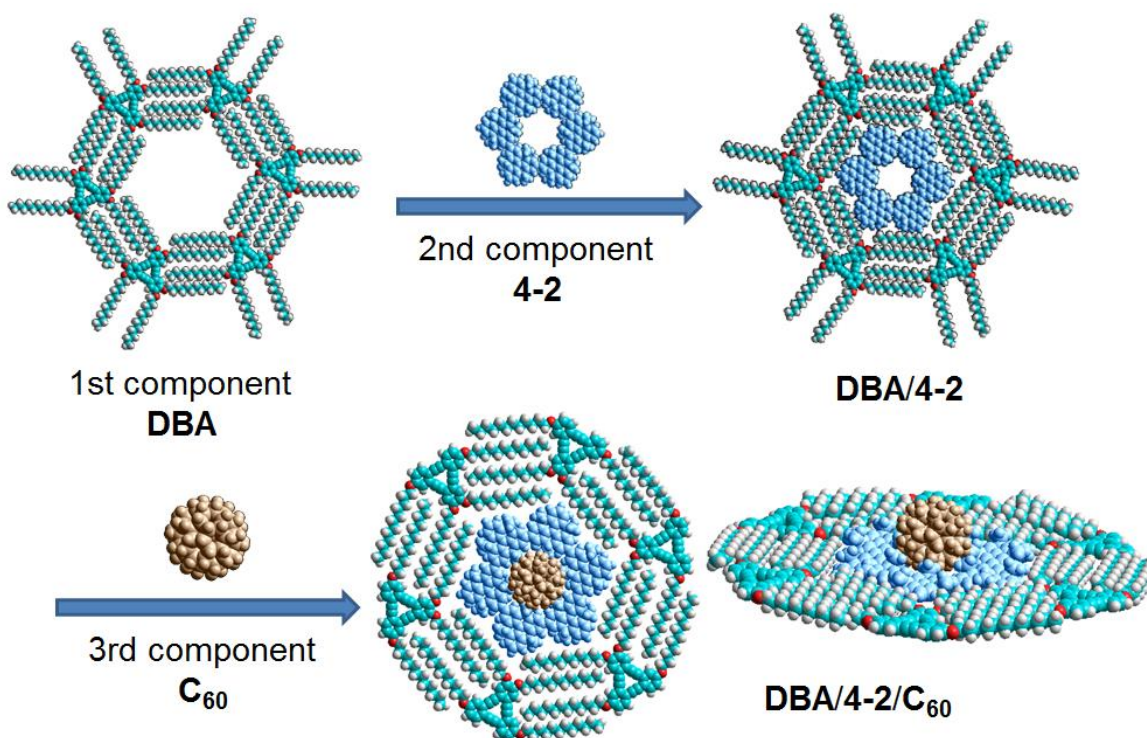
Scheme 4-10. Schematic representation of the hierarchical assembly of a three-component architecture based on the *N*-heterotriangulene macrocycle **4-2**.

Due to a diameter of ~2.8 nm (deduced from the X-ray crystallographic structure), **4-2** is expected to fill only the symmetrically formed cavities since the distorted pores offer a slightly smaller size than what is required for the adsorption of **4-2**. Due to the pore diameter of **4-2** (~1.3 nm), the fullerene C_{60} is anticipated to perfectly capture the central cavity of the *N*-heterotriangulene macrocycle as a third component resulting in a three-component architecture.

Before the fabrication of the multicomponent system, the adsorption behavior of **4-2** itself was studied on Au(111) films on mica. Thus, **4-2** was dissolved in a typical "STM" solvent, such as 1,2,4-trichlorobenzene. It was chosen as a solvent since it fulfills the technical criteria for the use in ambient STM, *e.g.*, high-boiling, non-conductive and stable under ambient conditions. Upon dropcasting from a 1,2,4-trichlorobenzene solution, **4-2** forms an ordered monolayer on Au(111) surface. Figure 4-24 shows a typical STM images of the monolayer formed by **4-2** at the 1,2,4-trichlorobenzene/Au(111) interface. Well-ordered arrays of **4-2** were found in which the molecules were arranged in a hexagonal lattice (Figure 4-24 a). The cell parameters of the unit cell of **4-2** on Au(111) are $a = 3.00 \pm 0.09$ nm, $b = 3.10 \pm 0.10$ nm and $\alpha = 60.0 \pm 1.0°$. The influence of the substrate lattice on the self-assembly is confirmed by the found hexagonal symmetry of the macrocycle arrangment indicating an epitaxial growth.
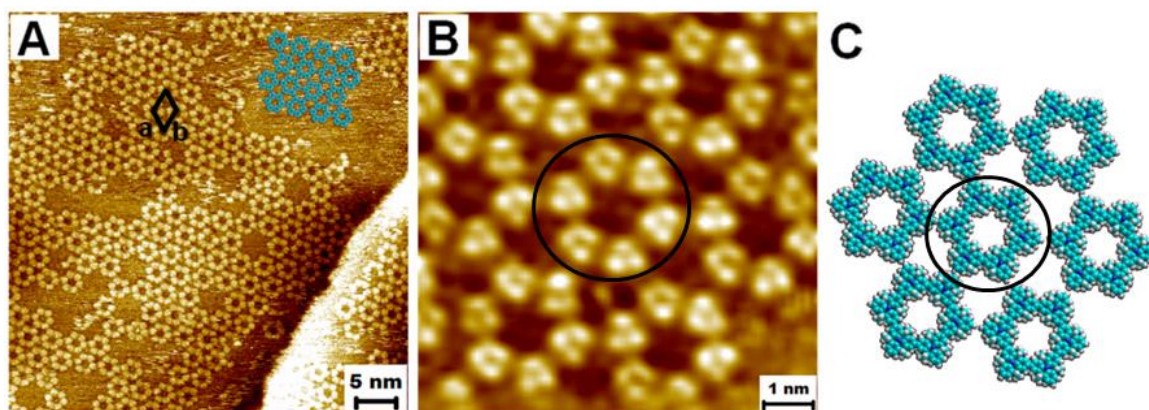
Figure 4-24. Typical large scale (a) and high-resolution (b) STM images of adlayers of **4-2** at the 1,2,4-trichlorobenzene/Au (111) interface ($c_{(4-2)} = 4.6 \times 10^{-6}$ M). The unit cell parameters are a = 3.0 ± 0.09 nm; 3.1 ± 0.10 nm; α = 60 ± 1.0°. (c) Molecular model of the self-assembled macrocycles. The black circles emphasizes the individual macrocycles in (b) and (c).

High-resolution STM images of monolayers show that the macrocycles show up as six units corresponding to the individual *N*-heterotriangulene subunits (Figure 4-24 b). In accordance with previous experiments, the individual *N*-heterotriangulene units are further visualized as three bright prostrusions, which correspond to perpendicularly oriented

dimethylmethylene groups (Figure 4-24 b and c). In addition, the central cavity of **4-2** can be visualized showing a diameter of 1.2 to 1.3 nm. Although the cavity appears to be empty in the STM images, it is normally filled by mobile solvent molecules which undergo adsorption-desorption dynamics that is too fast on the time scale of STM measurements. The observed pores are distorted in shape in the absence of a guest molecule.[103] The as-formed supramolecular networks of **4-2** were stable at room temperature could be visualized for a few hour after deposition. By considering these results together with the planar π-conjugated core with C_6 symmetry, **4-2** was expected to fit into the hexagonal cavities of the **DBA** host.
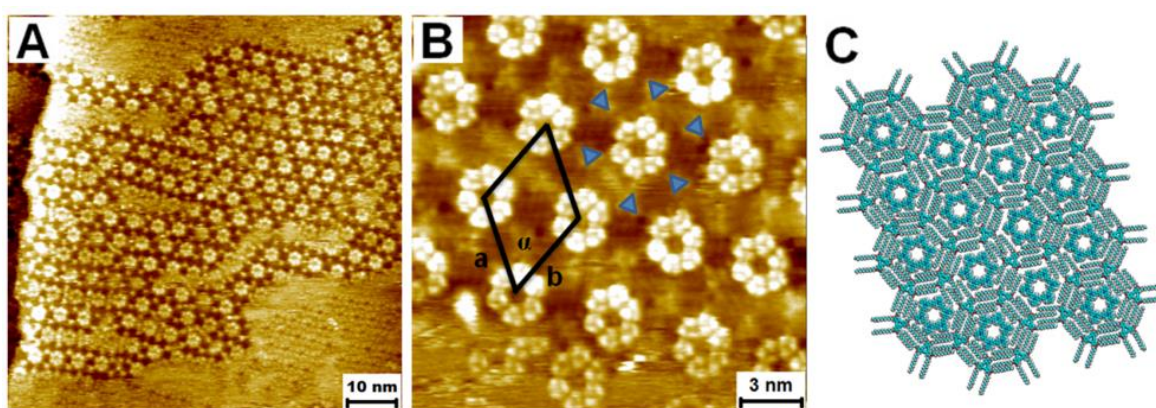
Figure 4-25. Large scale (a) and high-resolution (b) STM image of the two-component network of (**DBA**/**4-2**) at the 1,2,4-trichlorobenzene/Au(111) interface ($c_{(DBA)} = 4.0 \times 10^{-7}$ M, $c_{(4-2)} = 1.6 \times 10^{-6}$ M). The ratio of **DBA** to **4-2** is 1:2.6. The blue triangles depict the individual **DBA** host molecules. (c) A tentative model for the assembly of the two-component architecture.

Having characterized the single-component system involving only **4-2** adsorbed at the 1,2,4-trichlorobenzene/Au(111), a more complex two-component system was aimed. A premixed solution of **DBA** and **4-2** in 1,2,4-trichlorobenzene (molar ratio of **DBA**:**4-2** = 1:2.6) was used for this purpose. Deposition of the premixed solution on Au(111) led to the formation of a monolayer in which the molecules of **4-2** formed well-ordered arrays in a hexagonal lattice (Figure 4-25). Large-scale STM images revealed the presence of highly ordered domains of self-assembled networks extended over regions of a few hundred square nanometers in size. A characteristic feature of this monolayer is the increased periodicity of the molecules of **4-2** compared to the adsorbed one-component solution (Figure 4-24). The distance between adjacent molecules of **4-2**, when adsorbed from a two-component solution, is 4.5 nm which is significantly larger than that (3.0 nm) observed for the monolayer obtained from a single-component solution (*i.e.* only **4-2** in TCB). The origin of the increased periodicity lies in the templating effect of the **DBA** host

network. Although not clearly visible in the large scale STM image provided in Figure 4-25 a, the template layer of **DBA** molecules could be visualized in the high-resolution STM image provided in Figure 4-25 b. Each pore of the **DBA** network hosted a single molecule of **4-2**.[103, 104] A certain amount of uncomplexed macrocycles was however detected at this particular molar ratio, as it is visualized in Figure 4-25 a.
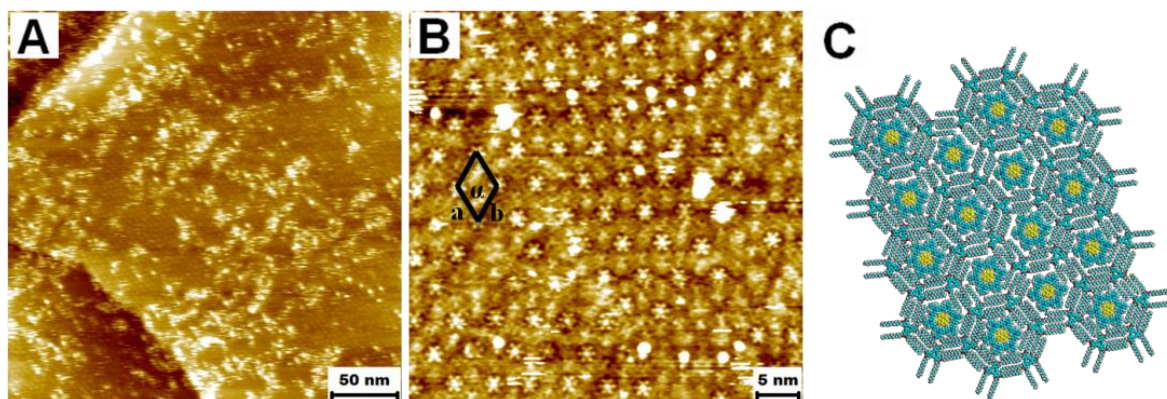
Figure 4-26. Large scale (a) and high-resolution (b) STM image of three-component architecture (**DBA**/**4-2**/C_{60}) at the trichlorobenzene/Au(111) interface ($c_{(DBA)} = 3.0 \times 10^{-7}$ M, $c_{(4-2)} = 1.2 \times 10^{-6}$ M, $c_{(C60)} = 2.0 \times 10^{-7}$ M). The unit cell parameters are a = 4.6 ± 0.2 nm; b = 4.5 ± 0.3 nm; α = 60 ± 2.0°. The ratio of **DBA**, **4-2** and C_{60} is 1:2.6:2.3. (c) A tentative model for the assembly of the three-component architecture.

Due to the empty cavity of **4-2** with sizes of around 1.3 nm, a third component was expected to adsorb to the remaining pores. The C_{60} fullerene was ideally suited for this incorporation, as a result of its diameter of 1 nm. In addition, the isotropic electron-accepting character of C_{60} was expected to interact favorably with electron-donating **4-2**. To fabricate the three-component system involving C_{60} molecules, a 1,2,4-trichlorobenzene solution of C_{60} (2.0×10^{-7} M) was applied to the Au(111) substrate which already contained the two-component monolayer. The STM images after the deposition of the C_{60} solution are shown in Figure 4-26. Again, highly ordered domains of self-assembled networks were observed over large areas of more than 100 nm^2. The high-resolution image revealed a unit cell with parameters of a = 4.6 ± 0.2 nm, b = 4.5 ± 0.3 nm and α = 60 ± 2.0° (Figure 4-26 b). These parameters essentially match with those obtained for the two-component system. The only difference was the central cavity of macrocycle **4-2** which appeared to be occupied by the C_{60} molecules displayed as bright protrusions. The experimental data, supported by molecular modeling calculations (Figure 4-26 c), confirmed that a molecule of **4-2**, which has incorporated a C_{60} molecule to its cavity, is in fact surrounded by an interdigitated hexamer of **DBA**. Adsorption of C_{60} to the voids of
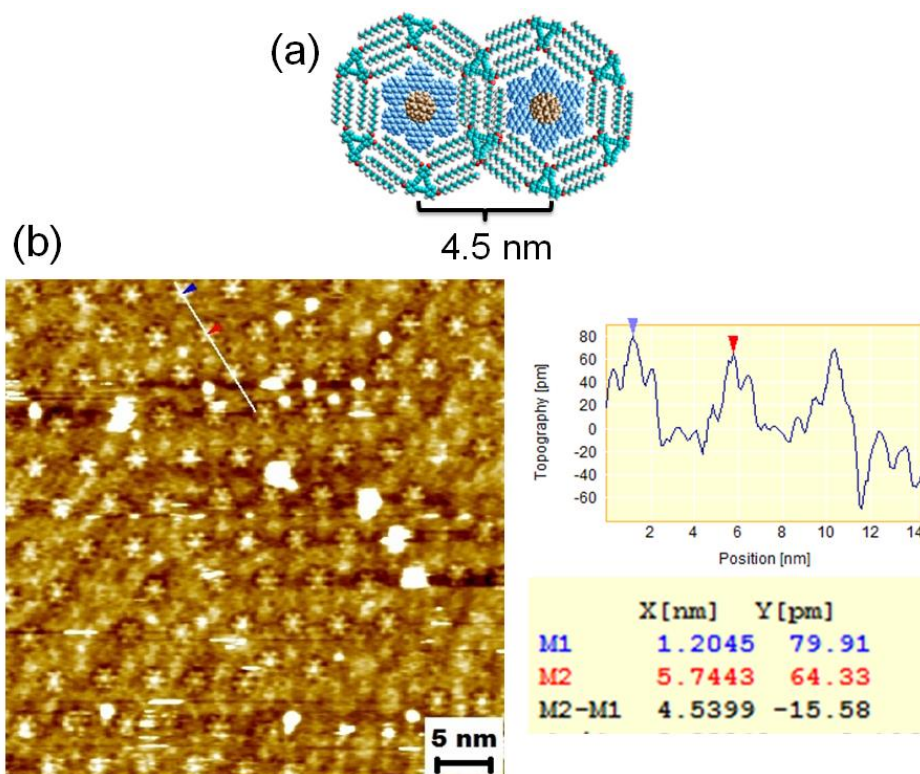
Figure 4-27. (a) Distance obtained by molecular modeling calculations between two C_{60} molecules adsorbed inside the three-component architecture. (b) Line profile analysis across the surface of three-component architecture.

macrocycle **4-2** did not affect the intrinsic honeycomb characteristics of the **DBA** host network. Some cavities remained, however, unfilled. To further corroborate the formation of the three-component architecture, a line profile analysis was conducted and compared with the results of the molecular modeling calculations (Figure 4-27). The latter one predicted a center-to-center distance between two imbedded fullerenes of 4.5 nm (Figure 4-27 a). Such distances can only be observed if (1) C_{60} is adsorbed to cavities of macrocycle **4-2**, (2) C_{60} and **4-2** are incorporated to pores of the **DBA** host network and (3) the alkyl chains of the host containing **4-2** and the fullerene are interdigitated toward a honeycomb network. Indeed, the line profile analysis indicated a center-to-center distance of 4.54 nm between two different assemblies (Figure 4-27 b). This unambiguously proved the successful self-assembly of the three-component architecture. These results suggested furthermore a recognition process between the DBA host, macrocycle **4-2** and C_{60} as a result of a selection based on the size, shape and symmetry commensurability as well as donor/acceptor interactions of the respective components.[105] To further elucidate this assumption, control experiments have to be carried out. By adding two additional components to the system, one having a slightly different size than **4-2** together with one slightly larger than C_{60}, would prove a size and shape recognition of the host network. The

utilization of different host networks, which have an intrinsically larger pore sizes should led furthermore to the fabrication of four- and five-component architectures.

4.5   Summary

In this chapter, the fabrication of a π-conjugated macrocycle (**4-2**) by two different synthetic concepts was shown for the first time. The analysis of the solution-based and surface-mediated one-step synthesis starting from the same precursor, revealed a preferential formation of the macrocycles compared to the linear oligomers on the surface. As a result of the precursor's (**4-1**) conformational and positional degrees of freedom, the solution-based cyclohexamerization has an intrinsically lower propensity for the formation of the macrocycle. On the Ag(111) surface, however, the precursor molecules are confined to two dimensions, which reduced the possible relative orientations of the reacting molecules and thus their degrees of freedom compared to the isotropic situation in solution. This advantage comes at the expense of scalability which was overcome by a stepwise protocol in solution affording the *N*-heterotriangulene macrocycle **4-2** in a reasonable overall yield of 12.4% over four steps on a several hundred milligram scale. Single crystal X-ray analysis confirmed the successful cyclization and revealed an edge-to-face orientation of the individual macrocycles in the unit cell. Bromination of **4-2** allowed further chemical extension such as the introduction of alky chains to study the mesophase formation. As a result of the perpendicular oriented dimethylmethylene bridging groups, however, efficient self-assembly of **4-2** in the bulk phase was impeded.

Focus then turned to the extension of **4-2** toward expanded macrocycles **4-12** and **4-17** mimicking monodisperse fractions of the hyperbanched polymer discussed in Chapter 3. However, the fabrication of the fused analogue of **4-17**, "heptacycle" **4-19**, remained challenging and its formation was therefore not conclusively proven.

Concerning the photophysical properties of the macrocyclic species **4-2**, **4-12** and **4-17**, the linear nonamer **4-9** and pristine *N*-heterotriangulene **3-4**, considerable differences have been found. Macrocycles **4-2**, **4-12** and **4-17** exhibited deep blue emissions in solution with the maxima close to the optimum value of around 450 nm together with a significant improvement in the PLQY with respect to parent *N*-heterotriangulene **3-4**.

Studying the electronic properties of **4-2** by electrochemical methods, a reasonable redox stability together with a HOMO level close to the work function of metallic gold ($\varphi = -5.1$ eV) was revealed.

Moreover, the utilization of macrocycle **4-2** for the selective self-assembly on Au(111) surfaces resulted in the successful formation of multi-component architectures, which were investigated by STM. Premixing **4-2** with a **DBA** host allowed for the generation of a honeycomb structured two-component architecture. By the addition of a fullerene, the C_{60} was imbedded to the central cavity of macrocycle **4-2** thus extending the system to a three-component architecture.

4.6   References

[1]   M. Iyoda, *Pure Appl. Chem.* **2010**, *82*, 831-841.

[2]   M. Iyoda, J. Yamakawa, M. J. Rahman, *Angew. Chem., Int. Ed.* **2011**, *50*, 10522-10553.

[3]   S. Höger, A. D. Meckenstock, H. Pellen, *J. Org. Chem.* **1997**, *62*, 4556-4557.

[4]   C. Grave, A. D. Schlüter, *Eur. J. Org. Chem.* **2002**, 3075-3098.

[5]   D. H. Zhao, J. S. Moore, *Chem. Commun.* **2003**, 807-818.

[6]   S. Höger, *Chem.-Eur. J.* **2004**, *10*, 1320-1329.

[7]   W. Zhang, J. S. Moore, *Angew. Chem., Int. Ed.* **2006**, *45*, 4416-4439.

[8]   Y. B. Song, C. A. Di, W. Xu, Y. Q. Liu, D. Q. Zhang, D. B. Zhu, *J. Mater. Chem.* **2007**, *17*, 4483-4491.

[9]   A. Ito, Y. Yokoyama, R. Aihara, K. Fukui, S. Eguchi, K. Shizu, T. Sato, K. Tanaka, *Angew. Chem., Int. Ed.* **2010**, *49*, 8205-8208.

[10]   L. Arnold, H. Norouzi-Arasi, M. Wagner, V. Enkelmann, K. Müllen, *Chem. Commun.* **2011**, *47*, 970-972.

[11]   P. K. Chen, F. Jäkle, *J. Am. Chem. Soc.* **2011**, *133*, 20142-20145.

[12]   M. G. Schwab, T. S. Qin, W. Pisula, A. Mavrinskiy, X. Feng, M. Baumgarten, H. Kim, F. Laquai, S. Schuh, R. Trattnig, E. J. W. List, K. Müllen, *Chem.-Asian J.* **2011**, *6*, 3001-3010.

[13]   P. K. Chen, R. A. Lalancette, F. Jäkle, *Angew. Chem., Int. Ed.* **2012**, *51*, 7994-7998.

[14]   F. Schlütter, F. Rossel, M. Kivala, V. Enkelmann, J. P. Gisselbrecht, P. Ruffieux, R. Fasel, K. Müllen, *J. Am. Chem. Soc.* **2013**, *135*, 4550-4557.

[15]   H. A. Staab, F. Binnig, *Chem. Ber.* **1967**, *100*, 293-305.

[16]   H. Bräunling, F. Binnig, H. A. Staab, *Chem. Ber.* **1967**, *100*, 880-888.

[17]   H. A. Staab, U. E. Meissner, B. Meissner, *Chem. Ber.* **1976**, *109*, 3875-3885.

[18]   W. Pisula, M. Kastler, C. Yang, V. Enkelmann, K. Müllen, *Chem.-Asian J.* **2007**, *2*, 51-56.

[19]   J. Zhang, X. Wang, Q. Su, L. J. Zhi, A. Thomas, X. Feng, D. S. Su, R. Schlögl, K. Müllen, *J. Am. Chem. Soc.* **2009**, *131*, 11296-11297.

[20]   M. J. Rahman, J. Yamakawa, A. Matsumoto, H. Enozawa, T. Nishinaga, K. Kamada, M. Iyoda, *J. Org. Chem.* **2008**, *73*, 5542-5548.

[21]   S. H. Jung, W. Pisula, A. Rouhanipour, H. J. Räder, J. Jacob, K. Müllen, *Angew. Chem., Int. Ed.* **2006**, *45*, 4685-4690.

[22]   J. E. Lovett, M. Hoffmann, A. Cnossen, A. T. J. Shutter, H. J. Hogben, J. E. Warren, S. I. Pascu, C. W. M. Kay, C. R. Timmel, H. L. Anderson, *J. Am. Chem. Soc.* **2009**, *131*, 13852-13859.

[23]   D. Mössinger, D. Chaudhuri, T. Kudernac, S. Lei, S. De Feyter, J. M. Lupton, S. Höger, *J. Am. Chem. Soc.* **2010**, *132*, 1410-1423.

[24]   D. Mössinger, J. Hornung, S. Lei, S. De Feyter, S. Höger, *Angew. Chem., Int. Ed.* **2007**, *46*, 6802-6806.

[25]   M. Hoffmann, C. J. Wilson, B. Odell, H. L. Anderson, *Angew. Chem., Int. Ed.* **2007**, *46*, 3122-3125.

[26]   M. Hoffmann, J. Karnbratt, M. H. Chang, L. M. Herz, B. Albinsson, H. L. Anderson, *Angew. Chem., Int. Ed.* **2008**, *47*, 4993-4996.

[27]   J. S. Zhang, D. J. Pesak, J. L. Ludwick, J. S. Moore, *J. Am. Chem. Soc.* **1994**, *116*, 4227-4239.

[28]   L. Lafferentz, V. Eberhardt, C. Dri, C. Africh, G. Comelli, F. Esch, S. Hecht, L. Grill, *Nat. Chem.* **2012**, *4*, 215-220.

[29]   J. Cai, P. Ruffieux, R. Jaafar, M. Bieri, T. Braun, S. Blankenburg, M. Muoth, A. P. Seitsonen, M. Saleh, X. Feng, K. Müllen, R. Fasel, *Nature* **2010**, *466*, 470-473.

[30]   M. Bieri, M. Treier, J. M. Cai, K. Ait-Mansour, P. Ruffieux, O. Groning, P. Groning, M. Kastler, R. Rieger, X. Feng, K. Müllen, R. Fasel, *Chem. Commun.* **2009**, 6919-6921.

[31]   M. Bieri, M. T. Nguyen, O. Groning, J. M. Cai, M. Treier, K. Ait-Mansour, P. Ruffieux, C. A. Pignedoli, D. Passerone, M. Kastler, K. Müllen, R. Fasel, *J. Am. Chem. Soc.* **2010**, *132*, 16669-16676.

[32]   M. O. Blunt, J. C. Russell, N. R. Champness, P. H. Beton, *Chem. Commun.* **2010**, *46*, 7157-7159.

[33]   M. Bieri, S. Blankenburg, M. Kivala, C. A. Pignedoli, P. Ruffieux, K. Müllen, R. Fasel, *Chem. Commun.* **2011**, *47*, 10239-10241.

[34] L. Lafferentz, F. Ample, H. Yu, S. Hecht, C. Joachim, L. Grill, *Science* **2009**, *325*, 148-148.

[35] J. A. Lipton-Duffin, O. Ivasenko, D. F. Perepichka, F. Rosei, *Small* **2009**, *5*, 592-597.

[36] N. R. Champness, *Nat. Chem.* **2012**, *4*, 149-150.

[37] T. Yamamoto, *Bull. Chem. Soc. Jpn.* **1999**, *72*, 621-638.

[38] T. Yamamoto, *Prog. Polym. Sci.* **1992**, *17*, 1153-1205.

[39] M. G. Schwab, Ph.D. thesis, Johannes Gutenberg-University Mainz **2011**.

[40] G. W. Parshall, *J. Am. Chem. Soc.* **1974**, *96*, 2360-2366.

[41] T. Yamamoto, T. Kohara, A. Yamamoto, *Bull. Chem. Soc. Jpn.* **1981**, *54*, 1720-1726.

[42] Z. H. Zhou, T. Yamamoto, *J. Organomet. Chem.* **1991**, *414*, 119-127.

[43] M. T. Nguyen, C. A. Pignedoli, D. Passerone, *Phys. Chem. Chem. Phys.* **2011**, *13*, 154-160.

[44] L. Cardenas, R. Gutzler, J. Lipton-Duffin, C. Fu, J. L. Brusso, L. E. Dinca, M. Vondracek, Y. Fagot-Revurat, D. Malterre, F. Rosei, D. F. Perepichka, *Chem. Sci.* **2013**, *4*, 3263-3268.

[45] A. Gourdon, *Angew. Chem., Int. Ed.* **2008**, *47*, 6950-6953.

[46] G. Franc, A. Gourdon, *Phys. Chem. Chem. Phys.* **2011**, *13*, 14283-14292.

[47] D. F. Perepichka, F. Rosei, *Science* **2009**, *323*, 216-217.

[48] L. Talirz, H. Sode, J. M. Cai, P. Ruffieux, S. Blankenburg, R. Jafaar, R. Berger, X. Feng, K. Müllen, D. Passerone, R. Fasel, C. A. Pignedoli, *J. Am. Chem. Soc.* **2013**, *135*, 2060-2063.

[49] Q. Fan, C. Wang, Y. Han, J. Zhu, W. Hieringer, J. Kuttner, G. Hilt, J. M. Gottfried, *Angew. Chem., Int. Ed.* **2013**, *52*, 4668-4672.

[50] S. Stepanow, N. Lin, D. Payer, U. Schlickum, F. Klappenberger, G. Zoppellaro, M. Ruben, H. Brune, J. V. Barth, K. Kern, *Angew. Chem., Int. Ed.* **2007**, *46*, 710-713.

[51] T. Ishiyama, M. Murata, N. Miyaura, *J. Org. Chem.* **1995**, *60*, 7508-7510.

[52] D. Qiu, F. Y. Mo, Z. T. Zheng, Y. Zhang, J. B. Wang, *Org. Lett.* **2010**, *12*, 5474-5477.

[53] T. Kanbara, N. Saito, T. Yamamoto, K. Kubota, *Macromolecules* **1991**, *24*, 5883-5885.

[54] A. N. Sobolev, V. K. Belsky, I. P. Romm, N. Y. Chernikova, E. N. Guryanova, *Acta Crystallogr. C* **1985**, *41*, 967-971.

[55] S. Höger, K. Bonrad, A. Mourran, U. Beginn, M. Möller, *J. Am. Chem. Soc.* **2001**, *123*, 5651-5659.

[56] M. Kastler, Ph.D. thesis, Johannes Gutenberg-University Mainz **2006**.

[57] J. J. Yin, M. P. Rainka, X. X. Zhang, S. L. Buchwald, *J. Am. Chem. Soc.* **2002**, *124*, 1162-1163.

[58] S. D. Walker, T. E. Barder, J. R. Martinelli, S. L. Buchwald, *Angew. Chem., Int. Ed.* **2004**, *43*, 1871-1876.

[59] T. E. Barder, S. D. Walker, J. R. Martinelli, S. L. Buchwald, *J. Am. Chem. Soc.* **2005**, *127*, 4685-4696.

[60] J. F. Van der Pol, E. Neeleman, J. C. Vanmiltenburg, J. W. Zwikker, R. J. M. Nolte, W. Drenth, *Macromolecules* **1990**, *23*, 155-162.

[61] D. H. Zhao, J. S. Moore, *J. Org. Chem.* **2002**, *67*, 3548-3554.

[62] M. Fischer, G. Lieser, A. Rapp, I. Schnell, W. Mamdouh, S. De Feyter, F. C. De Schryver, S. Höger, *J. Am. Chem. Soc.* **2004**, *126*, 214-222.

[63] B. Schmaltz, A. Rouhanipour, H. J. Räder, W. Pisula, K. Müllen, *Angew. Chem., Int. Ed.* **2009**, *48*, 720-724.

[64] W. Pisula, Z. Tomovic, C. Simpson, M. Kastler, T. Pakula, K. Müllen, *Chem. Mater.* **2005**, *17*, 4296-4303.

[65] R. Scholl, C. Seer, R. Weitzenbock, *Ber. Dtsch. Chem. Ges.* **1910**, *43*, 2202-2209.

[66] R. Scholl, C. Seer, *Ber. Dtsch. Chem. Ges.* **1911**, *44*, 1233-1240.

[67] R. Scholl, C. Seer, *Liebigs Ann. Chem.* **1912**, *394*, 111-177.

[68] B. T. King, J. Kroulik, C. R. Robertson, P. Rempala, C. L. Hilton, J. D. Korinek, L. M. Gortari, *J. Org. Chem.* **2007**, *72*, 2279-2288.

[69] W. Ishikawa, H. Inada, H. Nakano, Y. Shirota, *J. Phys. D: Appl. Phys.* **1993**, *26*, B94-B99.

[70] W. Ishikawa, K. Noguchi, Y. Kuwabara, Y. Shirota, *Adv. Mater.* **1993**, *5*, 559-561.

[71] T. Noda, H. Ogawa, N. Noma, Y. Shirota, *Adv. Mater.* **1997**, *9*, 720-722.

[72] Y. Shirota, H. Kageyama, *Chem. Rev.* **2007**, *107*, 953-1010.

[73] Z. Fang, T. L. Teo, L. P. Cai, Y. H. Lai, A. Samoc, M. Samoc, *Org. Lett.* **2009**, *11*, 1-4.

[74] Z. Fang, X. H. Zhang, Y. H. Lai, B. Liu, *Chem. Commun.* **2009**, 920-922.

[75]   Z. Fang, V. Chellappan, R. D. Webster, L. Ke, T. F. Zhang, B. Liu, Y. H. Lai, *J. Mater. Chem.* **2012**, *22*, 15397-15404.

[76]   R. Rieger, K. Müllen, *J. Phys. Org. Chem.* **2010**, *23*, 315-325.

[77]   M. Baumgarten, T. Yüksel, *Phys. Chem. Chem. Phys.* **1999**, *1*, 1699-1706.

[78]   D. Vak, B. Lim, S. H. Lee, D. Y. Kim, *Org. Lett.* **2005**, *7*, 4229-4232.

[79]   D. D. Bao, B. Millare, W. Xia, B. G. Steyer, A. A. Gerasimenko, A. Ferreira, A. Contreras, V. I. Vullev, *J. Phys. Chem. A* **2009**, *113*, 1259-1267.

[80]   *DigiElch v 6F, http://www.elchsoft.com/.*

[81]   M. Rudolph, D. P. Reddy, S. W. Feldberg, *Anal. Chem.* **1994**, *66*, 589-600.

[82]   P. Le Magueres, S. V. Lindeman, J. K. Kochi, *Org. Lett.* **2000**, *2*, 3567-3570.

[83]   N. Drolet, J. F. Morin, N. Leclerc, S. Wakim, Y. Tao, M. Leclerc, *Adv. Funct. Mater.* **2005**, *15*, 1671-1682.

[84]   E. J. Meijer, D. M. De Leeuw, S. Setayesh, E. Van Veenendaal, B. H. Huisman, P. W. M. Blom, J. C. Hummelen, U. Scherf, T. M. Klapwijk, *Nat. Mater.* **2003**, *2*, 678-682.

[85]   S. H. Yeh, C. Y. Tsai, C. Y. Huang, G. S. Liou, S. H. Cheng, *Electrochem. Commun.* **2003**, *5*, 373-377.

[86]   K. Y. Chiu, T. H. Su, C. W. Huang, G. S. Liou, S. H. Cheng, *J. Electroanal. Chem.* **2005**, *578*, 283-287.

[87]   T. F. Yang, K. Y. Chiu, H.-C. Cheng, J. W. Lee, M. Y. Kuo, Y. O. Su, *J. Org. Chem.* **2012**, *77*, 8627–8633.

[88]   S. Barlow, C. Risko, S. J. Chung, N. M. Tucker, V. Coropceanu, S. C. Jones, Z. Levi, J. L. Bredas, S. R. Marder, *J. Am. Chem. Soc.* **2005**, *127*, 16900-16911.

[89]   G. Zhou, M. Baumgarten, K. Müllen, *J. Am. Chem. Soc.* **2007**, *129*, 12211-12221.

[90]   D. Cortizo-Lacalle, S. Arumugam, S. E. T. Elmasly, A. L. Kanibolotsky, N. J. Findlay, A. R. Inigo, P. J. Skabara, *J. Mater. Chem.* **2012**, *22*, 11310-11315.

[91]   D. J. Cram, *Angew. Chem., Int. Ed.* **1988**, *27*, 1009-1020.

[92]   J. M. Lehn, *Angew. Chem., Int. Ed.* **1988**, *27*, 89-112.

[93]   C. J. Pedersen, *Angew. Chem., Int. Ed.* **1988**, *27*, 1021-1027.

[94]   S. De Feyter, F. C. De Schryver, *Chem. Soc. Rev.* **2003**, *32*, 139-150.

[95]   P. Samori, J. P. Rabe, *J. Phys.: Condens. Matter* **2002**, *14*, 9955-9973.

[96]   R. Otero, M. Schock, L. M. Molina, E. Laegsgaard, I. Stensgaard, B. Hammer, F. Besenbacher, *Angew. Chem., Int. Ed.* **2005**, *44*, 2270-2275.

[97]   B. A. Hermann, L. J. Scherer, C. E. Housecroft, E. C. Constable, *Adv. Funct. Mater.* **2006**, *16*, 221-235.

[98]   S. Furukawa, K. Tahara, F. C. De Schryver, M. Van der Auweraer, Y. Tobe, S. De Feyter, *Angew. Chem., Int. Ed.* **2007**, *46*, 2831-2834.

[99]   L. Grill, M. Dyer, L. Lafferentz, M. Persson, M. V. Peters, S. Hecht, *Nat. Nanotechnol.* **2007**, *2*, 687-691.

[100] H. Spillmann, A. Kiebele, M. Stohr, T. A. Jung, D. Bonifazi, F. Y. Cheng, F. Diederich, *Adv. Mater.* **2006**, *18*, 275-279.

[101] K. Tahara, S. Furukawa, H. Uji-I, T. Uchino, T. Ichikawa, J. Zhang, W. Mamdouh, M. Sonoda, F. C. De Schryver, S. De Feyter, Y. Tobe, *J. Am. Chem. Soc.* **2006**, *128*, 16613-16625.

[102] K. Tahara, S. B. Lei, J. Adisoejoso, S. De Feyter, Y. Tobe, *Chem. Commun.* **2010**, *46*, 8507-8525.

[103] T. Balandina, K. Tahara, N. Sandig, M. O. Blunt, J. Adisoejoso, S. B. Lei, F. Zerbetto, Y. Tobe, S. De Feyter, *ACS Nano* **2012**, *6*, 8381-8389.

[104] S. J. H. Griessl, M. Lackinger, F. Jamitzky, T. Markert, M. Hietschold, W. A. Heckl, *Langmuir* **2004**, *20*, 9403-9407.

[105] S. Lei, M. Surin, K. Tahara, J. Adisoejoso, R. Lazzaroni, Y. Tobe, S. De Feyter, *Nano Lett.* **2008**, *8*, 2541-2546.

5 *N*-Heterotriangulenes as Hole-Transport-Materials in Solid-State Dye-Sensitized Solar Cells

5.1 Introduction

Studying the electronic properties of *N*-heterotriangulene architectures (see above), revealed a reasonable redox stability together with HOMOs above the ground state level of dye molecules, such as perylene monoimides ($E_{HOMO} \approx -5.40$ eV). This enables their utilization as hole-transport material (HTM) in optoelectronic devices, such as dye-sensitized solar cells (DSSCs). DSSCs are among the most efficient organic photovoltaic devices nowadays.[1-6] Although DSSCs based on liquid electrolytes, such as iodide/triiodide (I^-/I_3^-) and Co^{2+}/Co^{3+} redox couples, have reached power conversion efficiencies (PCE) of 12.3%, they suffer from a limited device stability as a result of solvent evaporation and the corrosive nature of the electrolyte.[4, 6-10] The fabrication of multi-cell modules based on liquid electrolyte DSSCs is furthermore hampered due to difficulties in chemically separating the electrically connected cells on a single substrate.[4, 11, 12] Thus, much effort has been devoted to the replacement of the liquid electrolyte by solid-state hole-transport materials (HTMs) to make liquid electrolyte free, long-term stable and reliable solid-state dye-sensitized solar cells (sDSSCs) which are by far more attractive for industry.[13-19] *Grätzel* and coworkers reported in 1998 the first efficient sDSSC based on 2,2',7,7'-tetrakis(*N,N*'-di-*p*-methoxyphenylamine)-9,9'-spirobifluorene (spiro-MeOTAD, **I5-1**, Figure 5-1) as a HTM.[13]
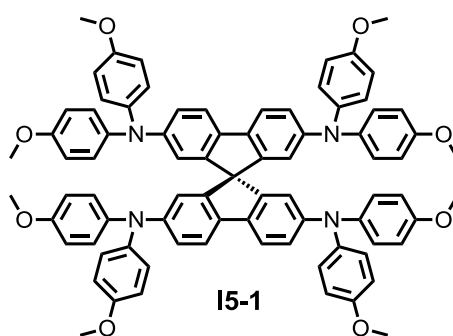
Figure 5-1. Chemical structure of spiro-MeOTAD **I5-1**.

By using **I5-1** in combination with $N(4-C_6H_4Br)_3SbCl_6$ and $Li[(CF_3SO_2)N]$ as additives, they were able to use a thin (~4.2 μm) mesoporous titanium dioxide together with a ruthenium dye to enhance the pore filling of HTM and thus the conductivity. As a result of the electron-rich character (*p*-type) such organic semiconductors serve in sDSSCs as a regenerator of the dye, which has injected an electron into the conduction band of the

titanium dioxide upon photoexcitation. The restoring of the sensitizer prevents the recapture of the electron in the TiO$_2$ conduction band by the oxidized dye. In the final step, the HTM is regenerated at the counter electrode and the circuit is completed *via* electron migration through the external load.[4, 20]

As a consequence of these processes, several criteria have to be fulfilled by the HTM for an efficient dye regeneration in sDSSCs:[21-23]

(1) The HOMO level of the organic HTM has to be located above the ground state level of the sensitizer in order to transfer the holes from the oxidized dye.

(2) An excellent pore filling of the HTM inside the porous layer of titanium dioxide is strongly required. Dissolving or degrading of the dye monolayer on the titanium dioxide nanocrystallites should be avoided by the respective processing technique.

(3) A sufficient hole mobility and conductivity in combination with a good thermal and photochemical stability of the HTM is required.

(4) It should be furthermore transparent in the visible part of the spectrum. However, if the HTM absorbs light, the electron injection has to be as efficient as from the dye.

With respect to these requirements, spiro-MeOTAD (**I5-1**) is nowadays one of the most commonly used HTMs in conventional sDSSCs with record PCEs of up to 7.2%.[23, 24] The lower efficiency is primarily a consequence of its somewhat lower conductivity (10^{-5} S cm^{-1}) compared to the liquid electrolyte (10^{-3} S cm^{-1}) leading to higher recombination losses.[25-27] Recent studies showed that the slow charge transport in **I5-1** significantly limits the maximum power point in the DSSC.[28] Thus, the maximum obtainable power in sDSSCs is limited to 10 to 20% when generating photocurrents of less than 10 mA cm^{-2}.[29] Although significant enhancements in the photocurrent generation have recently been achieved by utilizing organometallic halide Perovskites absorbers,[30, 31] the increase in charge carrier transport of the HTM can be considered as one of the major challenges in sDSSC research. Besides that, the crystallization tendency of **I5-1** reduces the operation hours at maximum power conversion and thus hampers the durability of sDSSCs.[32] This clearly reveals that besides the other main components of the sDSSC, such as the sensitizer and the electron transporting material, the HTM requires further enhancement to improve this technology.

5.2 *N*-Heterotriangulene-based Small Molecules as HTMs for sDSSCs

5.2.1 Synthesis and Characterization

As previously discussed in Chapter 3, *N*-heterotriangulene-based molecules combine reasonable hole-transport mobilities (~10^{-3} cm^2 V^{-1} s^{-1}) with excellent stability in OFETs. Both characteristics are highly relevant for the performance of sDSSCs and hence make *N*-heterotriangulenes potentially interesting as HTMs in organic photovoltaics (OPV). To evaluate this, two small molecules with different electron-donating abilities were initially designed based on the previously described functionalization strategy (Scheme 5-1).
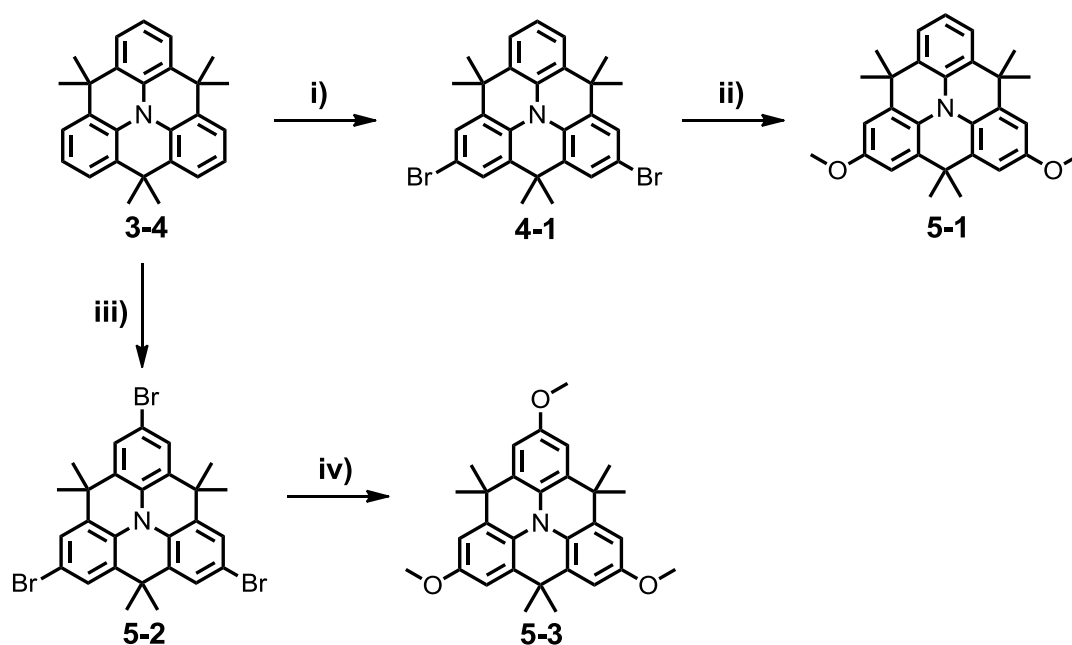
Scheme 5-1. Synthetic route for the selective methoxylation toward **5-1** and **5-3**. Conditions: i) 2 equiv. NBS, CHCl$_3$, 0 °C to RT, 2h, 77%; ii) NaOMe, CuI, DMF, 100 °C, 12h, 70%; iii) 3 equiv. NBS, CHCl$_3$, 0 °C to RT, 2h, 90%; iv) NaOMe, CuI, DMF, 100 °C, 12h, 88%.

The attachment of strong electron-donors such as methoxy groups was targeted, to stabilize the HOMO level of the *N*-heterotriangulene moiety and thus increase the ability to transfer holes from the sensitizer. By using a Cu-catalyzed *Ullmann*-type methoxylation reaction with sodium methoxide in the presence of copper(I) iodide, methoxy groups can be introduced to halogenated aryls.[33, 34] Dibromo **4-1** and tribromo *N*-heterotriangulene **5-2** were reacted under these conditions to provide methoxy-substituted **5-1** and **5-3** in 70 and 80% yield, respectively. Both compounds were prone to oxidation to the corresponding radical cation accompanied by the emergence of blue coloration during purification.

Nevertheless, in both cases the partially oxidized species could be reduced back to the colorless neutral compound upon addition of hydrazine.

Suprisingly, dimethoxy *N*-heterotriangulene **5-1** was obtained as colorless oil which solidified upon cooling, whereas **5-3** formed a colorless crystalline material. The difference might be explained by the unsymmetric substitution pattern of **5-1** which led to inefficient packing thus hampering the crystallization process. To slow down the partial oxidation, both compounds were stored in the absence of light in a fridge under argon atmosphere. **5-1** and **5-3** were excellently soluble in organic solvents, such as dichloromethane, THF, toluene and acetone thus enabling their characterization by NMR spectroscopy as representatively shown for **5-3** in Figure 5-2.
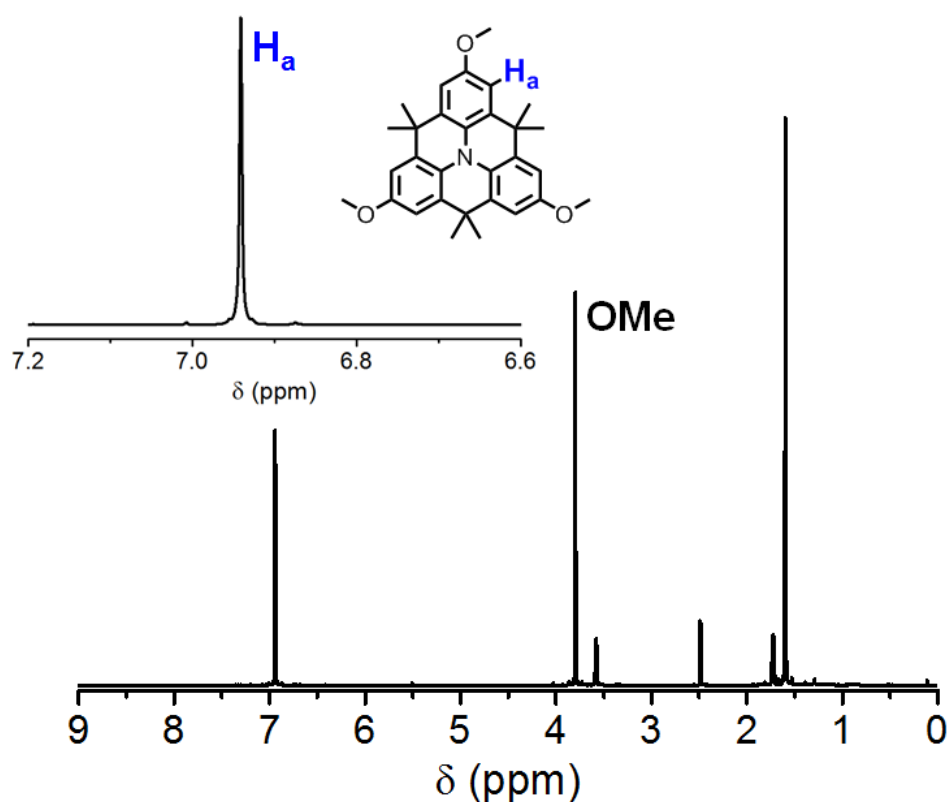
Figure 5-2. ^{1}H NMR spectrum of trismethoxy *N*-heterotriangulene **5-3** in THF-d$_8$ at 25 °C. Inset: Zoom into the aromatic region with proton assignment.

As a result of the symmetric nature of trimethoxy *N*-heterotriangulene **5-3**, three sets of sharp signals were obtained at 1.60, 3.80 and 6.94 ppm, which were unambiguously assigned to the methyl-, methoxy- and aromatic protons. In addition, single crystals suitable for X-ray diffraction analysis were grown by slow evaporation of a THF solution of **5-3** (Figure 5-3). The crystals belong to the triclinic system with a space group $P\bar{1}$ having two independent molecules per unit cell. The central nitrogens were found to have

(a)   (b)
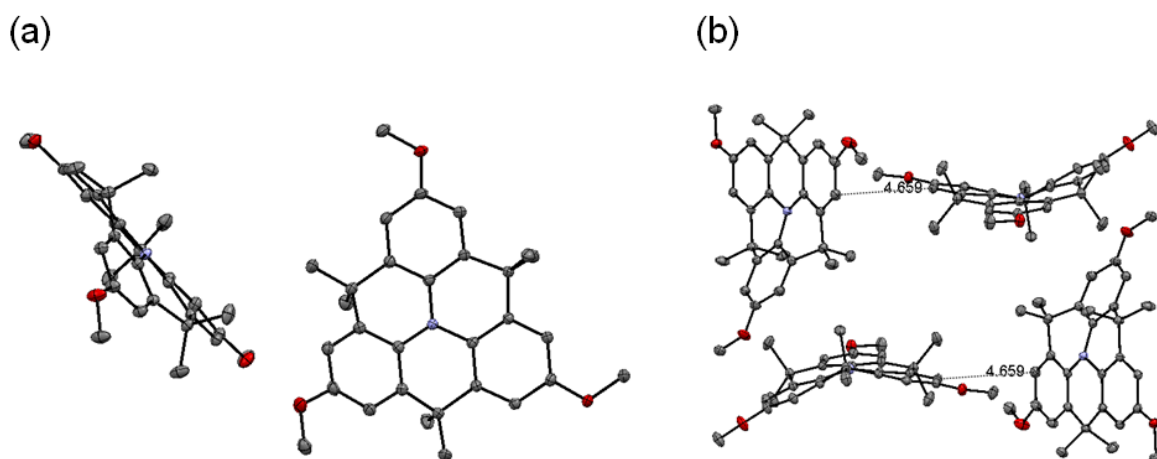
Figure 5-3. X-ray crystal structure of trismethoxy *N*-heterotriangulene **5-3**. (a) Top view (nitrogen atoms in blue, carbon atoms in grey, hydrogens omitted for clarity). (b) Side view of the unit cell. The dashed lines indicate the shortest distance between two molecules of 4.66 Å (hydrogens omitted for clarity).

small deviations from planarity as revealed by the sum of the three C−N−C angles (355.7(7)°). Furthermore, the average N−C(sp^2) bond length of 1.43 Å is not affected by the methoxy substituents (1.43 Å for **3-4**) and does not differ significantly from that in triphenylamine (1.42 Å).[35] Short distances were found for the edge-to-face oriented molecules in the unit cell with shortest *inter*molecular distances of 4.66 Å (Figure 5-3 b).

A key parameter for applications of the HTM in sDSSCs is a high transparency in the visible to NIR region.[36, 37] Therefore, the UV-vis absorption properties of **5-1** and **5-3** were measured in dichloromethane solutions and the respective absorption spectra are shown in Figure 5-4 a. Both compounds displayed longest wavelength absorptions in the spectral window between 275 to 375 nm, revealing their large band gap character. The additional methoxy group in **5-3** ($\lambda_{abs,max}$ = 299 nm, ε = 139 800 L mol^{-1} cm^{-1}; **5-1**: $\lambda_{abs,max}$ = 300 nm, ε = 55 000 L mol^{-1} cm^{-1}) influenced rather the extinction coefficient than the position of the absorption band. This ensured the required transparency in the visible region to minimize the absorption of the potential HTM in the sDSSC. The electron-donating character of a HTM is not only reflected in the absorption spectrum but also in the first ionization potentials (IP). Therefore, DFT calculations were performed on *N*-heterotriangulenes **5-1** and **5-3** in collaboration with ▮▮▮▮▮▮▮▮▮▮ and ▮▮▮▮▮▮▮▮▮▮ at BASF SE Ludwigshafen, Germany.[38-41] This revealed IPs of 4.92 eV and 4.76 eV for **5-1** and **5-3**, respectively. As expected, the additional methoxy groups increase the electron-donating character of **5-3** compared to **5-1**. Moreover, DFT calculations (B3LYP/6-31G*) revealed a *C$_3$* symmetric HOMO orbital of **5-3** with contributions at the central nitrogen and the methoxy groups (Figure 5-4 c).[38]
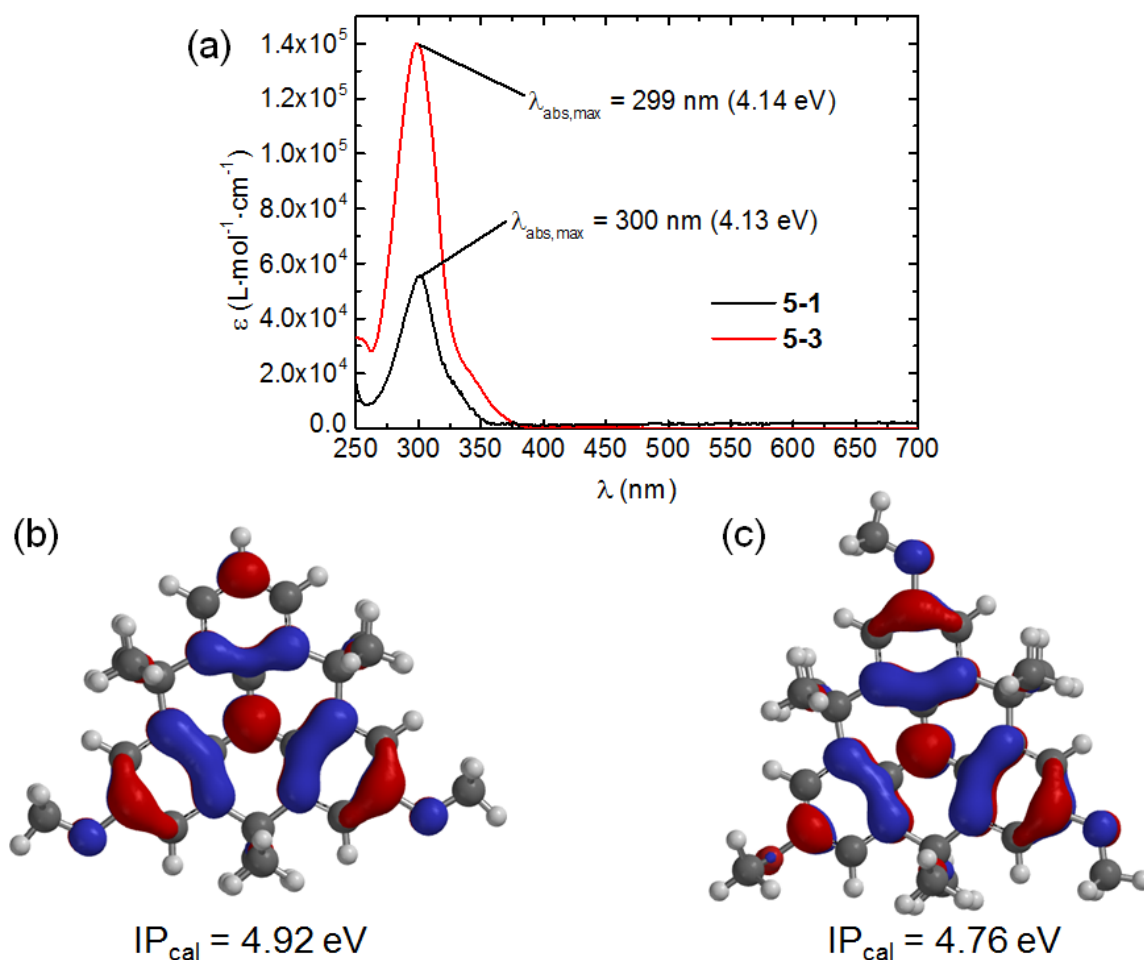
Figure 5-4. (a) UV-vis absorption spectra of **5-1** (black line) and **5-3** (red line). For all spectra: 1×10^{-6} M in CH$_2$Cl$_2$. Orbital surfaces of the HOMO levels of **5-1** (b) and **5-3** (c) obtained by DFT calculation (B3LYP/6-31G*) and the respective ionization potentials calculated by BASF SE.[38-41]

Due to the unsymmetric substitution, the HOMO orbital of **5-1** showed C_{2v} symmetry with main contributions at the nitrogen and both methoxy groups (Figure 5-4 b). Since the respective electron affinity and the LUMO level were considered to be marginally important for the hole-transport in sDSSCs, they will not be further discussed in the following.

The HOMO level of commonly used dyes in sDSSCs, such as perylene monoimide derivatives, are located around |5.1| to |5.4| eV, thus well above the ionization potential of **5-1** and **5-3** providing approximately 0.4 to 0.2 eV driving force for the hole-transport.[42] Moreover, the calculated ionization potential of trimethoxy *N*-heterotriangulene **5-3** (4.76 eV) is in the same region as that IP of the commonly used HTM spiro-MeOTAD **I5-1** (4.77 eV) thus revealing its potential for a successful hole-transport in sDSSCs.[26]

5.2.2 sDSSC Characterization

Solid-state dye-sensitized solar cells (sDSSCs) based on **5-1** and **5-3** as HTMs were processed and measured in collaboration with ███████████████████ und ████████████████ at BASF SE, Ludwigshafen. They were fabricated on a fluorine-doped tin oxide (FTO) covered glass substrate with titanium dioxide as the inorganic semiconductor. The electrode was sensitized in a toluene solution of organic additive and a perylene monoimide based dye (ID504) having a HOMO level of |5.40| eV.[43] The HTM (**5-1** or **5-3**) was subsequently spin-coated followed by evaporation of the silver counter electrode on top.
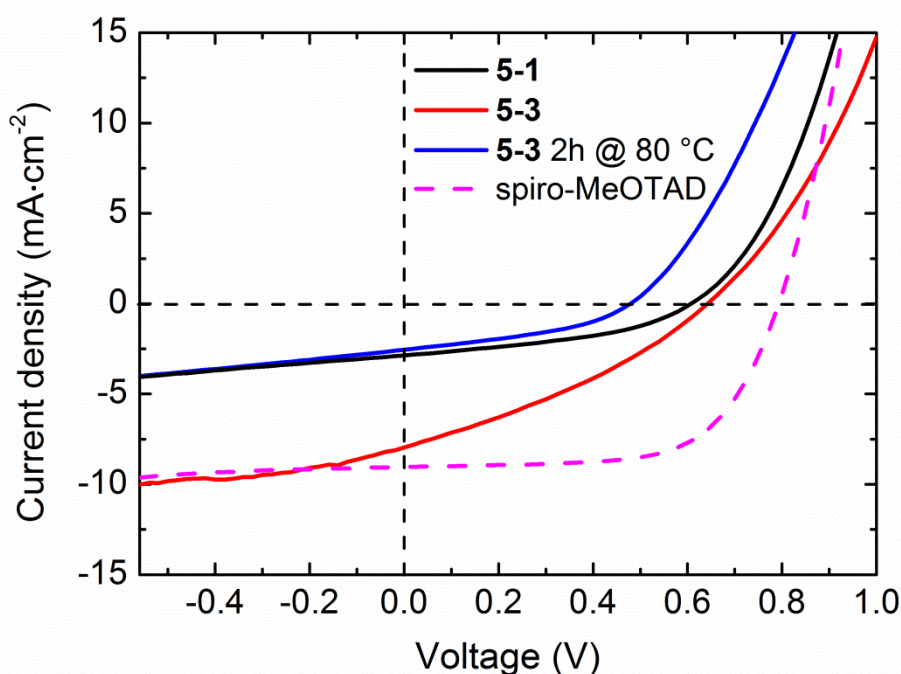
Figure 5-5. I-V-curves of sDSSCs with **5-1** (black line), **5-3** (red and blue line) and spiro-MeOTAD (magenta line) as hole-transport layer under AM 1.5G illumination.

Table 5-1. Photovoltaic performance of the HTMs **5-1**, **5-3** and spiro-MeOTAD (**I5-1**).

HTM	IP_{cal}[a] (eV)	ΔE[b] (eV)	$\sigma \times 10^{-5}$ (S cm^{-1})	V_{OC}[a] (mV)	I_{SC}[a] (mA cm^{-2})	FF[a] (%)	PCE[a] (%)
5-1	4.92	0.48	0.66	600	−2.87	41	0.7
5-3	4.76	0.64	1.04	640	−7.96	33	1.7
5-3	4.76	0.64	1.04	480[c]	−2.56[c]	39[c]	0.5[c]
I5-1	4.77	0.63	3.32	800	−9.06	64	4.6

[a] The cell preparation was undertaken by BASF SE. They were processed from toluene using ID504 as dye together with an additive. The cell performance was measured under 1 sun. [b] $\Delta E = |HOMO_{dye}| - IP_{cal}$. [c] Prior to the measurement, the hole-transport layer was annealed at 80 °C for two hours.

Measurements were carried out under simulated AM 1.5G illumination at 1 sun. In addition conductivity (σ) measurements of the pristine HTMs were carried out. The results are shown in Figure 5-5 and are summarized in Table 5-1.

The cell fabricated from dimethoxy *N*-heterotriangulene **5-1** as HTM revealed a short circuit current (I_{SC}) of -2.87 mA cm^{-2}, an open circuit voltage (V_{OC}) of 600 mV and a fill factor (FF) of 41%, which led to an overall power conversion efficiency (PCE) of 0.7% under 1 sun. The weak performance can be mainly attributed to the low short circuit current (I_{SC}) in comparison to the reference cell using spiro-MeOTAD (**I5-1**) as HTM having a PCE of 4.6%. In contrast to that, the cell using trimethoxy *N*-heterotriangulene **5-3** as HTM fabricated under identical conditions displayed a significantly increased I_{SC} of -7.96 mA cm^{-2} and a V_{OC} of 640 mV. The fill factor, however, remained low, compared with the reference cell using **I5-1** as HTM.
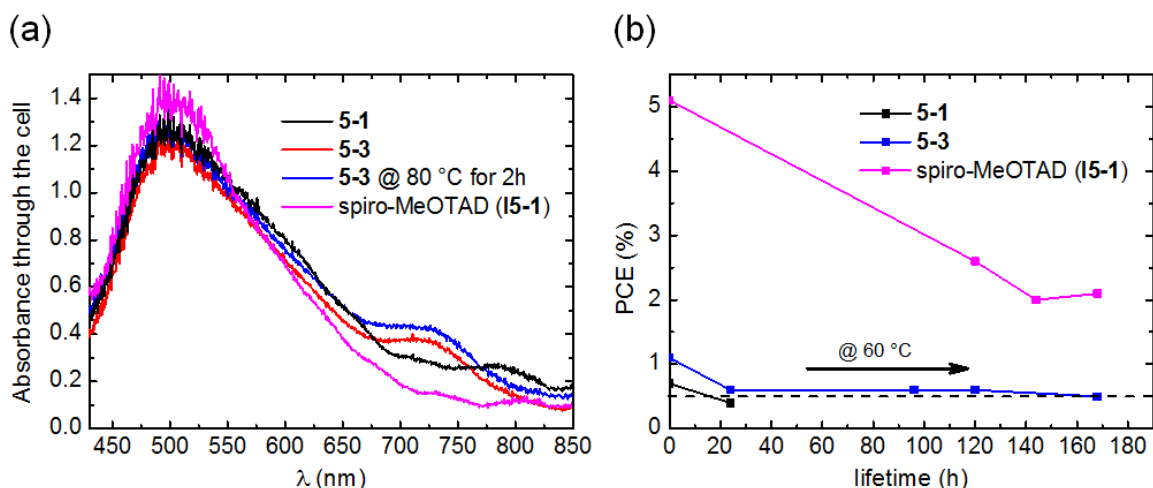
Figure 5-6. (a) UV-vis absorption spectrum measured through the whole sDSSC utilizing **5-1** (black line), **5-3** (red and blue line) and spiro-MeOTAD (magenta line) as HTMs. (b) Power conversion efficiency of the sDSSCs as a function of the lifetime utilizing **5-1** (black line), **5-3** (blue line) and spiro-MeOTAD (magenta line) as HTMs at 60 °C.

This resulted in an overall PCE of 1.7%. Further annealing of the hole-transport layer of **5-3** at 80 °C for two hours prior to the measurement had basically a detrimental influence on the outcome as a result of the decreased I_{SC}. The differences in the performance of **5-1** and **5-3** can be mainly attributed to the large deviation of both in the short circuit current (I_{SC}). Due to an increased IP of **5-1**, a weaker driving force for the regeneration of the dye is observed, which occurs by a hole-transport from the dye`s HOMO level to the HOMO of the HTM. Thus, the I_{SC} of the respective cell is intrinsically lowered. This observation is in agreement with previous reports of *Snaith* and *Kroeze*, showing an exponential decay (improvement) in I_{SC} by decreasing (increasing) the energy offset between the HTM and

the dye.[26, 36] Moreover, the conductivity of the HTM is a key parameter for an efficient hole-transport. With respect to this **5-1** ($\sigma = 0.66 \times 10^{-5}$ S cm^{-1}) and **5-3** ($\sigma = 1.04 \times 10^{-5}$ S cm^{-1}) showed a slightly lower conductivity than spiro-MeOTAD ($\sigma = 3.32 \times 10^{-5}$ S cm^{-1}). This might be attributed to the large *inter*molecular distances in the solid state of the *N*-heterotriangulene based HTMs (~4.66 Å, see Figure 5-3) as a result of the perpendicularly oriented dimethylmethylene bridging groups in **5-1** and **5-3**.

Investigation of the UV-vis absorption through the whole sDSSC revealed differences around 700 nm between the three HTMs (Figure 5-6 a). All cells displayed broad dye absorptions between 400 to 700 nm. In addition, the cells fabricated with **5-1** and **5-3** as HTMs led to the formation of an additional band between 700 and 850 nm. Such absorption bands are typically observed for radical cation species of triarylamines as shown in the previous chapter, suggesting a partial oxidation of **5-1** and **5-3** during the fabrication process.[44-46] This led to a change of the hole injection barrier which influenced simultaneously σ and I$_{SC}$. It changes furthermore the energy offset between the HTM and titanium dioxide thus affecting V$_{OC}$.

As discussed in the introduction, spiro-MeOTAD (**I5-1**) is nowadays the widely used HTM in sDSSC reaching record PCEs. Due to its crystallization tendency inside the titanium dioxide pores, however, the long-term stability of such sDSSCs is significantly hampered.[32] With respect to this destabilization, *N*-heterotriangulene derivatives **5-1** and **5-3** were examined regarding their thermal stability in sDSSCs (Figure 5-6 b) by constantly illuminating the cells under simulated AM 1.5G at 1 sun at a temperature of 60 °C, while recording the PCE. For comparison the reference cell with spiro-MeOTAD (**I5-1**) was treated under the same conditions. Experiments were stopped after reaching a PCE of 0.5%. The device using **5-1** as HTM showed thereby a drop of initially 0.7% to 0.4% PCE within one day and was therefore not further studied. A similar decline from 1.1% to 0.6% after one day was observed for the device using **5-3**. It is speculated that the initial drop might be a result of crystallization inside the titanium dioxide pores in combination with partial doping of the HTM, due to an oxidation of **5-1** and **5-3** to the radical cation species. In the following days (2 to 7 days), however, the PCE of the respective sDSSC remained practically constant and reached a PCE of 0.5% after one week. For comparison, the reference sDSSC utilizing spiro-MeOTAD (**I5-1**) as HTM showed a drop in PCE from initially 5.1% to 2.1%, reflecting again a restricted long term stability.

Although the overall photovoltaic performance of **5-1** and **5-3** showed virtually no improvement in comparison with spiro-MeOTAD (**I5-1**), the obtained results were encouraging for further optimization.

5.3 *N*-Heterotriangulene Oligomers as HTMs for sDSSCs

5.3.1 Synthesis and Characterization

Considering the excellent stability of the linear *N*-heterotriangulene polymer **P1** as active layer in OFETs, as previously shown in Chapter 3, the elongation of the π-conjugated backbone of the aforementioned small molecule HTMs might be a chance to overcome their drawbacks. By increasing the molecular size of the *N*-heterotriangulenes, the crystallization tendency was expected to be decreased which is beneficial from the viewpoint of long-term stability. Moreover, the variation of the π-conjugation length enables the tuning of the energy levels. The utilization of polymeric HTMs, however, is expected to have a more detrimental influence on the outcome of the sDSSCs as a result of a decreased pore filling of larger polymer chains.
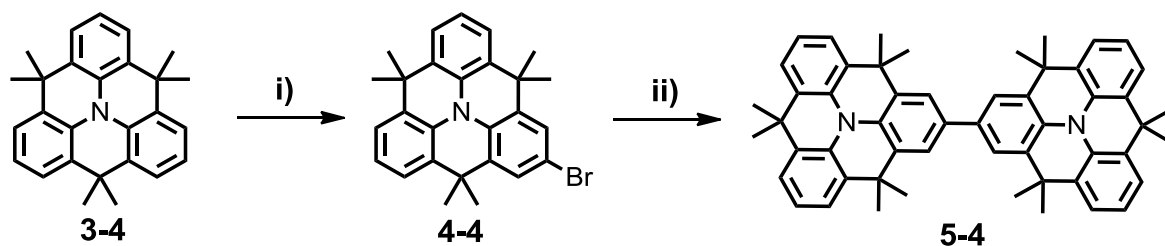
Scheme 5-2. Synthetic route toward *N*-heterotriangulene dime **5-4**. Conditions: i) 1 equiv. NBS, CHCl$_3$, 0 °C to RT, 2h, 90%; ii) bis(cycloocta-1,5-diene)nickel(0), cycloocta-1,5-diene, 2,2'-bipyridine, toluene/DMF, 85 °C, 2 days, 80%.

The synthesis of a *N*-heterotriangulene dimer (**5-4**) was initially aimed (Scheme 5-2). The reaction sequence started with a mono-bromination of **3-4** referring to the previous procedures. For a direct dimerization of mono-bromo *N*-heterotriangulene **4-4**, the *Yamamoto* reaction proved again to be the most suitable method and provided dimer **5-4** in 80% yield.[47, 48]

It showed an excellent solubility in organic solvents such as dichloromethane, THF, toluene and acetone thus enabling its characterization by NMR spectroscopy (Figure 5-7). Three sharp sets of aromatic signals with a ratio of 1 to 2 to 1 were observed in the ^{1}H NMR spectrum of **5-4**. The chemically unequal dimethylmethylene protons caused two distinct signals in the aliphatic region with correct signal intensities. The assignment of the
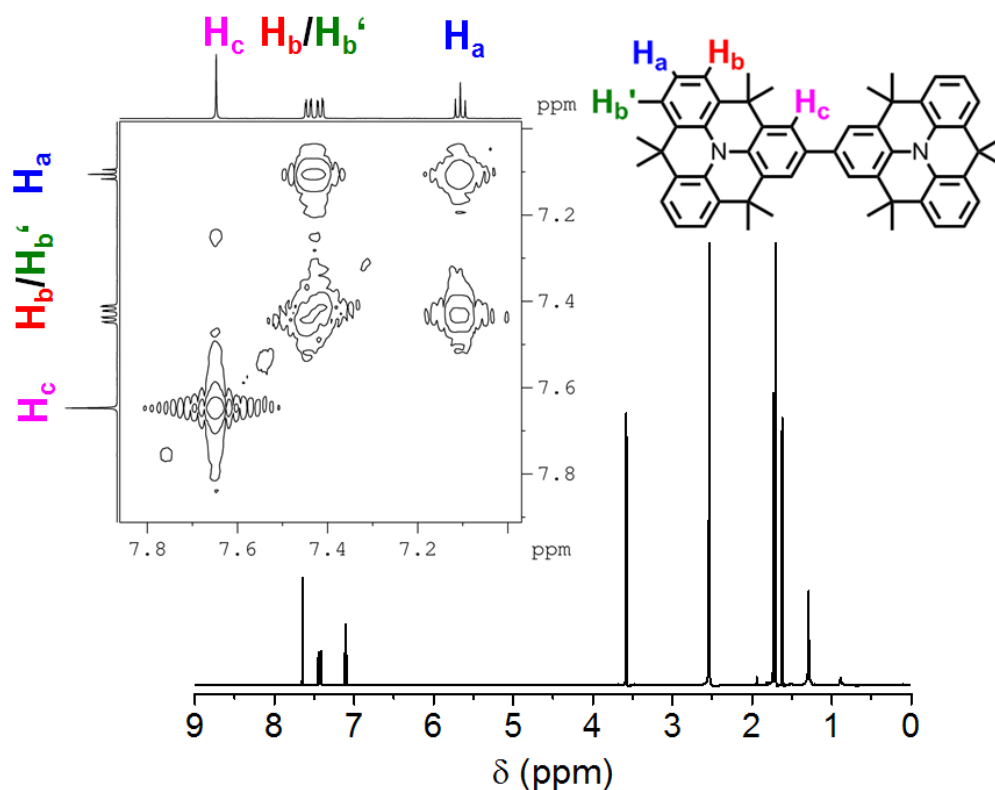
Figure 5-7. ^{1}H NMR spectrum of *N*-heterotriangulene dimer **5-4** in THF-d$_8$ at 25 °C. Inset: Two-dimensional proton correlation (^{1}H, ^{1}H COSY) of **5-4** with proton assignment.

aromatic protons was achieved with the help of their relative intensities and by two-dimensional proton correlation (^{1}H, ^{1}H COSY) NMR spectroscopy. The triplet at 7.06 ppm was therefore assigned to the protons, *para* to the central nitrogen (H$_a$) in agreement with previous findings. In addition, the doublet at 7.34 ppm originated from the unequal adjacent protons (H$_b$/H$_b$') giving rise to a cross peak in the ^{1}H, ^{1}H COSY spectrum as a result of *ortho*-coupling with H$_a$ (Figure 5-7, inset). Finally, the resonance at 7.55 ppm was attributed to the protons (H$_c$) in close proximity to the attached *N*-heterotriangulene moiety.

By slow evaporation of a dichloromethane/*n*-hexane solution, single crystals of **5-4** suitable for X-ray diffraction analysis were grown. The compound crystallizes in the monoclinic space group C2/*c* with six independent molecules in the unit cell (Figure 5-8). The angles at the central nitrogen sum up to 357.7(6)° in both *N*-heterotriangulene moieties indicating almost no pyramidalization at these atoms (for comparison 355.7(7)° in **5-3**). Furthermore, the average N−C(sp^2) bond length (1.42 Å) remains almost unaffected by the dimerization and does not differ significantly from that of pristine *N*-heterotriangulene **3-4** (1.43 Å) and triphenylamine (1.42 Å).[35] Surprisingly, the dihedral angle between the
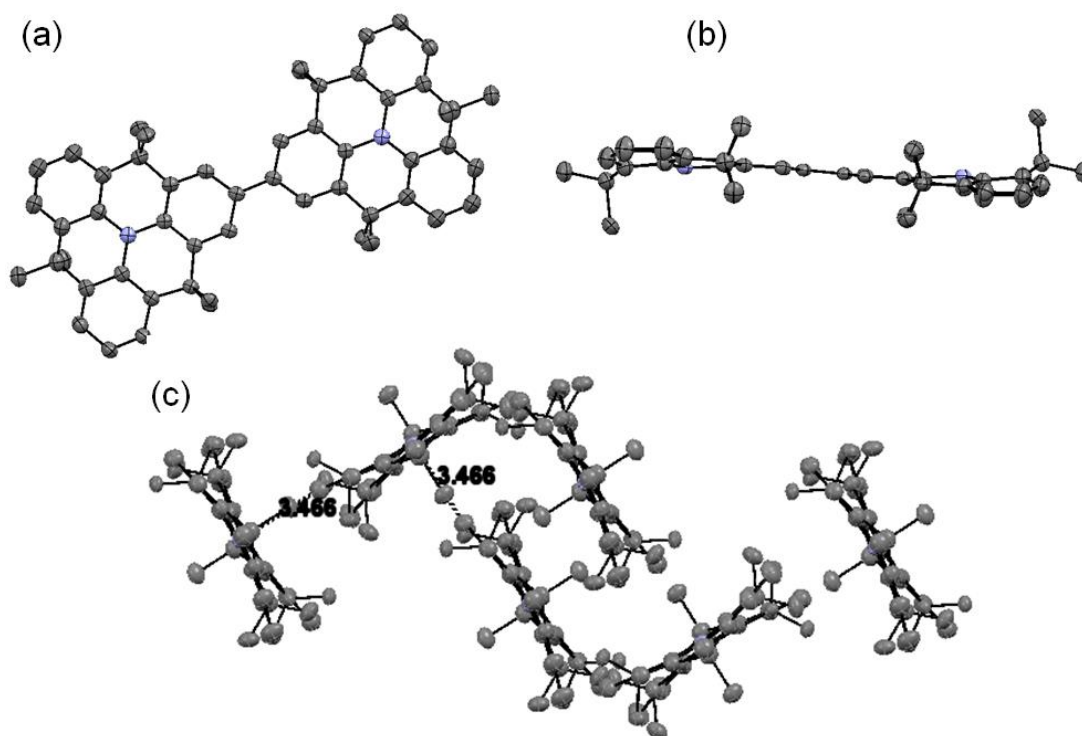
Figure 5-8. X-ray crystal structure of *N*-heterotriangulene dimer **5-4**. (a) Top view (nitrogen atoms in blue, carbon atoms in grey, hydrogens omitted for clarity) and (b) side view. (c) Side view of the unit cell. The dashed lines indicate the shortest distance between two molecules of 4.66 Å (hydrogens omitted for clarity).

covalently connected *N*-heterotriangulenes is extremely low (0.8(5)°) despite the sterical crowding of the *ortho-* protons and therefore significantly lower than in hexameric macrocycle **4-2** (13.8(9)° to 35.5(4)°, see above). For comparison, the dihedral angle observed in biphenyl is 44.4°. This comes, however, at the expense of a slightly elongated bond length of 1.47 Å between both *N*-heterotriangulenes (~1.44 Å for **4-2**). The independent molecules within the asymmetric unit are arranged in an edge-to-face orientation with virtually short average distances of 3.47 Å (**5-3**: 4.66 Å), which might be beneficial for the charge carrier transport in the sDSSC.

Upon dimerization, the facile crystallization of the *N*-heterotriangulene moiety retained, thus altering the sDSSC performance. Therefore, an *N*-heterotriangulene oligomer was aimed which was envisaged to show amorphous behavior in the solid state and to possess an adequate size for an efficient filling of the titanium dioxide pores.

During the course of the multistep macrocycle synthesis, discussed in Chapter 4, a linear nonamer **4-9** was obtained as a byproduct. With its monodisperse structure being composed of nine *N*-heterotriangulene units, **4-9** builds a link between the small molecules **5-1** and **5-3** and the linear polymer **P1** presented in Chapter 3. To obtain **4-9** in an
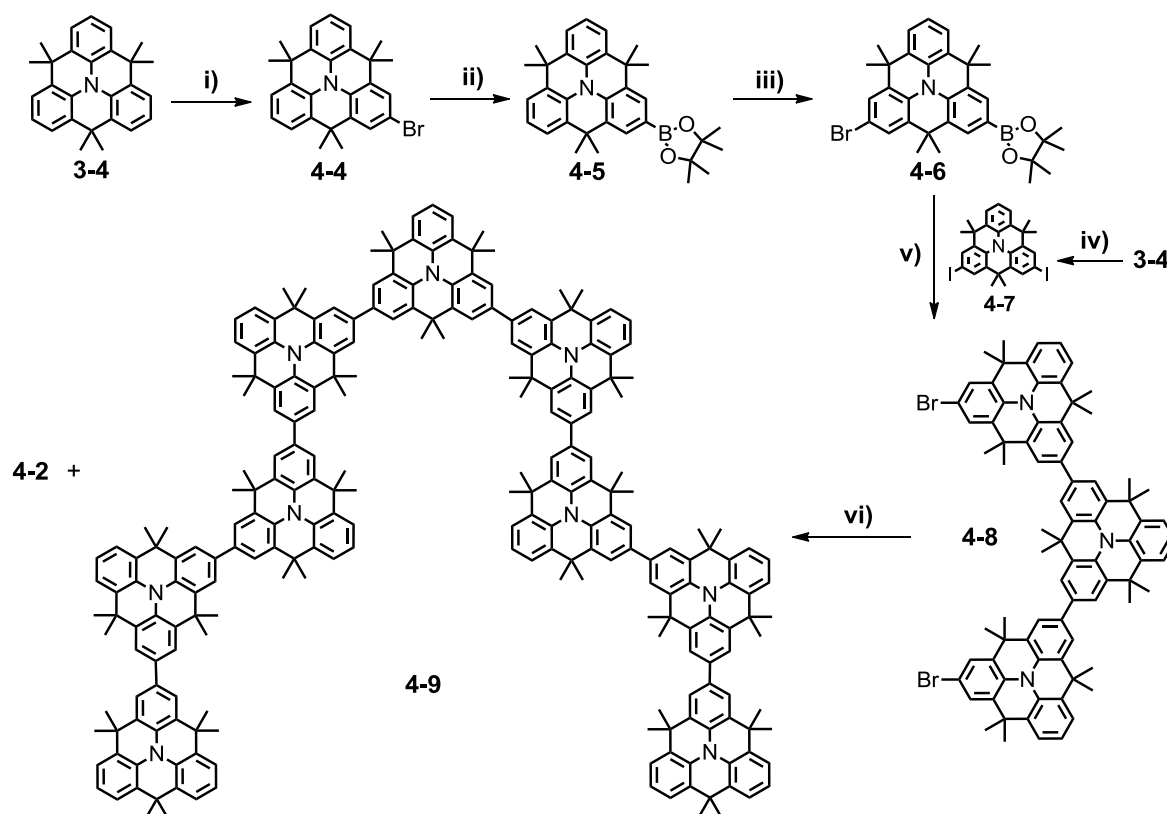
Scheme 5-3. Synthetic route of the stepwise synthesis toward *N*-heterotriangulene nonamer **4-9**. Conditions: i) 1 equiv. NBS, CHCl₃, 0 °C to RT, 2h, 90%; ii) Pd(dppf)Cl₂, KOAc, bis(pinacolato)diboron, DMF, 85 °C, 12h, 86%; iii) 1 equiv. NBS, CHCl₃, 0 °C to RT, 18h, 75%; iv) 2 equiv. NIS, CHCl₃, 0 °C to 50 °C, 96h, 89%; v) Pd(PPh₃)₄, 2 M aq. Na₂CO₃, toluene, *Aliquat 336*, 65 °C, 3 days, 55%; vi) bis(cycloocta-1,5-diene)nickel(0), cycloocta-1,5-diene, 2,2'-bipyridine, toluene/DMF, $c = 3.8 \times 10^{-3}$ M, 85 °C, 2 days, **4-9**: 15%.

appropriate quantity for the utilization as HTM in sDSSCs, the reaction sequence was repeated thus providing nonamer **4-9** on a several hundred milligram scale (Scheme 5-3). The analysis of the MALDI-TOF MS data can be found in Chapter 4. Due to its excellent solubility in organic solvents, it was further characterized by means of NMR spectroscopy. The ¹H NMR spectrum of **4-9** revealed the linear conformation of **4-9** by less symmetric and broadened signals being reminiscent of linear polymer **P1** (Figure 5-9). In line with the previously discussed *N*-heterotriangulene materials, the spectrum of **4-9** showed three sets of aromatic signals indicating three major types of aromatic protons. The appearance is mainly caused by the different types of protons located at the terminal *N*-heterotriangulene moieties (H$_a$, H$_b$, H$_b$', H$_c$) together with the protons located at the internal subunits (H$_e$, H$_f$, H$_f$', H$_d$). With the help of two-dimensional proton correlation (¹H, ¹H COSY) spectroscopy the signals were assigned to the appropriate protons, showing a cross peak between the different types of peripheral protons (H$_a$, H$_b$, H$_b$', H$_e$, H$_f$, H$_f$'). Moreover, the broadened
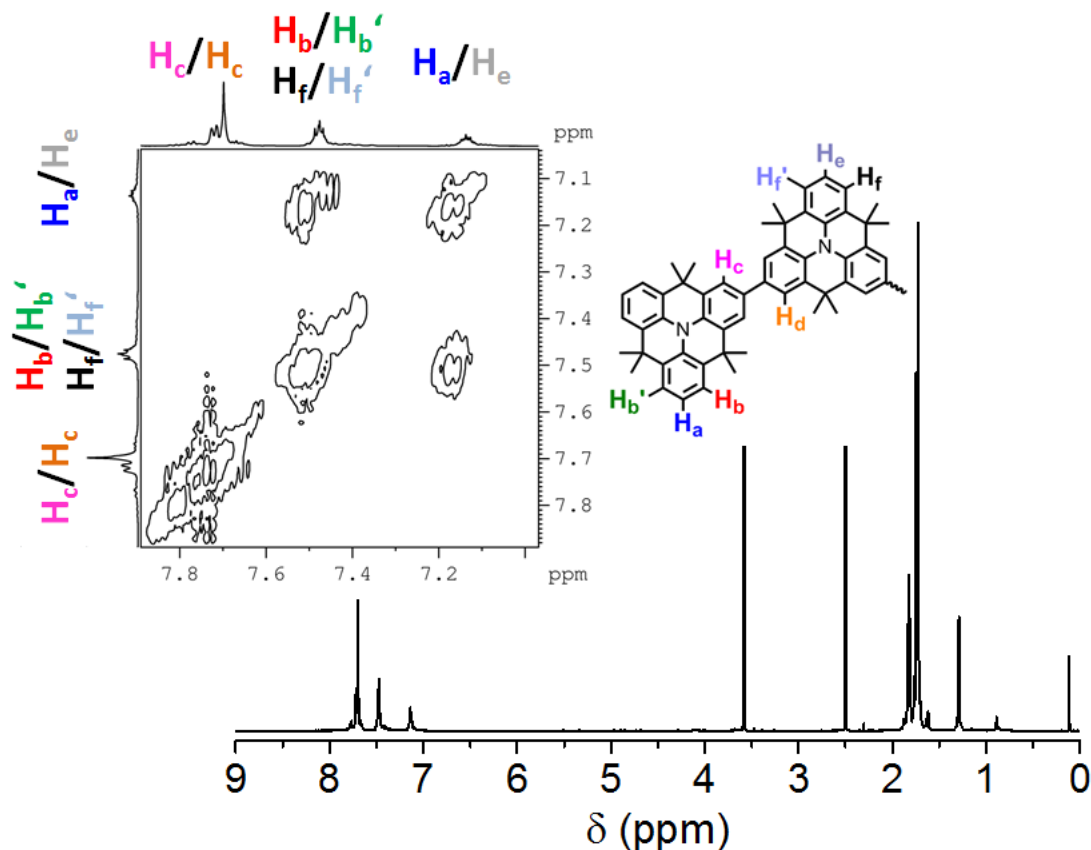
Figure 5-9. ^{1}H NMR spectrum of *N*-heterotriangulene nonamer **4-9** in THF-d$_8$ at 25 °C. Inset: Two-dimensional proton correlation (^{1}H, ^{1}H COSY) of **4-9** with proton assignment.

signal at 1.8 ppm corresponded to the bridging dimethylmethylene protons, showing correct signal intensities.

Dimer **5-4** and nonamer **4-9** were furthermore investigated by UV-vis absorption spectroscopy (Figure 5-10 a). Both compounds showed absorptions between 250 nm and 400 nm, respectively, reflecting a high level of transparency in the visible to near-IR region. The increased π-conjugation of **4-9** had a stronger impact on the extinction coefficient rather than on the position of the absorption band (**5-4**: $\lambda_{abs,max} = 364$ nm, $\varepsilon = 139\ 800$ L mol^{-1} cm^{-1}; **4-9**: $\lambda_{abs,max} = 383$ nm, $\varepsilon = 19\ 300$ L mol^{-1} cm^{-1}) reflecting the applicability of both compounds as HTMs in sDSSCs.

Calculation of the first ionization potentials for **5-4** and **4-9** resulted in IPs of 4.88 and 4.44 eV, respectively. Additionally, DFT calculations were carried out on dimer **5-4** displaying a totally symmetric HOMO level (B3LYP/6-31G*) with contributions of the central nitrogen and C−C connected benzene rings (Figure 5-10 b).[38] The increased electron-donating strength of **4-9** is displayed by a reduced IP. Similar orbital contributions were expected along the linear chain of nonamer **4-9**.
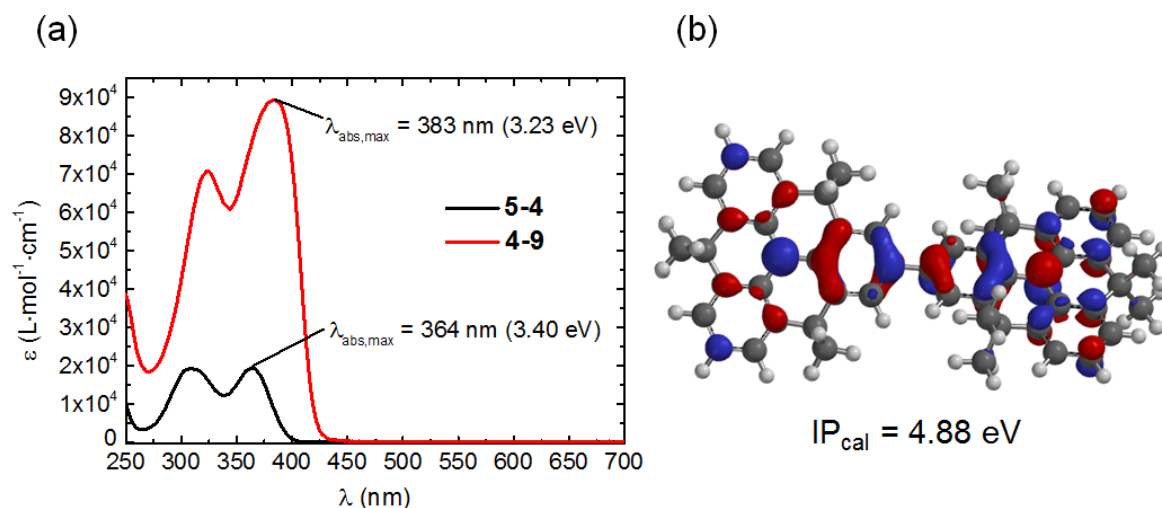
Figure 5-10. (a) UV-vis absorption spectra of **5-4** (black line) and **4-9** (red line). For all spectra: 1×10^{-6} M in CH_2Cl_2. Orbital surfaces of the HOMO level of **5-4** by DFT calculation (B3LYP/6-31G*) and the respective ionization potentials calculated by BASF SE.[38-41]

5.3.2 sDSSCs Characterization

To ensure comparability of the results, both HTMs were incorporated in sDSSCs following the same procedure as utilized for **5-1** and **5-3** (see above). The results are shown in Figure 5-11 and summarized in Table 5-2.

The cell fabricated using *N*-heterotriangulene dimer **5-4** revealed an I_{SC} of −4.27 mA cm^{-2}, a V_{OC} of 860 mV with a fill factor of 36%, which led to an overall PCE of 1.3% under 1 sun. Annealing the hole-transport layer prior to the measurement did not improve the output. In contrast to that the cell using nonamer **4-9** as HTM resulted in an I_{SC} of −6.30 mA cm^{-2}, a V_{OC} of 820 mV and a FF of 45%, giving rise to a PCE of 2.3%. By annealing of **4-9** at 80 °C for two hours, the V_{OC} and the fill factor were particularly enhanced as a result of an enlarged gap between the conduction band of titanium dioxide and the valence band of **4-9**. An increased PCE of 2.8% was thereby obtained, which still did not reach the performance of spiro-MeOTAD **I5-1** (PCE = 4.3%). However, this is so far one of the best values obtained for spiro-MeOTAD alternatives in sDSSCs.[23] The significant drop in the output characteristics of the sDSSCs after annealing of dimer **5-4** might be caused by an induced crystallization process inside the titanium dioxide pores thus hampering the dye regeneration. Similar observations have been made for trimethoxy *N*-heterotriangulene **5-3** (see above). Due to the increased size and thereby reduced crystallization tendency of nonamer **4-9**, the output characteristics were improved after annealing.
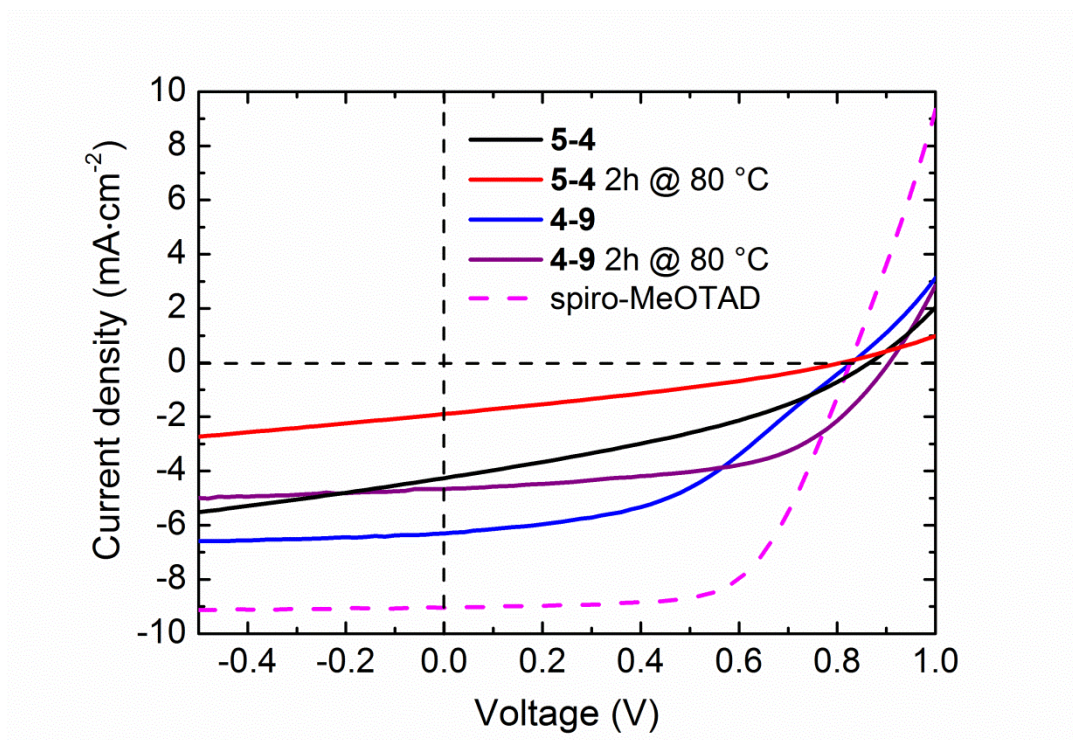
Figure 5-11. I-V-curves of sDSSCs with **5-4** (black line), **4-9** (red and blue line) and spiro-MeOTAD (magenta line) as hole-transport layer under AM 1.5G illumination.

Table 5-2. Photovoltaic performance of the HTMs **5-4**, **4-9** and spiro-MeOTAD (**I5-1**).

HTM	IP_{cal}[a] (eV)	$\varDelta E$[b] (eV)	V_{OC}[a] (mV)	I_{SC}[a] (mA cm^{-2})	FF[a] (%)	PCE[a] (%)
5-4	4.88	0.52	860	−4.27	36	1.3
5-4	4.88	0.52	800[c]	−1.90[c]	31[c]	0.5[c]
4-9	4.44	0.96	820	−6.30	45	2.3
4-9	4.44	0.96	900[c]	−5.35[c]	58[c]	2.8[c]
I5-1	4.77	0.63	860	−7.19	68	4.3

[a] The cell preparation was undertaken by BASF SE. They were processed from toluene using ID504 as dye together with an additive. The cell performance was measured under 1 sun. [b] $\varDelta E = |HOMO_{dye}|-IP_{cal}$. [c] Prior to the measurement, the hole-transport layer was annealed at 80 °C for two hours.

By taking a closer look at the thermal propertie of **4-9** with the help of differential scanning calorimetry (DSC), no phase transitions were revealed, reflecting the amorphous character of **4-9** (Figure 5-12). This indicated that no rearrangement of the local structure organization or an improvement of the *intra*molecular π-orbital overlap occurred upon heating of **4-9**, which would similarly explain an increase in V_{OC} and the fill factor. It is thus speculated that the annealing promoted a partial doping as a result of spontaneous oxidation of **4-9** to the corresponding radical cation species, which allowed for a more efficient hole-transport from the dye to the HTM. However, the differences between the
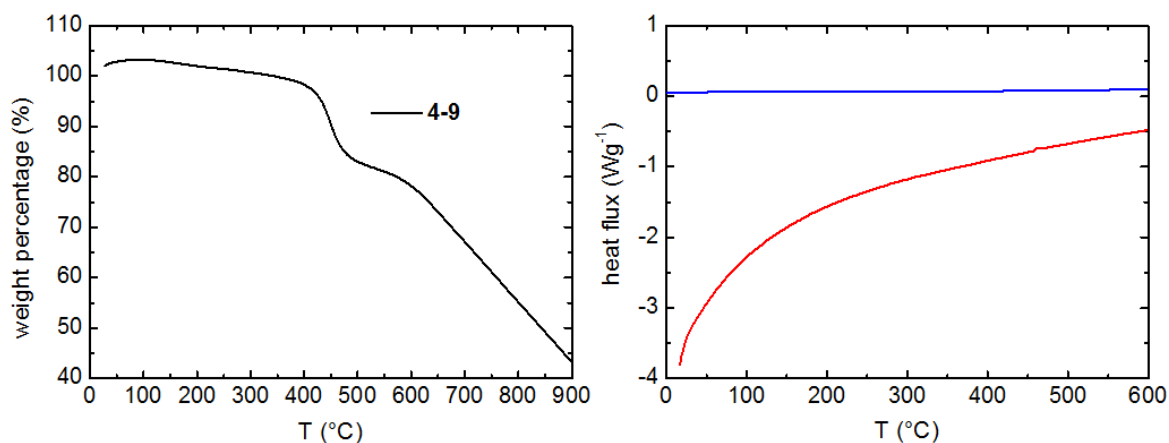
Figure 5-12. Left: Thermogravimetric analysis of *N*-heterotriangulene nonamer **4-9**. Right: DSC traces of **4-9** applying heating/cooling rates 10 °C/min (red line = heating, blue line = cooling).

PCE of the cell using **4-9** compared with the spiro-MeOTAD (**I5-1**) reference cell as the HTM were mainly attributed the corresponding I_{SC} caused by the too low IP of **4-9**. This, in combination with the rather high I_{SC} observed for trimethoxy *N*-heterotriangulene **5-3** (see above), suggested an ideal energy gap between the HOMO of the dye and the IP of the HTM of around 0.6 eV for an efficient hole-transport. In addition, thermal stability measurements were conducted at 60 °C of the sDSSCs fabricated from **5-4** and **4-9** and compared with the reference cell (Figure 5-13 a). Using *N*-heterotriangulene dimer **5-4** as HTM resulted thereby in a significant decrease in PCE from initially 0.7% to almost 0% after 3 days and was therefore not further studied. Again, this might be caused by the susceptibility of **5-4** to crystallization. Upon utilization of nonamer **4-9** as HTM, however, the PCE of the sDSSC stayed almost constant for 15 days with an initial drop from 2.8% to 2.5% within the first two days. By comparing these results with the reference cell using spiro-MeOTAD **I5-1** as HTM, a superiority of **4-9** is observed after approximately 5 days. While the reference cell showed a further decrease to 1.6%, the PCE of the cell based on **4-9** was measured to be still 2.4% after two weeks. In other words, after two weeks of operation, sDSSCs utilizing **4-9** as the HTM are working around 30% more efficient than the cells using spiro-MeOTAD (**I5-1**). By running the cell for additional four days at 85 °C the PCE slightly decreased, remained, however, constantly above 2%. Finally, it could not be figured out whether the decreased PCE at 85 °C was caused by decomposition of the HTM or by degradation of the cell encapsulation.

To gain further insight into the stability of the sDSSC utilizing **4-9** as the HTM, the changes of the individual photovoltaic characteristics were recorded as a function of time (Figure 5-13 b-d). In agreement with the PCE values, the I_{SC}, V_{OC} and the fill factor
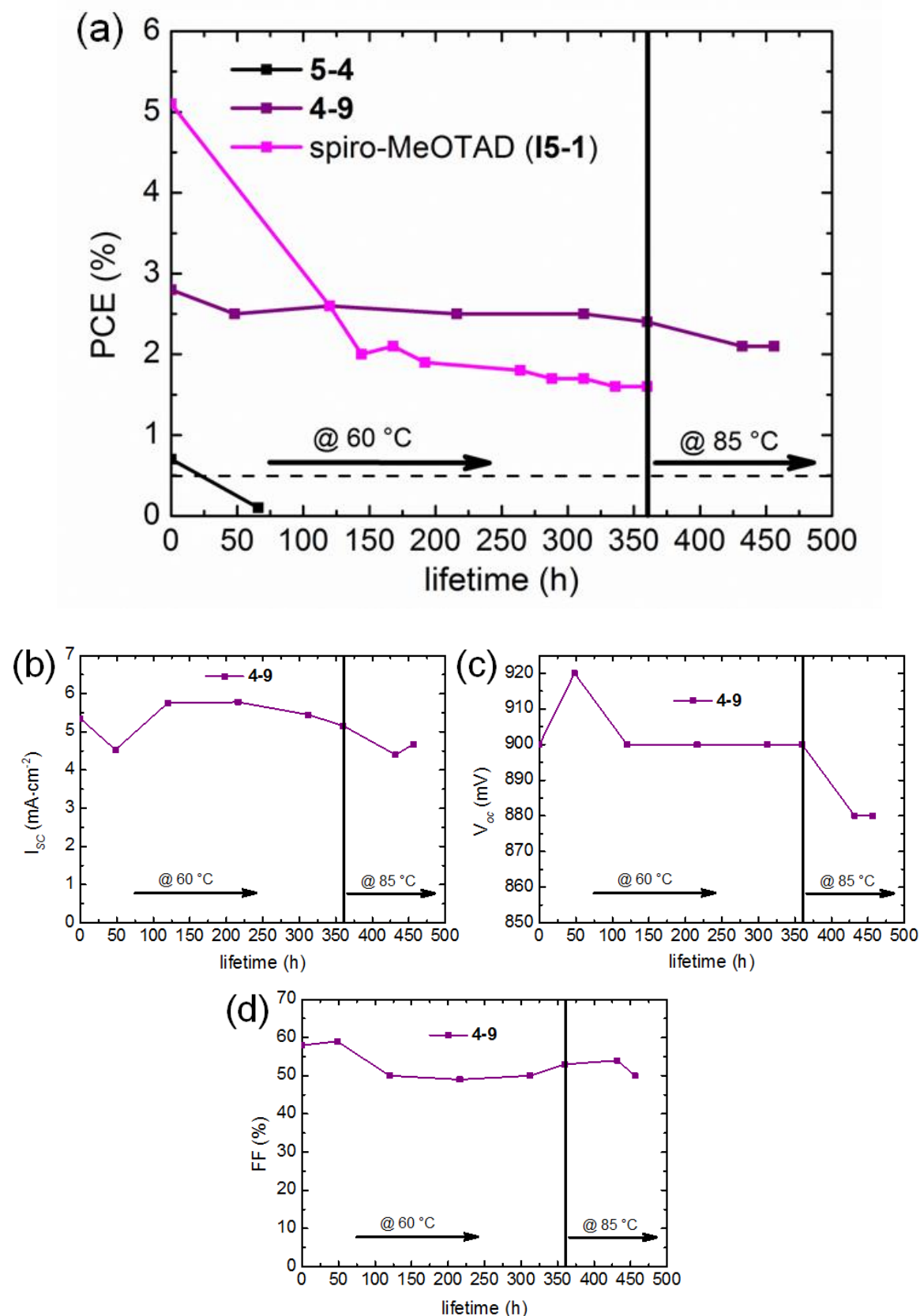
Figure 5-13. Power conversion efficiency (a), current density (b), open-circuit voltage (c) and fill factor (d) of the sDSSCs as a function of the lifetime utilizing **5-4** (black line), **4-9** (violet line) and spiro-MeOTAD (magenta line) as HTMs at 60 °C. Note: After 360 hours the temperature was increased from 60 to 85 °C.

retained more than 85% of their initial values after 19 days of irradiation. While the I_{SC} initially dropped after 2 days, the V_{OC} slightly increased in that time, thus leading to relatively constant values of $I_{SC} = -4.67\,\mathrm{mA\,cm^{-2}}$ and $V_{OC} = 880\,\mathrm{mV}$ after 19 days, respectively. During the same period the fill factor reached a value of 50%. This relatively small decrease in the photovoltaic performance after 450 hours confirmed the robustness of the TiO_2/ID504/**4-9** device architecture, and hence nicely illustrated the durability of this system compared to the spiro-MeOTAD (**I5-1**) counterpart.[49] The remarkable stability is attributed to the formation of an amorphous hole-transport layer of **4-9** at the mesoscopic titanium dioxide surface, thus preventing crystallization inside the pores as observed for devices based on spiro-MeOTAD (**I5-1**). These observations are in excellent agreement with the results of linear *N*-heterotriangulene polymer **P1**, forming highly stable amorphous films, which have been used for OFETs (Chapter 3).

However, it should be finally noted that the results of the herein presented HTMs derived from a first testing whereas **I5-1** has been the subject of optimization for several years. This means that further improvements are to be expected for the *N*-heterotriangulene-based systems.

5.4 Summary

A series of *N*-heterotriangulenes with increased electron-donating ability and extended π-conjugation length have been prepared by straightforward synthetic protocols and studied as alternative HTMs for sDSSCs. With these compounds PCE values of up to 2.8% were reached. Cells based on di- and trimethoxy-substituted small molecules **5-1** and **5-3** revealed respectable I_{SC} values, however, moderate stabilities of the devices. This was mainly addressed to an increased oxidation tendency in combination with a facile crystallization of the small molecule HTMs inside the titanium dioxide pores. By dimerization of *N*-heterotriangulene toward **5-4** neither the overall PCE nor the cell stability was improved. However, by further expanding the π-conjugated system of the *N*-heterotriangulene toward linear nonamer **4-9**, a significant increase in the output was obtained. This could be further enhanced up to a PCE of 2.8% by annealing the hole-transport layer. While the efficiency of the commonly used spiro-MeOTAD based cells has not been reached, an excellent thermal stability was observed for **4-9**. Compared to a spiro-MeOTAD (**I5-1**) reference cell, the *N*-heterotriangulene nonamer **4-9** containing cell, showed superior efficiencies already after 5 days of operation. The individually studied photovoltaic characteristics remained thereby relatively stable for at least 19 days at

elevated temperatures. The combination of reasonable efficiency, robust performance together with a good processability makes **4-9** to a viable alternative for commonly applied spiro-MeOTAD. Moreover, the utilization of **4-9** in Perovskite-based DSSCs provides further room for applications. In future efforts, the identification of an ideal compound is targeted. Upon careful investigation of *N*-heterotriangulene oligomers with shorter and longer chains as well as different architectures, such as star-shaped geometries, the penetration of the HTM into the TiO_2 pores can be further optimized.

5.5 References

[1]   B. O`Regan, M. Grätzel, *Nature* **1991**, *353*, 737-740.

[2]   M. K. Nazeeruddin, A. Kay, I. Rodicio, R. Humphrybaker, E. Muller, P. Liska, N. Vlachopoulos, M. Grätzel, *J. Am. Chem. Soc.* **1993**, *115*, 6382-6390.

[3]   M. Grätzel, *Nature* **2001**, *414*, 338-344.

[4]   B. Li, L. D. Wang, B. N. Kang, P. Wang, Y. Qiu, *Sol. Energ. Mat. Sol. Cells* **2006**, *90*, 549-573.

[5]   A. Hagfeldt, G. Boschloo, L. C. Sun, L. Kloo, H. Pettersson, *Chem. Rev.* **2010**, *110*, 6595-6663.

[6]   C. Li, M. Y. Liu, N. G. Pschirer, M. Baumgarten, K. Müllen, *Chem. Rev.* **2010**, *110*, 6817-6855.

[7]   B. E. Hardin, H. J. Snaith, M. D. McGehee, *Nat. Photonics* **2012**, *6*, 162-169.

[8]   M. K. Nazeeruddin, F. De Angelis, S. Fantacci, A. Selloni, G. Viscardi, P. Liska, S. Ito, T. Bessho, M. Grätzel, *J. Am. Chem. Soc.* **2005**, *127*, 16835-16847.

[9]   F. F. Gao, Y. Wang, J. Zhang, D. Shi, M. K. Wang, R. Humphry-Baker, P. Wang, S. M. Zakeeruddin, M. Grätzel, *Chem. Commun.* **2008**, 2635-2637.

[10]   A. Yella, H. W. Lee, H. N. Tsao, C. Y. Yi, A. K. Chandiran, M. K. Nazeeruddin, E. W. G. Diau, C. Y. Yeh, S. M. Zakeeruddin, M. Grätzel, *Science* **2011**, *334*, 629-634.

[11]   W. C. Sinke, M. M. Wienk, *Nature* **1998**, *395*, 544-545.

[12]   M. Matsumoto, Y. Wada, T. Kitamura, K. Shigaki, T. Inoue, M. Ikeda, S. Yanagida, *Bull. Chem. Soc. Jpn.* **2001**, *74*, 387-393.

[13]   U. Bach, D. Lupo, P. Comte, J. E. Moser, F. Weissortel, J. Salbeck, H. Spreitzer, M. Grätzel, *Nature* **1998**, *395*, 583-585.

[14]   U. Bach, Y. Tachibana, J. E. Moser, S. A. Haque, J. R. Durrant, M. Grätzel, D. R. Klug, *J. Am. Chem. Soc.* **1999**, *121*, 7445-7446.

[15]   U. Bach, K. De Cloedt, H. Spreitzer, M. Grätzel, *Adv. Mater.* **2000**, *12*, 1060-1063.

[16]   H. J. Snaith, M. Grätzel, *Appl. Phys. Lett.* **2006**, *89*.

[17]   H. J. Snaith, M. Grätzel, *Adv. Mater.* **2007**, *19*, 3643-3647.

[18]   H. J. Snaith, A. J. Moule, C. Klein, K. Meerholz, R. H. Friend, M. Grätzel, *Nano Lett.* **2007**, *7*, 3372-3376.

[19]   H. J. Snaith, L. Schmidt-Mende, *Adv. Mater.* **2007**, *19*, 3187-3200.

[20]   M. Grätzel, *J. Photochem. Photobiol., A* **2004**, *164*, 3-14.

[21]   K. Tennakone, G. R. R. A. Kumara, A. R. Kumarasinghe, K. G. U. Wijayantha, P. M. Sirimanne, *Semicond. Sci. Technol.* **1995**, *10*, 1689-1693.

[22]   G. P. Smestad, S. Spiekermann, J. Kowalik, C. D. Grant, A. M. Schwartzberg, J. Zhang, L. M. Tolbert, E. Moons, *Sol. Energ. Mat. Sol. Cells* **2003**, *76*, 85-105.

[23]   C. Y. Hsu, Y. C. Chen, R. Y. Y. Lin, K. C. Ho, J. T. Lin, *Phys. Chem. Chem. Phys.* **2012**, *14*, 14099-14109.

[24]   J. Burschka, A. Dualeh, F. Kessler, E. Baranoff, N. L. Cevey-Ha, C. Y. Yi, M. K. Nazeeruddin, M. Grätzel, *J. Am. Chem. Soc.* **2011**, *133*, 18042-18045.

[25]   I. K. Ding, N. Tetreault, J. Brillet, B. E. Hardin, E. H. Smith, S. J. Rosenthal, F. Sauvage, M. Grätzel, M. D. McGehee, *Adv. Funct. Mater.* **2009**, *19*, 2431-2436.

[26]   J. E. Kroeze, N. Hirata, L. Schmidt-Mende, C. Orizu, S. D. Ogier, K. Carr, M. Grätzel, J. R. Durrant, *Adv. Funct. Mater.* **2006**, *16*, 1832-1838.

[27]   A. Mishra, M. K. R. Fischer, P. Bäuerle, *Angew. Chem., Int. Ed.* **2009**, *48*, 2474-2499.

[28]   F. Fabregat-Santiago, J. Bisquert, L. Cevey, P. Chen, M. K. Wang, S. M. Zakeeruddin, M. Grätzel, *J. Am. Chem. Soc.* **2009**, *131*, 558-562.

[29]   A. Abate, T. Leijtens, S. Pathak, J. Teuscher, R. Avolio, M. E. Errico, J. Kirkpatrik, J. M. Ball, P. Docampo, I. McPherson, H. J. Snaith, *Phys. Chem. Chem. Phys.* **2013**, *15*, 2572-2579.

[30]   M. M. Lee, J. Teuscher, T. Miyasaka, T. N. Murakami, H. J. Snaith, *Science* **2012**, *338*, 643-647.

[31]   J. Burschka, N. Pellet, S. J. Moon, R. Humphry-Baker, P. Gao, M. K. Nazeeruddin, M. Grätzel, *Nature* **2013**, *499*, 316-+.

[32]   I. K. Ding, J. Melas-Kyriazi, N. L. Cevey-Ha, K. G. Chittibabu, S. M. Zakeeruddin, M. Grätzel, M. D. McGehee, *Org. Electron.* **2010**, *11*, 1217-1222.

[33] M. Tashiro, S. Mataka, Y. Takezaki, M. Takeshita, T. Arimura, A. Tsuge, T. Yamato, *J. Org. Chem.* **1989**, *54*, 451-458.

[34] T. Yamato, M. Fujimoto, A. Miyazawa, K. Matsuo, *J. Chem. Soc., Perkin Trans. 1* **1997**, 1201-1207.

[35] A. N. Sobolev, V. K. Belsky, I. P. Romm, N. Y. Chernikova, E. N. Guryanova, *Acta Crystallogr. C* **1985**, *41*, 967-971.

[36] M. Planells, A. Abate, D. J. Hollman, S. D. Stranks, V. Bharti, J. Gaur, D. Mohanty, S. Chand, H. J. Snaith, N. Robertson, *J. Mater. Chem. A* **2013**, *1*, 6949-6960.

[37] G. Y. Margulis, B. E. Hardin, I. K. Ding, E. T. Hoke, M. D. McGehee, *Adv. Energy. Mater.* **2013**.

[38] M. J. Frisch, G. W. Trucks, H. B. Schlegel, G. E. Scuseria, M. A. Robb, J. R. Cheeseman, J. Montgomery, J. A., T. Vreven, K. N. Kudin, J. C. Burant, J. M. Millam, S. S. Iyengar, J. Tomasi, V. Barone, B. Mennucci, M. Cossi, G. Scalmani, N. Rega, G. A. Petersson, H. Nakatsuji, M. Hada, M. Ehara, K. Toyota, R. Fukuda, J. Hasegawa, M. Ishida, T. Nakajima, Y. Honda, O. Kitao, H. Nakai, M. Klene, X. Li, J. E. Knox, H. P. Hratchian, J. B. Cross, V. Bakken, C. Adamo, J. Jaramillo, R. Gomperts, R. E. Stratmann, O. Yazyev, A. J. Austin, R. Cammi, C. Pomelli, J. W. Ochterski, P. Y. Ayala, K. Morokuma, G. A. Voth, P. Salvador, J. J. Dannenberg, V. G. Zakrzewski, S. Dapprich, A. D. Daniels, M. C. Strain, O. Farkas, D. K. Malick, A. D. Rabuck, K. Raghavachari, J. B. Foresman, J. V. Ortiz, Q. Cui, A. G. Baboul, S. Clifford, J. Cioslowski, B. B. Stefanov, G. Liu, A. Liashenko, P. Piskorz, I. Komaromi, R. L. Martin, D. J. Fox, T. Keith, M. A. Al-Laham, C. Y. Peng, A. Nanayakkara, M. Challacombe, P. M. W. Gill, B. Johnson, W. Chen, M. W. Wong, C. Gonzalez, J. A. Pople, *Gaussian 03, Revision C.02*, Gaussian, Inc., Wallingford CT, **2004.**

[39] J. P. Perdew, *Phys. Rev. B* **1986**, *33*, 8822-8824.

[40] A. D. Becke, *Phys. Rev. A* **1988**, *38*, 3098-3100.

[41] R. Ahlrichs, M. Bar, M. Haser, H. Horn, C. Kolmel, *Chem. Phys. Lett.* **1989**, *162*, 165-169.

[42] C. Li, H. Wonneberger, *Adv. Mater.* **2012**, *24*, 613-636.

[43] G. Sadoughi, V. Sivaram, R. Gunning, P. Docampo, I. Bruder, N. Pschirer, A. Irajizad, H. J. Snaith, *Phys. Chem. Chem. Phys.* **2013**, *15*, 2075-2080.

[44] S. H. Yeh, C. Y. Tsai, C. Y. Huang, G. S. Liou, S. H. Cheng, *Electrochem. Commun.* **2003**, *5*, 373-377.

[45] S. Barlow, C. Risko, S. J. Chung, N. M. Tucker, V. Coropceanu, S. C. Jones, Z. Levi, J. L. Bredas, S. R. Marder, *J. Am. Chem. Soc.* **2005**, *127*, 16900-16911.

[46] G. Zhou, M. Baumgarten, K. Müllen, *J. Am. Chem. Soc.* **2007**, *129*, 12211-12221.

[47] T. Kanbara, N. Saito, T. Yamamoto, K. Kubota, *Macromolecules* **1991**, *24*, 5883-5885.

[48] Z. H. Zhou, T. Yamamoto, *J. Organomet. Chem.* **1991**, *414*, 119-127.

[49] M. K. Wang, S. J. Moon, M. F. Xu, K. Chittibabu, P. Wang, N. L. Cevey-Ha, R. Humphry-Baker, S. M. Zakeeruddin, M. Grätzel, *Small* **2010**, *6*, 319-324.

6 Sterically π-Congested Poly(*para*phenylenes) – Synthetic Approaches toward Cubic Graphite Subunits

6.1 Introduction

Besides *N*-heterotriangulenes as efficiently working HTMs, which were discussed in the previous chapters, further benzene-based materials are required for the fabrication of useful organic optoelectronic devices. Benzene-rich architectures, such as oligo- and poly(*para*phenylenes) (OPPs and PPPs) have been extensively studied as active materials for use in OLEDs and are nowadays one of the most important classes of π-conjugated polymers.[1-14] These materials have been of particular interest as blue emitters due to their intrinsically large HOMO-LUMO distances (E_g). However, they usually suffer from poor solubility which severely limits their processability.[12, 15-18] While the attachment of long alkyl or alkoxy groups helps to overcome these drawbacks, it reduces the π-conjugative interactions along the *para*phenylene backbone which shifts the emission into the UV region.[19, 20] Moreover, the development of new phenylene-based nanostructures is driven by the fundamental interest in the connection between steric congestion, reactivity, and the resulting properties. Besides 1D and 2D structures, *e.g*, PPP and graphene, this includes the search for novel 3D poly(phenylenes), such as the so-called cubic graphite proposed by *Gibson* in 1946 (Figure 6-1 a).[21]
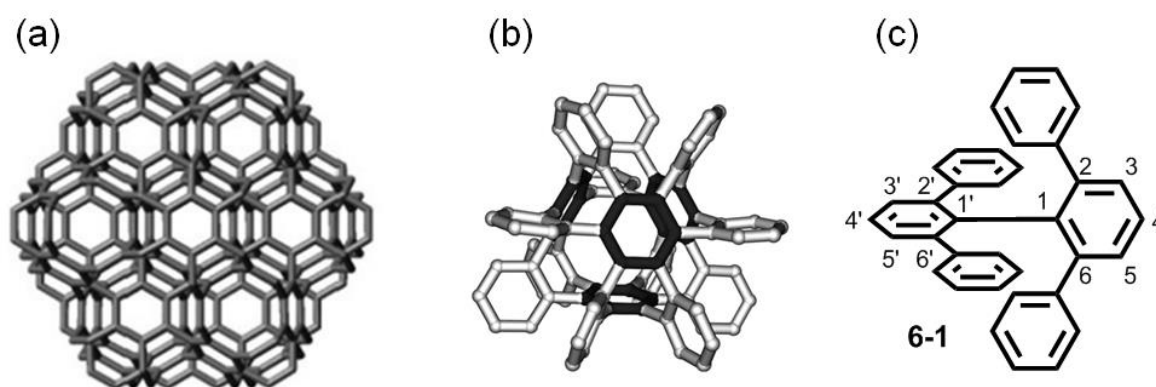
Figure 6-1. Schematic representation of a subunit of cubic graphite (a) and three-dimensional models of cubic graphite as (b) ball-and-stick representation.[22, 23] (c) Chemical structure of 2,2',6,6'-tetraphenyl-1,1'-biphenyl **6-1** and atom numbering.

In this hypothetical carbon allotrope each benzene ring is connected to six different rings while each benzene is a part of three equivalent PPP chains (Figure 6-1 b).[22, 24] This

arrangement leads to eight-membered cyclooctatetraphenylene (**COT**) rings with strong mutual twists between the individual phenyl units, resulting in overall equivalent carbon atoms. The material can be considered as a perfect 3D polyphenylene structure which should give rise to high thermal and mechanical stability.[22] Even though this carbon allotrope might never be accessible due to the extremely crowded arrangement of its hexaphenylbenzene (**HPB**) subunits, several extremely π-congested oligo(phenylenes) possessing highly unusual geometries have been synthesized in the last years.[22, 24-31] One of these systems is 2,2',6,6'-tetraphenyl-1,1'-biphenyl (**6-1**, Figure 6-1 c), having four surrounding phenyl moieties attached to the biphenyl core thus leading to a significant torsion between the mean planes of the central bond (~65°) with the peripheral phenyls being π-stacked in a face-to-face orientation. Although the solid state properties of this structural unit were intensively studied, the influence of the mutual twist and the π-stacked peripheral phenyls on the electronic properties in π-extended systems has not been investigated so far. The synthesis together with the X-ray crystallographic structure of **6-1** was reported by *Ozasa* and *Pascal Jr.*, further investigations were, however, precluded due to the low yields of their synthetic protocols.[25-27] In order to expand the π-conjugation of this structural motif, a straightforward synthetic method was aimed which furthermore allows for polymerization along the 4,4'-positions of **6-1**. Additionally, this could also provide access to a suitable precursors for subunits of cubic graphite.

6.2 Synthetic Approaches toward 2,2',6,6'-Tetraphenyl-1,1'-biphenyl

The synthesis of π-congested 2,2',6,6'-tetraphenyl-1,1'-biphenyl (**6-1**, Scheme 6-1) can be principally divided into two retrosynthetic concepts: (**1**) Dimerization of *m*-terphenyl (**1-I**) along the sterically unfavorable 2'-position of the central benzene ring (Scheme 6-1, left, red arrow). (**1-I**) can be obtained by previous attachment of the peripheral phenyls *via* selective twofold cross-coupling to (**1-II**) (Scheme 6-1, left, blue arrow). This approach basically refers to the work of *Ozasa* and *Pascal Jr.*[25-27] (**2**) To reduce the steric demand of one reaction partner, the peripheral phenyls were attached to a 2,2',6,6'-tetrahalo biphenyl (**2-I**) (Scheme 6-1, right, blue arrow). It can be obtained *via* selective dimerization of a sterically less crowded precursor (**2-II**) (Scheme 6-1, right, red arrow) bearing different functionalities.
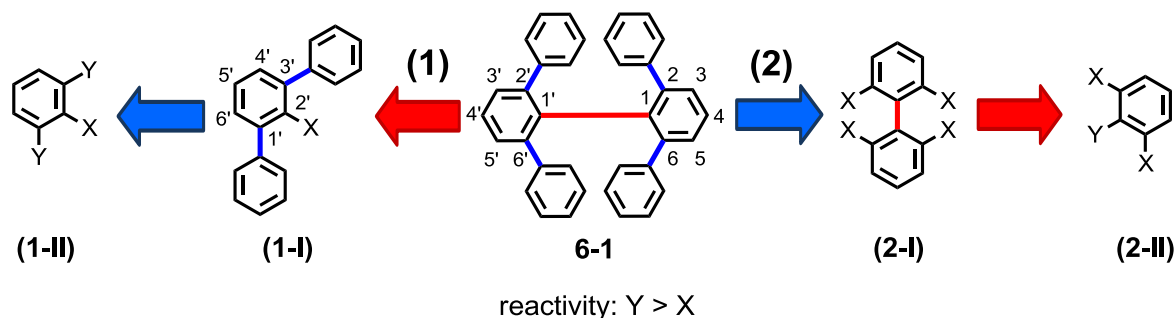
Scheme 6-1. Schematic representation of the two retrosynthetic approaches toward 2,2',6,6'-tetraphenyl-1,1'-biphenyl **6-1**. The colors of the arrows indicate the respective bond formation. Note the different numbering of **6-1** and (**1-I**).

However, it should be pointed out that the synthesis comprises either the combination of a facile twofold phenyl attachment with a subsequent sterically extraordinary hindered dimerization or a sterically less encumbered dimerization followed by a more ambitious fourfold phenyl attachment. It will be discussed in the following which concept allows a more efficient synthesis and gives access to the 4,4'-positions of **6-1** for further extensions. Initially, the efforts were focused on concept (1) for the synthesis of 2,2',6,6'-tetraphenyl-1,1'-biphenyl **6-1**. The work of *Ozasa* and *Pascal Jr.* was mainly based on repetitive C−C bond formations based on the Cu-mediated *Ullmann* coupling[32] which is a robust and versatile method, however, the isolated yields of **6-1** and its derivatives remained comparably low (~2% over four steps).[25-27] In recent years, considerable progress has been made in the development of highly efficient cross-coupling procedures for the $C(sp^2)$−$C(sp^2)$ bond formation based on transition metal complexes, such as the *Yamamoto*-,[33-36] the *Suzuki-Miyaura*-[37-48] and the *Stille*-reaction.[49-51]
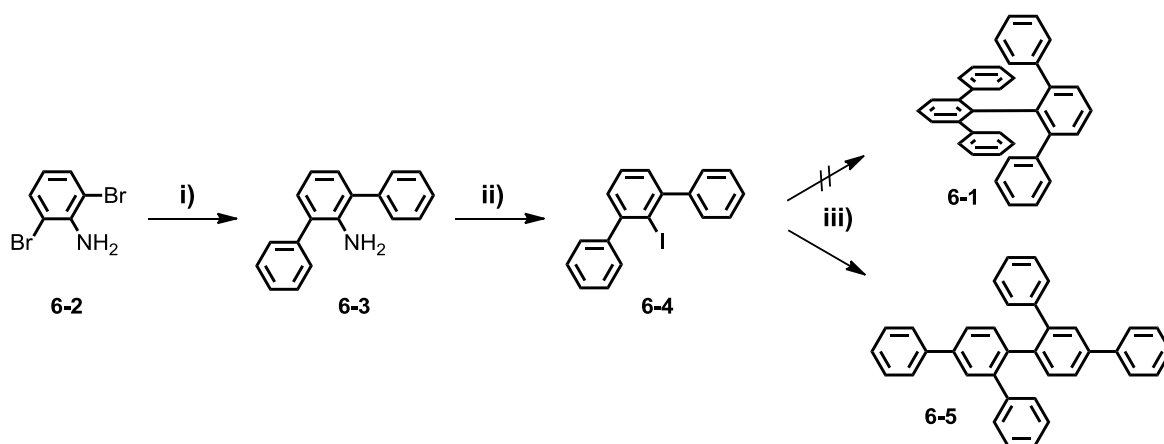
Scheme 6-2. Synthetic route toward 2,2',6,6'-tetraphenyl-1,1'-biphenyl **6-1** utilizing concept (1). Conditions: i) phenylboronic acid, Pd(PPh₃)₄, K₂CO₃, toluene, *Aliquat 336*, 100 °C, 12h, 93%; ii) NaNO₂, H₂SO₄, KI, 0 °C to 70 °C, 2h, 80%; iii) bis(cycloocta-1,5-diene)nickel(0), cycloocta-1,5-diene, 2,2'-bipyridine, toluene/DMF, 85 °C, 12h, **6-5**: 12%.

Owing to this, the highly versatile Ni^0-mediated *Yamamoto* reaction has been initially tested toward its practicability for the direct dimerization of 2'-iodo-1,1':3',1''-terphenyl (**6-4**). For this purpose, **6-4** was synthesized from commercially available 2,6-dibromoaniline (**6-2**) in two steps (Scheme 6-2). The introduction of the peripheral phenyl moieties was carried out by a twofold *Suzuki-Miyaura* reaction utilizing phenylboronic acid and tetrakis(triphenylphosphine)palladium(0) in the presence of potassium carbonate as base affording **6-3** in virtually quantitative yields. Diazotation of **6-3** under classical *Sandmeyer* conditions followed by treatment with potassium iodide led to 2'-iodo-1,1':3',1''-terphenyl (**6-4**) in 75% over two steps. Compound **6-4** was subjected to dimerization utilizing standard *Yamamoto* conditions in the absence of light.[35, 36] By column chromatography a blue fluorescent compound was isolated as the main fraction. Besides that, a significant amount of protodehalogenated precursor was obtained. Mass spectrometry confirmed the same stoichiometric composition as **6-1** (*m/z* = 458.20), however, NMR spectroscopy revealed complicated spectra, suggesting the absence of highly symmetric 2,2',6,6'-tetraphenyl-1,1'-biphenyl **6-1**. Thus, it was not possible to unambiguously assign the NMR spectrum to a molecular structure.
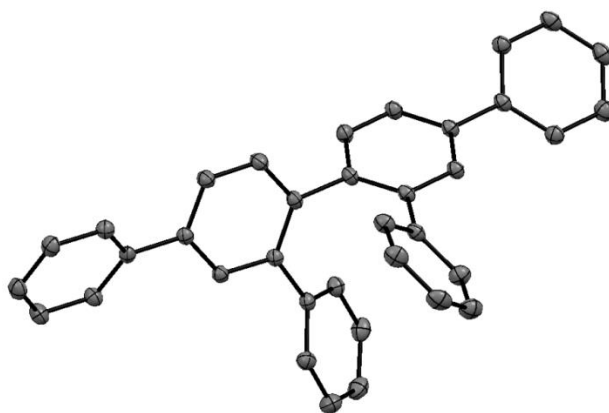
Figure 6-2. X-ray crystal structure of 4'',5'-diphenyl-1,1':2',1'':2'',1'''-quaterphenyl **6-5** (hydrogens omitted for clarity).

By slow evaporation of a toluene solution, single crystals suitable for X-ray diffraction analysis could be grown. Surprisingly, the analysis revealed the formation of an isomeric species of **6-1**, namely 4'',5'-diphenyl-1,1':2',1'':2'',1'''-quaterphenyl (**6-5**, Figure 6-2), having two phenyl moieties attached to the central position of a *p*-quaterphenyl backbone. The formation of **6-5** was apparently a result of a rearrangement during the cross-coupling, nevertheless, its exact origin could not be clarified so far. To elucidate the mechanism of its formation, a precursor having blocked 5'-position was synthesized. This was conducted
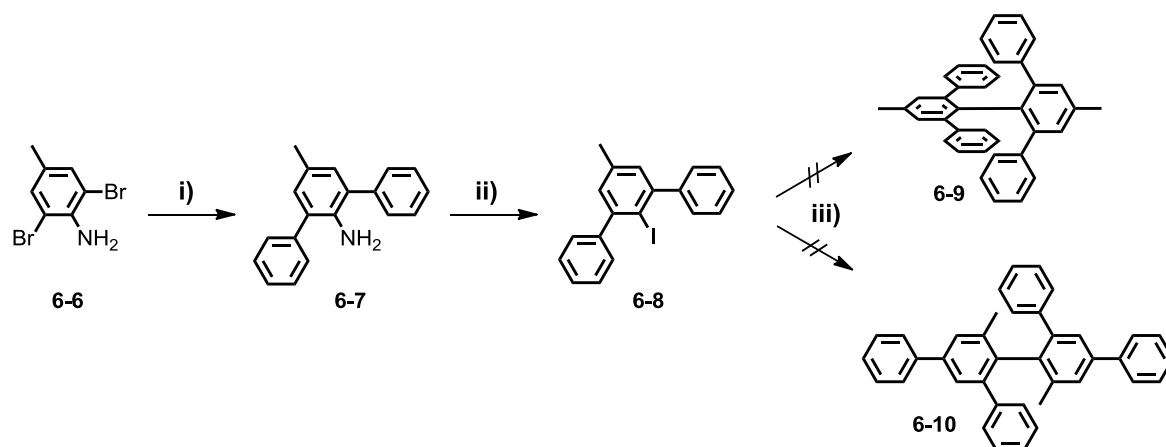
Scheme 6-3. Synthetic route of the model reaction. Conditions: i) phenylboronic acid, Pd(PPh$_3$)$_4$, K$_2$CO$_3$, toluene, *Aliquat 336*, 100 °C, 12h, 93%; ii) NaNO$_2$, H$_2$SO$_4$, KI, 0 °C to 70 °C, 2h, 53%; iii) bis(cycloocta-1,5-diene)nickel(0), cycloocta-1,5-diene, 2,2'-bipyridine, toluene/DMF, 85 °C, 12h.

according to the preparation of **6-4**, comprising a *Suzuki-Miyaura* reaction with 2,6-dibromo-4-methylaniline (**6-6**) and phenyl boronic acid followed by a iodination under *Sandmeyer* conditions (Scheme 6-3). The procedure afforded 2'-iodo-5'-methyl-1,1':3',1''-terphenyl (**6-8**) in an overall yield of 50% over two steps. Compound **6-8** was s subjected to the *Yamamoto* reaction under identical conditions as for **6-4**. According to the previous observations, this reaction would theoretically result in the formation of either **6-9** or **6-10**. After 12 hours, the reaction was quenched and the crude mixture was separated with the help of column chromatography. In this case, exclusively the protodehalogenated precursor was obtained. This observation could be explained with the help of a kinetic and theoretical study on low valent Ni-mediated cross-coupling reactions of *Nakamura* and coworkers.[52] Based on these investigations, the following mechanism was proposed for the dimerization of **6-4** and **6-8** toward 2,2',6,6'-tetraphenyl-1,1'-biphenyl derivatives (Scheme 6-4). By utilizing precursor **6-4** in situation (a), migration of the active Ni^0 species to the less hindered π-face occurs toward **6-4a**, as a result of a so-called "ring walk" of the Ni-complex.[52, 53] This is attributed to the formation of a η^2-complex with haloarene **6-4**, followed by an isomerization and subsequent C−I bond cleavage toward **6-4a**. This phenomenon was similarly observed for the Ni^0-catalyzed *Kumada-Tamao-Corriu* reaction as well as the *Kumada* catalyst-transfer polycondensation of sterically hindered substrates and could be ascribed to the d-electron donative character of Ni^0-complexes.[52-55] Subsequent to the migration process, a bond formation at the 4'-position of **6-4a** toward **6-5** is most likely. By utilizing precursor **6-8** in situation (b), however, the migration of the Ni^0 species does not result in a less hindered environment due to an equally shielded 2'-
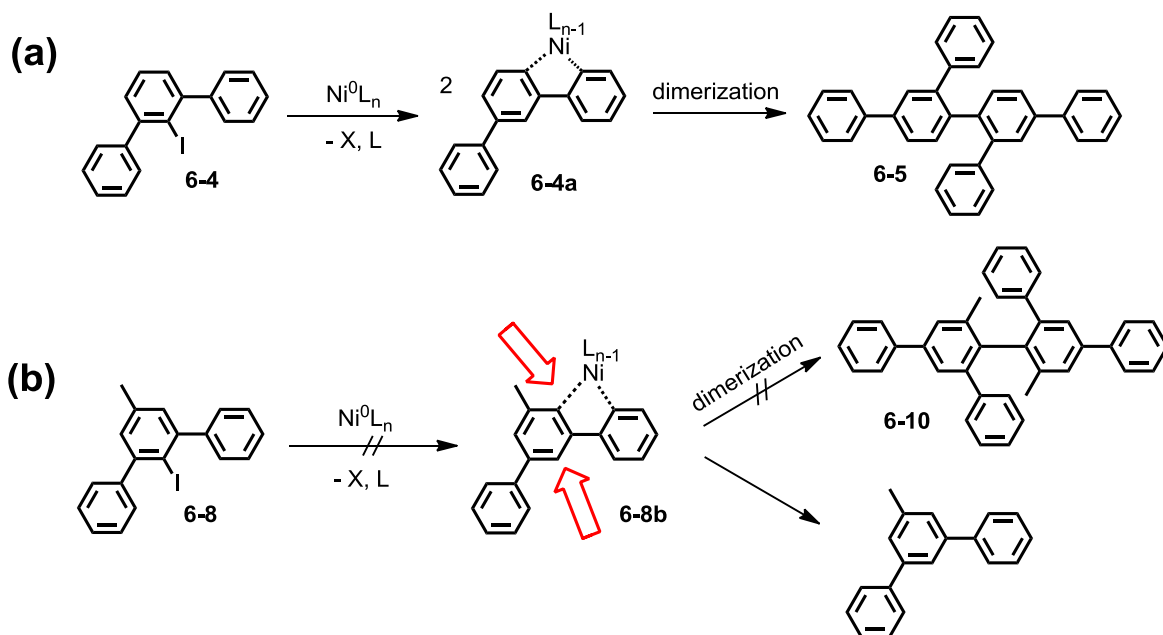
Scheme 6-4. Proposed reaction mechanisms during the Ni⁰-mediated *Yamamoto* reaction of derivatives **6-4** (a) and **6-8** (b). The red arrows indicate the equally hindered positions.

and 4'-positions (indicated by red arrows in Scheme 6-4). Thus, neither C−C bond formation at the 4'-position nor at the 2'-position is preferred which led finally to protodehalogenation. Owing to the fact that cross-coupling procedures comprising Ni⁰-complexes did not allow intrinsically for the fabrication of π-congested **6-1**, the synthetic strategy was modified.

The *Suzuki-Miyaura* reaction is among the Pd⁰-catalyzed cross-coupling procedures the most powerful and versatile $C(sp^2)$−$C(sp^2)$ bond forming transformation available to synthetic chemists nowadays because of its broad scope and wide functional group tolerance.[37, 48] In addition, several procedures for the formation of sterically crowded biaryls relying on chemoselective halogen transformations (I > Br > Cl) are available.[38-45] With respect to this, the bis(pinacol) ester of *m*-terphenyl boronic acid **6-11** was synthesized (Scheme 6-5). The ester was applied because the purification of esters is usually easier than the parent boronic acids due to their reduced polarity. Owing to the increased steric demand at the 2'-position of **6-4**, the introduction of the boronic ester utilizing a *Miyaura* borylation resulted mostly in protodehalogenation.[56] Therefore, the boron functionality was introduced with the help of a lithiation. The iodine-lithium exchange was carried out at room temperature to facilitate the lithiation process at the sterically hindered gulf region of 2'-iodo-1,1':3',1''- terphenyl **6-4**. Subsequent quenching with 2-isopropoxy-4,4,5,5-tetramethyl-1,3,2-dioxaborolane and purification by column
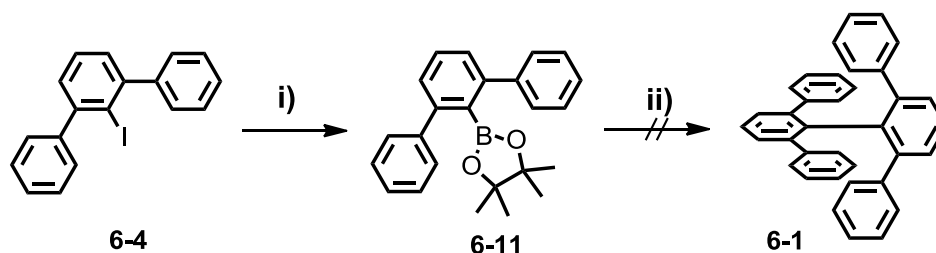
Scheme 6-5. Synthetic route toward **6-1** utilizing the *Suzuki-Miyaura* reaction. Conditions: i) *n*-BuLi, 2-isopropoxy-4,4,5,5-tetramethyl-1,3,2-dioxaborolane, Et$_2$O, RT, 0 °C to RT, 91%; ii) **6-4**, Pd(PPh$_3$)$_4$, 2 M aq. K$_2$CO$_3$, toluene, *Aliquat 336*, 100 °C, 24h.

chromatography led to the formation of **6-11** in 91% yield. It was subsequently subjected to the *Suzuki-Miyaura* reaction by screening different synthetic protocols (Table 6-1). Initially 2-dicyclohexylphosphino-2',6'-dimethoxybiphenyl (S-Phos) in combination with different Pd-sources was utilized. *Buchwald's* pioneering work afforded these catalytic systems as general method for the preparation of sterically hindered biaryls at low temperature with low catalyst loadings, however, they were not utilized for the dimerization of 2'-halo-1,1':3',1''-terphenyls so far.[39, 42, 43] Screening different Pd-sources resulted basically in protodehalogenation and protodeboronation without the formation of **6-1** or any of its isomers (Table 6-1, entry 1 and 2). The nature of the applied base influences the outcome of the cross-coupling to a great extent.[38, 45] However, the utilization of different bases, such as caesium carbonate and thallium(I) carbonate did not allow for the formation of **6-1** and led only to protodehalogenation and protodeboronation (Table 6-1, entry 3 to 6).

Table 6-1. Optimization of the reaction conditions for the sterically hindered *Suzuki-Miyaura* coupling between **6-4** and **6-11**.

Entry	Catalyst System	T (°C)	t (h)	Base	Yield (%)[a]
1	Pd$_2$dba$_3$ + S-Phos	100	24	K$_3$PO$_4$	-[b]
2	Pd(OAc)$_2$ + S-Phos	100	24	K$_3$PO$_4$	-[b]
3	Pd(OAc)$_2$ + PPh$_3$	100	24	K$_3$PO$_4$	-[b]
4	Pd(PPh$_3$)$_4$	100	24	K$_3$PO$_4$	-[b]
5	Pd(PPh$_3$)$_4$	100	24	Cs$_2$CO$_3$	-[b]
6	Pd(PPh$_3$)$_4$	100	24	Tl$_2$CO$_3$	-[b]
7	Pd(PPh$_3$)$_4$ + *Aliquat 336*	100	24	Na$_2$CO$_3$	-[b], [c]
8	**Pd(PPh$_3$)$_4$ + *Aliquat 336***	**100**	**24**	**K$_2$CO$_3$**	**20[d]**

[a] Yield of the isolated, analytically pure compound. [b] Besides protodehalogenation and protodeboronation, no product was detected. [c] Na$_2$CO$_3$ was used as a 2 M aqueous solution. [d] Isolated yield of 5',5''''-dichloro-sexiphenyl **6-17**.
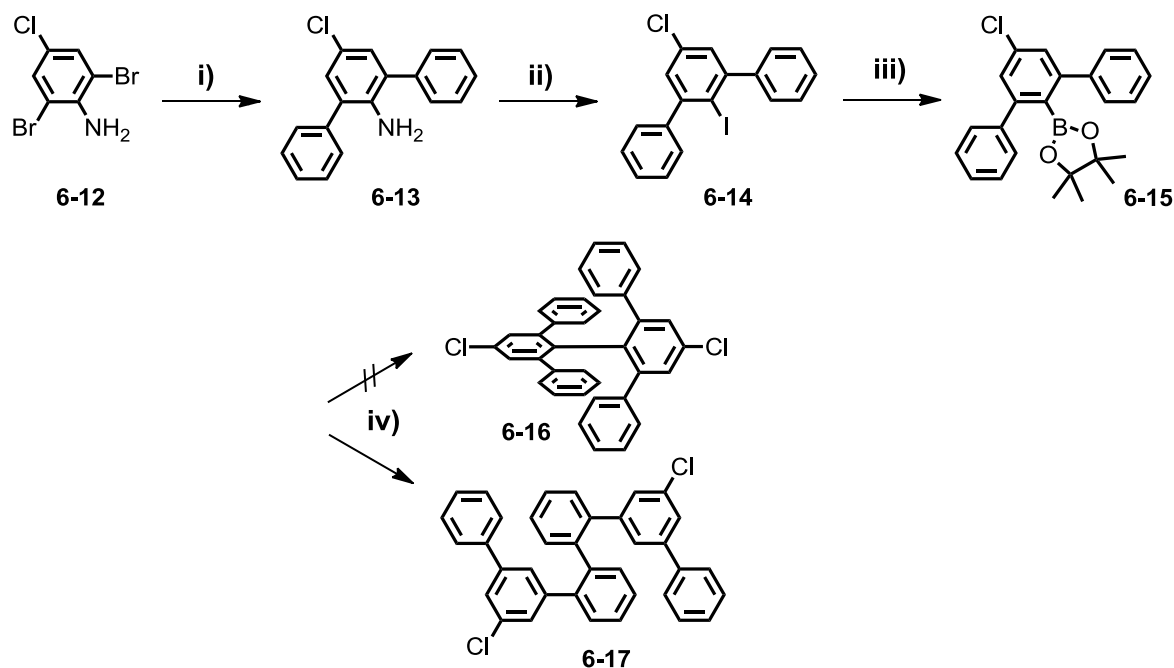
Scheme 6-6. Synthetic route toward **6-16** utilizing the *Suzuki-Miyaura* reaction. Conditions: i) phenylboronic acid, Pd(PPh$_3$)$_4$, K$_2$CO$_3$, toluene, *Aliquat 336*, 100 °C, 12h, 94%; ii) NaNO$_2$, H$_2$SO$_4$, KI, 0 °C to 70 °C, 2h, 58%; iii) *n*-BuLi, 2-isopropoxy-4,4,5,5-tetramethyl-1,3,2-dioxaborolane, Et$_2$O, RT, 0 °C to RT, 91%; iv) **6-14**, *Suzuki-Miyaura* conditions see Table 6-1.

Surprisingly, aqueous potassium carbonate in combination with a few drops of phase transfer catalyst *Aliquat 336* and tetrakis(triphenylphosphine)palladium(0) led to the formation of a species showing the molar mass of **6-1** (*m/z* = 458.20) in 20% yield. The analysis of this compound by ^{1}H NMR spectroscopy revealed a complex spectrum, suggesting the formation of an isomer of **6-1**. However, the exact structure of the obtained product could not be assigned due to an insufficient crystallization of the product. In order to elucidate the structure of the cross-coupling product and the mechanism of its formation, the reaction sequence was repeated utilizing a 5'-chloro *m*-terphenyl (Scheme 6-6). The chloro substituent was chosen to induce crystallinity and to allow for additional functionalization at the 5'-position. Precursors **6-14** and **6-15** were obtained in good overall yields by utilizing analogue procedures as shown previously. Subsequently, they were subjected to identical *Suzuki-Miyaura* cross-coupling conditions (Table 6-1, entry 8). After one day, the reaction was stopped and the crude mixture was separated by column chromatography resulting in a main fraction having the exact stoichiometric composition as **6-16** (*m/z* = 527.48). In agreement with the previous results, a second fraction was obtained which contained the protodehalogenated and protodeboronated precursors **6-14** and **6-15**. By utilizing two-dimensional proton correlation (^{1}H, ^{1}H COSY) spectroscopy
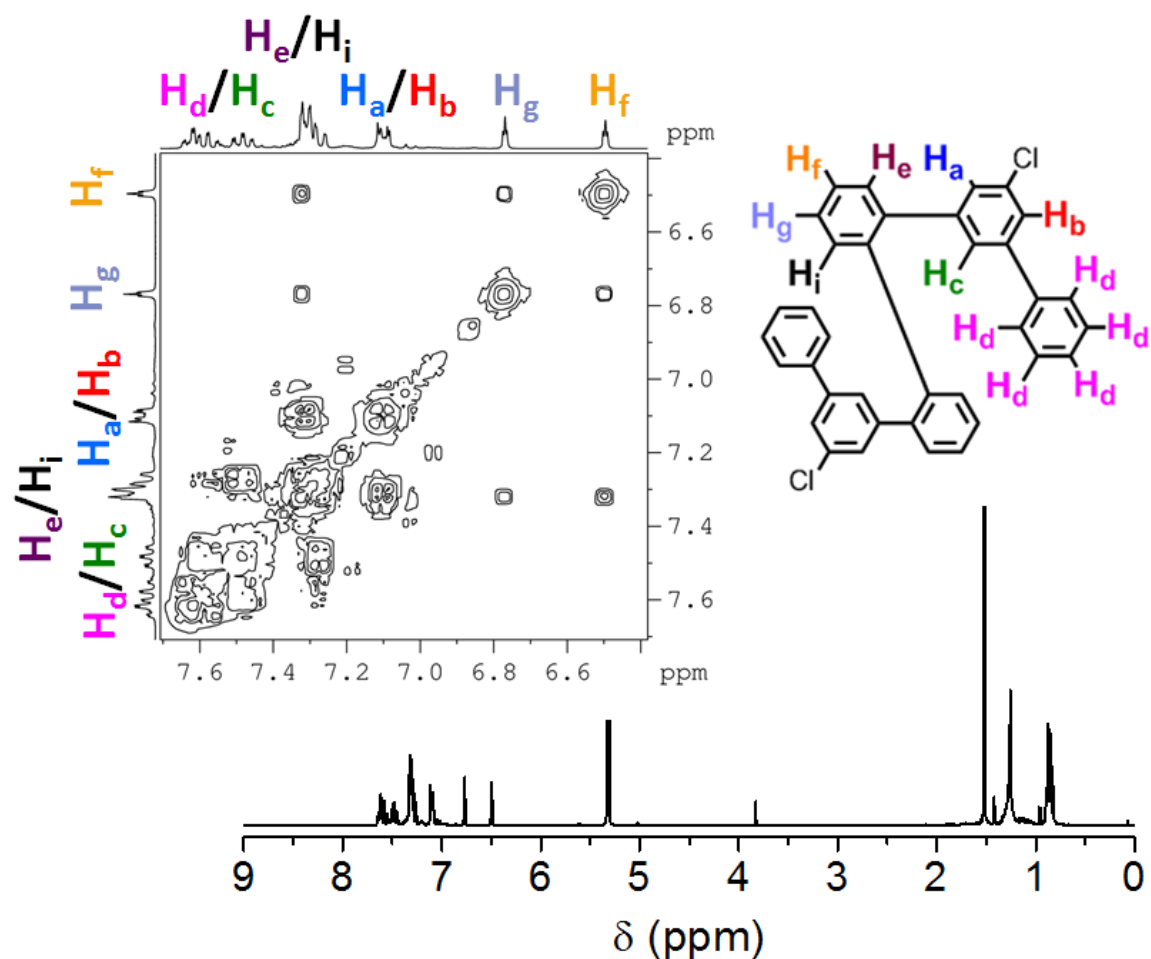
Figure 6-3. ^{1}H NMR spectrum of 5',5''''-dichloro-sexiphenyl **6-17** in CD_2Cl_2 at 25 °C. Inset: Two-dimensional proton correlation (^{1}H, ^{1}H COSY) of **6-17** with proton assignment.

(Figure 6-3), the formation of 5',5''''-dichloro-sexiphenyl **6-17** was indicated (Scheme 6-6). As a result of the asymmetric substitution on the peripheral phenyl rings, signals at 6.50 and 6.77 ppm (H_f and H_g) gave rise to a cross peaks due to *ortho*-coupling with the neighboring protons (H_e and H_i). In addition, the protons located next to the chlorine substituent (H_a/H_b) showed a cross peak to the *ortho* protons (H_e/H_d) at the peripheral phenyl rings caused by their close spatial contact. This was similarly observed for the proton located at the gulf region (H_c) of the *m*-terphenyl subunit. However, the proton assignment remained an indication rather than a final proof for the formation of **6-17**. In this particular case, single crystals suitable for X-ray diffraction analysis were grown by slow evaporation of a solution of dichloromethane and methanol. The structural analysis confirmed the formation of **6-17**, having the C−C bonds connected at the peripheral 2/2''-positions of the individual *m*-terphenyl subunits (Figure 6-3).

Figure 6-4. X-ray crystal structure of 5',5'''''-dichloro-1,1':3',1'':2'',1''':2''',1'''':3'''',1'''''-sexiphenyl **6-17**.
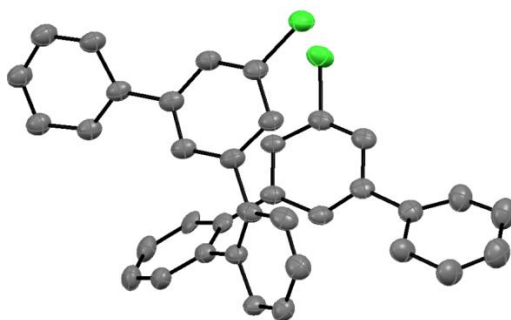
These findings suggested a migration of the Pd-complex in the course of the cross-coupling, which will be discussed in the following on the basis of the catalytic cycle of the *Suzuki-Miyaura* reaction. The proposed reaction sequence is depicted in Scheme 6-7. The activation of the Pd^0-complex occurs initially by the dissociation of two ligands towards **C-1**. This step is followed by an insertion of the palladium atom into the carbon-iodine bond (*i.e.* oxidative addition) of *m*-terphenyl derivative (**6-4** or **6-14**) toward complex **C-2** (step **A**). This is followed by the replacement of the halogen by one molecule of base.[57-59] During this step it is plausible that an *intra*molecular C−H activation by the palladium at the peripheral phenyl ring of the *m*-terphenyl occurs thus leading to the formation of Pd^{II}-complex **C-3** (step **B**). The Pd-complex is thereby surrounded by only one phenyl moiety, which results in a sterically less crowded environment compared with the situation at the 2'-position. Very recently, this behavior was similarly observed for the Pd^0-catalyzed synthesis of a π-congested pentahelicene by *Perez* and *Pena*.[60] The subsequent transmetalation (step **C**) of the activated boronic acid led to the formation of complex **C-4** which is expected to comprise an additional *intra*molecular C−H activation at the peripheral phenyl ring of the second *m*-terphenyl. These migrations result in a decreased steric demand of the C−C bond formation in combination with a more favorable conformation, thus leading to the cross-coupling product (**CP**) upon reductive elimination (step **D**) which is followed by the release of the regenerated complex **C-1**.[61]

Both dimerization procedures of 2'-functionalized *m*-terphenyls resulted in undesired migration or rearrangement as a result of the sterically unfavorable environment around the 2'-position. This led to a change of the strategy for the synthesis of 2,2',6,6'-tetraphenyl-1,1'-biphenyl (**6-1**) toward concept (**2**) comprising a less hindered dimerization which is followed by a fourfold phenyl attachment (Scheme 6-1). In line with this, a 2,2',6,6'-tetrahalo-1,1'-biphenyl precursor (**2-I**) was aimed, having a methyl-group in the 4,4'-position to enhance crystallinity and for the utilization as marker for NMR measurements.
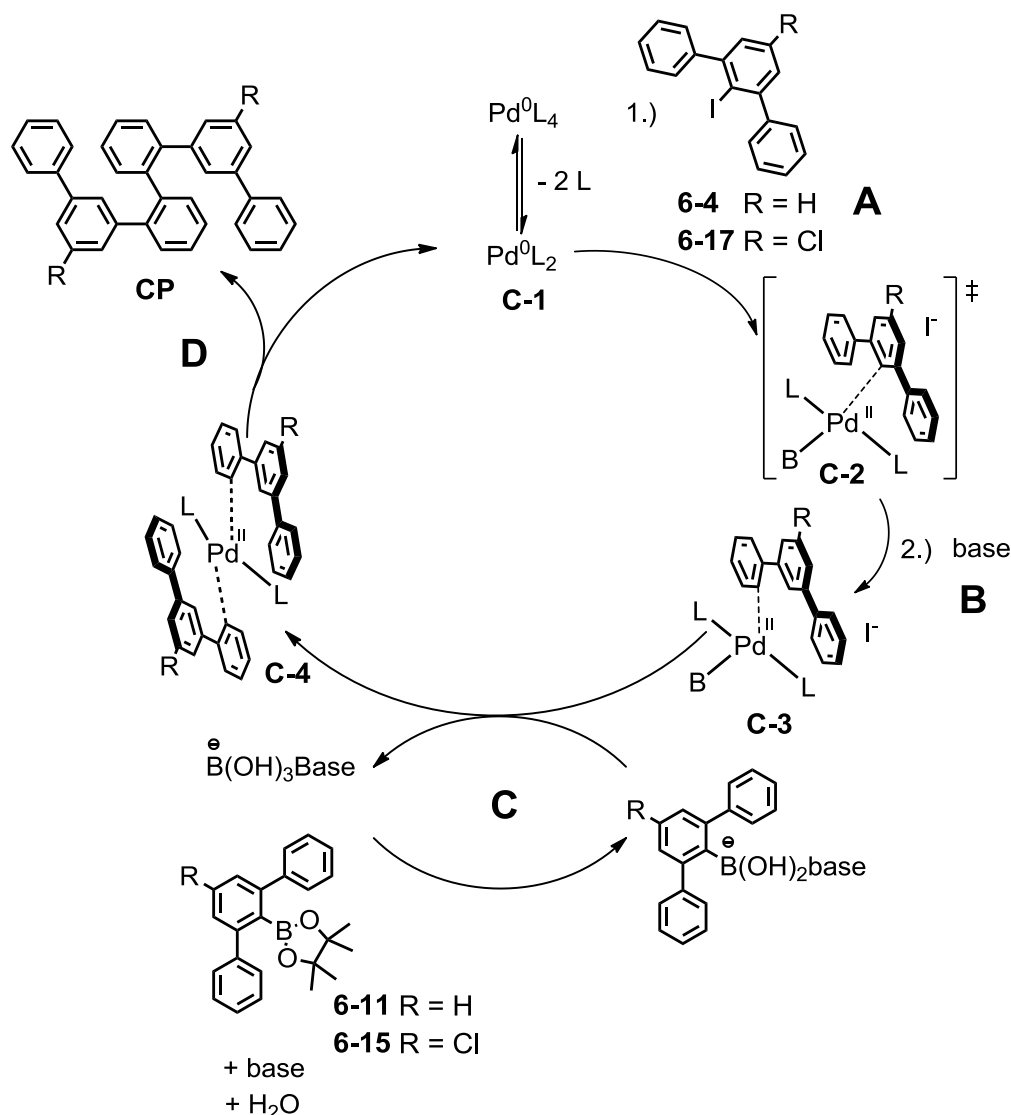
Scheme 6-7. Proposed catalytic cycle for the *Suzuki-Miyaura* cross-coupling toward **6-17**. (**A**) oxidative addition; (**B**) C-H activation during and reaction with the base; (**C**) C-H activation during transmetallation (the *cis-trans* isomerization is omitted for clarity); (**D**) reductive elimination.

The synthesis route toward **6-20** (Scheme 6-8) started with a *Sandmeyer* diazotation adapted from literature of the commercially available 2,6-dibromo-4-methylaniline followed by treatment with potassium iodide to the iodo analogue **6-19**.[62] This was followed by oxidative dimerization along the 2-position of **6-19**. The lithiation was conducted selectively by the slow addition of *n*-BuLi at -78 °C, to minimize the competing bromine-lithium exchange. The generated organometallic species was dimerized by the addition of anhydrous copper(II) chloride as oxidant, followed by column chromatographic separation affording **6-20** in 47% overall yield on a gram scale.[62] As a result of the smaller van der Waals radius of the bromine atoms compared with the phenyl substituents in **6-4** and **6-14**, the dimerization of **6-19** proceeded efficiently already at -78 °C in good
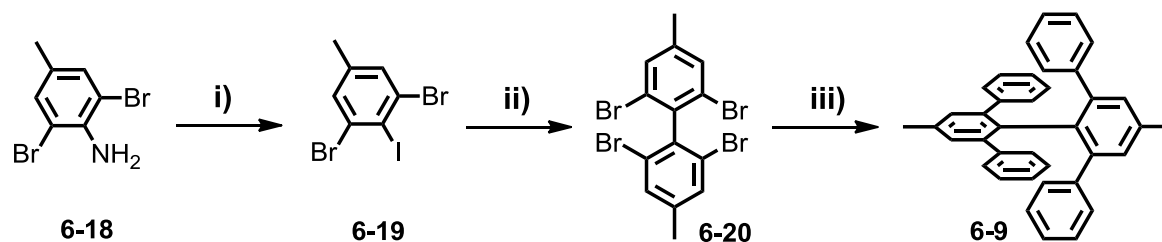
Scheme 6-8. Synthetic route toward 4,4'-dimethyl-2,2',6,6'-tetraphenyl-1,1'-biphenyl **6-9** utilizing concept (2). Conditions: i) NaNO$_2$, HCl, KI, 0 °C to 70 °C, 2h, 85%; ii) *n*-BuLi, CuCl$_2$, Et$_2$O, -78 °C to RT, 55%; iii) phenylboronic acid, *Suzuki-Miyaura* conditions see Table 6-2.

Table 6-2. Optimization of the reaction conditions for the fourfold *Suzuki-Miyaura* coupling toward **6-9**.

Entry	Catalyst System	T (°C)	t (h)	Base	Yield (%)[a]
1	Pd$_2$dba$_3$ + S-Phos	100	24	K$_3$PO$_4$	20[b]
2	Pd(OAc)$_2$ + PPh$_3$	100	24	K$_3$PO$_4$	-[c]
3	Pd(PPh$_3$)$_4$	100	24	K$_3$PO$_4$	12
4	Pd(PPh$_3$)$_4$	100	24	Cs$_2$CO$_3$	23
5	Pd(PPh$_3$)$_4$ + *Aliquat 336*	100	24	Na$_2$CO$_3$	33[d]
6	**Pd(PPh$_3$)$_4$ + *Aliquat 336***	**100**	**24**	**K$_2$CO$_3$**	**47**

[a] Yield of the isolated, analytically pure compound. [b] The purification was complicated by a large amount of protodehalogenated **4a**. [c] No product was detected. [d] Na$_2$CO$_3$ was used as a 2 M aqueous solution.

yields without significant side reactions. With compound **6-20** at hand, the attention was focused on the subsequent fourfold cross-coupling. The *Suzuki-Miyaura* reaction was chosen again, due to its broad scope and versatility in combination with readily available catalytic systems. Screening different Pd-sources and ligand combinations for the *Suzuki-Miyaura* reaction with **6-20** and phenylboronic acid (Table 6-2), resulted in the formation of a compound with the same molecular weight as **6-9** (*m/z* = 486.23) for almost all tested procedures. By optimizing the reaction conditions, tetrakis(triphenyl-phosphine)palladium(0) in the presence of solid potassium carbonate and phase transfer catalyst *Aliquat 336* was found to be most effective (Table 6-2, entry 6). After purification by column chromatography and recrystallization from *n*-hexane, a weakly fluorescent material with limited solubility in organic solvents was obtained. ^{1}H NMR spectroscopy at elevated temperatures proved the successful formation of **6-9** thus confirming the absence of migrations and rearrangements during the reaction (Figure 6-5). As it can be seen from the ^{1}H NMR spectrum three sharp signals were obtained in the aromatic region with a ratio of 1 to 3 to 2. A preliminary assignment was achieved by a simple integration of the signals, showing correct intensities by comparing them with the isolated methyl resonance
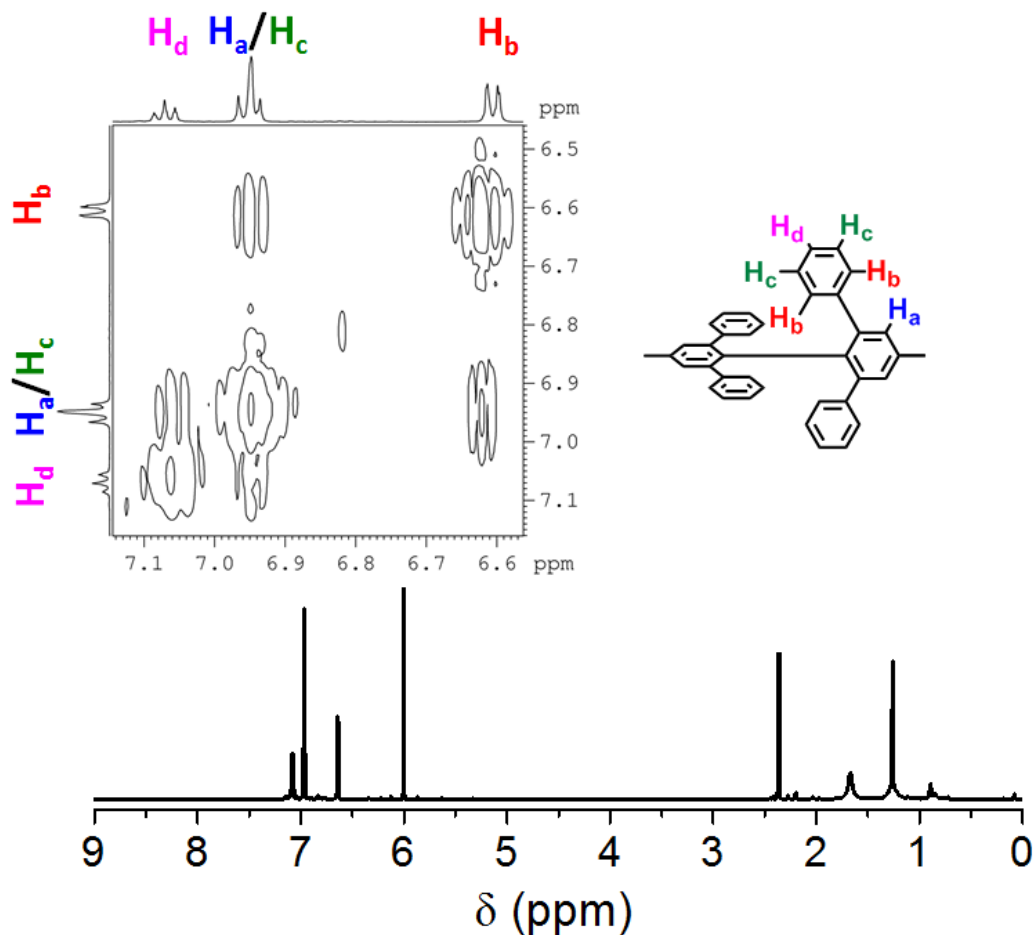
Figure 6-5. ^{1}H NMR spectrum of 4,4'-dimethyl-2,2',6,6'-tetraphenyl-1,1'-biphenyl (**6-9**) in C$_2$D$_2$Cl$_4$ at 50 °C. Inset: Two-dimensional proton correlation (^{1}H, ^{1}H COSY) of **6-9** with proton assignment.

at 2.36 ppm. Moreover, the ^{1}H, ^{1}H COSY NMR spectrum confirmed an *ortho*-coupling between the doublet at 6.60 ppm and the triplet at 6.95 ppm, corresponding to the two H$_c$ and three H$_b$ protons located at the peripheral phenyl moieties. As expected, the protons at the *para*-position of the peripheral phenyl rings (7.07 ppm, H$_d$) gave rise to a triplet and showed an *ortho*-coupling to the neighboring H$_c$. The singlet of the isolated protons at the biphenyl core (7.07 ppm, H$_a$), however, overlap with the triplet of H$_c$ which is supported by the respective integral.

By slow evaporation of a solution of **6-9** in dichloromethane and methanol, single crystals were obtained. They were analyzed by X-ray diffraction proving unequivocally the structure of **6-9** which crystallizes in the centrosymmetric space group C2/*c* (Figure 6-6). Expectedly, the shape is reminiscent of a handshake. Its static geometry is described by several parameters (Figure 6-6 c), such as the dihedral angle of the central bond d_1 (2, 1, 1', 2') and the central bond length r_1.[31] The analysis revealed a mutual twist of 65.8° along the 1,1'-position of the biphenyl core. Moreover, the central bond showed a relatively ordinary length (r_1 = 1.49(1) Å) despite the large amount of strain induced by the
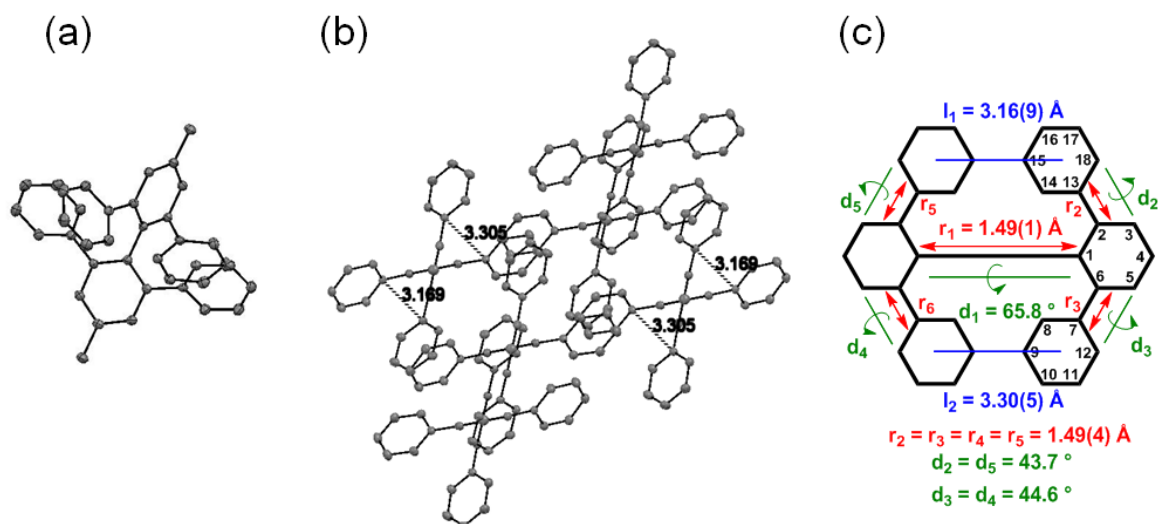
Figure 6-6. X-ray crystal structure of **6-9**. (a) Top view. (b) Side view of the unit cell along the 4,4'-positions together with the distances between the peripheral phenyl rings (hydrogens omitted for clarity in both views). (c) Numbering and characteristic metrics of **6-9**.

π-congested environment. The peripheral aryls showed a π-stacking distance I_1 and I_2 of 3.16(9) Å and 3.30(5) Å, respectively, which is slightly elongated in comparison with related [2.2]*para*cyclophanes (~3.09 Å).[63, 64]

By utilizing the retrosynthetic concept (2), π-congested methyl-substituted 2,2',6,6'-tetraphenyl-1,1'-biphenyl was synthesized with an overall yield of 22% over three steps. This corresponds to an improvement of one order of magnitude compared with the procedure reported by *Ozasa* and *Pascal Jr.* (~2% over four steps),[25-27] thus enabling the synthesis of 2,2',6,6'-tetraphenyl-1,1'-biphenyl on a gram scale.

6.3 Extension of the π-Conjugation of 2,2',6,6'-Tetraphenyl-1,1'-biphenyl

6.3.1 Monomer Synthesis and Polymerization

To expand the π-conjugation of sterically π-congested 2,2',6,6'-tetraphenyl-1,1'-biphenyl toward OPPs and PPPs, the synthesis of an *AA*-monomer with the structural motif of **6-1** was targeted by utilizing the halogen selectivity of concept (2). In addition, the attachment of alkyl substituents such as *tert*-butyl groups was essential to ensure solubility of the resulting π-extended compounds.

For this purpose, the reaction sequence comprising concept (2) was adapted accordingly (Scheme 6-9). Initial diazotation of commercially available 2,6-dibromo-4-chloroaniline (**6-21**), followed by treatment with potassium iodide under *Sandmeyer* conditions afforded 1,3-dibromo-5-chloro-2-iodobenzene (**6-22**) in 55% yield.[62] The oxidative dimerization of
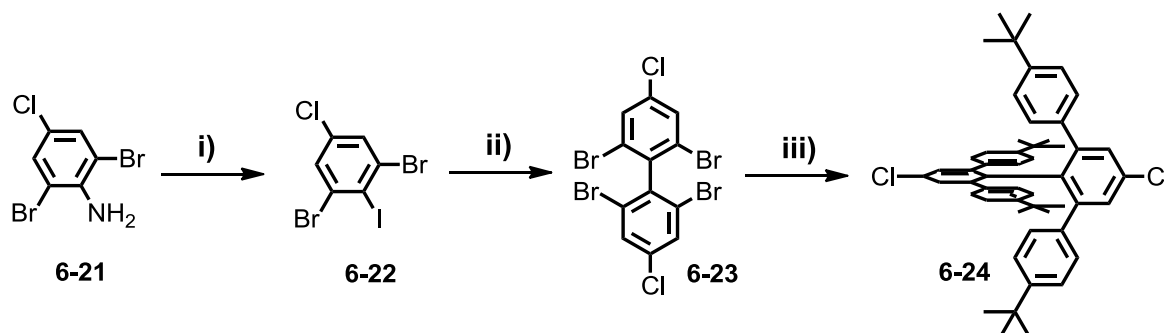
Scheme 6-9. Synthetic route toward monomer **6-24** utilizing concept (2). Conditions: i) NaNO$_2$, HCl, KI, 0 °C to 70 °C, 2h, 55%; ii) *n*-BuLi, CuCl$_2$, Et$_2$O, -78 °C to RT, 12h 50%; iii) (4-(*tert*-butyl)phenyl)boronic acid, Pd(PPh$_3$)$_4$, K$_2$CO$_3$, toluene, *Aliquat 336*, 100 °C, 24h, 47%.

6-22 was accomplished by selective iodine-lithium exchange followed by the addition of copper(II) chloride provided 2,2',6,6'-tetrabromo-4,4'-dichloro-1,1'-biphenyl (**6- 23**) in 28% overall yield.[62] By applying the previously established *Suzuki-Miyaura* coupling conditions, the crucial fourfold attachment of the peripheral phenyl moieties was achieved using (4-(*tert*-butyl)phenyl) boronic acid. The reactivity of the bromine substituents was sufficiently high at the applied conditions to exclude thereby a possible attack of the chlorine atoms in 4,4'-position, which were required for subsequent π-extensions. The reaction showed full conversion after 24 hours, as revealed by thin-layer chromatography
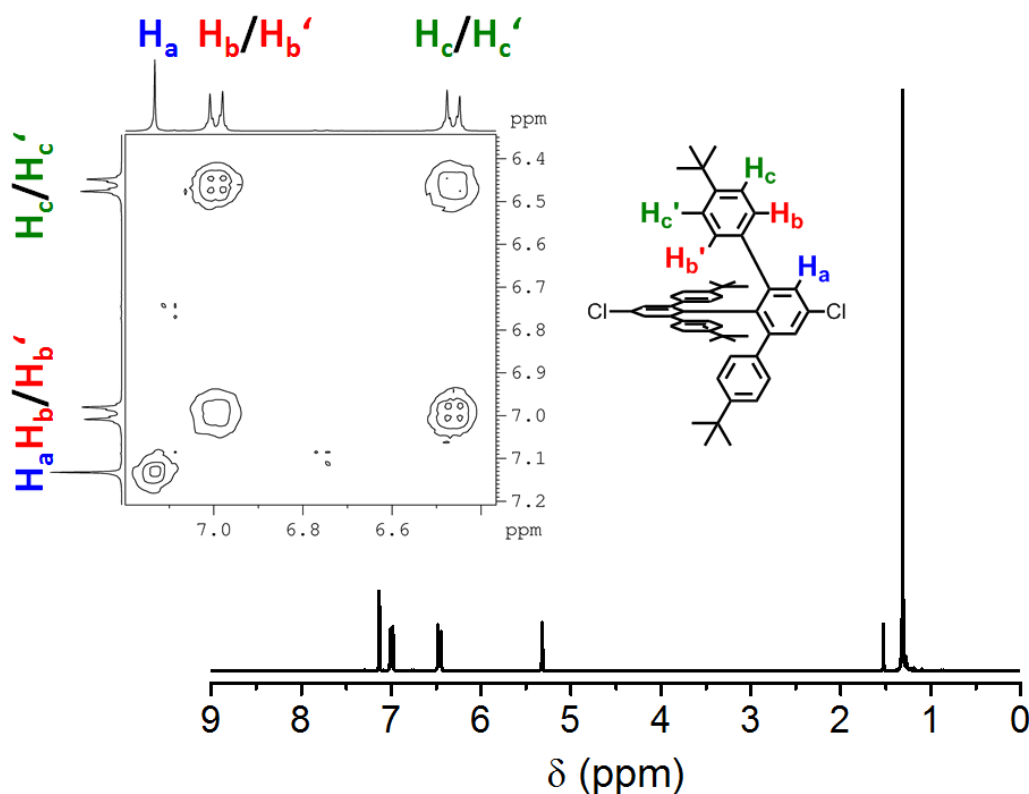
Figure 6-7. ^{1}H NMR spectrum of monomer **6-24** in CD$_2$Cl$_2$ at 25 °C. Inset: Two-dimensional proton correlation (^{1}H, ^{1}H COSY) of **6-24** with proton assignment.
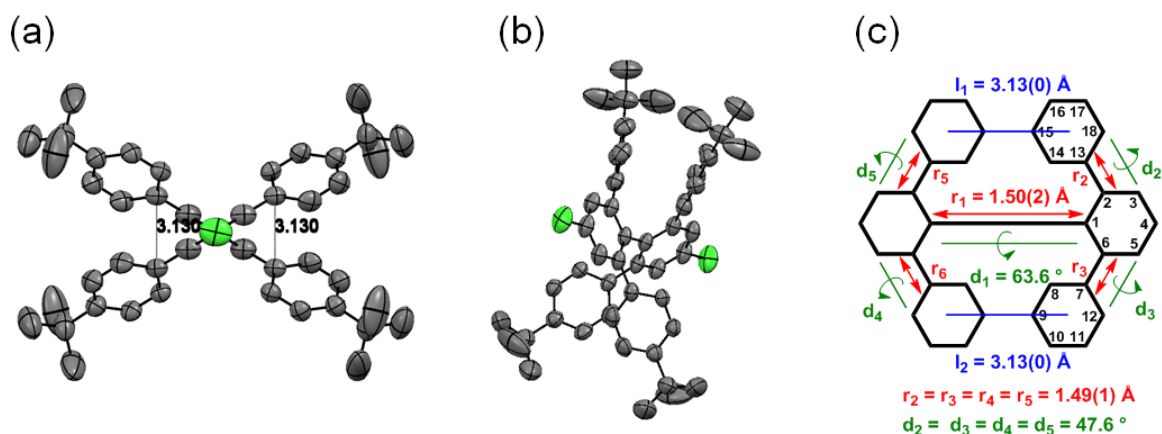
Figure 6-8. X-ray crystal structure of **6-24**. (a) View along the 4,4'-positions and (b) side view of the individual molecules together with the distances between the peripheral phenyl rings (hydrogens omitted for clarity in both views). (c) Numbering and characteristic metrics of **6-24**.

and FD-MS. Column chromatographic separation of the reaction mixture followed by recrystallization, afforded **6-24** in 47% yield. Its identity was confirmed by ^{1}H NMR spectroscopy, revealing three sets of signals with a ratio of 1 to 2 to 2 in the aromatic region (Figure 6-7). Based on the above considerations for model compound **6-9** and with the help of the integrals, the signals were readily assigned. In line with that, the singlet at 7.13 ppm corresponds to the protons located at the biphenyl core (H_a). The remaining two doublets at 6.99 and 6.46 ppm were assigned to the four protons at the peripheral phenyl rings (H_b, H_b', H_a, H_a'), giving rise to a AA'XX' system. This resulted in an *ortho*-coupling among them as displayed by the ^{1}H, ^{1}H COSY NMR spectrum. As a result of the ring current of the adjacent biphenyl core, the signals of H_b and H_b' were shifted downfield to 6.99 ppm. This data proved furthermore the high level of purity of **6-24** which is a key parameter to guarantee for a high degree of polymerization (see above).

Single crystals obtained by slow evaporation of a dichloromethane solution of **6-24** were analyzed by X-ray diffraction (Figure 6-8). They confirmed the successful formation of **6-24** and revealed similar parameters as observed for model compound **6-9**. However, the dihedral angle ($d_1 = 63.6°$) was measured to be slightly reduced compared with **6-9**. Additionally, the π-π distances among the peripheral phenyl rings ($I_1 = I_2 = 3.13(0)$ Å) were shortened.

As a result of the dichloro-functionalities at the 4,4'-position, **6-24** can be considered as an *AA*-monomer suitable for polymerization in "*para*" direction. Referring to this, the Ni^0-mediated *Yamamoto* dehalogenation polycondensation was shown to be an efficient cross-coupling procedure to overcome the drawbacks of *AB*-type polymerizations. This has
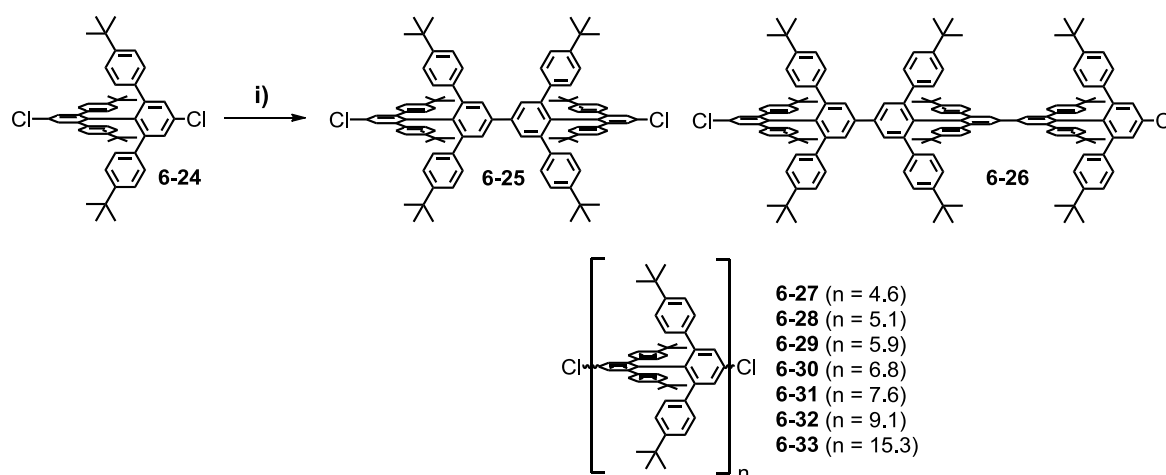
Scheme 6-10. Synthetic route of the polymerization of **6-24** utilizing the *Yamamoto* reaction. Conditions: i) bis(cycloocta-1,5-diene)nickel(0), cycloocta-1,5-diene, 2,2'-bipyridine, toluene/DMF, 110 °C, microwave irradiation, 2 days, **6-25**: 9%, **6-26**: 5%, **6-27**: 2%, **6-28**: 2%, **6-29**: 1%, **6-30**: 1%, **6-31**: 0.5%, **6-32**: 0.3%, **6-33**: 2%.

previously been demonstrated for the polymerization of the *AA*-monomers dibromo *N*-heterotriangulene **3-5** (see above).[34-36] Thus, the polymerization reaction of **6-24** was carried out in the established *Yamamoto* protocol by utilizing an overall 2/1 mixture of toluene/DMF with a concentration of 25×10^{-3} M. After subsequent activation at 65 °C, the solution of **6-24** was added to the Ni-complex and the reaction was allowed to proceed for several days in the dark. However, after one week at 85 °C, the MALDI-TOF MS revealed the presence of mainly dimers, trimers and tetramers (Figure 6-9, black line). By further increasing the temperature, the conversion remained unaffected which indicated an already deactivated Ni^0-complex. This was mainly attributed to the lower reactivity of the two chloro-functionalities. Thus, the concentration of the reaction mixture was increased (55×10^{-3} M) and the polymerization was repeated under microwave irradiation at 110 °C to enhance the *inter*molecular C−C bond formation. After running the reaction for two days, an excess amount of chlorobenzene was added as endcapping agent and the reaction was continued for another 12 hours. The quenching of the reaction and decomposition of the nickel residues was achieved by adding the reaction mixture to dilute methanolic hydrochloric acid. The white precipitate was filtered and re-precipitated from a dichloromethane/methanol mixture. Initial analysis of the polymeric mixture by SEC in THF with a PPP standard revealed a M_n of 3 500 g/mol. MALDI-TOF MS indicated the presence of a regular pattern which extended up to molecular weights of 13 000 g/mol (Figure 6-9, red line). The number of repeating units was around 19, which corresponds to 38 linearly connected benzene rings. In general, the MALDI-TOF MS was measured in the
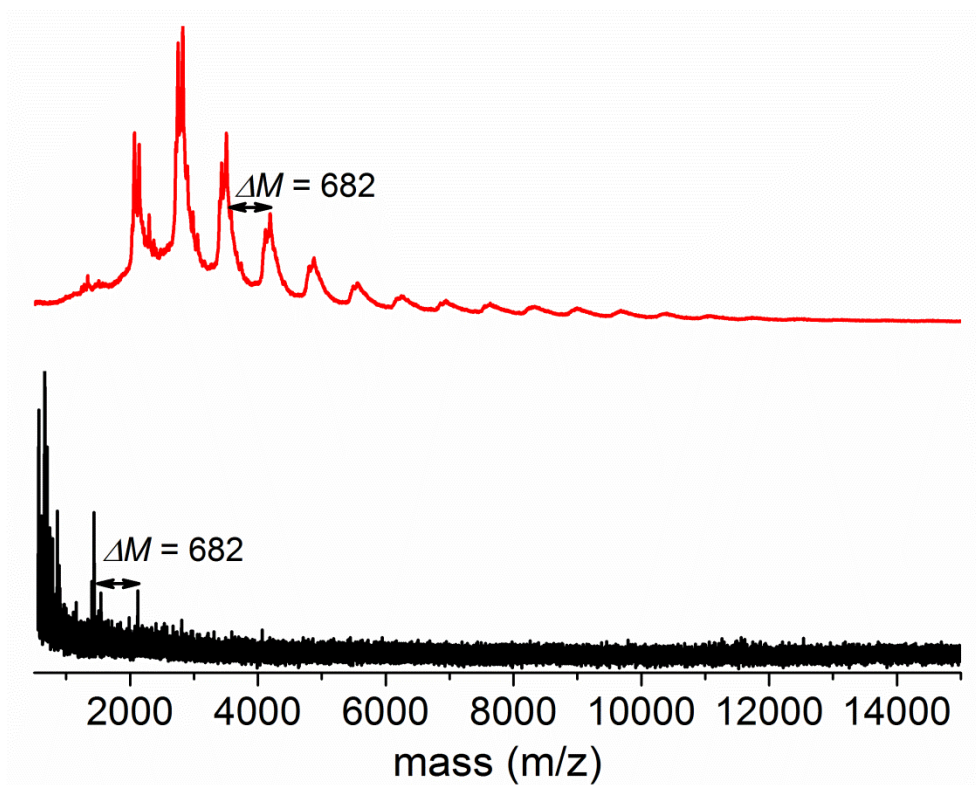
Figure 6-9. MALDI-TOF MS obtained after *Yamamoto* polymerization of **6-24** by conventional heating (black line, reflector mode) and under microwave irradiation (red line, linear mode).

so-called "linear mode" which allows for the detection of high molecular species but leads to broad signals preventing their detailed investigations such as an end group analysis. The obtained polymer was subjected to preparative SEC with toluene as eluent for the fractionation of the oligomers, in order to study the impact of the chain length on the photophysical properties. This allowed for the separation of the obtained polymer into the

Table 6-3. Characteristics of the individual fractions **6-25** to **6-33**.

Fraction	M_n[a] (g/mol)	M_w[a] (g/mol)	PDI[b]	DP[c]	$n_{phenylene}$[d]
6-25	1 432[e]	1 432[e]	1.00	2	4
6-26	2 113[e]	2 113[e]	1.00	3	6
6-27	3 100	3 550	1.15	4.6	9.2
6-28	3 500	4 000	1.14	5.1	10.2
6-29	4 000	4 750	1.19	5.9	11.8
6-30	4 600	5 500	1.20	6.8	13.6
6-31	5 200	6 250	1.20	7.6	15.2
6-32	6 200	7 400	1.19	9.1	18.1
6-33	10 400	14 000	1.35	15.3	30.6

[a] Molecular wights were determined by SEC in THF ousing PPP as standard. [b] *PDI* = M_w/M_n. [c] DP = M_n/M_0. [d] Number of 1,4-connected phenylene. [e] Absolut molecular weights.
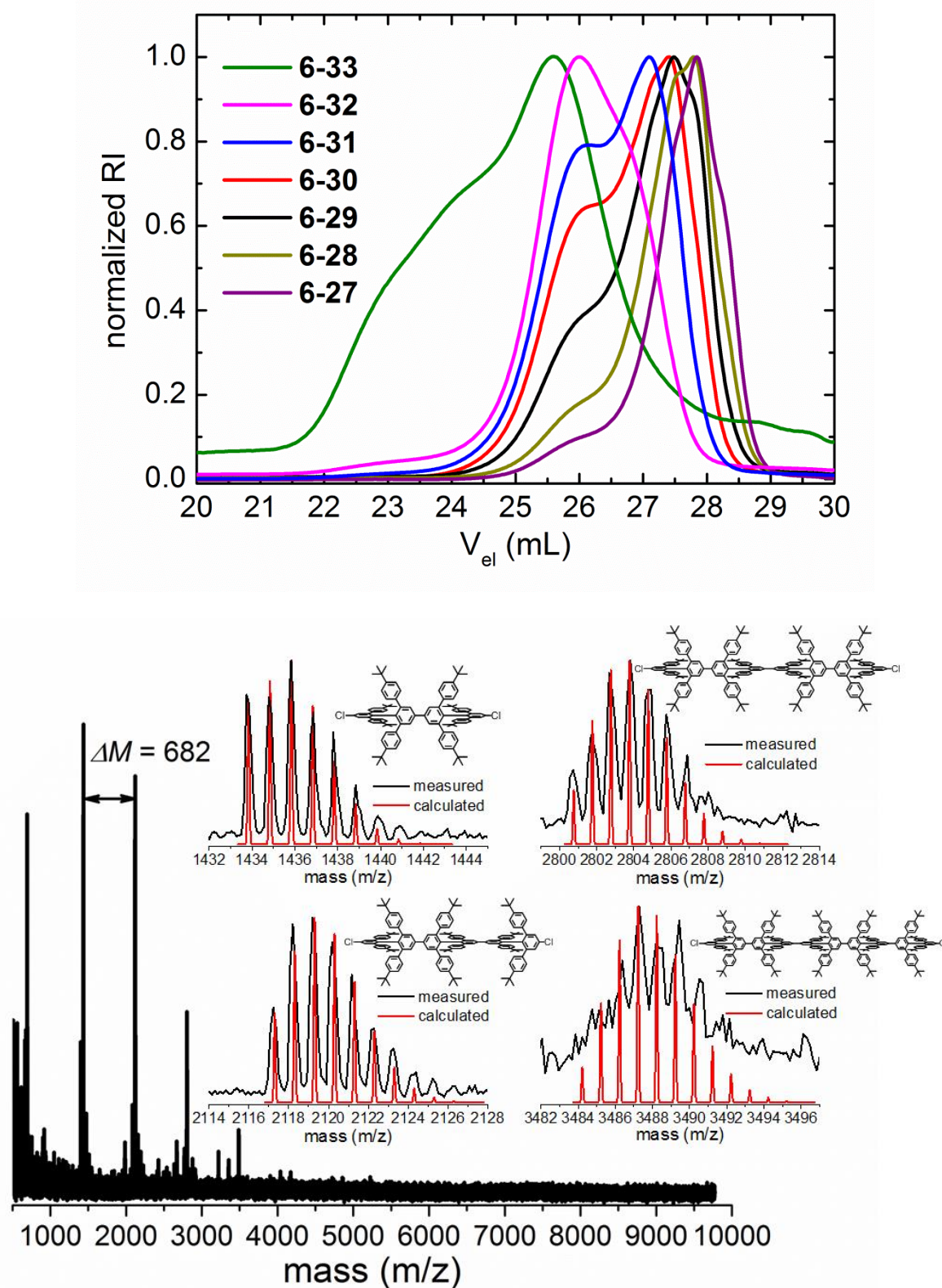
Figure 6-10. Top: SEC analysis of the separated oligomeric fractions **6-27** to **6-33** (THF, PPP standard). Bottom: MALDI-TOF MS of the polymeric fraction **6-33** reflecting the presence of up to pentamers. Inset: Measured and calculated isotopic patterns of the dimer, trimer, tetramer and pentamer.

monodisperse dimer **6-25** and trimer **6-26**, as well as seven polydisperse fractions **6-27** to **6-33** (Scheme 6-10, Table 6-3). The composition of dimer **6-25**, trimer **6-26**, separated oligomers **6-27** to **6-32** and polymer **6-33** was analyzed by SEC in THF utilizing a PPP standard (Table 6-3, Figure 6-10, top). As a result of its rigidity, a PPP standard was expected to be structurally closely related to the π-congested compounds thus allowing for an accurate estimation of the molecular weights of **6-27** to **6-33**. The SEC analysis revealed a gradually decreased elution volume (V_{el}) of the obtained SEC curves corresponding to the extended hydrodynamic volume of the fractions and consequently an increase in their chain length. Polymer **6-33** was obtained as first fraction having a $M_n = 10\,400$ g/mol with a PDI of 1.35 which corresponds to approximately 15 repeating units and thus 30 to 32 1,4-phenylene moieties. The characteristics of the remaining fractions are illustrated in Table 6-3. Moreover, polymer fraction **6-33** could be analyzed with MALDI-TOF MS utilizing the "reflector mode" which is characterized by a narrow signal width thus rendering endgroup analysis possible (Figure 6-10, bottom). The MALDI-TOF spectrum revealed clearly resolved isotopic patterns up to 3 500 g/mol. By comparing these signals with the calculated isotopic patterns of the dimer, trimer, tetramer and pentamer, the presence of chlorine endgroups was revealed suggesting an unsuccessful endcapping process. As a result of the decreased ionization tendency of the larger chains under the applied MALDI-TOF conditions, the endgroup analysis based on mass spectrometry was limited to the smaller species.

By characterizing dimer **6-25** and trimer **6-26** with the help of ^{1}H and ^{1}H, ^{1}H COSY NMR spectroscopy, well resolved spectra with distinct signals in the aromatic region were obtained due to their monodisperse composition. The spectrum of trimer **6-26** is shown in Figure 6-11 (top) and the signal assignment is representatively discussed in the following. Due to the three different types of *m*-terphenyl subunits in **6-26**, three sharp singlets of the *tert*-butyl protons were observed between 1.28 and 1.31 ppm showing correct signal intensities (1:1:1). In the aromatic region five sharp signals were furthermore detected, having a ratio of 2 to 1 to 6 to 2 to 4. The singlets at 7.48 and 7.14 ppm, which were similarly observed for dimer **6-25**, could be assigned to the coalescing internal (H_b and H_c) and the four external protons (H_a) located at the biphenyl core thus indicating the presence of chlorine endgroups. The remaining three aromatic signals resulted from three individual AA'XX' systems located at the peripheral phenyl rings. In agreement with the ^{1}H NMR spectrum of the monomer **6-24** (Figure 6-7) the signals of the 12 internal protons of the peripheral phenyls ($H_d'/H_e'/H_f'$) overlapped at 6.99 ppm in a pseudo triplet, which showed
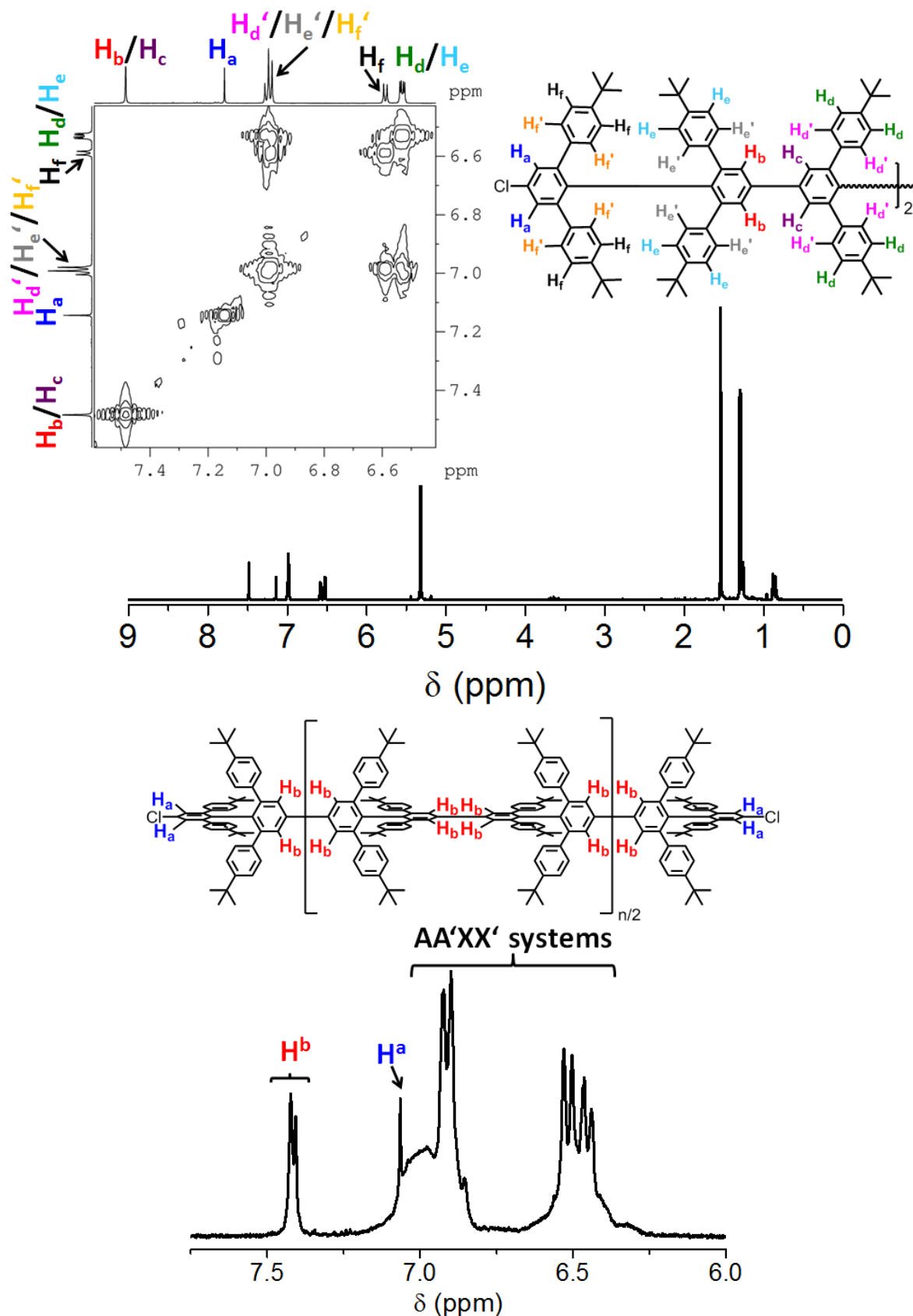
**Figure 6-11.** Top: ^{1}H NMR spectrum of trimer **6-26** in CD$_2$Cl$_2$ at 25 °C. Inset: Two-dimensional proton correlation (^{1}H, ^{1}H COSY) of **6-26** with proton assignment. Bottom: ^{1}H NMR spectrum of the polymeric fraction **6-33** in CD$_2$Cl$_2$ at 25 °C.

an *ortho*-coupling to its neighboring protons ($H_d/H_e/H_f$). The four protons of the peripheral phenyl moieties located at the external *m*-terphenyls (H_f) were slightly downfield shifted (6.58 ppm) in comparison to their internal counterparts (H_d/H_e, two doublets at 6.53 ppm). By comparing the ^{1}H NMR spectra of the polymeric fraction **6-33** with dimer **6-25** and trimer **6-26** (Figure 6-11, bottom), the appearance of a broadened signal at 7.49 ppm together with two coalescing singlets at 7.14 ppm was observed. These signals originated from the isolated protons at the biphenyl core (H_a, H_b) thus confirming the similar presence of chlorine endgroups at the polymeric chains as for **6-25** and **6-26**.

6.3.2 Photophysical and Electronic Properties

Having the π-congested dimer **6-25**, trimer **6-26** and polymeric fractions **6-27** to **6-33** in hand, UV-vis absorption and emission properties were investigated in dichloromethane solutions (Figure 6-12). To gain further insights into the electronic properties of π-congested PPPs, time-dependent DFT calculations (TD-DFT, B3LYP/6-31G*) on simplified derivatives **6-24$_{th}$**, **6-25$_{th}$** and **6-26$_{th}$** were carried out in collaboration with ▮▮▮▮▮▮▮▮▮▮▮▮▮▮ at the MPI-P Mainz, Germany.[65]
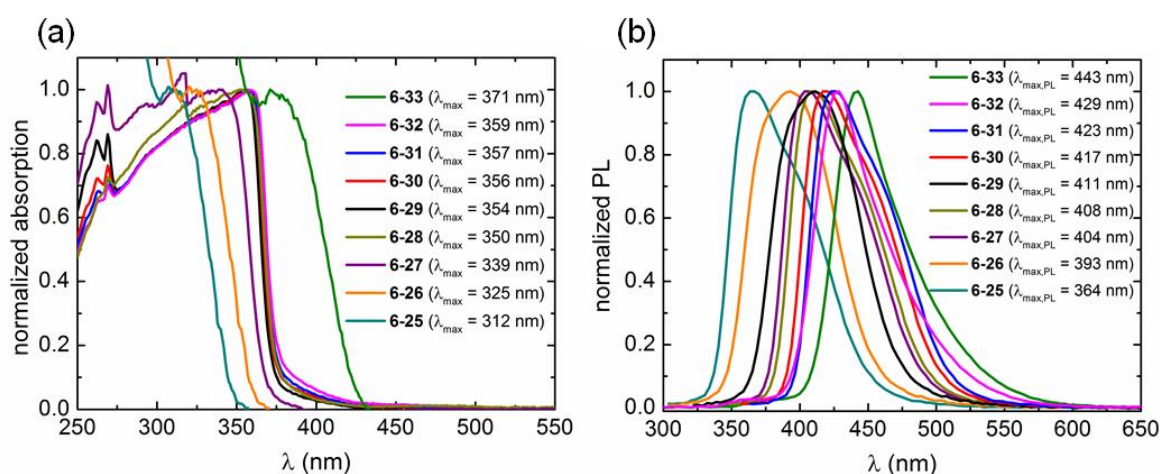
Figure 6-12. UV-vis absorption (a) and emission (b) spectra of the individual fractions **6-25**-**6-33**. For all spectra: 1×10^{-6} M in CH$_2$Cl$_2$.

The UV-vis absorption spectra of all compounds displayed characteristic transitions below 300 nm and between 310 nm to 360 nm (Figure 6-12 a). They were assigned upon TD-DFT calculations as HOMO−1 to LUMO+1 and HOMO−LUMO absorptions (Figure 6-13). By extending the π-conjugation toward **6-25** to **6-33**, bathochromic shifts by about 10 and 30 nm were observed. The position of the longest wavelength absorptions is thereby in excellent agreement with the transitions of the calculated spectra. These absorptions
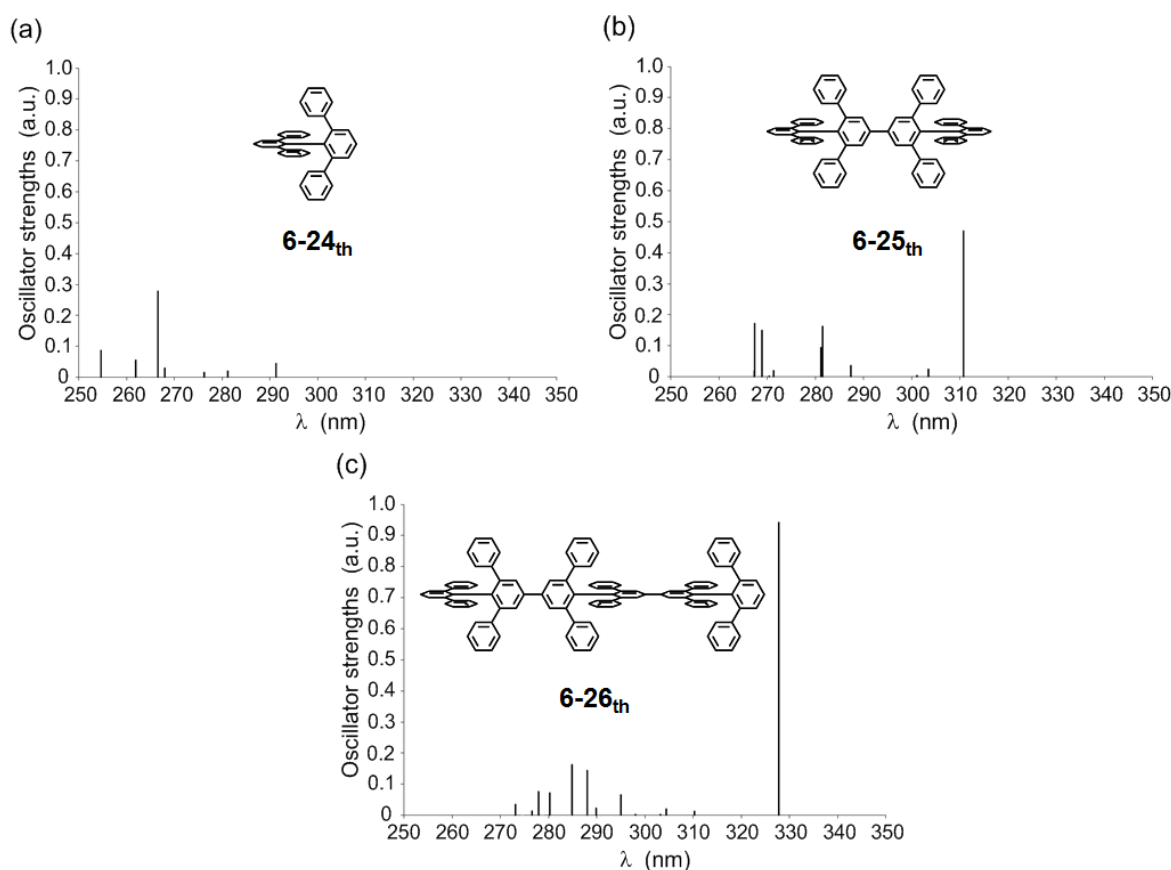
Figure 6-13. Calculated UV-vis absorptions spectra of (a) **6-24**th, (b) **6-25**th, and (c) **6-26**th obtained with the help of TD-DFT calculations (B3LYP/6-31G*).

feature simultaneously a significant increase in the oscillator strength. In addition, deep blue emissions in the range of 360 nm to 450 nm were observed for **6-25** to **6-33** (Figure 6-12 b). The emission of polymer **6-33** ($\lambda_{PL,max}$ = 443 nm) is thereby located in the ideal range for pure blue luminescence between 440 and 450 nm.[66-68] This holds promise for their future applications in OLEDs.

Even though a large mutual twist in the central biphenyl units was observed, the red-shifts in absorption upon π-extension indicated an effective π-conjugation along the *para*-positions of the sterically π-crowded subunits. A closer look at the frontier orbitals of simplified derivatives **6-24**th, **6-25**th and **6-26**th, revealed HOMO and LUMO orbitals fully delocalized over the entire molecules (Figure 6-14). The peripheral phenyl moieties led to a considerable increase of the π-electron density along the *para*phenylene backbone in dimer **6-25** and trimer **6-26** (Figure 6-14 b and c). For the sake of comparability with unsubstituted OPPs, calculations were carried out on the *p*-quaterphenyl and *p*-sexiphenyl possessing identical dihedral angles in the biphenyl core. By comparing the HOMO orbitals of **6-25**th and **6-26**th with the unsubstituted OPPs, significant π-orbital interactions were observed in the π-congested biphenyl units, which were absent in the unsubstituted *p*-
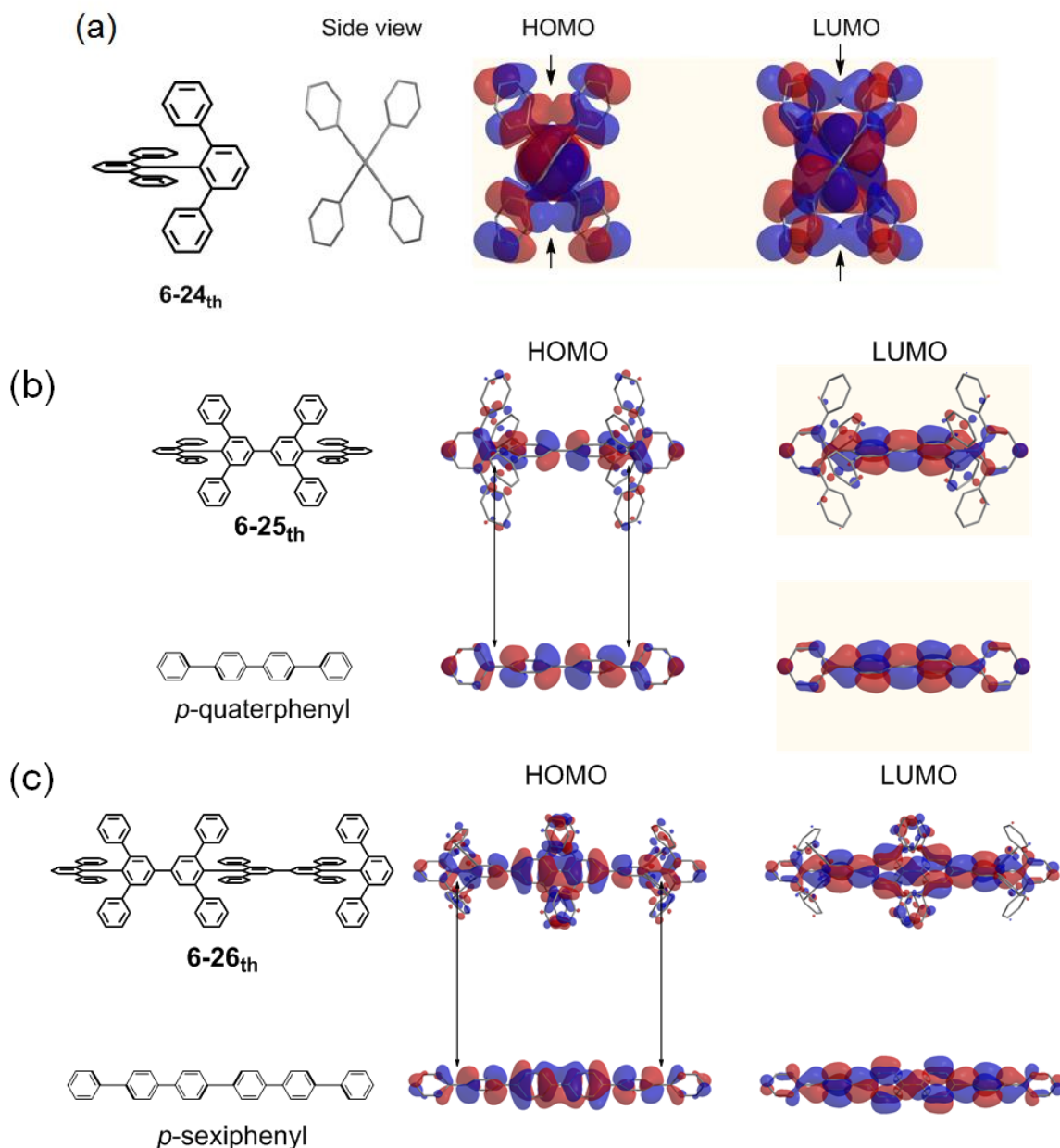
Figure 6-14. (a) HOMO and LUMO orbitals of **6-24_{th}**. The arrows indicate a through-space π-conjugation among the peripheral phenyl rings. HOMO and LUMO orbitals of (b) **6-25_{th}** and *p*-quaterphenyl and (c) **6-26_{th}** and *p*-sexiphenyl. The arrows indicate the increased electron density in **6-25_{th}** and **6-26_{th}** compared to the unsubstituted OPPs.

quaterphenyl and *p*-sexiphenyl at the same isocounter values (Figure 6-14 b and c). Due to the lack of electron density along the unsubstituted backbone, the π-conjugative interactions in PPPs were drastically decreased and the individual 1,4-phenylene subunits were widely referred to as virtually independent chromophores.[6, 69-71] Besides that, an *intra*molecular through-space conjugation was identified among the cofacially oriented π-orbitals of the peripheral phenyl rings of π-congested **6-24_{th}** (Figure 6-14 a). As a result of the unique architecture of the 2,2',6,6'-tetraphenyl-1,1'-biphenyl subunit, the peripheral

phenyls were constrained to stack on the top of each other related to [2.2]*para*cyclophanes and π-stacked poly(fluorenes).[72-74] Both characteristics contribute to the observed bathochromic shifts of the absorption maxima at the longest wavelength for dimer **6-25** and trimer **6-26**, compared with the analogous *p*-quaterphenyl and *p*-sexiphenyl. These aspects were further elucidated by comparing the absorption maxima of π-congested polymer **6-33** (M_n = 10 400 g/mol, DP ≈ 15, $n_{phenylene}$ ≈ 31) at λ_{max} = 371 nm with a non-congested *n*-hexyl substituted PPP (M_n = 7 600 g/mol, $n_{phenylene}$ ≈ 31) at λ_{max} ≈ 300 nm, which was reported by *Rehahn*, *Schlüter* and *Wegner*.[7] As a consequence of the intrinsic dihedral angle between the phenylene subunits upon alkyl substitution, such PPPs loose the electronic properties of π-conjugated polymers. In contrast to that, **6-33** absorption maximum is bathochromically shifted of about 71 nm, even though it is composed of the same number of benzene units as the non-congested PPP along the *para*phenylene main chain. Thus, the π-orbital interactions along the polymer backbone of **6-33** in combination with the through-space conjugation compensate for the adverse dihedral angles.

In general, the π-conjugation in conjugated polymers and oligomers is limited to a certain number of repeating units along their backbone. In this context, a fundamental question is the extent to which polymer properties can be predicted on extrapolation from oligomer data.[75] A valuable parameter for these purposes is the effective conjugation length. It defines the convergence of photophysical and electronic parameters such as absorption, photoluminescence or redox characteristics, with increasing chain length of the π-conjugated system and thus the overall size of the π-system, which is necessary to reach size-independent electronic properties.[69, 76-78] The effective conjugation length and the associated absorption maxima of π-conjugated polymers with sufficiently high molecular weights can be estimated from the empirical relation between the number of repeating units (n) with the absorption maxima (λ_{max}) of the π-conjugated oligomers according to equation (1):[69, 78, 79]

$$E_n = E_\infty + {E}/{n_{phenylene}} \; with \; E_n = {h}/{\lambda_{max}} \quad and \; h = 6.626 \times 10^{-34} J \, s \qquad (1)$$

In line with this, the optical absorption energies E_n of the π-congested oligomers **6-25** to **6-32** were plotted against the inverse chain length $1/n_{phenylene}$ ($n_{phenylene}$: number of 1,4-connected phenylene units) and were correlated to the absorption data of the known oligophenyls (Figure 6-15). This resulted in a linear correlation with small deviations of the values as expressed by the high R factor of 0.98 (Figure 6-15 a).[75, 78-80] The resulting
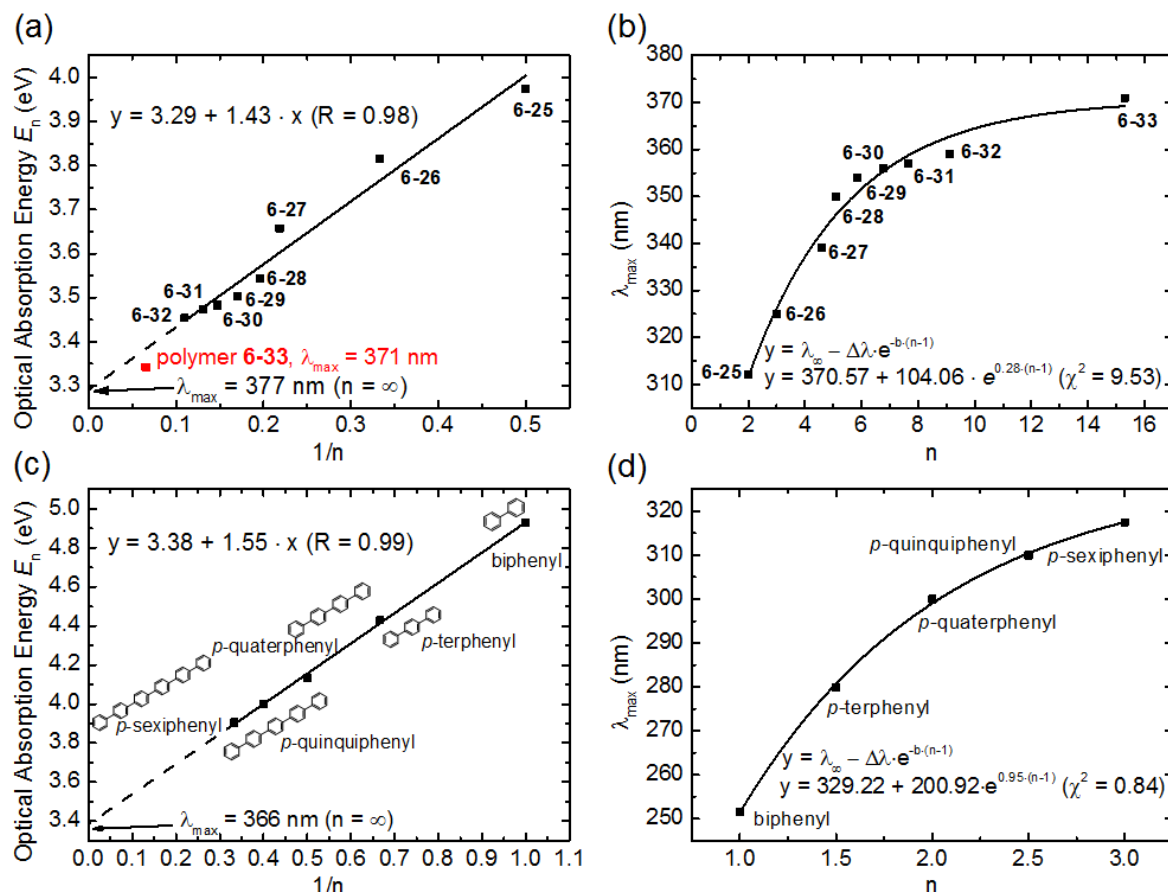
Figure 6-15. Correlation of the optical absorption energy (E_n) of (a) **6-25** to **6-33** and (c) unsubstituted oligophenyls[82] with the inverse number of repeating units. The black line corresponds to the linear fit. Plot of the absorption maxima (λ_{max}) of (b) **6-25** to **6-33** and (d) unsubstituted oligophenyls[82] with the number of the repeating units. The black line corresponds to the exponential fit.[79] For all spectra: 1×10^{-6} M in CH_2Cl_2 or $CHCl_3$.

extrapolation to an infinite number of repeating units (n = ∞) provided an absorption maximum of 377 nm ($E_\infty = 3.29$ eV). However, the expected asymptotical behavior of E_n and λ_{max} of higher oligomers was not reflected by this correlation. In other words, for higher values of n the linear correlation merges to a non-linear regime.[81] Therefore, the absorption maxima of **6-25** to **6-32** were plotted against the number of repeating units approaching a limit of convergence (Figure 6-15 b). This convergence was first reported by *Stalmach* and *Meier* utilizing the following equation:[79]

$$\lambda_{max}(n) = \lambda_\infty - \Delta\lambda \cdot e^{-b(n-1)} \qquad (2)$$

with $\Delta\lambda = \lambda_\infty - \lambda_1$ representing the overall effect of π-conjugation. Moreover, the empirical parameter b indicates how fast the limit of convergence is reached. The excellent fit (small χ^2 value) of the measured absorptions of **6-25** to **6-32** by using equation (2) provided the following data:

$$\lambda_\infty = 371 \text{ nm}; \Delta\lambda = 104 \text{ nm}; b = 0.28; \chi^2 = 9.53$$

thus corresponding to a maximum absorption energy E_∞ of 3.34 eV, which is in fairly good agreement with the results of the linear correlation. The limiting values λ_∞ and E_∞ correspond thereby to λ_{16} and E_{16} obtained for the polymeric fraction **6-33** (n = 16). Thus, the effective conjugation length is reached for 16 π-congested repeating units, which means that polymeric chains with more than 16 repeating units have no additional effect on the absorption energies and thus on E_g.

To compare this data with unsubstituted OPPs, the above mentioned procedures were repeated (Figure 6-15 b and d) with biphenyl, *p*-terphenyl, *p*-quaterphenyl, *p*-quinquiphenyl and *p*-sexiphenyl by utilizing the absorption data measured in chloroform, which was reported by *Gillam* and *Hey* providing the following parameters:[82]

linear correlation: $\lambda_\infty = 366 \text{ nm}; E_\infty = 3.38 \text{ eV}$;

exponential correlation: $\lambda_\infty = 330 \text{ nm}; \Delta\lambda = 201 \text{ nm}; b = 0.95; \chi^2 = 0.84$.

The absorption maximum at the longest wavelength is consequently shifted by approximately 10−40 nm to higher wavelengths by using the 2,2',6,6'-tetraphenyl-1,1'-biphenyl subunit instead of unsubstituted phenylenes. These results confirmed the enhancement of the π-conjugation by the attachment of additional phenyl moieties, due to significant π-orbital interactions along the *para*phenylene backbone of the π-congested systems, together with a through–space conjugation among the π-orbitals of the peripheral phenyls. Compared to classical PPP without having these beneficial interactions, an increased effective conjugation length is observed. Furthermore, it elucidates that planarization of the aromatic π-system is not the only beneficial aspect for enhancing the communication along the PPP backbone. With respect to potential applications in organic solar cells, the attachment of donor and acceptor moieties is expected to further increase the bathochromic shift by an *intra*molecular charge transfer.

An extended chain stiffness and thus an increased persistence length was moreover anticipated for the discussed π-congested PPPs compared to its unsubstituted counterparts, due to the contorted and rigid architecture of the 2,2',6,6'-tetraphenyl-1,1'-biphenyl subunits. However, the comparably low molecular weights of polymer **6-33** (M_n = 10 400 g/mol) hampered the estimation of the persistence lengths so far. A polymerization method with an increased efficiency toward chlorine-functionalities could help to overcome this and allow for a persistence length determination by dynamic light scattering (DLS).

6.4 Expansion of the Phenyl Density

In continuation of these encouraging findings, synthetic pathways were pursued for expanding the density of benzene rings in 2,2',6,6'-tetraphenyl-1,1'-biphenyl (**6-1**). Due to the remaining 3,3',4,4',5,5'-positions of **6-1**, the attachment of further phenyl moieties was considered to be possible by utilizing the established *Suzuki-Miyaura* procedure (Scheme 6-11). The steric demand during the cross-coupling process in this particular situation was expected to be further increased as a result of the sequential C−C bond formation along the *ortho*-positions of the biphenyl core (**6-34**, Scheme 6-11).
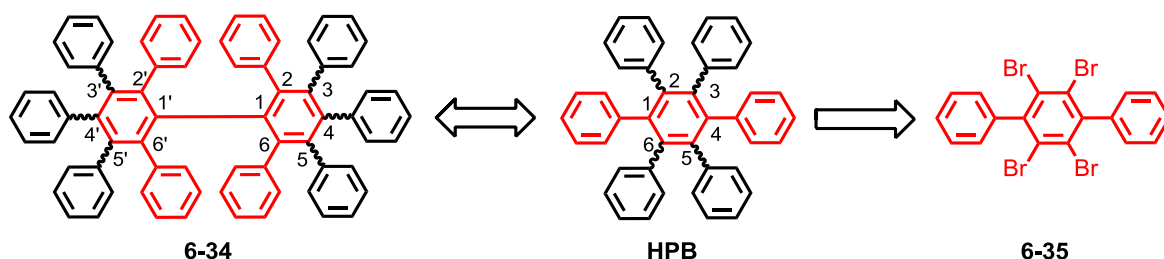
Scheme 6-11. Strategy for the attachment of the additional phenyl density to the core of **6-1** toward **6-34** having a direct relation to **HPB** which can be generated from **6-35**. The crucial benzene rings are shown in red.

Initially, a test reaction was aimed which models the steric environment during the formation of **6-34** toward 2,2',3,3',4,4',5,5',6,6'-decaphenyl-1,1'-biphenyl (**6-34**). Thus, 2',3',5',6'-tetrabromo-1,1':4',1''-terphenyl (**6-35**) was expected to fulfill this requirement and enable the synthesis of HPBs which itself mimics a segment of **6-34** (Scheme 6-11 and 6-12). Functionalized *p*-terphenyl **6-38** was built from commercially available 1,2,4,5-tetrabromobenzene (**6-36**) by adopting a literature-known synthetic procedure.[83]
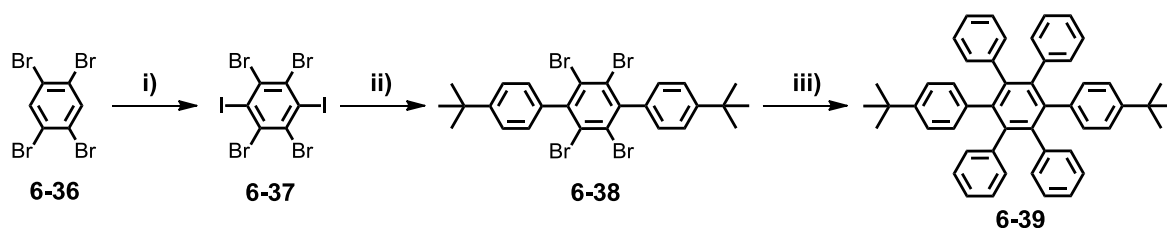
Scheme 6-12. Synthetic route of the model reaction toward hexaphenylbenzene **6-39**. Conditions: i) I_2, KIO_3, H_2SO_4, RT, 48h, 73%; ii) 1-(*tert*-butyl)-4-iodobenzene, Cu, 200 °C, 14h, 27%; iii) phenylboronic acid, Pd(PPh$_3$)$_4$, K_2CO_3, toluene, H_2O, *Aliquat 336*, 100 °C, 24h, 87%.

Iodination of the 3,6-positions was achieved by treatment of **6-36** with iodine in sulfuric acid in the presence of potassium iodate yielding 1,2,4,5-tetrabromo-3,6-diiodobenzene (**6-37**) in 73%. The subsequent twofold *Ullmann* coupling of **6-38** with commercially available 1-(*tert*-butyl)-4-iodobenzene afforded the functionalized *p*-terphenyl **6-38** in 27%
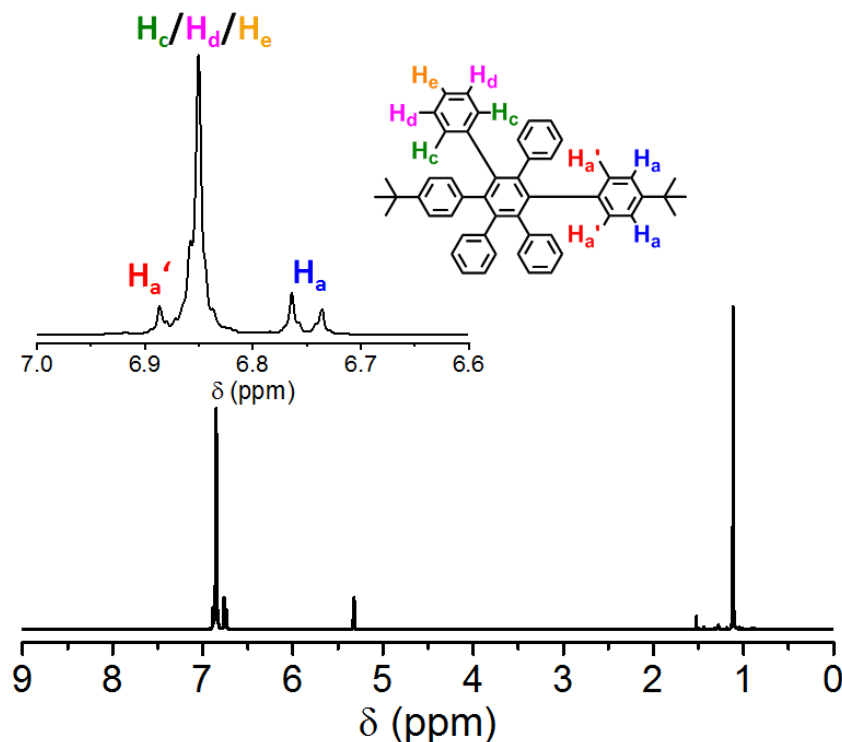
Figure 6-16. ^{1}H NMR spectrum of monomer **6-39** in CD$_2$Cl$_2$ at 25 °C. Inset: Zoom into the aromatic region of **6-39** with proton assignment.

available 1-(*tert*-butyl)-4-iodobenzene afforded the functionalized *p*-terphenyl **6-36** in 27% yield. As a result of an almost equal reactivity of the bromo and iodo functionalities at the applied reaction temperature, the yield of **6-38** was significantly lowered, due to the formation of several byproducts, which were removed by standard column chromatography. Nevertheless, **6-38** was obtained on a several hundred milligram scale. For determination of the optimum reaction conditions, **6-38** was reacted under the previously established *Suzuki-Miyaura* protocol utilizing phenylboronic acid and tetrakis(triphenylphosphine)palladium(0) in the presence of aqueous potassium carbonate and *Aliquat 336*. FD-MS indicated full conversion after one day at 100 °C by a single peak at the expected molecular weight of **6-39** ($m/z = 646.36$). After aqueous workup and column chromatographic separation, **6-39** was obtained in 87% yield. Screening different cross-coupling conditions, however, did not further improve the outcome of the reaction (see Table 6-2).

HPB **6-39** showed a reasonable solubility in organic solvents enabling its characterization by NMR spectroscopy (Figure 6-16). The spectra are in agreement with literature-known HPB derivatives.[84, 85] Besides the singlet at 1.12 ppm originating from the protons of the *tert*-butyl groups, the ^{1}H NMR spectrum showed the expected three sets of sharp aromatic
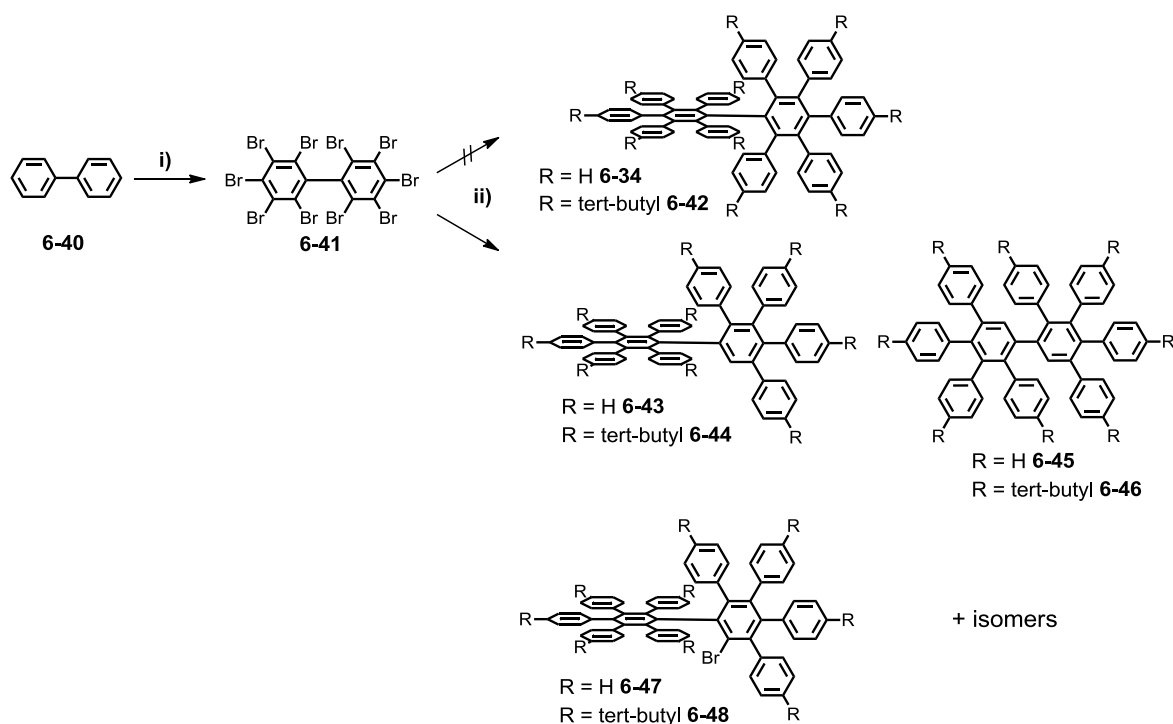
Scheme 6-13. Synthetic route toward 2,2',3,3',4,4',5,5',6,6'-decaphenyl-1,1'-biphenyls **6-34** and **6-42**. Conditions: i) Br$_2$, Fe, 0 to 40 °C, 24h, 91%; ii) phenylboronic acid or (4-(*tert*-butyl)phenyl)boronic acid, Pd(PPh$_3$)$_4$, K$_2$CO$_3$, toluene, H$_2$O, *Aliquat 336*, 100 °C, 96h.

signals with a ratio of 1 to 2.5 to 1 confirming the structure of **6-39**. As a result of the AA'XX' system of two phenyl rings (H$_a$, H$_a$'), two doublets at 6.75 and 6.87 ppm were observed. The latter one overlap with the broad multiplet at 6.85 ppm corresponding to the three protons located at the remaining four phenyl rings (H$_c$, H$_d$, H$_e$).

The discussed model reaction provided reasonable yields so that its applicability was tested for the synthesis of π-extended 2,2',3,3',4,4',5,5',6,6'-decaphenyl-1,1'-biphenyl (**6-34**). In addition, the reaction sequence depicts an alternative route for the straightforward synthesis of unsymmetrically substituted hexa-*peri*-hexabenzocoronenes (HBCs), which are easily accessed *via* the *Scholl* reaction from the obtained HPBs such as **6-39**.[45, 86-89]

With the optimized conditions available, the synthesis of a perhalogenated precursor for the generation of decaphenyl-1,1'-biphenyl (**6-34**) was required (Scheme 6-13). This was accomplished by treatment of 1,1'-biphenyl (**6-40**) with bromine in the presence of catalytic amounts of iron.[31] Quenching the reaction with sodium sulfite afforded perbromo-1,1'-biphenyl (**6-41**) in almost quantitative yields. It was subjected to the *Suzuki-Miyaura* reaction utilizing the established protocol with phenylboronic acid. Monitoring the reaction by thin-layer chromatography and FD-MS revealed fast conversion of the starting materials, however, **6-34** was not detected. Instead, a broad variety of byproducts was found having lower masses than **6-34**. Extended reaction times, higher temperatures as
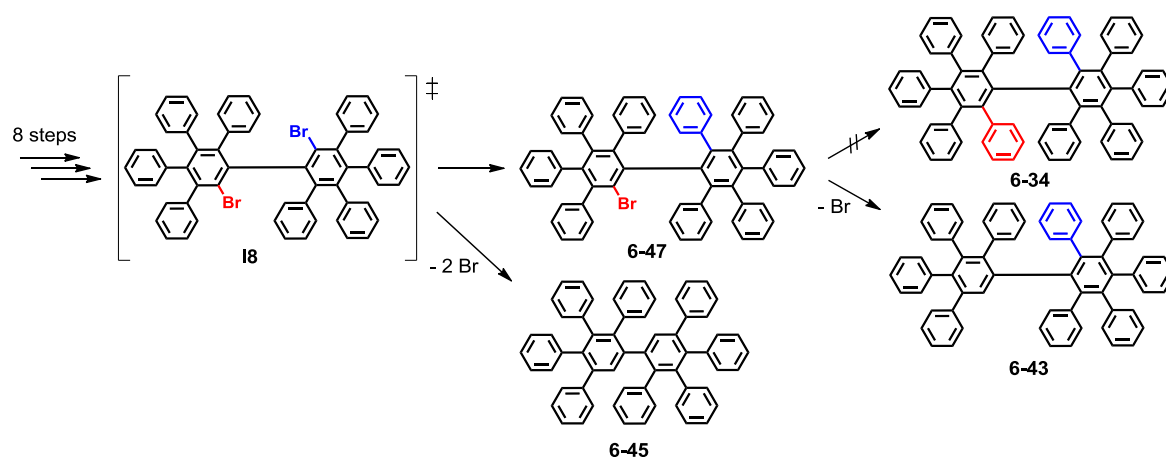
Scheme 6-14. Proposed reaction mechanism during the *Suzuki-Miyaura* reaction toward 2,2',3,3',4,4',5,5',6,6'-decaphenyl-1,1'-biphenyls **6-34**.

well as additional amounts of the Pd^0-source did not facilitate the formation of the desired product. Column chromatographic separation of the reaction mixture allowed for the isolation of two main fractions. Mass spectrometry confirmed an incomplete C−C coupling in combination with partial protodehalogenation giving rise to compounds **6-43**, **6-45** and **6-47**. NMR spectroscopy revealed furthermore the presence of several isomers, thus hampering the isolation of pure samples of **6-43**, **6-45** and **6-47**. Changing the catalytic system to *Buchwald`s* ligand S-Phos in combination with either palladium(II) acetate or tris(dibenzylideneacetone)dipalladium(0) solely increased the amount of protodehalogenation.[39, 42, 43]

To induce crystallinity and to allow for an unambiguous structural assignment, the *Suzuki-Miyaura* reaction utilizing the optimized conditions was repeated with (4-(*tert*-butyl)phenyl)boronic acid (Scheme 6-13). Similarly, the reaction did not result in the formation of the desired product **6-42** rather than a broad variety of byproducts. Unfortunately, neither **6-44**, **6-46** and **6-48** nor its isomers could be isolated by crystallization.

In contrast to the formation of 2,2',6,6'-tetraphenyl-1,1'-biphenyls **6-9** and **6-24** (four C−C coupling steps), the reaction toward decaphenyl-1,1'-biphenyl **6-34** comprises in total ten C−C bond connections which intrinsically lowers its efficiency. Considering a reasonable yield of 85 to 90% for each C−C bond formation, the theoretical limit for the formation of **6-34** will not exceed 20%. In addition, with the progress of the cross-coupling, the steric demand of the intermediate further increases which facilitates the protodehalogenation during the remaining steps (Scheme 6-14). One could speculate that after eight successful C−C bond formations, intermediate **I8** with the bromines in 2,2'-position is formed. This means that the following connection has to occur in a sterically very unfavorable

environment, which decreases the yield of **6-47** and simultaneously increases the chance for protodehalogenation toward **6-45**. However, the steric demand of the final C−C bond formation at **6-47** is even more increased thus preventing the cross-coupling toward **6-34** and decreasing the activation barrier for protodehalogenation (**6-43**).

6.5 Synthetic Approaches toward Cubic Graphite Substructures

Owing to the insufficient formation of π-extended decaphenyl-1,1'-biphenyl derivatives, the work was directed to the expansion of the readily obtained 2,2',6,6'-tetraphenyl-1,1'-biphenyls toward cubic graphic subunits. Thus, cyclooctatetraphenylene (**COT**, Figure 6-16 a), being composed of four 1,2-connected benzene moieties, can be considered as the smallest subunit of the theoretically hitherto unknown carbon allotrope cubic graphite.[90-92] The connection of the *ortho*-positions among the peripheral aryls of 2,2',6,6'-tetraphenyl-1,1'-biphenyl results in the consequent expansion of **COT**, namely bis-cyclooctatetraphenylene (**bis-COT**). This structural motif is composed of two annulated eight-membered rings having a boat conformation (Figure 6-16 b). Both **COT** rings are arranged in a double helical structure. The linear connecting of **bis-COT** units lead to a PPP type structure, mimicking a one-dimensional strand of cubic graphite.
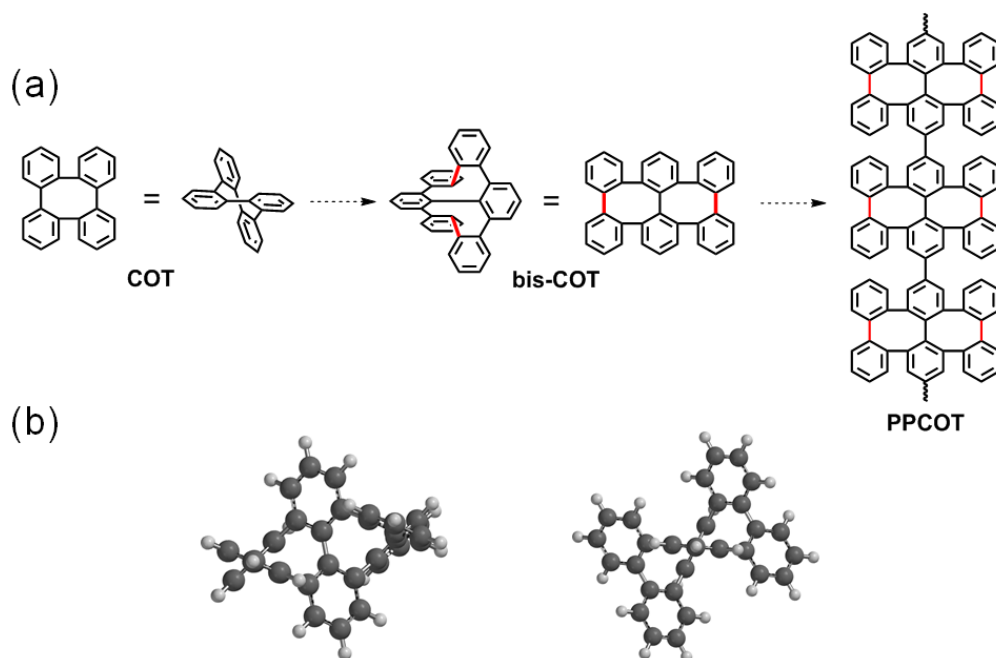
Figure 6-17. (a) Structure of cyclooctatetraphenylene and two views of bis-cyclooctatetraphenylene. The red bonds highlight the positions of the respective bond formation. (b) Two different views of an optimized structure of bis-cyclooctatetraphenylene (**bis-COT**).
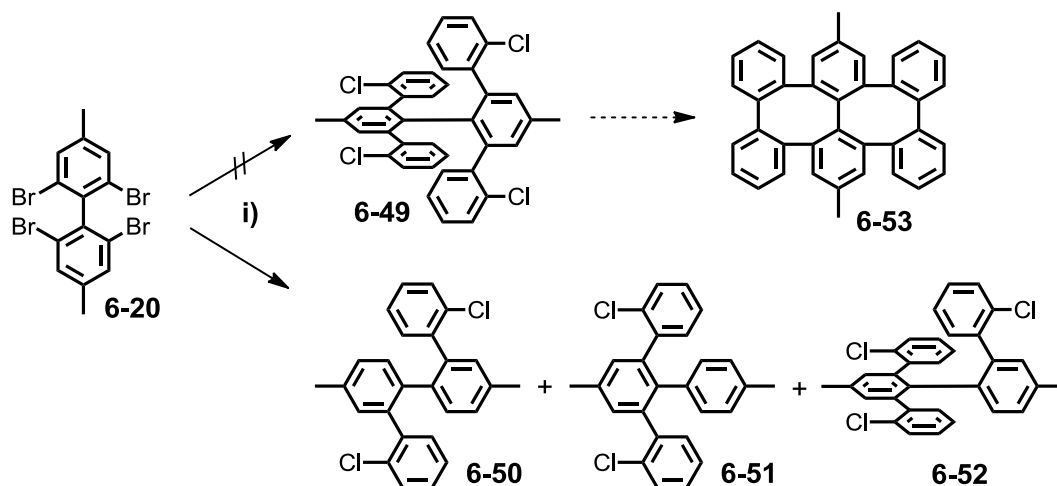
Scheme 6-15. Synthetic route toward **6-49**. Conditions: i) (2-chlorophenyl)boronic acid, Pd(PPh$_3$)$_4$, K$_2$CO$_3$, toluene, *Aliquat 336*, 100 °C, 24h.

In contrast to the widely applied *Scholl* reaction, which generates a new C−C bond between two unfunctionalized aryl vertices toward a new benzene moiety, no such synthetic concept is available for the direct formation of larger ring sizes. Owing to this fact, the introduction of functionalities to the appropriate positions of the aryl is required, which enables the subsequent cyclization *via* cross-coupling techniques. To introduce halogens at the *ortho*-positions of the peripheral aryls of 2,2',6,6'-tetraphenyl-1,1'-biphenyl, previously synthesized **6-20** was subjected to a *Suzuki-Miyaura* reaction with (2-chlorophenyl)boronic acid (Scheme 6-15). Chlorine substituents were chosen due to the fact that they show a weaker reactivity in Pd^0-catalyzed cross-couplings compared to bromine and iodine and hence remain basically unaffected during *Suzuki-Miyaura* reaction. Moreover, the atomic radius of chlorine is smaller in comparison to other halogens or leaving groups, which reduces the additional steric hindrance during the reaction. Nevertheless, chloro-subsituents are prone to subsequent mutual coupling by utilizing, *e.g.*, *Yamamoto* conditions.

The reaction was conducted on the basis of the previous results, utilizing tetrakis(triphenylphosphine)palladium(0) in the presence of solid potassium carbonate and *Aliquat 336* phase transfer catalyst. The progress of the reaction was monitored by FD-MS. After 24 hours at 100 °C, however, no desired product (**6-49**) was detected. Instead, the formation of two (**6-50** and **6-51**) and three (**6-52**) C−C bonds was revealed in combination with protodehalogenation of the residual bromines. Neither standard column chromatography nor preparative SEC or crystallization allowed for the separation of analytically pure samples. This was mainly attributed to similar polarities and almost identical sizes of **6-50**, **6-51** and **6-52**.
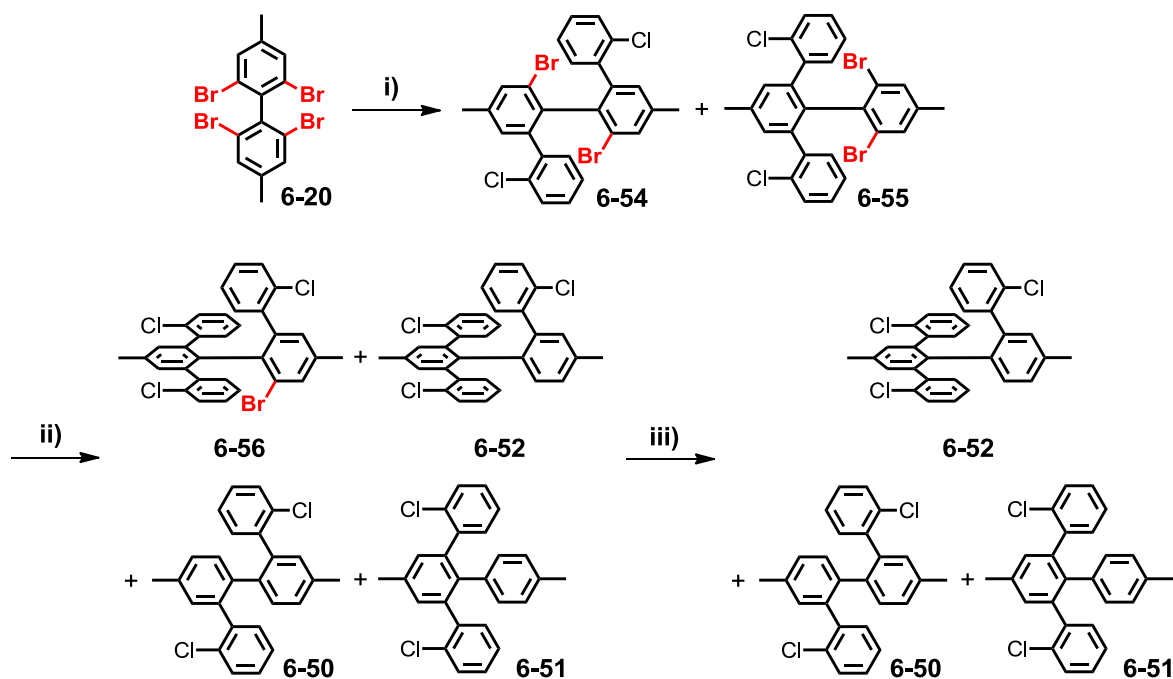
Scheme 6-16. Synthetic route during the kinetically controlled *Suzuki-Miyaura* reaction of **6-20**. For a better visualization the bromines are highlighted in red. Conditions: i) (2-chlorophenyl)boronic acid, Pd(PPh$_3$)$_4$, K$_2$CO$_3$, toluene, *Aliquat 336*, 60 °C, 72h; ii) addition of (2-chlorophenyl)boronic acid and Pd(PPh$_3$)$_4$, 80 °C, 48h; iii) addition of (2-chlorophenyl)boronic acid and Pd(PPh$_3$)$_4$, 90 °C, 48h.

The reaction was repeated at lower temperatures to minimize protodehalogenation and to gain further insights into its mechanism (Scheme 6-16). During the course of 24 hours at 60 °C under the previously used conditions, the sequential formation of 2,2'-diphenyl-6,6'-dibromo-1,1'-biphenyl (**6-54**) was observed, which was most likely accompanied by its isomer 2,6-diphenyl-2,6'-1,1'-biphenyl (**6-55**). Running the reaction for additional 24 hours together with the further addition of (2-chlorophenyl)boronic acid and catalyst did not change the outcome. Increasing the temperature to 80 °C led to the formation of 2,2',6'-triphenyl-6-bromo-1,1'-biphenyl (**6-56**). At this temperature, however, protodehalogenation was already detected (**6-50**, **6-51** and **6-52**) in an equal amount compared to **6-56**. Isolation attempts of **6-56** remained unsuccessful due to the almost identical polarities and sizes of the formed species. Further addition of the boronic acid and the Pd^0-source at 90 °C resulted in complete protodehalogenation toward **6-50**, **6-51** and **6-52** thus impeding the formation of 2,2',6,6'-tetra(2-chlorophenyl)-1,1'-biphenyl **6-49**.

This study clearly showed that by utilizing boronic acids with *ortho*-substituents in combination with sterically demanding substrates, such as 2,2',6,6'-tetrabromo-4,4'-dimethyl-1,1'-biphenyl (**6-20**), the limit of *Suzuki-Miyaura* reactions has apparently been reached.
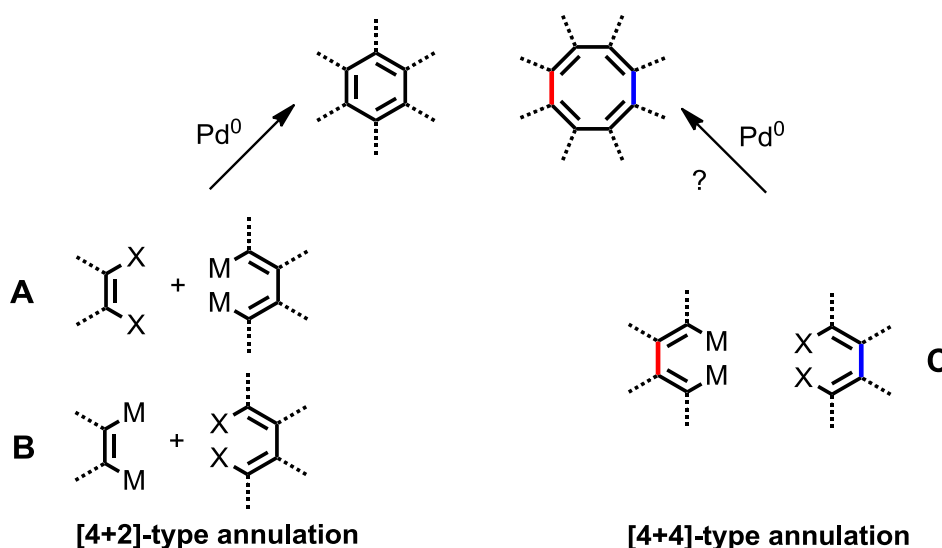
Scheme 6-17. Schematic representation of the [4+2]- and [4+4]-type annulation strategy.[93, 94] The crucial bonds are highlight in red and blue.

To find alternative ways to approach the **bis-COT**, the investigations were focused on a double annulation by a twofold cross-coupling as developed by *Shimizu* and *Hiyama*.[93, 94] This method essentially comprises the Pd[0]-catalyzed twofold cross-coupling of a 1,4-dimetal reagent and a 1,2-dihaloarene (method A, Scheme 6-17) or a 1,2-dimetal reagent with a 2,2'-dihalobiaryl in a [4+2]-type annulation (method B, Scheme 6-17), giving rise to a new benzene moiety. Adapting this approach for a [4+4]-type annulation of a 2,2'-dihalobiaryls with 1,4-dimetal reagents, would theoretically result in the formation of **COT** (method C, Scheme 6-17). This has, however, not been reported so far. With this sequence, the crucial *ortho*-connections (Scheme 6-17, blue and red bonds) are directly introduced during the annulation thus avoiding further bond formations.

In order to test the feasibility of such annulation, the attention was focused on a 9-stannafluorene as a typical 1,4-dimetal analogue, which is readily accessible from the corresponding 2,2'-dihalobiphenyls (Scheme 6-18). Therefore, 2,2'-dibromo-1,1'-biphenyl (**6-57**) was lithiated at -78 °C and quenched with chlorotrimethylstannane which afforded 9-stannafluorene (**6-58**) after recrystallization in 47% yield. Compound **6-58** was subsequently reacted under *Stille*-type annulation conditions with 2,2'-dibromo-1,1'-biphenyl (**6-57**) in the presence of catalytic amounts of highly reactive bis(tri-*tert*-butylphosphine)palladium(0).[93, 94] After running the reaction at 100 °C for two days, however, **COT** has not been detected. As a result of protodehalogenation and protostannylation, 1,1'-biphenyl was observed as the only product. To enhance the cross-coupling, the reaction was repeated in the presence of caesium fluoride. Fluoride additives
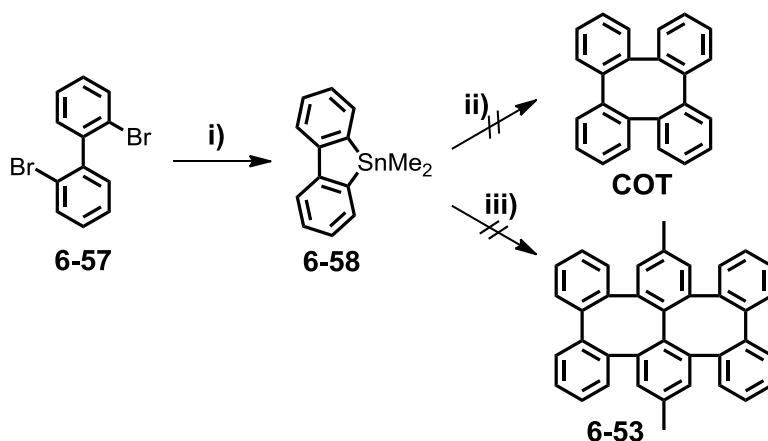
Scheme 6-18. Synthetic route toward **COT** and **6-53**. Conditions: i) *n*-BuLi, Me₃SnCl, THF, -78 °C to RT, 12h, 47%; ii) **6-57**, Pd(P*t*Bu₃)₂, CsF, 60 to 100 °C, 72h; iii) **6-20**, Pd(P*t*Bu₃)₂, CsF, 60 to 100 °C, 72h.

are known to accelerate the transmetallation step of *Stille* reactions by the *in situ* generation of stannates.[51, 94] However, the outcome of the reaction remained unaffected. Nonetheless, 9-stannafluorene (**6-58**) was used for the twofold annulation with 2,2',6,6'-tetrabromo-4,4'-dimethyl-1,1'-biphenyl (**6-20**) by applying *Shimizu* and *Hiyama's* protocol. Besides the previously observed cleavage of the bromines and tin functionalties, no further products were observed, which did not even change upon increasing the temperature and/or utilizing fluoride additives. It might be speculated that these observations were mainly attributed to the different distances between the involved functionalities in the [4+2]-type and the [4+4]-type annulation. *Shimizu* and *Hiyama's* work was either based on a 1,2-dihaloarene or a 1,2-dimetal reagent in which both functionalities were in a comparably close distance (~1.4 Å) thus enabling an efficient cross-coupling. Whereas in the [4+4]-type situation both reaction partners were based on 1,1'-biphenyl derivatives thus increasing the distance between the functionalities in the 2,2'-positions to approximately 3.4 Å. The latter was shown to be unfavorable for the annulation which intrinsically favors protodefunctionalization processes.

6.6 Summary

Synthetic approaches toward the synthesis of 2,2',6,6'-tetraphenyl-1,1'-biphenyls have been presented in this chapter. The synthesis of 4,4'-dimethyl-2,2',6,6'-tetraphenyl-1,1'-biphenyl (**6-9**) was thereby improved by using an efficient three-step protocol comprising the attachment of the peripheral phenyl rings through a four-fold *Suzuki-Miyaura* coupling in the crucial step. In contrast to that, the direct dimerization of preorganized *m*-terphenyl derivatives resulted in migrations and rearrangements of the phenyl moieties.

In this way, the 2,2',6,6'-tetraphenyl-1,1'-biphenyl monomer **6-24** was readily obtained and was subsequently polymerized at the 4,4'-positions, giving rise to π-congested PPP. Preparative SEC allowed for the separation of the polymer into oligomeric fractions which were analyzed by UV-vis absorption and emission spectroscopy. The results were compared with unsubstituted OPPs and PPPs thus revealing pronounced bathochromic shifts in absorption for the π-congested systems despite the large mutual twist of the monomer. Supported by TD-DFT calculations, this could be attributed to significant π-orbital interactions along the *para*phenylene backbone of the π-congested compounds which were accompanied by a through-space conjugation among the π-orbitals of the peripheral aryls. An effective conjugation length is achieved with approximately 16 repeating units resulting in an absorption maximum of 371 nm (3.34 eV). Additionally, the emission of polymer **6-33** was shown to be in the ideal range for pure blue luminescence thus holding promise for future application in OLEDs.

As an extension of the research above, strategies toward cubic graphite substructures have been pursued. The initial approach comprised the extension of the phenyl densitiy in 2,2',6,6'-tetraphenyl-1,1'-biphenyl. By doing this, an alternative synthesis toward unsymmetric HPBs and its associated HBCs was developed which was, however, not applicable for the formation of targeted decaphenyl-1,1'-biphenyl **6-34**.

Moreover, different methods have been tested for the formation of bis-cyclooctatetraphenylene (**bis-COT**) being an expansion of cyclooctatetraphenylene (**COT**) on the way to subunits of cubic graphite. Although neither the desired **bis-COT** nor its precursors could be obtained *via* sterically demanding cross-coupling approaches, the results highlight the strengths and the weaknesses of the developed methodology at the same time. While 2,2',6,6'-tetraphenyl-1,1'-biphenyls **6-9** and **6-24** were obtained in reasonable yields by reducing the steric hindrance of one reaction partner, the fourfold reaction with an *ortho*-substituted derivative, such as (2-chlorophenyl)boronic acid, severely suffered from incompletion and protodehalogenation. Summarizing these aspects, Pd^0-catalyzed cross-coupling procedures work most efficiently, if one reaction partner is sterically unhindered. However, if both reactants bear sterically demanding substituents, the reaction is strongly retarded and accompanied by undesired side reactions.

6.7 References

[1]   C. S. Marvel, G. E. Hartzell, *J. Am. Chem. Soc.* **1959**, *81*, 448-452.

[2]   S. B. Mainthia, P. L. Kronick, M. M. Labes, *J. Chem. Phys.* **1962**, *37*, 2509-2510.

[3]   M. Akiyama, Y. Iwakura, Shiraish.S, Y. Imai, *J. Polym. Sci., Part B: Polym. Lett.* **1966**, *4*, 305-308.

[4]   P. Kovacic, Marchion.Vj, F. W. Koch, J. Oziomek, *J. Org. Chem.* **1966**, *31*, 2467-2470.

[5]   M. Rehahn, A. D. Schlüter, G. Wegner, W. J. Feast, *Polymer* **1989**, *30*, 1060-1062.

[6]   M. Rehahn, A. D. Schlüter, G. Wegner, W. J. Feast, *Polymer* **1989**, *30*, 1054-1059.

[7]   M. Rehahn, A. D. Schlüter, G. Wegner, *Macromol. Chem. Phys.* **1990**, *191*, 1991-2003.

[8]   U. Scherf, K. Müllen, *Makromol. Chem., Rapid Commun.* **1991**, *12*, 489-497.

[9]   U. Scherf, K. Müllen, *Polymer* **1992**, *33*, 2443-2446.

[10]   U. Scherf, K. Müllen, *Synthesis* **1992**, 23-38.

[11]   M. B. Goldfinger, T. M. Swager, *J. Am. Chem. Soc.* **1994**, *116*, 7895-7896.

[12]   A. C. Grimsdale, K. Müllen, *Adv. Polym. Sci.* **2006**, *199*, 1-82.

[13]   K. Müllen, U. Scherf, *Organic Light Emitting Devices: Synthesis, Properties and Applications*, John Wiley & Sons, Weinheim, **2006**.

[14]   C. Li, M. Y. Liu, N. G. Pschirer, M. Baumgarten, K. Müllen, *Chem. Rev.* **2010**, *110*, 6817-6855.

[15]   A. Kraft, A. C. Grimsdale, A. B. Holmes, *Angew. Chem., Int. Ed.* **1998**, *37*, 402-428.

[16]   U. Mitschke, P. Bäuerle, *J. Mater. Chem.* **2000**, *10*, 1471-1507.

[17]   A. C. Grimsdale, K. Müllen, *Adv. Polym. Sci.* **2008**, *212*, 1-48.

[18]   B. Schmaltz, T. Weil, K. Müllen, *Adv. Mater.* **2009**, *21*, 1067-1078.

[19]   A. D. Schlüter, G. Wegner, *Acta Polym.* **1993**, *44*, 59-69.

[20]   K. C. Park, L. R. Dodd, K. Levon, T. K. Kwei, *Macromolecules* **1996**, *29*, 7149-7154.

[21]   J. Gibson, M. Holohan, H. L. Riley, *J. Chem. Soc.* **1946**, 456-461.

[22]   D. Wasserfallen, G. Mattersteig, V. Enkelmann, K. Müllen, *Tetrahedron* **2006**, *62*, 5417-5420.

[23]   D. Türp, T. T. T. Nguyen, M. Baumgarten, K. Müllen, *New J. Chem.* **2012**, *36*, 282-298.

[24]   X. F. Shen, D. M. Ho, R. A. Pascal, *Org. Lett.* **2003**, *5*, 369-371.

[25]   S. Ozasa, Y. Fujioka, J. Kikutake, E. Ibuki, *Chem. Pharm. Bull.* **1983**, *31*, 1572-1581.

[26]   Y. Fujioka, S. Ozasa, K. Sato, E. Ibuki, *Chem. Pharm. Bull.* **1985**, *33*, 22-29.

[27]   L. Tong, H. Lau, D. M. Ho, R. A. Pascal, *J. Am. Chem. Soc.* **1998**, *120*, 6000-6006.

[28]   R. A. Pascal, N. Hayashi, D. M. Ho, *Tetrahedron* **2001**, *57*, 3549-3555.

[29]   J. Lu, D. M. Ho, N. J. Vogelaar, C. M. Kraml, R. A. Pascal, *J. Am. Chem. Soc.* **2004**, *126*, 11168-11169.

[30]   X. F. Shen, D. M. Ho, R. A. Pascal, *J. Am. Chem. Soc.* **2004**, *126*, 5798-5805.

[31]   C. L. Hilton, J. M. Crowfoot, P. Rempala, B. T. King, *J. Am. Chem. Soc.* **2008**, *130*, 13392-13399.

[32]   F. Ullmann, *Chem. Ber.* **1903**, *36*, 2382-2384.

[33]   T. Yamamoto, T. Kohara, A. Yamamoto, *Bull. Chem. Soc. Jpn.* **1981**, *54*, 1720-1726.

[34]   T. Kanbara, N. Saito, T. Yamamoto, K. Kubota, *Macromolecules* **1991**, *24*, 5883-5885.

[35]   Z. H. Zhou, T. Yamamoto, *J. Organomet. Chem.* **1991**, *414*, 119-127.

[36]   T. Yamamoto, *Prog. Polym. Sci.* **1992**, *17*, 1153-1205.

[37]   N. Miyaura, A. Suzuki, *Chem. Rev.* **1995**, *95*, 2457-2483.

[38]   H. Chaumeil, S. Signorella, C. Le Drian, *Tetrahedron* **2000**, *56*, 9655-9662.

[39]   J. J. Yin, M. P. Rainka, X. X. Zhang, S. L. Buchwald, *J. Am. Chem. Soc.* **2002**, *124*, 1162-1163.

[40]   G. Altenhoff, R. Goddard, C. W. Lehmann, F. Glorius, *Angew. Chem., Int. Ed.* **2003**, *42*, 3690-3693.

[41]   G. Altenhoff, R. Goddard, C. W. Lehmann, F. Glorius, *J. Am. Chem. Soc.* **2004**, *126*, 15195-15201.

[42]   S. D. Walker, T. E. Barder, J. R. Martinelli, S. L. Buchwald, *Angew. Chem., Int. Ed.* **2004**, *43*, 1871-1876.

[43]   T. E. Barder, S. D. Walker, J. R. Martinelli, S. L. Buchwald, *J. Am. Chem. Soc.* **2005**, *127*, 4685-4696.

[44]   K. L. Billingsley, T. E. Barder, S. L. Buchwald, *Angew. Chem., Int. Ed.* **2007**, *46*, 5359-5363.

[45]   X. Y. Yang, X. Dou, K. Müllen, *Chem. Asian J.* **2008**, *3*, 759-766.

[46]   M. G. Organ, S. Calimsiz, M. Sayah, K. H. Hoi, A. J. Lough, *Angew. Chem., Int. Ed.* **2009**, *48*, 2383-2387.

[47]   T. Kinzel, Y. Zhang, S. L. Buchwald, *J. Am. Chem. Soc.* **2010**, *132*, 14073-14075.

[48]   A. Suzuki, *Angew. Chem., Int. Ed.* **2011**, *50*, 6722-6737.

[49]   D. Milstein, J. K. Stille, *J. Am. Chem. Soc.* **1978**, *100*, 3636-3638.

[50]   J. K. Stille, *Angew. Chem., Int. Ed.* **1986**, *25*, 508-523.

[51]   P. Espinet, A. M. Echavarren, *Angew. Chem., Int. Ed.* **2004**, *43*, 4704-4734.

[52]   N. Yoshikai, H. Matsuda, E. Nakamura, *J. Am. Chem. Soc.* **2008**, *130*, 15258-15259.

[53]   H. Komber, V. Senkovskyy, R. Tkachov, K. Johnson, A. Kiriy, W. T. S. Huck, M. Sommer, *Macromolecules* **2011**, *44*, 9164-9172.

[54]   K. Tamao, K. Sumitani, M. Kumada, *J. Am. Chem. Soc.* **1972**, *94*, 4374-4376.

[55]   J. P. Corriu, J. P. Masse, *J. Chem. Soc., Chem. Commun.* **1972**, 144-&.

[56]   T. Ishiyama, M. Murata, N. Miyaura, *J. Org. Chem.* **1995**, *60*, 7508-7510.

[57]   J. K. Stille, K. S. Y. Lau, *Acc. Chem. Res.* **1977**, *10*, 434-442.

[58]   G. B. Smith, G. C. Dezeny, D. L. Hughes, A. O. King, T. R. Verhoeven, *J. Org. Chem.* **1994**, *59*, 8151-8156.

[59]   A. L. Casado, P. Espinet, *Organometallics* **1998**, *17*, 954-959.

[60]   D. Rodriguez-Lojo, D. Perez, D. Pena, E. Guitian, *Chem. Commun.* **2013**, *49*, 6274-6276.

[61]   B. H. Ridgway, K. A. Wörpel, *J. Org. Chem.* **1998**, *63*, 458-460.

[62]   M. Shimizu, H. Tatsumi, K. Mochida, K. Oda, T. Hiyama, *Chem. Asian J.* **2008**, *3*, 1238-1247.

[63]   C. J. Brown, A. C. Farthing, *Nature* **1949**, *164*, 915-916.

[64]   D. J. A. De Ridder, K. Goubitz, M. Fontijn, P. Capkova, E. Dova, H. Schenk, *Acta Crystallogr. B* **2001**, *57*, 780-790.

[65]   M. J. Frisch, G. W. Trucks, H. B. Schlegel, G. E. Scuseria, M. A. Robb, J. R. Cheeseman, J. Montgomery, J. A., T. Vreven, K. N. Kudin, J. C. Burant, J. M. Millam, S. S. Iyengar, J. Tomasi, V. Barone, B. Mennucci, M. Cossi, G. Scalmani, N. Rega, G. A. Petersson, H. Nakatsuji, M. Hada, M. Ehara, K. Toyota, R. Fukuda, J. Hasegawa, M. Ishida, T. Nakajima, Y. Honda, O. Kitao, H. Nakai, M. Klene, X. Li, J. E. Knox, H. P. Hratchian, J. B. Cross, V. Bakken, C. Adamo, J. Jaramillo, R. Gomperts, R. E. Stratmann, O. Yazyev, A. J. Austin, R. Cammi, C. Pomelli, J. W. Ochterski, P. Y. Ayala, K. Morokuma, G. A. Voth, P. Salvador, J. J. Dannenberg, V. G. Zakrzewski, S. Dapprich, A. D. Daniels, M. C. Strain, O. Farkas, D. K. Malick, A. D. Rabuck, K. Raghavachari, J. B. Foresman, J. V. Ortiz, Q. Cui, A. G. Baboul, S. Clifford, J. Cioslowski, B. B. Stefanov, G. Liu, A. Liashenko, P. Piskorz, I. Komaromi, R. L. Martin, D. J. Fox, T. Keith, M. A. Al-Laham, C. Y. Peng, A. Nanayakkara, M. Challacombe, P. M. W. Gill, B. Johnson, W. Chen, M. W. Wong, C. Gonzalez, J. A. Pople, *Gaussian 03, Revision C.02*, Gaussian, Inc., Wallingford CT, **2004.**

[66]   M. G. Schwab, Ph.D. thesis, Johannes Gutenberg-University Mainz **2011**.

[67]   M. Baumgarten, T. Yüksel, *Phys. Chem. Chem. Phys.* **1999**, *1*, 1699-1706.

[68]   D. Vak, B. Lim, S. H. Lee, D. Y. Kim, *Org. Lett.* **2005**, *7*, 4229-4232.

[69]   J. Grimme, M. Kreyenschmidt, F. Uckert, K. Müllen, U. Scherf, *Adv. Mater.* **1995**, *7*, 292-295.

[70]   J. F. Jia, H. S. Wu, Z. H. Chen, Y. R. Mo, *Eur. J. Org. Chem.* **2013**, 611-616.

[71]   S. Menning, M. Kramer, B. A. Coombs, F. Rominger, A. Beeby, A. Dreuw, U. H. F. Bunz, *J. Am. Chem. Soc.* **2013**, *135*, 2160-2163.

[72]   R. Rathore, S. H. Abdelwahed, I. A. Guzei, *J. Am. Chem. Soc.* **2003**, *125*, 8712-8713.

[73]   Y. Morisaki, S. Ueno, A. Saeki, A. Asano, S. Seki, Y. Chujo, *Chem. Eur. J.* **2012**, *18*, 4216-4224.

[74]   H. L. Qi, J. H. Chang, S. H. Abdelwahed, K. Thakur, R. Rathore, A. J. Bard, *J. Am. Chem. Soc.* **2012**, *134*, 16265-16274.

[75]   J. L. Bredas, R. Silbey, D. S. Boudreaux, R. R. Chance, *J. Am. Chem. Soc.* **1983**, *105*, 6555-6559.

[76]   M. D. Watson, A. Fechtenkötter, K. Müllen, *Chem. Rev.* **2001**, *101*, 1267-1300.

[77]   H.-H. Hörhold, M. Helbig, D. Raabe, J. Opfermann, U. Scherf, R. Stockmann, D. Weiß, *Z. Chem.* **1987**, *27*, 126-137.

[78]   H. Meier, U. Stalmach, H. Kolshorn, *Acta Polym.* **1997**, *48*, 379-384.

[79]   U. Stalmach, H. Kolshorn, I. Brehm, H. Meier, *Liebigs Ann.* **1996**, 1449-1456.

[80]   L. M. Tolbert, *Acc. Chem. Res.* **1992**, *25*, 561-568.

[81]   J. Rissler, *Chem. Phys. Lett.* **2004**, *395*, 92-96.

[82]   A. E. Gillam, D. H. Hey, *J. Chem. Soc.* **1939**, 1170-1177.

[83]   M. Standera, R. Hafliger, R. Gershoni-Poranne, A. Stanger, G. Jeschke, J. D. van Beek, L. Bertschi, A. D. Schlüter, *Chem. Eur. J.* **2011**, *17*, 12163-12174.

[84]   X. L. Feng, J. S. Wu, M. Ai, W. Pisula, L. J. Zhi, J. P. Rabe, K. Müllen, *Angew. Chem., Int. Ed.* **2007**, *46*, 3033-3036.

[85]   L. Y. Zhai, R. Shukla, R. Rathore, *Org. Lett.* **2009**, *11*, 3474-3477.

[86]   R. Scholl, C. Seer, R. Weitzenbock, *Ber. Dtsch. Chem. Ges.* **1910**, *43*, 2202-2209.

[87]   R. Scholl, C. Seer, *Ber. Dtsch. Chem. Ges.* **1911**, *44*, 1233-1240.

[88]   R. Scholl, C. Seer, *Liebigs Ann. Chem.* **1912**, *394*, 111-177.

[89]   B. T. King, J. Kroulik, C. R. Robertson, P. Rempala, C. L. Hilton, J. D. Korinek, L. M. Gortari, *J. Org. Chem.* **2007**, *72*, 2279-2288.

[90]   A. Rajca, A. Safronov, S. Rajca, R. Shoemaker, *Angew. Chem., Int. Ed.* **1997**, *36*, 488-491.

[91]   A. Rajca, H. Wang, P. Bolshov, S. Rajca, *Tetrahedron* **2001**, *57*, 3725-3735.

[92]   S. M. H. Kabir, M. Hasegawa, Y. Kuwatani, M. Yoshida, H. Matsuyama, M. Iyoda, *J. Chem. Soc., Perkin Trans. 1* **2001**, 159-165.

[93]   M. Shimizu, I. Nagao, Y. Tomioka, T. Hiyama, *Angew. Chem., Int. Ed.* **2008**, *47*, 8096-8099.

[94]   I. Nagao, M. Shimizu, T. Hiyama, *Angew. Chem., Int. Ed.* **2009**, *48*, 7573-7576.

7 Tetrafunctionalized Biphenylenes – Molecular Precursors for the Synthesis of Isomeric Graphene Nanostructures

7.1 Introduction

While the transition between one-dimensional PPP and the three-dimensional carbon allotrope cubic graphite was described in the previous chapter, the final part of this work is devoted to a new type of two-dimensional benzene-based materials. The three hybridization states of carbon (sp^3, sp^2 and sp) allow for numerous combinations for the C−C bond connection which result in several carbon allotropes, such as naturally occurring diamond (sp^3) and graphite (sp^2), as well as various carbon allotropes with different dimensionalties comprising fullerenes (sp^2, 0D),[1] carbon nanotubes (sp^2, 1D),[2] graphene (sp^2, 2D),[3, 4] and the previously discussed cubic graphite (sp^2, 3D).[5-10] The search for novel carbon allotropes and carbon-rich materials has always been associated with the development of unusual structural, electronic and optical properties.[11-17] Among all these materials, the family of sp^2-carbon allotropes, including fullerenes, carbon nanotubes and graphene has sparked considerable attention, due to their remarkable properties and potential applications in many fields of technology. However, all of them are composed of benzene moieties.[18] By considering naphthalene, a $C_{10}H_8$ isomer with two benzenes sharing one edge, and azulene, a $C_{10}H_8$ isomer where a seven- and a five-membered ring share one edge, the impact of isomerization becomes visible. Naphtalene is colorless, whereas azulene is deep blue. Shifting one bond by one position completely alters the electronic properties.[19] A scientifically relevant question therefore is, whether sp^2-connected carbons allows for the construction of alternative networks with a structural motif different from that of graphene. In line with this, biphenylene (**I7-1**, Figure 7-1) can be anticipated as a structural unit of new carbon allotropes such as doubly stranded polymer **I7-3** or graphenylene **I7-5**.[20-25] The latter one, for example is predicted to be a semiconductor with an intrinsic bandgap, in contrast to the semi-metal graphene (*i.e.* zero bandgap) which hampers its potential application in optoelectronic devices such as FETs. In addition, its periodically distributed pores of about 3.2 Å in diameter may render graphenylene (**I7-5**) as a potential two-dimensional sieve for gas separation.[18] Biphenylene itself combines the aromatic and antiaromatic motifs of benzene and
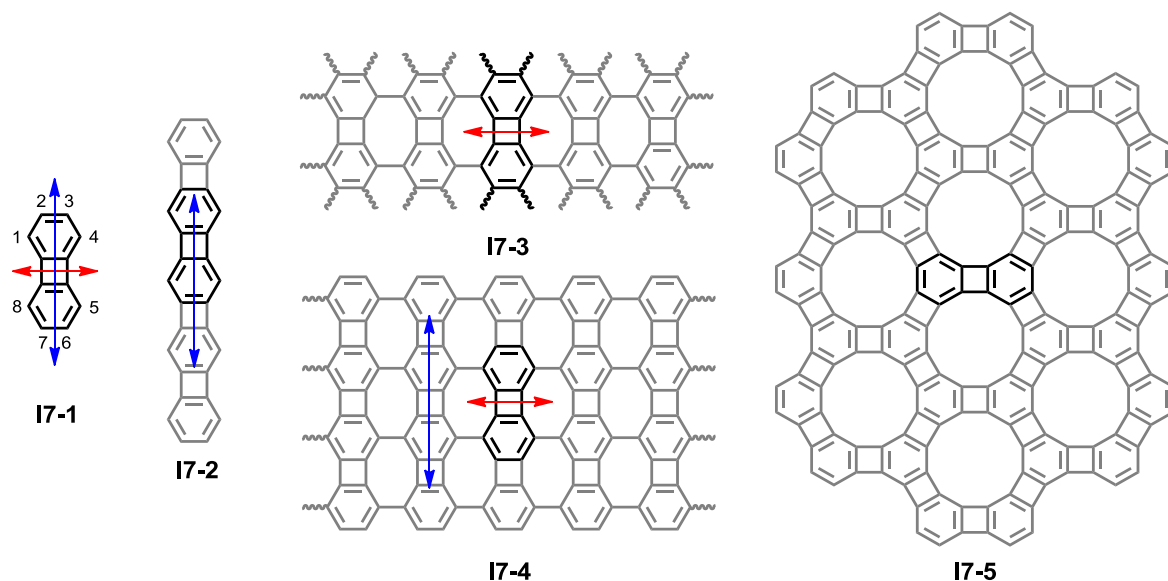
Figure 7-1. Chemical structure of [5]phenylene **I7-2**, isomeric GNRs **I7-3** and **I7-4** and a section of graphenylene **I7-5** based on biphenylene **I7-1** as structural motif. The arrows indicate the direction of the expansion: along the 1,4,5,8-positions ("East-West", red) and the 2,3,6,7-positions ("North-South", blue).

cyclobutadiene in a single structure, which makes it intriguing from the viewpoint of aromaticity. Many synthetic efforts have thus been made toward selective functionalization of **I7-1** to enable its utilization as a building block for new carbon allotropes. Pioneering work of *Vollhardt* based on a [2+2+2]-cyclotrimerization of suitably functionalized alkynes allowed, for example, for the functionalization of the 2,3,6,7-positions of **I7-1** to provide access to further expansions such as the [N]phenylenes series, with N = 3, 4 and 5 (**I7-2**).[26-32] *Vollhardt`s* approach allowed for the expansion of biphenylene along the so-called "North-South" direction (Figure 7-1, blue arrow). The controlled functionalization of the 1,4,5,8-positions of **I7-1** remained, however, elusive and hence, apart from a dimer, the synthesis of "East-West" connected biphenylene oligomers has not been reported to date (Figure 7-1, red arrow).[22] To further extend the biphenylene motif, a synthetic method was required which allows a straightforward functionalization of the 1,4,5,8-positions of **I7-1** for an "East-West" expansion (**I7-3**) and, in the best scenario, a subsequent extension along its "North-South" direction giving rise to constitutional isomers of graphene nanoribbons (GNRs), such as **I7-3** or **I7-4**.

7.2 Synthesis of 1,4,5,8-Tetrahalobiphenylene

A broad variety of synthetic methods have been used to connect benzenes *via* a four-membered ring toward biphenylene structures. These synthetic protocols include dimerization of benzyne,[33] the *Ullmann* coupling of 2,2'-dihalobiphenyl,[34, 35] *Vollhardt`s* method utilizing $Co^0$-catalyzed cyclizations,[26-28, 36, 37] and *Iyoda`s* Cu^{II}-catalyzed oxidative coupling of highly air-sensitive organozinc precursors.[23-25] These synthetic approaches were, however, limited to the generation of 2,3,6,7- or 1,8-functionalized biphenylenes.[22] To gain access to the 1,4,5,8-positions a different methodology is necessary and was therefore the subject of the following investigations.
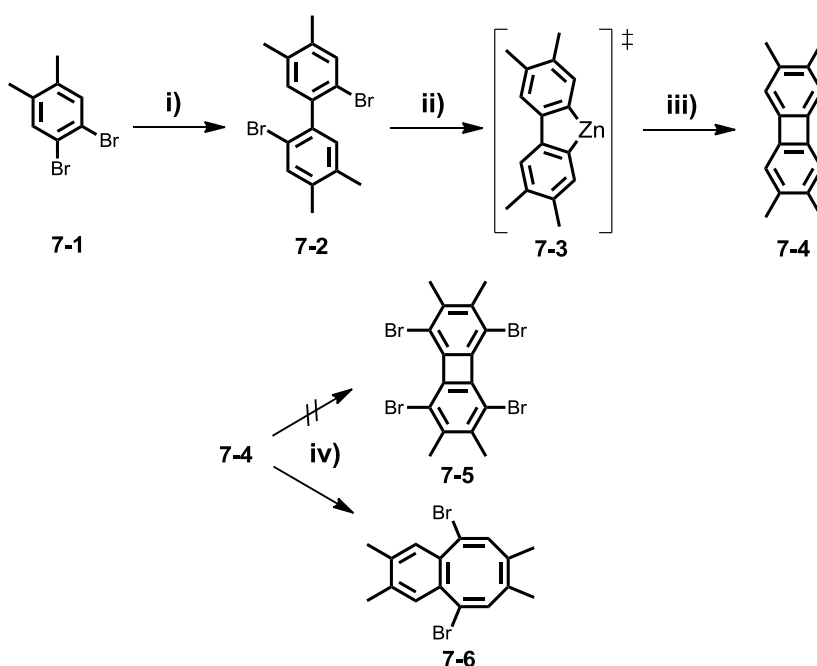
Scheme 7-1. Synthetic route toward 1,4,5,8-tetrabromobiphenylene **7-5**. Conditions: i) 0.5 equiv. *n*-BuLi, THF, -78 °C to RT, 3h, 76%; ii) *n*BuLi, $ZnCl_2$, THF, -78 °C to -50 °C, 2h; iii) $CuCl_2$, THF, -78 C to RT, 14h, 16%; iv) Br_2, pyridine, $CHCl_3$, RT, 12h.

The introduction of halogens at the 1,4,5,8-positions was initially attempted by a classical electrophilic aromatic substitution involving the synthesis of 2,3,6,7-tetramethylbiphenylene (**7-4**) by adapting the literature-known procedure from *Iyoda* and coworkers (Scheme 7-1).[23-25] Thus, commercially available 1,2-dibromo-4,5- dimethyl-benzene (**7-1**) was dimerized using 0.5 equivalents of *n*-butyllithium, yielding 2,2'-dibromo-4,4',5,5'-tetramethyl-1,1'-biphenyl (**7-2**) in 76%. The reaction of **7-2** with *n*-butyllithium produced the 2,2'-dilithiobiphenyl which was subsequently treated with anhydrous zinc(II) chloride, providing *in situ* the arylzinc species **7-3**. This was followed
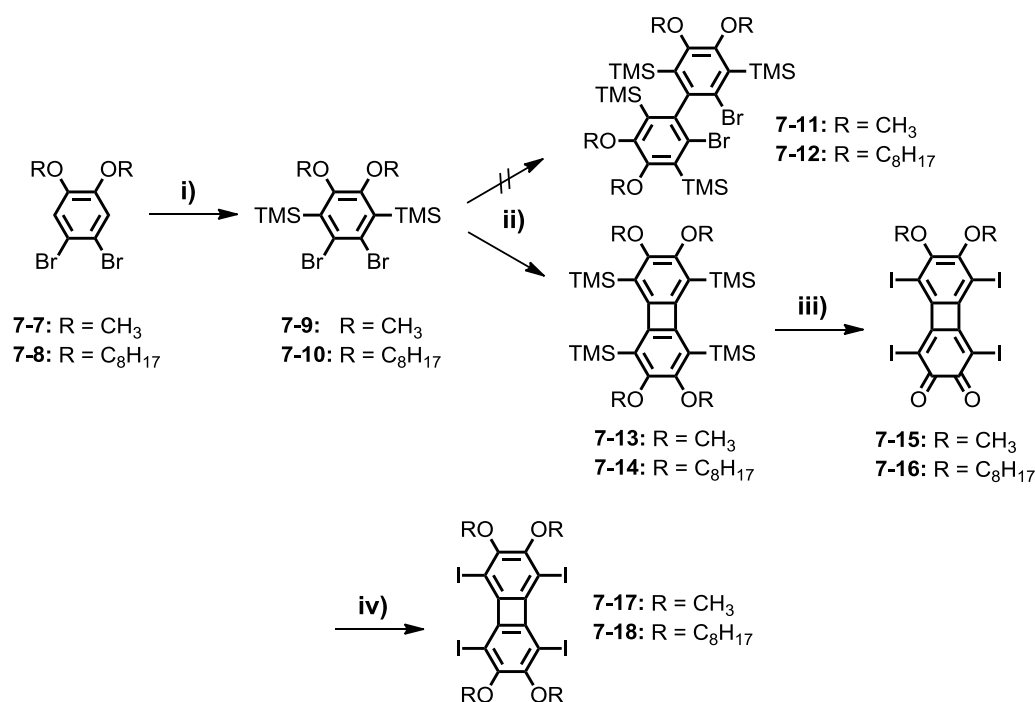
Scheme 7-2. Synthetic route toward 1,4,5,8-tetraiodo-2,3,6,7-tetraalkoxybiphenylenes **7-17** and **7-18**. Conditions: i) LDA, Me₃SiCl, THF, -78 °C to RT, 12h, **7-9**: 90%, **7-10**: quantitative; ii) 1 equiv. *n*-BuLi, THF, -78 °C to RT, 12h, **7-13**: 17%, **7-14**: 10%; iii) 1 M ICl, CH₂Cl₂, -78 °C to RT, 24h, **7-15**: 92%, **7-16**: 91%, iv) Na₂S₂O₄, Me₂SO₄ or C₈H₁₇Br, Bu₄NBr, H₂O/THF, 40 °C or 100 °C, 24h, **7-17**: 97%, **7-18**: 20%.

by treatment with copper(II) chloride producing 2,3,6,7-tetramethylbiphenylene **7-4** in 16% yield. As a result of partial protodehalogenation and the formation of a COT derivative, the yield of the reaction was comparably low. The bromination was conducted in a standard protocol by treating **7-4** with bromine in chloroform and in the presence of pyridine as scavenger for the evolving hydrobromic acid.[38] Although **7-4** was completely consumed after 12 hours, neither the formation of 1,4,5,8-tetrabromo-2,3,6,7-tetramethylbiphenylene (**7-5**) nor its less brominated counterparts were detected. Instead, the opening of the central cyclobutadiene ring was observed giving rise to 5,10-dibromo-2,3,7,8-tetramethylbenzocyclooctene (**7-6**), which can be explained by an addition of the bromine rather than an electrophilic substitution. This observation was attributed to the partial antiaromatic character of the central cyclobutadiene ring which intrinsically impeded the electrophilic substitution at the 1,4,5,8-positions of **7-4**.[39, 40] The aromaticity or the antiaromaticity of benzene-rich materials is thereby expressed by their nucleus-independent chemical shift (NICS) values which provides the chemical shift of a point nucleus at any given position in a molecule (NICS(1) indicates the NICS value 1 Å above the ring center).[41] Negative NICS values denote an aromatic ring (NICS(0)$_{benzene}$ = −12.5 ppm) whereas positive values indicate an antiaromatic contribution (NICS(0)$_{cyclobutadiene}$ = 15.1 ppm). The reported NICS(0) values for biphenylene are

−8.0 ppm and 7.0 ppm for the six- and four-membered rings, respectively, thus showing the antiaromatic nature of biphenylene`s central four-membered ring.[41]

Since the post-halogenation of **7-4** by electrophilic substitution was not feasible, the synthetic strategy was modified. From a retro-synthetic point of view, this problem can potentially be solved by introducing the functionalities prior to the formation of the biphenylene core which can be achieved by using protecting groups such as trimethylsilyl. Among other possibilities, trimethylsilyl groups can be introduced at alkoxydibromobenzenes *via* a straightforward deprotonation-silylation sequence. It is known that the positions between an alkoxy- and a bromo-substituent can be readily deprotonated by lithium di-*iso*-propylamide (LDA) due to their cooperative *ortho*-directing and acidifying effects.[42, 43] This procedure was adapted for the functionalization of 1,2-dibromo-4,5-dimethoxybenzene (**7-7**, Scheme 7-2). For this purpose, **7-7** was treated with LDA in the presence of chlorotrimethylsilane at -78 °C. The reaction proceeded smoothly without the undesired protodehalogenation which resulted in (2,3-dibromo-5,6-dimethoxy-1,4-phenylene)bis(trimethylsilane) (**7-9**) in excellent yields after recrystallization. By utilizing 1,2-dibromo-4,5-bis(octyloxy)benzene (**7-8**),[44] **7-10** was obtained in quantitative yield thus proving the versatility of this method toward alkyl chains of different lengths.

Treatment of **7-9** with 0.5 equivalents *n*-butyllithium was expected to result in dimerization toward **7-11** referring to *Iyoda`s* protocol.[23-25] Instead, the formation of biphenylene **7-13** was observed. This suggests the involvement of an aryne intermediate during the reaction undergoing a [2+2]-cyclodimerization to afford **7-13** (Scheme 7-3 a). It is therefore reasonable to assume that the lithiation of **7-9** at -78 °C led to intermediate **I1** which forms instantaneously an aryne species **I2** after cleavage of the remaining bromine. The resulting aryne **I2** can subsequently undergo a [2+2]-cycloaddition with a second molecule giving rise to biphenylene **7-13**.[45-48] Besides that, protodehalogenation toward **7-19** was detected as a side reaction which decreased the yield of the biphenylene.

To study the effect of the trimethylsilyl groups, 1,2-dibromo-4,5-dimethoxybenzene (**7-7**) was treated in a model reaction under identical conditions (Scheme 7-3 b). In contrast to the lithiation of **7-9**, this resulted in 1,2-dimethoxybenzene (**7-22**) in virtually quantitative yields. The crucial influence of the trimethylsilyl groups for the [2+2]-cycloaddition was thereby revealed. It is very likely that π-backbonding from the aryne to the d-orbitals of the adjacent silicon atoms increases the lifetime of **I2** significantly and hence allows for the [2+2]-cycloaddition as reasonable reaction pathway. By using **7-7**, however, the π-backbonding is not available and therefore solely protodehalogenation occurs.

(a)
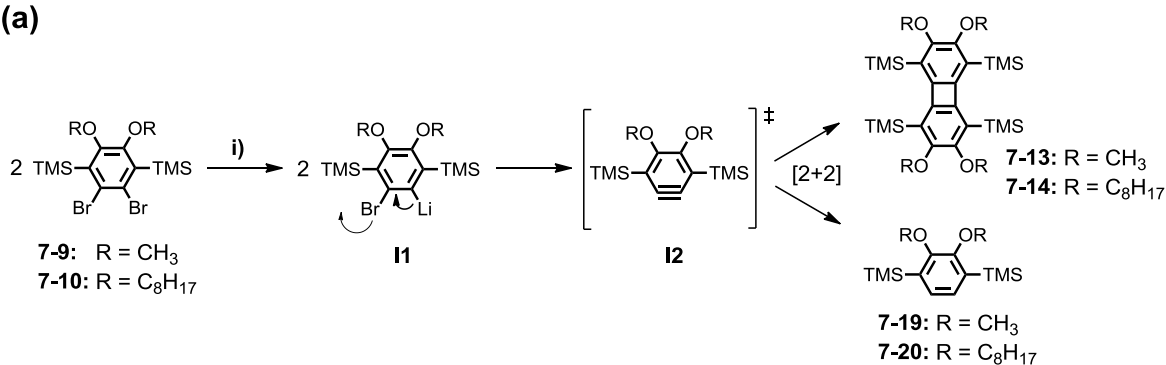
(b)
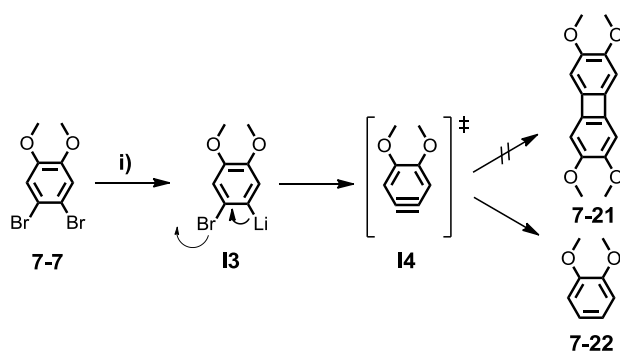
Scheme 7-3. (a) Proposed reaction mechanism of the formation of biphenylenes **7-13** and **7-14**. (b) Model reaction for the base induced dimerization of **7-7**. Conditions: i) 1 equiv. *n*-BuLi, THF, -78 °C to RT, 12h, **7-22**: 92%.

Repeating the reaction with the *n*-octyl-substituted precursor **7-10** led to the formation of biphenylene **7-14** in similar yields. Increasing the amount of *n*-butyllithium did not affect the outcome of the reaction. Although the yields of the [2+2]-dimerization were comparably low, **7-13** and **7-14** could be obtained on a gram scale due to the easy accessibility of their precursors and the prevention of a multistep procedure. Subsequent to the biphenylene synthesis, trimethylsilyl-iodine exchange was targeted. Therefore, **7-13** was treated with a 1 M solution of iodine monochloride in dichloromethane. To favor the deprotective iodination and to suppress the addition of iodine to the four-membered ring of **7-13**, the reaction was carried out at -78 °C. Utilizing two equivalents of iodine monochloride per trimethylsilyl group resulted in precipitation of an orange solid in the course of the reaction. FD-MS confirmed the successful iodination together with the removal of two methyl groups suggesting the possible formation of **7-15**. Owing to decreased solubility of the obtained product, characterization by NMR spectroscopy was impeded. Thus, the reaction was repeated with **7-14** under identical conditions, which similarly resulted in the fourfold iodination and removal of two *n*-octyl chains. The obtained product showed reasonable solubility in organic solvents, which enabled its characterization by ^{13}C NMR spectroscopy (Figure 7-2). The corresponding spinecho
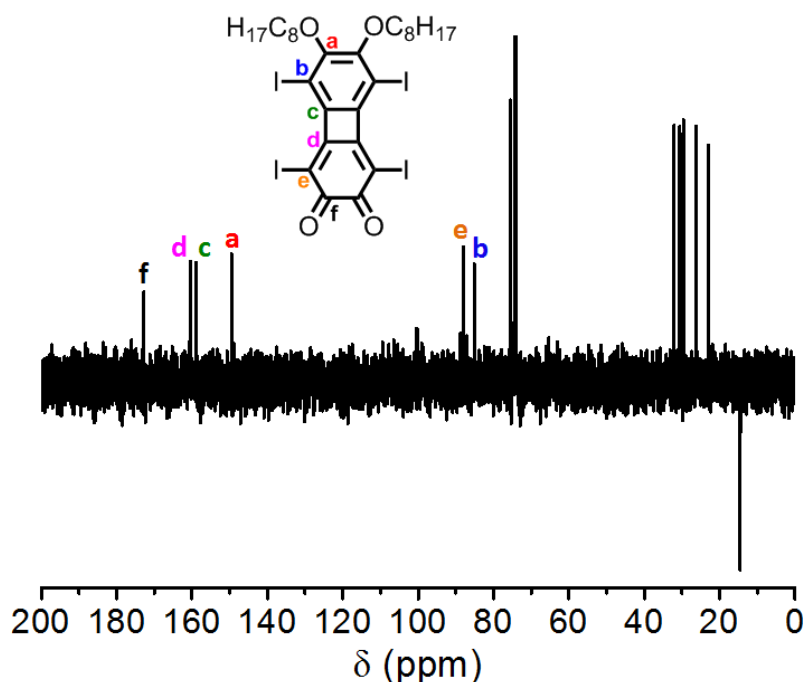
Figure 7-2. Spinecho ^{13}C NMR spectrum of 1,4,5,8-tetraiodo-6,7-bis(octyloxy)biphenylene-2,3-dione **7-16** with carbon assignment in $C_2D_2Cl_4$ at 25 °C.

^{13}C NMR spectrum showed the presence of six aromatic carbons with positive signals for quaternary carbons and CH_2 groups together with negative signals for CH- and CH_3 groups, thus proving the unsymmetric substitution of **7-16**. The presence of a 1,2-diketone (C_f) was revealed by a positive signal at 172.8 ppm, whereas the carbon located at the *n*-octyloxy chain (C_a) was shifted to 149.5 ppm. Moreover, the signals at 160.5 and 159.0 ppm, caused by the unsymmetric substitution of **7-16**, were assigned to the cyclobutadiene ring (C_c and C_d). The successful iodination (C_b and C_e) was evidenced by two signals at 88.1 and 85.1 ppm and the absence of a TMS signal at around 0 ppm.

The formation of 1,2-diketones **7-15** and **7-16** was rather unexpected, but could be explained by the Lewis acidity and the oxidative nature of iodine monochloride which led to the alkyl removal and subsequent oxidation toward the 1,2-diketones. Their utilization for further amine condensations toward pyrazine derivatives might be interesting for the generation of new donor-acceptor molecules. They are further relevant from the viewpoint of aromaticity, due to the combination of aromatic, antiaromatic and quinoid motifs in a single molecule.
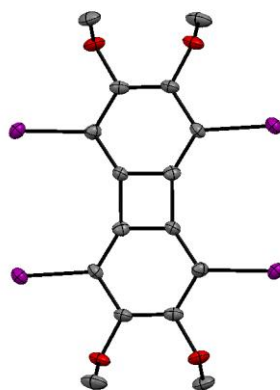
Figure 7-3. X-ray crystal structure of 1,4,5,8-tetraiodo-2,3,6,7-tetramethoxybiphenylene (**7-17**) (iodine atoms in violet, oxygen atoms in red, carbon atoms in grey, hydrogens omitted for clarity).

To enhance the solubility, the re-alkylation of **7-15** and **7-16** was intended. Reductive alkylation was performed with sodium dithionite and subsequent addition of an alkylation reagent adapting a procedure developed by *Müllen* and coworkers.[49-52] In case of **7-15**, dimethyl sulfate gave the methylated species **7-17** in 97% yield. On the other hand, by the addition of 1-bromooctane **7-18** was obtained in 20% yield which proved the versatility of this method. The different yields of **7-17** and **7-18** were attributed to a reduced electrophilicity of 1-bromooctane compared with dimethyl sulfate. Both materials were obtained on a several hundred milligram scale.

The successful formation of **7-17** and **7-18** was confirmed by MALDI-TOF MS with signals at $m/z = 777$ and 1 169, respectively. Only ^{13}C NMR spectroscopy allowed for a reliable characterization due to the absence of aromatic protons in **7-17** and **7-18**. Gratifingly, slow evaporation of a dichloromethane solution of **7-17** provided yellow crystals suitable for X-ray crystallography which unambiguously proved the successful iodination as well as the re-alkylation (Figure 7-3). As a result of the four-membered ring, the biphenylene core showed only small deviations (<1°) from planarity.

As described above, the newly developed tetrafunctionalization of the 1,4,5,8-positions of biphenylene proceeded selectively with an overall yield of around 10 to 15% over four steps. This is in a similar range as for the synthesis of non-functionalized biphenylenes by *Iyoda`s* protocol (**7-4**: 12% over two steps, see above).

7.3 Synthesis of 2,3,6,7-Tetrabromo-1,4,5,8-tetraiodo-biphenylene

Having proven applicability and, thus versatility of the protocol on both **7-17** and **7-18**, the focus turned now on the perfunctionalization of biphenylene toward subsequent "North-South" expansions (Figure 7-1).

Based on the above mentioned procedure for the introduction of trimethylsilyl groups at alkoxydibromobenzenes *via* a deprotonation-silylation sequence, the applicability of this method was studied in the following for 1,2,4,5-tetrabromobenzene (**7-23**, Scheme 7-4).
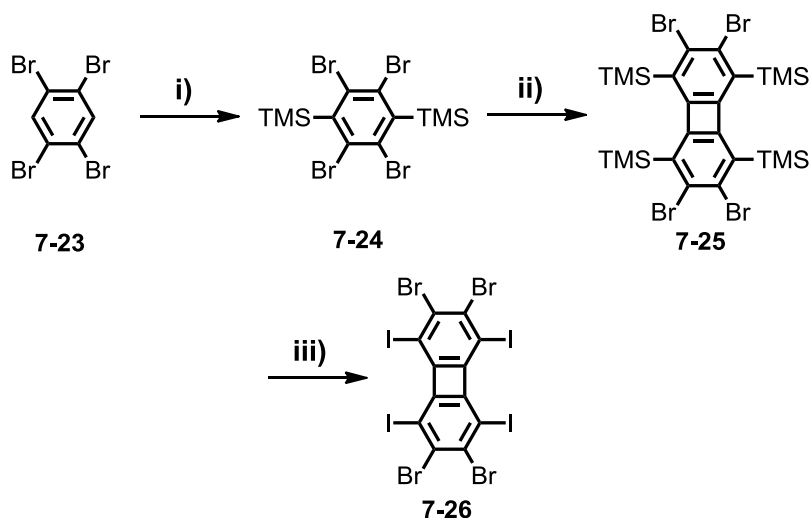
Scheme 7-4. Synthetic route toward 2,3,6,7-tetrabromo-1,4,5,8-tetraiodobiphenylene (**7-26**). Conditions: i) 2 equiv. LDA, Me$_3$SiCl, THF, -78 °C to RT, 78%; ii) 1 equiv. *n*-BuLi, THF, -78 °C to RT, 12%; iii) 1 M ICl, CH$_2$Cl$_2$, 0 °C to RT, 65%.

Therefore, **7-23** was similarly treated with LDA in the presence of chlorotrimethylsilane at -78 °C. In contrast to **7-7** and **7-8**, the amount of LDA had to be reduced to two equivalents to minimize protodehalogenation of **7-23**. The so obtained mixture was successfully separated by repeated column chromatography affording **7-24** in 78% yield. It was subsequently reacted with one equivalent of *n*-butyllithium. Owing to the ditopic nature of **7-24**, a precise control of the stoichiometry was of crucial importance to allow for a selective formation of biphenylene **7-25**. Hence, the lithiation was conducted in the course of one hour to minimize the amount of [N]phenylene byproducts, which were expected to form *via* repetitive [2+2]-cycloadditions. FD-MS revealed the formation of **7-25** together with partially protodehalogenated precursor **7-24** and small amounts of [3]phenylene and [4]phenylene. Extending the addition times of *n*-butyllithium did not change the outcome of the reaction. Column chromatographic separation and
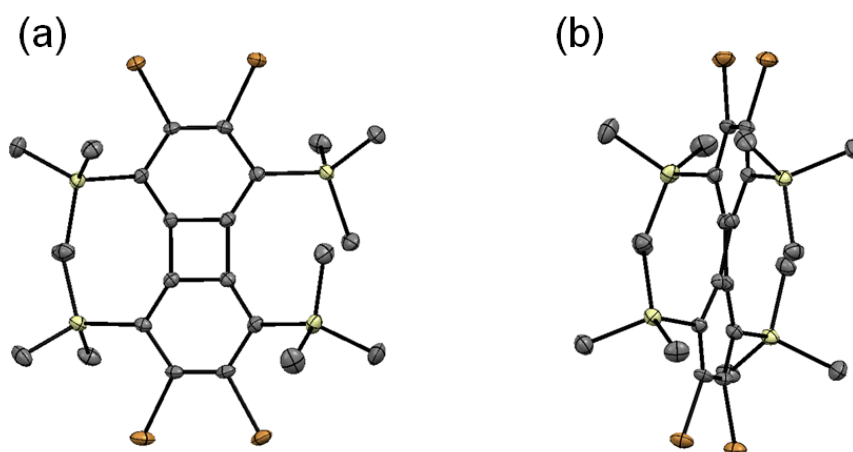
Figure 7-4. X-ray crystal structure of 2,3,6,7-tetrabromo-1,4,5,8-tetra(trimethylsilyl)biphenylene (**7-25**) in (a) the front view and (b) side view (silicon atoms in yellow, bromine atoms in orange, carbon atoms in grey, hydrogens omitted for clarity).

recrystallization allowed for the removal of the byproducts thus affording **7-25** in 12% yield as yellow solid soluble in common organic solvents. Besides mass spectrometry and NMR spectroscopic characterization, the structure of **7-25** was confirmed by X-ray crystallographic analysis (Figure 7-4). Due to the sterically demanding trimethylsilyl groups, the biphenylene core is significantly twisted (32.9° between the mean planes of the benzene units).

Iodination of **7-25** was conducted under the previously applied conditions. Besides iodination the exchange of the bromine atoms to chlorines was observed at 0 and
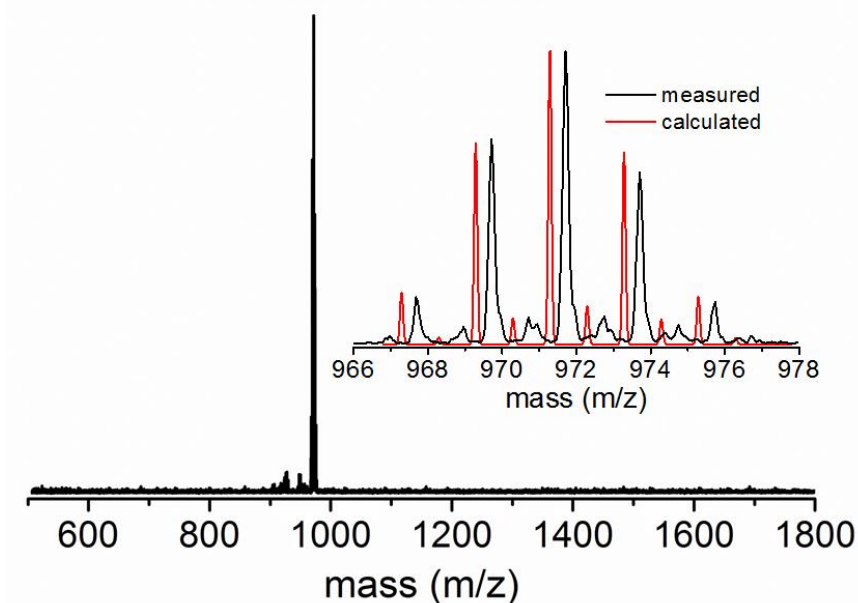
Figure 7-5. MALDI-TOF MS spectrum (matrix: TCNQ) of 2,3,6,7-tetrabromo-1,4,5,8-tetraiodobiphenylene (**7-26**). Inset: Measured and calculated isotopic patterns of **7-26**.

-78 °C. This underlined once again the reactivity of the 2,3,6,7-positions of biphenylene in the presence of iodine monochloride. To avoid the bromine-chlorine exchange, iodine monobromide was used instead. This led, however, to partial protodesilylation most probably caused by the reduced electrophilicity of iodine monobromide. The utilization of silver(I) salts as chloride scavengers resulted similarly in incomplete deprotection of the trimethylsilyl groups.[53] By carefully screening the reaction times and the amount of the iodine source, it was shown that slow addition of iodine monochloride at 0 °C in combination with 12 hours in the absence of light minimized bromine-chlorine exchange and allowed for a complete iodination. This enabled the successful formation of 2,3,6,7-tetrabromo-1,4,5,8-tetraiodobiphenylene (**7-26**) in 65% yield on a several hundred milligram scale. Due to the insolubility of **7-26** in organic solvents, purification was achieved by consecutive washing of the crude product with methanol, tetrahydrofuran and dichloromethane. MALDI-TOF MS clearly indicated the successful iodination with a targeted mass of $m/z = 967$ (Figure 7-5). The decreased solubility of **7-26** did not allow for further characterization by NMR spectroscopy.

7.4 "East-West" Expansion of the Biphenylenes

7.4.1 Solution-Based Polymerization

Having functionalized biphenylenes **7-17**, **7-18** and **7-26** in hand, expansion along their "East–West" direction *via* repetitive C−C bond formation was targeted (Figure 7-1). In contrast to the one-dimensional polymerizations of dibromo *N*-heterotriangulene **3-5** (see Chapter 3) and 2,2',6,6'-tetraphenyl-1,1'-biphenyl **6-24** (see above), the expansion of biphenylene **7-17** and **7-18** would theoretically result in a two-dimensional ladder-type polymer. The complexity of the *inter-* and *intra*molecular C−C bond formations is thereby significantly increased. To avoid the detrimental effects of A_4B_4-type polycondensations (see Chapter 3 for details), an efficient A_4-type coupling method was targeted. One of the most versatile methods for an *AA*-type coupling is the Ni⁰-mediated *Yamamoto* polycondensation, as described in the previous chapters.[54-58] Thus, the polymerization of **7-17** was conducted in a standard *Yamamoto* protocol in a toluene/DMF (3/1) mixture with a concentration of 20×10^{-3} M to favor both *inter-* and *intra*molecular C−C bond formation (Scheme 7-5).[54, 55] After usual work-up, analysis of the crude mixture by FD- and MALDI-TOF MS showed neither the presence of oligomers nor polymeric chains (**7-27**). Instead, the formation of 3,3',4,4'-tetramethoxy-1,1'-biphenyl (**7-28**) was observed as
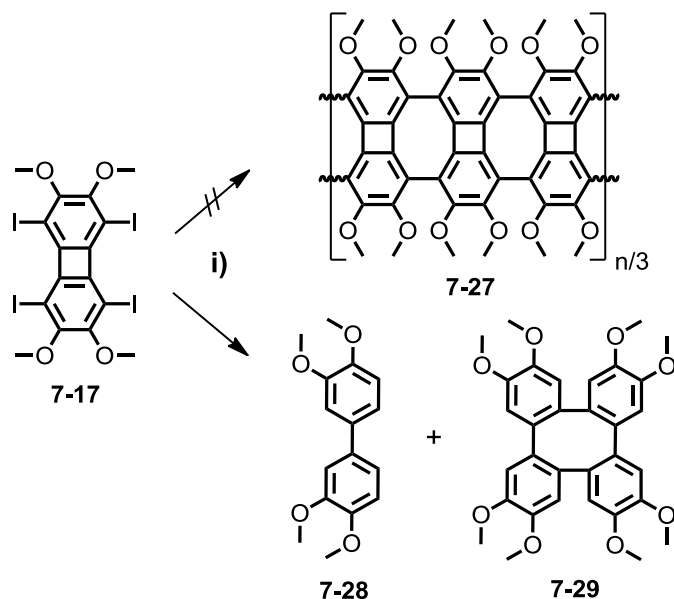
Scheme 7-5. The *Yamamoto* reaction of 1,4,5,8-tetraiodo-2,3,6,7-tetramethoxybiphenylene **7-17**. Conditions: i) bis(cycloocta-1,5-diene)nickel(0), cycloocta-1,5-diene, 2,2'-bipyridine, toluene/DMF, 85 °C, 4 days, **7-28**: 27%, **7-29**: 4%.

the main product together with a minor amount of COT (**7-29**). This observation can be explained with the help of mechanistic studies on the catalytic conversion of biphenylene to COT by *Johnson* and coworkers (Scheme 7-6).[59]
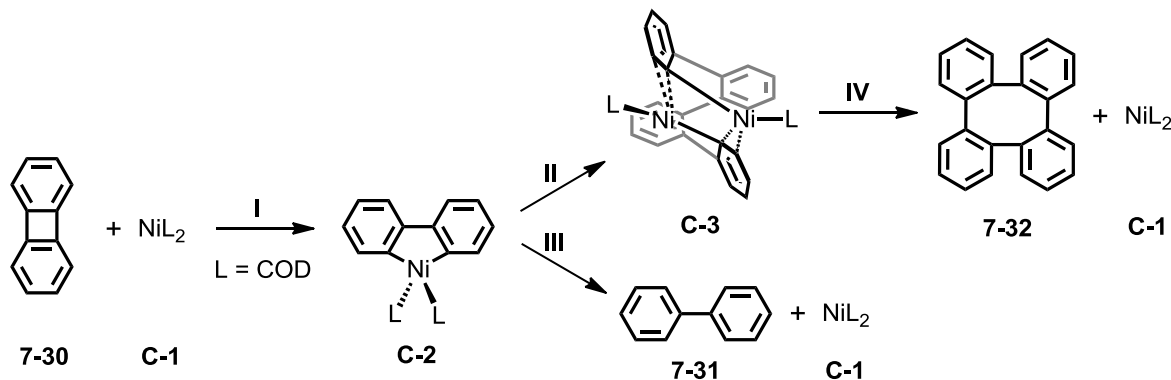
Scheme 7-6. Reaction mechanism of the Ni⁰-mediated ring opening and dimerization of biphenylene **7-30**.[59] **I** Insertion to the four-membered ring; **II** first C−C coupling step; **III** reductive elimination of biphenyl; **IV** second C−C coupling step and reductive elimination of COT. The methoxy and iodine substituents are omitted for clarity.

In the course of the *Yamamoto* reaction, insertion of the nickel atom of complex **C-1** into the C−C bond of the four-membered ring leads to the formation of complex **C-2** (step **I**). At this step, complex **C-2** is capable of an *inter*molecular C−C coupling to a second molecule yielding dinuclear complex **C-3** (step **II**). It is very likely that due to the steric demand of the *inter*molecular C−C coupling step (step **II**) a reductive elimination toward biphenyl (**7-31**) additionally occurs (step **III**). Dinuclear complex **C-3** can subsequently

undergo an *intra*molecular C−C coupling toward COT **7-32** which is followed by reductive elimination and the subsequent release of the reactivated complex **C-1** (step **IV**). According to the generation of **7-28** and **7-29** (Scheme 7-5), protodehalogenation is expected to occur during these reaction step.

Although the formation of COT derivatives by *Yamamoto* dimerization of biphenylene holds promise for the potential fabrication of subunits of cubic graphite, polymerization of **7-17** was impeded by this method.

Alternatively, the utilization of the *Suzuki-Miyaura* reaction was tested. The preparation of a biphenylene boronate as reaction partner was therefore necessary. Due to the lack of an asymmetric functionalization of biphenylene **7-17** toward an A_2B_2-type monomer, the formation of a B_4-type monomer was targeted (**7-33** and **7-34**, Scheme 7-7). Hence, the halogen-lithium exchange was conducted by treating **7-17** with an excess of *n*-butyllithium
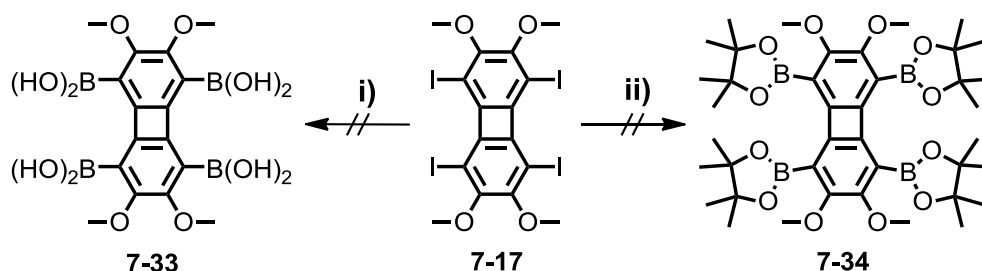
Scheme 7-7. Synthetic route toward biphenylene boronic acid **7-33** and boronate **7-34**. Conditions: i) *n*-BuLi, 2-isopropoxy-4,4,5,5-tetramethyl-1,3,2-dioxaborolane, 1 N aq. HCl, THF, -78 °C to RT; ii) Pd(dppf)Cl₂ or Pd(PPh₃)₄, KOAc, bis(pinacolato)diboron, DMF, 85 °C or 100 °C, 12 h.

at -78 °C followed by the addition of 2-isopropoxy-4,4,5,5-tetramethyl-1,3,2-dioxaborolane and subsequent quenching with hydrochloric acid. However, only the formation of the tri-, di- and monoboronic acids was revealed. Purification was furthermore hampered by concurrent protodehalogenation leading to the inevitable formation of constitutional isomers of the diboronic acid and the high polarity of the boronic acids. The synthetic approach was therefore changed to a Pd-catalyzed *Miyaura* borylation, which enables the introduction of boronates under cross-coupling conditions.[60] The iodine-boronate exchange, however, did not proceed and a broad variety of protodehalogenated products was obtained. Despite different catalytic systems and temperatures were tested, the formation of **7-34** was not achieved.

Owing to the incomplete borylation of **7-17**, the synthetic strategy was changed to the Cu-mediated *Ullmann* reaction. This robust and versatile method has long been employed to generate a C−C bond between two aromatic carbon atoms and is known for its broad

7-35 (n = 7.6)
7-36 (n = 12.9)
7-37 (n = 17.2)
7-38 (n = 24.1)
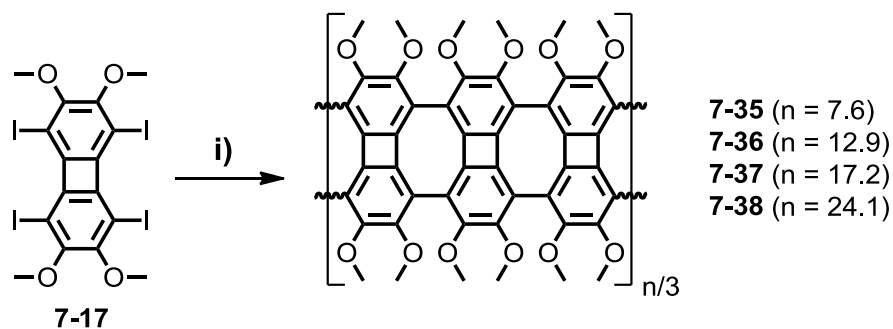
Scheme 7-8. Synthetic route toward the "East-West" expansion of 1,4,5,8-tetraiodo-2,3,6,7-tetramethoxybiphenylene (**7-17**) *via* the *Ullmann* reaction. Conditions: i) *Ullmann* conditions see Table 7-1, **7-35**: 36%, **7-36**: 26%, **7-37**: 14%, **7-38**: 20%.

Table 7-1. Optimization of the reaction conditions of the *Ullmann* polymerization of **7-17**.

Entry	Catalyst System	T (°C)	t (h)	Solvent	Polymerization[a]
1	Cu^0	120	96	DMSO	No[b]
2	Cu^0	190	96	DMSO	No[b]
3	Cu^0	120	96	DMF	No[b]
4	Cu^0	170	96	DMF	No[b]
5	Cu^0	210	96	*o*-DCB	No[b]
6	activated Cu^0	180	96	*o*-DCB+DMF	No[b]
7	**activated Cu^0**	**210**	**96**	**_o_-DCB**	**Yes**

DMSO: dimethyl sulfoxide; DMF: *N,N*-dimethylformamide; *o*-DCB: 1,2-dichlorobenzene. [a] Determined by MALDI-TOF MS and SEC. [b] Besides products of protodehalogenation and starting material, no product was detected.

functional group tolerance.[61-64] Different *Ullmann* conditions were therefore screened by using biphenylene **7-17** as monomer (Scheme 7-8 and Table 7-1). Typically, the aryl halide is reacted with a finely powdered copper in a molar ratio of 2/1 at elevated temperatures to form a biaryl and copper halide. As a result of the heterogeneous nature of the *Ullmann* reaction, the applied Cu^0 source can potentially act as template to enhance analogous to the previously discussed surface-confined reaction (see Chapter 4).

The concentration of all tested reactions was set to 30×10^{-3} M to ensure efficient *inter*molecular coupling and to favor at the same time *intra*molecular bond formations. Biphenylene **7-17** was initially reacted in high boiling solvents such as dimethylsulfoxide and *N,N*-dimethylformamide in the presence of commercially available copper powder under an argon argon atmosphere. Different temperatures were thereby tested ranging from 120 to 190 °C (Table 7-1, entries 1-4). Analyzing the reaction mixtures by MALDI-TOF MS and SEC, however, revealed unreacted **7-17** together with protodehalogenation. By further increasing the temperature to 210 °C with 1,2-dichlorobenzene as solvent (entry 5), the reaction remained almost unaffected. Activated Cu^0 is known to enhance the biaryl
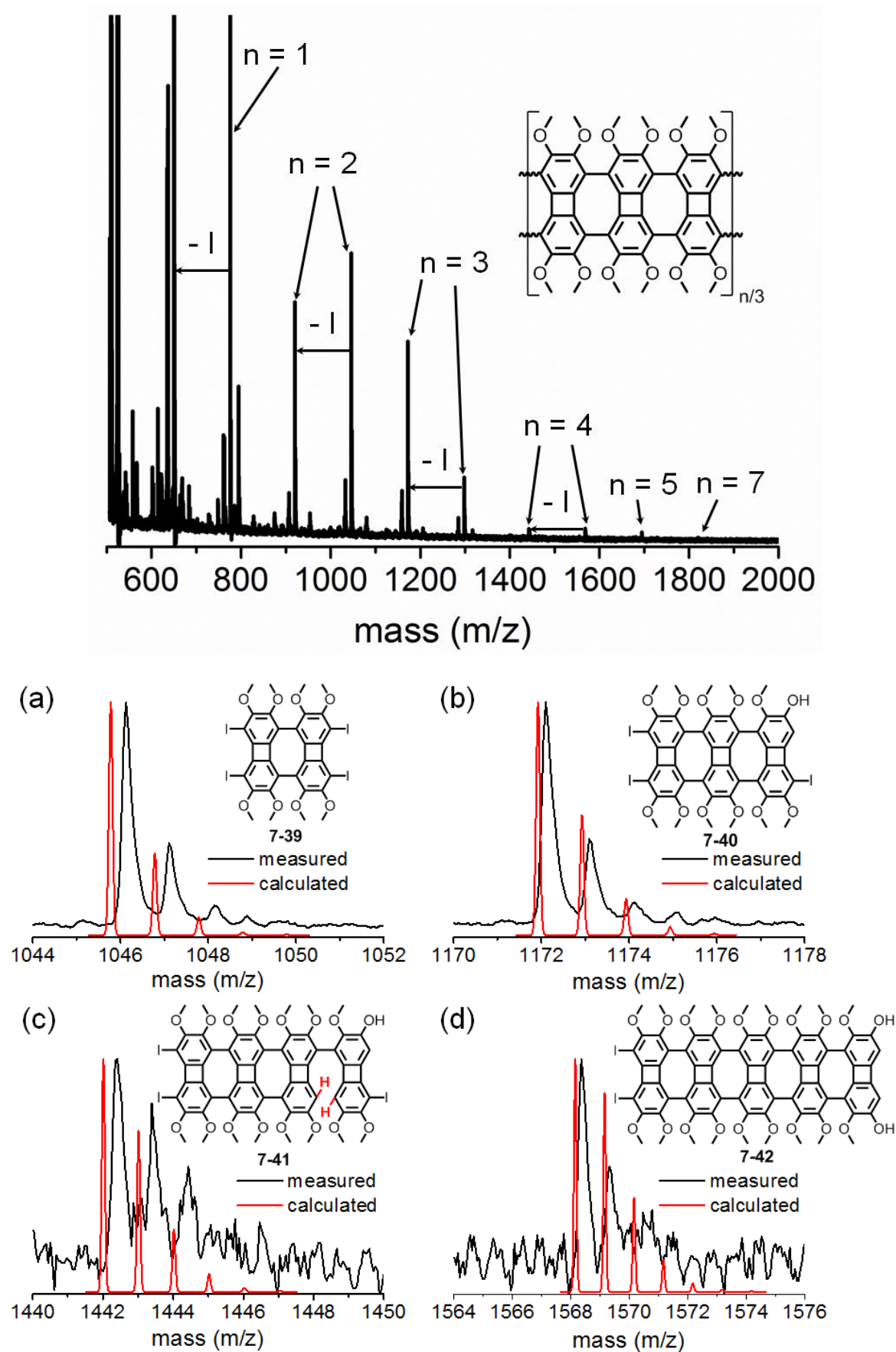
Figure 7-6. Top: MALDI-TOF MS (matrix: dithranol, reflector mode) of the polymeric fraction reflecting the presence of up to heptamers. Bottom: Measured and calculated isotopic patterns of (a) dimer **7-39**, (b) trimer **7-40** (c) tetramer **7-41** and (d) pentamer **7-42**.
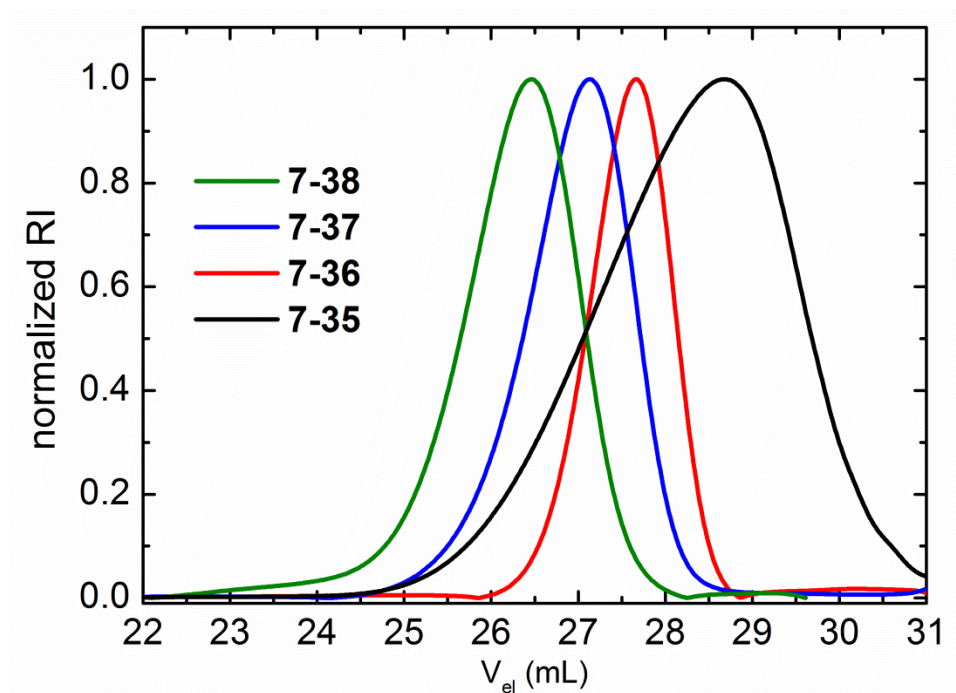
Figure 7-7. SEC analysis of the separated isomeric GNR fractions **7-35** to **7-38** (THF, PPP standard).

Table 7-2. Characteristics of the individual fractions **7-35** to 7-**38**.

Fraction	M_n[a] (g/mol)	M_w[a] (g/mol)	PDI[b]	DP[c]	Yield (%)
7-35	2 050	2 880	1.40	5.8	30
7-36	3 460	3 630	1.05	11.0	15
7-37	4 620	5 110	1.11	15.3	13
7-38	6 460	7 810	1.21	22.2	26

[a] Molecular wights were determined by SEC in THF using PPP as standard. [b] $PDI = M_w/M_n$. [c] DP = $(M_n - 4 \times 127)/M_0$ = number of biphenylenes.

formation of the *Ullmann* reaction.[65] It is generated by cleaning commercially available copper powder with hydrochloric acid and aqueous ammonia, which removes cuprous ions from the copper surface.[66] Subsequently, it was used in combination with *N*,*N*-dimethylformamide and 1,2-dichlorobenzene as solvent mixture at 180 °C (entry 6). The outcome of the reaction remained essentially the same. However, a further increase of the temperature to 210 °C by using 1,2-dichlorobenzene as solvent led to the detection of oligomers by MALDI-TOF MS after four days. The reaction was allowed to proceed for further seven days at 210 °C and was quenched by the addition of aqueous ammonium chloride. After removal of the inorganic residues, the crude reaction mixture was added to dilute methanolic hydrochloric acid. The MALDI-TOF MS of the precipitate indicated the presence of oligomeric species up to $m/z = 1\,900$ (Figure 7-6, top) which corresponds up to seven biphenylene units. Besides the [M+H]$^+$ peak, the scission of one or two methyl

groups and the cleavage of iodine was observed for all species during the reaction. Clearly resolved isotopic patterns were obtained up to $m/z = 1\,600$ (Figure 7-6, bottom). Comparing these patterns with the calculated ones for dimer **7-39**, trimer **7-40** and pentamer **7-42**, the formation structures with alternating four- and eight-membered rings was revealed. The tetramer peak, however, showed the presence of two additional protons suggesting the incomplete formation of one eight-membered ring toward **7-41**. Although the obtained structures were expected to be not completely defect-free they reflect isomers of graphene nanoribbons. Thus, they will be denoted in the following as isomeric GNRs.

In parallel *n*-octyloxy substituted biphenylene **7-18** was reacted under identical *Ullmann* conditions. In contrast to **7-17** this led, however, neither to the formation of a polymer nor any oligomeric species which might be attributed to the sterically more demanding *n*-octyl chains of **7-18**.

The obtained ribbon-type structures based on methoxy substituted **7-17** showed good solubility in organic solvents such as dichloromethane, THF and toluene which enabled its fractionation by preparative SEC to study the impact of the chain length on the photophysical properties. This allowed for the separation of the obtained ribbons into four polydisperse fractions **7-35** to **7-38**. The composition of **7-35** to **7-38** was analyzed by SEC in THF using a PPP standard which revealed a gradual decreased elution volume (V_{el}) of the obtained SEC curves (Table 7-2, Figure 7-7). Fraction **7-38** was obtained at first having a $M_n = 6\,460$ g/mol with a PDI of 1.21. By considering four residual iodine endgroups per polymer chain, **7-38** consists of at least 22 biphenylenes even though a smaller number of iodine endgroups is more likely. This corresponds to a linear dimension of at least 9.1 nm according to geometry optimizations.[67] A more precise determination of the molecular weights of the fractions **7-35** to **7-38** was, however, impeded due to the lack of a more appropriate SEC standard and a limited detection of polydisperse samples by MALDI-TOF MS. The polymer characteristics of the remaining fractions are illustrated in Table 7-2.

For more detailed information about the perfection of the isomeric GNRs, ^{1}H NMR spectroscopy of **7-38** was conducted (Figure 7-8). Two sets of signals were basically observed having a ratio of 2 to 33 which was not significantly changed upon heating or cooling the sample. In agreement with monomer **7-17**, the broadened signal at 3.76 ppm was assigned to the methoxy protons at the periphery (H_a) of the isomeric GNR **7-38**. The broadened aromatic signal between 6.75 and 7.62 ppm was attributed to the remaining protons obtained from incompletely fused eight-membered rings (H_b) together with proton
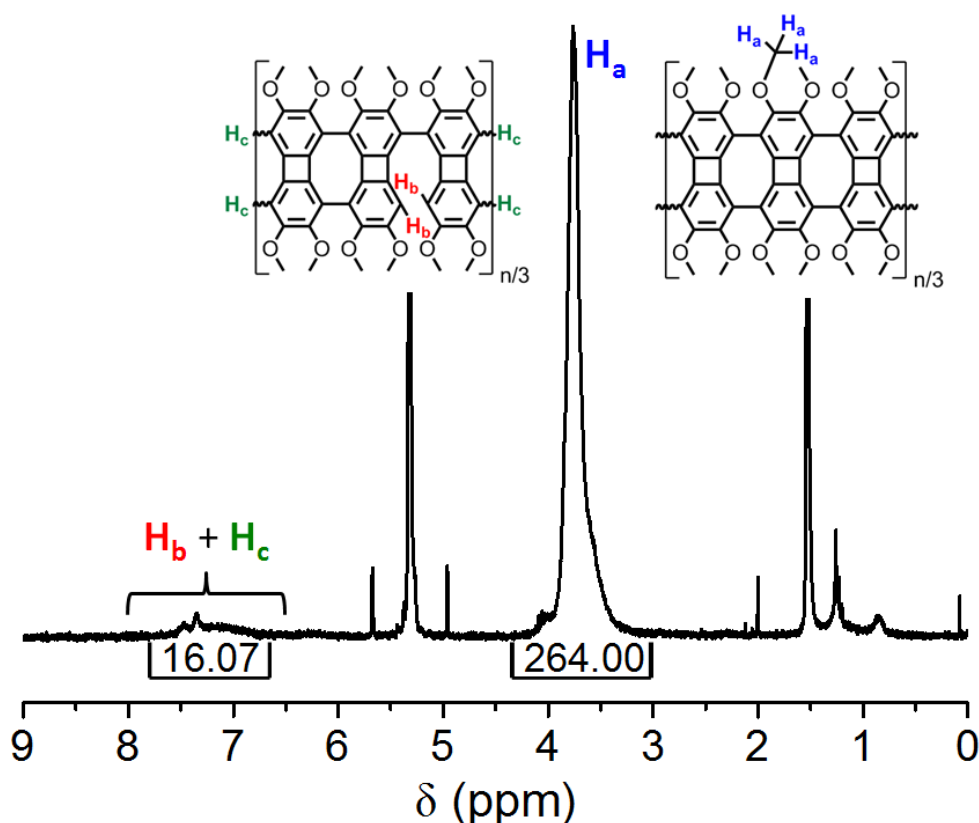
Figure 7-8. ^{1}H NMR spectrum of isomeric GNR fraction **7-38** in CD_2Cl_2 at 25 °C together with proton assignment.

endgroups (H_c). Combining the signal intensities with the previous SEC analysis allowed for a determination of the non-fused eight-membered rings of **7-38** and thus an estimation of the amount of defects. Based on the assumption that all methoxy groups remained intact during polymerization the obtained aromatic signals correspond to approximately 16 protons resulting from 8 non-fused eight-membered rings. This analysis considered four iodine endgroups per chain. However, taking (partial) protodehalogenation into account (four proton endgroups per chains), six non-fused eight-membered rings were revealed. In other words, at least 13 to 15 eight-membered rings were expected for isomeric GNR **7-38** even though the exact position of these rings could not be determined.

To gain further insights to the structural composition, isomeric GNR **7-38** was characterized by vibrational spectroscopy. Raman spectroscopy theoretically provides information about the expansion of the π-system and the associated π-conjugation length.[68-73] The sample was therefore homogenized and subsequently irradiated with an excitation wavelength of 488 nm. Two characteristic bands are usually obtained for graphene and all-benzenoid PAHs. The D-band (disorder) is caused by defects in the graphene and by edge effects, which is absent for infinitely large and defect-free graphene.
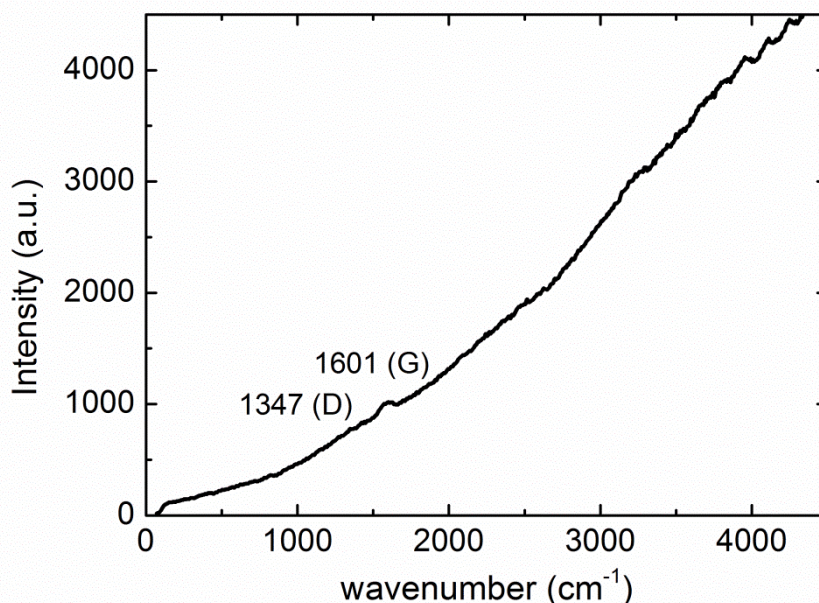
Figure 7-9. Raman spectrum of isomeric GNR **7-38** on a quartz glass slide (λ_{exc} = 488 nm).

The G-band, however, is a result of C−C vibrations in the graphitic material and is observed for almost every material based on sp^2-carbons. The Raman measurement of **7-38** was accompanied by fluorescence which significantly decreased the resolution of the characteristic bands (Figure 7-9). However, two bands at around 1600 and 1350 cm^{-1} were observed. Although the intensities were very low, the positions of these two bands are similar to reported values for polyphenylene-based GNRs, confirming the PAH character of **7-38**.[73-75] The overlay of fluorescence, however, did not allow for a reliable calculation of the dimension of the isomeric GNR **7-38**.

UV-vis absorption and emission properties of **7-35**, **7-36**, **7-37** and **7-38** were investigated in dichloromethane and compared to the data of monomer **7-17**. To ensure comparability, the concentration in all experiments was set to 1×10^{-6} M. All spectra are depicted in Figure 7-10 and the obtained values are listed in Table 7-3.

Owing to the limited molecular weight determination of polymeric samples, such as **7-35**, **7-36**, **7-37** and **7-38**, normalized spectra are shown. The UV-vis absorption spectrum of monomer **7-17** is characterized by two sets of transitions, a very intense band at 308 nm and a progression of weak bands between 350 and 400 nm. The latter one was thereby assigned to electric dipole-forbidden HOMO-LUMO excitations, which were however observed as a result of the methoxy and iodine substitution of **7-17**.[22, 76-78] Consequently, an E_g^{opt} of 2.96 eV was calculated for **7-17**. By increasing the molecular weight toward isomeric GNRs **7-35**, **7-36**, **7-37**, and **7-38** small hypsochromic shifts for the longest
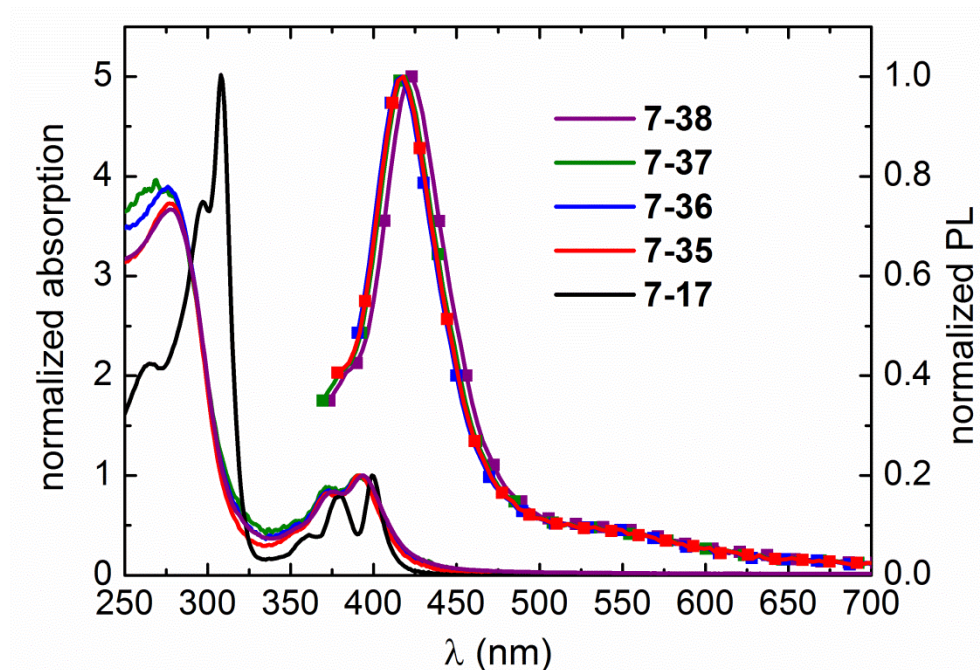
Figure 7-10. UV-vis absorption (solid line) and emission (symbol line) spectra of **7-17** (black), **7-35** (red), **7-36** (blue), **7-37** (green) and **7-38** (violet). For all spectra: 1×10^{-6} M in CH_2Cl_2.

Table 7-3. Selected photophysical data of **7-17**, **7-35**, **7-36**, **7-37**, and **7-38**.

	$\lambda_{abs,max}$[a] (nm)	$\lambda_{PL,max}$[a,b] (nm)	Stokes shift (cm^{-1})	E_g^{opt} [c] (eV)
7-17	265(s), 297(s), 308, 361(s), 380(s), 399	-	-	2.96
7-35	277, 351(s), 373(s), 392	418	1 590	2.87
7-36	276, 353(s), 373(s), 391	417	1 595	2.84
7-37	269, 353(s), 372(s), 390	419	1 775	2.83
7-38	278, 353(s), 376(s), 394	423	1 740	2.81

[a] For all spectra: 10^{-6} M in CH_2Cl_2. [b] Excited at the absorption maxima. [c] $E_g^{opt} = h \cdot c / \lambda_{0.1max}$. (s) = shoulder.

wavelength transitions were revealed. Due to a broadened absorption tail, the respective band gaps increased to around 2.8 eV which is surprisingly large compared with other types of GNRs and reflect the large band gap character of the described isomeric GNRs.[73, 75, 79] In contrast to monomer **7-17**, emissions at around 420 nm were detected for **7-35**, **7-36**, **7-37** and **7-38** which proved the increased π-conjugation. A moderate level of reorganization in the excited state was revealed by comparably low Stokes shifts of around 1 700 cm^{-1}. To explain the surprisingly large optical band gaps (E_g^{opt}) of the isomeric
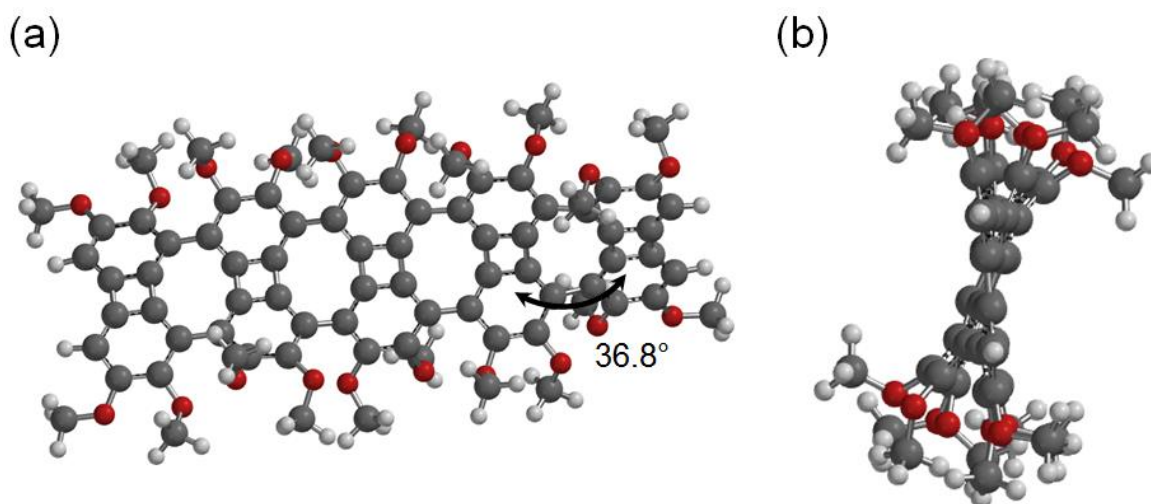
Figure 7-11. Pentamer **7-43** obtained by a geometry-optimized DFT calculation (B3LYP, 6-31G*).

GNRs, a DFT geometry optimization (DFT, B3LYP/6-31G*) on a model compound with hydrogen endgroups (**7-43**) was carried out (Figure 7-11).[67] Pentamer **7-43** consists of individual biphenylene dimers which can be considered as COTs planarized by cyclobutadiene moieties thus preventing the characteristic boat conformation of COT. The dihedral angles in COT are 65° *vs.* ~22° for the individual dimers in **7-43**. Therefore, an out-of-plane distortion along the ribbon chain is observed which is expressed by dihedral angles between the individual biphenylenes ranging from 22.1 to 36.8° (Figure 7-11 a and b). This is basically attributed to the sterical repulsion among the methoxy groups at the neighboring biphenylene subunits. As a result of this mutual twist, the π-conjugation along the chains is significantly decreased and hence led to size independent photophysical properties similiar to monomer **7-17**. The individual biphenylene moieties in **7-35**, **7-36**, **7-37** and **7-38** are therefore virtually isolated which leads to comparably large band gaps. Additionally, the observed defects are expected to further weaken the π-conjugation.

7.4.2 Surface-Assisted Polymerization

Although different lengths of isomeric GNRs were accessible by the solution-based polymerization of biphenylene **7-17**, the obtained ribbon-type structures were not structurally perfect. Based on the surface-assisted *Ullmann* reaction, however, different types of polyphenylene-based GNRs have been prepared by controlling the topology, the width and edge periphery by the appropriate choice of the precursor monomer.[79-81] The formation of defect free ribbons was thereby attributed to the confinement of the motion of the precursor monomers to two dimensions which enforces planar growth. To study this
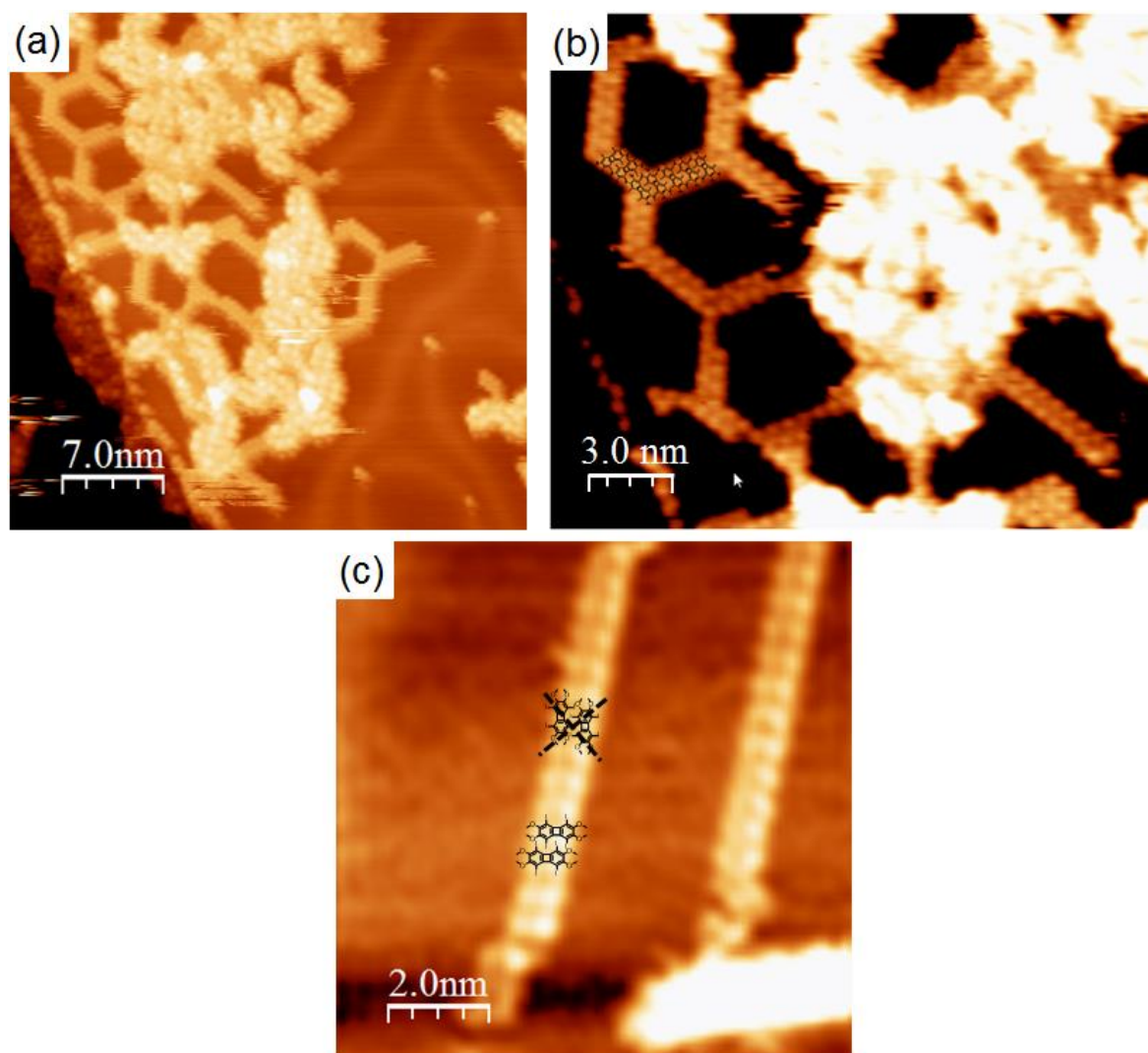
Figure 7-12. (a) STM images of 1,4,5,8-tetraiodo-2,3,6,7-tetramethoxybiphenylene (**7-17**) on Au(111) after annealing at 100 °C. (b) Zoom into the upper left area of (a) with a molecular model. (c) Close-up view of ribbon-type structures (4.5 ×12 Å) with two possible orientations of **7-17**.

effect on the outcome of the formation of isomeric GNRs, 1,4,5,8-tetraiodo-2,3,6,7-tetramethoxybiphenylene **7-17** was applied for the STM-monitored surface reaction under UHV conditions. The respective STM experiments were carried out in collaboration with ████████████████ in the group of ████████████████ at the EMPA Dübendorf, Switzerland.

To guarantee high purity of the monomer, **7-17** was several times recrystallized and rigorously dried in high vacuum. With its molecular weight of 776 g/mol and the temperature- and transition metal-sensitive four-membered ring it was initially uncertain whether sublimation would be possible for precursor **7-17**. Gratifingly, it could be successfully deposited on Au(111) substrate at a temperature of 160 °C in UHV (~10^{-7} mbar). After annealing for 10 minutes at 100 °C, the Au(111) substrate was covered with different structures that formed from monomer **7-17** (Figure 7-12 a and b). It appeared

that the molecules of **7-17** adopt ribbon-type structures in a regular and planar conformation suggesting a covalent C−C bond formation already at this temperature. They were partly arranged to quasi hexagons with lengths of up to 20 nm. Bright islands were additionally observed, which might be explained by partially cleaved methyl groups and iodine atoms.

From these results it could not be definitely judged whether the individual molecules of **7-17** were covalently bonded due to the accessible resolution of the STM images. By performing a line profile analysis with the STM tip, however, parts of the ribbons could be moved (Figure 7-13 a and b). This clearly evidenced a self-assembly of **7-17** to ribbon-like structures instead of a covalent C−C bond formation. The biphenylene molecules are thereby parallel orientated to each other and stabilized by van der Waals attractions between the iodine and the oxygen atoms of **7-17** (Figure 7-12 c). This was additionally confirmed by the dimensions of the structures (4.5×12 Å) which ruled out other arrangements.
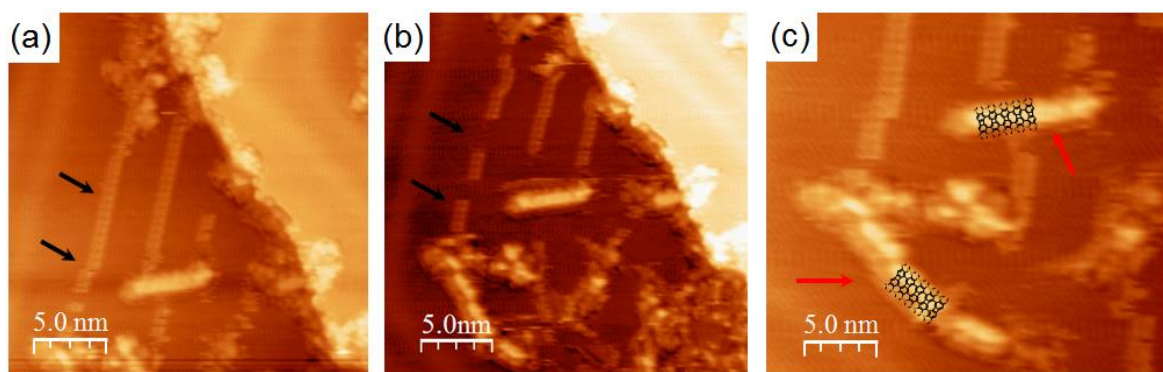
Figure 7-13. STM images of the ribbon-type structures (a) before and (b) after the the line profile analysis with the STM tip. The black arrows indicate the movement of the molecules by the STM tip. (c) Close-up view of brighter ribbons which remained intact with a molecular model. They are indicated by red arrows.

Even though several ribbons were non-covalently bond a few structures remained intact after the line profile analysis with the STM tip (Figure 7-13 c). These features were identified as successfully polymerized ribbons with lengths of up to 10 nm. It has to be kept in mind that after the initial C−C bond formation the molecules can adopt a twisted structure on the substrate which might hamper the second C−C bond formation toward the eight-membered ring. Owing to the limited resolution of the STM images, however, the defect-free nature of the obtained ribbons could not be finally proven.

Increasing the temperature to 200 °C, however, did not result in the formation of larger ribbons (Figure 7-14). Due to the increased size of bright islands, decomposition of **7-17** is very probable. Nonetheless, three types of ribbons were observed. The first type is

composed of an odd number of benzene moieties (Figure 7-14 a, black arrow), which indicated the decomposition of the central four-membered ring at the applied temperature. A second, very thin ribbon type (5 ×12 Å, height 1.2 Å) confirmed the partial cleavage of benzene rings (Figure 7-14 b, blue arrow). In addition, thicker ribbons (7 ×18 Å, height 2.0 Å) indicated partial polymerization of **7-17** toward the targeted isomeric GNRs (Figure 7-14 b, red arrow), although the observed structures have a comparably low molecular weight. Increasing the temperature further to 350 °C led to complete decomposition of the obtained structures and only bright clusters were obtained.
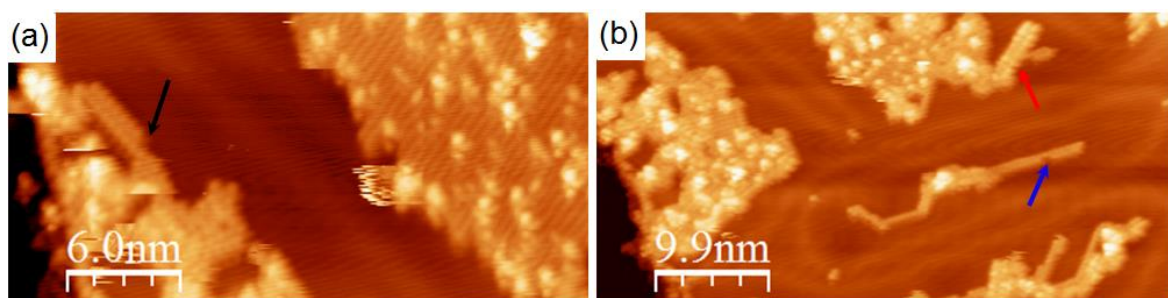
Figure 7-14. STM images after annealing to 200 °C. The three types of ribbons are indicated by the black, blue and red arrows.

The results of the experiments suggested that increasing the halogen reactivity might lead to a more efficient polymerization at lower temperatures and thereby an increase of the molecular weight. It has been discussed in Chapter 4 that one of the key steps of the surface protocol is the formation of a radical immediately after the monomer contacts the metal surface from the gas phase. Electron-rich biphenylene **7-17**, however, did not dehalogenate during this step thus requiring elevated temperatures. It can be assumed that decreasing the strength of the carbon-halogen bond could beneficially support the formation of the active site and thus lead to a more efficient polymerization. The steric demand of the methoxy groups was furthermore expected to be detrimental to the efficient C−C bond formation. Based on these considerations it became clear that the utilization of electron-poor 2,3,6,7-tetrabromo-1,4,5,8-tetraiodobiphenylene (**7-26**) could help to overcome the encountered difficulties. With this precursor the expansion along the "North-South" direction was expected to be possible.

7.5 "East-West" and "North-South" Expansion of the Biphenylenes

7.5.1 Solution-Based Polymerization and Expansion of 7-26

It has been theoretically and experimentally demonstrated that both width and edge structure of GNRs strongly govern their electronic characteristics.[73, 75, 82-84] Although the intrinsic properties of isomeric GNRs **7-35**, **7-36**, **7-37** and **7-38** are mainly determined by the biphenylene moieties, their lateral expansion is expected to similarly influence the nature of these materials. As it was shown for the synthesis of polyphenylene based GNRs *via* the well-known bottom-up approach of *Müllen* and coworkers, the molecular precursor dictates the GNR geometry.[73, 75, 79, 81] Adapting this concept for the fabrication of laterally extended isomeric GNRs was targeted in the following.

Due to the presence of different halogen functionalities, 2,3,6,7-tetrabromo-1,4,5,8-tetraiodobiphenylene (**7-26**) was expected to polymerize initially along the 1,4,5,8-positions toward **7-44** (Scheme 7-9). Subsequent reaction of the remaining bromine atoms should theoretically result in the formation of two types of isomeric GNRs **7-45** and **7-46**. In the former type the individual biphenylene chains are connected by four- and eight-membered rings whereas in **7-46** the ribbons are exclusively fused by benzene rings.
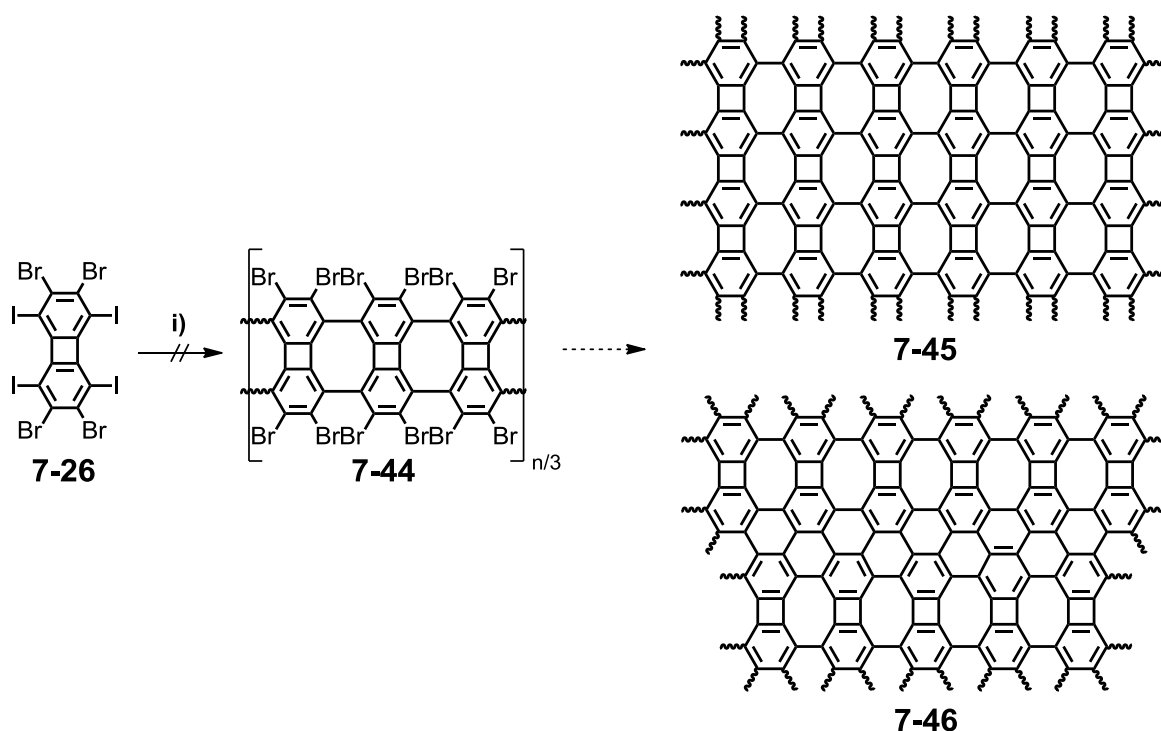
Scheme 7-9. The "East-West" and "North-South" expansion of 2,3,6,7-tetrabromo-1,4,5,8-tetraiodobiphenylene **7-26**. Conditions: i) *Ullmann* conditions see Table 7-4.

Table 7-4. Optimization of the reaction conditions of the *Ullmann* polymerization of **7-26**.

Entry	Catalyst System	T (°C)	t (h)	Solvent	Polymerization[a]
1	activated Cu^0	100	96	*o*-DCB	No[b]
2	activated Cu^0	120	96	*o*-DCB	No[b]
3	activated Cu^0	140	96	*o*-DCB	No[b]
4	activated Cu^0	180	96	*o*-DCB	No[b]
5	activated Cu^0	160	96	DMF	No[b]
6	activated Cu^0	160	96	DMSO	No[b]
7	Cu^0	180	96	*o*-DCB	No[b]
8	CuI + L-proline	110	96	DMSO	No[b]

DMSO: dimethyl sulfoxide; DMF: *N,N*-dimethylformamide; *o*-DCB: 1,2-dichlorobenzene. [a] Determined by MALDI-TOF MS and SEC. [b] Besides protodehalogenation, no product was detected.

Owing to the fact that the generation of **7-45** is expected to comprise the involvement of various aryne intermediates, the occurrence of both ribbon types is most likely. The previously established *Ullmann* protocol using activated Cu^0 was therefore utilized for the polymerization of **7-26**. To exclude a possible involvement of the bromine atoms, the reaction was conducted at lower temperatures (Table 7-4, entry 1-4). As a result of the decreased solubility of **7-26** in organic solvents the reaction did not proceed between 100 to 120 °C. Increasing the temperature to 140 °C partially dissolved **7-26** but led mainly to protodeiodination (Table 7-4, entry 3). A further temperature increase to 180 °C resulted in protodehalogenation of both the iodine and the bromine atoms (Table 7-4, entry 4). The formation of C−C bonds by this procedure was neither detected by MALDI-TOF MS nor by SEC. Alternatively, high boiling solvents, such as dimethylsulfoxide and *N,N*-dimethylformamide, did not affect the outcome of the reaction (Table 7-4, entry 5 and 6). Expectedly, nonactivated Cu^0 did not show any superiority over activated copper (Table 7-4, entry 7). An alternative pathway for enhancing sterically demanding *Ullmann*-type homocouplings involved copper(I) iodide in combination with L-proline and potassium carbonate.[85] Utilizing this procedure for the polymerization of **7-26**, however, showed only partial protodehalogenation (Table 7-4, entry 8). Unfortunately, other cross-coupling procedures, such as the *Suzuki-Miyaura* and the *Yamamoto* reaction, provided no feasible alternative owing to the poor solubility of **7-26** in typical *Suzuki-Miyaura* solvents, *e.g.*, toluene and tetrahydrofuran together with its sensitivity to transition metals. Solid-state polymerization, however, could help to overcome these drawbacks in the future and might enable a selective activation of the iodine and bromine functionalities upon controlled heating.

Due to the fact that the targeted polymer **7-44** was so far not accessible *via* conventional solution-based methods, its polymerization and the subsequent two dimensional expansion was aimed *via* the already described surface-assisted *Ullmann* protocol (see above).

7.5.2 Surface-Assisted Polymerization and Expansion of 7-26

In contrast to the surface-assisted polymerization of **7-17**, 2,3,6,7-tetrabromo-1,4,5,8-tetraiodobiphenylene (**7-26**) possesses two different halogen functionalities thus allowing for a sequential activation. Hence, the specific bond dissociation energy and activation temperature should be adjustable *via* the type of halogen atom.[86]

Although the molecular weight of **7-26** (M = 971.36 g/mol) is higher than in the previous case, UHV sublimation could be realized at a temperature of 250 °C without any degradation. The molecules of **7-26** initially ordered to molecular islands with an apparent height of 2.3 Å on the Au(111) substrate held at room temperature. Subsequent annealing to 100 °C for 20 minutes, resulted in the formation of quasi hexagonal ribbon networks (Figure 7-15), which resemble the structures obtained for 1,4,5,8-tetraiodo-2,3,6,7-tetra-methoxybiphenylene (**7-17**) (see above). Again, bright islands were observed, most probably caused by cleaved iodine and bromine atoms. However, the ribbon-type structures could be moved by the STM tip thus showing that no covalent C−C bonds have been formed. This suggested that adsorption of **7-26** to the Au(111) surface did not result in the efficient generation of radical species, due to an increased bond dissociation energy of the C−I bond.
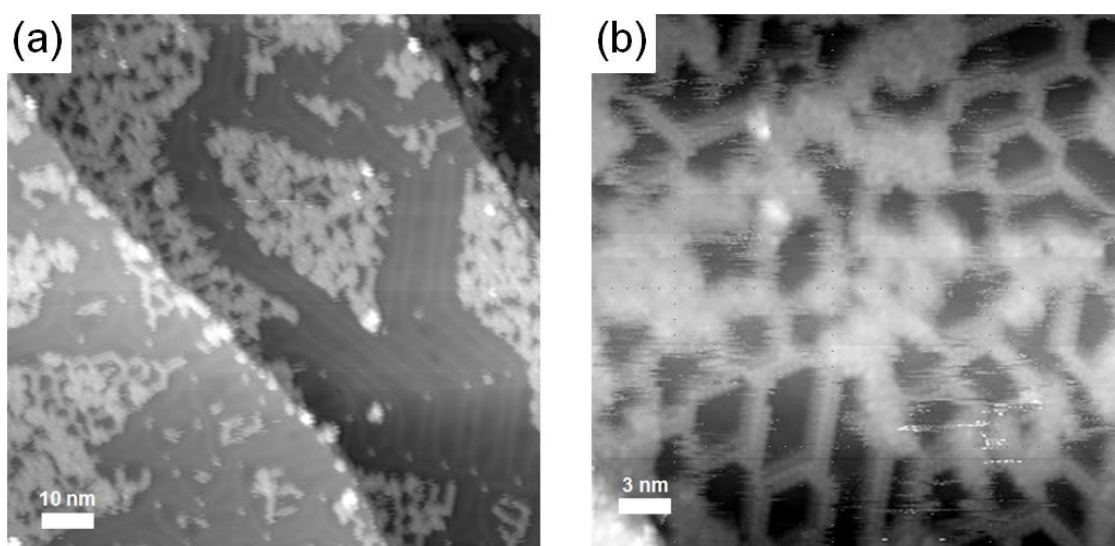
Figure 7-15. (a) STM image of 2,3,6,7-tetrabromo-1,4,5,8-tetraiodobiphenylene (**7-26**) on Au(111) after annealing at 100 °C. (b) Zoom into the lower left corner of (a).

To activate this functionality, the temperature has been further increased to 200 °C. The formation of elongated ribbon-type features was observed with linear sections up to 15 nm. Along these rows consecutive maxima with distances of 4.7 Å were observed, which is slightly longer than the calculated distance of ~4.3 Å (DFT) for the covalently bound biphenylene tetramer **7-43** (Figure 7-11).[67] The row width of 11 Å suggested the presence of bromine atoms at the 2,3,6,7-positions. By performing a line profile analysis with the STM tip these ribbon-type structures could still be moved.

The annealing temperature was therefore further increased to 300 °C. This led, however, to a reduced number of rows and to an extended formation of disordered structures suggesting decomposition of the biphenylene molecules very similar to the results of **7-17** (Figure 7-16 c).
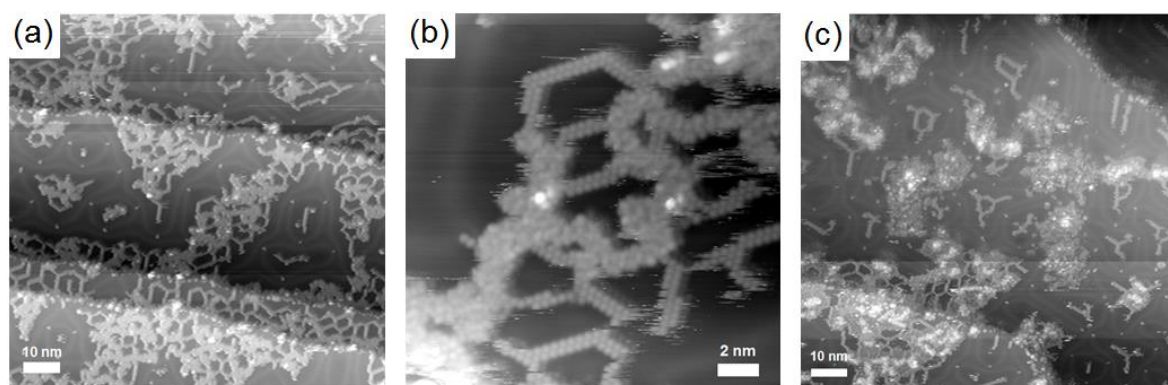
Figure 7-16. (a) STM image after annealing to 200 °C. (b) Zoom into the middle of (a). (c) STM image after annealing to 300 °C.

Although **7-26** is more electron-deficient than **7-17**, the specific bond dissociation energies of the carbon-halogen bonds are still above its decomposition energy. Moreover, the sterically demanding bromine atoms are expected to hinder an efficient C−C bond formation. These aspects prevented so far the formation of isomeric GNRs and their laterally extended analogues by surface-assisted protocols. Nevertheless, the results obtained thus far give motivation to optimize this experimental system within the scope of future studies in the group of ███████████████ (EMPA Dübendorf, Switerland). Also, the improvement of the molecular design by reducing the steric demand at the 2,3,6,7-positions of 1,4,5,8-tetrahalobiphenylenes can be envisaged upon chlorine or even fluorine substitution.

7.6 Octaarylbiphenylenes – Potential Precusors toward Isomeric Nanographenes

7.6.1 Synthesis and Characterization

In recent years, *Müllen* and coworkers developed a synthetically valuable concept for the bottom-up synthesis of PAHs, comprising the formation of a fully soluble oligophenylene precursor which is subsequently planarized by oxidative cyclodehydrogenation to the corresponding PAH.[14, 15, 87-92] Most important, the targeted carbon framework of the PAH is already present in the well-soluble precursor compounds. This allowed for the fabrication of extremely large PAHs with up to 222 carbon atoms, so-called nanographenes, being monodisperse model compounds for graphite.[89]
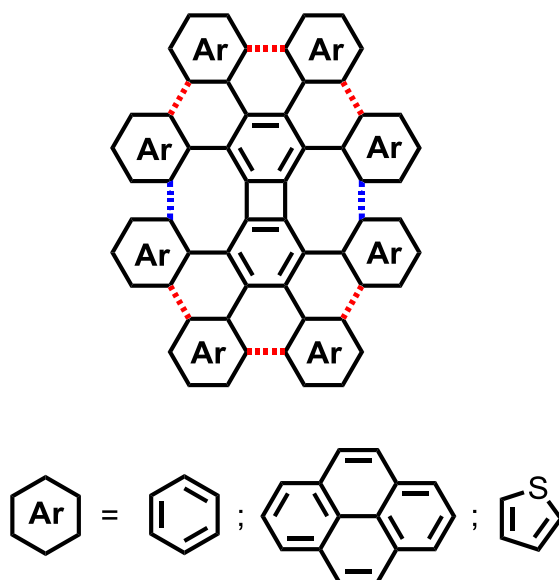
Scheme 7-10. Schematic represenation of octaarylbiphenylenes with different aryl substituents. The crucial bonds for the cyclodehydrogenation toward a [6+4] nanographene are highlighted in red. The fusion of the additional blue bonds will lead to a [8+6+4] nanographene.

Much of the success in this chemistry can be attributed to the formation of strain-free six-membered rings from crowded starting materials. The utilization of this concept for the synthesis of other ring size combinations toward isomeric nanographene molecules, however, has been rarely described.[93] Such defects influence the physical (electronic and thermal conductivity, electronic structure) and chemical (reactivity, activation of adsorbed molecules) properties of graphite.[94, 95] It is well known that structural defects enhance the reaction of molecular oxygen with graphite.[96] Next to the model substances with different peripheral structures the synthesis of specific graphitic segments with selectively introduced defects is of importance to study their influence on the resulting properties.
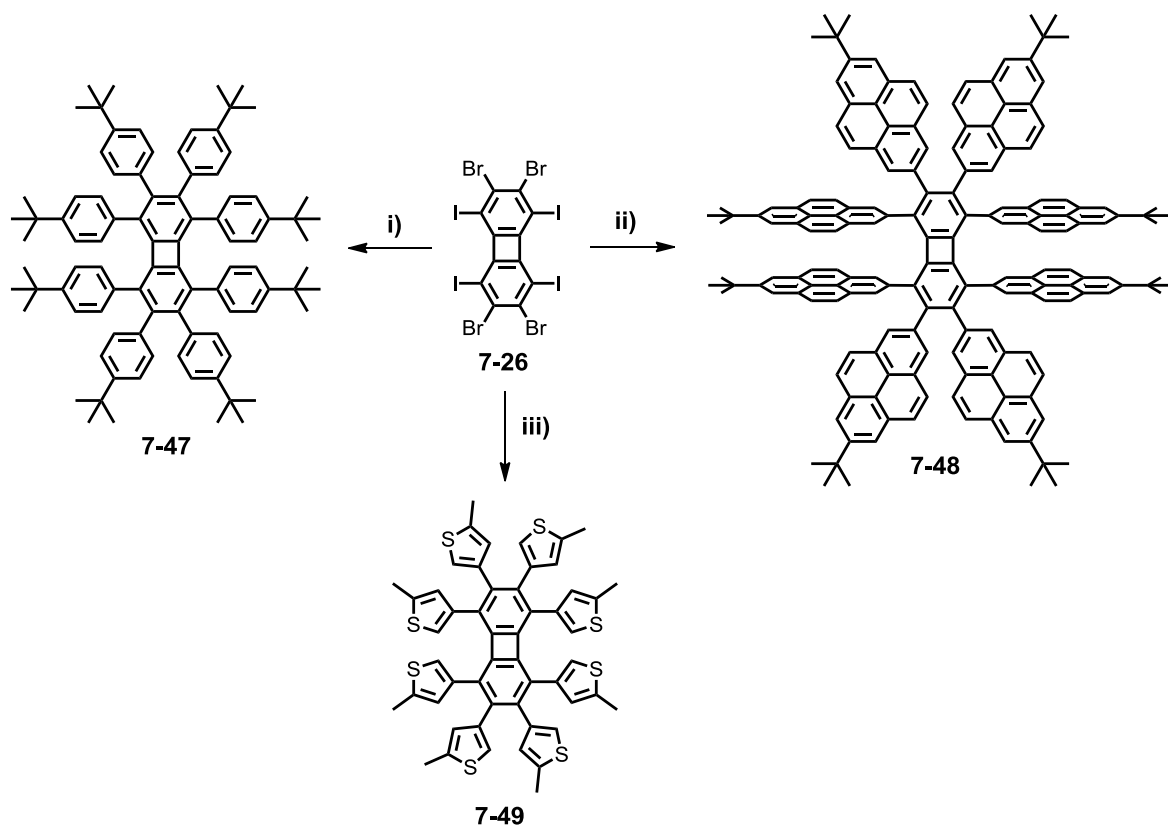
Scheme 7-11. Synthetic route toward octaarylbiphenylenes **7-47**, **7-48** and **7-49**. Conditions: i) (4-(*tert*-butyl)phenyl)boronic acid, Pd(PPh$_3$)$_4$, 2 M aq. K$_2$CO$_3$, toluene, *Aliquat 336*, 115 °C, 4 days, 33%; ii) 2-(7-(*tert*-butyl)pyren-2-yl)-4,4,5,5-tetramethyl-1,3,2-dioxaborolane, Pd(PPh$_3$)$_4$, 2 M aq. K$_2$CO$_3$, toluene, *Aliquat 336*, 115 °C, 24h, 53%; iii) 4,4,5,5-tetramethyl-2-(5-methylthiophen-3-yl)-1,3,2-dioxaborolane, Pd(PPh$_3$)$_4$, 2 M aq. K$_2$CO$_3$, toluene, *Aliquat 336*, 115 °C, 2 days, 70%.

Besides its application as potential monomer for the fabrication of isomeric GNRs (see above), 2,3,6,7-tetrabromo-1,4,5,8-tetraiodobiphenylene (**7-26**) is an interesting building block for the construction of of octaarylbiphenylenes (Scheme 7-10). Due to the central cyclobutadiene moiety, these molecules represent oligophenylene precursors for the formation of PAHs with unprecedented ring size combinations such as six- and four-membered rings. Theoretically, it would be furthermore possible to introduce eight-membered rings between the *ortho*-positions of the aryl moieties at the equatorial positions (Scheme 7-10, blue bonds). In view of the facts above, octaarylbiphenylenes can be considered as isomeric analogues of HPB, which itself is a precursor for HBC.

Precursor molecules **7-47**, **7-48** and **7-49** are easily accessed by a one-step protocol utilizing Pd^0-catalyzed reactions (Scheme 7-11). Once again, the *Suzuki-Miyaura* reaction was chosen for the eightfold cross-coupling because of its broad scope and the toleration of sterically demanding substrates.[97-104] The applied boronic acids and esters were either commercially available or were obtained by simple one-pot reactions.
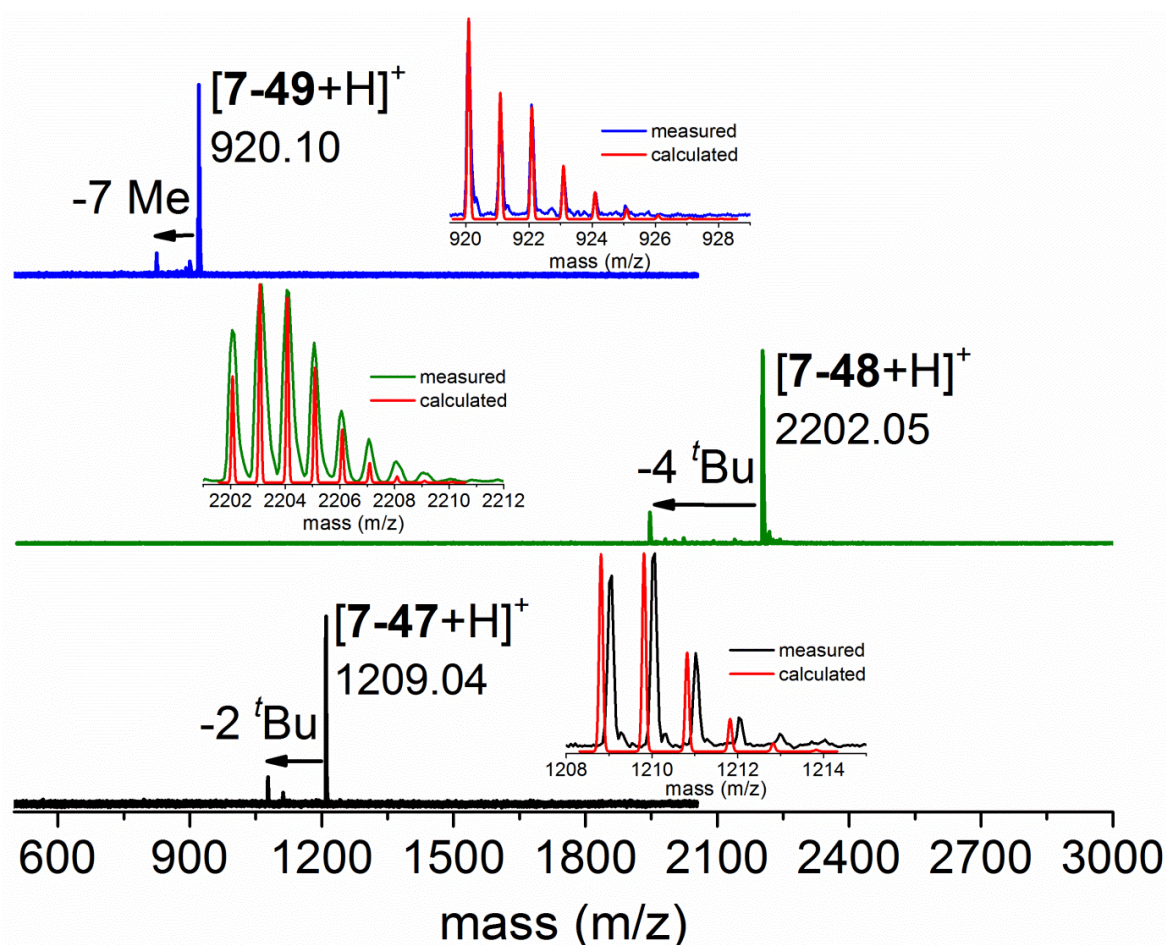
Figure 7-17. MALDI-TOF MS spectra (matrix: TCNQ) of octaarylbiphenylenes **7-47** (black line), **7-48** (green line) and **7-49** (blue line). Inset: Measured and calculated isotopic patterns of **7-47**, **7-48** and **7-49**.

Octaphenylbiphenylene **7-47** was therefore synthesized by utilizing the previously established *Suzuki-Miyaura* protocol for sterically hindered substrates (see Chapter 6). 2,3,6,7-Tetrabromo-1,4,5,8-tetraiodobiphenylene (**7-26**) and (4-(*tert*-butyl)phenyl)boronic acid were reacted with tetrakis(triphenylphosphine)palladium(0) in the presence of solid potassium carbonate and phase transfer catalyst *Aliquat 336* affording **7-47** in 33% yield. The procedure was repeated by using 2-(7-(*tert*-butyl)pyren-2-yl)-4,4,5,5-tetramethyl-1,3,2-dioxaborolane and 4,4,5,5-tetramethyl-2-(5-methylthiophen-3-yl)-1,3,2-dioxaborolane,[105, 106] toward octapyrenylbiphenylene **7-48** and octathienobiphenylene **7-49**. Both reactions showed full conversion after 24 and 48 hours, respectively. Purification of the materials was achieved by column chromatography and subsequent precipitation, thus yielding **7-48** and **7-49** in 53 and 70% yield, respectively. MALDI-TOF MS clearly confirmed the eightfold attachment of the aryl moieties for **7-47**, **7-48**, and **7-49** by virtually single peaks at *m/z* = 1 209, 920 and 2 202, respectively (Figure 7-17). Depending on the applied laser power the partial cleavage of alkyl fragments was observed for all materials.
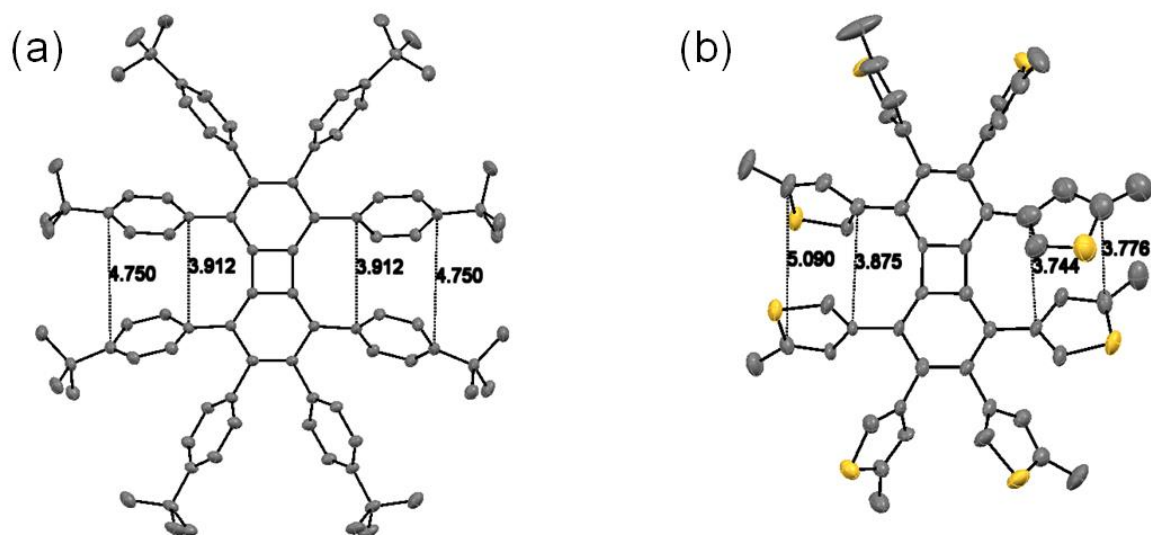
Figure 7-18. X-ray crystal structure of octaphenylbiphenylene **7-47** and octathienobiphenylene **7-49** (sulfur atoms in yellow, carbon atoms in grey, hydrogens omitted for clarity).

As a consequence of the highly twisted aryl moieties, octaarylbiphenylenes **7-47**, **7-48** and **7-49** showed excellent solubility in organic solvents, such as dichloromethane, chloroform and 1,1,2,2-tetrachloroethane. By slow evaporation of a dichloromethane/*n*-hexane solution of **7-47** and **7-49** single crystals were obtained. They were analyzed by X-ray diffraction proving unequivocally the structure of **7-47** and **7-49** (Figure 7-18). Both molecules are characterized by two sets of different external aryl moieties, which are located at the 1,4,5,8- (equatorial) and the 2,3,6,7-positions (axial). Expectedly, they are significantly twisted for both molecules, whereas the biphenylene core remained almost planar. The dihedral angles range from 54.1 to 74.7° and 42.9 to 68.8° for **7-47** and **7-49**, respectively, which is slightly smaller than the average dihedral of the six external phenyls in HPB (~82.5°).[107] In addition, the equatorially located aryl moieties are basically coplanar with distances of 4.33(1) Å and 4.48(3) Å for **7-47** and **7-49**, respectively. In contrast to 2,2',6,6'-tetraphenyl-1,1'-biphenyl **6-9** (3.23(7) Å, see Chapter 6) and [2.2]*para*cyclophanes (~3.09 Å),[108, 109] these values are significantly elongated thus suggesting the absence of through-space π-conjugation.

The large size and amorphous nature of octapyrenylbiphenylene **7-48**, however, did not allow for the growth of single crystals suitable for X-ray diffraction. Nonetheless, ^{1}H NMR spectroscopy proved to successful formation of **7-48** by four sets of aromatic and two sets of aliphatic signals caused by two different types of magnetically non-equivalent pyrene substituents (Figure 7-19). As a result of both a diatropic and a paratropic ring current induced by the biphenylene, the two singlets at 7.69 and 7.68 ppm were assigned to the two protons at the 1-position of the pyrene (H_a and H_d).
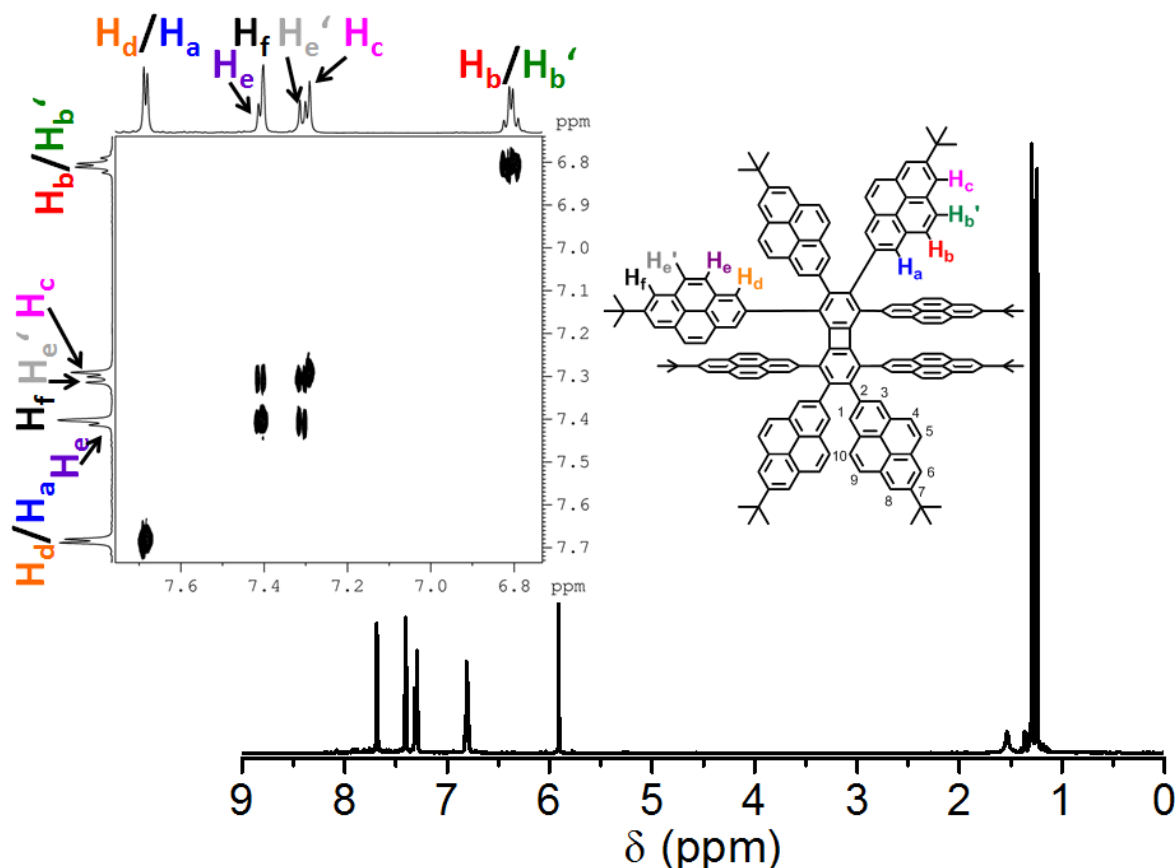
Figure 7-19. ^{1}H NMR spectrum of **7-48** in $C_2D_2Cl_4$ at 25 °C. Inset: Two-dimensional proton correlation (^{1}H, ^{1}H COSY) of **7-48** with proton assignment and pyrene numbering.

The coplanar orientation of the pyrenes at the 1,4,5,8-positions led to a downfield shift of the respective protons thus enabling a distinction to the pyrenes at the equatorial positions. The two singlets at 7.40 and 7.29 ppm could be therefore assigned to the protons at the 8-position of the pyrene in close proximity to the *tert*-butyl group (H_f and H_c). Additionally, the four signals of the two AA'XX' systems were observed at 7.41 and 7.31 ppm as well as at 6.82 and 6.79 ppm, which could be assigned to H_b and H_b' as well as to H_e and H_e', respectively.

7.6.2 Cyclodehydrogenation

With octaarylbiphenylenes **7-47**, **7-48** and **7-49** in hand, the subsequent *intra*molecular cyclodehydrogenation was targeted. The so-called *Scholl* reaction is generally achieved by the reaction of the oligophenylene precursor in the presence of Lewis acids, such as iron(III) chloride or molybdenum(V) chloride.[110-113] Due to the susceptibility of the biphenylene toward transition metals, the utilization of this method for the cyclodehydrogenation of **7-47**, **7-48** and **7-49** was impeded. *Rathore* and coworkers
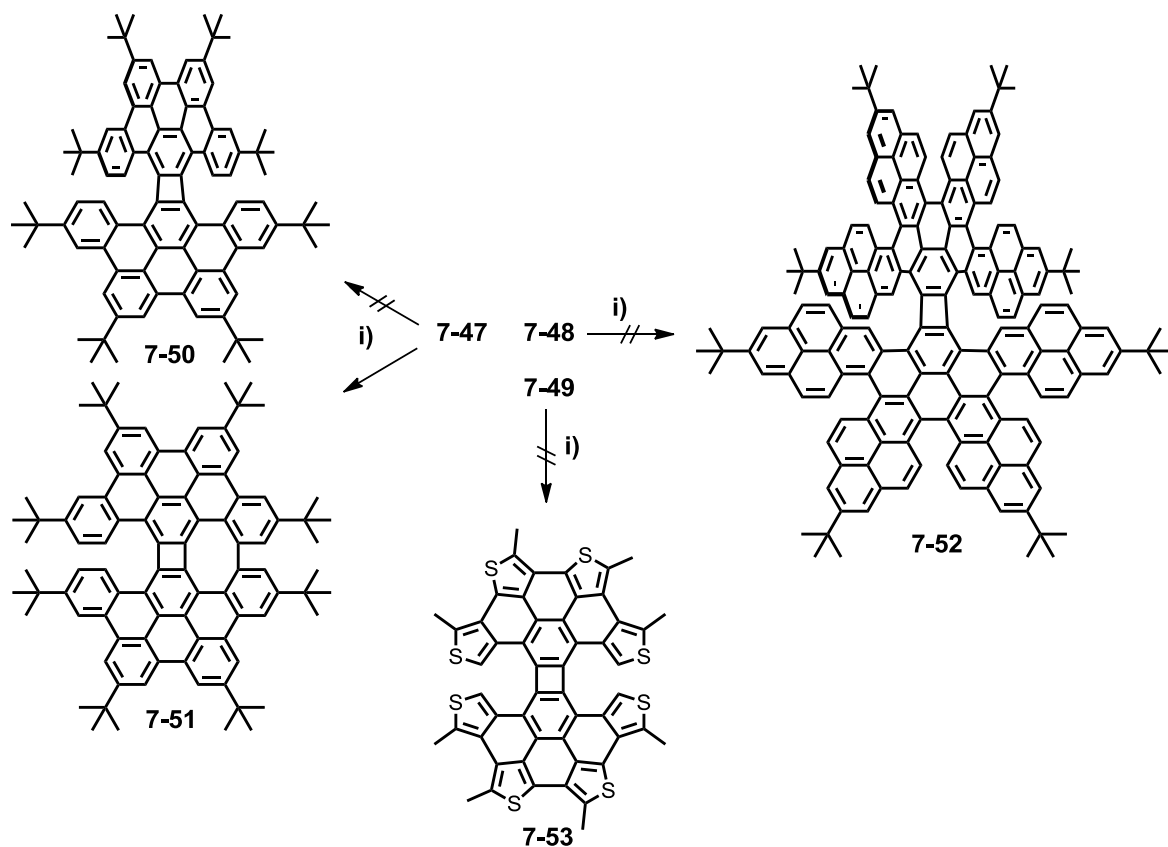
Scheme 7-12. Synthetic route of the oxidative cyclodehydrogenation attempts of octaarlybiphenylenes **7-47**, **7-48** and **7-49**. Conditions: i) DDQ, CH$_3$SO$_3$H, CH$_2$Cl$_2$, 0 °C to RT, 24h, **7-51**: 90%.

showed that dichlorodicyano-*p*-benzoquinone (DDQ) in combination with a (Lewis) acid readily oxidizes a variety of oligophenylenes to HBCs and triphenylenes.[114] This method additionally avoids the formation of chlorinated byproducts, which is frequently observed when using iron(III) chloride or molybdenum(V) chloride.[115] Thus, a 0.01 M solution of octaphenylbiphenylene **7-47** in a 10/1 mixture of dichloromethane and methanesulfonic acid was treated with DDQ at 0 °C (Scheme 7-12). After eight hours reaction time at this temperature, no conversion was observed. Therefore, the reaction mixture was allowed to warm up to room temperature. The subsequent MALDI-TOF MS showed a new peak at $m/z = 1\,219$ and $1\,195$ as well as a minor peak at $m/z = 1\,209$ corresponding to **7-47**. The latter one did not decrease by further extending the reaction times. Aqueous workup with sodium bicarbonate and subsequent precipitation from a dichloromethane/methanol mixture resulted in weakly soluble yellow material. Analyzing the obtained solid by MALDI-TOF MS revealed basically one major peak at $m/z = 1\,218.71$ (Figure 7-20), which was identified as **7-51** being ionized with one sodium cation. Besides the expected cyclodehydrogenation toward **7-50**, the additional formation of one eight-membered ring is therefore very likely. This was further confirmed by a peak at $m/z = 1\,194.75$,
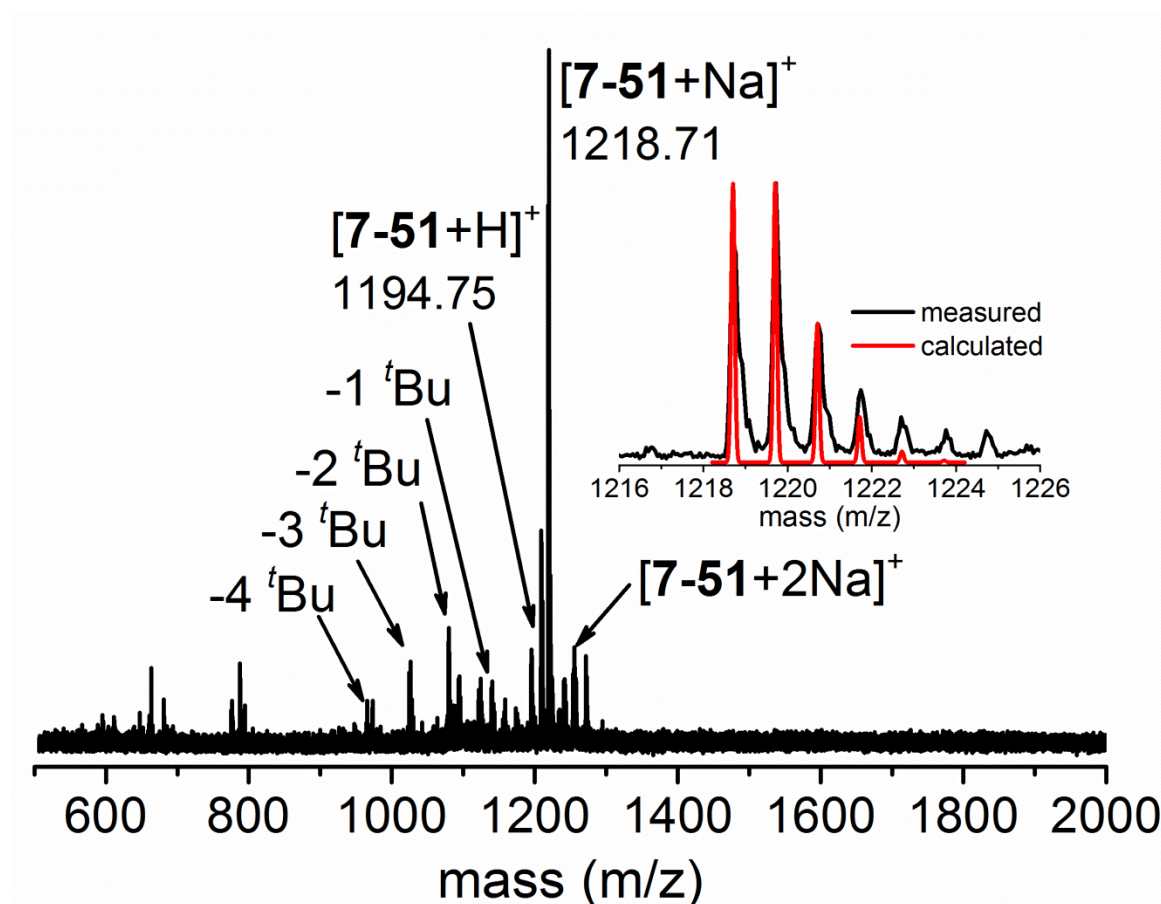
Figure 7-20. MALDI-TOF MS spectra (matrix: TCNQ) of **7-51**. Inset: Measured and calculated isotopic pattern of **7-51**.

corresponding to the $[M+H]^+$ species of **7-51**. Surprisingly, the signal intensity of the $[M+Na]^+$ peak was significantly higher than $[M+H]^+$ peak which was observed for the first time in the presented work. During the ionization process one sodium ion is most probably intercalated inside the "open" equatorial position of **7-51**, thus leading to the preferential formation of the $[M+Na]^+$ species.

Structural analysis of **7-51** by NMR spectroscopy was, however, not possible due to the presence of aggregates in solution. Moreover, the growth of single crystals for X-ray diffraction analysis failed, as a result of the decreased solubility of **7-51** in organic solvents, such as dichloromethane, chloroform, 1,1,2,2-tetrachloroethane and 1,2-dichlorobenzene. Although the structural characterization of **7-51** was limited to mass spectrometry, a highly accurate agreement between the calculated and the measured isotopic pattern ($\Delta m/z = 0.009$) allowed for proposing the structure of **7-51** (Figure 7-20, inset).

DFT geometry optimizations (B3LYP/6-31G*) carried out on the proposed structure of **7-51** revealed a distorted structure caused by the combination of eight-, six- and four-

membered rings in this sheet of carbon atoms, having dimensions of 13×15 Å (Figure 7-21).[67] Four-membered rings embedded in a hexagonal lattice impart planarity, but eight-membered rings introduce so-called "negative curvature".[93, 116, 117] The accumulation of both kinds of even-membered ring defects in **7-51** led to its unique distortion. The central biphenylene moiety is twisted by 16.8° (Figure 7-21 b) which enabled together with the contorted boat conformation of the eight-membered ring a deformation of the molecule. This was expressed by height differences at the edges of 5 and 6 Å, respectively, thus leading to an expanded helicene (Figure 7-21 b and c).
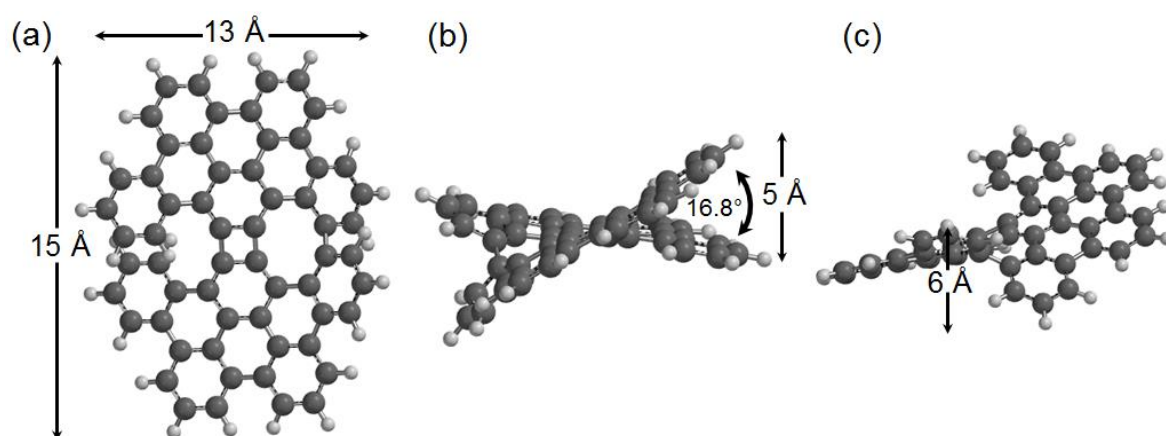
Figure 7-21. Geometry optimized DFT calculation (B3LYP/6-31G*) of **7-51**.[67] (a) Front view with molecule dimensions. (b) Side view indicating the height difference at the "open" side. (c) Side view indicating the height difference at the "closed" side.

The cyclodehydrogenation procedure was subsequently applied for octapyrenylbiphenylene **7-48** (Scheme 7-12). Surprisingly the *Scholl* reaction yielded neither the aimed PAH **7-52** nor any other products. Independent of the amount of used oxidant (<60 equiv.), the reaction did not proceed and only the starting material could be isolated. By increasing the reaction temperature, the results remained essentially the same. The utilization of more reactive Lewis acids, such as scandium(III) trifluoromethanesulfonate,[118] in combination with DDQ was however not applicable due to the coordinative ring opening reaction of transition metals with biphenylene. The reason why the *Scholl* reaction did not proceed is not apparent. It can be thus speculated that the steric repulsion of the pyrene protons at the positions 4,5,9 and 10 do not allow the pyrenes to come into close proximity, which is necessary for a C−C bond formation between the usually very reactive 1- and 3-positions.[119]

Utilizing the same protocol for octathienobiphenylene **7-49** did not allow for the formation of PAH **7-53**. After the addition of DDQ, the solution turned immediately black and a dark

precipitate formed. MALDI-TOF MS analysis of the precipitate revealed a broad distribution with *m/z* up to 1 500 together with the absence of the aimed PAH **7-53** and starting material. This observation suggested polymerization of the **7-49** during the *Scholl* reaction which might occur at β-position of the thiophene substituents.

The described results emphasized the difficulty to predict the outcome of the *Scholl* reaction. An alternative approach might be therefore, the STM controlled surface cyclodehydrogenation which has been demonstrated for the transformation of hexaalkoxy-substituted hexaphenylbenzene to the corresponding HBC and of cyclic oligoarylenes to triangular-shaped nanographene molecules.[120, 121]

7.6.3 Photophysical Properties

Electronic absorption and emission spectroscopy is an important tool in the field of PAH chemistry as it provides a facile insight into the optoelectronic nature of the molecules.[92, 122] According to the original nomenclature of *Clar*, the absorption spectra of PAHs feature typically three main bands which are denoted as *α-*, *β-* and *p*-bands.[123] They originate from S_0 ground state excitations into higher orbitals with their transition probabilities governed by the *Franck-Condon* factors. As a result of the increased level of π-conjugation of the PAHs the absorptions are typically shifted to intermediate and long wavelengths.[92, 122, 123]

UV-vis absorption and emission spectroscopy enabled investigation of the electronic properties of octaarlybiphenylenes **7-47**, **7-48** and **7-49** (Figure 7-22, top and Table 7-5), and allowed for a comparison with PAH **7-51** with a dodecyl-substituted HBC derivative. Octaarlybiphenylenes **7-47**, **7-48** and **7-49** featured two sets of sharp bands between 300 and 320 nm and at 390 nm which indicated the presence of virtually two independent chromophores. The transition at shorter wavelengths was assigned to the individual tetraarylbenzene moieties whereas the transition at the longest wavelength was attributed to the electric dipole-forbidden HOMO-LUMO excitation of biphenylene.[76, 77] As a result of the weak π-conjugation between the tetraarylbenzene moieties through the four-membered ring, similar band gaps (E_g^{opt}) at around 2.9 eV were obtained for all of the materials. The planarization of the aromatic core toward **7-51** resulted in three major significantly broadened transitions (Figure 7-22, bottom). The first two bands were thereby observed at similar wavelengths ($\lambda_{abs} = 299$ and 395 nm) as for precursor **7-47** thus confirming again a reduced communication through the cyclobutadiene moiety. Due to its
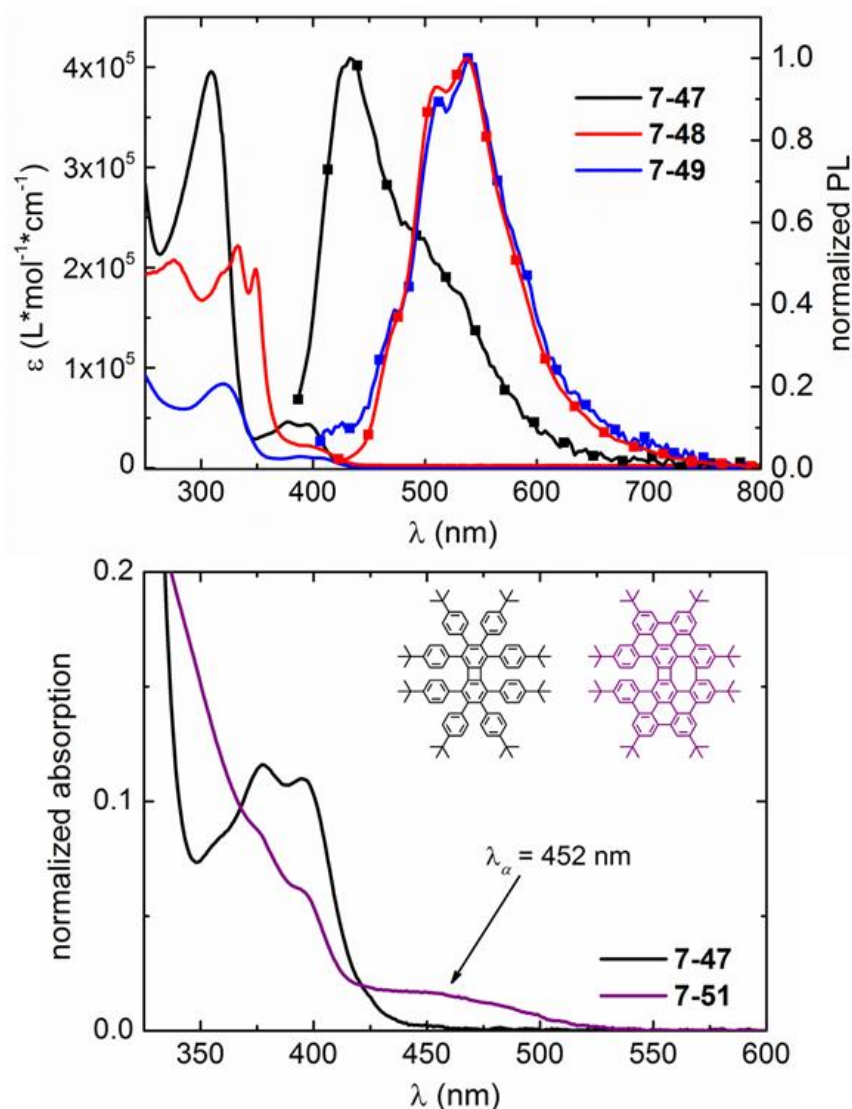
Figure 7-22. Top: UV-vis absorption (solid line) and emission (symbol line) spectra of octaarylbiphenylenes **7-47** (black), **7-48** (red) and 7-**49** (blue). Bottom: Comparison of the normalized UV-vis absorption spectra of octaphenylbiphenylene **7-47** and PAH **7-51**. For all spectra: 1×10^{-6} M in CH_2Cl_2.

Table 7-5. Selected photophysical data of **7-47**, **7-48**, **7-49** and **7-51**.

	$\lambda_{abs,max}$ [a] (nm)	$\lambda_{PL,max}$ [a,b] (nm)	$\varepsilon \times 10^4$ [a,c] (M^{-1} cm^{-1})	Stokes shift (cm^{-1})	E_g^{opt} [d] (eV)
7-47	309, 378, 394	433	4.3	2 290	2.90
7-48	276, 320(s), 333, 349, 393	510(s), 538	2.2	6 860	2.84
7-49	320, 388,	512(s), 538	1.1	7 190	2.84
7-51	299, 395(s), 452	-	-	-	2.74
HBC	362, 392, 465[e]	490[e]	-	1 100[e]	2.66[e]

[a] For all spectra: 10^{-6} M in CH_2Cl_2. [b] Excited at the absorption maxima. [c] Extinction coefficients of the lowest energy absorption band. [d] $E_g^{opt} = h \cdot c / \lambda_{0.1max}$. (s) = shoulder. [e] Values were taken from Ref.[124]

intensity and its lower wavelength in comparison to the other bands of this spectrum, the prominent band at 299 nm is thereby identified as *β*-band according to *Clar`s* classification. It typically arises from a transition involving the HOMO and the second lowest unoccupied orbital (LUMO+1).[123, 124] At an order of magnitude lower a shoulder is detected at 395 nm which corresponds to the *p*-band of the PAH. In accordance with **7-47**, this band can be attributed to the dipole-forbidden HOMO-LUMO excitation of biphenylene. The small signal at 452 nm can be assigned to the α-band which is typically found at longer wavelengths and low intensities. This transition, which is absent for precursor **7-47**, confirmed the increased π-conjugation of **4-51** and thus the formation of one eight-membered ring. Experimentally, the influence of the even-membered ring defects on the optical properties can be seen by comparing the UV-vis absorption data of **7-51** versus that of HBC (Table 7-5).[124] The *α*-band in the spectrum of the planar HBC ($\lambda_{abs} = 465$ nm) is located at a longer wavelength than that of **7-51**. Expectedly, the distorted structure of **7-51** caused a larger HOMO-LUMO distance than for HBC. In contrast to HBC ($\lambda_{PL,max} = 490$ nm), no photoluminescence has been detected for **7-51**. These differences might be a consequence of having combined both eight- and four-membered rings, thus providing insights into the impact of multiple defects in a nanographene molecule.

7.7 Summary

A reliable delivery of chemically defined graphene materials to molecular electronics and material science remains an unsolved challenge. This chapter described various approaches toward the bottom-up synthesis of isomeric GNRs and graphene nanostructures having unique ring-size combinations. This was based on a successful functionalization strategy of the 1,4,5,8-positions of biphenylene. The synthetic strategy toward the biphenylene core relied on an *ortho*-directed silylation of tetrafunctionalized benzenes which was followed by a subsequent lithiation-induced [2+2]-cyclodimerization *via* an aryne intermediate. An optimized deprotective iodination allowed for the successful synthesis of 1,4,5,8-tetraiodo-2,3,6,7-tetraalkoxybiphenylenes **7-17** and **7-18** and 2,3,6,7-tetrabromo-1,4,5,8-tetraiodobiphenylene **7-26**.

The expansion of these A_4-monomers toward "East-West" connected ladder-type polymers was targeted in the following. Due to the combination of eight-, six- and four-membered rings these materials were defined as isomeric GNRs. Due to the susceptibility of the biphenylene toward various transition metal mediated reactions, polymerization of **7-17**

was achieved by application of an alternative *Ullmann* approach. This resulted in the formation of isomeric GNRs with at least 13 to 15 eight-membered rings having linear expansion of up to 9.1 nm. The surface-assisted polymerization, however, indicated that the iodine groups of **7-17** were not sufficiently activated to promote an efficient growth of isomeric GNRs on Au(111).

The electronic properties of isomeric GNRs **7-35**, **7-36**, **7-37** and **7-38** obtained *via* the solution-based approach were governed by the characteristics of biphenylene and hence behaved as large band gap materials. Although the obtained isomeric GNRs were not defect-free, the large band gap could enable their utilization as active material optoelectronic devices. This might allow a switching between the "on" and "off" state in OFETs, which is impeded for semi-metallic graphene.

To laterally expand the GNR structures, 2,3,6,7-tetrabromo-1,4,5,8-tetraiodobiphenylene (**7-26**) was used for the polymerization initially along the "East-West" direction. The fusion of these ribbons would theoretically result in laterally extended, isomeric GNRs. Despite great efforts, the targeted structures could neither be obtained by a solution-based synthesis nor by surface-supported reaction.

For fabrication of isomeric nanongraphenes, octaarylbiphenylenes **7-47**, **7-48** and **7-49** decorated with phenyl, pyrenyl and thieno-substituents were prepared by a *Suzuki-Miyaura* reaction from 2,3,6,7-tetrabromo-1,4,5,8-tetraiodobiphenylene **7-26**. The subsequent oxidative with DDQ and methanesulfonic acid proved to be successful solely in the case of phenyl-substituted **7-47**. The resulting isomeric nanographene **7-51** combined eight-, six- and four-membered rings thus leading to a significant bending. That distortion perturbs the optoelectronic properties in comparison with HBC. The ease, with which this intriguing 18-ring system can be synthesized, highlights the potential of the presented synthetic strategy. The intercalation of alkali metal ions into the equatorial aryls of **7-47**, **7-48** and **7-49** could moreover enable their utilization in the field of Li-ion batteries.

Altogether it has been shown in this chapter, that the developed methods could open new perspectives for carbon-rich π-conjugated materials.

7.8 References

[1]   H. W. Kroto, J. R. Heath, S. C. Obrien, R. F. Curl, R. E. Smalley, *Nature* **1985**, *318*, 162-163.
[2]   S. Iijima, *Nature* **1991**, *354*, 56-58.
[3]   K. S. Novoselov, A. K. Geim, S. V. Morozov, D. Jiang, Y. Zhang, S. V. Dubonos, I. V. Grigorieva, A. A. Firsov, *Science* **2004**, *306*, 666-669.
[4]   G. X. Li, Y. L. Li, H. B. Liu, Y. B. Guo, Y. J. Li, D. B. Zhu, *Chem. Commun.* **2010**, *46*, 3256-3258.
[5]   J. Gibson, M. Holohan, H. L. Riley, *J. Chem. Soc.* **1946**, 456-461.
[6]   R. H. Baughman, C. Cui, *Synth. Met.* **1993**, *55*, 315-320.
[7]   X. F. Shen, D. M. Ho, R. A. Pascal, *Org. Lett.* **2003**, *5*, 369-371.
[8]   X. F. Shen, D. M. Ho, R. A. Pascal, *J. Am. Chem. Soc.* **2004**, *126*, 5798-5805.
[9]   D. Wasserfallen, G. Mattersteig, V. Enkelmann, K. Müllen, *Tetrahedron* **2006**, *62*, 5417-5420.
[10]   D. Türp, T. T. T. Nguyen, M. Baumgarten, K. Müllen, *New J. Chem.* **2012**, *36*, 282-298.
[11]   F. Diederich, Y. Rubin, *Angew. Chem., Int. Ed.* **1992**, *31*, 1101-1123.
[12]   H. R. Karfunkel, T. Dressler, *J. Am. Chem. Soc.* **1992**, *114*, 2285-2288.
[13]   F. Diederich, *Nature* **1994**, *369*, 199-207.
[14]   A. J. Berresheim, M. Müller, K. Müllen, *Chem. Rev.* **1999**, *99*, 1747-1785.
[15]   M. D. Watson, A. Fechtenkötter, K. Müllen, *Chem. Rev.* **2001**, *101*, 1267-1300.
[16]   F. Diederich, M. Kivala, *Adv. Mater.* **2010**, *22*, 803-812.
[17]   A. Hirsch, *Nat. Mater.* **2010**, *9*, 868-871.
[18]   Q. Song, B. Wang, K. Deng, X. L. Feng, M. Wagner, J. D. Gale, K. Müllen, L. J. Zhi, *J. Mater. Chem. C* **2013**, *1*, 38-41.
[19]   B. T. King, *Nat. Chem.* **2013**, *5*, 730-731.
[20]   L. Friedman, D. F. Lindow, *J. Am. Chem. Soc.* **1968**, *90*, 2324-2328.
[21]   L. Mindach, K. Müllen, *Adv. Mater.* **1996**, *8*, 504-507.
[22]   A. Rajca, A. Safronov, S. Rajca, C. R. Ross, J. J. Stezowski, *J. Am. Chem. Soc.* **1996**, *118*, 7272-7279.
[23]   M. Iyoda, S. M. H. Kabir, A. Vorasingha, Y. Kuwatani, M. Yoshida, *Tetrahedron Lett.* **1998**, *39*, 5393-5396.
[24]   S. M. H. Kabir, M. Iyoda, *Synthesis* **2000**, 1839-1842.
[25]   S. M. H. Kabir, M. Hasegawa, Y. Kuwatani, M. Yoshida, H. Matsuyama, M. Iyoda, *J. Chem. Soc., Perkin Trans. 1* **2001**, 159-165.
[26]   B. C. Berris, G. H. Hovakeemian, Y. H. Lai, H. Mestdagh, K. P. C. Vollhardt, *J. Am. Chem. Soc.* **1985**, *107*, 5670-5687.
[27]   H. Schwager, S. Spyroudis, K. P. C. Vollhardt, *J. Organomet. Chem.* **1990**, *382*, 191-200.
[28]   R. H. Schmidtradde, K. P. C. Vollhardt, *J. Am. Chem. Soc.* **1992**, *114*, 9713-9715.
[29]   K. P. C. Vollhardt, *Pure Appl. Chem.* **1993**, *65*, 153-156.
[30]   D. Holmes, S. Kumaraswamy, A. J. Matzger, K. P. C. Vollhardt, *Chem. Eur. J.* **1999**, *5*, 3399-3412.
[31]   M. J. Eichberg, K. N. Houk, J. Lehmann, P. W. Leonard, A. Marker, J. E. Norton, D. Sawicka, K. P. C. Vollhardt, G. D. Whitener, S. Wolff, *Angew. Chem., Int. Ed.* **2007**, *46*, 6894-6898.
[32]   P. I. Dosa, Z. Gu, D. Hager, W. L. Karney, K. P. C. Vollhardt, *Chem. Commun.* **2009**, 1967-1969.
[33]   F. M. Logullo, A. H. Seitz, L. Friedman, *Org. Synth. Coll.* **1973**, *5*, 54-59.
[34]   W. C. Lothrop, *J. Am. Chem. Soc.* **1941**, *63*, 1187-1191.
[35]   J. C. Salfeld, E. Baume, *Tetrahedron Lett.* **1966**, 3365-3367.
[36]   B. C. Berris, Y. H. Lai, K. P. C. Vollhardt, *J. Chem. Soc., Chem. Commun.* **1982**, 953-954.
[37]   P. I. Dosa, G. D. Whitener, K. P. C. Vollhardt, A. D. Bond, S. J. Teat, *Org. Lett.* **2002**, *4*, 2075-2078.
[38]   W. Baker, J. W. Barton, J. F. W. Mcomie, *J. Chem. Soc.* **1958**, 2666-2674.
[39]   H. Kidokoro, M. Sato, S. Ebine, *Bull. Chem. Soc. Jpn.* **1982**, *55*, 3204-3207.
[40]   H. Kidokoro, Y. Saito, M. Sato, S. Ebine, S. Sato, T. Hata, C. Tamura, *Bull. Chem. Soc. Jpn.* **1983**, *56*, 1192-1195.
[41]   M. M. Haley, R. R. Tykwinski, *Carbon-Rich Compounds: From Molecules to Materials*, John Wiley & Sons, Weinheim, **2006**.
[42]   F. Mongin, M. Schlosser, *Tetrahedron Lett.* **1997**, *38*, 1559-1562.
[43]   M. Dabrowski, J. Kubicka, S. Lulinski, J. Serwatowski, *Tetrahedron Lett.* **2005**, *46*, 4175-4178.
[44]   D. Waghray, W. Nulens, W. Dehaen, *Org. Lett.* **2011**, *13*, 5516-5519.
[45]   L. Friedman, F. M. Logullo, *J. Am. Chem. Soc.* **1963**, *85*, 1549-1549.
[46]   P. G. Gassman, H. P. Benecke, *Tetrahedron Lett.* **1969**, 1089-1092.
[47]   M. Jones, R. H. Levin, *J. Am. Chem. Soc.* **1969**, *91*, 6411-6415.
[48]   D. Pérez, D. Peña, E. Guitián, *Eur. J. Org. Chem.* **2013**, 5981-6013.

[49] L. Zöphel, D. Beckmann, V. Enkelmann, D. Chercka, R. Rieger, K. Müllen, *Chem. Commun.* **2011**, *47*, 6960-6962.
[50] L. Zöphel, V. Enkelmann, R. Rieger, K. Müllen, *Org. Lett.* **2011**, *13*, 4506-4509.
[51] L. Zöphel, K. S. Mali, P. S. Reddy, M. Wagner, S. De Feyter, W. Pisula, K. Müllen, *Chem. Eur. J.* **2012**, *18*, 3264-3276.
[52] L. Zöphel, V. Enkelmann, K. Müllen, *Org. Lett.* **2013**, *15*, 804-807.
[53] L. A. Jacob, B. L. Chen, D. Stec, *Synthesis* **1993**, 611-614.
[54] T. Yamamoto, *Prog. Polym. Sci.* **1992**, *17*, 1153-1205.
[55] T. Yamamoto, *Bull. Chem. Soc. Jpn.* **1999**, *72*, 621-638.
[56] T. Kanbara, N. Saito, T. Yamamoto, K. Kubota, *Macromolecules* **1991**, *24*, 5883-5885.
[57] K. Chmil, U. Scherf, *Makromol. Chem., Rapid Commun.* **1993**, *14*, 217-222.
[58] A. C. Grimsdale, K. Müllen, *Adv. Polym. Sci.* **2006**, *199*, 1-82.
[59] R. Beck, S. A. Johnson, *Chem. Commun.* **2011**, *47*, 9233-9235.
[60] T. Ishiyama, M. Murata, N. Miyaura, *J. Org. Chem.* **1995**, *60*, 7508-7510.
[61] F. Ullmann, J. Bielecki, *Ber. Dtsch. Chem. Ges.* **1901**, *34*, 2174-2185.
[62] P. E. Fanta, *Chem. Rev.* **1946**, *38*, 139-196.
[63] P. E. Fanta, *Synthesis* **1974**, 9-21.
[64] J. Hassan, M. Sevignon, C. Gozzi, E. Schulz, M. Lemaire, *Chem. Rev.* **2002**, *102*, 1359-1469.
[65] A. J. Paine, *J. Am. Chem. Soc.* **1987**, *109*, 1496-1502.
[66] A. H. Lewin, M. J. Zovko, W. H. Rosewater, T. Cohen, *Chem. Commun.* **1967**, 80-81.
[67] *Spartan `08, Version 1.2.0*, Wavefunction, Inc., Irvine CA, **2008.**
[68] C. Mapelli, C. Castiglioni, G. Zerbi, *Chem. Phys. Lett.* **1999**, *314*, 189-193.
[69] C. Mapelli, C. Castiglioni, G. Zerbi, K. Müllen, *Phys. Rev. B* **1999**, *60*, 12710-12725.
[70] C. Castiglioni, C. Mapelli, F. Negri, G. Zerbi, *J. Chem. Phys.* **2001**, *114*, 963-974.
[71] M. Rigolio, C. Castiglioni, G. Zerbi, F. Negri, *J. Mol. Struct.* **2001**, *563*, 79-87.
[72] F. Negri, C. Castiglioni, M. Tommasini, G. Zerbi, *J. Phys. Chem. A* **2002**, *106*, 3306-3317.
[73] L. Dössel, L. Gherghel, X. L. Feng, K. Müllen, *Angew. Chem., Int. Ed.* **2011**, *50*, 2540-2543.
[74] A. C. Ferrari, J. C. Meyer, V. Scardaci, C. Casiraghi, M. Lazzeri, F. Mauri, S. Piscanec, D. Jiang, K. S. Novoselov, S. Roth, A. K. Geim, *Phys. Rev. Lett.* **2006**, *97*.
[75] M. G. Schwab, A. Narita, Y. Hernandez, T. Balandina, K. S. Mali, S. De Feyter, X. L. Feng, K. Müllen, *J. Am. Chem. Soc.* **2012**, *134*, 18169-18172.
[76] E. P. Carr, L. W. Pickett, D. Voris, *J. Am. Chem. Soc.* **1941**, *63*, 3231-3232.
[77] R. Hochstrasser, *Can. J. Chem.* **1961**, *39*, 765-772.
[78] T. Hoshi, H. Yamamoto, T. Miyauchi, S. Mori, M. Kobayashi, Y. Tanizaki, *Ber. Bunsen-Ges. Phys. Chem.* **1982**, *86*, 330-335.
[79] J. M. Cai, P. Ruffieux, R. Jaafar, M. Bieri, T. Braun, S. Blankenburg, M. Muoth, A. P. Seitsonen, M. Saleh, X. L. Feng, K. Müllen, R. Fasel, *Nature* **2010**, *466*, 470-473.
[80] C. Bronner, S. Stremlau, M. Gille, F. Brausse, A. Haase, S. Hecht, P. Tegeder, *Angew. Chem., Int. Ed.* **2013**, *52*, 4422-4425.
[81] L. Talirz, H. Sode, J. M. Cai, P. Ruffieux, S. Blankenburg, R. Jafaar, R. Berger, X. Feng, K. Müllen, D. Passerone, R. Fasel, C. A. Pignedoli, *J. Am. Chem. Soc.* **2013**, *135*, 2060-2063.
[82] Z. H. Chen, Y. M. Lin, M. J. Rooks, P. Avouris, *Physica E* **2007**, *40*, 228-232.
[83] M. Y. Han, B. Özyilmaz, Y. B. Zhang, P. Kim, *Phys. Rev. Lett.* **2007**, *98*.
[84] F. Schwierz, *Nat. Nanotechnol.* **2010**, *5*, 487-496.
[85] H. L. Qian, Z. H. Wang, W. Yue, D. B. Zhu, *J. Am. Chem. Soc.* **2007**, *129*, 10664-+.
[86] L. Lafferentz, V. Eberhardt, C. Dri, C. Africh, G. Comelli, F. Esch, S. Hecht, L. Grill, *Nat. Chem.* **2012**, *4*, 215-220.
[87] V. S. Iyer, M. Wehmeier, J. D. Brand, M. A. Keegstra, K. Müllen, *Angew. Chem., Int. Ed.* **1997**, *36*, 1604-1607.
[88] V. S. Iyer, K. Yoshimura, V. Enkelmann, R. Epsch, J. P. Rabe, K. Müllen, *Angew. Chem., Int. Ed.* **1998**, *37*, 2696-2699.
[89] C. D. Simpson, J. D. Brand, A. J. Berresheim, L. Przybilla, H. J. Räder, K. Müllen, *Chem. Eur. J.* **2002**, *8*, 1424-1429.
[90] B. Schmaltz, T. Weil, K. Müllen, *Adv. Mater.* **2009**, *21*, 1067-1078.
[91] C. Li, M. Y. Liu, N. G. Pschirer, M. Baumgarten, K. Müllen, *Chem. Rev.* **2010**, *110*, 6817-6855.
[92] R. Rieger, K. Müllen, *J. Phys. Org. Chem.* **2010**, *23*, 315-325.
[93] K. Kawasumi, Q. Zhang, Y. Segawa, L. T. Scott, K. Itami, *Nat. Chem.* **2013**, *5*, 739-744.
[94] F. Atamny, A. Baiker, R. Schlogl, *Fresen. J. Anal. Chem.* **1997**, *358*, 344-348.
[95] J. Osing, I. V. Shvets, *Surf. Sci.* **1998**, *417*, 145-150.
[96] B. Henschke, H. Schubert, J. Blocker, F. Atamny, R. Schlogl, *Thermochim. Acta* **1994**, *234*, 53-83.
[97] H. Chaumeil, S. Signorella, C. Le Drian, *Tetrahedron* **2000**, *56*, 9655-9662.

[98]   J. J. Yin, M. P. Rainka, X. X. Zhang, S. L. Buchwald, *J. Am. Chem. Soc.* **2002**, *124*, 1162-1163.
[99]   G. Altenhoff, R. Goddard, C. W. Lehmann, F. Glorius, *Angew. Chem., Int. Ed.* **2003**, *42*, 3690-3693.
[100]   G. Altenhoff, R. Goddard, C. W. Lehmann, F. Glorius, *J. Am. Chem. Soc.* **2004**, *126*, 15195-15201.
[101]   S. D. Walker, T. E. Barder, J. R. Martinelli, S. L. Buchwald, *Angew. Chem., Int. Ed.* **2004**, *43*, 1871-1876.
[102]   T. E. Barder, S. D. Walker, J. R. Martinelli, S. L. Buchwald, *J. Am. Chem. Soc.* **2005**, *127*, 4685-4696.
[103]   K. L. Billingsley, T. E. Barder, S. L. Buchwald, *Angew. Chem., Int. Ed.* **2007**, *46*, 5359-5363.
[104]   X. Y. Yang, X. Dou, K. Müllen, *Chem. Asian J.* **2008**, *3*, 759-766.
[105]   T. M. Figueira-Duarte, S. C. Simon, M. Wagner, S. I. Drtezhinin, K. A. Zachariasse, K. Müllen, *Angew. Chem., Int. Ed.* **2008**, *47*, 10175-10178.
[106]   L. H. Wang, J. Y. Li, X. L. Cui, Y. S. Wu, Z. W. Zhu, Y. J. Wu, *Adv. Synth. Catal.* **2010**, *352*, 2002-2010.
[107]   J. C. J. Bart, *Acta Crystallogr. B* **1968**, *B 24*, 1277-1287.
[108]   C. J. Brown, A. C. Farthing, *Nature* **1949**, *164*, 915-916.
[109]   D. J. A. De Ridder, K. Goubitz, M. Fontijn, P. Capkova, E. Dova, H. Schenk, *Acta Crystallogr. B* **2001**, *57*, 780-790.
[110]   R. Scholl, C. Seer, R. Weitzenbock, *Ber. Dtsch. Chem. Ges.* **1910**, *43*, 2202-2209.
[111]   R. Scholl, C. Seer, *Ber. Dtsch. Chem. Ges.* **1911**, *44*, 1233-1240.
[112]   R. Scholl, C. Seer, *Liebigs Ann. Chem.* **1912**, *394*, 111-177.
[113]   B. T. King, J. Kroulik, C. R. Robertson, P. Rempala, C. L. Hilton, J. D. Korinek, L. M. Gortari, *J. Org. Chem.* **2007**, *72*, 2279-2288.
[114]   L. Y. Zhai, R. Shukla, R. Rathore, *Org. Lett.* **2009**, *11*, 3474-3477.
[115]   P. Rempala, J. Kroulik, B. T. King, *J. Am. Chem. Soc.* **2004**, *126*, 15002-15003.
[116]   M. Fujita, M. Yoshida, E. Osawa, *Fullerene Sci. Technol.* **1995**, *3*, 93-105.
[117]   R. B. King, *J. Phys. Chem.* **1996**, *100*, 15096-15104.
[118]   Y. Li, Z. H. Wang, *Org. Lett.* **2009**, *11*, 1385-1387.
[119]   T. M. Figueira-Duarte, K. Müllen, *Chem. Rev.* **2011**, *111*, 7260-7314.
[120]   K. Weiss, G. Beernink, F. Dötz, A. Birkner, K. Müllen, C. H. Woll, *Angew. Chem., Int. Ed.* **1999**, *38*, 3748-3752.
[121]   M. Treier, C. A. Pignedoli, T. Laino, R. Rieger, K. Müllen, D. Passerone, R. Fasel, *Nat. Chem.* **2011**, *3*, 61-67.
[122]   M. G. Schwab, Ph.D. thesis, Johannes Gutenberg-University Mainz **2011**.
[123]   E. Clar, *The Aromatic Sextet*, John Wiley & Sons, London, **1972**.
[124]   M. Kastler, J. Schmidt, W. Pisula, D. Sebastiani, K. Müllen, *J. Am. Chem. Soc.* **2006**, *128*, 9526-9534.

8 Conclusion and Outlook

In the course of this work, various synthetic protocols and functionalization strategies of *N*-heterotriangulene, 2,2',6,6'-tetraphenyl-1,1'-biphenyl and biphenylene were described, which enabled the preparation of new benzene-based π-conjugated materials. In order to tailor the application-relevant properties, the main objective was the synthesis of different architectures with varying dimensionality such as linear and hyperbranched polymers, macrocycles and small molecules. This should provide a deeper understanding how structural variations influence the electronic characteristics and hence the device performance of the materials. Each chapter of this work addressed thereby different research objectives having benzene-rich materials as the central element.

Within the scope of Chapter 3, a facile functionalization strategy of the *N*-heterotriangulene for the preparation of an *AA*- and *A₂B*-monomer has been developed. The substitution pattern of the monomers controlled thereby the geometry of the resulting polymers, providing linear and hyperbranched structures. Two distinct polycondensation procedures based on the *Yamamoto* and *Suzuki-Miyaura* reaction have been successfully applied to build up the linear (**P1**) and the hyperbranched (**P2**) *N*-heterotriangulene polymers (Figure 8-1).
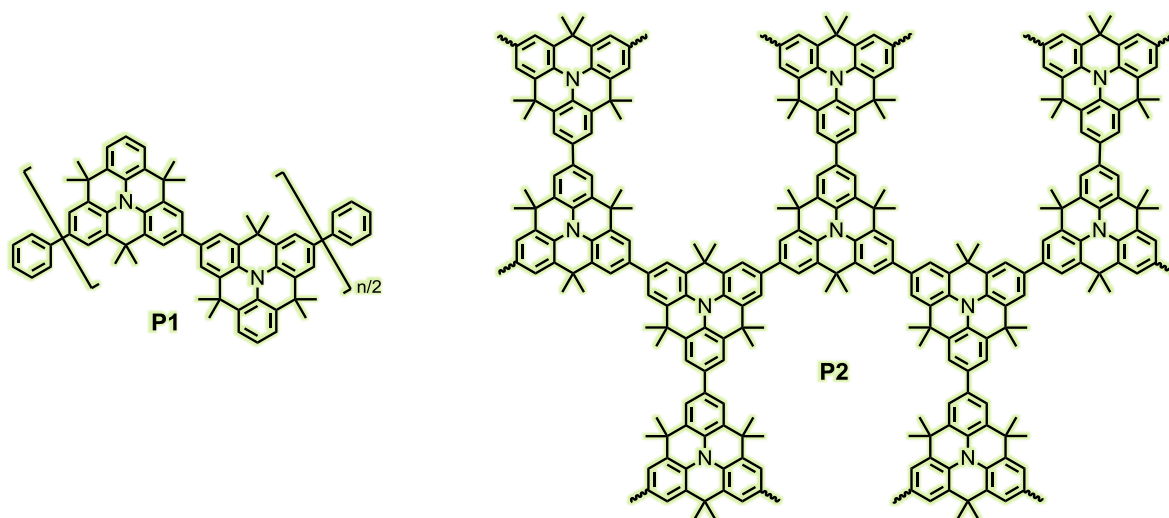
Figure 8-1. Chemical Structures of *N*-heterotriangulene polymers **P1** and **P2** (Chapter 3).

Both materials have been investigated in BG/BC OFETs. By optimization of the electrode- and dielectric-polymer interfaces, a charge carrier mobility of 4.2×10^{-3} cm^2 V^{-1} s^{-1} and an on/off current ratio of ~10^5 was obtained for **P1**. The linear geometry of **P1** represents a compromise between a good solubility and an efficient charge transport among the

individual polymer chains. Besides its promising pH-sensing ability **P1** showed an excellent stability over months compared to commonly used P3HT. The hyperbranched structure resulted, however, in a decreased solubility of **P2** in organic solvents and therefore in the formation of inhomogeneous films. Thus, a significantly lower charge carrier mobility ($\mu_{sat} = 5 \times 10^{-5}$ cm^2 V^{-1} s^{-1}) was observed for **P2** in BG/BC OFETs compared with the linear analogue **P1**. The studies presented in this chapter, highlighted the structural impact of the active material on the device performance. The linear arrangement increased the solubility and the *inter*chain transport; the hyperbranched arrangement reduced the solubility which hampered the device fabrication.

By using the C_3-symmetric shape of the *N*-heterotriangulene and applying the previously developed functionalization strategy, Chapter 4 focused on the fabrication of a π-conjugated *N*-heterotriangulene macrocycle **4-2** (Figure 8-2), combining features of both linear and hyperbranched structures. Initially, a solution-based and surface-mediated one-step synthesis starting from the same precursor was compared. Although the precursor was characterized by an ideal 120 ° angle between the functional groups, the direct cyclohexamerization in solution afforded mainly linear oligomers. Through the reduction
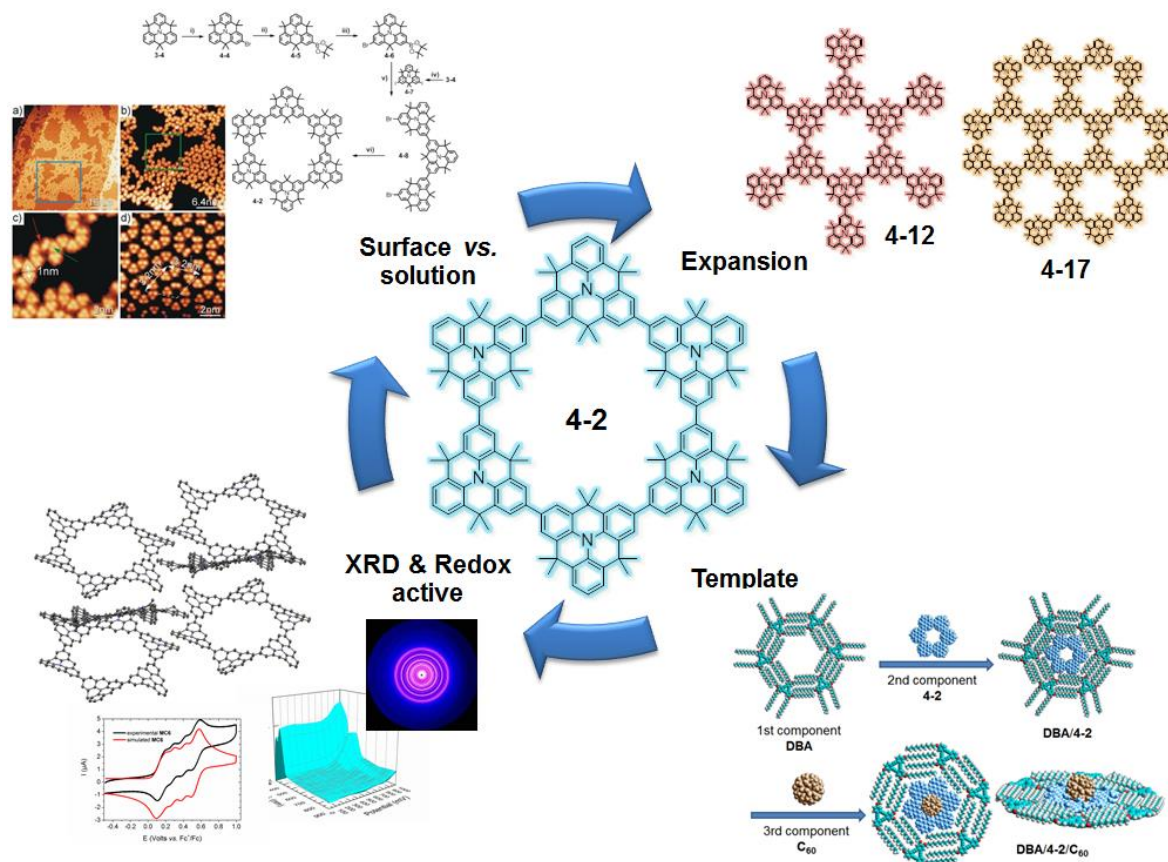
Figure 8-2. Overview of the most striking features of the *N*-heterotriangulene macrocycle **4-2** (Chapter 4).

of conformational and positional degrees of freedom, the surface-assisted synthesis based on an *Ullmann* coupling on Ag(111) facilitated greatly the formation of **4-2** thus proving the superiority of the surface chemistry toward the synthesis of sophisticated two-dimensional structures. However, a few criteria have to be fulfilled to improve the applicability of this method for an industrial application in organic electronics: (1) the fabrication process has to be scaled up to provide macroscopic quantities, (2) it has to be run under ambient conditions, to avoid the need for UHV, (3) it has work on non-metallic surfaces, such as SiO_2, TiO_2 or graphene. By reducing the total number of cyclization steps, macroscopic quantities of **4-2** have been prepared in a multistep synthesis based on a *Yamamoto* cyclodimerization in the final step. In combination with the *AA*-polymerization discussed in the first part, the cyclization highlights the enormous synthetic flexibility of the Ni^0-mediated *Yamamoto* protocol. Macrocycle **4-2** was successfully expanded toward **4-12** and **4-17** mimicking monodisperse fractions of hyperbranched polymer **P2**. These compounds were characterized in terms of their photophysical and electronic properties thus proving a reasonable redox stability together with a HOMO level of **4-2** close to the work function of metallic gold ($\varphi = -5.1$ eV) (Figure 8-2). These results reflect once more the great impact of comparably small structural modifications on the electronic characteristics of the materials. In addition, the cavity of **4-2** offered an efficient accommodation for guest species, such as fullerenes, toward the formation of three-component supramolecular architectures. Altogether it has been shown, that the interplay of photophysical and electronic properties together with the thermal stability makes *N*-heterotriangulene macrocycle **4-2** not only to an appealing candidate for potential hole-transport applications in organic electronics but moreover to a versatile precursor for the fabrication of sophisticated structures.

Based on their electron-rich nature and redox stability, *N*-heterotriangulenes have been applied in Chapter 5 as alternative HTMs for the fabrication of sDSSCs, to replace commonly used spiro-MeOTAD. The efforts aimed at an efficient synthesis of *N*-heterotriangulenes with increased electron-donating ability and extended π-conjugation length and their utilization as HTMs in sDSSCs (Figure 8-3). With increasing π-conjugation the solar cell performance and the long-term stability was significantly improved. While the cells based on di- and trimethoxy-substituted small molecules **5-1** and **5-3** and dimer **5-4** revealed respectable I_{SC} values together with moderate stabilities, a significant increase in the output characteristics was obtained for linear nonamer **4-9** with
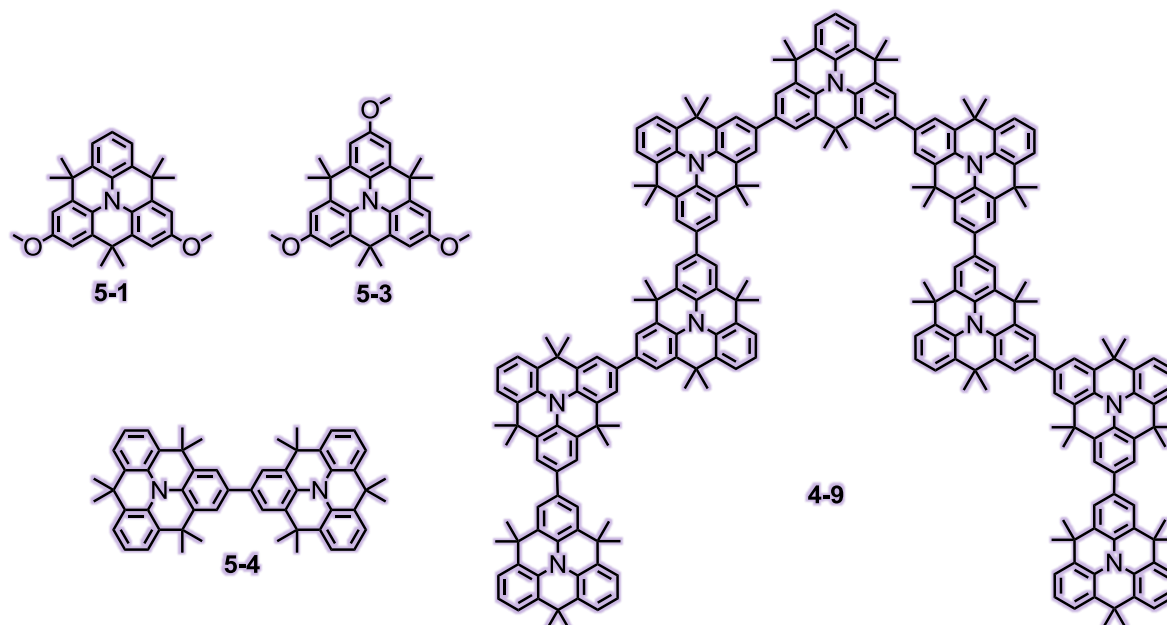
Figure 8-3. Chemical structures of the *N*-heterotriangulene based HTMs tested in sDSSCs (Chapter 5).

PCEs of up to 2.8%. This remarkable efficiency was accompanied by an excellent thermal stability. Already after 5 days of operation, the cells based on **4-9** as HTM showed superior efficiencies and relatively stable individual photovoltaic characteristics compared to the spiro-MeOTAD reference cell. These parameters remained constant for at least 19 days at elevated temperatures. With respect to the OFET studies of Chapter 3, the sDSSCs results illustrate the exceptional stability of *N*-heterotriangulene architectures gained upon extension of the π-conjugation. These exciting initial results, represent a great opportunity to design further *N*-heterotriangulene-based HTMs with enhanced conductivity, charge carrier mobility and the stability. Star-shaped or even dendritic geometries might be particularly promising possibilities to achieve this goal. Upon blocking possible radical migration pathways by substitution of the activated *para*-positions with different functionalities could moreover help to enlighten the prerequisites of the very stable hole transport.

Besides hole-transport applications, benzene-based semiconductors, such as PPPs, are attractive candidates for the use as emissive materials in OLEDs. Thus, the focus shifted toward sterically encumbered 2,2',6,6'-tetraphenyl-1,1'-biphenyl as central element in Chapter 6. The yield of its synthesis was initially improved by of one order of magnitude compared with literature protocols. The key step, of the efficient three-step sequence was a four-fold *Suzuki-Miyaura* coupling to attach the peripheral phenyls moieties. Adapting this procedure for the synthesis of monomer **6-24** allowed for subsequent linear
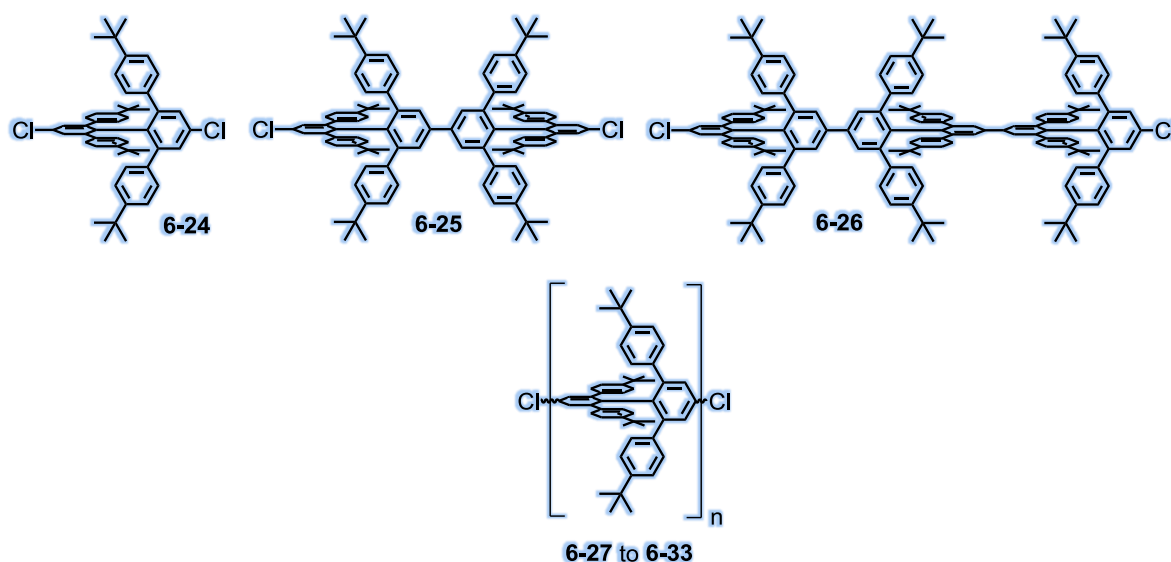
Figure 8-4. Chemical structures of 2,2',6,6'-tetraphenyl-1,1'-biphenyl based oligomers and polymers (Chapter 6).

polymerization, providing a new class of π-congested PPPs (Figure 8-4). Again, the Ni^0-mediated *Yamamoto* reaction played a key role. Surprisingly, a significantly increased effective conjugation length and pronounced bathochromic shifts were revealed by comparing the photophysical and electronic properties of **6-24** to **6-33** with classical OPPs and PPPs. Despite the large mutual twist in the biphenyl core, the emission properties of the π-congested structures were in the ideal range for pure blue luminescence thus holding promise for future application in OLEDs. The studies presented in this chapter, provide important guidelines to understand and control π-conjugation effects and hence the photophysical properties in different PPP-type structures, which might direct future developments in this field. Moreover, various strategies have been pursued to approach three-dimensional cubic graphite substructures by further increasing the phenyl density in 2,2',6,6'-tetraphenyl-1,1'-biphenyl and attempting the formation of bis-cyclooctatetraphenylene. Despite of extensive synthetic efforts, none of the targeted structures could be obtained. In the course of these attempts, however, an alternative synthesis toward HPBs was developed, which provides access to unsymmetric HBCs.

In the last section, the possibility to construct two-dimensional isomeric graphene structures with combinations of eight-, six- and four-membered rings was studied. The fundamental basis was therefore the successful functionalization of the 1,4,5,8-positions of biphenylene. An *ortho*-lithiation with subsequent silylation of 1,2,4,5-functionalized benzenes followed by a base-induced [2+2]-cyclodimerization *via* an aryne intermediate and the deprotective iodination were the key steps in the synthetic sequence toward
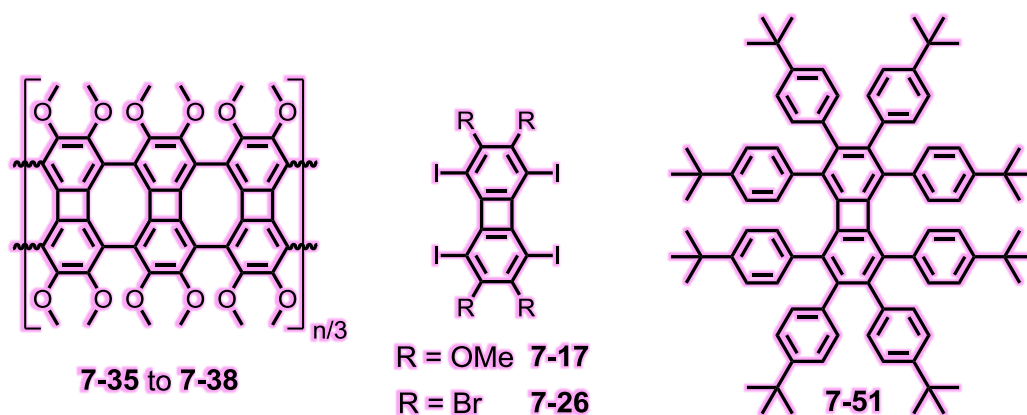
Figure 8-5. Chemical structures of isomeric GNR structure and octaarylbiphenylenes based on tetrafunctionalized biphenylenes.

1,4,5,8- and perfunctionalized biphenylenes. The *Ullmann*-type polymerization of A_4-monomer 1,4,5,8-tetraiodo-2,3,6,7-tetramethoxybiphenylene (**7-17**) provided in solution isomeric GNRs **7-35** to **7-38** with at least 13 to 15 eight-membered rings having linear expansion of up to 9.1 nm (Figure 8-5). Visualization of the obtained ribbon structures by STM can provide more precise information about the nature and amount of defects. A solution-based polymerization of **7-17** in the presence of templates, such as single-layer graphene or hexagonal metal surfaces, could help in the future to decrease the defects by reducing the conformational degrees of freedom. Investigation of the photophysical properties, however, confirmed the anticipated large band gap character of isomeric GNRs **7-35** to **7-38**. This could enable a switching between the "on" and "off" state in optoelectronic applications, such as OFETs, which is impeded for semi-metallic graphene. Moreover, several pathways were pursued for the solution-based polymerization of 2,3,6,7-tetrabromo-1,4,5,8-tetraiodobiphenylene **7-26** and the subsequent "North-South" expansion. As a consequence of its decreased solubility in organic solvents, all attempts failed to achieve laterally extended isomeric GNRs through this method. Solid-state polymerization could help to overcome the limitations of solution-based chemistry by enabling a selective activation of the iodine and bromine functionalities upon controlled heating. Unfortunately, the STM-controlled surface polymerization of both monomers was unsuccessful. This highlighted again the importance of sufficiently reactive and sterically accessible functional groups to promote an efficient *Ullmann*-type C−C coupling on the surface. Further weakening of the C−X bond through the attachment of small acceptor groups, such as cyano- or trifluoromethyl-groups could help to solve these issues. 2,3,6,7-Tetrabromo-1,4,5,8-tetraiodobiphenylene (**7-26**) was successfully applied for the synthesis of different octaarylbiphenylene species. The subsequent oxidative cyclodehydrogenation

proved to be successful soley for octaphenyl-substituted **7-47** under the applied conditions. The resulting isomeric nanographene **7-51** combined eight-, six- and four-membered rings leading to a significant bending which significantly altered the photophysical properties in comparison with HBC. As shown in the first three chapters, the incorporation of heteroatoms, such as nitrogen or sulfur, greatly influences semiconductor properties. Thus, the oxidative cyclodehydrogenation of octathienobiphenylene **7-49** or the utilization of nitrogen or sulfur containing biphenylene monomers could lead to selectively doped isomeric graphene nanostructures with a well-defined number of exactly located heteroatoms. Combining the dynamic features of supramolecular chemistry with the beneficial aspects of the herein reported molecular architectures by the aid of dynamic covalent chemistry could enable further synthetic improvements of the described isomeric GNRs as well as the hyperbranched *N*-heterotriangulene frameworks **P2** and **4-2** (Chapter 3 and 4).

In summary, next to the synthesis of new materials holding promise for organic electronics, new concepts have been developed which allow, *e.g.*, for a simple functionalization of *N*-heterotriangulene, 2,2',6,6'-tetraphenyl-1,1'-biphenyl and biphenylene at its 1,4,5,8-positions. These strategies provide access toward great structural diversity. Together with the extensive interdisciplinary studies of the newly prepared molecular architectures, this mark one more step forward on the way to a precise structure-property relationship.

9 Experimental Part

9.1 General Methods

Chemicals and Solvents

All used chemicals and solvents were obtained from the companies ABCR, Acros Organics, Alpha-Aesar, Bio-Rad Laboratories Inc., Fluka, Merck, Sigma-Aldrich, Strem Chemicals and TCI Europe. Unless otherwise mentioned, they were used as received without further purification.

Chromatography

Preparative column chromatography was performed on silica gel from Merck with a grain size of 63−200 μm (silica gel) or 40−63 μm (flash silica gel). For analytical thin layer chromatography (TLC), silica gel coated substrates "60 F_{254}" from Merck were used. Compounds were detected by fluorescence quenching at 254 nm or self-fluorescence at 366 nm. For eluents, analytically pure solvents (p.a. or technical grade) were used.

Inert Atmosphere

Oxygen- or moisture-sensitive reactions were carried out under argon atmosphere (grade 4.8, Westfalen AG). Reactions were degassed by purging a stream of argon through the reaction mixture.

Microwave-assisted Reactions

Some reactions were performed in a microwave oven (CEM GmbH, Kamp-Lintfort, Germany, model: Discover) using the maximum power to heat the system. The temperature was adjusted by changing the flow rate for a jet of air around the glass reaction vessel. The reaction vessels were sealed and could hold a pressure of up to 10 bars.

9.2 Analytical Techniques

Melting Points

Melting points were determined on a Büchi Melting Point B-545 apparatus and are uncorrected.

Mass Spectrometry

Field-desorption (FD) mass spectra were obtained on a VG Instruments ZAB 2-SE-FPD spectrometer. MALDI-TOF mass spectrometry was conducted on a Bruker Reflex II-TOF spectrometer, utilizing a 337 nm nitrogen laser. If not specifically mentioned, 1,8-dihydroxyanthracen-9(10*H*)-one (dithranol) or tetracyanoquinodimethane (TCNQ) was used as the matrix substance.

High resolution (HR) mass spectrometry was performed on an ESI-Q-TOF system (maXis, Bruker Daltonics, Germany). The instrument was operated in wide pass quadrupole mode, for MS experiments, with the TOF data being collected between m/z 100–5000 with low-collision energy of 10-15 eV.

NMR Spectroscopy

^{1}H NMR, ^{13}C NMR, H,H-COSY and C,H-COSY spectra were measured in different deuterated solvents and at temperatures as stated on Bruker DPX 250, Bruker AMX 300, Bruker DRX 500 or a Bruker DRX 700 spectrometer. The spectra were referenced as follows from the deuterated solvents: for CHDCl$_2$ $\delta(^1\text{H}) = 5.32$ ppm and CD$_2$Cl$_2$ $\delta(^{13}\text{C}) = 54.00$ ppm; for CHCl$_3$ $\delta(^1\text{H}) = 7.24$ ppm and $\delta(^{13}\text{C}) = 77.23$ ppm; for THF-d$_7$H $\delta(^1\text{H}$ low field signal$) = 3.58$ ppm and THF-d$_8$ $\delta(^{13}\text{C}) = 67.57$ ppm; for C$_2$HDCl$_4$ $\delta(^1\text{H}) = 5.91$ ppm and C$_2$D$_2$Cl$_4$ $\delta(^{13}\text{C}) = 74.20$ ppm; for DMSO-d$_5$H $\delta(^1\text{H}) = 2.50$ ppm and DMSO-d$_6$ $\delta(^{13}\text{C}) = 39.51$ ppm. The temperature dependent experiments were performed between 298 and 393 K and regulated by a standard ^{1}H methanol (low temperature) and glycol (high temperature) NMR sample. For the ^{13}C-spectra with the PAQXI probe a 90° pulse of 14.5 μs was used.

Elemental Analysis

Elemental analysis of solid samples was carried out on a Foss Heraeus Vario EL as a service measurement at the Institute for Organic Chemistry, Johannes-Gutenberg-Universität of Mainz. All samples were dried under vacuum in order to remove possible residuals of solvent molecules and humidity. Values for some samples show higher variance than 0.40% from calculated values. The entrapment of solvent molecules and atmospheric gases such as CO$_2$ is a common phenomenon in the analysis of aromatic hydrocarbons.[1] Moreover, the high carbon content of the synthesized compounds complicated the detection of the elements. Although all combustions were complete (no soot formation), the analysis in most of the cases lacked reproducibility. Repetitive

measurements on the same sample gave strongly varying contents of the analyzed elements. This problem could not be solved so far, therefore the given results are associated with some uncertainty.

UV-vis Spectroscopy

The spectra are recorded in given concentrations and solvents on a Perkin-Elmer Lambda 100 UV/Vis/NIR spectrometer. The molar extinctions are given in the unit $L\,mol^{-1}\,cm^{-1}$. Unless otherwise noted, a concentration of $10^{-6}\,mol\,L^{-1}$ was used. Solvents of spectroscopic grade were used. Prior to the measurement the baseline was corrected by subtracting a measurement of the cuvette filled with the neat solvent.

Emission Spectroscopy

Solution emission spectra were recorded at room temperature on a J&M TIDAS spectrofluorometer. Quartz cuvettes from Hellma with 1 cm thickness were applied. Absolute photoluminescence quantum yields (PLQY) were evaluated at 298 K on a Hamamatsu Photonic Multi-Channel Analyzer C 10027 at the Laboratory of Organic and Macromolecular Chemistry at the Friedrich-Schiller University Jena, Germany.

Raman Spectroscopy

Raman spectra were recorded on a Bruker RFS/100s using a Nd:YAG Laser with a wavelength of 1066 nm (400 mW). The samples were homogenized and placed on aluminum sample holder.

Analytical Size-Exclusion Chromatography (SEC)

Analytical size-exclusion chromatography (SEC) was performed on SDV (PSS) columns (106, 104, and 500 Å porosity) connected to a RI ERC 7512 (ERMA) detector and a UV S-3702 (SOMA) detector ($\lambda = 254$ nm) against polystyrene standards and calibrated for 1,4-poly(*para*phenylene) (PPP) with THF as an eluting solvent at 298 K.

Electrochemical Measurements

Electrochemical measurements were carried out in CH_2Cl_2 containing 0.1 M n-Bu_4NPF_6 in a classical three-electrode cell by cyclic voltammetry (CV) and rotating-disk voltammetry (RDV). The working electrode was a glassy C disk (3 mm in diameter), the auxiliary electrode a Pt wire, and the reference electrode a Pt wire used as pseudo reference electrode. At the end of the studies, ferrocene was added to the solution. The cell was

connected to an Autolab PGSTAT30 potentiostat (Eco Chemie, Holland) driven by a GPSE software running on a personal computer. All potentials are given *vs*. Fc^+/Fc used as internal reference and are uncorrected from ohmic drop. Digital simulation of the electron transfers for some compounds were carried out using the DigiElch software for CV studies and the Digisim software for RDV studies.[2, 3] Simulation allowed to fit the experimental curves. Some of the measurements were carried out by ██████████████ at the Laboratoire d'Electrochimie et de Chimie Physique du Corps Solide at the Université de Strasbourg, France.

Spectroelectrochemistry

The experiments were carried out by ██████████ in the group of ██████████████ at the University of Strathclyde Glasgow, United Kingdom. For spectroelectrochemical measurements a CH_2Cl_2 solution of the sample (1 mg/mL) was drop-casted on top of an ITO slide. The measurements were carried out under argon and in the presence of a 0.1 M *n*-Bu_4NPF_6 solution in anhydrous acetonitrile as supporting electrolyte. The ITO slide was used as the working electrode, a platinum wire as counter electrode and silver wire as the reference electrode. The three electrodes were immersed to a solution of the electrolyte in a sealed quartz glass cuvette. Upon repetitive cycling between 0 to 1000 mV, the UV-vis spectra were recorded between 300 to 900 nm.

Thermogravimetric Analysis (TGA)

Thermogravimetric analysis (TGA) was acquired on a Mettler TGA/SDTA 851e at a heating rate of 10 K/min under a nitrogen atmosphere.

Differential Scanning Calorimetry (DSC)

Differential scanning calorimetry (DSC) was measured on a Mettler DSC 30 with heating and cooling rates of 10 K/min in the range from -100 °C until thermal decomposition. The peak values of the second heating cycle were given to exclude influences from the thermal history.

Organic Field-Effect Transistors (OFETs)

Organic field-effect transistors (OFET) devices were fabricated by ██████████████ in the group of ██████████████ at the NanoTecCenter Weiz, Austria in a bottom-gate/bottom-contact (BG/BC) architecture on silicon substrates (1 inch x 1 inch). The heavily doped silicon (n^{++}-Si) was used as common bottom gate and the 200 nm thermally

grown SiO_2 as gate dielectric ($C_i = 17.3$ nF cm^{-2}). 50 nm gold source/drain (S/D) electrodes with 2 nm chrome adhesion layer were structured using conventional lift-off processing. The channel width and the channel length were 2.85 mm and 25 μm, respectively. The semiconductor material and regioregular poly(3-hexylthiophene) (Plexcore® OS, purchased from Sigma-Aldrich) were dissolved in toluene with a concentration of 2 g L^{-1} and 3 g L^{-1}. In order to optimize the wetting behavior of the semiconductor and the device performance, the surface of some samples was modified before depositing the semiconductor. Hexamethyldisilazane (97% purity degree, SSE Optihot VB20 hotplate) was applied via vapor phase deposition for various exposure times. Certain samples were treated by UV/ozone or O_2 plasma to hydrophilize the surface and form a thin AuO_x layer on the gold electrodes.[4] A UV-lamp 6035 Hg (Ar) was used for 10 min UV-light exposure of the SiO_2 surface and the gold electrodes. The O_2-plasma treatment was done using a Femto plasma etch plant (Diener electronic) with exposure times of 5 min and a power of 100 W. All devices were assembled under inert atmosphere, except those used for ambient stability investigations. In order to remove adsorbed water on the SiO_2, the substrates were also annealed at 120°C in high vacuum for 1 h before the application of the semiconductors (only for inert assembling). After spin-coating the semiconductor, the films were first dried at 60 °C in Argon (Ar) for ~10 min and subsequently at 120 °C under high vacuum (p ~ 4×10^{-5} mbar) for 1 h.

The charge carrier mobilities were calculated with the help of

$$\mu_{sat} = \frac{2 \cdot I_{SD} \cdot L}{W \cdot C_i \cdot (V_{GS} - V_{th})^2}$$

with the current in the saturation regime I_{SD}, the channel width W, channel length L, capacitance C_i per unit area of the gate insulator, gate voltage V_{GS}, the saturated charge-carrier field-effect mobility μ_{sat} and the threshold voltage V_{th}.

Single Crystal X-Ray Analysis

Single crystal X-ray measurements were carried out by ████████████████ at 120 K with Mo Kα radiation (λ = 0.71073 Å) on a Nonius KCCD diffractometer. The structure was solved by direct methods and refined on F by full-matrix least-squares cycles.

2D Wide Angle X-Ray Scattering (2D WAXS)

2D wide angle X-ray scattering (2D WAXS) measurements of oriented filaments were conducted by WOJCIECH ZAJACZKOWSKI using a rotating anode (Rigaku 18 kW) X-ray beam (CuKα, pinhole collimation, double graphite monochromator) and CCD camera. The

patterns were recorded with vertical orientation of the filament axis and with the beam perpendicular to the filament.

Scanning Tunneling Microscopy (STM)

Scanning tunneling microscopy (STM) measurements were carried out in collaboration with ███████████████ in the group of ███████████████, EMPA Duebendorf, Switzerland. The Ag(111) crystal was cleaned by standard cycles of Ar^+ sputtering and subsequent annealing (470 °C, 30 min) in a preparation chamber with a base pressure in the 10^{-10} mbar range. After sample cleaning, dibromo-substituted heterotriangulene was deposited onto the substrate held at room temperature by sublimation from a resistively heated quartz crucible at 115 °C, which resulted in deposition rates of about 0.2 monolayers (ML) per minute monitored by a quartz crystal microbalance. Subsequently, the sample is thermally annealed for a period of 10 min. Annealing of the Ag(111) crystal at temperatures of 200 °C after molecule deposition results in dehalogenation of the precursor molecules and coordination of the so-obtained surface-stabilized bi-radical species to Ag atoms to form metal-coordination networks. By annealing the sample at temperatures of 300 °C covalent networks are formed. After annealing, the sample was transferred to the analysis chamber for investigation (base pressure in the low 10^{-11} mbar range). The experiments were carried out with an Omicron variable-temperature scanning tunneling microscope (VT-STM) operating at a temperature of about 30 K (liquid helium). Voltages indicated for STM images correspond to sample bias.

Additional STM experiments were done in collaboration with ███████████████ (group of ███████████████, Katholieke Universiteit Leuven, Belgium). All experiments were performed at room temperature (20-24 °C) using a PicoSPM (Agilent) system operating in constant-current mode with the tip immersed in the supernatant liquid. STM tips were prepared by mechanical cutting of Pt/Ir wire (80%/20%, diameter 0.25 mm). Au(111) films on mica (Georg Albert PVD Company) have been used as substrate. Prior to use, Au(111) substrates were annealed in a butane flame. Reconstruction lines of Au (111) were not always visible after sample annealing. For each measurement an 8 µL drop of the desired solution was applied directly to the prepared substrates and STM imaging commenced immediately. The experiments were repeated in several sessions using different tips to check for reproducibility and to avoid experimental artifacts, if any. The unit cell parameters were determined by examining at least 10 images and only the average values are reported. After the determination of the unit cell from the acquired STM images,

a molecular model of the observed monolayer is constructed using HyperChem program. C_{60} (Sigma, 99%) and 1,2,4-trichlorobenezene (TCB, Sigma-Aldrich, 99%) were used without further purification. The synthesis of dehydrobenzo[12]annulene (**DBA**) derivatives is reported elsewhere.[5]

9.3 Synthesis

9.3.1 *N*-Heterotriangulene Polymers

4,4,8,8,12,12-Hexamethyl-8,12-dihydro-4*H*-benzo[1,9]quinolizino[3,4,5,6,7-*defg*]acridine (3-4)

3-4
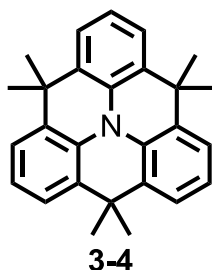
4,4,8,8,12,12-Hexamethyl-8,12-dihydro-4*H*-benzo[1,9]quinolizino[3,4,5,6,7-*defg*]acridine (**3-4**) was synthesized according to literature.[6, 7]

2,6-Dibromo-4,4,8,8,12,12-hexamethyl-8,12-dihydro-4*H*-benzo[1,9]quinolizino-[3,4,5,6,7-*defg*]acridine (3-5)

3-5
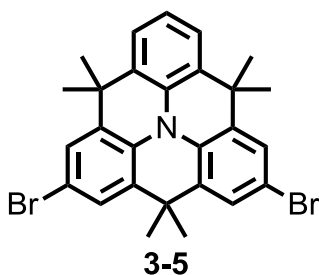
N-Bromosuccinimide (487 mg, 2.74 mmol) was added to a solution of *N*-heterotriangulene[6, 7] **3-4** (500 mg, 1.37 mmol) in CHCl$_3$ (40 mL) at 0 °C over a period of 20 min. While warming up to room temperature, the resulting solution was stirred in the dark overnight. The reaction was quenched with a saturated aqueous solution of Na$_2$S$_2$O$_3$. The resulting mixture was extracted with CH$_2$Cl$_2$ (3x) and the combined organic fractions were dried with MgSO$_4$. After filtration and evaporation of the solvent, the residue was subjected to column chromatography (silica, *n*-hexane/CH$_2$Cl$_2$ 4:1). Final recrystallization from ethanol yielded **3-5** as a white powder (550 mg, 77%). Mp: 170 °C. ^{1}H NMR (CDCl$_3$, 250 MHz, δ): 1.51 (s, 6H), 1.53 (s, 12H), 7.08 (t, $J_1 = J_2 = 6.3$ Hz, 1H), 7.29 (d, $J = 7.5$ Hz, 2H), 7.37 (dd, $J_1 = J_2 = 2.5$ Hz, 4H). ^{13}C NMR (CDCl$_3$, 63 MHz, δ): 132.2, 131.6, 131.5, 131.2, 131.0, 129.4, 126.5, 126.1, 123.5, 115.8, 35.6, 33.0, 32.5, 29.7. FD-MS (8kV): *m/z* = 521.9 (100%, M$^+$). ESI-HR MS calcd for C$_{27}$H$_{25}$Br$_2$N ([M+H]$^+$) 522.0432, found 522.0441. Anal. Calcd. for C$_{27}$H$_{25}$Br$_2$N: C 61.97%, H 4.82%, N 2.68%. Found: C 61.89%, H 4.94%, N 2.67%.

Linear *N*-Heterotriangulene Polymer (P1)

P1   n/2
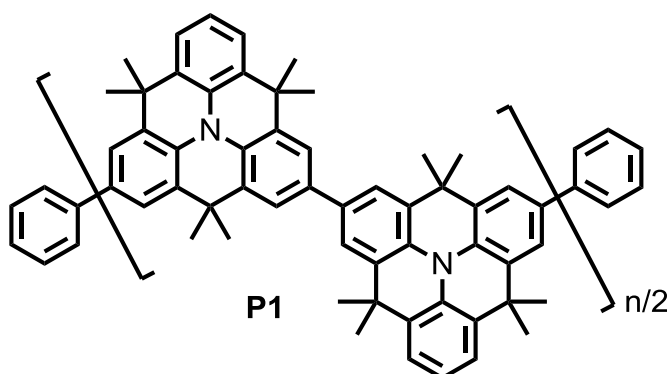
Bis(1,5-cycloocatdiene)nickel(0) (460 mg, 1.67 mmol), 1,5-cyclooctadiene (181 mg, 0.21 mL, 1.67 mmol) and 2,2'-bipyridine (261 mg, 1.67 mmol) were added to a flame-dried 100 mL Schlenk flask, dissolved in 7 mL anhydrous toluene and *N*,*N*-dimethylformamide (2:1) and stirred for 30 min at 65 °C in the absence of light. A solution of dibromo *N*-heterotriangulene **3-5** (350 mg, 0.67 mmol) in 23 mL anhydrous toluene at 65 °C was added quickly *via* a double-tipped needle and the resulting mixture was stirred for two days at 85 °C in the absence of light. After addition of 1 mL bromobenzene the mixture was stirred for additional two hours. Subsequently the reaction mixture was poured into 160 mL MeOH/HCl (30:1) and was stirred for one hour and the precipitate was filtered. After repeated precipitation in MeOH/HCl, the polymer was subjected to Soxhlet extraction using acetone and *n*-hexane. Final precipitation lead to **P1** as a white solid (160 mg, 66%). ¹H NMR (CD$_2$Cl$_2$, 250 MHz, δ): 1.67 (br, 6H), 1.76 (br, 12H), 7.09 (br, 1H), 7.40 (br, 2H), 7.62 (br, 4H). SEC (THF, PS-standard): M_w = 17 800 g/mol, PDI = 1.7, DP ~ 49. Anal. Calcd. for C$_{27}$H$_{25}$N: C 89.21%, H 6.93%, N 3.85%. Found: C 89.11%, H 6.70%, N 3.91%.

2-Bromo-4,4,8,8,12,12-hexamethyl-8,12-dihydro-4*H*-benzo[1,9]quinolizino[3,4,5,6,7-*defg*]acridine (3-6/4-4)

3-6
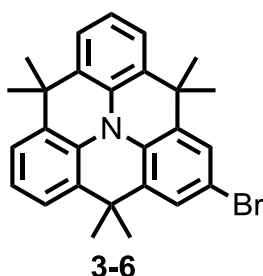
To a solution of *N*-heterotriangulene[6, 7] **3-4** (5.0 g, 13.68 mmol) in CHCl$_3$ (133 mL) at 0 °C was added *N*-bromosuccinimide (2.44 g, 13.68 mmol) over a periode of 20 min. While warming up to room temperature, the resulting solution was stirred in the absence of light overnight. The reaction was quenched with a saturated aqueous solution of Na$_2$S$_2$O$_3$. The

resulting mixture was extracted with CH_2Cl_2 (3x) and the combined organic fractions were dried with $MgSO_4$. After filtration and evaporation of the solvent, the residue was subjected to column chromatography (silica, *n*-hexane/CH_2Cl_2 4:1). Final recrystallization from ethanol yielded **3-6/4-4** as a white powder (5.6 g, 92%). Mp: 169 °C. ^{1}H NMR (CD_2Cl_2, 250 MHz, δ): 1.63 (s, 12H), 1.66 (s, 6H), 7.18 (t, $J_1 = J_2 = 7.5$ Hz, 2H), 7.43 (m, 4H), 7.51 (s, 2H). ^{13}C NMR (CD_2Cl_2, 63 MHz, δ): 32.0, 131.5, 129.9, 129.3, 126.5, 126.1, 123.7, 123.3, 123.1, 115.5, 35.6, 35.4, 33.2, 32.8. FD-MS (8kV): $m/z = 442.8$ (100%, M^+). ESI-HR MS calcd for $C_{27}H_{26}BrN$ ([M+H]$^+$) 444.1327, found 444.1331.

4,4,8,8,12,12-Hexamethyl-2-(4,4,5,5-tetramethyl-1,3,2-dioxaborolan-2-yl)-8,12-dihydro-4*H*-benzo[1,9]quinolizino[3,4,5,6,7-*defg*]acridine (3-7/4-5)

3-7
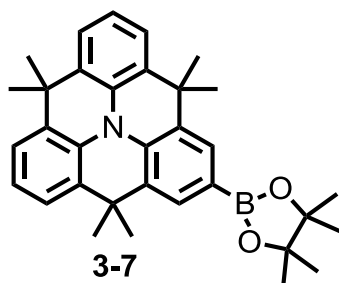
A flame-dried 250 mL Schlenk flask was equipped with monobromo *N*-heterotriangulene (**3-6/4-4**) (5.12 g, 11.52 mmol), bispinacolato diboron (3.66 g, 14.40 mmol) and KOAc (4.07 g, 41.47 mmol). The mixture was suspended in anhydrous *N*,*N*-dimethylformamide (96 mL) and degassed with argon for 1.5 hours. Subsequently, Pd(dppf)Cl$_2 \cdot$ CH$_2$Cl$_2$ (282 mg, 4 mol%) was added and the resulting mixture was stirred under an argon atmosphere for 15 hours at 85 °C. The reaction was stopped by addition of water and the resulting mixture was extracted with CH_2Cl_2 (3x). The combined organic fractions were dried with $MgSO_4$, filtered and the solvents were evaporated. The crude product was purified by column chromatography (silica, *n*-hexane/CH_2Cl_2 2:3) yielding **3-7/4-5** as a colorless, crystalline solid (4.88 g, 86%). Mp: 272 °C. ^{1}H NMR (CDCl$_3$, 250 MHz, δ): 1.41 (s, 12H), 1.68 (s, 18H), 7.19 (t, $J_1 = J_2 = 8.75$ Hz, 2H), 7.45 (d, $J = 7.5$ Hz, 4H), 7.82 (s, 2H). ^{13}C NMR (CDCl$_3$, 63 MHz, δ): 25.1, 33.2, 33.6, 35.8, 84.0, 123.6, 123.9, 124.1, 129.1, 130.3, 130.4, 130.8, 132.0, 134.9. ESI-HR MS calcd for $C_{33}H_{39}BNO_2$ ([M+H]$^+$) 492.3074, found 492.3004. Anal. Calcd. for $C_{33}H_{38}BNO_2$: C 80.65%, H 7.79%, N 2.85%. Found: C 80.86%, H 8.17%, N 2.77%.

2,6-Dibromo-4,4,8,8,12,12-hexamethyl-10-(4,4,5,5-tetramethyl-1,3,2-dioxaborolan-2-yl)-8,12-dihydro-4*H*-benzo[1,9]quinolizino[3,4,5,6,7-*defg*]acridine (3-8)
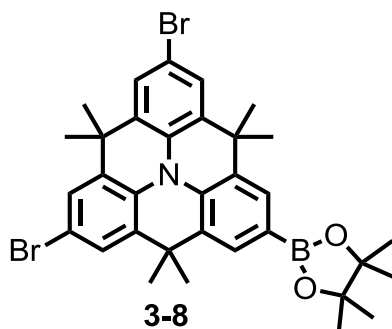
To a solution of *N*-heterotriangulene monoboronic ester **3-7** (250 mg, 0.51 mmol) in CHCl$_3$ (10 mL) at 0 °C was added *N*-bromosuccinimide (190 mg, 1.07 mmol) over a period of 20 min. While warming up to room temperature, the resulting solution was stirred in the absence of light overnight. The reaction was quenched with a saturated aqueous solution of Na$_2$S$_2$O$_3$. The resulting mixture was extracted with CH$_2$Cl$_2$ (3x) and the combined organic fractions were dried with MgSO$_4$. After filtration and evaporation of the solvent, the residue was subjected to column chromatography (silica, *n*-hexane/CH$_2$Cl$_2$ 2:3) yielding **3-8** as a white powder (240 mg, 73%). Mp: 275 °C. ^{1}H NMR (CD$_2$Cl$_2$, 250 MHz, δ): 1.35 (s, 12H), 1.58 (s, 6H), 1.61 (s, 12H), 7.46 (d, *J* = 2.5 Hz, 2H), 7.50 (d, *J* = 2.5 Hz, 2H), 7.76 (s, 2H). ^{13}C NMR (CD$_2$Cl$_2$, 75 MHz, δ): 25.1, 32.9, 33.0, 35.9, 36.1, 84.1, 116.5, 126.6, 126.9, 128.9, 130.5, 132.2, 133.2, 135.6. ESI-HR MS calcd for C$_{33}$H$_{36}$BBr$_2$NO$_2$ ([M+H]$^+$) 650.2714, found 650.2709. Anal. Calcd. for C$_{33}$H$_{36}$BBr$_2$NO$_2$: C 61.05%, H 5.59%, N 2.16%. Found: C 60.38%, H 5.72%, N 2.16% (see general remarks "Elemental Analysis").

Hyperbranched *N*-Heterotriangulene Polymer (P2)
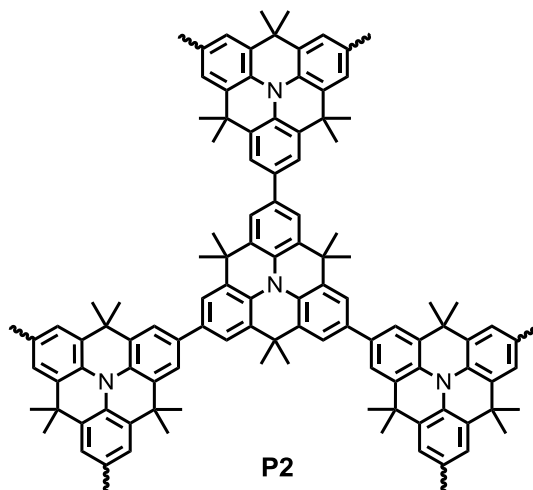
A 250 mL Schlenk tube was equipped with **3-8** (110 mg, 0.17 mmol) followed by three times evacuating and backfilling with argon. After the addition of 18 mL toluene, 9 mL of an aqueous 2 M Na_2CO_3 solution and three drops of *Aliquat 336* the resulting mixture was degassed with argon for one hour. To this mixture $Pd(PPh_3)_4$ (12 mg, 3 mol%) was added and it was stirred under an atmosphere of argon at 90 °C for six days. After addition of 1 mL bromobenzene and 1 mg $Pd(PPh_3)_4$ the mixture was stirred for additional two hours, followed by the addition of 1 g phenylboronic acid and stirring for two hours. Subsequently the reaction mixture was poured into 160 mL MeOH/HCl (30:1), was stirred for one hour and the precipitate was subsequently filtered. After repeated precipitation in MeOH/HCl, the polymer was subjected to Soxhlet extraction using acetone and hexane. Final precipitation lead to **P2** as a light yellow solid (43 mg, 70%). ^{1}H NMR (CD_2Cl_2, 250 MHz, δ): 1.67 (br, 6H), 1.76 (br, 12H), 7.00 (br m), 7.51 (br), 7.75 (br). SEC (THF, PS-standard): $M_w = 22\,400$ g/mol, PDI = 2.3, DP ~ 61. Anal. Calcd. for $C_{27}H_{24}N$: C 89.46%, H 6.67%, N 3.86%. Found: C 87.93%, H 6.42%, N 3.76%.

9.3.2 *N*-Heterotriangulene Macrocycles

2-Bromo-4,4,8,8,12,12-hexamethyl-6-(4,4,5,5-tetramethyl-1,3,2-dioxaborolan-2-yl)-8,12-dihydro-4*H*-benzo[1,9]quinolizino[3,4,5,6,7-*defg*]acridine (4-6)

4-6
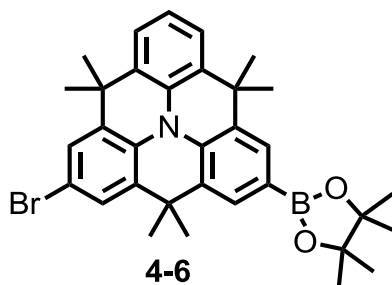
To a solution of *N*-heterotriangulene monoboronic ester **4-5** (2.1 g, 4.27 mmol) in CHCl$_3$ (77 mL) at 0 °C was added *N*-bromosuccinimide (0.76 g, 4.27 mmol) over a period of 20 min. While warming up to room temperature, the resulting solution was stirred in the absence of light overnight. The reaction was quenched with a saturated aqueous solution of Na$_2$S$_2$O$_3$. The resulting mixture was extracted with CH$_2$Cl$_2$ (3x) and the combined organic fractions were dried with MgSO$_4$. After filtration and evaporation of the solvent, the residue was subjected to column chromatography (silica, *n*-hexane/CH$_2$Cl$_2$ 2:3). Final recrystallization from ethanol yielded **4-6** as a white powder (1.87 g, 77%). Mp: 212 °C. ^{1}H NMR (CDCl$_3$, 250 MHz, δ): 1.40 (s, 12H), 1.65 (s, 12H), 1.67 (s, 6H), 7.20 (t, $J_1 = J_2 = 8.75$ Hz, 1H), 7.44 (dd, $J_1 = 8.75$ Hz, $J_2 = 1.5$ Hz, 2H), 7.52 (s, 2H), 7.81 (d, $J = 7.5$ Hz, 2H). ^{13}C NMR (CDCl$_3$, 75 MHz, δ): 25.1, 32.8, 33.2, 33.3, 84.0, 123.9, 124.0, 124.2, 126.5, 126.7, 130.2, 130.6 (12 out of 17 expected). ESI-HR MS calcd for C$_{33}$H$_{37}$BBrNO$_2$ ([M+H]$^+$) 570.2179, found 570.2190. Anal. Calcd. for C$_{33}$H$_{37}$BBrNO$_2$: C 69.49%, H 6.54%, N 2.46%. Found: C 69.57%, H 7.97%, N 2.43%.

Direct Macrocyclization

(i)   Yamamoto coupling c = 4 × 10^{-3} M (3.5 × 10^{-4} M)

Bis(1,5-cyclooctadiene)nickel(0) (105 mg, 0.38 mmol), 1,5-cyclooctadiene (41 mg, 0.17 mL, 0.38 mmol) and 2,2'-bipyridine (60 mg, 0.38 mmol) were added to a flame-dried 25 mL Schlenk flask, dissolved in 8 mL (10 mL) anhydrous *N,N*-dimethylformamide and stirred for 30 min at 65 °C in the absence of light. A solution of 2,6-dibromo-4,4,8,8,12,12-hexamethyl-8,12-dihydro-4*H*-benzo[1,9]quinolizino[3,4,5,6,7-*defg*]acridine (**3-5**) (100 mg, 0.19 mmol) in 40 mL (550 mL) anhydrous toluene at 65 °C was added slowly *via* a double-tipped needle and the resulting mixture was stirred for five days at 85 °C. The reaction was quenched by adding 10% aqueous hydrochloric acid, extracted with CH$_2$Cl$_2$ (3x) and the organic phase was dried with MgSO$_4$. After having removed the solvents *in*

vacuo, the residue was subjected to preparative size exclusion chromatography (BioBeads S-X3, CH_2Cl_2).

Further separation was attempted by column chromatography (silica, *n*-hexane/EtOAc 5:1).

For $c = 3.5 \times 10^{-4}$ M only unreacted **3-5** was isolated.

(ii) Suzuki coupling $c = 4 \times 10^{-4}$ M

A 250 mL Schlenk tube was equipped with 2-bromo-4,4,8,8,12,12-hexamethyl-6-(4,4,5,5-tetramethyl-1,3,2-dioxaborolan-2-yl)-8,12-dihydro-4*H*-benzo[1,9]quinolizino[3,4,5,6,7-*defg*]acridine (**4-6**) (36 mg, 0.06 mmol) followed by three times evacuating and backfilling with argon. After the addition of 115 mL toluene, 45 mL ethanol and 7 mL of an aqueous 2 M K_2CO_3 solution, the resulting mixture was degassed with argon for 30 min. To this mixture $Pd(PPh_3)_4$ (1 mg, 1.5 mol%) was added and it was stirred under an atmosphere of argon at 85 °C for two days. Washing the aqueous phase three times with toluene, drying the combined organic phases with $MgSO_4$ and evaporating of the solvent *in vacuo* resulted in a crude mixture which was subjected to column chromatography (silica, *n*-hexane/EtOAc 3:1).

2,6-Diiodo-4,4,8,8,12,12-hexamethyl-8,12-dihydro-4*H*-benzo[1,9]quinolizino[3,4,5,6,7-*defg*]acridine (4-7)

4-7
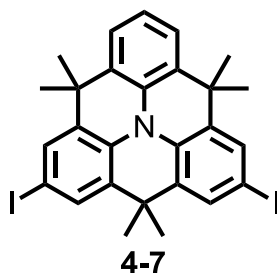
To a solution *N*-heterotriangulene **3-4** (1.52 g, 4.17 mmol) in $CHCl_3$ (40 mL) at 0 °C was added *N*-iodosuccinimide (2.38 g, 10.58 mmol) over a period of 20 min (for completion of the reaction an excess of NIS was necessary). After slowly warming up to room temperature, the resulting solution was stirred at 50 °C in the absence of light for 96 hours. The reaction was quenched with a saturated aqueous solution of $Na_2S_2O_3$. The resulting mixture was extracted with CH_2Cl_2 (3x) and the combined organic fractions were dried with $MgSO_4$. After filtration and evaporation of the solvent, the residue was subjected to column chromatography (silica, *n*-hexane/CH_2Cl_2 4:1). Final recrystallization from ethanol yielded **4-7** as a white powder (2.3 g, 89%). Mp: 185 °C. ^{1}H NMR (CDCl_3, 250 MHz, δ): 1.55 (s, 6H), 1.58 (s, 12H), 7.15 (t, $J_1 = J_2 = 8.75$ Hz, 1H), 7.39 (d, $J = 8.75$ Hz, 2H), 7.63

(dd, J_1 = 5 Hz, J_2 = 2.5 Hz, 4H). ^{13}C NMR (CDCl$_3$, 63 MHz, δ): 132.2, 131.6, 131.5, 131.2, 131.0, 129.4, 126.5, 126.1, 123.7, 123.5, 115.8, 35.6, 33.0, 32.5, 29.7. ESI-HR MS calcd for C$_{27}$H$_{25}$I$_2$N ([M+H]$^+$) 618.0155, found 618.0161. Anal. Calcd. for C$_{27}$H$_{25}$I$_2$N: C 52.53%, H 4.08%, N 2.27%. Found: C 52.35%, H 3.23%, N 2.31%.

N-Heterotriangulene Trimer (4-8)
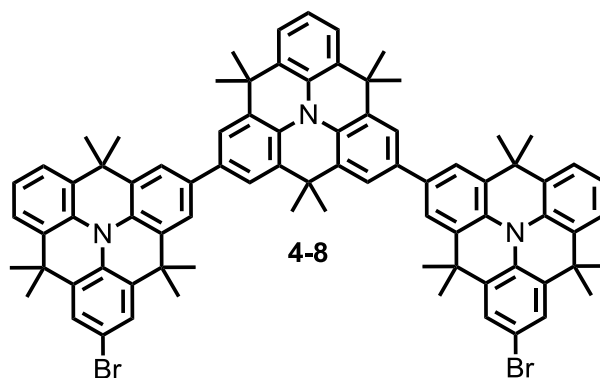
A 250 mL Schlenk tube was equipped with monobromo N-heterotriangulene boronic ester **4-6** (0.75 g, 1.21 mmol) and diiodo N-heterotriangulene **4-7** (1.42 g, 2.49 mmol) followed by three times evacuating and backfilling with argon. After the addition of 55 mL toluene, 27.5 mL of an aqueous 2 M Na$_2$CO$_3$ solution and three drops of *Aliquat 336* the resulting mixture was degassed with argon for one hour. To this mixture Pd(PPh$_3$)$_4$ (112 mg, 4 mol%) was added and it was stirred under an atmosphere of argon at 65 °C for three days. Washing the aqueous phase three times with toluene, drying the combined organic phases with MgSO$_4$ and evaporating of the solvent *in vacuo* resulted in a crude mixture which was subjected to column chromatography (silica, *n*-hexane/CH$_2$Cl$_2$ 3:1). **4-8** was obtained as pale yellow solid (0.84 mg, 55%). Mp: 391 °C decomp. ^{1}H NMR (CD$_2$Cl$_2$, 250 MHz, δ): 1.54 (s, 12H), 1.65 (m, 36H), 1.73 (s, 6H), 7.09 (t, J_1 = J_2 = 7.5 Hz, 3H), 7.37 (m, 10H), 7.57 (m, 8H). ^{13}C NMR (CD$_2$Cl$_2$, 75 MHz, δ): 136.2, 132.6, 132.5, 131.1, 131.0, 130.3, 129.8, 126.6, 124.3, 123.9, 123.7, 122.5, 122.1, 115.9, 50.8, 36.2, 36.0, 33.6, 33.1, 33.0. FD-MS (8kV): *m/z* = 1250.4 (100%, M$^+$), 624.8 (85%, M^{2+}). MALDI-TOF MS (dithranol): *m/z* = 1248.65 (100%) [M+H]$^+$. ESI-HR MS calcd for C$_{81}$H$_{75}$Br$_2$N$_3$ ([M+H]$^+$) 1248.4406, found 1248.4392. Anal. Calcd. for C$_{81}$H$_{75}$Br$_2$N$_3$: C 77.81%, H 6.05%, N 3.36%. Found: C 78.10%, H 5.84%, N 3.43%.

N-Heterotriangulene Macrocycle (4-2) + Nonamer (4-9)
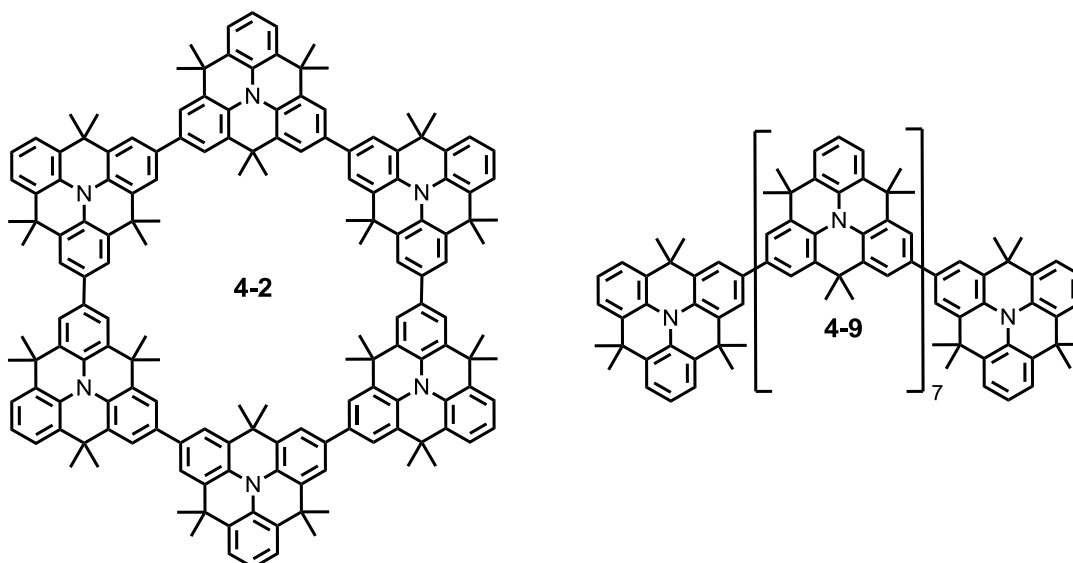
Bis(1,5-cyclooctadiene)nickel(0) (381 mg, 1.39 mmol), 1,5-cyclooctadiene (150 mg, 0.17 mL, 1.39 mmol) and 2,2'-bipyridine (216 mg, 1.39 mmol) were added to a flame-dried 250 mL Schlenk flask, dissolved in 30 mL anhydrous *N*,*N*-dimethylformamide and stirred for 30 min at 65 °C in the absence of light. A solution of trimer **4-8** (825 mg, 0.66 mmol) in 141 mL anhydrous toluene at 65 °C was added in the course of one hour *via* a double-tipped needle and the resulting mixture was stirred for two days at 85 °C. The reaction was quenched by adding 10% aqueous hydrochloric acid, extracted three times with CH_2Cl_2 and the organic phase was dried with $MgSO_4$. After having removed the solvents *in vacuo*, the residue was filtered over a plug of silica (*n*-hexane/CH_2Cl_2 1:1). Finally, macrocycle **4-2** was removed from the linear nonamer **4-9** (108 mg, 15%) with the help of preparative size exclusion chromatography (BioBeads S-X1, toluene) and obtained as a yellow solid (273 mg, 38%). Crystals suitable for X-ray analysis were grown by slow diffusion of diethyl ether to a chloroform solution of **4-2**.

4-2: Mp > 400 °C. ^{1}H NMR (THF-d_8, 700 MHz, δ): 1.81 (s, 72H), 1.88 (s, 36H), 7.20 (t, $J_1 = J_2 = 7.5$ Hz, 6H), 7.54 (d, $J = 7.5$ Hz, 12H), 7.81 (d, $J = 1.9$ Hz, 12H), 7.82 (d, $J = 1.9$ Hz, 12H). ^{13}C NMR (THF-d_8, 176 MHz, δ): 30.1, 33.5, 33.6, 36.2, 36.4, 121.9, 122.15, 123.5, 124.2, 125.6, 128.6, 129.4, 130.3, 130.8, 130.9, 131.3, 132.1, 135.6. SEC (THF, PPP-standard): $M_w = 1520$ g/mol, PDI = 1.02. FD-MS (8kV): $m/z = 2180.0$ (65%, M$^+$), 1089.0 (100%, M^{2+}). MALDI-TOF MS (dithranol): $m/z = 2181.01$ (100%) [M+H]$^+$. ESI-HR MS calcd for $C_{162}H_{150}N_6$ ([M+H]$^+$) 2180.2000, found 2180.2009. Anal. Calcd. for $C_{162}H_{150}N_6$: C 89.21%, H 6.93%, N 3.85%. Found: C 89.51%, H 6.73%, N 3.46%.

4-9: Mp > 400 °C. ^{1}H NMR (THF-d$_8$, 700 MHz, δ): 1.73 (s, 108H), 1.82 (s, 54H), 7.14 (broad m, 11H), 7.48 (br m, 18H), 7.71 (br m, 36H). ^{13}C NMR (THF-d$_8$, 176 MHz, δ): 33.2, 33.3, 36.3, 36.5, 122.3, 122.6, 123.8, 124.2, 124.3, 130.6, 130.9, 131.6, 131.7, 132.4, 132.5, 136.5, 136.9, 137.0. FD-MS (8kV): m/z = 3273.7 (100%, M$^+$), 1636.8 (50%, M^{2+}). MALDI-TOF MS (dithranol): m/z = 3270.01 (100%) [M+H]$^+$. Anal. Calcd. for C$_{243}$H$_{227}$N$_9$: C 89.16%, H 6.99%, N 3.85%. Found: C 88.78%, H 7.29%, N 3.76 %.

Hexabromo *N*-Heterotriangulene Macrocycle (4-10)
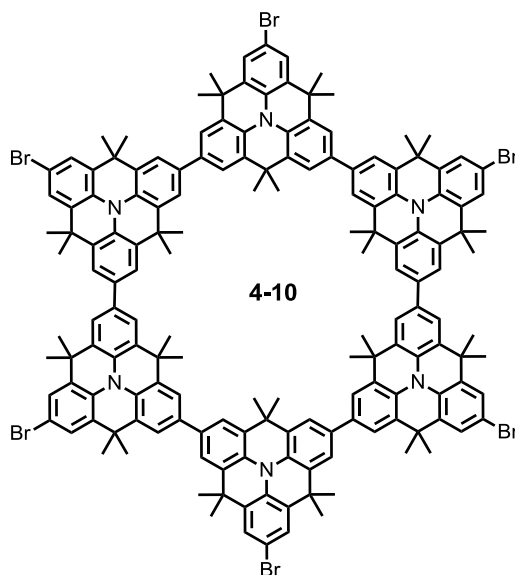
To a solution of heterotriangulene macrocycle **4-2** (75 mg, 0.03 mmol) in CHCl$_3$ (3 mL) at 0 °C was added *N*-bromosuccinimide (61 mg, 0.34 mmol). While warming up to room temperature, the resulting solution was stirred in the absence of light overnight. The reaction was quenched with a saturated aqueous solution of Na$_2$S$_2$O$_3$. The resulting mixture was extracted with CH$_2$Cl$_2$ (3x) and the combined organic fractions were dried with MgSO$_4$. Filtration and evaporation of the solvent afforded **4-10** as a hardly soluble, yellow material (63 mg, 69%). The compound was used without further purification. Mp > 400 °C. FD-MS (8kV): m/z = 2651.2 (100%, M$^+$), 1326.6 (90%, M^{2+}). MALDI-TOF MS (dithranol): m/z = 2652.31 (100%) [M+H]$^+$.

Hexakis(4-dodecylphenyl)-substituted *N*-Heterotriangulene Macrocycle (4-11)
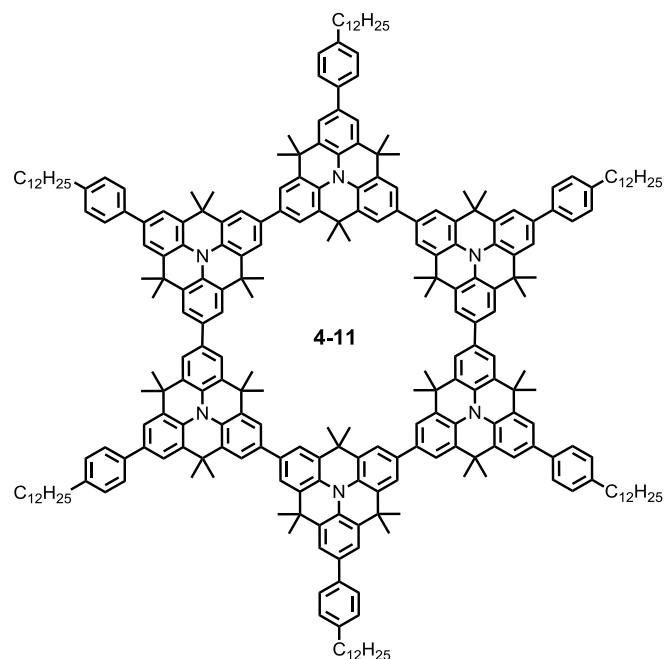
A 10 mL microwave tube was equipped with the hexabromo *N*-heterotriangulene macrocycle **4-10** (17 mg, 0.006 mmol) and (4-dodecylphenyl)boronic acid[8] (22 mg, 0.77 mmol), K_3PO_4 (16 mg, 0.77 mmol), $Pd(OAc)_2$ (0.2 mg, 2 mol%) and dicyclohexyl(2',6'-dimethoxy-[1,1'-biphenyl]-2-yl)phosphine (S-Phos) (0.7 mg, 4 mol%) in a glovebox. This mixture was suspended in 2.5 mL of anhydrous toluene and 0.25 mL H_2O (degassed with argon prior to use), the reaction vial was sealed and heated under microwave irradiation at 130 °C overnight. The reaction was stopped by the addition of water. Washing the aqueous phase three times with toluene, drying the combined organic phases with $MgSO_4$ and evaporating of the solvent *in vacuo* resulted in a crude mixture which was subjected to column chromatography (silica, *n*-hexane/CH_2Cl_2 1:1). Compound **4-11** was finally obtained after precipitation from MeOH as a yellow solid (10 mg, 43%). Mp: 233 °C. ^{1}H NMR (CD$_2$Cl$_2$, 300 MHz, δ): 0.90 (m, 18H), 1.26-1.30 (m, 120H), 1.85 (s, 72H), 1.88 (s, 36H), 2.68 (t, $J_1 = J_2 = 9$ Hz, 12H), 7.32 (d, $J = 9$ Hz, 12H), 7.63 (d, $J = 6$ Hz, 12H), 7.71 (s, 12H), 7.79 (d, $J = 3$ Hz, 24H). ^{13}C NMR (CD$_2$Cl$_2$, 75 MHz, δ): 14.3, 23.1, 25.6, 27.3, 29.8, 29.9, 30.1, 32.0, 32.1, 32.3, 100.4, 117.4, 121.7, 122.0, 123.7, 126.8, 129.2, 132.3, 136.0, 140.8, 147.9, 160.5 (22 out of 34 expected). MALDI-TOF MS (dithranol): $m/z = 3647.06$ (100%) $[M+H]^+$. ESI-HR MS calcd for $C_{270}H_{318}N_6$ ($[M+H]^+$) 3644.5068, found 3644.5071.

First Generation Expanded *N*-Heterotriangulene Macrocycle (4-12)
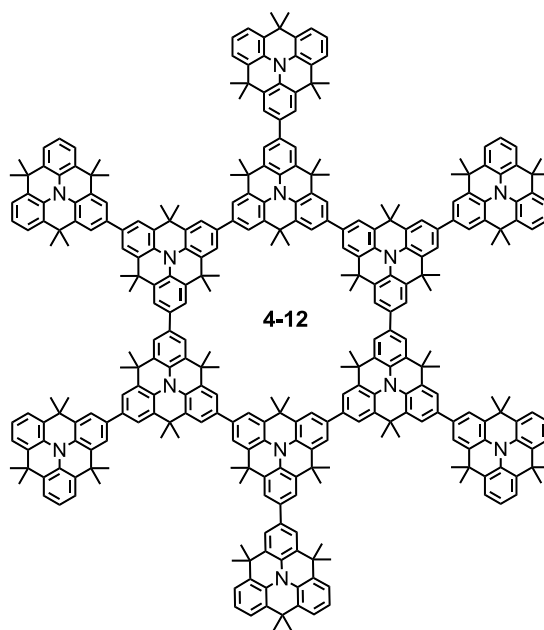

A 10 mL microwave tube was equipped with the hexabromo *N*-heterotriangulene macrocycle **4-10** (24 mg, 0.01 mmol) and *N*-heterotriangulene monoboronic ester **4-5** (44 mg, 0.09 mmol), K_3PO_4 (23 mg, 0.11 mmol), $Pd(OAc)_2$ (0.4 mg, 4 mol%) and dicyclohexyl(2',6'-dimethoxy-[1,1'-biphenyl]-2-yl)phosphine (S-Phos) (2 mg, 8 mol%) within a glovebox. This mixture was suspended in 3 mL of anhydrous toluene and 0.3 mL H_2O (degassed with argon prior to use), the reaction vial was sealed and heated under microwave irradiation at 130 °C overnight. The reaction was stopped by the addition of water. Washing the aqueous phase three times with toluene, drying the combined organic phases with $MgSO_4$ and evaporating of the solvent *in vacuo* resulted in a crude mixture which was subjected to column chromatography (silica, *n*-hexane/CH_2Cl_2 3:2 to 1:1). **4-12** was obtained as a yellow solid (15 mg, 38%). Mp > 400 °C. ^{1}H NMR (THF-d_8, 700 MHz, δ): 1.44 (s, 48H), 1.74 (s, 68H), 1.89 (s, 102H), 7.12 (t, $J_1 = J_2 = 7.5$ Hz, 12H), 7.44 (d, $J = 7.5$ Hz, 12H), 7.47 (d, $J = 7.5$ Hz, 12H), 7.71 (s, 12H), 7.76 (s, 14H), 7.84 (d, $J = 7.0$ Hz, 24H). ^{13}C NMR (THF-d8, 176 MHz, δ): 30.6, 30.7, 30.8, 33.7, 33.9, 119.7, 119.9, 120.1, 121.0, 121.5, 121.6, 127.8, 127.9, 128.3, 128.4, 128.8, 129.0, 129.1, 129.8, 134.1, 134.5 (21 out of 27 expected). MALDI-TOF MS (dithranol): *m/z* = 4347.83 (100%) [M-CH$_3$]$^+$. ESI-HR MS calcd for $C_{324}H_{300}N_{12}$ ([M+H]$^{2+}$) 2180.6966, found 2180.6900.

2-Bromo-6,10-diiodo-4,4,8,8,12,12-hexamethyl-8,12-dihydro-4*H*-

benzo[1,9]quinolizino-[3,4,5,6,7-*defg*]acridine (4-14)

4-14
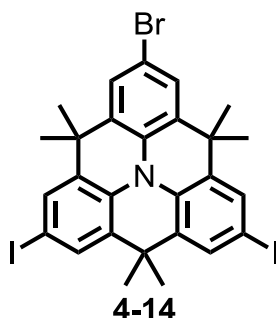
To a suspension of monobromo *N*-heterotriangulene **4-4** (1.0 g, 2.25 mmol) in 50 mL acetic acid was added KI (0.83 g, 5.00 mmol) and KIO$_3$ (1.07 g, 5.00 mmol). The resulting mixture was stirred at 85 °C for two hours. The reaction was stopped by the addition water and the mixture was washed with Na$_2$SO$_3$ solution, extracted three times with CH$_2$Cl$_2$ and the organic phase was dried with MgSO$_4$. After having removed the solvents *in vacuo*, the residue was filtered over a plug of silica (*n*-hexane/CH$_2$Cl$_2$ 4:1). Compound **4-14** was obtained as white solid (1.46 g, 93%). Mp: 288 °C. ^{1}H NMR (CD$_2$Cl$_2$, 250 MHz, δ): 1.60 (s, 6H), 1.61 (s, 12H), 7.51 (s, 2H), 7.67 (s, 4H). ^{13}C NMR (CD$_2$Cl$_2$, 63 MHz, δ): 132.2, 131.6, 131.5, 131.2, 131.0, 129.4, 126.5, 126.1, 123.7, 123.5, 115.8, 35.6, 33.0, 32.5, 29.7. Anal. Calcd. for C$_{27}$H$_{24}$BrI$_2$N: C 46.58%, H 3.47%, N 2.01%. Found: C 46.83%, H 4.16%, N 1.65%.

Monobromo *N*-Heterotriangulene Trimer (4-15)

4-15
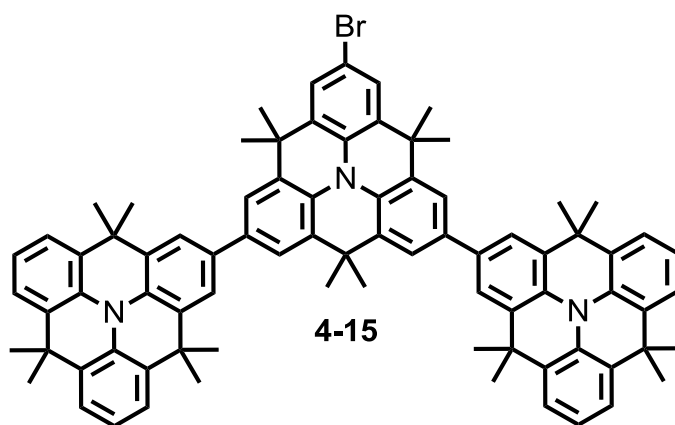
A 100 mL Schlenk tube was equipped with *N*-heterotriangulene monoboronic ester **4-5** (507 mg, 1.03 mmol) and monobromo-diiodo *N*-heterotriangulene **4-14** (350 mg, 0.50 mmol) followed by three times evacuating and backfilling with argon. After the addition of 23 mL toluene, 11.5 mL of an aqueous 2 M Na$_2$CO$_3$ solution and three drops of *Aliquat 336* the resulting mixture was degassed with argon for one hour. To this mixture Pd(PPh$_3$)$_4$

(47 mg, 4 mol%) was added and it was stirred under an atmosphere of argon at 65 °C for four days. Washing the aqueous phase three times with toluene, drying the combined organic phases with MgSO$_4$ and evaporating of the solvent *in vacuo* resulted in a crude mixture which was subjected to column chromatography (silica, *n*-hexane/CH$_2$Cl$_2$ 2:1). Trimer **4-15** was obtained after recrystallization from ethanol as pale yellow solid (250 mg, 43%). Mp > 400 °C. ^{1}H NMR (CD$_2$Cl$_2$, 250 MHz, δ): 1.54 (s, 12H), 1.63 (s, 36H), 1.73 (s, 6H), 7.05 (t, $J_1 = J_2 = 7.5$ Hz, 4H), 7.33 (m, 8H), 7.46 (s, 2H), 7.55 (m, 8H). ^{13}C NMR (CD$_2$Cl$_2$, 75 MHz, δ): 136.5, 135.8, 132.1, 131.6, 130.9, 130.8, 130.1, 126.7, 123.9, 123.4, 122.6, 122.1, 36.0, 36.1, 33.4, 30.1. FD-MS (8kV): *m/z* = 1170.4 (100%, M$^+$). ESI-HR MS calcd for C$_{81}$H$_{76}$BrN$_3$ ([M+H]$^+$) 1170.5301, found 1170.5309.

Monoboronate *N*-Heterotriangulene Trimer (4-16)

4-16
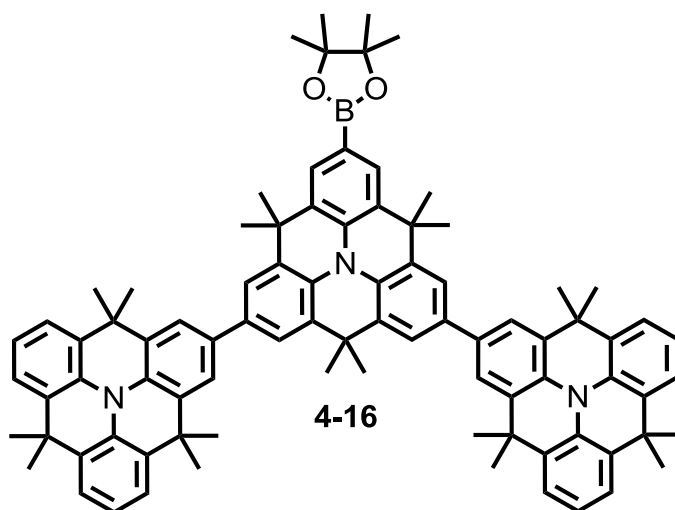
A flame-dried 50 mL Schlenk flask was equipped with the monobromo *N*-heterotriangulene trimer **4-15** (200 mg, 0.17 mmol), bispinacolato diboron (54 mg, 0.21 mmol) and KOAc (60 mg, 0.61 mmol). The mixture was suspended in anhydrous *N,N*-dimethylformamide (6 mL) and degassed with argon for 1.5 hours. Subsequently, Pd(dppf)Cl$_2 \cdot$ CH$_2$Cl$_2$ (8 mg, 6 mol%) was added and the resulting mixture was stirred under an argon atmosphere at 85 °C overnight. The reaction was stopped by addition of water and the resulting mixture was extracted with CH$_2$Cl$_2$ (3x). The combined organic fractions were dried with MgSO$_4$, filtered and the solvents were evaporated. The crude product was purified by column chromatography (silica, *n*-hexane//CH$_2$Cl$_2$ 2:1 to 1:1) yielding **4-16** as a colorless, crystalline solid (116 mg, 56%). Mp > 400 °C. ^{1}H NMR (CD$_2$Cl$_2$, 250 MHz, δ): 1.30 (s, 12H) 1.56 (s, 12H), 1.65 (m, 36H), 1.74 (s, 6H), 7.07 (t, $J_1 = J_2 = 7.5$ Hz, 4H), 7.35 (m, 8H), 7.58 (d, $J_1 = 5$ Hz, 8H), 7.76 (s, 2H). ^{13}C NMR (CD$_2$Cl$_2$, 75 MHz, δ): 135.8, 135.6, 132.1, 131.5, 130.9, 130.7, 130.1, 126.7, 123.9, 123.4,

123.4, 122.2, 84.0, 83.3, 36.0, 33.4, 30.1, 25.1 (18 out of 20 expected). FD-MS (8kV): $m/z = 1271.3$ (100%, M$^+$). ESI-HR MS calcd for $C_{87}H_{88}BN_3O_2$ ([M+H]$^+$) 1218.7048, found 1218.7054.

Second Generation Expanded *N*-Heterotriangulene Macrocycle (4-17)
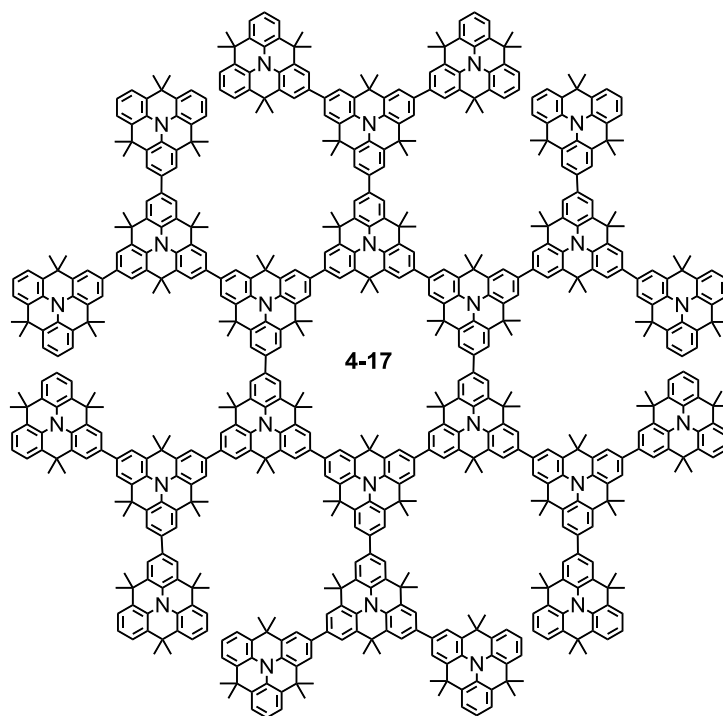
A 10 mL microwave tube was equipped with the hexabromo *N*-heterotriangulene macrocycle **4-10** (13 mg, 0.005 mmol) and monoboronate *N*-heterotriangulene trimer **4-16** (48 mg, 0.04 mmol), K_3PO_4 (13 mg, 0.06 mmol), Pd(OAc)$_2$ (0.3 mg, 4 mol%) and dicyclohexyl(2',6'-dimethoxy-[1,1'-biphenyl]-2-yl)phosphine (S-Phos) (1 mg, 8 mol%) in a glovebox. The mixture was suspended in 2.5 mL of anhydrous toluene and 0.25 mL H$_2$O (degassed with argon prior to use), the reaction vial was sealed and heated under microwave irradiation at 130 °C overnight. The reaction was stopped by the addition of water. Washing the aqueous phase with toluene (3x), drying the combined organic phases with MgSO$_4$ and evaporating of the solvent *in vacuo* resulted in a crude mixture which was subjected to preparative size exclusion chromatography (BioBeads S-X1, toluene). **4-17** was finally obtained after repeated precipitation from MeOH as a yellow solid (8 mg, 18%). Mp > 400 °C. ^{1}H NMR (CD$_2$Cl$_2$, 700 MHz, δ): 1.56 (s, 72H), 1.66 (s, 144H), 1.81 (m, 216H), 7.06 (t, $J_1 = 5$ Hz, $J_2 = 7.5$ Hz, 24H), 7.35 (m, 48H), 7.64 (m, 96H). ^{13}C NMR (CD$_2$Cl$_2$, 176 MHz, δ): 30.1, 33.3, 33.4, 33.6, 36.0, 36.4, 103.1, 121.0, 121.1, 122.2, 123.4, 123.5, 123.9, 124.4, 127.4, 130.2, 130.3, 130.7, 131.5, 132.1, 134.1, 134.5, 134.6, 134.7

(24 out of 38 expected). MALDI-TOF MS (DCTB): $m/z = 8717.41$ (100%) $[M+H]^{+}$. ESI-HR MS could not be obtained due to the low ionization tendency of **4-17**.

Brominated Second Generation Expanded *N*-Heterotriangulene Macrocycle (4-18)
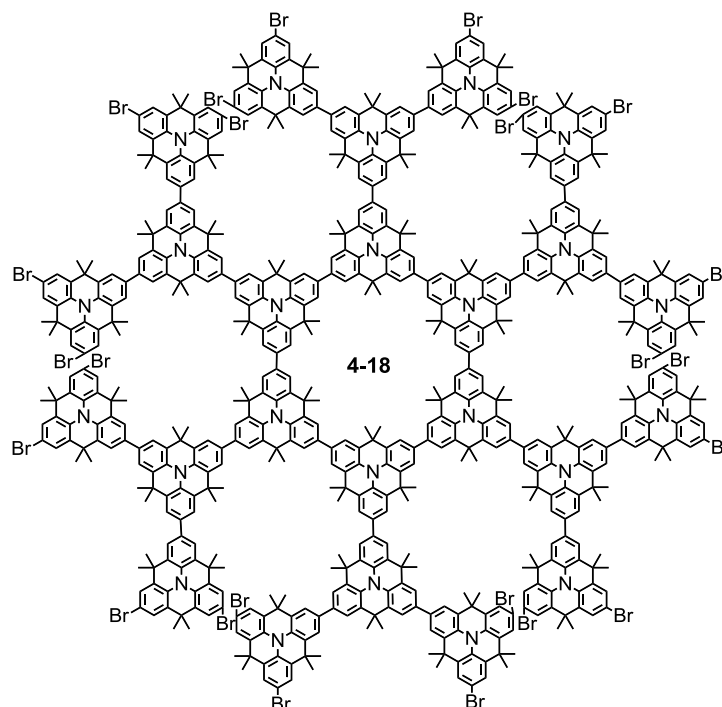
To a solution of heterotriangulene macrocycle **4-17** (38 mg, 0.01 mmol) in CHCl$_3$ (1.5 mL) at 0 °C was added *N*-bromosuccinimide (19 mg, 0.11 mmol). While warming up to room temperature, the resulting solution was stirred in the absence of light for four days. The reaction was quenched with a saturated aqueous solution of Na$_2$S$_2$O$_3$. The resulting mixture was extracted with CH$_2$Cl$_2$ (3x) and the combined organic fractions were dried with MgSO$_4$. Filtration and evaporation of the solvent afforded the **4-18** as a hardly soluble yellow material, which was identified as a complex mixture of brominated species. The compound was used without further purification. MALDI-TOF MS (DCTB + Ag^{+}): $m/z = 8000{-}14000$ (100%).

Attempt toward *N*-Heterotriangulene Heptacycle (4-19)

4-19
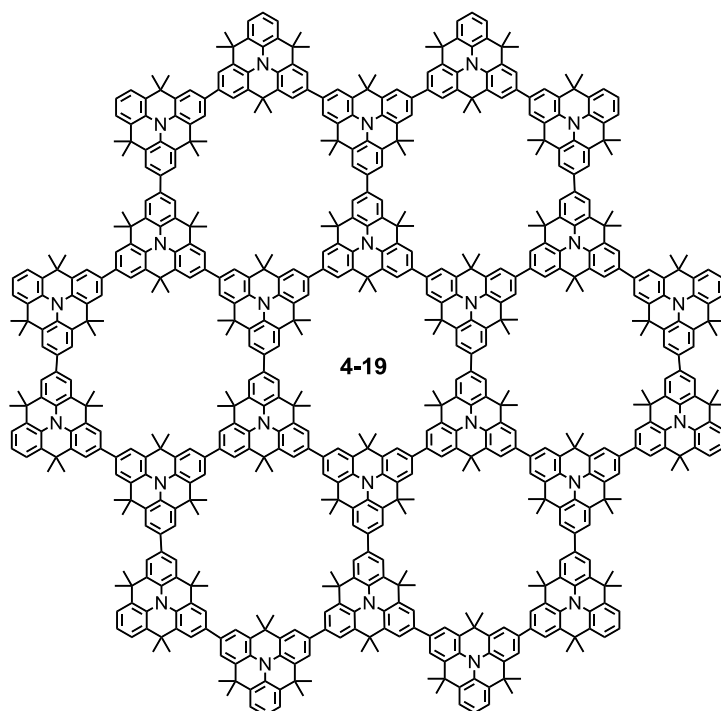
Bis(1,5-cyclooctadiene)nickel(0) (64 mg, 0.23 mmol), 1,5-cyclooctadiene (25 mg, 0.03 mL, 0.03 mmol) and 2,2'-bipyridine (36 mg, 0.23 mmol) were added to a flame-dried 25 mL Schlenk flask, dissolved in 1 mL anhydrous *N,N*-dimethylformamide and stirred for 30 min at 65 °C in the absence of light. A solution of **4-18** (82 mg, 0.01 mmol) in 1.5 mL anhydrous toluene at 65 °C was added slowly *via* a double-tipped needle and the resulting mixture was stirred for four days at 85 °C. The reaction was quenched by adding 10% aqueous hydrochloric acid, extracted with CH_2Cl_2 (3x) and the organic phase was dried with $MgSO_4$. After having removed the solvents *in vacuo*, the residue was separated with the help of preparative size exclusion chromatography (BioBeads S-X1, toluene) giving rise to a yellow solid which was identified as a complex mixture of fused and non-fused isomers of **4-19**. ^{1}H NMR (THF-d$_8$, 700 MHz, 60 °C δ): 1.40−1.70 (br), 6.52 (br), 7.14 (br), 7.42 (br). MALDI-TOF MS could not be obtained due to the low ionization tendency of the obtained species.

9.3.3   *N*-Heterotriangulenes as HTMs for sDSSCs

2,6-Dimethoxy-4,4,8,8,12,12-hexamethyl-8,12-dihydro-4*H*-benzo[1,9]quinolizino-[3,4,5,6,7-*defg*]acridine (5-1)

5-1
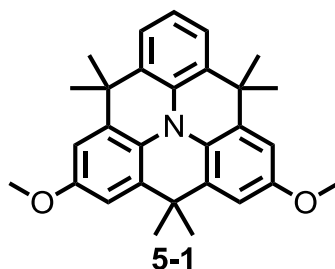
A flame-dried 50 mL Schlenk flask was equipped with sodium methanolate (1.90 g, 35.1 mmol, 6.5 mL; 5.4 M in MeOH), copper(I) iodide (0.77 g, 4.05 mmol) and dibromo *N*-heterotriangulene **3-5** (0.21 g, 0.40 mmol), suspended in *N*,*N*-dimethylformamide (12.4 mL) and degassed with argon for 30 min. This mixture was stirred under an atmosphere of argon at 100 °C overnight. The reaction was stopped by addition of aqueous NH$_4$Cl solution and the resulting mixture was extracted with CH$_2$Cl$_2$ (3x). The combined organic fractions were dried with MgSO$_4$, filtered and the solvents were evaporated. The crude product was purified by column chromatography (silica, *n*-hexane/EtOAc 8:1) yielding **5-1** as a colorless oil (0.120 g, 70%), which solidified upon cooling and became greenish after a few days in the presence of light.

Mp: 73 °C. ^{1}H NMR (CD$_2$Cl$_2$, 250 MHz, δ): 1.49 (s, 12H), 1.52 (s, 6H), 3.74 (broad s, 6H), 6.84 (s, 4H), 7.24 (m, 3H). ^{13}C NMR (CD$_2$Cl$_2$, 63 MHz, δ): 30.1, 32.2, 55.8, 109.5, 110.5, 116.5, 123.0, 123.7, 123.9, 139.1 (10 out of 11). FD-MS (8kV): *m/z* = 425.7 (100%, M$^+$). ESI-HR MS calcd for C$_{28}$H$_{31}$NO$_2$ ([M+H]$^+$) 426.2433, found 426.2438.

2,6,10-Tribromo-4,4,8,8,12,12-hexamethyl-8,12-dihydro-4*H*-benzo[1,9]quinolizino-[3,4,5,6,7-*defg*]acridine (5-2)

5-2
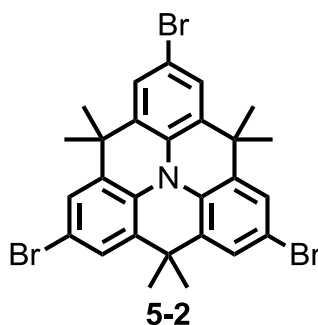
To a solution of *N*-heterotriangulene$^{[6, 7]}$ **3-4** (516 mg, 1.41 mmol) in CHCl$_3$ (30 mL) at 0 °C was added *N*-bromosuccinimide (754 mg, 4.24 mmol). While warming up to room

temperature, the resulting solution was stirred in the absence of light overnight. The reaction was quenched with a saturated aqueous solution of $Na_2S_2O_3$. The resulting mixture was extracted with CH_2Cl_2 (3x) and the combined organic fractions were dried with $MgSO_4$. After filtration and evaporation of the solvent, the residue was subjected to column chromatography (silica, n-hexane/CH_2Cl_2 4:1). Final recrystallization from ethanol yielded **5-2** as a white powder (760 mg, 90%). Mp: 210 °C. ^{1}H NMR (CDCl_3, 250 MHz, δ): 1.61 (s, 18H), 7.47 (s, 6H). ^{13}C NMR (CDCl_3, 63 MHz, δ): 29.7, 32.5, 115.8, 123.6, 126.5, 131.8. FD-MS (8kV): m/z = 600.5 (100%, M[+]). Anal. Calcd. for $C_{27}H_{24}Br_3N$: C 53.85%, H 4.02%, N 2.33%. Found: C 54.20%, H 3.76%, N 1.95%.

2,6,10-Trimethoxy-4,4,8,8,12,12-hexamethyl-8,12-dihydro-4H-benzo[1,9]quinolizino-[3,4,5,6,7-*defg*]acridine (5-3)

5-3
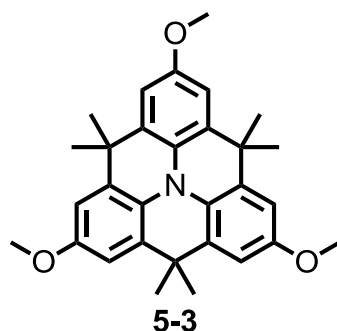
A flame-dried 50 mL Schlenk flask was equipped with sodium methanolate (5.24 g, 96.9 mmol, 17.9 mL; 5.4 M in MeOH), copper(I) iodide (0.68 g, 3.59 mmol) and tribromo N-heterotriangulene **5-2** (0.22 g, 0.36 mmol), suspended in N,N-dimethylformamide (11 mL) and degassed with argon for 30 min. This mixture was stirred under an atmosphere of argon at 100 °C overnight. The reaction was stopped by addition of aqueous NH_4Cl solution and the resulting mixture was extracted with CH_2Cl_2 (3x). The combined organic fractions were dried with $MgSO_4$, filtered and the solvents were evaporated. The crude product was purified by column chromatography (silica, n-hexane/EtOAc 8:1) yielding **5-3** as a white, crystalline solid (0.15 g, 88%). Crystals suitable for X-ray analysis were grown by slow evaporation of a THF solution of **5-3**. Mp: 142 °C. ^{1}H NMR (THF-d_8, 700 MHz, δ): 1.60 (s, 18H), 3.80 (s, 9H), 6.94 (s, 6H). ^{13}C NMR (CD_2Cl_2, 63 MHz, δ): 27.1, 30.1, 55.8, 92.5, 103.2, 107.8, (6 out of 7). FD-MS (8kV): m/z = 455.7 (100%, M[+]). ESI-HR MS calcd for $C_{30}H_{33}NO_3$ ([M][+]) 455.2455, found 455.2459. Anal. Calcd. for $C_{30}H_{33}NO_3$: C 79.09%, H 7.30%, N 3.07%. Found: C 78.15%, H 7.44%, N 2.80%.

N-Heterotriangulene Dimer (5-4)

5-4
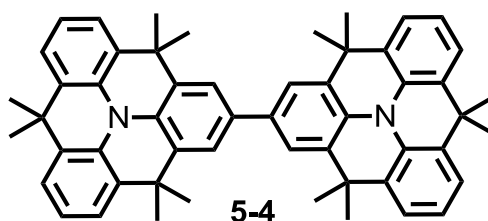
Bis(1,5-cyclooctadiene)nickel(0) (193 mg, 0.70 mmol), 1,5-cyclooctadiene (8 mg, 0.09 mL, 0.70 mmol) and 2,2'-bipyridine (109 mg, 0.70 mmol) were added to a flame-dried 100 mL Schlenk flask, dissolved in 9.4 mL anhydrous N,N-dimethylformamide and stirred for 30 min at 65 °C in the absence of light. A solution of monobromo N-heterotriangulene **4-4** (250 mg, 0.56 mmol) in 18.8 mL anhydrous toluene at 65 °C was added slowly *via* a double-tipped needle and the resulting mixture was stirred for two days at 85 °C. The reaction was quenched by adding 10% aqueous hydrochloric acid, extracted with CH_2Cl_2 (3x) and the organic phase was dried with $MgSO_4$. After having removed the solvents *in vacuo*, the residue was subjected to column chromatography (silica, n-hexane/CH_2Cl_2 3:1) leading to triangulene dimer as a white crystalline solid (165 mg, 80%). Crystals suitable for X-ray analysis were grown by slow evaporation of a dichloromethane/n-hexane solution of **5-4**. Mp> 380 °C decomp. ^{1}H NMR (THF-d$_8$, 700 MHz, δ): 1.62 (s, 12H), 1.70 (s, 24H), 7.11 (t, $J_1 = J_2 = 7.7$ Hz, 4H), 7.42 (dd, $J_1 = 7.6$ Hz, $J_2 = 1.5$ Hz, 4H), 7.44 (dd, $J_1 = 7.6$ Hz, $J_2 = 1.5$ Hz, 4H) 7.65 (s, 4H). ^{13}C NMR (THF-d$_8$, 176 MHz, δ): 30.5, 33.2, 33.3, 36.1, 36.3, 122.5, 123.6, 124.1, 124.2, 130.5, 130.9, 131.6, 132.5, 136.7. FD-MS (8kV): m/z = 728.1 (100%, M$^+$), 364.5 (10%, M^{2+}). ESI-HR MS calcd for $C_{54}H_{52}N_2$ ([M+H]$^+$) 729.4203, found 729.4193.

9.3.4   Sterically π-Congested Poly(*para*phenylenes)

4'',5'-Diphenyl-1,1':2',1'':2'',1'''-quaterphenyl (6-5)
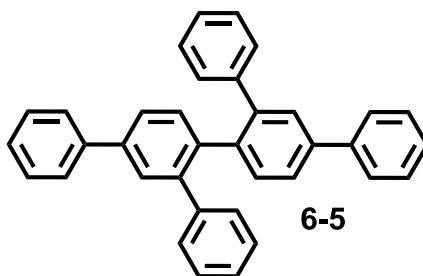
Bis(1,5-cyclooctadiene)nickel(0) (255 mg, 0.93 mmol), 1,5-cyclooctadiene (100 mg, 0.11 mL, 0.93 mmol) and 2,2'-bipyridine (145 mg, 0.93 mmol) were added to a flame-dried 100 mL Schlenk flask, dissolved in 10 mL anhydrous *N,N*-dimethylformamide and stirred for 30 min at 65 °C in the absence of light. A solution of 2'-iodo-1,1':3',1''-terphenyl[9-11] (**6-4**) (300 mg, 0.84 mmol) in 20 mL anhydrous toluene at 65 °C was added *via* a double-tipped needle and the resulting mixture was stirred overnight at 85 °C. The reaction was quenched by adding 1N aqueous hydrochloric acid, extracted with CH_2Cl_2 (3x) and the organic phase was dried with $MgSO_4$. After having removed the solvents *in vacuo*, the residue was subjected to column chromatography (silica, *n*-hexane/CH_2Cl_2 3:1 to 2:1). **6-5** was obtained as a white solid (41 mg, 21%). Crystals suitable for X-ray analysis were grown by slow evaporation of a toluene solution of **6-5**. Mp: 239 °C. ^{1}H NMR (CD_2Cl_2, 250 MHz, δ): 6.45–7.65 (m, 26H). ^{13}C NMR (CD_2Cl_2, 63 MHz, δ): 125.1, 126.0, 126.5, 127.4, 127.9, 128.4, 128.9, 130.1, 130.3, 132.1, 132.3. FD-MS (8kV): m/z = 458.7 (100%, M$^+$). FD-MS (8kV): m/z = 480.9 (100%, M$^+$), ESI-HR MS calcd for $C_{36}H_{26}$ ([M+Na]$^+$) 481.1923, found 481.1931.

5'-Methyl-[1,1':3',1''-terphenyl]-2'-amine (6-7)
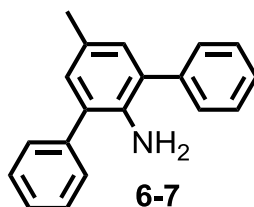
A 250 mL Schlenk tube was equipped with 2,6-dibromo-4-methylaniline (**6-6**) (1.5 g, 5.66 mmol) and phenylboronic acid (2.07 g, 16.98 mmol) followed by three times evacuating and backfilling with argon. After the addition of 100 mL toluene, solid K_2CO_3 (7.82 g, 56.62 mmol) and three drops of *Aliquat 336* the resulting mixture was degassed with argon for one hour. To this mixture Pd(PPh$_3$)$_4$ (262 mg, 4 mol%) was added and it was stirred under an atmosphere of argon at 100 °C overnight. The addition of water,

washing the aqueous phase with toluene (3x), drying the combined organic phases with MgSO$_4$ and evaporating of the solvent *in vacuo* resulted in a crude mixture which was subjected to column chromatography (silica, *n*-hexane/CH$_2$Cl$_2$ 1:2). Amine **6-7** was obtained as colorless oil (1.37 g, 93%). ^{1}H NMR (CD$_2$Cl$_2$, 250 MHz, δ): 2.41 (s, 3H), 7.05 (s, 2H), 7.40–7.65 (m, 10H). ^{13}C NMR (CD$_2$Cl$_2$, 75 MHz, δ): 20.6, 127.6, 128.4, 129.2, 129.7, 130.8, 138.8, 139.2 140.5. FD-MS (8kV): *m/z* = 259.3 (100%, M$^+$).

2'-Iodo-5'-methyl-1,1':3',1''-terphenyl (6-8)

6-8
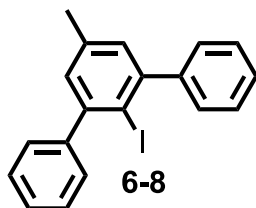
A solution of 5'-methyl-[1,1':3',1''-terphenyl]-2'-amine (**6-7**) (1.37 g, 5.27 mmol) in acetic acid (6.5 mL) was added dropwise to a suspension of solid NaNO$_2$ (0.38 g, 5.54 mmol) in conc. sulfuric acid (4.5 mL) at 0 °C. After vigorously stirring for one hour at 0 °C, the diazonium salt was added to a solution of KI (0.92 g, 5.54 mmol) in H$_2$O (12 mL) at 50 °C and stirred at 70 °C for one hour. The reaction was quenched by the addition of water and the mixture was extracted with CH$_2$Cl$_2$ (3x). The combined organic phase was dried with MgSO$_4$, filtered and the solvents were evaporated *in vacuo*. Compound **6-8** was obtained after column chromatographic separation (silica, *n*-hexane/CH$_2$Cl$_2$ 1:1 to 4:1) as colorless oil (1.04 g, 53%). ^{1}H NMR (CD$_2$Cl$_2$, 250 MHz, δ): 2.21 (s, 3H), 7.00 (s, 2H), 7.20 – 7.32 (m, 10H). ^{13}C NMR (CD$_2$Cl$_2$, 75 MHz, δ): 21.0, 127.9, 128.3, 129.9, 131.5, 137.4, 142.6, 143.9 (8 out of 9 expected). FD-MS (8kV): *m/z* = 370.4 (100%, M$^+$). ESI-HR MS calcd for C$_{19}$H$_{15}$I ([M+H]$^+$) 371.0297, found 371.0301.

2-([1,1':3',1''-Terphenyl]-2'-yl)-4,4,5,5-tetramethyl-1,3,2-dioxaborolane (6-11)

6-11
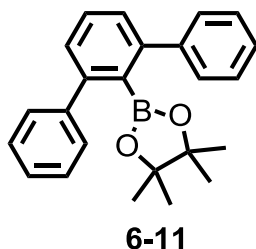
2'-Iodo-1,1':3',1''-terphenyl[9-11] (**6-4**) (1 g, 2.81 mmol) was added to a flame-dried 50 mL Schlenk flask and dissolved in 12.5 mL anhydrous Et$_2$O under an argon atmosphere. To the resulting solution was added dropwise *n*-BuLi (2.11 mL, 3.37 mmol, 1.6 M in *n*-hexane) at room temperature and stirred for additional two hours. The solution was subsequently

cooled to -78 °C and 2-isopropoxy-4,4,5,5-tetramethyl-1,3,2-dioxaborolane (1.04 g, 1.15 mL, 5.61 mmol) was added with a syringe. After warming up to room temperature overnight, the reaction mixture was quenched with 1 N aqueous hydrochloric acid, extracted with CH_2Cl_2 (3x), the combined organic phases were dried with $MgSO_4$ and filtered. The solvents were evaporated *in vacuo* and the residue was subjected to column chromatography (silica, *n*-hexane/CH_2Cl_2 1:1 to 1:2) yielding **6-11** as a white crystalline solid (900 mg, 91%). Mp: 142 °C. ^{1}H NMR (CD_2Cl_2, 250 MHz, δ): 0.76 (s, 12H), 7.18–7.40 (m, 13H). ^{13}C NMR (CD_2Cl_2, 75 MHz, δ): 25.1, 84.1, 127.5, 127.8, 127.9, 128.4, 128.9, 129.6, 130.0, 143.8, 146.8. FD-MS (8kV): m/z = 355.1 (100%, M$^+$). ESI-HR MS calcd for $C_{24}H_{25}BO_2$ ([M+H]$^+$) 357.2026, found 357.2035.

5'-Chloro-[1,1':3',1''-terphenyl]-2'-amine (6-13)
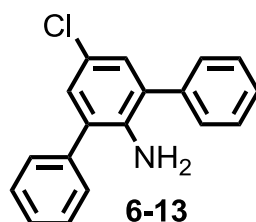
A 250 mL Schlenk tube was equipped with 2,6-dibromo-4-chloroaniline (**6-12**) (6.0 g, 21.03 mmol) and phenylboronic acid (6.41 g, 52.56 mmol) followed by three times evacuating and backfilling with argon. After the addition of 150 mL toluene, solid K_2CO_3 (43.6 g, 315.39 mmol) and three drops of *Aliquat 336* the resulting mixture was degassed with argon for one hour. To this mixture Pd(PPh$_3$)$_4$ (729 mg, 3 mol%) was added and it was stirred under an atmosphere of argon at 100 °C overnight. The addition of water, washing the aqueous phase with toluene (3x), drying the combined organic phases with $MgSO_4$ and evaporating of the solvent *in vacuo* resulted in a crude mixture which was subjected to column chromatography (silica, *n*-hexane/CH_2Cl_2 2:1). Compound **6-13** was obtained as colorless oil (5.55 g, 94%). ^{1}H NMR (CD_2Cl_2, 250 MHz, δ): 6.98 (s, 2H), 7.23–7.41 (m, 10H). ^{13}C NMR (CD_2Cl_2, 75 MHz, δ): 122.7, 128.1, 129.4, 129.5, 129.6, 139.0, 140.2 (7 out of 8 expected). FD-MS (8kV): m/z = 278.1 (100%, M$^+$).

5'-Chloro-2'-iodo-1,1':3',1''-terphenyl (6-14)
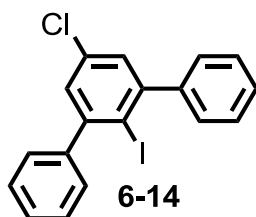
To a suspension of 5'-chloro-[1,1':3',1''-terphenyl]-2'-amine (**6-13***)* (5.55 g, 19.84 mmol) in conc. hydrochloric acid (15 mL) was added dropwise to a solution of NaNO$_2$ (1.49 g, 21.62 mmol) in H$_2$O (6.6 mL) at 0 °C. After vigorously stirring for 1.5 hours at 0 °C, the diazonium salt was added to a solution of KI (27.43 g, 165.25 mmol) in H$_2$O (37.5 mL) and stirred at room temperature overnight. The reaction was quenched by the addition of aqueous Na$_2$SO$_3$ solution and the mixture was extracted with CH$_2$Cl$_2$ (3x). The combined organic phase was dried with MgSO$_4$, filtered and the solvents were evaporated *in vacuo*. The residue was recrystallized from EtOH, yielding **6-14** as colorless needles (4.50 g, 58%). Mp: 129 °C. ^{1}H NMR (CD$_2$Cl$_2$, 250 MHz, δ): 7.34 (s, 2H), 7.37–7.56 (m, 10H). ^{13}C NMR (CD$_2$Cl$_2$, 75 MHz, δ): 100.4, 101.5, 128.4, 128.5, 128.8, 129.6, 144.5, 149.9. FD-MS (8kV): *m/z* = 389.3 (100%, M$^+$). ESI-HR MS calcd for C$_{18}$H$_{12}$ClI ([M+H]$^+$) 390.9750, found 390.9763.

2-(5'-Chloro-[1,1':3',1''-terphenyl]-2'-yl)-4,4,5,5-tetramethyl-1,3,2-dioxaborolane (6-15)
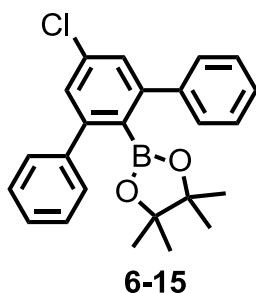
5'-Chloro-2'-iodo-1,1':3',1''-terphenyl (**6-14**) (1 g, 2.56 mmol) was added to a flame-dried 50 mL Schlenk flask and dissolved in 12.5 mL anhydrous Et$_2$O under an argon atmosphere. To the resulting solution was added dropwise *n*-BuLi (1.92 mL, 3.07 mmol, 1.6 M in hexane) at room temperature and stirred for additional two hours. The solution was subsequently cooled to -78 °C and 2-isopropoxy-4,4,5,5-tetramethyl-1,3,2-dioxaborolane (0.95 mg, 1.05 mL, 5.11 mmol) was added with a syringe. After warming up to room temperature overnight, the reaction mixture was quenched with 1 N aqueous hydrochloric acid, extracted with CH$_2$Cl$_2$ (3x), the combined organic phases were dried with MgSO$_4$ and filtered. The solvents were evaporated *in vacuo* and the residue was

subjected to column chromatography (silica, *n*-hexane/CH$_2$Cl$_2$ 1:1 to 1:2), yielding **6-15** as a white crystalline solid (0.91 g, 91%). Mp: 212 °C. ^{1}H NMR (CD$_2$Cl$_2$, 250 MHz, δ): 0.75 (s, 12H), 7.17 – 7.42 (m, 12H). ^{13}C NMR (CD$_2$Cl$_2$, 75 MHz, δ): 25.3, 84.1, 127.7, 127.9, 128.0, 128.4, 128.9, 129.6, 130.0, 143.8, 146.8. FD-MS (8kV): *m/z* = 389.9 (100%, M$^+$). ESI-HR MS calcd for C$_{24}$H$_{25}$BClO$_2$ ([M+H]$^+$) 391.1636, found 391.1655.

5',5'''''-Dichloro-1,1':3',1'':2'',1''':2''',1'''':3'''',1'''''-sexiphenyl (6-17)

6-17
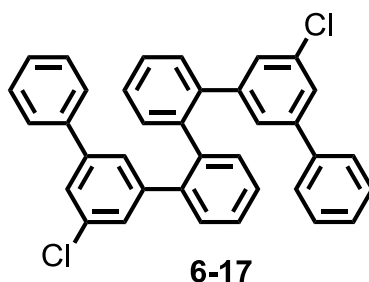
A 100 mL Schlenk tube was equipped with 2-(5'-chloro-[1,1':3',1''-terphenyl]-2'-yl)-4,4,5,5-tetramethyl-1,3,2-dioxaborolane (**6-15**) (300 mg, 0.77 mmol) and 5'-chloro-2'-iodo-1,1':3',1''-terphenyl (**6-14**) (300 mg, 0.77 mmol) followed by three times evacuating and backfilling with argon. After the addition of 30 mL toluene, aqueous 2 M K$_2$CO$_3$ solution (15 mL) and three drops of *Aliquat 336* the resulting mixture was degassed with argon for one hour. To this mixture Pd(PPh$_3$)$_4$ (35 mg, 4 mol%) was added and it was stirred under an atmosphere of argon at 100 °C for one day. After the addition of water, washing the aqueous phase with toluene (3x), drying the combined organic phases with MgSO$_4$ and evaporating of the solvent *in vacuo*, the crude mixture was subjected to column chromatography (silica, *n*-hexane/CH$_2$Cl$_2$ 4:1). Compound **6-17** was obtained as a white solid (42 mg, 21%). Crystals suitable for X-ray analysis were grown by slow evaporation of a CH$_2$Cl$_2$/MeOH solution of **6-17**. Mp: 187 °C. ^{1}H NMR (CD$_2$Cl$_2$, 250 MHz, δ): 5.91 (d, *J* = 7.5 Hz, 2H), 6.30 (d, *J* = 10 Hz, 2H), 6.53 (s, 4H) 6.67 – 7.47 (m, 16H). ^{13}C NMR (CD$_2$Cl$_2$, 63 MHz, δ): 125.3, 126.2, 126.6, 127.4, 127.9, 128.4, 128.9, 130.3, 130.5, 142.1, 142.3 (11 out of 16 expected). FD-MS (8kV): *m/z* = 525.1 (100%, M$^+$). ESI-HR MS calcd for C$_{36}$H$_{24}$Cl$_2$ ([M+H]$^+$) 527.1333, found 527.1322.

1,3-Dibromo-2-iodo-5-methylbenzene (6-19)

6-19
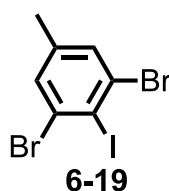
To a suspension of 2,6-dibromo-4-methylaniline (**6-18**) (6.00 g, 22.65 mmol) in conc. hydrochloric acid (15 mL) was added dropwise a solution of $NaNO_2$ (1.72 g, 24.91 mmol) in H_2O (7.8 mL) at 0 °C. After vigorously stirring for 2 hours at 0 °C, the diazonium salt was added to a solution of KI (31.32 g, 188.64 mmol) in H_2O (44 mL) and stirred at room temperature overnight. The reaction was quenched by the addition of aqueous Na_2SO_3 solution and the mixture was extracted with CH_2Cl_2 (3x). The combined organic phases were dried with $MgSO_4$, filtered and the solvents were evaporated *in vacuo*. The residue was recrystallized from EtOH, yielding **6-19** as a white solid (7.23 g, 85%). Mp: 70 °C. ^{1}H NMR (CD_2Cl_2, 250 MHz, δ): 2.30 (s, 3h), 7.47 (s, 2H). ^{13}C NMR (CD_2Cl_2, 75 MHz, δ): 21.4, 107.6, 131.4, 131.8, 135.8. FD-MS (8kV): m/z = 375.6 (100%, M$^+$).

2,2',6,6'-Tetrabromo-4,4'-dimethyl-1,1'-biphenyl (6-20)
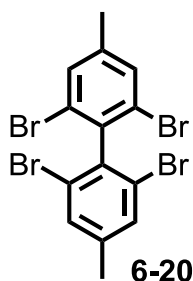
1,3-Dibromo-2-iodo-5-methylbenzene (**6-19**) (4.2 g, 11.18 mmol) and anhydrous $CuCl_2$ (9.0 g, 67.05 mmol) was added to a flame-dried 100 mL Schlenk flask and suspended in 37 mL anhydrous Et_2O under an argon atmosphere. The resulting mixture was cooled to -78 °C and *n*-BuLi (7.54 mL, 12.07 mmol, 1.6 M in *n*-hexane) was added dropwise over 2.5 hours. After warming up to room temperature overnight, the reaction mixture was quenched with aqueous NH_4Cl solution, extracted with CH_2Cl_2 (3x), the combined organic phases were dried with $MgSO_4$ and filtered. The solvents were evaporated *in vacuo* and the residue was subjected to column chromatography (silica, *n*-hexane), yielding **6-20** as a white crystalline solid (1.53 g, 55%). Mp: 215 °C. ^{1}H NMR (CD_2Cl_2, 250 MHz, δ): 2.43 (s, 6H), 7.55 (s, 4H). ^{13}C NMR (CD_2Cl_2, 75 MHz, δ): 20.9, 124.4, 132.8, 142.2, 153.6. FD-MS (8kV): m/z = 498.1 (100%, M$^+$). Anal. Calcd. for $C_{14}H_{10}Br_4$: C 33.78%, H 2.02%. Found: C 33.51%, H 1.95%.

4,4'-Dimethyl-2,2',6,6'-tetraphenyl-1,1'-biphenyl (6-9)

6-9
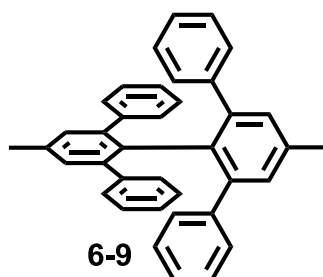
A 50 mL Schlenk tube was equipped with 2,2',6,6'-tetrabromo-4,4'-dimethyl-1,1'-biphenyl (**6-20**) (150 mg, 0.30 mmol) and phenylboronic acid (220 mg, 1.81 mmol) followed by three times evacuating and backfilling with argon. Afterwards 30 mL toluene, solid K_2CO_3 (1.67 g, 12.05 mmol) and three drops of *Aliquat 336* were added. The resulting mixture was degassed with argon for 1.5 hours. To this mixture $Pd(PPh_3)_4$ (35 mg, 2.5 mol%) was added and it was stirred under an atmosphere of argon at 100 °C for two days. After the addition of water, washing the aqueous phase with toluene (3x), drying the combined organic phases with $MgSO_4$ and evaporating of the solvent *in vacuo*, the crude mixture was subjected to column chromatography (silica, *n*-hexane/CH_2Cl_2 4:1). Finally the product fraction was recrystallized from *n*-hexane, yielding **6-9** as a white solid (69 mg, 47%). Crystals suitable for X-ray analysis were grown by slow evaporation of a CH_2Cl_2/MeOH solution of **6-9**. Mp: 288 °C. ^{1}H NMR (CD_2Cl_2, 500 MHz, δ): 2.38 (s, 6H), 6.63 (d, J = 10 Hz, 8H), 6.99 (m, 12H), 7.11 (t, $J_1 = J_2 = 5$ Hz, 4H). ^{13}C NMR ($CDCl_3$, 176 MHz, 323 K, δ): 21.1, 125.6, 127.1, 129.2, 130.6, 132.9, 137.0, 141.7, 142.0. FD-MS (8kV): m/z = 486.7 (100%, M$^+$). Anal. Calcd. for $C_{38}H_{30}$: C 91.79%, H 6.21%. Found: C 91.48%, H 5.92%.

1,3-Dibromo-5-chloro-2-iodobenzene (6-22)

6-22
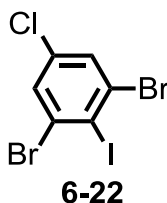
A suspension of 2,6-dibromo-4-chloroaniline (**6-21**) (10.0 g, 35.04 mmol) in conc. hydrochloric acid (19 mL) was added dropwise to a solution of $NaNO_2$ (2.6 g, 38.20 mmol) in H_2O (12 mL) at 0 °C. After vigorously stirring for 2 hours at 0 °C, the diazonium salt was added to a solution of KI (48.5 g, 291.91 mmol) in H_2O (68 mL) and the resulting mixture was stirred at room temperature overnight. The reaction was quenched by the addition of aqueous Na_2SO_3 solution and the mixture was extracted with

CH$_2$Cl$_2$ (3x). The combined organic phase was dried with MgSO$_4$, filtered and the solvents were evaporated *in vacuo*. The residue was recrystallized (3x) from EtOH, yielding **6-22** as off-white needles (7.6 g, 55%). Mp: 104 °C. ^{1}H NMR (CD$_2$Cl$_2$, 250 MHz, δ): 7.47 (s, 2H). ^{13}C NMR (CD$_2$Cl$_2$, 75 MHz, δ): 107.6, 131.4, 131.8, 135.8. FD-MS (8kV): m/z = 395.7 (100%, M$^+$).

2,2',6,6'-Tetrabromo-4,4'-dichloro-1,1'-biphenyl (6-23)
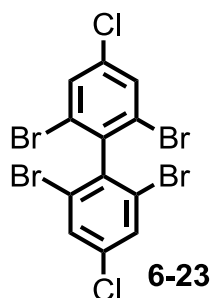
1,3-Dibromo-5-chloro-2-iodobenzene (**6-22**) (3.5 g, 8.83 mmol) and anhydrous CuCl$_2$ (7.1 g, 53.00 mmol) was added to a flame-dried 100 mL Schlenk flask and suspended in 28 mL anhydrous Et$_2$O under an argon atmosphere. The resulting mixture was cooled to -78 °C and *n*-BuLi (5.96 mL, 9.54 mmol, 1.6 M in *n*-hexane) was added dropwise over 2.5 hours. After warming up to room temperature overnight, the reaction mixture was quenched with aqueous NH$_4$Cl solution, extracted with CH$_2$Cl$_2$ (3x), the combined organic phases were dried with MgSO$_4$ and filtered. The solvents were evaporated *in vacuo* and the residue was subjected to column chromatography (silica, *n*-hexane) yielding **6-23** as a white crystalline material (1.91 g, 50%). Mp: 95 °C. ^{1}H NMR (CD$_2$Cl$_2$, 250 MHz, δ): 7.77 (s, 4H). ^{13}C NMR (CD$_2$Cl$_2$, 75 MHz, δ): 124.8, 132.2, 136.2 (3 out of 4 expected). FD-MS (8kV): m/z = 539.3 (100%, M$^+$). Anal. Calcd. for C$_{12}$H$_4$Br$_4$Cl$_2$: C 26.76%, H 0.75%. Found: C 26.92%, H 0.88%.

4,4'-Dichloro-2,2',6,6'-tetraphenyl-1,1'-biphenyl (6-24)
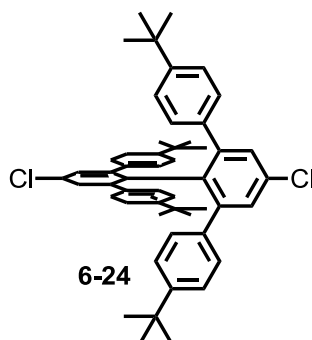
A 50 mL Schlenk tube was equipped with 2,2',6,6'-tetrabromo-4,4'-dichloro-1,1'-biphenyl (**6-23**) (1.0 g, 1.86 mmol) and (4-(*tert*-butyl)phenyl)boronic acid (1.98 g, 11.14 mmol)

followed by three times evacuating and backfilling with argon. Subsequently, 55 mL toluene, solid K_2CO_3 (10.26 g, 74.26 mmol) and three drops of *Aliquat 336* were added and the resulting mixture was degassed with argon for 2 hours. To this mixture $Pd(PPh_3)_4$ (215 mg, 2.5 mol%) was added and it was stirred under an atmosphere of argon at 100 °C for four days. After the addition of water, washing the aqueous phase with toluene (3x), drying the combined organic phases with $MgSO_4$ and evaporating of the solvent *in vacuo*, the crude mixture was subjected to column chromatography (silica, petrolether/CH_2Cl_2 20:1). Finally the product fraction was crystallized from petrolether/CH_2Cl_2 solution, yielding **6-24** as a white, crystalline solid (0.65 g, 47%). Crystals suitable for X-ray analysis were grown by slow evaporation of a CH_2Cl_2 solution of **6-24**. Mp: 319 °C. ^{1}H NMR (CD_2Cl_2, 250 MHz, δ): 1.23 (s, 36H), 6.38 (d, $J = 10$ Hz, 8H), 6.91 (d, $J = 10$ Hz, 8H), 7.05 (s, 4H). ^{13}C NMR (CD_2Cl_2, 75 MHz, δ): 31.3, 34.6, 124.7, 128.9, 129.4, 133.7, 133.8, 137.4, 144.3, 149.9. FD-MS (8kV): $m/z = 753.4$ (100%, M^+). Anal. Calcd. for $C_{52}H_{56}Cl_2$: C 83.06%, H 7.51%. Found: C 82.98%, H 7.03%.

Polymerization Procedure of 6-24

Bis(1,5-cyclooctadiene)nickel(0) (121 mg, 0.44 mmol), 1,5-cyclooctadiene (47 mg, 0.05 mL, 0.44 mmol) and 2,2'-bipyridine (69 mg, 0.44 mmol) were added to a flame-dried 10 mL microwave vial, dissolved in 1.6 mL anhydrous *N,N*-dimethylformamide, sealed and stirred for 30 min at 65 °C in the absence of light. A solution of **6-24** (150 mg, 0.20 mmol) in 2.4 mL anhydrous toluene at 65 °C was added *via* a double-tipped needle and the resulting mixture was heated in a CEM microwave at 300 W and activated cooling, keeping the temperature at 110 °C for two days. The reaction mixture was precipitated in 150 mL MeOH/conc. HCl (10:1) and stirred for 2 hours resulting in a white solid after filtration (119 mg, 79%). The polymer was separated by preparative size-exclusion chromatography (BioBeads S-X1, $CHCl_3$) to allow isolation of **6-25** (25 mg, 9%), **6-26** (18 mg, 5%), **6-27** (10 mg, 2%), **6-28** (11 mg, 2%), **6-29** (8 mg, 1%), **6-30** (8 mg, 1%), **6-31** (5 mg, 0.5%), **6-32** (4 mg, 0.3%) and **6-33** (30 mg, 2%). Compounds **6-25** to **6-28** were identified with the help of mass spectrometry, while their ^{1}H NMR spectra showed broadened and less distinct signals.

π-Congested Dimer (6-25)

6-25
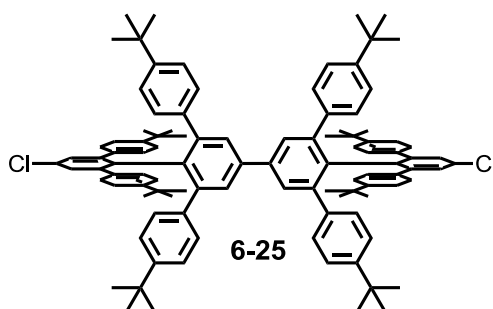
6-25 was obtained as white solid (25 mg, 9%). ^{1}H NMR (CD$_2$Cl$_2$, 700 MHz, δ): 1.34 (s, 36H), 1.35 (s, 36H), 6.57 (dd, J_1 = 6 Hz, J_2 = 2.5 Hz, 16H), 7.03 (t, J_1 = J_2 = 7.5 Hz 16H), 7.19 (s, 4H), 7.51 (s, 4H). ^{13}C NMR (CD$_2$Cl$_2$, 63 MHz, δ): 33.0, 33.1, 33.6, 36.0, 36.2, 115.9, 122.1, 122.5, 123.7, 123.9, 124.3, 126.6, 129.8, 130.3, 131.0, 131.1, 132.5, 132.6, 136.2 (19 out of 20 expected). FD-MS (8kV): m/z = 1434.4 (100%, M$^+$). MALDI-TOF MS (dithranol): m/z = 1435.82 (100%) [M+H]$^+$. ESI-HR MS calcd for C$_{104}$H$_{112}$Cl$_2$ ([M+Na]$^+$) 1453.8039, found 1453.7991.

π-Congested Trimer (6-26)

6-26
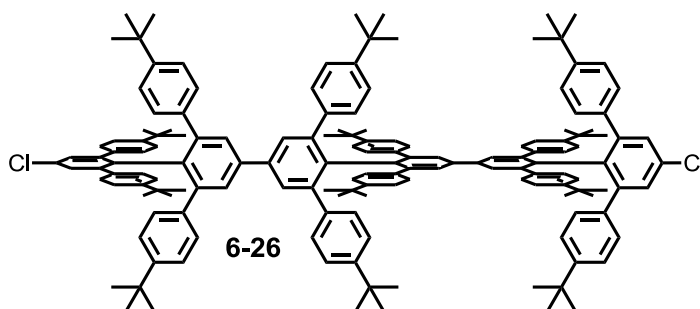
6-26 was obtained as white solid (18 mg, 5%). ^{1}H NMR (CD$_2$Cl$_2$, 700 MHz, δ): 1.33 (s, 36H), 1.34 (s, 36H), 1.35 (s, 36H), 6.57 (dd, J_1 = 6 Hz, J_2 = 2.2 Hz, 16H), 6.63 (d, J = 8 Hz, 8H), 7.03 (m, 24H), 7.19 (s, 4H), 7.53 (s, 8H). ^{13}C NMR (CD$_2$Cl$_2$, 176 MHz, δ): 29.2, 29.7, 31.1, 34.2, 118.5, 124.2, 124.3, 125.0, 127.6, 128.6, 128.7, 128.8, 129.0, 130.7, 133.0, 133.9, 134.3, 134.5, 134.9, 137.3, 137.6, 138.3, 138.6, 138.8, 139.2, 142.8, 142.9, 144.0, 148.9, 149.0, 149.4, 153.7. FD-MS (8kV): m/z = 2113.4 (100%, M$^+$). MALDI-TOF MS (dithranol): m/z = 2114.34 (100%) [M+H]$^+$. ESI-HR MS calcd for C$_{156}$H$_{168}$Cl$_2$ ([M+Na]$^+$) 2134.2421, found 2134.2405.

Polymer (6-33)

6-33
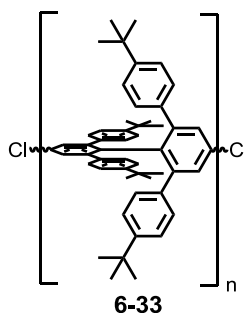
6-33 was obtained as an off-white solid (30 mg, 2%). ^{1}H NMR (CD$_2$Cl$_2$, 300 MHz, δ): 1.29 (br s, 36H), 6.56 (br m, 8H), 7.04 (br m, 8H), 7.48 (br s, 2H), 7.50 (br s, 2H). SEC (eluent: THF, poly(*para*phenylene) calibration): M_n = 10 400 g/mol, PDI = 1.35, DP ~ 15.3. Anal. Calcd. for C$_{780}$H$_{840}$Cl$_2$: C 91.08%, H 8.23%. Found: C 89.46%, H 7.97%.

**2',3',5',6'-Tetrabromo-4,4''-di-*tert*-butyl-1,1':4',1''-terphenyl (6-38)**

6-38
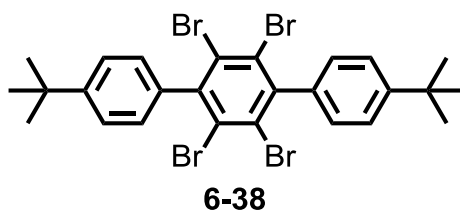
1,2,4,5-Tetrabromo-3,6-diiodobenzene (1.60 g, 2.48 mmol) and copper powder (3.78 g, 59.48 mmol) were added to a flame-dried 50 mL Schlenk flask and the mixture was thoroughly mixed. To this 1-(*tert*-butyl)-4-iodobenzene (3.12 g, 12 mmol) was subsequently added and the resulting suspension was vigorously stirred at 200 °C under an atmosphere of argon overnight. The reaction mixture was diluted with CH$_2$Cl$_2$ and filtered to remove the inorganic residues. The solvent was subsequently evaporated and the mixture was subjected to column chromatography (silica, *n*-hexane). Compound **6-38** was obtained as a white solid (0.44 g, 27%). The product fraction was contaminated by a minute amount of 2',4',5'-tribromo-4,4''-di-*tert*-butyl-1,1':3',1''-terphenyl, which could not be completely removed. Mp: 364 °C. ^{1}H NMR (C$_2$D$_2$Cl$_4$, 500 MHz, δ): 1.45 (s, 18H), 7.17 (d, J = 8 Hz, 4H), 7.53 (d, J = 8 Hz, 4H). ^{13}C NMR (C$_2$D$_2$Cl$_4$, 125 MHz, δ): 31.4, 34.6, 125.2, 127.2, 128.2, 141.0, 145.9, 151.5. FD-MS (8kV): m/z = 655.7 (100%, M$^+$). Anal. Calcd. for C$_{26}$H$_{26}$Br$_4$: C 47.45%, H 3.98%. Found: C 46.95%, H 4.69%.

1,4-Bis(4'-*tert*-butylphenyl)-2,3,5,6-tetrakisphenyl-benzene (6-39)

6-39
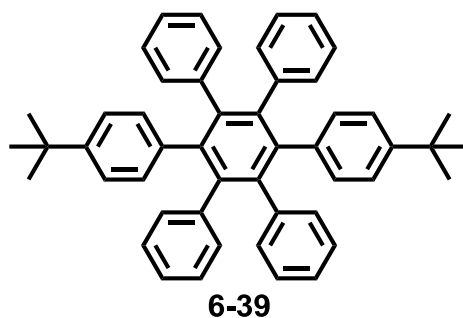
A 50 mL Schlenk tube was equipped with 2',3',5',6'-tetrabromo-4,4''-di-*tert*-butyl-1,1':4',1''-terphenyl (**6-38**) (0.15 mg, 0.23 mmol) and phenylboronic acid (0.17 g, 1.37 mmol) followed by three times evacuating and backfilling with argon. After the addition of 6.8 mL toluene, solid K_2CO_3 (1.26 g, 9.12 mmol) and three drops of *Aliquat 336* the resulting mixture was degassed with argon for 1.5 hours. To this mixture $Pd(PPh_3)_4$ (26 mg, 2.5 mol%) was added and it was stirred under an atmosphere of argon at 100 °C overnight. After the addition of water, washing the aqueous phase three times with toluene, drying the combined organic phases with $MgSO_4$ and evaporating of the solvent *in vacuo*, the crude mixture was subjected to column chromatography (silica, *n*-hexane/CH_2Cl_2 4:1). Finally **6-39** was obtained as a white solid (0.13 g, 87%). Mp: 383 °C. ^{1}H NMR (CD_2Cl_2, 300 MHz, δ): 1.12 (s, 18H), 6.75 (d, $J = 5$ Hz, 4H), 6.85 (m, 20H), 6.88 (d, $J = 5$ Hz, 4H). ^{13}C NMR (CD_2Cl_2, 75 MHz, δ): 31.5, 34.6, 123.8, 125.6, 127.0, 131.6, 132.0, 138.2, 140.8, 141.0, 141.6, 148.6. FD-MS (8kV): $m/z = 646.4$ (100%, M$^+$). Anal. Calcd. for $C_{50}H_{46}$: C 92.83%, H 7.17%. Found: C 90.80%, H 8.53% (see general remarks "Elemental Analysis").

9.3.5   Tetrafunctionalized Biphenylenes

(2,3-Dibromo-5,6-dimethoxy-1,4-phenylene)bis(trimethylsilyl) (7-9)

7-9
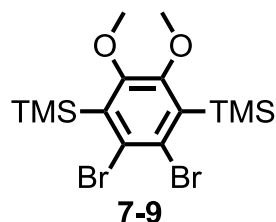
1,2-Dibromo-4,5-dimethoxybenzene (15.0 g, 50.70 mmol) and chlorotrimethylsilane (32.2 mL, 253.4 mmol) were dissolved anhydrous THF (77 mL) in a flame-dried 500 mL Schlenk flask and cooled to -78 °C. Subsequently a solution of LDA (2 M, 126.7 mL, 253.40 mmol) was added in the course of 30 min. The resulting solution was stirred at -78 °C for additional 45 minutes, warmed up to room temperature overnight, quenched with 1 N HCl solution and extracted with CH_2Cl_2 (3x). The combined organic fractions were dried with $MgSO_4$. After filtration and evaporation of the solvent, the residue was dissolved in MeOH and stored in a refrigerator. This led to the precipitation of **7-9** as colorless needles, which were filtered and dried (20.1 g, 90%). Mp: 96 °C. ^{1}H NMR (CD_2Cl_2, 300 MHz, δ): 0.44 (s, 18H), 3.72 (s, 6H). ^{13}C NMR (CD_2Cl_2, 75 MHz, δ): 2.9, 60.9, 127.9, 139.3, 158.2. FD-MS (8kV): $m/z = 440.6$ (100%, M$^+$). Anal. Calcd. for $C_{14}H_{24}Br_2O_2Si_2$: C 38.19%, H 5.49%. Found: C 38.48%, H 5.63%.
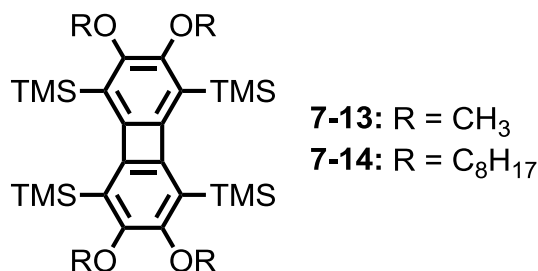
(2,3-Dibromo-5,6-bis(octyloxy)-1,4-phenylene)bis(trimethylsilyl) (7-10)

7-10
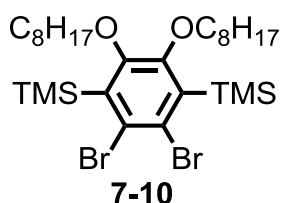
1,2-Dibromo-4,5-bis(octyloxy)benzene[12] (4.0 g, 8.10 mmol) and trimethylsilyl chloride (5.2 mL, 40.60 mmol) were dissolved anhydrous THF (110 mL) in a flame-dried 250 mL Schlenk flask and cooled to -78 °C. Subsequently a solution of LDA (2 M, 20.3 mL, 40.60 mmol) was added in the course of 30 min. The resulting solution was stirred at -78 °C for additional 45 minutes, warmed up to room temperature overnight, quenched with 1 N HCl solution and extracted with CH_2Cl_2 (3x). The combined organic fractions were dried with $MgSO_4$. After filtration and evaporation of the solvent, the residue was subjected to column chromatography (silica, n-hexane/CH_2Cl_2 3:1). Compound **7-10** was obtained as colorless liquid which solidified upon cooling (5.1 g, quantitative). Mp: 43 °C.

^{1}H NMR (CD$_2$Cl$_2$, 300 MHz, δ): 0.27 (s, 18H), 0.89 (t, J_1 =J_2 = 9 Hz, 6H), 1.30 (m, 20H), 1.72 (m, 4H), 3.83 (t, J_1 =J_2 = 9 Hz, 4H). ^{13}C NMR (CD$_2$Cl$_2$, 75 MHz, δ): 1.5, 14.5, 23.3, 26.8, 29.9, 30.3, 30.8, 32.4, 73.6, 129.1, 155.2, 158.0. FD-MS (8kV): m/z = 955.1 (100%, M$^+$).

**(2,3,6,7-Tetramethoxybiphenylene-1,4,5,8-tetrayl)tetrakis(trimethylsilyl) (7-13/7-14)**

7-13: R = CH$_3$
7-14: R = C$_8$H$_{17}$

To a solution of (2,3-dibromo-5,6-dialkoxy-1,4-phenylene)bis(trimethylsilane) (**7-9/7-10**) (1 equiv.) in anhydrous THF at -78 °C under argon, n-BuLi (1 equiv.) was added over 30 min. After warming up to room temperature overnight, the reaction mixture was quenched with 1 N aqueous HCl solution, extracted with CH$_2$Cl$_2$ (3x), the combined organic phases were dried with MgSO$_4$ and filtered. The solvents were evaporated *in vacuo* and the residue was subjected to silica column chromatography yielding (2,3,6,7-tetraalkoxybiphenylene-1,4,5,8-tetrayl)tetrakis(trimethylsilyl) as yellow materials.

**(2,3,6,7-Tetramethoxybiphenylene-1,4,5,8-tetrayl)tetrakis(trimethylsilane) (7-13)**:
Chromatography n-hexane/CH$_2$Cl$_2$ 6:1 to 4:1; 261 mg, 0.89 mmol, 17%; Mp: 240 °C. ^{1}H NMR (CD$_2$Cl$_2$, 300 MHz, δ): 0.27 (s, 36H), 3.70 (s, 12H). ^{13}C NMR (CD$_2$Cl$_2$, 75 MHz, δ): 1.5, 60.4, 128.4, 155.9, 157.6. FD-MS (8kV): m/z = 560.1 (100%, M$^+$). Anal. Calcd. for C$_{28}$H$_{48}$O$_4$Si$_4$: C 59.94%, H 8.62%. Found: C 60.31%, H 9.85%.

(2,3,6,7-Tetraoctyloxybiphenylene-1,4,5,8-tetrayl)tetrakis(trimethylsilane) (7-14):
Chromatography n-hexane; 300 mg, 0.31 mmol, 10%; Mp: 120 °C. ^{1}H NMR (CD$_2$Cl$_2$, 300 MHz, δ): 0.26 (s, 36H), 0.89 (t, J_1 =J_2 = 6 Hz, 12H), 1.31 (m, 40H), 1.72 (m, 8H), 3.83 (t, J_1 =J_2 = 9 Hz, 8H). ^{13}C NMR (CD$_2$Cl$_2$, 75 MHz, δ): 1.5, 14.5, 23.3, 26.8, 29.9, 30.3, 30.8, 32.4, 73.6, 129.1, 155.2, 158.0. FD-MS (8kV): m/z = 955.1 (100%, M$^+$). Anal. Calcd. for C$_{56}$H$_{104}$O$_4$Si$_4$: C 70.52%, H 10.99%. Found: C 70.28%, H 10.19%.
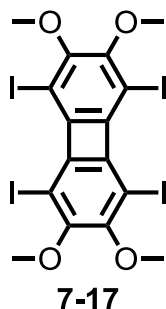
1,4,5,8-Tetraiodo-6,7-dimethoxybiphenylene-2,3-dione (7-15)

7-15
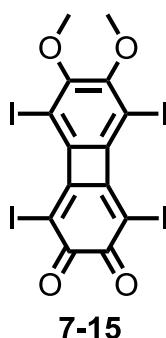
A 1 M iodine monochloride solution in CH_2Cl_2 (48.13 mL, 48.13 mmol) was added over 20 min to **7-13** (1.35 g, 2.41 mmol) in anhydrous CH_2Cl_2 (78 mL) at -78 °C under argon. After warming up to room temperature, the reaction was allowed to proceed for 2 days. The reaction was quenched by the addition of an aqueous Na_2SO_3 solution. The precipitate was filtered and extensively washed with water and MeOH, yielding **7-15** as an orange solid (1.65 g, 92%). The compound was used without further purification. FD-MS (8kV): $m/z = 746.1$ (100%, M^+).

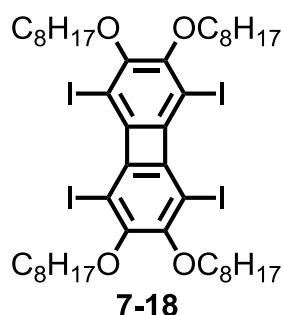### 1,4,5,8-Tetraiodo-6,7-bis(octyloxy)biphenylene-2,3-dione (7-16)

7-16
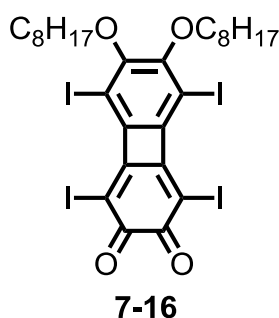
A 1 M iodine monochloride solution in CH_2Cl_2 (79.16 mL, 79.16 mmol) was added over 20 min to **7-14** (3.02 g, 3.17 mmol) in anhydrous CH_2Cl_2 (50 mL) at -78 °C under argon. After warming up to room temperature, the reaction was allowed to proceed for 2 days. The reaction was quenched by the addition of an aqueous Na_2SO_3 solution, extracted with CH_2Cl_2 (3x), the combined organic phases were dried with $MgSO_4$ and filtered. The solvents were evaporated *in vacuo* and the residue was subjected to column chromatography (silica, *n*-hexane/CH_2Cl_2 1:2 to 1:10). Finally **7-16** was obtained as an orange solid (2.88 g, 91%). Mp: 245 °C. ^1H NMR ($C_2D_2Cl_4$, 500 MHz, δ): 0.82 (t, $J_1 = J_2 = 7$ Hz, 6H), 1.23 (m, 16H), 1.44 (m, 4H), 1.81 (m, 4H), 4.03 (t, $J_1 = J_2 = 9$ Hz, 4H). ^{13}C NMR ($C_2D_2Cl_4$, 126 MHz, δ): 14.6, 23.1, 26.4, 29.5, 29.6, 30.5, 32.1, 75.5, 85.1, 88.1, 149.5, 159.0, 160.5, 172.8. FD-MS (8kV): $m/z = 944.0$ (100%, M^+). Anal. Calcd. for $C_{28}H_{34}I_4O_4$: C 35.69%, H 3.64%. Found: C 36.27%, H 3.97%.

### 1,4,5,8-Tetraiodo-2,3,6,7-tetramethoxybiphenylene (7-17)

7-17

1,4,5,8-Tetraiodo-6,7-dimethoxybiphenylene-2,3-dione **7-15** (1.20 g, 1.61 mmol), n-Bu$_4$NBr (0.36 g, 1.13 mmol) and Na$_2$S$_2$O$_4$ (0.84 g, 4.83 mmol) were suspended in THF (24 mL) and water (14.4 mL). Me$_2$SO$_4$ (1.06 g, 8.37 mmol) was added, followed by a 4.5 M aqueous KOH solution (4.4 mL) and the reaction mixture was stirred under an argon atmosphere at 40 °C overnight. The reaction was stopped by the addition of CH$_2$Cl$_2$, the organic phase was extracted, dried over MgSO$_4$ and the organic solvents were removed under vacuum. Column chromatography (silica, n-hexane/CH$_2$Cl$_2$ 1:3), followed by crystallization from MeOH gave **7-17** (1.21 g, 97%) as a light yellow solid. Crystals suitable for X-ray analysis were grown by slow evaporation of a CH$_2$Cl$_2$ solution of **7-17**. Mp: 331 °C. ^{1}H NMR (C$_2$D$_2$Cl$_4$, 500 MHz, 80 °C, δ): 3.74 (s, 12H). ^{13}C NMR (C$_2$D$_2$Cl$_4$, 126 MHz, 80 °C δ): 61.0, 82.8, 149.9, 152.7. FD-MS (8kV): $m/z = 776.5$ (100%, M$^+$). MALDI-TOF MS (dithranol): $m/z = 776.93$ (100%) [M+H]$^+$. Anal. Calcd. for C$_{16}$H$_{12}$I$_4$O$_4$: C 24.77%, H 1.56%. Found: C 24.96%, H 1.46%.

1,4,5,8-Tetraiodo-2,3,6,7-tetraoctyloxybiphenylene (7-18)

7-18

1,4,5,8-Tetraiodo-6,7-bis(octyloxy)biphenylene-2,3-dione **7-16** (1.60 g, 1.70 mmol), n-Bu$_4$NBr (0.16 g, 0.51 mmol) and Na$_2$S$_2$O$_4$ (0.89 g, 5.13 mmol) were suspended in THF (15 mL) and water (15 mL) and stirred vigorously for 5 min at room temperature. 1-Bromooctane (1.65 g, 8.54 mmol) and a 4.5 M aqueous KOH solution (15 mL) were added and the reaction mixture was stirred under an argon atmosphere at 100 °C overnight. After dilution with CH$_2$Cl$_2$, the organic phase was extracted, dried over MgSO$_4$ and the organic

solvents were removed under vacuum. Column chromatography (silica, *n*-hexane/CH$_2$Cl$_2$ 1:1), followed by precipitation from MeOH gave **7-18** (0.39 g, 20%) as a light yellow solid. Mp: 137 °C. ^{1}H NMR (C$_2$D$_2$Cl$_4$, 500 MHz, 80 °C, δ): 0.86 (t, $J_1 = J_2 = 6$ Hz, 12H), 1.27 (m, 32H), 1.43 (m, 8H), 1.76 (m, 8H), 3.86 (t, $J_1 = J_2 = 7$ Hz, 8H). ^{13}C NMR (C$_2$D$_2$Cl$_4$, 126 MHz, 80 °C, δ): 14.0, 22.6, 26.1, 29.2, 29.4, 29.7, 30.2, 31.8, 83.2, 149.5, 151.7. FD-MS (8kV): $m/z = 1167.6$ (100%, M$^+$). Anal. Calcd. for C$_{44}$H$_{68}$I$_4$O$_4$: C 45.22%, H 5.86%. Found: C 45.45%, H 6.30%.

1,4-Bis(trimethylsilyl)-2,3,5,6-tetrabromobenzene (7-24)

7-24
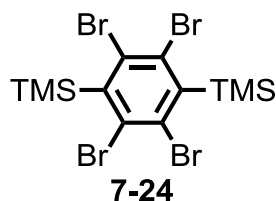
1,2,4,5-Tetrabromobenzene (20.0 g, 50.8 mmol) and chlorotrimethylsilane (14.2 mL, 111.8 mmol) were suspended in anhydrous THF (300 mL) in a flame-dried 500 mL Schlenk flask and cooled to -78 °C. Subsequently, a solution of LDA (2 M, 55.9 mL, 111.8 mL) was added to this suspension in the course of 30 min. The resulting solution was warmed up to room temperature overnight, quenched with 1 N HCl solution and extracted with CH$_2$Cl$_2$ (3x). The combined organic fractions were dried over MgSO$_4$. After filtration and evaporation of the solvent, the residue was subjected to repeated column chromatography (silica, *n*-hexane). Compound **7-24** was obtained as a colorless liquid, which slowly crystallized upon standing in the refrigerator (14.4 g, 72%). Mp: 46 °C. ^{1}H NMR (CD$_2$Cl$_2$, 250 MHz, δ): 0.62 (s, 18H). ^{13}C NMR (CD$_2$Cl$_2$, 63 MHz, δ): 2.8, 127.8, 158.4. FD-MS (8kV): $m/z = 537.1$ (100%, M$^+$).

2,3,6,7-Tetrabromo-1,4,5,8-tetraiodobiphenylene (7-25)

7-25
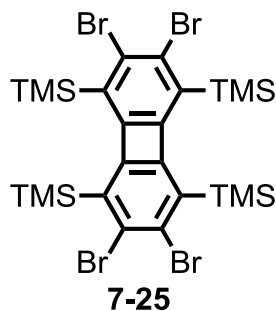
To a solution of **7-24** (5.0 g, 9.29 mmol) in anhydrous THF (40 mL) at -78 °C under argon, *n*-BuLi (5.8 mL, 9.29 mmol, 1.6 M in *n*-hexane) was added over one hour. After warming up to room temperature overnight, the reaction mixture was quenched with 1 N aqueous

HCl solution, extracted with CH_2Cl_2 (3x), the combined organic phases were dried over $MgSO_4$ and filtered. The solvents were evaporated *in vacuo* and the residue was subjected to column chromatography (silica, *n*-hexane to *n*-hexane/CH_2Cl_2 6:1), followed by precipitation from MeOH to give **7-25** (0.85 g, 12%) as a yellow solid. Crystals suitable for X-ray analysis were grown by slow evaporation of a *n*-hexane/CH_2Cl_2 solution of **7-25**. Mp: 322 °C. ^1H NMR (CD_2Cl_2, 250 MHz, δ): 0.39 (s, 36H). ^{13}C NMR (CD_2Cl_2, 63 MHz, δ): 1.9, 132.7, 137.0, 161.5. FD-MS (8kV): $m/z = 757.5$ (100%, M^+). Anal. Calcd. for $C_{24}H_{36}Br_4Si_4$: C 38.10%, H 4.80%. Found: C 38.31%, H 5.48%.

2,3,6,7-Tetrabromo-1,4,5,8-tetraiodobiphenylene (7-26)

7-26
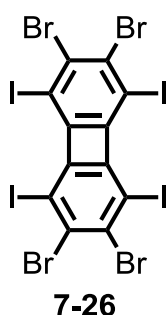
In the absence of light a 1 M iodine monochloride solution in CH_2Cl_2 (7.93 mL, 7.93 mmol) was added dropwise over 15 min to **7-25** (300 mg, 0.40 mmol) in anhydrous CH_2Cl_2 (18 mL) at 0 °C under argon. After warming up to room temperature overnight, the reaction was quenched by the addition of an aqueous Na_2SO_3 solution. The precipitate was filtered and extensively washed with water, MeOH, CH_2Cl_2 and THF, yielding **7-26** as a light yellow solid (250 mg, 65%). The compound was used without further purification. Mp: 380 °C decomp. ^1H and ^{13}C NMR spectra could not be obtained due to the limited solubility of **7-26** in organic solvents. FD-MS (8kV): $m/z = 971.0$ (100%, M^+). MALDI-TOF MS (TCNQ): $m/z = 967.68$ (100%) $[M+H]^+$. Anal. Calcd. for $C_{24}Br_4I_4$: C 14.84%, H 0.00%. Found: C 14.95%, H 0.43%.

Polymerization Procedure of 7-17

7-35 (n = 7.6)
7-36 (n = 12.9)
7-37 (n = 17.2)
7-38 (n = 24.1)
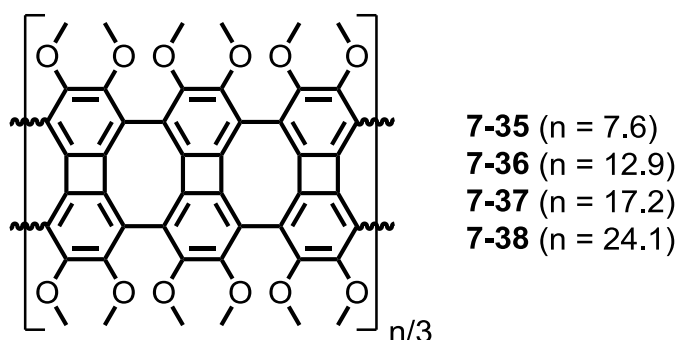
In a flame-dried 50 mL Schlenk flask **7-17** (200 mg, 0.26 mmol) was suspended in anhydrous 1,2-dichlorobenzene and the resulting mixture was stirred at 90 °C under argon until complete dissolution. Subsequently activated copper powder[13] (164 mg, 2.58 mmol) was added and the reaction mixture was stirred at 210 °C for 12 days. The solvent was evaporated *in vacuo*, the residue was dissolved in CH_2Cl_2, filtered and the insoluble material was extensively washed with CH_2Cl_2 and THF. The filtrate was poured into 100 mL MeOH/HCl (50:1) and was stirred for one hour and the precipitate was filtered. After repeated precipitation in MeOH/HCl, the polymer was subjected to preparative size exclusion chromatography (BioBeads S-X1, toluene) to allow isolation of **7-35** (25 mg, 36%), **7-36** (18 mg, 26%), **7-37** (10 mg, 14%) and **7-38** (14 mg, 20%). MALDI-TOF MS (dithranol): $m/z = 523.90$ (100%), 649.92 (95%), 775.84 (50%), 920.05 (20%), 146.13 (30%), 1172.10 (20%), 1298.12 (10%), 1442.30 (2%), 1568.40 (1%).

Polymer (7-35)

7-35 was obtained as a tan yellow solid (25 mg, 36%). SEC (eluent: THF, poly(*para*phenylene) calibration): $M_n = 2\ 050$ g/mol, PDI = 1.40, DP ~ 5.8. Anal. Calcd. for $C_{78}H_{57}I_3O_{20}$: C 55.27%, H 3.39%. Found: C 54.67%, H 3.40%.

Polymer (7-36)

7-36 was obtained as a tan yellow solid (18 mg, 26%). SEC (eluent: THF, poly(*para*phenylene) calibration): $M_n = 3\ 460$ g/mol, PDI = 1.05, DP ~ 11.0. Anal. Calcd. for $C_{138}H_{76}I_4O_{40}$: C 57.52%, H 2.66%. Found: C 54.69%, H 3.67%.

Polymer (7-37)

7-37 was obtained as a tan yellow solid (10 mg, 14%). SEC (eluent: THF, poly(*para*phenylene) calibration): $M_n = 4\ 620$ g/mol, PDI = 1.11, DP ~ 15.3. Anal. Calcd. for $C_{214}H_{128}I_4O_{60}$: C 61.68%, H 3.10%. Found: C 54.67%, H 3.40%.

Polymer (7-38)

7-38 was obtained as a tan yellow solid (14 mg, 20%). ^{1}H NMR (CD_2Cl_2, 300 MHz, δ): 3.76 (br s, 264H), 6.77–7.57 (br m, 16H). SEC (eluent: THF, poly(*para*phenylene) calibration): $M_n = 6\ 460$ g/mol, PDI = 1.21, DP ~ 22.2. Anal. Calcd. for $C_{332}H_{238}I_2O_{88}$: C 67.71%, H 4.07%. Found: C 59.67%, H 3.36%.

Octaphenylbiphenylene (7-47)
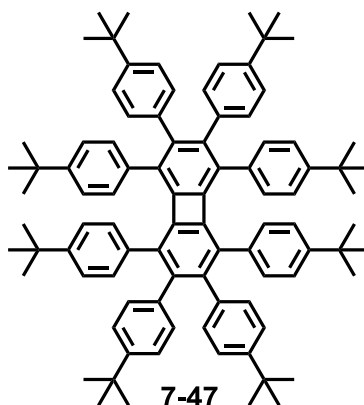
A 50 mL Schlenk tube was equipped with **7-26** (125 mg, 0.13 mmol) and (4-(*tert*-butyl)phenyl)boronic acid (1.47 g, 8.24 mmol) followed by three times evacuating and backfilling with argon. After the addition of toluene (9.2 mL), solid K_2CO_3 (1.42 g, 10.29 mmol) and three drops of *Aliquat 336*, the resulting mixture was degassed with argon for 2 hours. To this mixture $Pd(PPh_3)_4$ (48 mg, 4 mol%) was added and it was stirred under an atmosphere of argon at 115 °C for four days. After the addition of water, washing the aqueous phase with toluene (3x), drying the combined organic phases over $MgSO_4$ and evaporating of the solvent *in vacuo*, the crude mixture was subjected to column chromatography (silica, *n*-hexane /CH_2Cl_2 3:1). Finally the product fraction was recrystallized from *n*-hexane, yielding **7-47** as a light yellow solid (52 mg, 33%). Crystals suitable for X-ray analysis were grown by slow evaporation of a *n*-hexane/CH_2Cl_2 solution of **7-47**. Mp: 367 °C. ^{1}H NMR (CD_2Cl_2, 700 MHz, δ): 1.07 (s, 36H), 1.08 (s, 36H), 6.44 (d, $J = 8$ Hz, 8H), 6.52 (d, $J = 8$ Hz, 8H), 6.57 (d, $J = 8$ Hz, 8H), 6.74 (d, $J = 8$ Hz, 8H). ^{13}C NMR (CD_2Cl_2, 175 MHz, δ): 29.7, 30.9, 31.1, 122.8, 123.0, 129.4, 130.9, 134.4, 137.7, 142.3, 143.6, 146.5, 147.8, 148.2 (14 out of 15 expected). FD-MS (8kV): $m/z = 1208.3$ (100%, M$^+$). MALDI-TOF MS (TCNQ): $m/z = 1209.05$ (100%) [M+H]$^+$. Anal. Calcd. for $C_{92}H_{104}$: C 91.34%, H 8.66%. Found: C 88.99%, H 8.68% (see general remarks "Elemental Analysis").

Octapyrenylbiphenylene (7-48)

7-48
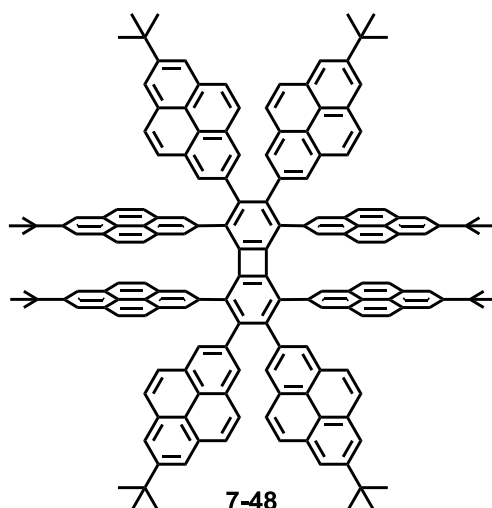
A 50 mL Schlenk tube was equipped with **7-26** (80 mg, 0.08 mmol) and 2-(7-(*tert*-butyl)pyren-2-yl)-4,4,5,5-tetramethyl-1,3,2-dioxaborolane[14]   (950 mg,   2.47 mmol) followed by three times evacuating and backfilling with argon. After the addition of toluene (5 mL) and water (2.5 mL), solid K_2CO_3 (911 mg, 6.59 mmol) and three drops of *Aliquat 336* the resulting mixture was degassed with argon for 2 hours. To this mixture $Pd(PPh_3)_4$ (31 mg, 4 mol%) was added and it was stirred under an atmosphere of argon at 115 °C overnight. After the addition of water, washing the aqueous phase with toluene (3x), drying the combined organic phases over $MgSO_4$ and evaporating of the solvent *in vacuo*, the crude mixture was subjected to column chromatography (silica, *n*-hexane /CH_2Cl_2 1:1). Finally the product fraction was precipitated from EtOH, yielding **7-48** as a yellow solid (96 mg, 53%). Mp > 400 °C. ^{1}H NMR ($C_2D_2Cl_4$, 700 MHz, δ): 1.24 (s, 36H), 1.29 (s, 36H), 6.79 (d, $J = 9$ Hz, 8H), 6.82 (d, $J = 9$ Hz, 8H), 7.29 (s, 8H), 7.31 (d, $J = 9$ Hz, 8H), 7.40 (s, 8H), 7.41 (d, $J = 9$ Hz, 8H), 7.68 (s, 8H), 7.69 (s, 8H). ^{13}C NMR ($C_2D_2Cl_4$, 175 MHz, δ): 31.8, 31.9, 34.8, 34.9, 120.4, 120.9, 121.2, 121.3, 121.5, 122.1, 122.2, 122.3, 125.8, 125.9, 126.1, 126.7, 127.2, 128.0, 128.9, 129.3, 129.8, 130.5, 133.1, 134.3, 137.2, 142.8, 147.3, 148.2, 149.4. FD-MS (8kV): $m/z = 2201.6$ (100%, M[+]). MALDI-TOF MS (TCNQ): $m/z = 2202.07$ (100%) [M+H][+]. Anal. Calcd. for $C_{172}H_{136}$: C 93.78%, H 6.22%. Found: C 92.23%, H 5.58% (see general remarks "Elemental Analysis").

Octathienobiphenylene (7-49)

7-49
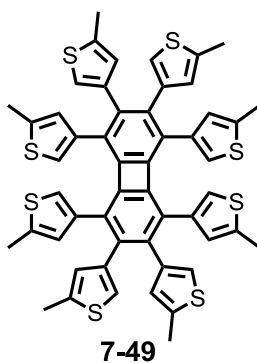
A 50 mL Schlenk tube was equipped with 7-**26** (100 mg, 0.10 mmol) and 4,4,5,5-tetramethyl-2-(5-methylthiophen-3-yl)-1,3,2-dioxaborolane (689 g, 3.09 mmol) followed by three times evacuating and backfilling with argon. After the addition of toluene (6.6 mL), water (3.3 mL), solid K_2CO_3 (1.14 g, 8.24 mmol) and three drops of *Aliquat 336*, the resulting mixture was degassed with argon for 2 hours. To this mixture $Pd(PPh_3)_4$ (38 mg, 4 mol%) was added and it was stirred under an atmosphere of argon at 115 °C for two days. After the addition of water, washing the aqueous phase with toluene (3x), drying the combined organic phases over $MgSO_4$ and evaporating of the solvent *in vacuo*, the crude mixture was subjected to column chromatography (silica, *n*-hexane /CH_2Cl_2 2:1). Finally the product fraction was precipitated from MeOH, yielding **7-49** as a yellow, crystalline material (66 mg, 70%). Crystals suitable for X-ray analysis were grown by slow evaporation of a *n*-hexane/CH_2Cl_2 solution of **7-49**. Mp: 290 °C decomp. ^{1}H NMR (CD_2Cl_2, 500 MHz, δ): 2.14 (s, 12H), 2.25 (s, 12H), 5.93 (m, 4H), 6.10 (m, 4H), 6.14 (d, $J = 1.25$ Hz, 4H), 6.27 (d, $J = 1.5$ Hz, 4H). ^{13}C NMR (CD_2Cl_2, 126 MHz, δ): 15.1, 121.8, 122.0, 127.1, 127.4, 128.6, 137.1, 137.4, 137.5, 137.6, 140.5, 147.6 (12 out of 13 expected). FD-MS (8kV): $m/z = 920.3$ (100%, M^+). MALDI-TOF MS (TCNQ): $m/z = 921.07$ (100%) $[M+H]^+$. Anal. Calcd. for $C_{52}H_{40}S_8$: C 67.78%, H 4.38%, S 27.84%. Found: C 68.13%, H 4.58%, S 26.30% (see general remarks "Elemental Analysis").

Isomeric Nanographene (7-51)

7-51
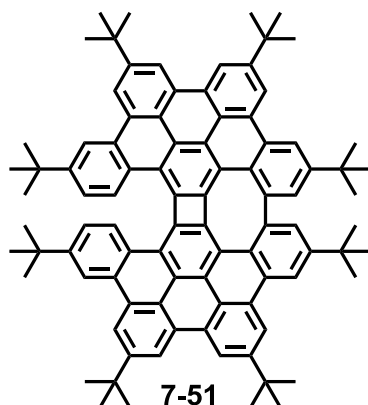
To a solution of **7-47** (10 mg, 0.01 mmol) in anhydrous CH_2Cl_2 (1.5 mL) and methanesulfonic acid (167 mg, 1.74 mmol) was added dichlorodicyano-*p*-benzoquinone (15 mg, 0.08 mmol) at 0 °C under argon. The reaction mixture was stirred for eight hours at 0 °C and was subsequently warmed up to room temperature overnight. After addition of an aqueous $NaHCO_3$ solution, washing the aqueous phase three times with CH_2Cl_2 drying the combined organic phases with $MgSO_4$ and evaporating of the solvent *in vacuo*, the crude mixture was precipitated from a dichloromethane/methanol mixture yielding **7-51** (9 mg, 90%) as poorly soluble yellow material. FD-MS (8kV): m/z = 1195.5 (100%, M^+). MALDI-TOF MS (TCNQ): m/z = 1218.71 (100%) $[M+Na]^+$, 1194.77 (20%) $[M+H]^+$, 1239.80 (10%) $[M+2Na]^+$.

9.4 Crystal Data

The single crystal analysis was performed on a Nonius-KCCD diffractometer with a Mo-K$_\alpha$ ($\lambda = 0.71923$ Å, graphite monochromatized) at a temperature of 250 to 120 K. The structures were solved by direct methods (ShelXS) and refined on F with anisotropic temperature factors for all non-hydrogen atoms. The H atoms were refined with fixed isotropic temperature factors in the riding mode.
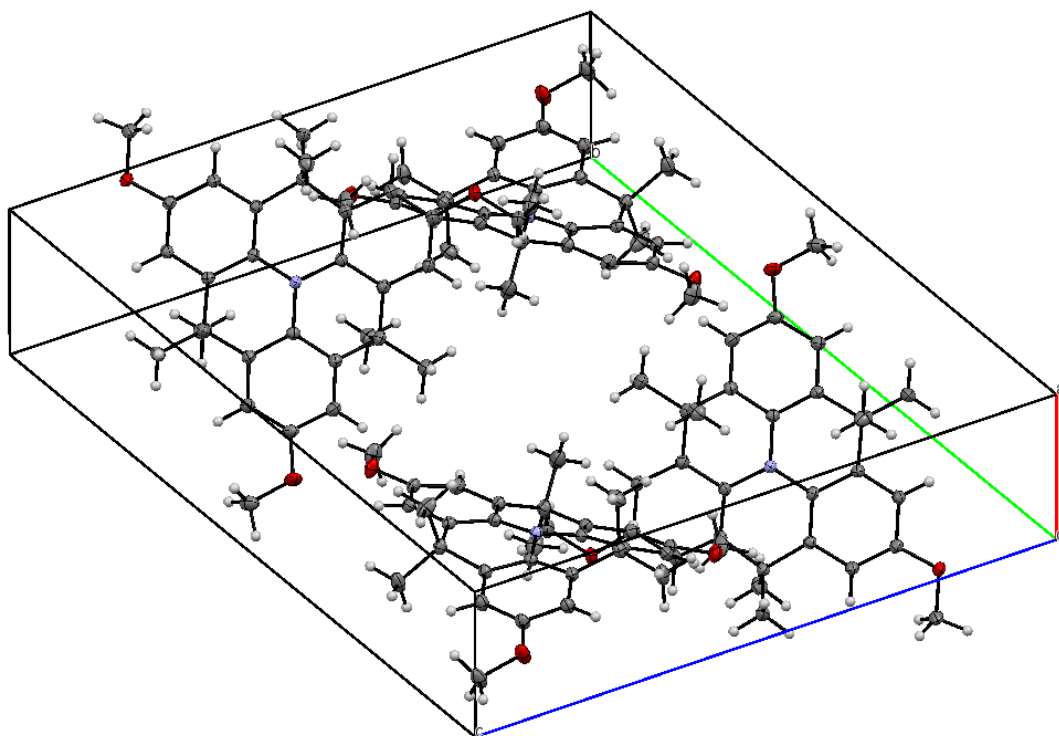
N-Heterotriangulene Macrocycle (4-2)
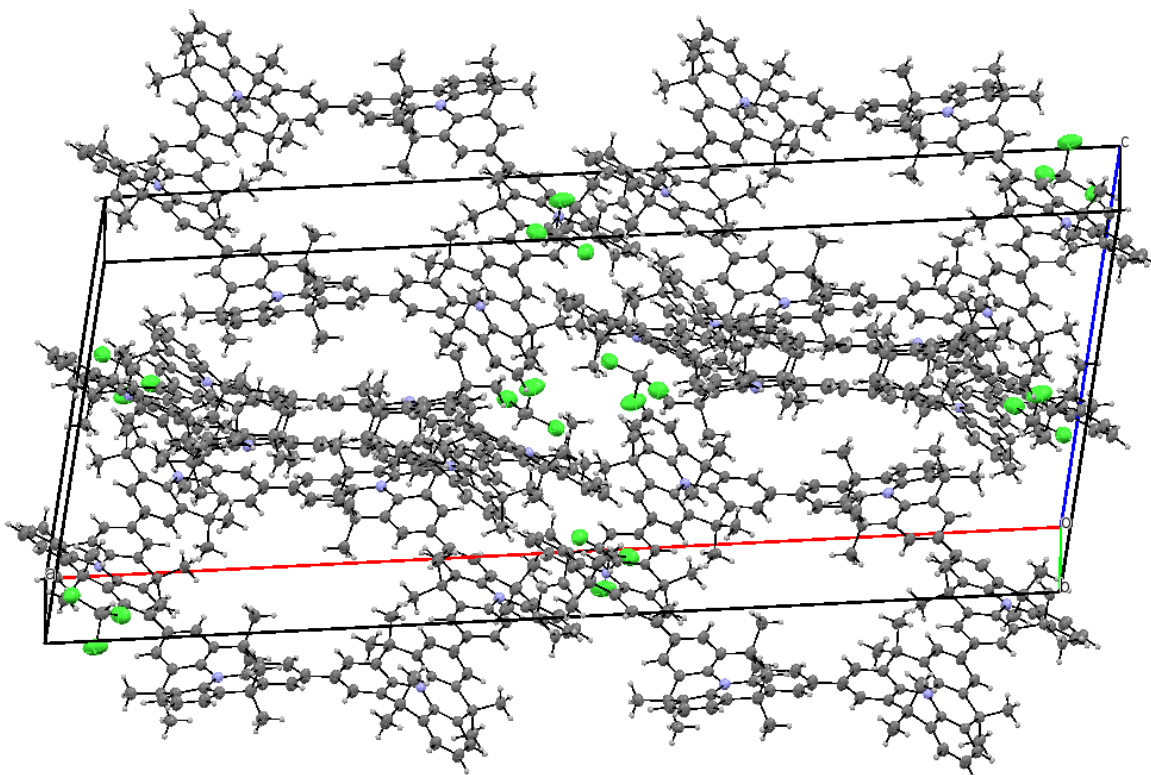
C$_{162}$H$_{150}$N$_6$, M$_r$ = 2419.62 g/mol, monoclinic, space group C2/*c*, a = 49.2578(9) Å, b = 15.0524(6) Å, c = 19.1141(7) Å, β = 101.6894(11)°, V = 13878.2(8) Å^3. R = 0.0506, R$_w$ = 0.0587.

Cambridge Crystallographic Data Centre identifier: CCDC-892865

2,6,10-Trimethoxy-4,4,8,8,12,12-hexamethyl-8,12-dihydro-4*H*-benzo[1,9]quinolizino-[3,4,5,6,7-*defg*]acridine (5-3)

$C_{30}H_{33}NO_3$, $M_r = 455.57$ g/mol,   triclinic,   space   group   *P-1*,   a = 8.4749(2) Å, b = 17.5197(4) Å, c = 17.7553(4) Å, $\alpha = 65.7932(13)°$, $\beta = 84.8456(12)°$, $\gamma = 87.8347(14)$, V = 2394.74(10) Å^3. R = 0.0471, R$_w$ = 0.0569.

N-Heterotriangulene Dimer (5-4)
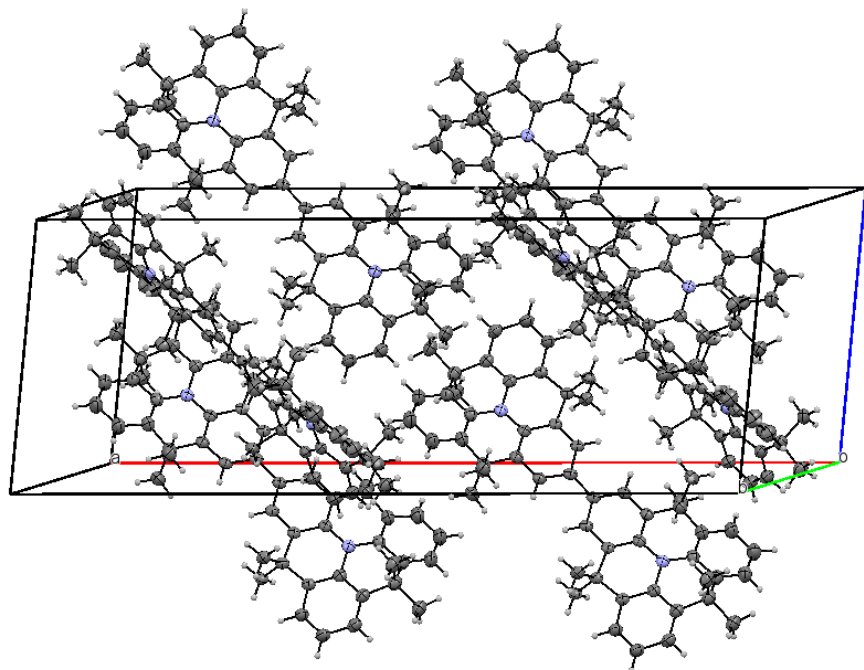
$C_{54}H_{52}N_2$, $M_r = 728.98$ g/mol, monoclinic, space group C2/*c*, a = 35.9549(9) Å, b = 9.4019(9) Å, c = 12.2861(9) Å, β = 100.525(4)°, V = 4083.4(5) Å^3. R = 0.0544, $R_w = 0.0589$.

Cambridge Crystallographic Data Centre identifier: CCDC-954071

4'',5'-Diphenyl-1,1':2',1'':2'',1'''-quaterphenyl (6-5)
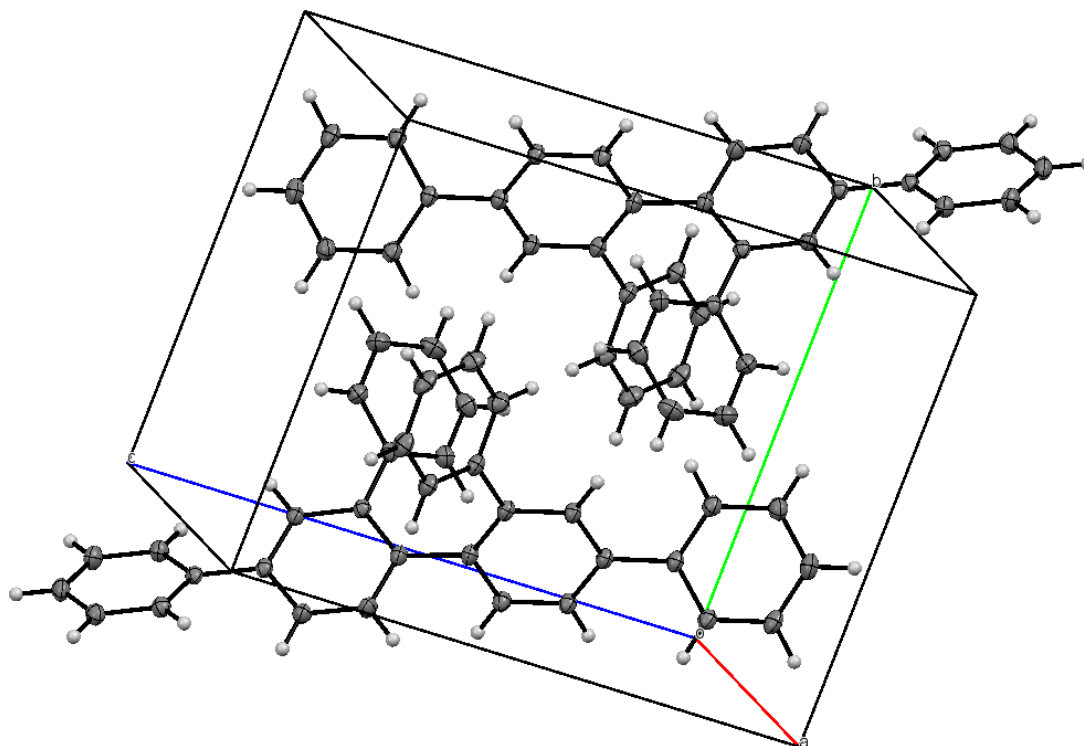
$C_{36}H_{26}$, M_r = 458.60 g/mol, triclinic, space group *P-1*, a = 9.9080(2) Å, b = 10.7787(3) Å, c = 12.7321(3) Å, α = 97.6691(12)°, β = 94.7545(14)°, γ = 115.8972(11)°, V = 1196.95(5) Å^3. R = 0.0482, R_w = 0.0590.

Cambridge Crystallographic Data Centre identifier: CCDC-918310

5',5'''''-Dichloro-1,1':3',1'':2'',1''':2''',1'''':3'''',1'''''-sexiphenyl (6-17)
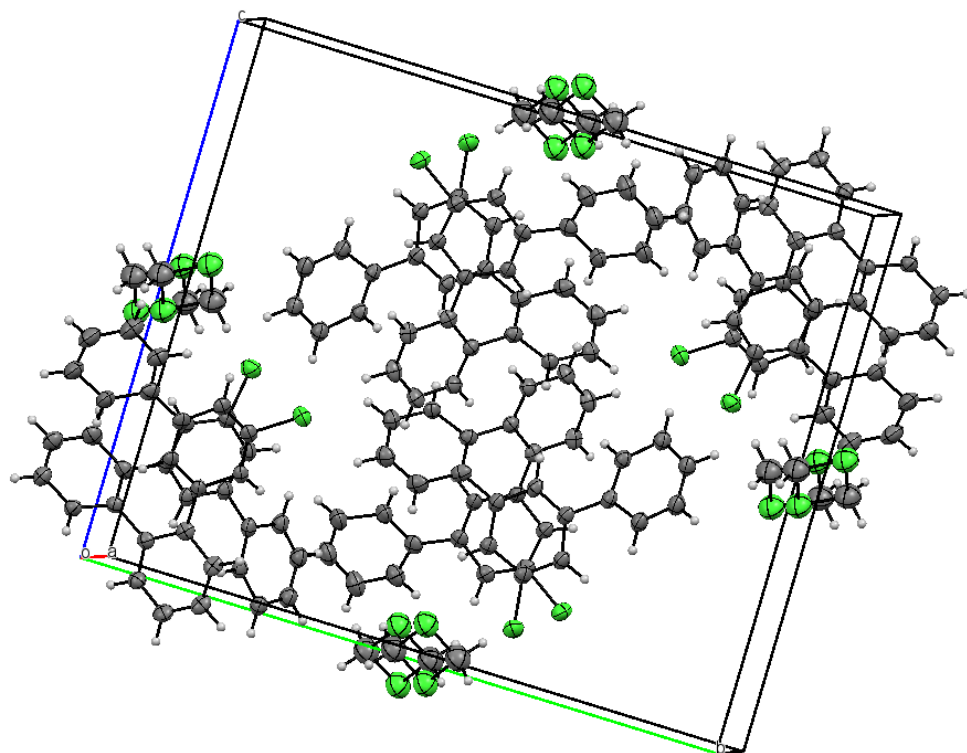
$C_{36.5}H_{25}Cl_3$, M_r = 569.96 g/mol,   monoclinic,   space   group   *P21/c*,   a = 7.5317(7) Å, b = 21.0519(9) Å,   c = 17.7743(8) Å,   β = 94.802(5)°,   V = 2808.3(3) Å^3.   R = 0.0464, R_w = 0.0571.

Cambridge Crystallographic Data Centre identifier: CCDC-918311

4,4'-Dimethyl-2,2',6,6'-tetraphenyl-1,1'-biphenyl (6-9)
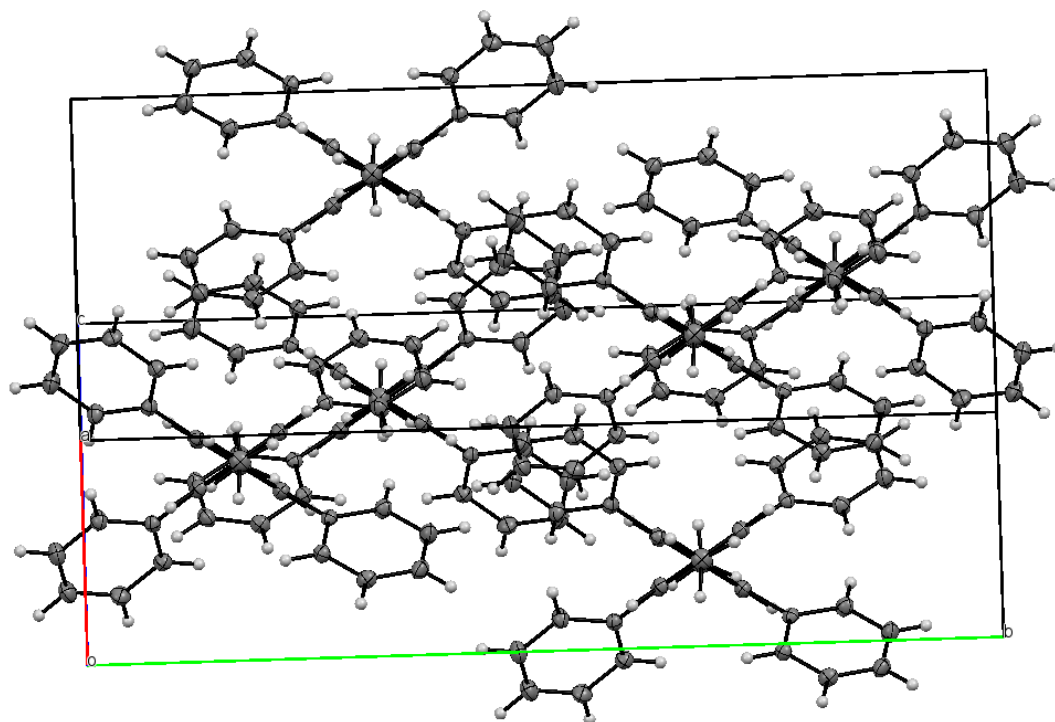
$C_{38}H_{30}$, $M_r = 486.66$ g/mol, monoclinic, space group C2/c, a = 7.3789(2) Å, b = 22.1571(8) Å, c = 16.3043(5) Å, β = 102.0571(18)°, V = 2606.87(14) Å^3. R = 0.0423, $R_w = 0.0502$.

Cambridge Crystallographic Data Centre identifier: CCDC-918312

4,4'-Dichloro-2,2',6,6'-tetraphenyl-1,1'-biphenyl (6-24)
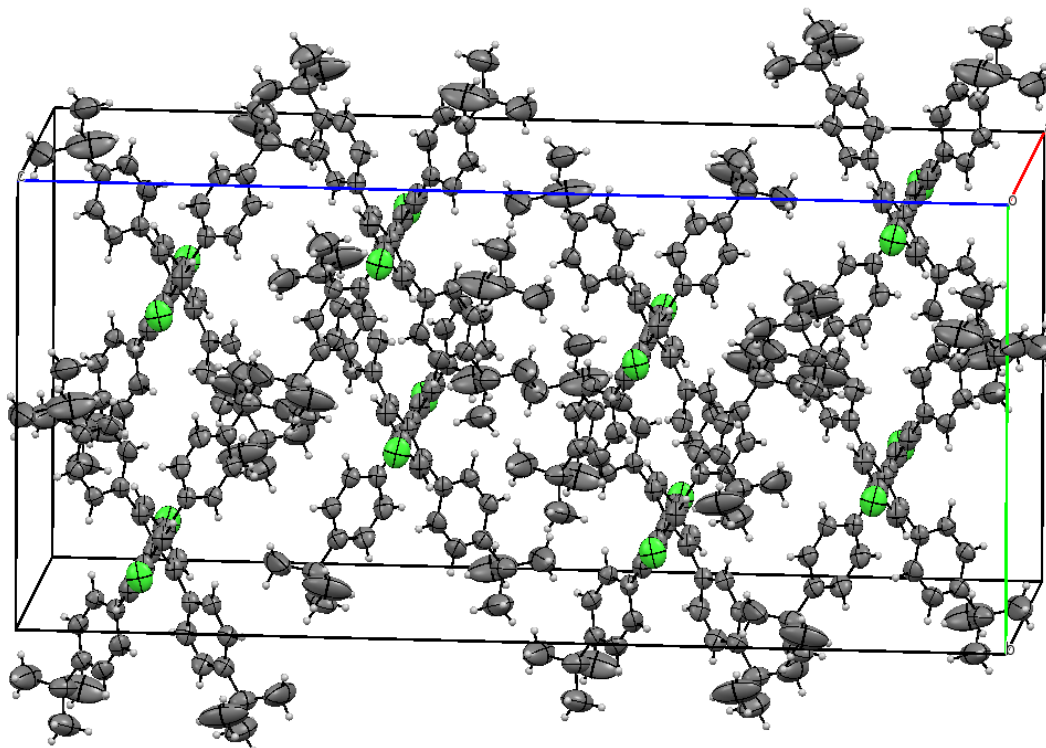
$C_{52}H_{56}Cl_2$, $M_r = 751.92$ g/mol, orthorhombic, space group *Fddd*, a = 13.8723(4) Å, b = 17.3314(3) Å, c = 37.5890(5) Å, β = 90.0000(00)°, V = 9037.4(3) Å^3. R = 0.0601, R_w = 0.0766.

Cambridge Crystallographic Data Centre identifier: CCDC-918313

1,4,5,8-Tetraiodo-2,3,6,7-tetramethoxybiphenylene (7-17)
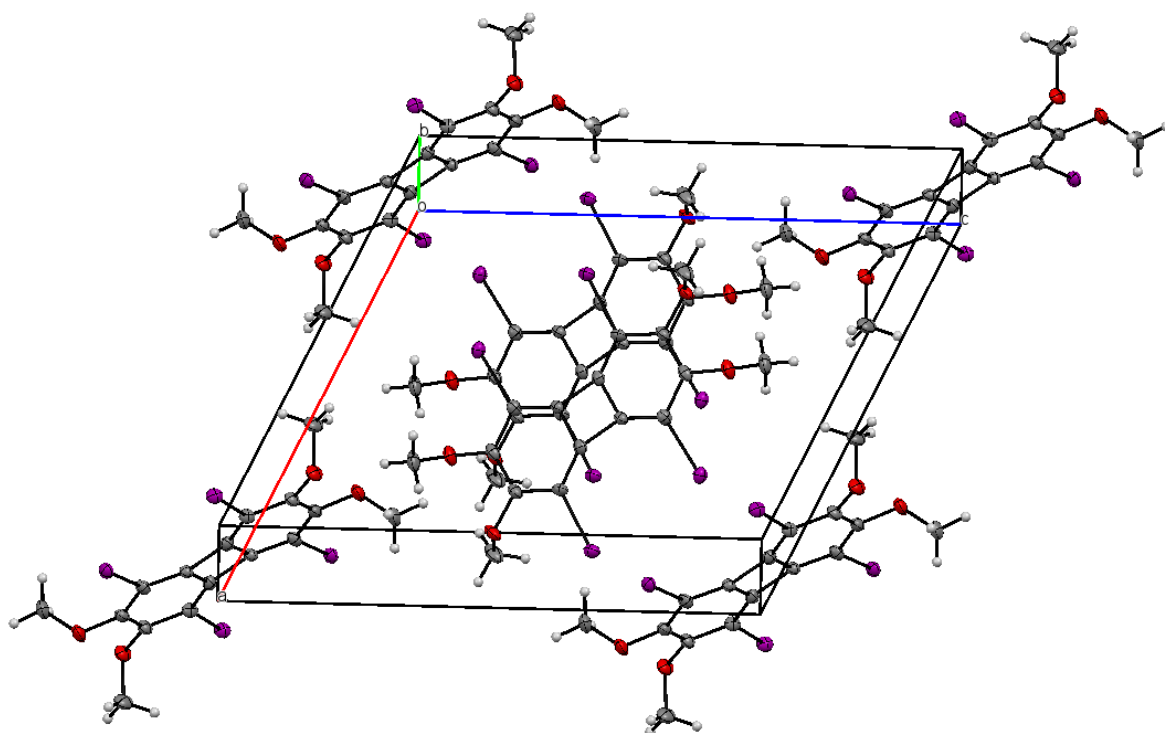
$C_{16}H_{12}I_4O_4$, M_r = 775.86 g/mol, monoclinic, space group $P2_1/n$, a = 13.9869(6) Å, b = 4.8425(1) Å, c = 15.7497(7) Å, β = 113.2499(18)°, V = 980.12(7) Å^3. R = 0.0402, R_w = 0.0479.

Cambridge Crystallographic Data Centre identifier: CCDC-954062

2,3,6,7-Tetrabromo-1,4,5,8-tetraiodobiphenylene (7-25)
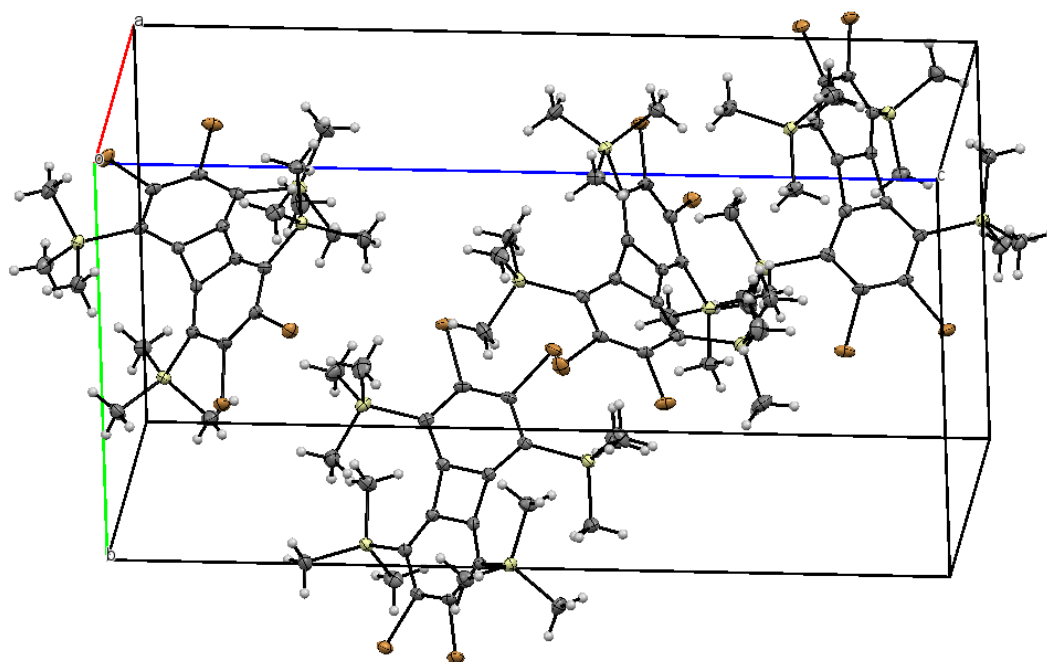
$C_{24}H_{36}Br_4Si_4$, $M_r = 756.49$ g/mol, orthorhombic, space group $P2_12_12_1$, a = 9.9033(2) Å, b = 12.5963(2) Å, c = 24.6330(5) Å, β = 90.0000(00)°, V = 3072.84(10) Å^3. R = 0.0271, R_w = 0.0338.

Cambridge Crystallographic Data Centre identifier: CCDC-954063

Octaphenylbiphenylene (7-47)
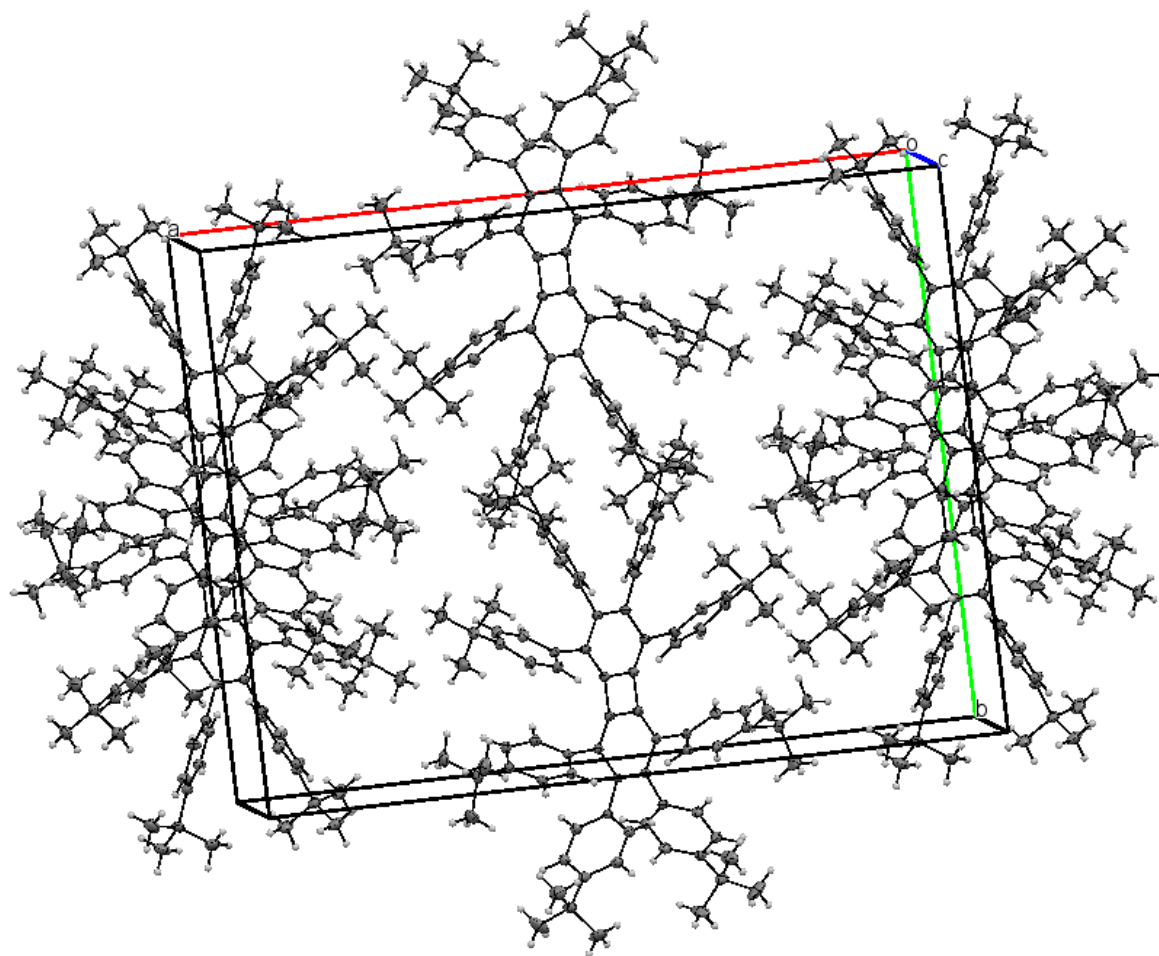
$C_{92}H_{104}$, $M_r = 1209.75$ g/mol, monoclinic, space group $C2/c$, $a = 28.5306(6)$ Å, $b = 21.7729(6)$ Å, $c = 12.7464(2)$ Å, $\beta = 102.1184(13)°$, $V = 7741.5(3)$ Å^3. $R = 0.0508$, $R_w = 0.0594$.

Cambridge Crystallographic Data Centre identifier: CCDC-954064

Octathienobiphenylene (7-49)
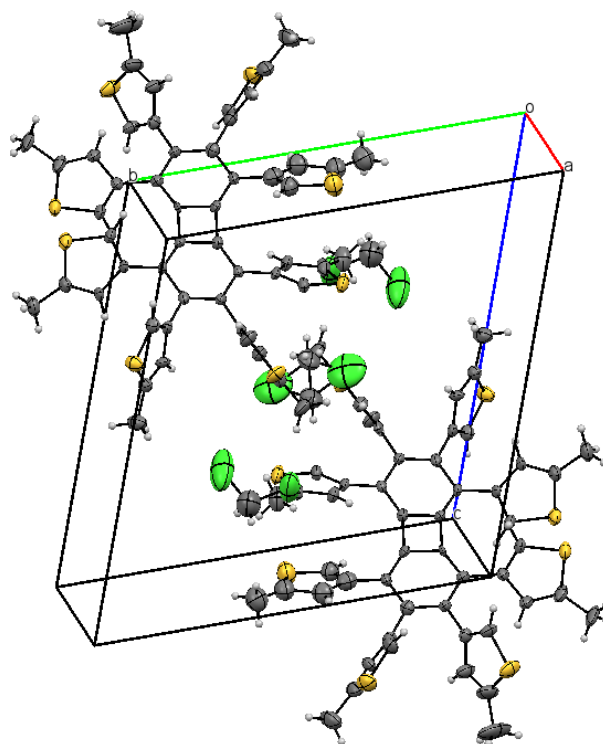
$C_{107}H_{84}Cl_6S_{16}$, M_r = 2095.56 g/mol,   triclinic,   space   group   *P-1*,   a = 11.9053(5) Å,
b = 15.3421(9) Å,   c = 15.7230(8) Å, α = 69.419(2)°, β = 73.405(3)°, γ = 87.754(3)°,
V = 2570.6(2) Å^3. R = 0.0399, R_w = 0.0470.

Cambridge Crystallographic Data Centre identifier: CCDC-954065

9.5   References

[1]   M. G. Schwab, Ph.D. thesis, Johannes Gutenberg-University Mainz **2011**.

[2]   *DigiElch v 6F, http://www.elchsoft.com/.*

[3]   M. Rudolph, D. P. Reddy, S. W. Feldberg, *Anal. Chem.* **1994**, *66*, 589-600.

[4]   S. Rentenberger, A. Vollmer, E. Zojer, R. Schennach, N. Koch, *J. Appl. Phys.* **2006**, *100*, 053701.

[5]   K. Tahara, S. Furukawa, H. Uji-I, T. Uchino, T. Ichikawa, J. Zhang, W. Mamdouh, M. Sonoda, F. C. De Schryver, S. De Feyter, Y. Tobe, *J. Am. Chem. Soc.* **2006**, *128*, 16613-16625.

[6]   Z. Fang, T. L. Teo, L. P. Cai, Y. H. Lai, A. Samoc, M. Samoc, *Org. Lett.* **2009**, *11*, 1-4.

[7]   Z. Fang, X. H. Zhang, Y. H. Lai, B. Liu, *Chem. Commun.* **2009**, 920-922.

[8]   D. Wasserfallen, Ph.D. thesis, Johannes Gutenberg-University Mainz **2006**.

[9]   S. Ozasa, Y. Fujioka, J. Kikutake, E. Ibuki, *Chem. Pharm. Bull.* **1983**, *31*, 1572-1581.

[10]   Y. Fujioka, S. Ozasa, K. Sato, E. Ibuki, *Chem. Pharm. Bull.* **1985**, *33*, 22-29.

[11]   L. Tong, H. Lau, D. M. Ho, R. A. Pascal, *J. Am. Chem. Soc.* **1998**, *120*, 6000-6006.

[12]   D. Waghray, W. Nulens, W. Dehaen, *Org. Lett.* **2011**, *13*, 5516-5519.

[13]   A. H. Lewin, M. J. Zovko, W. H. Rosewater, T. Cohen, *Chem. Commun.* **1967**, 80-81.

[14]   T. M. Figueira-Duarte, S. C. Simon, M. Wagner, S. I. Drtezhinin, K. A. Zachariasse, K. Müllen, *Angew. Chem., Int. Ed.* **2008**, *47*, 10175-10178.

10 List of Publications

10.2 Scientific Publications

[1]   <u>F. Schlütter</u>, F. Rossel, M. Kivala, V. Enkelmann, J.-P. Gisselbrecht, P. Ruffieux,
        R. Fasel, K. Müllen, *J. Am. Chem. Soc.* **2013**, *135*, 4550-4557.

[2]   <u>F. Schlütter</u>, T. Nishiuchi, V. Enkelmann, K. Müllen, *Polym. Chem.* **2013**, *4*, 2963-
        2967.

[3]   K. Schmoltner, <u>F. Schlütter</u>, M. Kivala, M. Baumgarten, S. Winkler, R. Trattnig,
        N. Koch, A. Klug, E.J.W. List, K. Müllen, *Polym. Chem.* **2013**, *4*, 5337-5344.

[4]   K. Mali, <u>F. Schlütter</u>, M. Kivala, K. Müllen, S. De Feyter, *in preparation*.

[5]   A. Wild, A. Teichler, C.-L. Ho, X.Z. Wang, H. Zhan, <u>F. Schlütter</u>, A. Winter,
        M.D. Hager, W.-Y. Wong, U.S. Schubert, *J. Mater. Chem. C*, **2013**, *1*, 1812-1822.

[6]   A.M. Breul, J. Schäfer, C. Friebe, <u>F. Schlütter</u>, R.M. Paulus, G. Festag, M.D.
        Hager, A. Winter, B. Dietzek, Jürgen Popp, Ulrich S. Schubert, *Macromol. Chem.
        Phys.* **2012**, *213*, 808-819.

[7]   <u>F. Schlütter</u>, G.M. Pavlov, J.-F. Gohy, A. Wild, A. Winter, M.D. Hager, S.
        Hoeppener, U.S. Schubert, *J. Polym. Sci. A, Polym. Chem.* **2011**, *49*, 1396-1408.

[8]   R. Siebert, C. Hunger, J. Guthmüller, <u>F. Schlütter</u>, A. Winter, U.S. Schubert,
        L. Gonzalez, B. Dietzek, J. Popp, *J. Phys. Chem. C* **2011**, *115*, 12677-12688.

[9]   R. Siebert, <u>F. Schlütter</u>, A. Winter, M. Presselt, H. Görls, U.S. Schubert,
        B. Dietzek, J. Popp, *Cent. Eur. J. Chem.* **2011**, *9*, 990-999.

[10]   A. Wild, A. Winter, <u>F. Schlütter</u>, U.S. Schubert, *Chem. Soc. Rev.*, **2011**, *40*, 1459-
        1511.

[11]   <u>F. Schlütter</u>, A. Wild, A. Winter, M.D. Hager, A. Baumgaertel, C. Friebe,
        U.S. Schubert, *Macromolecules* **2010**, *43*, 2759-2771.

[12]   A. Wild, <u>F. Schlütter</u>, G. M. Pavlov, C. Friebe, G. Festag, A. Winter, M.D. Hager,
        V. Cimrova, U.S. Schubert, *Macromol. Rapid Commun.* **2010**,*31*, 868-874.

[13]   A. Wild, S. Hornig, <u>F. Schlütter</u>, J. Vitz, C. Friebe, M.D. Hager, A. Winter,
        U.S. Schubert, *Macromol. Rapid Commun.* **2010**,*31*, 921-927.

10.3 Patent

F. Schlütter, M. Kivala, K. Müllen, H. Wonneberger, I. Bruder, R. Send „Thermally stable p-conducting triangulene oligomers for application in photovoltaic cells" US61/752509.

11 Acknowledgements

██

█████████

██

██

██

██

███

██

██

██

██████████████████

██

███

██

██████████████████████████████████

██

██

██

██

██

████████████████████████████████████

██

- ██

  ████████████████████████████

- ██

  ████████████████████████████████

- ██

  ██████████████████████████████████

- ██
  ████████████████████████████████████

- ██
  ██
  ██████████████████

- ██
  ████████████████████████████████████

- ██
  ███████████████████████████████

- ██
  ███████████████████████████

██
██
██
██
████████████████████████

██
██
██
██
██████████████

██
██
██
██
███

12 Lebenslauf

■ Persönliche Daten

Name: Florian Schlütter

Geburtsdatum/-ort: 30.12.1984 in Suhl

Nationalität: deutsch

■ Ausbildung

■ Praktische Erfahrungen

◼ Präsentationen

- ███████████████████████████████████
  ████████████████

- ███████████████████████████████████
  █████████████████████

- ███████████████████████████████████
  █████████████

Mainz, 10.12.2013

██████████████████████████
██████████████████████████
██████████████████████████
██████████████████████████